

Authors: Webb, W. Richard; Muller, Nestor L.; Naidich, David P.

Title: *High-Resolution CT of the Lung, 3rd Edition*

Copyright ©2001 Lippincott Williams & Wilkins

> Table of Contents > Chapter 1 - Technical Aspects of High-Resolution Computed Tomography

Chapter 1

Technical Aspects of High-Resolution Computed Tomography

Although the introduction of computed tomography (CT) revolutionized the radiologic diagnosis of chest diseases, the ability of early CT scanners to evaluate pulmonary parenchymal diseases was limited by their resolving power [1]. Specifically, CT obtained with long scan times (18 seconds) and 1-cm collimation provided insufficient anatomic detail to allow a precise evaluation of normal and abnormal pulmonary anatomy, at least to the degree that it would surpass the information available on plain radiographs.

Attempts to improve the resolution of CT for diagnosing lung abnormalities were first described relative to the assessment of focal lung disease and lung nodules. In 1980, Siegelman et al. [2] emphasized the necessity of using 5-mm collimation for the detection of calcification in lung nodules. As thinner collimation became available on commercial scanners, simultaneous with other developments in CT technology, the use of CT for the precise anatomic definition of diffuse lung diseases became possible and was reported by several authors. The first use of the term high-resolution CT (HRCT) has been attributed to Todo, Itoh, and

others [3], who described the potential use of this technique for assessing lung disease in 1982. The first reports of HRCT in English date to 1985, including landmark descriptions of HRCT findings by Nakata, Naidich, and Zerhouni [4, 5, 6]. HRCT techniques developed since then are capable of imaging the lung with excellent spatial resolution, providing anatomic detail similar to that available from gross pathologic specimens or lung slices [7, 8, 9, 10]. HRCT can demonstrate the normal and abnormal lung interstitium and morphologic characteristics of both localized and diffuse parenchymal abnormalities; in this regard, HRCT is clearly superior to plain radiographs and conventional CT. HRCT has become established as an important diagnostic modality and has significantly contributed to our understanding of diffuse lung diseases. In this chapter, we review the CT techniques that are appropriate in obtaining HRCT, spiral HRCT techniques, scan protocols recommended in specific clinical settings, expiratory HRCT, the spatial resolution of HRCT, the radiation dose associated with HRCT, and common HRCT artifacts.

TABLE 1-1. *Summary of HRCT
technique*

Recommended

Collimation: thinnest available collimation (1.0-1.5 mm).

Reconstruction algorithm: high-spatial frequency or **"sharp" algorithm (i.e., GE "bone")**.

Scan time: as short as possible (1 sec or less).

kV(p), 120-140; mA, 240.

Matrix size: largest available (512 × 512).

Windows: At least one consistent lung window setting is necessary. Window mean/width values of -600 HU to -700 HU/1,000 HU to 1,500 HU are appropriate. Good combinations are -700/1,000 HU or -600/1,500 HU.

Soft-tissue windows of approximately 50/350 HU should also be used for the mediastinum, hila, and pleura.

Image display: photography of lung windows 12 on 1.

Optional

kV(p)/mA: Increased kV(p)/mA (i.e., 140/340).

Recommended in large patients. Otherwise optional.

Reduced mA (low-dose HRCT): 40-80 mA.

Targeted reconstruction: (15- to 25-cm field of view).

Windows: Windows may need to be customized; a low-window mean (-800 to -900 HU) is optimal for diagnosing emphysema. For viewing the mediastinum, 50/350 HU is recommended. For viewing pleuro-parenchymal disease, -600/2,000 HU is recommended.

Image display: Photography of lung windows 6 on 1.

High-Resolution Computed Tomography Technique

The HRCT technique attempts to optimize the demonstration of lung anatomy. Although each of the three of us performs HRCT in a slightly different manner, experienced radiologists generally agree as to what technical **modifications constitute a “high-resolution” CT study.** This section reviews the effect of various technical factors on the appearance of HRCT and summarizes our recommendations for techniques that are either necessary or optional for obtaining an adequate examination.

The most important modifications of CT technique used to increase spatial resolution are the uses of thin collimation and image reconstruction with a high-spatial frequency (sharp) algorithm. Increased kilovolt (peak) [kV(p)] or milliamperes (mA) and targeted image reconstruction may also be used to improve image quality and increase spatial resolution, but these techniques are optional (Table 1-1) [7, 8, 9, 10, 11, 12, 13]. The use of appropriate window settings and methods of image display are also necessary to obtain optimal diagnostic images.

Scan Collimation

With thick (7- to 10-mm) collimation, volume averaging within the plane of scan significantly reduces the ability of CT to resolve small structures. Therefore, scanning with the thinnest possible collimation (1- to 1.5-mm) is essential if spatial resolution is to be optimized [4, 6, 10, 11] (Table 1-1). The use of 3- to 5-mm collimation should not be considered for HRCT.

Murata et al. [13] compared the ability of HRCT scans performed with 1.5- and 3-mm collimation to allow the identification of small vessels, bronchi, interlobular septa, and some pathologic findings. With 1.5-mm collimation, greater contrast was evident between vessels and surrounding lung parenchyma, more branches of small vessels were seen, and small bronchi were more often recognizable than with 3-mm collimation [13]. Also, slight increases in lung attenuation (as in early interstitial disease), or decreases in attenuation (as in emphysema) were better resolved with 1.5-mm collimation. On the other hand, the authors concluded that certain pathologic findings, such as thickened interlobular septa, were similarly visible on images with 1.5- and 3-mm collimation [13].

There are several differences in how lung structures are visualized on scans performed with thin collimation compared to more thickly collimated scans. With thin collimation, it is more difficult to follow the courses of vessels and bronchi than it is with 7- to 10-mm collimation. With thick collimation, for example, vessels that lie in the plane of scan look like vessels (i.e., they appear cylindrical or branching) and can be clearly identified as such. With thin collimation, vessels can appear nodular, because only short segments may lie in the plane of scan; this finding may lead to confusion (Fig. 1-1), but with experience, this difficulty is avoided easily.

Also, with thin collimation, the diameter of a vessel that lies in or near the plane of scan can appear larger than it does with 1-cm collimation, because less volume averaging is occurring between the rounded edge of the vessel and the adjacent air-filled lung (Fig. 1-1); thin collimation scans

more accurately reflect vessel diameter in this setting, analogous to the better estimation of the diameter of a lung nodule that is possible with thin collimation. Furthermore, with 1-mm collimation, bronchi that are oriented obliquely relative to the scan plane are much better defined than they are with 1-cm collimation, and their wall thicknesses and luminal diameters are more accurately assessed [14]. The diameters of vessels or bronchi that lie perpendicular to the scan plane appear the same with both thin and thick collimation.

Reconstruction Algorithm

The inherent or maximum spatial resolution of a CT scanner is determined by the geometry of the data collecting system and the frequency at which scan data are sampled during the scan sequence [11]. The spatial resolution of the image produced is less than the inherent resolution of the scan system, depending on the reconstruction algorithm that is used, the matrix size, and the field of view (FOV), all of which in turn determine pixel size. In HRCT, these parameters are optimized to increase the spatial resolution of the image.

With conventional body CT, scan data are usually reconstructed with a relatively low-spatial frequency **algorithm (e.g., "standard" or "soft-tissue" algorithms)**, that smoothes the image, reduces visible image noise, and improves the contrast resolution to some degree [12, 15]. Low-spatial frequency simply means that the frequency of information recorded in the final image is relatively low; it is the same as saying that the algorithm is low-resolution rather than high-resolution.

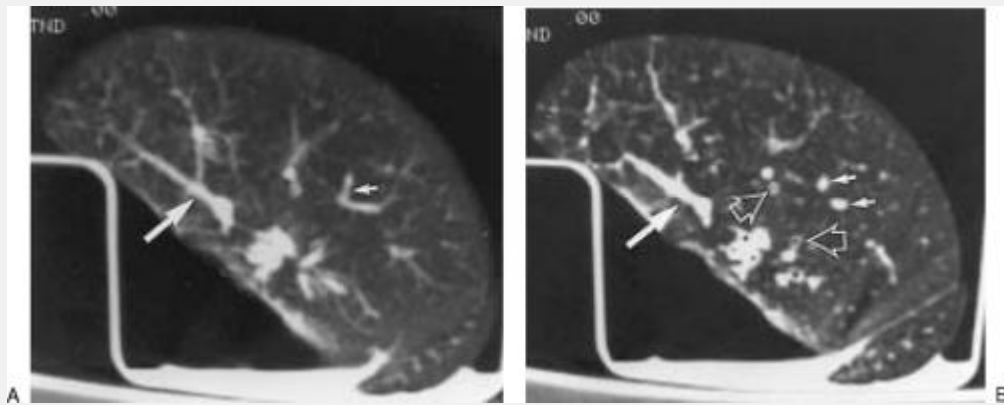


FIG. 1-1. Effects of collimation on resolution. A: Conventional CT of a fresh inflated human lung obtained with 1-cm collimation and reconstructed with the standard algorithm. Several cylindrical or branching pulmonary arteries (small arrow) are visible. A large pulmonary artery branch (large arrow) lies in the plane of scan. B: CT at the same level with 1.5-mm collimation; technical parameters and reconstructed algorithm are otherwise identical. Pulmonary arteries seen as branching or cylindrical on the scan obtained using 1-cm collimation appear nodular on the scan with 1.5-mm collimation (small arrows). Small bronchi (open arrows) are much better seen with thin collimation. Note that the large pulmonary vessel that lies in the plane of scan appears to have a greater diameter with thin collimation (large arrow) than it does with 1-cm collimation.

P. 3

Reconstruction of the image using a high-spatial frequency algorithm—in other words, a high-resolution algorithm (e.g., General Electric “bone” algorithm), reduces image

smoothing and increases spatial resolution, making structures appear sharper (Fig. 1-2) [4, 11, 13]. In one study of HRCT techniques [11], a quantitative improvement in spatial resolution was found when the bone, instead of the standard, algorithm was used to reconstruct scan data (Fig. 1-3); in this study, subjective image quality was also rated more highly with the bone

P.4

algorithm. In another study of HRCT [13], small vessels and bronchi were better seen when images were reconstructed with the bone algorithm than when the standard algorithm was used. The use of a sharp algorithm has also been recommended for routine chest CT performed using 1-cm collimation, to improve spatial resolution [16].

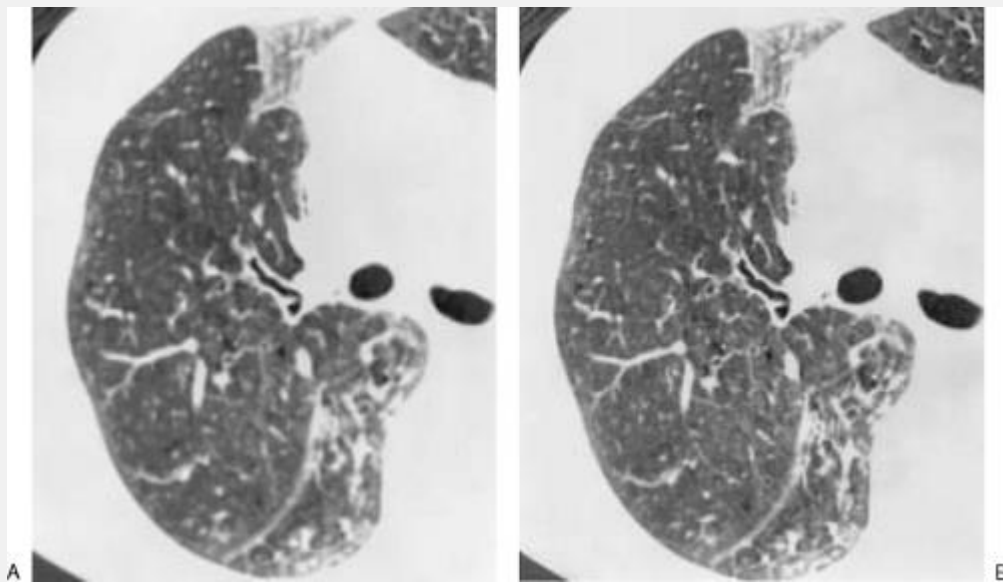


FIG. 1-2. Effect of reconstruction algorithm on resolution. A CT scan obtained with 1.5-mm collimation has been reconstructed using a smoothing (standard) algorithm (A) and a sharp (bone) algorithm (B). Lung structures appear

much sharper with the bone algorithm.

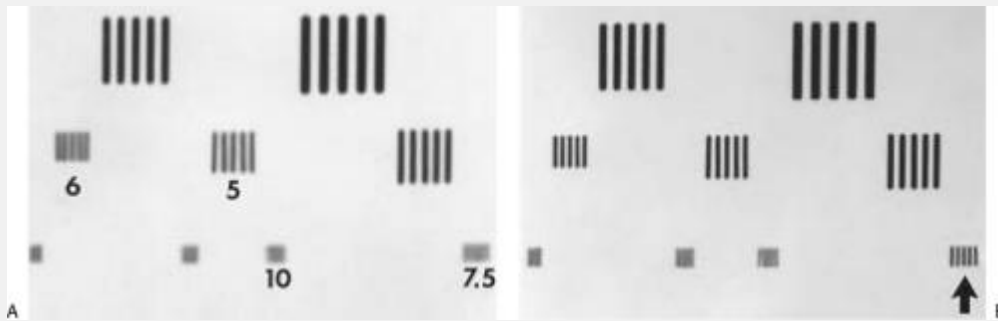


FIG. 1-3. Effect of reconstruction algorithm on spatial resolution. A: HRCT of a line-pair phantom obtained with 1.5-mm collimation and reconstructed with the standard algorithm. Numbers indicate the resolution in line pairs per cm. The resolution with this technique is 6-line pairs per cm. B: When the same scan is reconstructed using the bone algorithm, spatial resolution improves. Also, in contrast to the scan reconstructed using the standard algorithm, 7.5-line pairs are easily resolved (arrow), and edges are considerably sharper. (From Mayo JR, Webb WR, Gould R, et al. High-resolution CT of the lungs: an optimal approach. *Radiology* 1987;163:507, with permission.)

Using a sharp, or high-resolution, algorithm is a critical element in performing HRCT (Table 1-1) [12, 15].

Kilovolt (Peak), Milliamperes, Scan Time, and Low-Dose High-Resolution Computed Tomography

In HRCT, image noise is more apparent than with standard CT. This noise usually appears as a graininess or mottle that can be distracting and may obscure anatomic detail (Fig. 1-4) [11]. High-resolution techniques using a sharp reconstruction algorithm, in addition to increasing image detail, increase the visibility of noise in the CT image [12, 15]. Because much of this noise is quantum-related and thus decreases with increased technique (number of photons), increasing the mA or kV(p) used during scanning, or increasing scan time, can reduce noise and improve scan quality (Fig. 1-5) [11]; noise is inversely proportional to the number of photons absorbed (precisely, it is inversely proportional to the square root of the product of the mA and scan time).

Increasing scan time is not generally desirable with lung CT. Because of patient motion, longer scan times can result in an increase in motion-related artifacts. When available, a scan time of 1 second or less is most appropriate for HRCT and is recommended (Table 1-1).

mA and kV(p) can be easily increased when obtaining HRCT, which results in a reduction in visible image noise. In one study [11], a measure of image noise was reduced by approximately 30% when kV(p)/mA were increased from 120/100 to 140/170 (2-second scan time) (Fig. 1-5), and the scans with increased kV(p) and mA settings were rated by observers as being of better quality 80% of the time (Fig. 1-6) [11]. It should also be kept in mind, however, that increasing scan technique also increases the patient's radiation dose [17], although with HRCT, radiation is limited to a few thin scan levels (as discussed below).

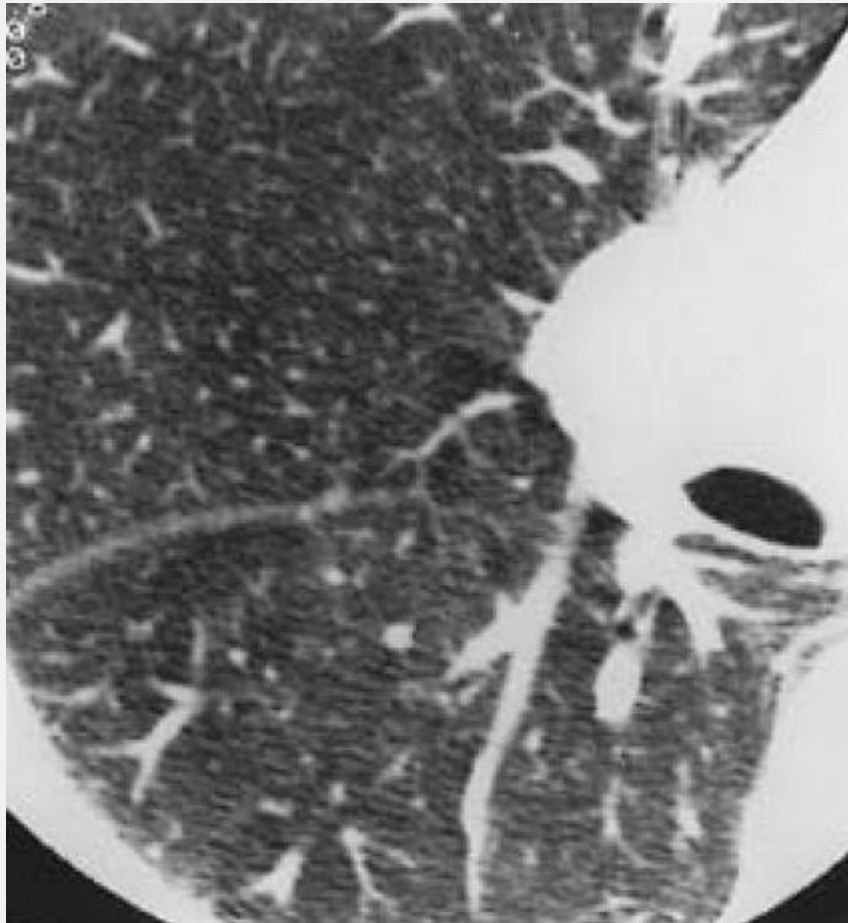


FIG. 1-4. Image noise. Detailed view of an HRCT image of the right lung. The mottled appearance, which is most evident posteriorly, represents image noise. Very thin linear streaks, best seen in the anterior part of the image, represent "aliasing" artifacts.

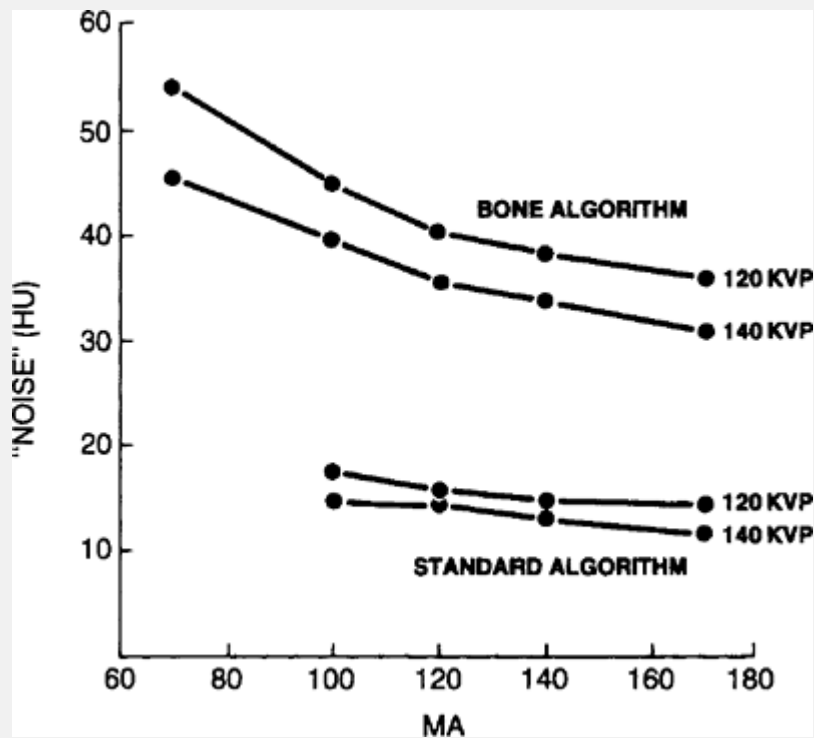


FIG. 1-5. Effect of algorithm, kV(p), and mA on image noise. Graph of HRCT image noise (standard deviation of Hounsfield unit measurements) in an anthropomorphic CT phantom [21] as related to the reconstruction algorithm and scan technique. Noise increases when the bone algorithm is used instead of the standard algorithm. With the bone algorithm, noise decreases approximately 30% with increased kV(p) and mA settings. (From Mayo JR, Webb WR, Gould R, et al. High-resolution CT of the lungs: an optimal approach. *Radiology* 1987;163:507, with permission.)

P.5

Although increasing kV(p) and mA reduces image noise, this modification is not generally necessary with current scanners. Adequate diagnostic scans can be obtained in most patients using routine techniques for chest CT [18],

although image quality may not be quite as good as when technique is increased. Use of current scanners capable of a 1-second scan time, scan techniques of 120 to 140 kV(p), and mA values of approximately 240 has proven quite satisfactory [19].

Furthermore, the efficacy of low-dose HRCT has been assessed in several studies [20, 21, 22, 23]. In a study by Zwirerich et al. [20], scans with 1.5-mm collimation, and 2-second scan time, and at 120 kV(p), were obtained using both 20 mA (low-dose HRCT) and 200 mA (conventional-dose HRCT) at selected levels in the chests of 31 patients. Observers evaluated the visibility of normal structures, various parenchymal abnormalities, and artifacts using both techniques. Low-dose and conventional-dose HRCT were equivalent for the demonstration of vessels, lobular and segmental bronchi, and structures of the secondary pulmonary lobule and in characterizing the extent and distribution of reticular abnormalities, honeycomb cysts, and thickened interlobular septa. However, the low-dose technique failed to demonstrate ground-glass opacity in two of ten cases, and emphysema in one of nine cases, although they were evident but subtle on the usual-dose HRCT. Linear streak artifacts were also more prominent on images acquired with the low-dose technique, but the two techniques were judged equally diagnostic in 97% of cases. The authors concluded that HRCT images acquired at 20 mA yield anatomic information equivalent to that obtained with 200-mA scans in the majority of patients without significant loss of spatial resolution or image degradation due to streak artifacts.

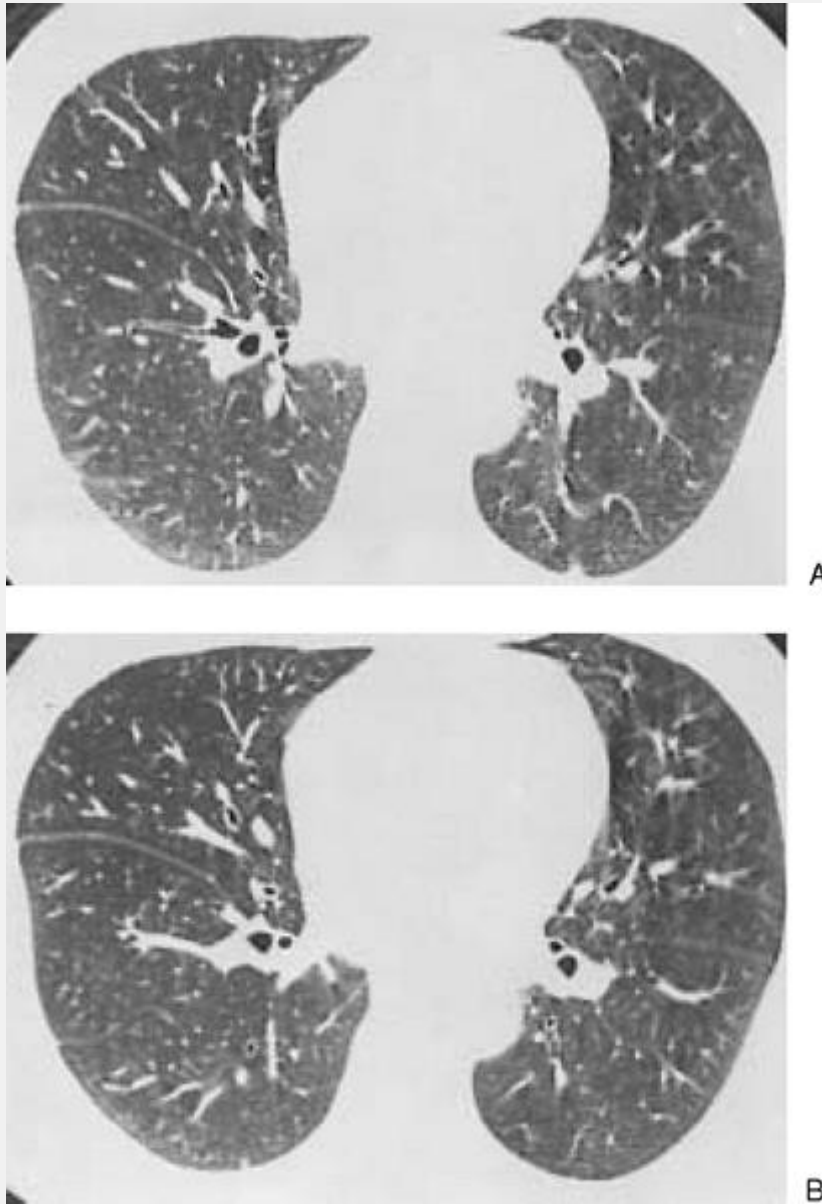


FIG. 1-6. Effect of kV(p) and mA on image noise. HRCT scans obtained with kV(p)/mA settings of 120/100 (A) and 140/170 (B). Noise is most evident posteriorly and in the paravertebral regions. Although noise is greater in A, the difference is probably not significant clinically. Nonetheless, increasing the kV(p)/mA is optimal. Also note pulsation ("star") artifacts in the left lung on both images and a "double" left major fissure. (From Mayo JR, Webb WR, Gould

R, et al. High-resolution CT of the lungs: an optimal approach. *Radiology* 1987;163:507, with permission.)

In a subsequent study [21], the diagnostic accuracies of chest radiographs, low-dose HRCT [80 mA; 120 kV(p), 40 mA, 2 seconds] and conventional-dose HRCT [340 mA; 120 kV(p), 170 mA, 2 seconds] were compared in 50 patients with chronic infiltrative lung disease and ten normal controls. For each HRCT technique, only three images were used, obtained at the levels of the aortic arch, tracheal carina, and 1 cm above the right hemidiaphragm. A correct first-choice diagnosis was made significantly more often with either HRCT technique than with radiography; the correct

P.6

diagnosis was made in 65% of cases using radiographs, 74% of cases with low-dose HRCT ($p < .02$), and 80% of conventional HRCT ($p < .005$). A high confidence level in making a diagnosis was reached in 42% of radiographic examinations, 61% of the low-dose HRCT examinations ($p < .01$), and 63% of the conventional-dose HRCT examinations ($p < .005$), and it was correct in 92%, 90%, and 96% of the studies, respectively. Although conventional-dose HRCT was more accurate than low-dose HRCT, this difference was not significant, and both techniques provided quite similar anatomic information (Figs. 1-7 and 1-8) [21].

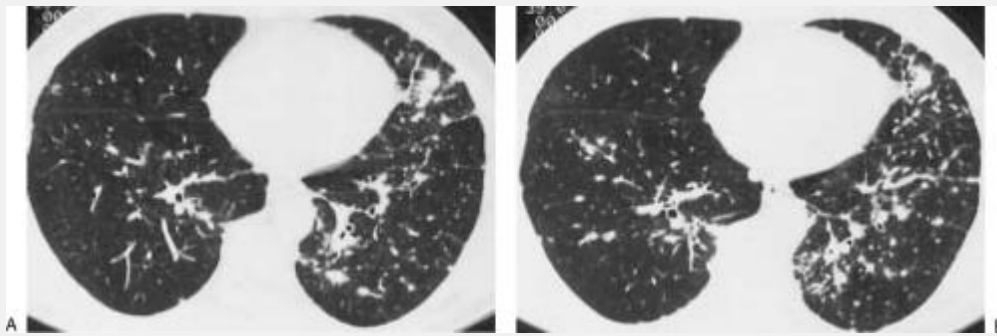


FIG. 1-7. Low-dose (A) and conventional-dose (B) HRCT in a patient with sarcoidosis. Both techniques demonstrate the presence of small peribronchovascular, septal, and subpleural nodules typical of this disease. Despite the increased noise on the low-dose image, the pattern and extent of abnormalities are equally well seen with both techniques. (From Lee KS, Primack SL, Staples CA, et al. Chronic infiltrative lung disease: comparison of diagnostic accuracies of radiography and low- and conventional-dose thin-section CT. *Radiology* 1994;191:669, with permission.)

Majurin et al. [22] compared a variety of low-dose techniques in 45 patients with suspected asbestos-related lung disease. Of the 37 patients with CT evidence of lung fibrosis, HRCT images obtained with mA as low as 120 (60 mA/2 seconds) clearly showed parenchymal bands, curvilinear opacities, and honeycombing. However, reliable identification of interstitial lines or areas of ground-glass opacity required a minimum technique of 160 mA (80 mA/2 seconds). Furthermore, these authors showed that using the lowest possible dosage (30 mA/2 seconds) HRCT was

sufficient only for detecting marked pleural thickening and areas of gross lung fibrosis.

Although optimizing resolution may require the use of increased mA and kV(p), this is optional and uncommonly used with current scanners (Table 1-1). In the majority of patients, diagnostic scans will be obtained without increased P.7

ing scan technique. Because noise is usually a bigger problem in large patients (because more x-ray photons are attenuated by the patient) (Fig. 1-9) and in the posterior part of the scan image (because of photon attenuation by the spine), it would be most important to use increased technical factors when studying large patients or patients with suspected posterior lung disease [11]. Low-dose HRCT should not be routinely used for the initial evaluation of patients with lung disease, although it can be valuable in following patients with a known lung abnormality or in screening large populations at risk for lung disease. Optimal low-dose techniques will likely vary with the clinical setting and indication for the study, and they remain to be established.

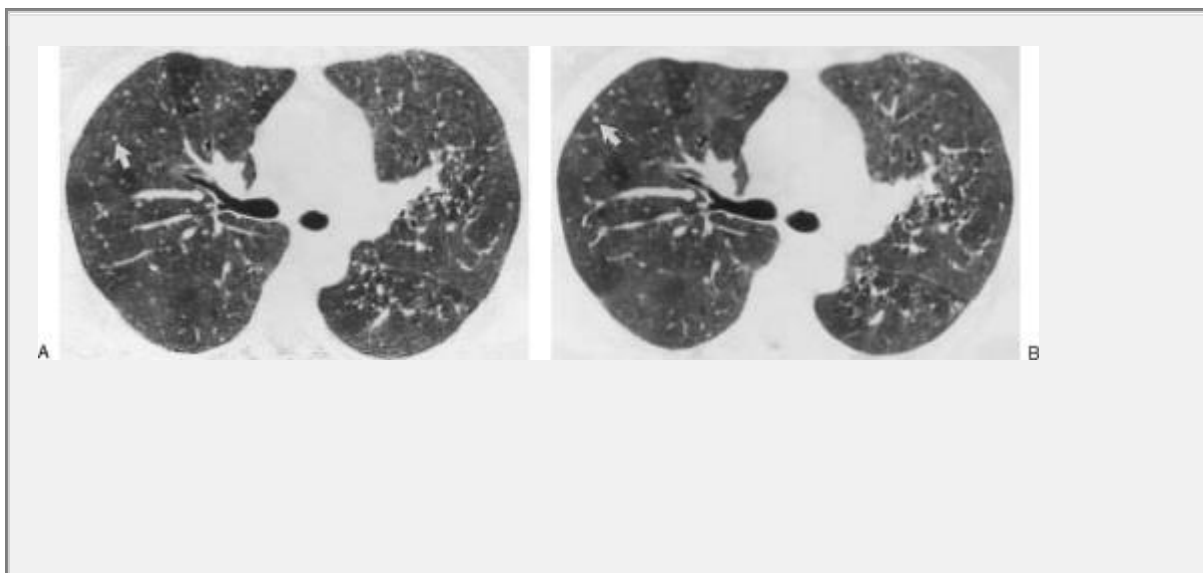


FIG. 1-8. Low-dose (A) and conventional-dose (B) HRCT in a patient with hypersensitivity pneumonitis. Although noise is much more obvious on the low-dose image, areas of ground-glass opacity and ill-defined nodules (arrows) are visible with both techniques. (From Lee KS, Primack SL, Staples CA, et al. Chronic infiltrative lung disease: comparison of diagnostic accuracies of radiography and low- and conventional-dose thin-section CT. *Radiology* 1994;191:669, with permission.)

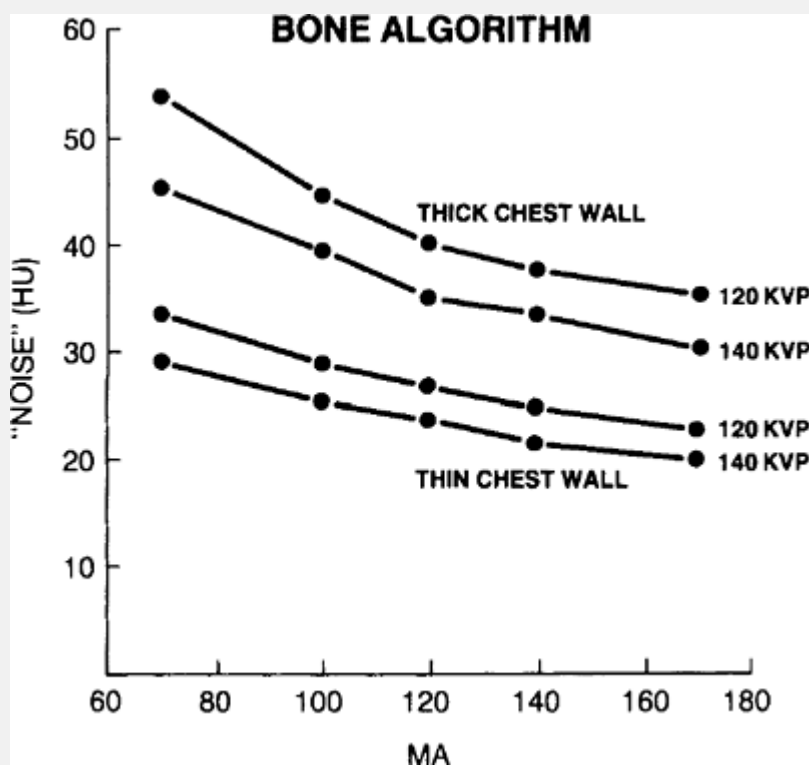


FIG. 1-9. Relationship of noise to patient size. Graph of image noise measured using an anthropomorphic chest phantom [21], with simulated thick and thin chest walls. Noise significantly increases with the thick chest wall. (From Mayo JR, Webb WR, Gould R, et al. High-resolution CT of the lungs: an optimal approach. *Radiology* 1987;163:507, with

permission.)

Matrix Size, Field of View, and the Use of Targeted Reconstruction

The largest matrix available should be used routinely in image reconstruction, to reduce pixel size [4, 11, 13]. The largest available matrix is usually 512×512.

Scanning should be performed using an FOV large enough to encompass the patient (e.g., 35 cm). Retrospectively targeting image reconstruction to a single lung instead of the entire thorax, using a smaller FOV, significantly reduces the image pixel size and thus increases spatial reso

P.8

lution (Fig. 1-10) [11, 18]. For example, with a 40-cm reconstruction circle (FOV) and a 512 × 512 matrix, pixel size measures 0.78 mm. With targeted image reconstruction using a 25-cm FOV, pixel size is reduced to 0.49 mm, and the spatial resolution is correspondingly increased (Fig. 1-11). Using a 15-cm FOV further reduces pixel size to 0.29 mm, but this FOV is usually insufficient to view an entire lung and is not often used clinically. It should be recognized, however, that the improvement in resolution obtainable by targeting is limited by the intrinsic resolution of the detectors. For example, with a General Electric 9800 system, optimal matching of the inherent spatial resolution of the scanner and pixel size occurs at a reconstruction diameter of approximately 13 cm and a pixel size of 0.25 mm [11, 12, 15]; further reduction in the FOV would be of no benefit in improving spatial resolution.

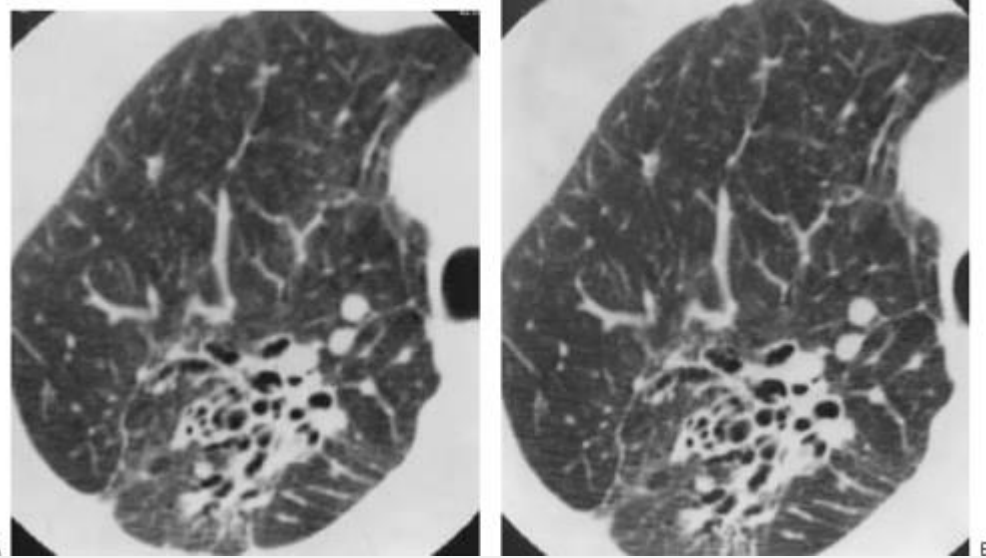


FIG. 1-10. Effect of targeted reconstruction on resolution. A: CT image in a patient with end-stage sarcoidosis obtained with a 38-cm field of view (FOV) and 1.5-mm collimation, and reconstructed using the bone algorithm and a 38-cm reconstruction circle. B: The same CT scan has been reconstructed using a targeted FOV (15 cm), reducing image-pixel diameter. Image sharpness is improved compared to A.

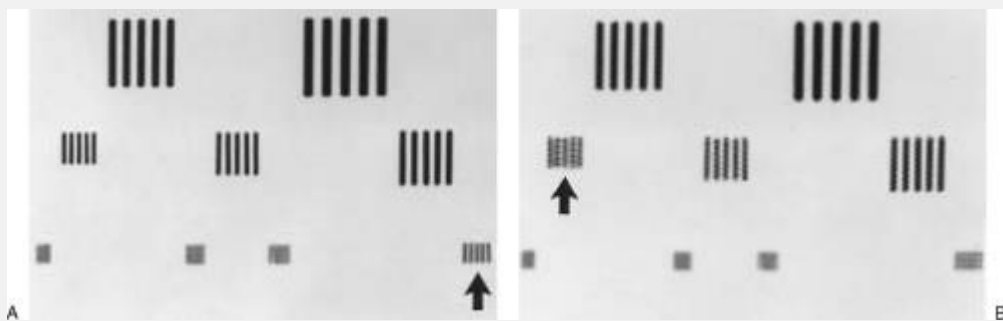


FIG. 1-11. Effect of targeted reconstruction on spatial

resolution. A: HRCT of a line-pair phantom. The scan was obtained with a 40-cm field of view (FOV), and reconstructed using a targeted FOV of 25 cm. The resolution with this technique is 7.5-line pairs (arrow). B: The same scan viewed without targeting shows the effects of larger pixel size. Only 6-line pairs can be resolved (arrow), and the margins of the lines appear jagged or wavy. (From Mayo JR, Webb WR, Gould R, et al. High-resolution CT of the lungs: an optimal approach. *Radiology* 1987;163:507, with permission.)

The use of image targeting, or targeted reconstruction, is often a matter of personal preference. In clinical practice, use of image targeting is uncommon because it requires additional reconstruction time, the raw scan data must be saved until targeting is performed, and additional filming is required to display all the images. Also, with a nontargeted reconstruction, the ability to see both lungs on the same image allows a quick comparison of one lung to the other; this can be quite helpful in diagnosis and is preferred to the marginal increase in resolution achieved with targeting. Image targeting is considered to be optional (Table 1-1) and is recommended only when optimal resolution is desired.

Window Settings

The window mean and width used for photography have a significant impact on the appearance of the lung parenchyma and the dimensions of visualized structures (Fig. 1-12) [14, 24]. If the display technique used is not appropriate, normal structures can be made to look abnormal, or subtle abnormalities may be overlooked.

The most important window setting to use in photography is the so-called lung window. It should be emphasized that there is no single correct or ideal window setting for the demonstration of lung anatomy on HRCT, and several combinations of window mean and width may be appropriate [25]. Within limits, the precise window width and levels chosen are a matter of personal preference; the values indicated below should serve only as guidelines. However, it is important that a single lung window setting be used consistently in all patients. Unless this is done, it is difficult to compare one case to another, develop an understanding of what appearances are normal and abnormal, and compare sequential examinations in the same patient. Although it is not inappropriate to use some additional window settings in specific cases, depending on what abnormality is being sought, the effects of the variations in window settings on the appearance of the resulting images must be kept in mind.

Level and width settings of approximately -700/1,000 Hounsfield units (HU) are appropriate for a routine lung window (Fig. 1-12). Some authors prefer using a window width of 1,500 HU when viewing the lung, with a window mean of -600 to -700 HU; such settings should also be considered appropriate for routine lung imaging. It should be recognized, however, that an extended window width reduces contrast between lung parenchymal structures, such as vessels, bronchi, and the air-containing alveoli, and may make interstitial structures appear less conspicuous or thinner than they actually are. On the other hand, extended windows may be of some value in detecting abnormalities of overall lung attenuation [26, 27] and are also useful in evaluating the relationship of peripheral parenchymal

abnormalities to the pleural surfaces. A window width of less than 1,000 HU is not generally appropriate for viewing lung parenchyma, as it unnecessarily increases contrast and may result in an apparent increase in the size of soft-tissue
P.9

P.10

structures. For example, the effect of window mean and level on the HRCT appearance of bronchial walls has been assessed using inflation-fixed lungs [24]. In this study, window widths less than 1,000 HU resulted in a substantial overestimation of bronchial wall thickness, whereas window widths greater than 1,400 HU resulted in an underestimation of bronchial wall thickness (Fig 1-13).

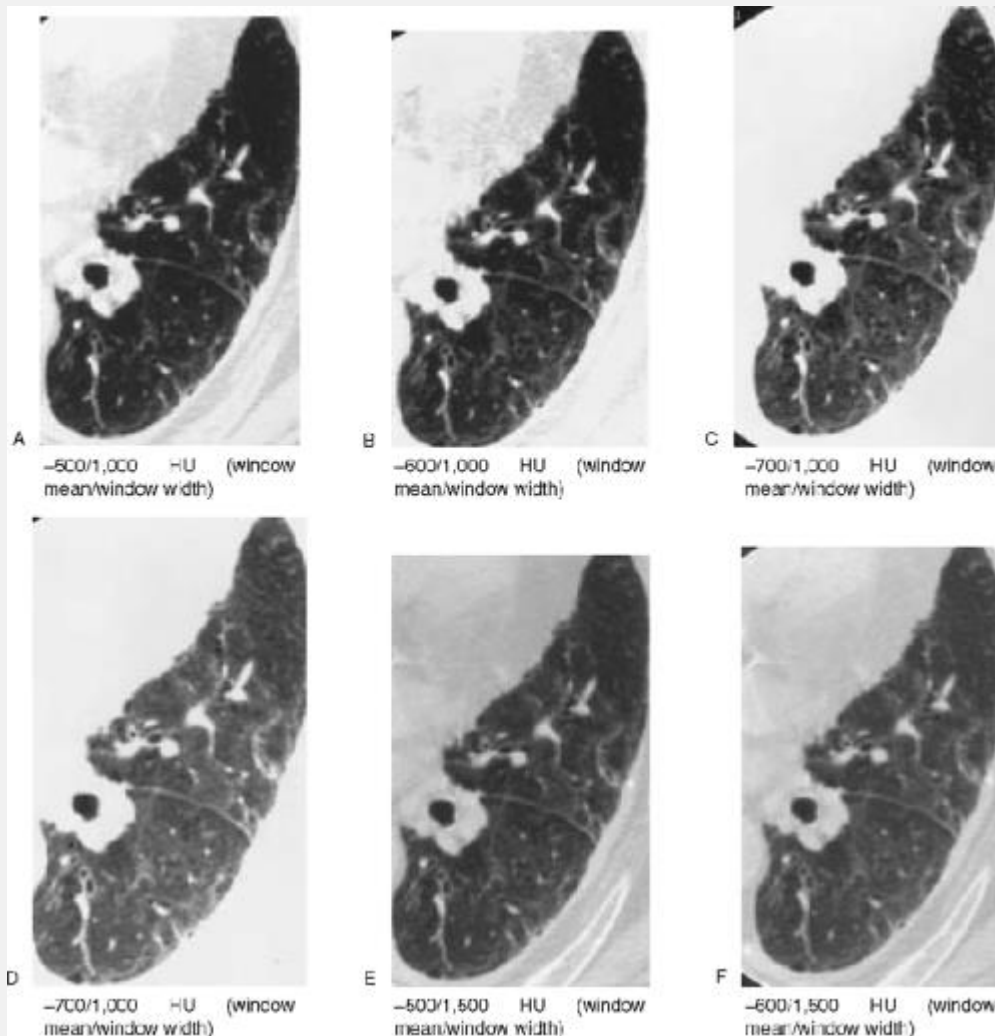


FIG. 1-12. Effects of window mean and width on the appearance of lung and soft tissues in a patient with asbestosis. Window means decrease from left to right. Window widths increase from top to bottom. A-D: A window width of 1,000 HU and a window mean of -700 HU (C) provides good contrast between soft-tissue structures in the lung (vessels and interstitial abnormalities) and lung parenchyma, allows areas of lung with varying attenuation to be distinguished, and allows air-filled structures (e.g., bronchi, cysts) to be contrasted with lung parenchyma. Abnormal reticular opacities and areas of increased lung and

decreased lung attenuation are all visible in C. Higher window means (A) make lung opacities more difficult to see or make them appear smaller. A lower window mean (D) accentuates the visibility of lung opacities and allows air-filled structures to be contrasted with lung parenchyma, but can also make normal lung appear abnormally dense. E-G: Wider window settings result in less contrast between soft-tissue lung structures and lung parenchyma. Those images with window levels of -600 and -700 HU (F, G) and a width of 1,500 HU provide information comparable to -700/1,000 HU. H, I: With a window width of 2,000 HU, much less contrast between normal and abnormal lung regions is visible. However, with this window setting, pleural thickening and calcification are visible.

Viewing soft-tissue windows is also important in reading HRCT. Window level/width settings of 50/350 HU or 50/450 HU are best for evaluation of the mediastinum, hila, and pleura. Mediastinal and pleural abnormalities are sometimes of value in interpreting HRCT of the lung (Table 1-1). For example, the presence of lymph node enlargement, esophageal dilatation, calcification, or pleural thickening may be helpful in making a correct diagnosis of lung disease. When performing an HRCT study, images are routinely displayed using both lung and soft-tissue windows. As stated, choosing different window levels can be advantageous in individual cases, despite the fact they may not be optimal for all indications (Fig. 1-12). Low-window settings

P.12

P.13

P.14

(-800 to -900 HU) with narrow-window widths (500 HU) can be valuable in contrasting emphysema or air-filled cystic lesions with normal lung parenchyma. With such a low-window mean, normal lung parenchyma looks gray, whereas areas of emphysema remain black. On the other hand, using this same window to image the lung interstitium would be improper. Such a low-window mean, particularly combined with a narrow-window width, would make the lung interstitium appear much more prominent than it really is and could make a normal case appear abnormal. This window would also result in overestimations of the size of vessels and of bronchial wall thickness.

FIG. 1-13. Effects of window mean and width on the visibility of bronchi and vessels in a normal subject. Using a narrow window width (500 HU), a high window mean (e.g., -300 HU) (A) makes bronchi and bronchial walls difficult to see, whereas a low window mean (e.g., -900 HU) (D) accentuates the apparent thickness of bronchial walls and the diameter of vessels. This effect decreases with increasing window width (i.e., 1,500 HU) (I-L). A window mean of approximately -450 HU and width of 1,000 to 1,400 HU have been shown to be best suited to measuring

bronchial wall thickness.

A window width of 2,000 HU is not generally suitable for viewing lung parenchyma, as contrast is significantly reduced. However, window settings of -500 to -700/2,000 HU may be used and are particularly useful when pleuro-parenchymal abnormalities are being evaluated (Fig. 1-12H and I) [9, 18].

Image Photography and Display

Proper photography is important in allowing the images to be interpreted accurately. A 12-on-1 format is acceptable for lung window images. However, large images are much easier to read, and using a 6-on-1 format when photographing lung windows is advantageous, particularly if both lungs are shown on the same slice. A 12-on-1 format is satisfactory for photographing of images reconstructed with a small FOV, and is satisfactory for photographing soft-tissue window images.

Cameras used to photograph CT images for viewing on film are capable of interpolating or smoothing the CT data, producing smaller pixels in the resultant image than are present in the scan itself. A similar process occurs in CT workstations. Although individual CT pixels are clearly visible on close inspection of an unprocessed HRCT image, this is not generally the case when viewing a study on film or on a workstation. In fact, if unprocessed CT images (raw CT

P.15

pixels) are viewed, the appearance can be disconcerting, and the images may be difficult to read. Cameras are

capable of photographing CT scans using a range of settings, from sharp to smooth. If the camera is set on sharp, individual CT pixels will be visible; on a smooth setting, the data are interpolated, and image pixel size is reduced (Fig. 1-14). Although it might seem that a sharp setting would be best for HRCT, this is not the case. Resolution of fine structures is better with a smooth setting, and image interpretation is easier.

The use of an electronic workstation to view HRCT images is helpful and recommended. Scans may be viewed at a larger size than generally possible on film, making small or subtle abnormalities much easier to see. It is also of diagnostic value to toggle rapidly between different preset window settings (e.g., lung window, wide lung window, soft-tissue window) at a given scan level. Having preset windows available is important; in one study assessing the utility of workstation viewing, interpreting HRCT studies with a fixed-window (-500/2,000 HU) setting proved to be more accurate than viewing them with operator-varied window settings [26]. Having preset windows available also markedly reduces the time required to interpret the images.

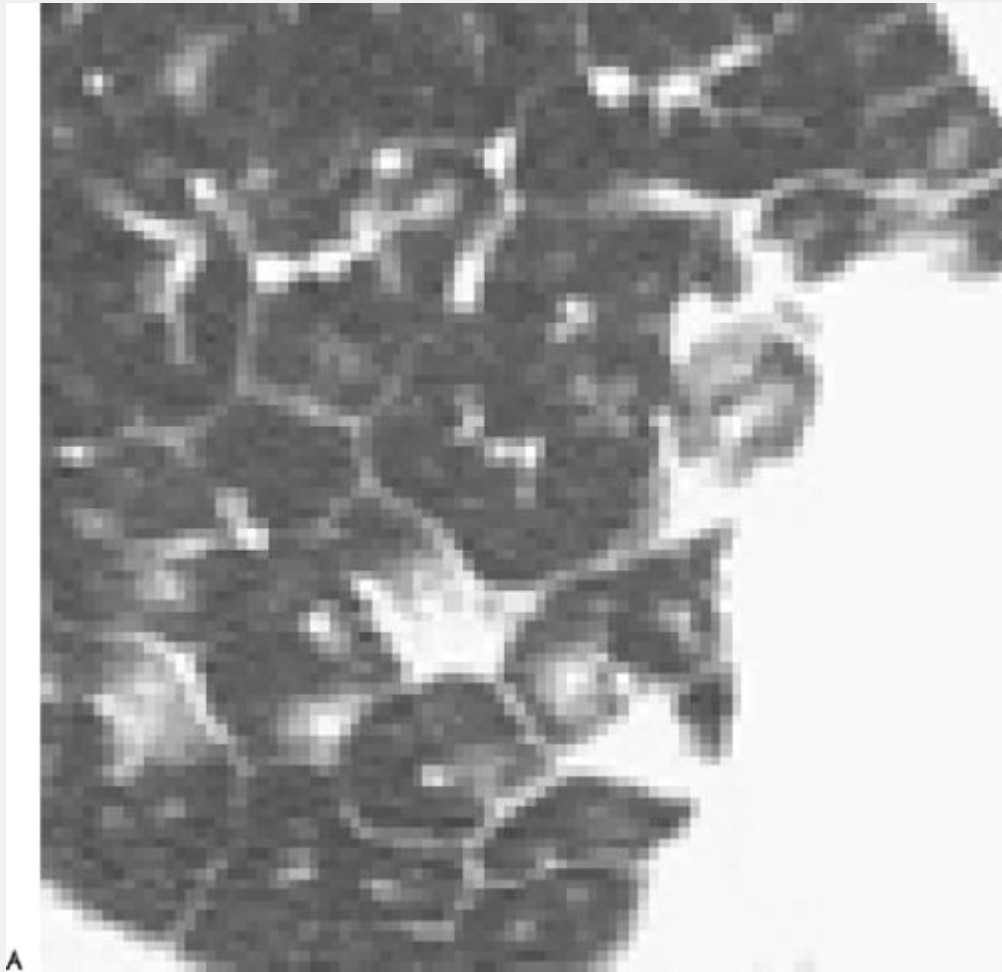


FIG. 1-14. Image interpolation and pixel size. a: Actual CT pixels are displayed on this HRCT image in a patient with interlobular septal thickening. The thickening septa have a stair-step appearance, and centrlobular arteries appear square. B: With interpolation, the appearance of the image is considerably improved. Note that a small centrlobular bronchiole clearly seen on this image (arrow) cannot be recognized on the original image (A).

High-Resolution Computed Tomography Examination: Technical Modifications

HRCT is usually performed using single slices at spaced intervals. Several technical modifications may be used, depending on the clinical indication for the study. Patient position and scan spacing are most often varied.

Inspiratory Level

Routine HRCT is obtained during suspended full inspiration, which (i) optimizes contrast between normal structures, abnormal soft tissue, and normal aerated lung parenchyma and (ii) reduces transient atelectasis, a finding that may mimic or obscure significant abnormalities. Selected scans obtained during or after forced expiration may also be valuable in diagnosing patients with obstructive lung disease or airway abnormalities. The use of expiratory HRCT is discussed below, and in Chapters 2 and 3.

Patient Position and the Use of Prone Scanning

Scans obtained with the patient supine are adequate in most instances. However, scans obtained with the patient positioned prone are sometimes necessary for diagnosing subtle lung disease. Atelectasis is commonly seen in the dependent lung in both normal and abnormal subjects, resulting in a so-called dependent density or a subpleural line (Fig. 1-15) [28]. These normal findings can closely mimic the appearance of early lung fibrosis, and they can be impossible to distinguish from true pathology on supine scans alone. However, if scans are obtained in both supine

and prone positions, dependent density easily can be differentiated from true pathology (Fig. 1-15). Normal dependent density disappears in the prone position (Fig. 1-16); a true abnormality remains visible regardless of whether it is dependent or nondependent (Figs. 1-17 and 1-18).

In a study by Volpe et al. [29], prone scans were considered helpful in 17 of 100 consecutive patients having HRCT. However, it should be pointed out that dependent density results in a diagnostic dilemma only in patients who have normal lungs or subtle lung abnormalities. In patients with obvious abnormalities, such as honeycombing, or who have diffuse lung disease, dependent density is not usually a diagnostic problem. Thus, if the patient being studied has evidence of moderate to severe lung disease on plain radiographs, prone scans are not likely to be needed. On the other hand, if the patient is suspected of having an

P.17

interstitial abnormality and the plain radiograph is normal or near normal or the results of chest radiographs are unknown, the supine scan sequence must be closely monitored or prone scans should be obtained. Volpe et al. [29] assessed the usefulness of prone scans in patients who had chest radiographs read as normal, possibly abnormal, or definitely abnormal. Prone HRCT scans were helpful in confirming or ruling out posterior lung abnormalities in 10 of 36 (28%) patients who had normal findings on chest radiographs, five of 18 (28%) patients who had possibly abnormal findings on chest radiographs, and only two of 46 (4%) patients who had definitely abnormal findings on chest radiographs. The proportion of patients who benefited from

prone scans was significantly lower among the patients with abnormal findings on chest radiographs than among the patients with normal ($p = .008$) or possibly abnormal ($p = .02$) findings. The two patients who had abnormal findings on radiographs and in whom CT scans obtained with the patient prone were helpful had minimal radiographic abnormalities.

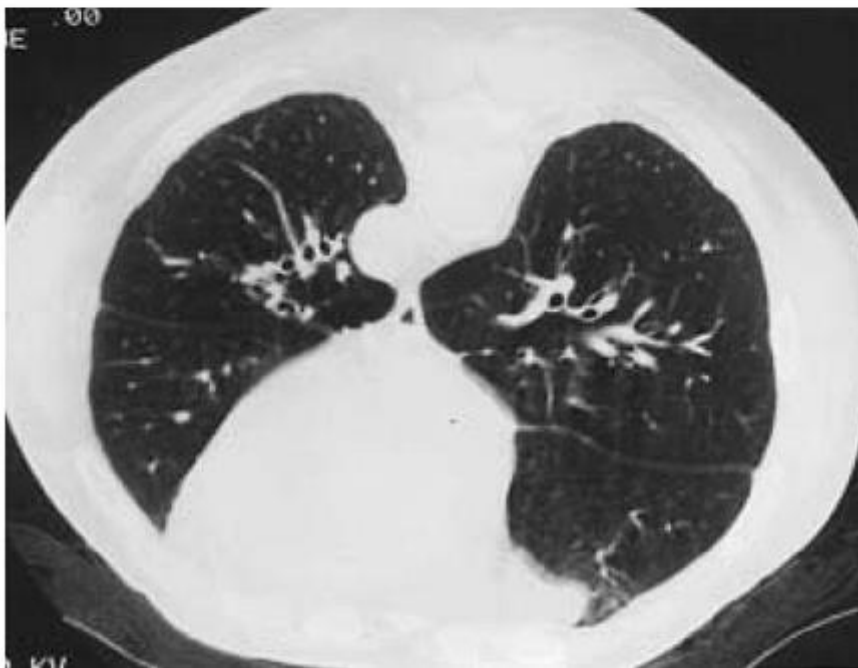


FIG. 1-15. Supine and prone scans with normal “dependent density.” A: Supine scan in a normal patient shows an ill-defined opacity in the posterior aspect of both lungs (arrows). It is impossible to know whether this represents lung disease or is normal atelectasis. B: Prone scan done at same level shows no evidence of an abnormality.

Some investigators [18, 30] obtain HRCT in the prone position only when dependent lung collapse is problematic [31]; however, this approach requires that the scans be closely monitored or that the patient be called back for P.18

additional scans. Others use prone scanning routinely; this approach has proved particularly valuable in detecting early lung fibrosis [28, 32]. In patients who are suspected of having an airway disease, such as bronchiectasis, or another obstructive lung disease, dependent atelectasis is not usually a diagnostic problem, and prone scans are not usually needed.

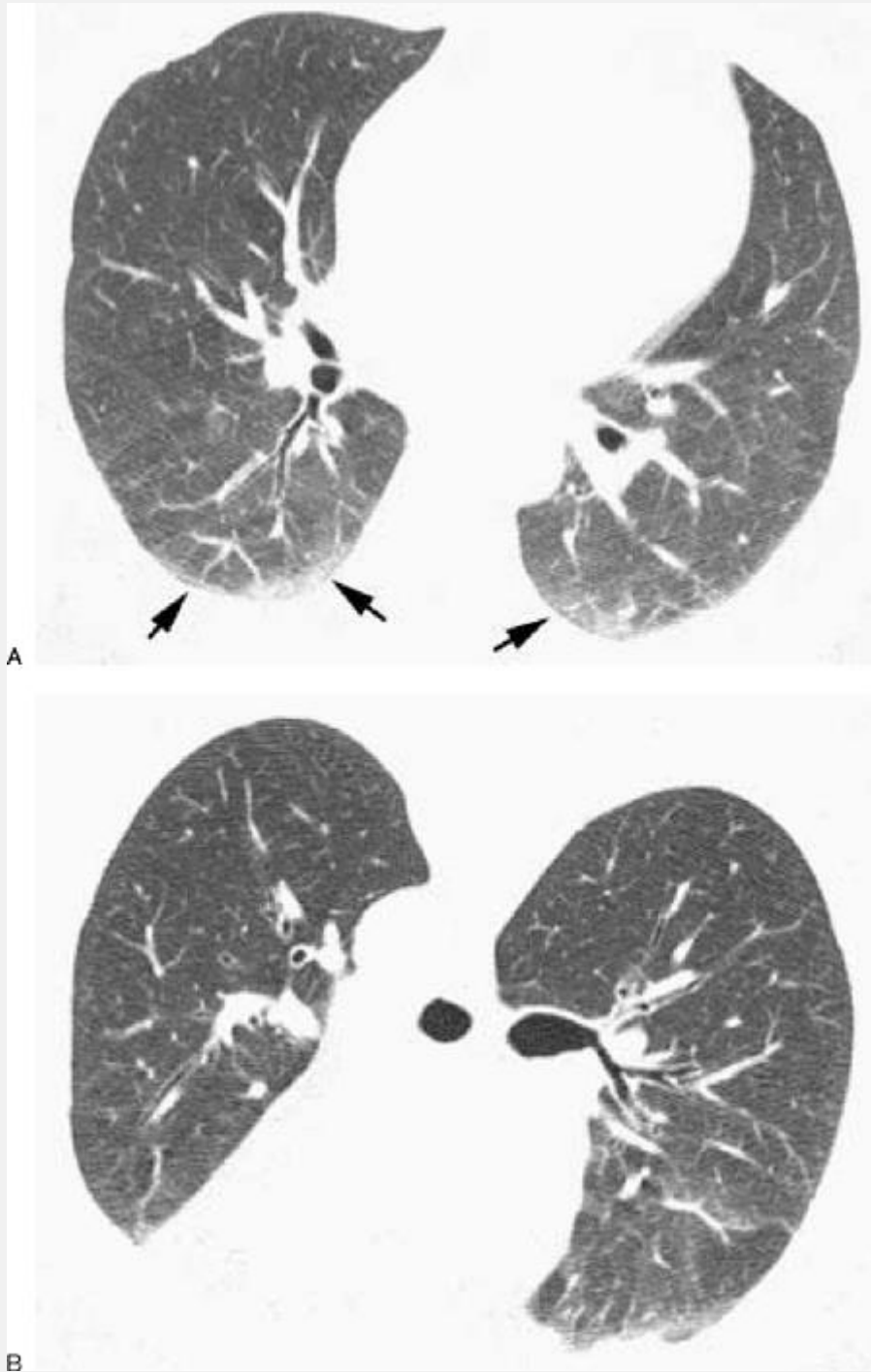


FIG. 1-16. Transient dependent density. A: Supine scan shows ill-defined opacity in the posterior lungs (arrows). B: On a prone image, the posterior lung appears normal. Note some dependent opacity is now visible in the anterior lung.

Scan Spacing

HRCT is generally performed by obtaining single slices at spaced intervals, from the lung apices to the lung bases during suspended respiration. In this manner, HRCT is **intended to "sample" lung anatomy, with the presumptions** that a diffuse lung disease will be visible in at least one of the levels sampled

P.19

and that the findings seen at the levels scanned will be representative of what is present throughout the lung. These presumptions have proven valid during years of experience with HRCT.

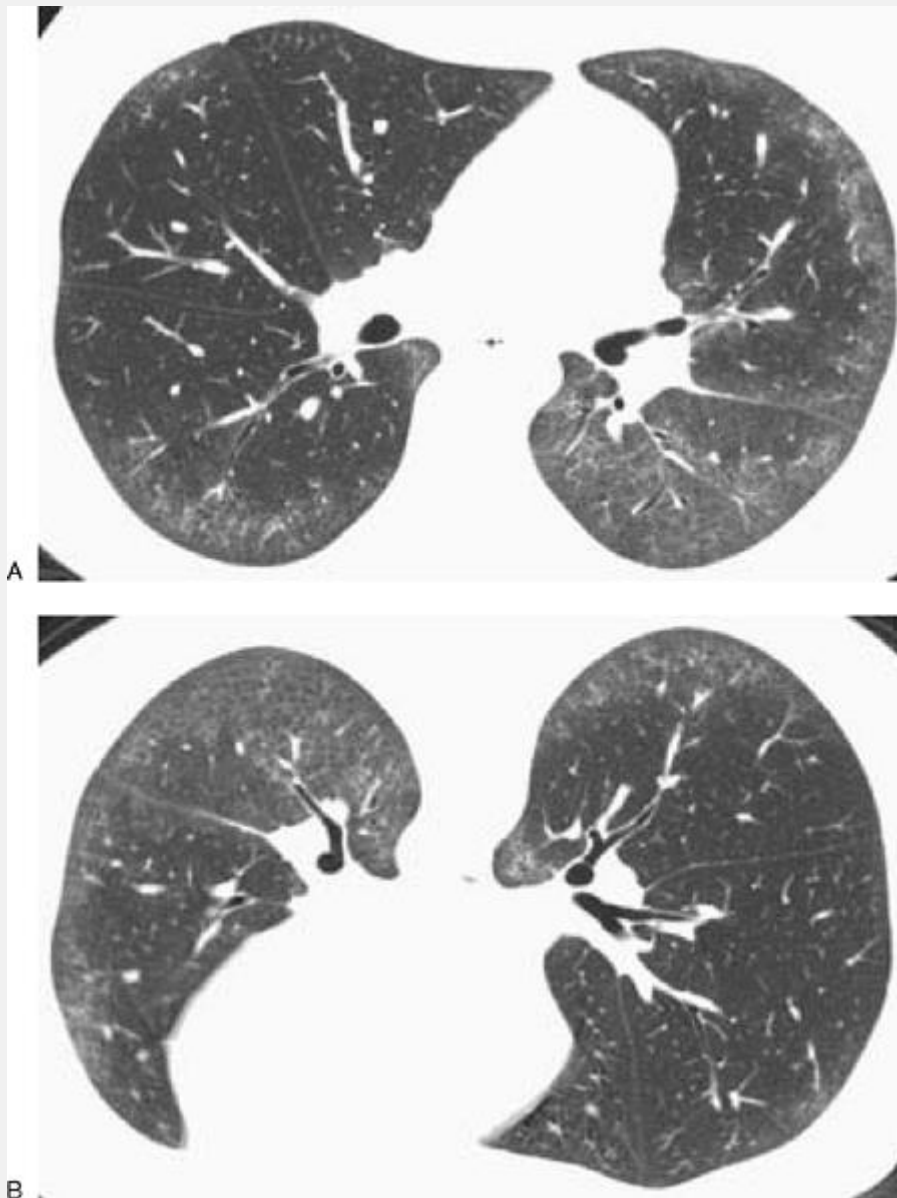


FIG. 1-17. Persistent opacity in the posterior lung in a patient with pulmonary fibrosis. A: Supine scan shows ill-defined opacity in the posterior lungs and in a subpleural region anteriorly. B: On a prone image, the posterior is unchanged in appearance, indicative of lung disease.

Two fundamentally different approaches to HRCT may be used, at least partially determined by the indications for the examination. The first approach is to obtain HRCT in combination with a conventional CT study, in which the

entire thorax is imaged using 7- to 10-mm collimation scans [12, 18, 30]. This technique is most appropriate when the primary indication for the study is an evaluation of the entire chest, or when the disease being evaluated necessitates comprehensive imaging. For example, even though mediastinal abnormalities are usually visible on HRCT images obtained at spaced intervals, in some patients with both mediastinal and pulmonary abnormalities suspected radiographically, obtaining a conventional CT study is appropriate. Similarly, in a patient with suspected lymphangitic spread of carcinoma who is having HRCT for diagnosis, obtaining a contrast-enhanced CT would be appropriate to look for or determine the extent of a primary carcinoma. Depending on the indication for the study, either HRCT or conventional CT may be obtained first and monitored to determine the need for additional imaging. The second approach is to obtain only HRCT images, in lieu of performing a conventional CT examination. Because HRCT is most often obtained to evaluate a patient suspected of having diffuse lung disease [9], and HRCT is optimized for imaging lung parenchyma, obtaining a conventional CT examination is not usually necessary for diagnosis. The great majority of HRCT studies in current clinical practice are obtained in this manner.

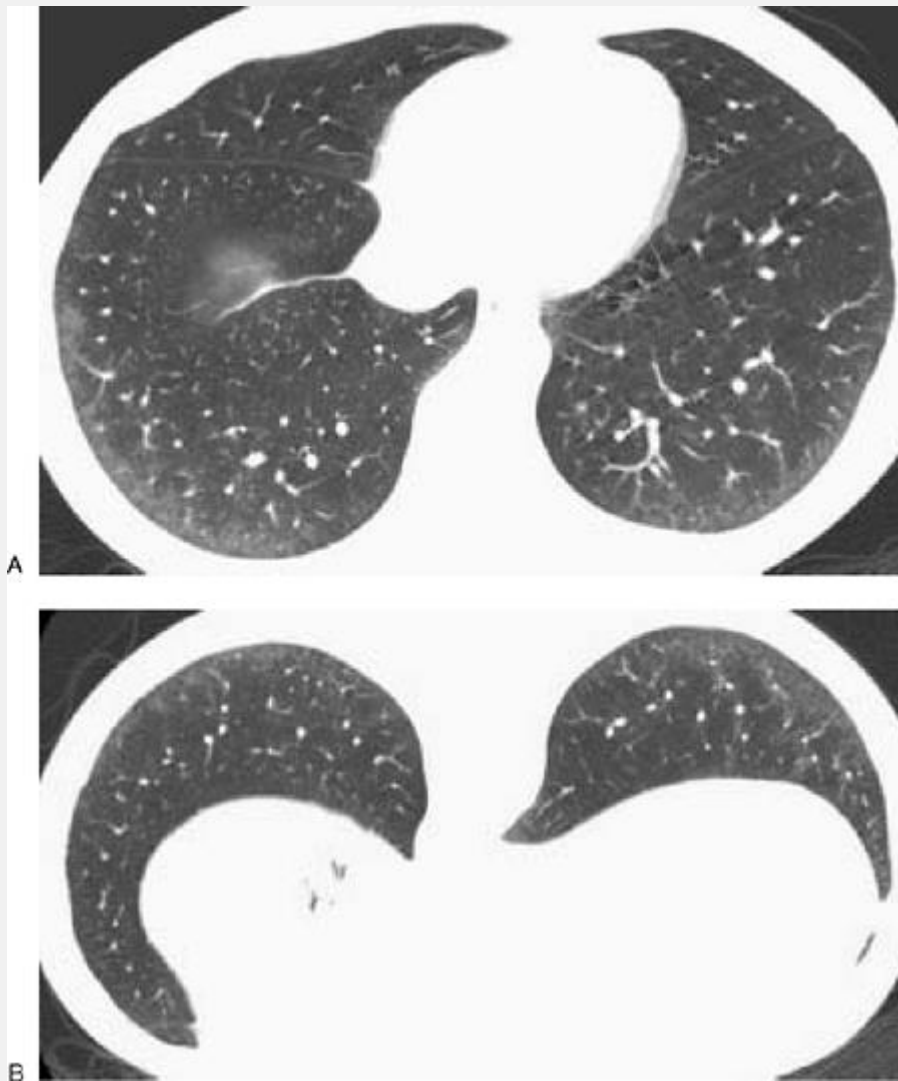


FIG. 1-18. Persistent posterior lung opacity on prone scans in a patient with scleroderma and interstitial pneumonia. A: Supine scan shows ill-defined opacity in the posterior lungs. B: On a prone image, the posterior subpleural lung opacity is unchanged in appearance, and the presence of true lung disease can be diagnosed.

P.20

We consider scans obtained at 1-cm intervals, from the lung apices to bases, to be the most appropriate routine scanning

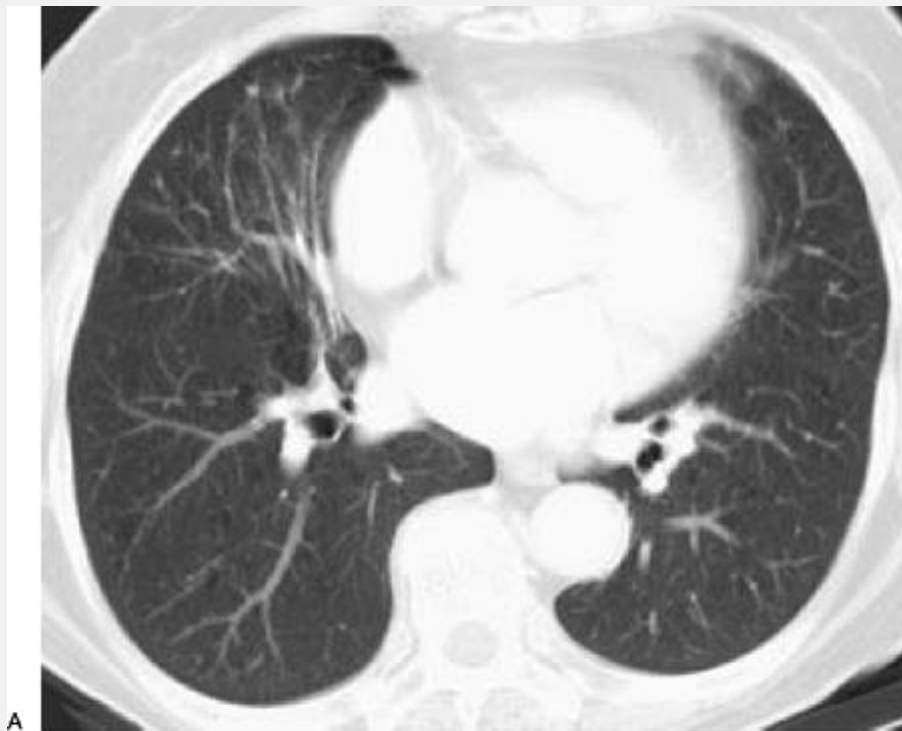
protocol, allowing a complete sampling of the lung and lung disease regardless of its distribution. Obtaining scans at smaller intervals or obtaining contiguous scans is not usually necessary for diagnosis and would not be desirable because of the increased radiation dose involved. Scanning at 1-cm intervals is currently used by most investigators, although in early reports, HRCT scanning was performed at 2-, 3-, and even 4-cm intervals [9, 31]; at three preselected levels [30]; or at one or two levels through the lower lungs [18]. HRCT is performed for a variety of reasons, and to some extent, the number of scans obtained and their levels can vary depending on the clinical indications for the study.

Although obtaining scans at 1-cm intervals is recommended for initial diagnosis, it should be pointed out that in patients with a known disease, a limited number of HRCT images may be sufficient to assess disease extent. In one study [33], the ability of HRCT obtained at three selected levels (limited HRCT) to show features of idiopathic pulmonary fibrosis (IPF) was compared to that of HRCT obtained at 10-mm increments (complete HRCT). HRCT fibrosis scores strongly correlated with pathology fibrosis scores for the complete ($r = 0.53$, $p = .0001$) and limited ($r = 0.50$, $p = .0001$) HRCT examinations. HRCT ground-glass opacity scores correlated with the histologic inflammatory scores on the complete ($r = 0.27$, $p = .03$) and limited ($r = 0.26$, $p = .03$) HRCT examinations. As another example, in evaluating patients with asbestos exposure, several investigators have suggested that a limited number of scans should be sufficient for the diagnosis of asbestosis [28,32,34, 35, 36, 37]. Obtaining four or five scans near the lung bases has proved to have good sensitivity in patients with suspected

asbestosis [38]. Conventional CT combined with a few HRCT images has also been applied to patients with suspected diffuse lung disease and has been shown to be clinically efficacious [30]; HRCT scans obtained at the levels of the aortic arch, carina, and 2 cm above the right hemidiaphragm allow the assessment of the lung regions in which lung biopsies are most frequently performed [12]. In patients who are likely to require prone images, several prone scans can be added to the routine supine sequence obtained with 1-cm scan spacing; a reasonable protocol would

P.21

include additional prone scans at 2- to 4-cm intervals. Alternatively, scans can be obtained at 2-cm intervals from lung apices to bases, in both supine and prone positions. Because the prone and supine images will be slightly different, even if obtained at the same level, the number of images obtained will be equivalent to a supine position scan protocol using 1-cm spacing.



A



B

FIG. 1-19. Gantry angulation in a patient with right middle lobe bronchiectasis. A: HRCT image obtained with the gantry vertical shows bronchial wall thickening in the right middle lobe. B: HRCT image obtained with the gantry angulated 20

degrees allows right middle lobe bronchi (arrows) to be imaged along their axes.

It may be appropriate to customize the number or location of scans, depending on the patient's suspected disease, clinical findings, or the location of plain radiographic abnormalities. For example, if the lung disease being studied predominates in a certain region of lung, as determined by chest radiographs, conventional CT [18], or other imaging studies, it makes sense that more scans should be obtained in the most abnormal area. In patients with suspected asbestosis, it has been recommended that more scans be performed near the diaphragm than in the upper lobes because of the typical basal distribution of this disease, even if the chest radiograph does not suggest an abnormality in this region [28, 32].

P.22

Some support for this approach has been lent by a paper [39] describing theoretical methods useful in selecting the appropriate number of HRCT images for estimating any quantitative parameter of lung disease; a marked reduction in the number of images necessary for quantification of a desired parameter can be achieved by using a stratified sampling technique based on prior knowledge of the disease distribution.

Gantry Angulation

It has been suggested that, in patients with bronchiectasis, angling the gantry 20 degrees caudally with the patient supine (i.e., the lower gantry is angled toward the feet)

improves visibility of the segmental and subsegmental bronchi, particularly in the middle lobe and lingula, by aligning them parallel to the plane of scan (Fig. 1-19) [40]. This technique may be valuable in assessing patients with bronchiectasis [41]. However, in the majority of patients with bronchiectasis, HRCT without gantry angulation is sufficient for diagnosis.

Electrocardiographically Triggered High-Resolution Computed Tomography

HRCT scans obtained in a routine fashion may be degraded by cardiac motion. Several motion-related artifacts may be seen, particularly in the left paracardiac region (see High-Resolution Computed Tomography Artifacts). HRCT scans may be obtained using electrocardiographic (ECG) triggering of scan acquisition in an attempt to reduce these artifacts [42]. In a recent study using a spiral scanner capable of 0.75-second gantry rotation, 500-millisecond HRCT scans, representing a 240-degree rotation of the gantry, were initiated at 50% of the R-R interval. Because of the shorter-than-routine scan time, images were reconstructed using a somewhat smoother algorithm than is usually used for HRCT. In 35 patients, Schoepf et al. [42] found that ECG triggering significantly reduced artifacts caused by cardiac motion, such as distortion of pulmonary vessels, double images, or blurring of the cardiac border, when compared to routine images. Furthermore, in patients with a heart rate of 75 beats per minute or less, ECG triggering significantly improved image quality. It should be noted, however, that

this technique was not found to improve diagnostic accuracy.

Use of Contrast Agents

At present, there is no routine indication for the use of contrast agents with HRCT, except when studying a focal lung lesion or solitary nodule [43] or in patients being studied for concomitant vascular disease. Because the lung window settings routinely used for HRCT are intended to accentuate the contrast between air and tissue, vascular opacification is not visible in patients receiving an injection of intravenous contrast. Using a soft-tissue window, opacification of segmental and subsegmental vessels may be seen on HRCT.

Volumetric High-Resolution Computed Tomography

Volumetric HRCT may be performed using several different techniques, including conventional HRCT with multiple contiguous slices, single detector-row spiral CT, and multidetector-row spiral CT. In each, a volume of lung is examined for the purpose of viewing contiguous slices or the volumetric reconstruction of scan data. With spiral technique, this can be accomplished during a single breath hold, although the volume of lung imaged will vary with the type of scanner.

Volumetric HRCT has several potential advantages. It would allow (i) complete lung imaging, (ii) viewing of contiguous slices for the purpose of better defining lung abnormalities, (iii) a better understanding of the three-dimensional (3D) distribution of abnormalities relative to lung structures, and (iv) the 3D reconstruction of scan data for the purpose of

viewing images in nontransaxial planes or obtaining maximum or minimum intensity projections. However, at present, evidence that volumetric imaging improves diagnostic accuracy in patients with diffuse lung disease is limited to several specific situations. Therefore, the use of volumetric HRCT should generally be limited to selected cases.

In an early attempt at volumetric imaging [44], four contiguous HRCT scans were obtained without using spiral technique at each of three locations (the aortic arch, carina, and 2 cm above the right hemidiaphragm) in 50 consecutive patients with interstitial lung disease or bronchiectasis. At each level, the diagnostic information obtainable from the set of four scans was compared to that obtainable from the first scan in the set of four. When the full set of four scans was considered, more findings of disease were identified. The sensitivity of the first scan as compared to the set of four was 84% for the detection of bronchiectasis, 97% for ground-glass opacity, 88% for honeycombing, 88% for septal thickening, and 86% for nodular opacities. However, it is more likely that the improvement in sensitivity found using the set of four scans reflects the number of scans viewed rather than the fact that they were obtained in contiguity.

Other studies have used spiral CT technique with thin collimation and maximum- or minimum-intensity projections (MinIPs) to acquire and display volumetric HRCT data for a slab of lung [45, 46, 47]. In this setting, maximum intensity projections (MIPs) have been used primarily for the diagnosis of nodular lung disease. MIP images increase the detection of small lung nodules and can be helpful in demonstrating their anatomic distribution (Fig. 1-20).

Coakley et al. [46] assessed the use of MIP images in the detection of pulmonary nodules by spiral CT. Forty pulmonary nodules of high density were created by placement of 2- and 4-mm beads into the peripheral airways of five dogs. MIP images were generated from overlapped slabs of seven consecutive 3-mm slices, reconstructed at 2-mm intervals and acquired at pitch 2. MIP imaging increased the odds of nodule detection by more than two, when compared to spiral images, and reader confidence for nodule detection was significantly higher with MIP images.

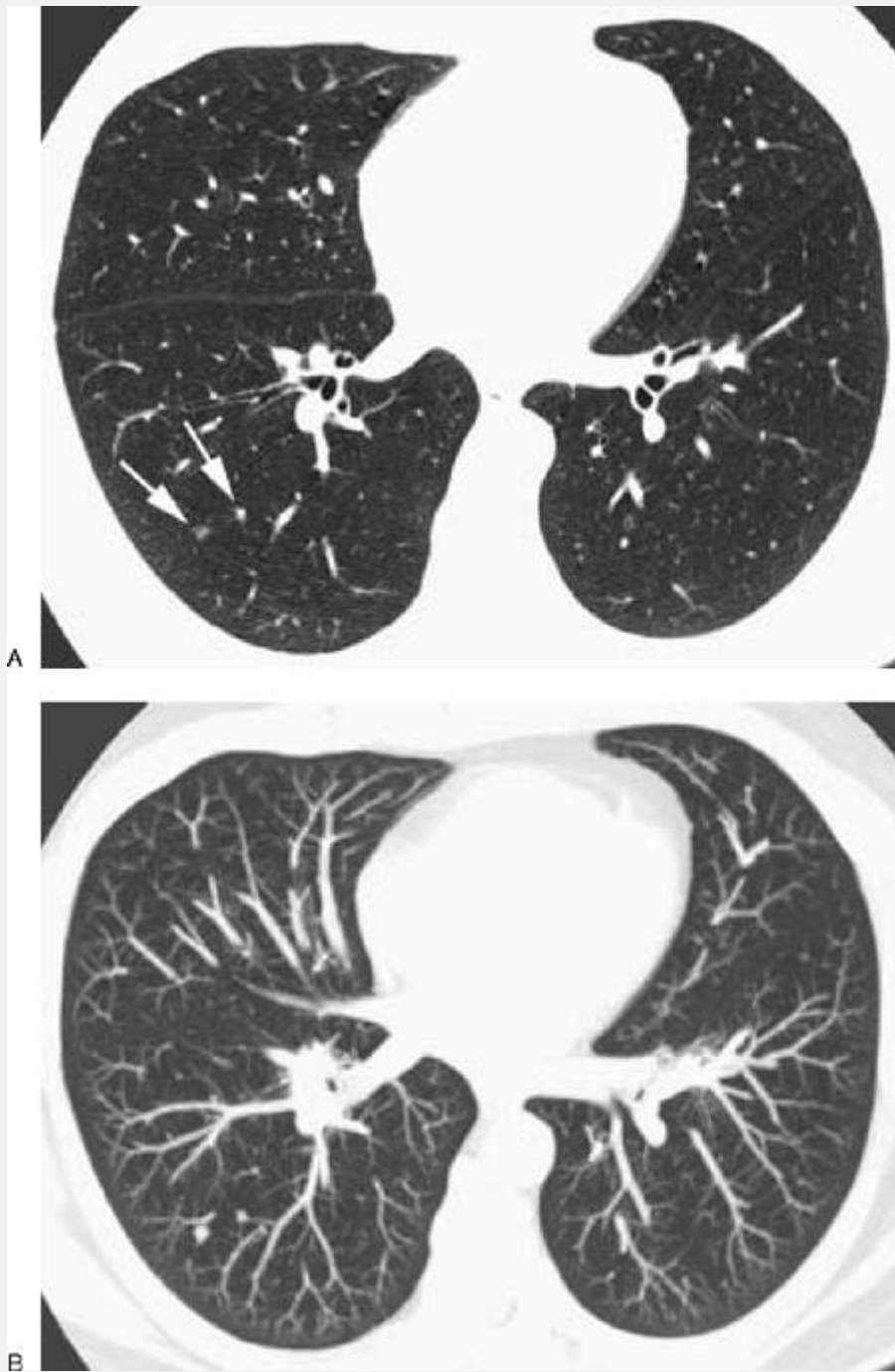


FIG. 1-20. Maximum-intensity projection (MIP) image in a patient with small lung nodules obtained using a multidetector-row spiral CT scanner with 1.25-mm detector width and a pitch of 6. A: A single HRCT image shows two small nodules (arrows) that are difficult to distinguish from

vessels. B: An MIP image consisting of eight contiguous HRCT images, including A, allows the two small nodules to be easily distinguished from surrounding vessels.

P.23

In a study by Bhalla et al. [45], the use of helical HRCT and MIP images was compared in patients with nodular lung disease. Because of the markedly improved visualization of peripheral pulmonary vessels and improved spatial orientation, MIP images were considered superior to helical scans for identifying pulmonary nodules and specifying their location as peribronchovascular or centrilobular, a finding of great value in differential diagnosis.

In another study [47], sliding-thin-slab MIP reconstructions were used in 81 patients with a variety of lung diseases associated with small nodules. In this study, patients were studied using 1- and 8-mm-thick conventional CT and focal spiral CT with generation of 3-, 5- and 8-mm-thick MIP reconstructions. When conventional CT findings were normal, MIPs did not demonstrate additional abnormalities. When conventional CT findings were inconclusive, MIPs enabled detection of micronodules (i.e., nodules 7 mm or less in diameter) involving less than 25% of the lung. When conventional CT scans showed micronodules, MIPs showed the extent and distribution of micronodules and associated

P.24

bronchiolar abnormalities to better advantage. The sensitivity of MIPs (3-mm-thick MIP, 94%; 5-mm-thick MIP, 100%; 8-mm-thick MIP, 92%) was significantly higher than

that of conventional CT (8-mm-thick, 57%; 1-mm-thick, 73%) in the detection of micronodules ($p < .001$). The authors [47] concluded that sliding-thin-slab MIPs may help to detect micronodular lung disease of limited extent and may be considered a valuable tool in the evaluation of diffuse infiltrative lung disease. On the other hand, in patients with extensive abnormalities, MIPs result in a confusing superimposition of opacities that tends to obscure anatomic detail (Fig. 1-21).

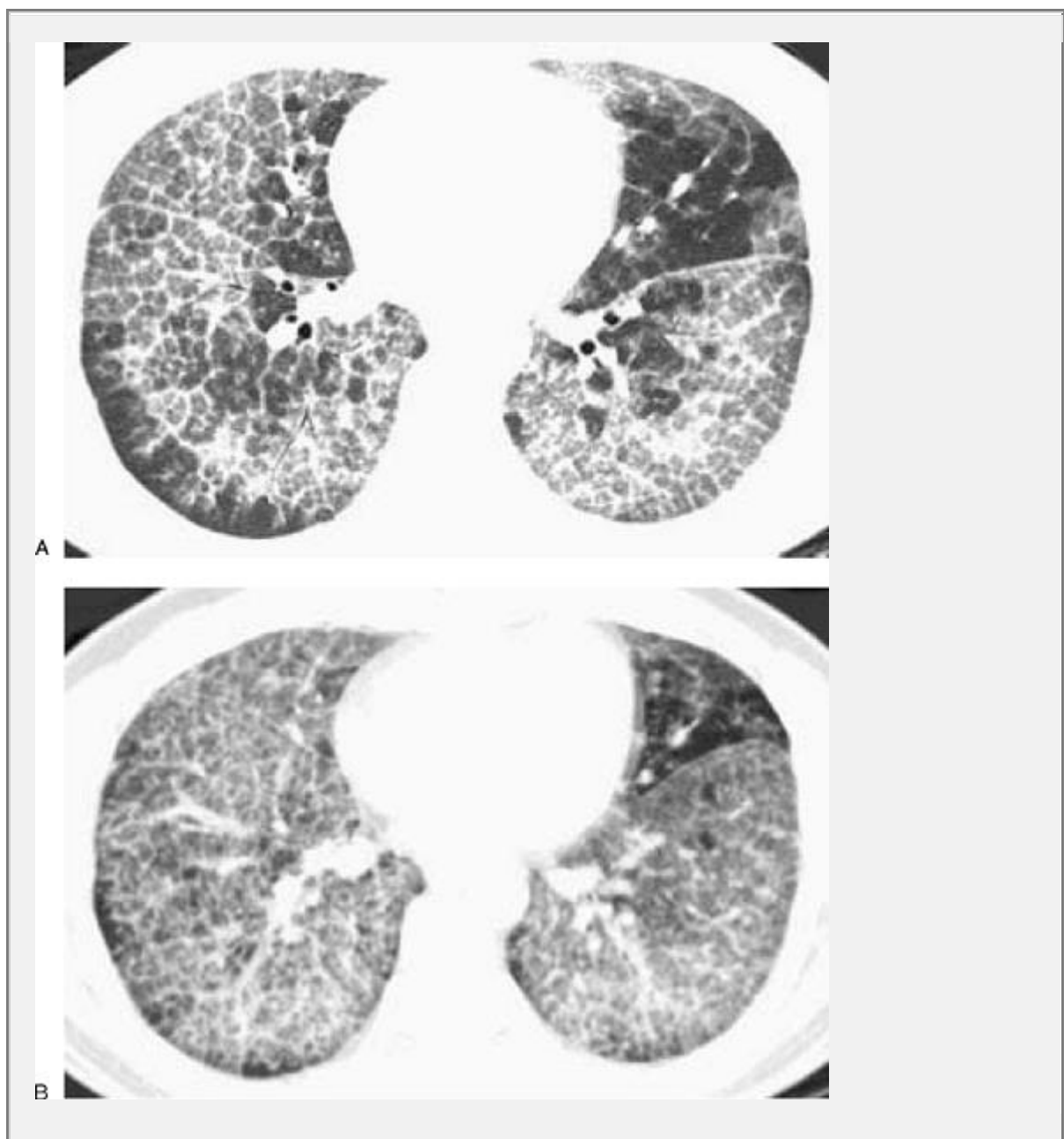


FIG. 1-21. Maximum-intensity projection (MIP) image in a patient with extensive abnormalities due to alveolar proteinosis obtained using a multidetector-row spiral CT scanner with 1.25-mm detector width and a pitch of 6. A: A single HRCT image shows a typical patchy distribution of interlobular septal thickening and ground-glass opacity typical of alveolar proteinosis. B: An MIP image consisting of five contiguous HRCT images, including (A), results in a confusing superimposition of opacities. Septal thickening is more difficult to diagnose.

The utility of MinIP images has also been evaluated (Fig. 1-22) [45]. In one study [45], MinIP images were more accurate than routine HRCT scans in identifying (i) the lumina of central airways (Fig. 1-23), (ii) areas of abnormal low attenuation (e.g., emphysema or air-trapping) (Fig. 1-23; see Fig. 7-36), and (iii) ground-glass opacity. In the study by Bhalla et al. [45], when compared to conventional HRCT, volumetric MIP and MinIP images demonstrated additional findings in 13 of 20 (65%) cases. However, although an advantage has been described for volumetric HRCT with MIP or MinIP image reconstruction in demonstrating small nodules of limited extent and subtle areas of increased or decreased lung density, conventional HRCT is advantageous in depicting fine linear structures, such as the walls of dilated small airways and interlobular septa.



FIG. 1-22. Minimum-intensity projection (MinIP) image in the patient shown in Fig. 1-17A, and at the same anatomic level. Normal lung parenchyma appears relatively homogeneous. Pulmonary vessels disappear on MinIP images.

P.25

Single Detector-Row Spiral Computed Tomography

Single detector-row spiral CT scanners have the ability to obtain a volumetric CT data set, with a 1- or 2-cm-thick slab of lung being scanned during a single breath hold, using 1-mm collimation and a pitch of 1. Obtaining scans with a spiral technique results in a small increase in effective slice thickness (compared to scans obtained

without table motion), and results in some loss of spatial resolution [48, 49], although this effect is minimal with proper technique [50]. Using a pitch of 2 broadens the effective slice thickness by approximately 30% [51, 52]. Thus, using 1-mm collimation, effective slice thickness is approximately 1.3 mm. An increase in pitch may also result in some decrease in signal-to-noise ratio, but this is not generally a problem in diagnosis. Although this technique is of potential value in demonstrating the 3D distribution of abnormalities in patients with diffuse lung disease and is an appealing concept, because of the limited volume of lung assessed during a single breath hold, volumetric HRCT using a single detector-row scanner is of considerably more value in assessing patients with focal lung disease or discrete lung nodules [49, 53]. The ability to perform this type of thin- or thick-slab volumetric imaging is not a major advantage in assessing most patients with diffuse lung disease; HRCT in patients with suspected diffuse lung disease requires a sampling of lung anatomy in different lung regions, rather than a more detailed volumetric assessment at a few levels. In general, in patients suspected of having diffuse infiltrative lung disease, HRCT obtained with a single detector-row spiral should be performed without table motion, using thin (1-mm) collimation, scans at spaced intervals, a scan time of 1 second or less, and a high-resolution reconstruction algorithm.

Multidetector-Row Spiral High-Resolution Computed Tomography

Multidetector-row spiral CT scanners make use of multiple adjacent detector rows that acquire scan data simultaneously and may be used independently or in

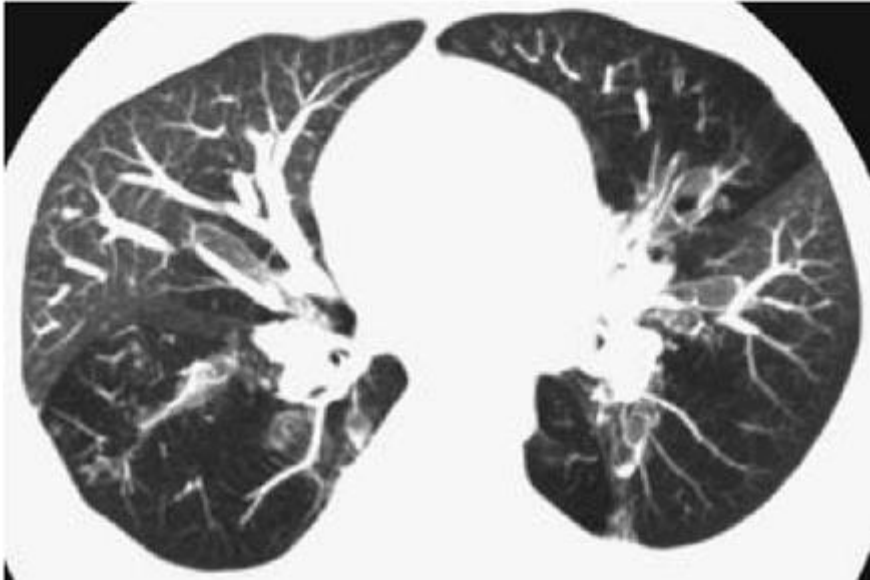
combination to generate images of different thickness. Such scanners typically use high orders of pitch (e.g., 6), and are capable of imaging the entire thorax during a single breath hold with the volumetric reconstruction of thin, high-resolution slices. For example, using one currently available scanner, data may be simultaneously acquired from four 1.25-mm detector rows, with table movement of 7.5 mm per second and a gantry rotation time of 0.8 seconds. Assuming that 25 cm is required for imaging the lungs, volumetric HRCT of the entire lung volume using these parameters would require approximately 27 seconds. Although single detector-row spiral CT does not offer a significant advantage in patients with diffuse lung disease when compared to conventional HRCT performed with individual spaced slices, multidetector-row CT has the potential to fundamentally change the way HRCT is performed, at least in some patients. The volumetric data resulting from this mode of scanning allow near-isotropic imaging and HRCT assessment of lung morphology in a continuous fashion from lung apex to base, the production of MIP and MinIP images at any desired level (Figs. 1-20, 1-21, 1-22 and 1-23), and the viewing of the scan volume in nontransaxial planes (Figs. 1-24, 1-25, 1-26 and 1-27; see Fig. 7-36).



A



B



C

FIG. 1-23. Multidetector-row spiral (HRCT) image with contrast enhancement in a patient with bronchiolitis obliterans and a clinical suspicion of pulmonary embolism. No pulmonary embolism was found. A: A single HRCT image obtained with 1.25-mm detector width and a pitch of 6 shows bronchiectasis and patchy lung attenuation with reduced artery size in lucent lung regions due to air-trapping and mosaic perfusion. B: A 10-mm-thick minimum-intensity projection image (MinIP) at the same level as A accentuates the differences in attenuation between normal lung and lucent lung, but pulmonary arteries cannot be assessed. Bronchiectasis is well seen using MinIP imaging. C: A maximum-intensity projection at the same level as B shows reduced vessel size in the lucent lung regions. Inhomogeneous lung attenuation is also visible. The bronchiectasis is difficult to see.

P.26

P.27

The spiral acquisition of HRCT data using this technique results in some broadening of the scan profile, but the effective slice thickness using this technique would still be sufficient for HRCT diagnosis in most cases. With 1.25-mm detector width, effective slice thickness is approximately 1.6 mm when a pitch of 6 (table travel 7.5 mm per gantry rotation) is used. Furthermore, depending on the technique used and how data from the various detector rows are combined, images of different thickness may be produced

retrospectively from the same study. Using the protocol described above, in addition to viewing images generated from data acquired by the individual 1.25-mm detectors, data from the detector rows may be combined to produce images representing thicker slices (i.e., 2.5 mm). Thus, this **technique enables HRCT and "routine" or thick-section chest imaging to be combined as a single examination, blurring the distinction between these studies.**

Combining a volumetric chest CT examination with HRCT by using multidetector-row CT may be of value in patients being studied primarily for diffuse lung disease, for which HRCT would be the examination of choice, and in patients being evaluated for disease usually studied using conventional spiral technique. For example, in patients being evaluated before volume reduction surgery for emphysema or before lung transplantation, volumetric lung imaging might be of value in the diagnosis of associated lung carcinoma, which has an incidence of up to 5% in this patient population, or other significant abnormalities [54]. In patients with hemoptysis, thin and thick image reconstruction may be of value in demonstrating small or large airway disease, respectively. Another advantage of multidetector-row CT would be in patients requiring a **"conventional" CT for the diagnosis of thoracic disease, such as evaluation of a lung nodule.** In such patients, scan data may be reconstructed with a thickness appropriate for the detection of lung nodules and bronchial abnormalities and for assessment of mediastinal and hilar lymph nodes. At the same time, and without additional scanning, high-resolution images could be reconstructed for the purpose of delineating nodule morphology and attenuation, or for the diagnosis of associated lymphangitic spread.

Similarly, in patients with suspected pulmonary vascular disease, HRCT with contrast enhancement may be obtained using multidetector-row spiral CT, allowing the detailed assessment of both vasculature and pulmonary parenchyma (Figs. 1-23, 1-26, 1-27; see Figs. 9-4, and 9-5). In patients having spiral CT for the diagnosis of acute or chronic pulmonary embolism, scan data can also be reconstructed using thin collimation to look for lung disease that could be associated with similar symptoms (Figs. 1-23 and 1-26). On the other hand, in patients being assessed using HRCT for known diffuse lung disease, such as IPF, the need for volumetric scanning or thicker slices is less clear, and the additional radiation dose required by volumetric imaging would not seem warranted. Another disadvantage of obtaining volumetric

P.28

P.29

HRCT is the large number of images produced. Unless scans are reviewed using a workstation, reading a volumetric study would be cumbersome and would require the use of a large number of films.

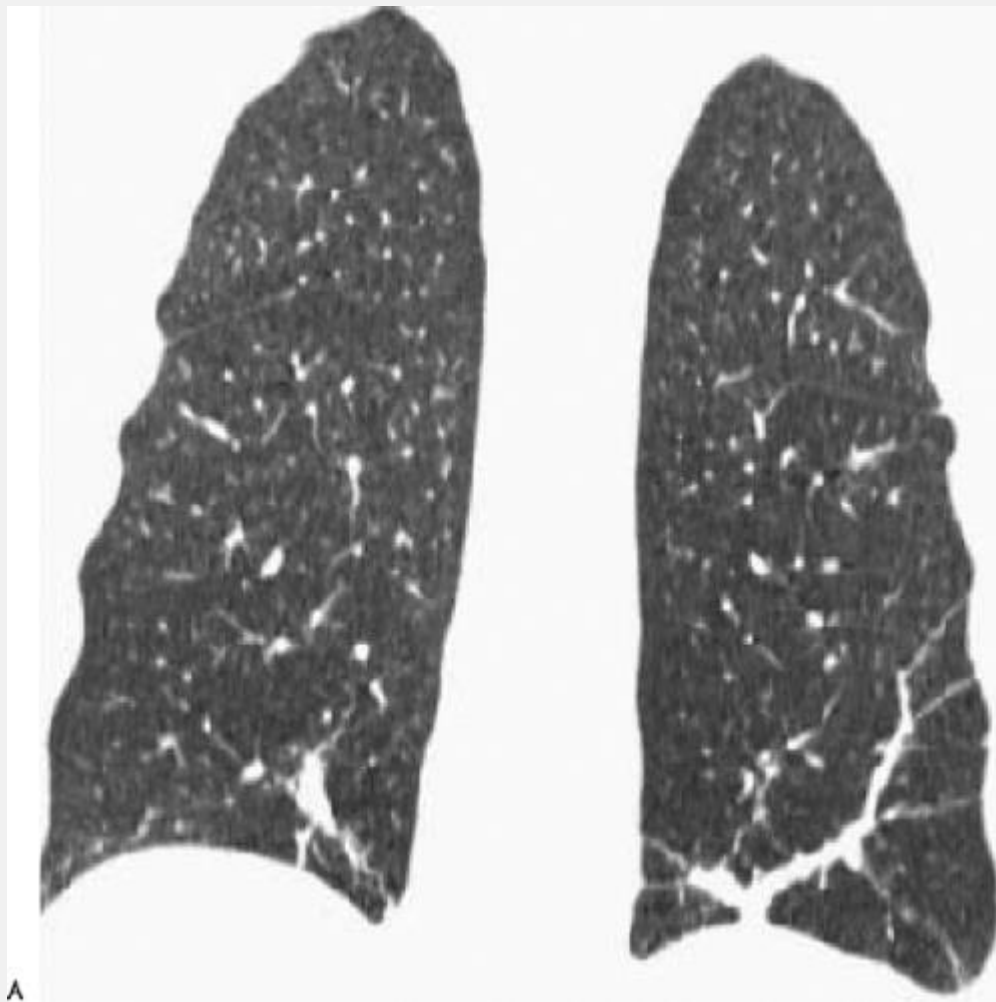


FIG. 1-24. Coronal and sagittal image reconstruction from multidetector-row spiral HRCT in a normal subject. A: Coronal reconstruction from a multidetector-row spiral CT obtained using 1.25-mm detectors, and a pitch of 6 relative to detector width, during a single breath hold. Small peripheral vessels are visible. The posterior portion of the major fissures are visible as thin stripes of opacity. B: Parasagittal reconstruction from the same HRCT data set shows the minor and major fissures.

Although some patients may be able to hold their breath for a volumetric spiral acquisition using this technique (e.g., 27 seconds), dyspneic patients will not. An advantage of

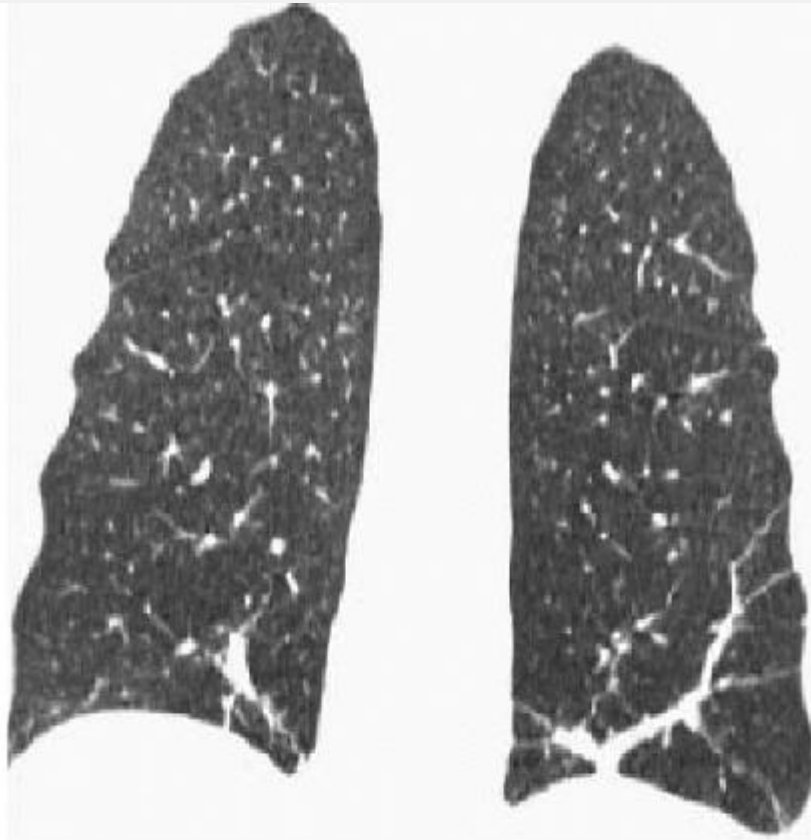
obtaining HRCT with single slices is that a breath hold of 1 second or less is required.

Standardized protocols for performing volumetric multidetector-row HRCT have not been established.

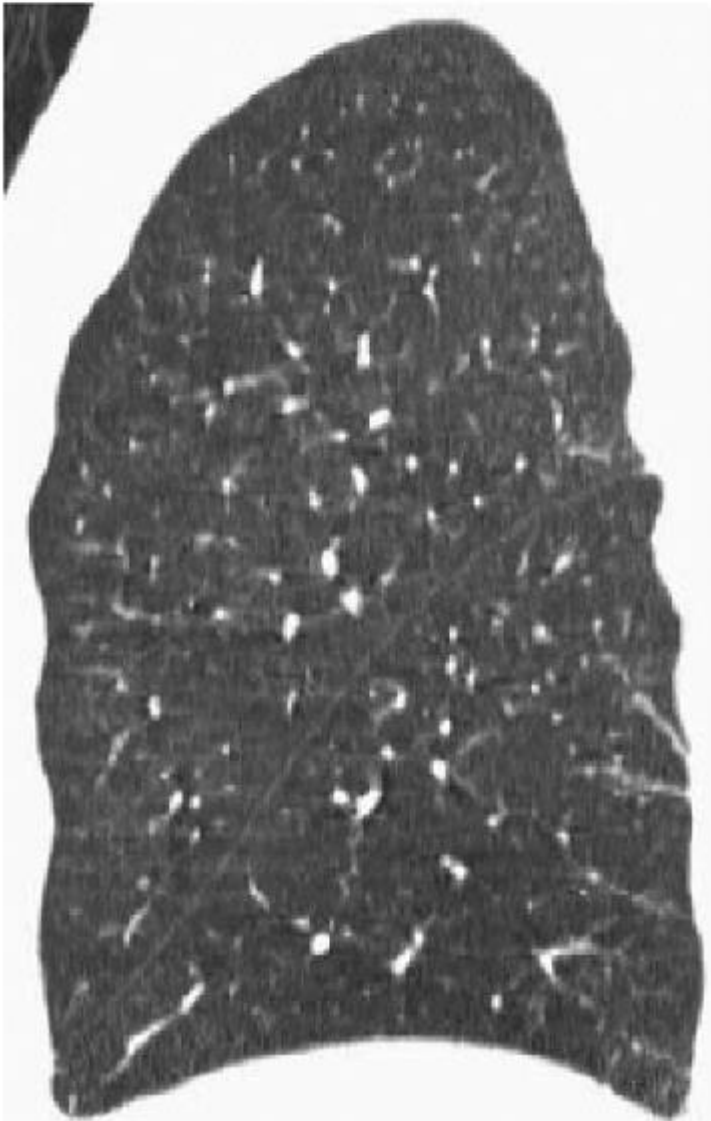
However, in patients who may not be able to hold their breath for a complete volumetric study, logic dictates that the scan protocol be modified according to the distribution of the disease suspected. For diseases likely to have a basal predominance, such as IPF, scanning should begin near the diaphragm and proceed in a cephalad direction. In this way, the more important basal lung will be imaged at the beginning of the scan sequence, and if the patient begins to breathe during scanning, only images through the less important upper lobes will be degraded by respiratory motion. For the same reason, in a patient suspected of having a disease with an upper-lobe predominance (e.g., sarcoidosis), it may be appropriate to begin scanning in the lung apices. Because lung movement with respiration is greatest at the lung bases, an alternative approach would be to scan from the bases to apices in all patients. If the patient breathes during the scan, the upper lobes would be less affected. In a dyspneic patient, breaking up the scan sequence into smaller volumes with several breath holds might also be helpful. Experience indicates that using a detector thickness of 1.25 mm and a pitch of 6 (table movement of 7.5 mm per gantry rotation), with reconstruction using a high-resolution algorithm, provides excellent lung detail. Depending on the indication for the study, this may be performed with or without contrast infusion.

With multidetector-row spiral scanners, contiguous HRCT images may also be obtained without table motion, with

each detector row acquiring a separate image. Using this technique, clusters of four contiguous scans could be obtained at selected levels (e.g., at 1.5- to 2-cm intervals). The individual scans could be viewed independently, as with conventional HRCT, or could be processed to produce MIP or MinIP images.

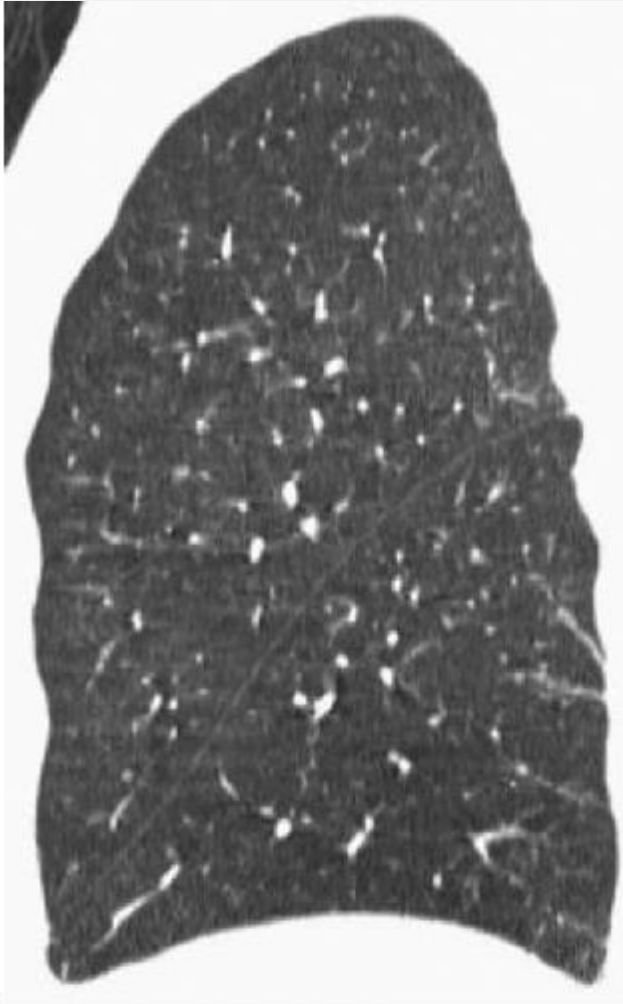


A

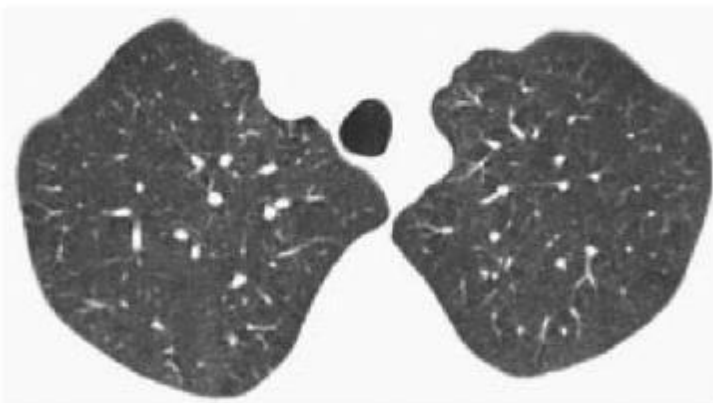


B

FIG. 1-25. Coronal and sagittal image reconstruction from multidetector-row spiral HRCT in a patient with disc atelectasis in the posterior lungs. A: Coronal reconstruction from a multidetector-row spiral CT obtained using 1.25-mm detectors, and a pitch of 6 relative to detector width, during a single breath hold. Linear areas of increased attenuation reflect disc atelectasis. B: Parasagittal reconstruction shows linear subpleural opacities representing disc atelectasis.



B



A



B

FIG. 1-26. HRCT obtained using multidetector-row HRCT with 1.25-mm detectors and a pitch of 6 relative to detector width, in an AIDS patient with pulmonary hypertension and a differential diagnosis, including chronic pulmonary embolism, vasculitis, and lung disease. Transaxial (A, B) and parasagittal reconstructed (C) HRCTs obtained during a single breath hold show normal findings. D: Transaxial image shows enlargement of main pulmonary artery consistent with pulmonary hypertension, but no evidence of pulmonary embolism. The presence of pulmonary hypertension in the absence of pulmonary embolism or lung disease suggests plexogenic arteriopathy.

FIG. 1-27. Contrast-enhanced spiral HRCT obtained in a 19-year-old woman with significant hypoxemia. Scans were obtained using multidetector-row HRCT with 1.25-mm detectors and a pitch of 6 relative to detector width. Transaxial (A, B) images showed numerous very small subpleural arteriovenous malformations (arrows). One-centimeter-thick maximum-intensity projection images in the transaxial (C,D) and coronal (E) planes show the malformations (arrows) and their vascular supply to better advantage. She was subsequently found to have Osler-Weber-Rendu disease.

P.30

P.31

P.32

P.33

P.34

P.35

Expiratory High-Resolution Computed Tomography

As an adjunct to routine inspiratory images, expiratory HRCT scans have proved useful in the evaluation of patients with a variety of obstructive lung diseases [55, 56]. On expiratory scans, focal or diffuse air-trapping may be diagnosed in patients with large or small airway obstruction or emphysema. It has been shown that the presence of air-trapping on expiratory scans (i) correlates to some degree with pulmonary function test abnormalities [57, 58], (ii) can confirm the presence of obstructive airway disease in patients with subtle or nonspecific abnormalities visible on inspiratory scans, (iii) allows the diagnosis of significant lung disease in some patients with normal inspiratory scans [59], and (iv) can help distinguish between obstructive disease and infiltrative disease as a cause of inhomogeneous lung opacity seen on inspiratory scans [60]. In most lung regions of normal subjects, lung parenchyma increases uniformly in attenuation during expiration

[6,61,62,63,64,65], but in the presence of air-trapping, lung parenchyma remains lucent on expiration and shows little change in volume. Focal, multifocal, or diffuse air-trapping is visible as areas of abnormally low attenuation on expiratory or postexpiratory CT. On expiratory scans, visible differences in attenuation between normal and obstructed lung regions are visible using standard lung window settings and can be quantitated using regions of interest. Differences in attenuation between normal lung regions and regions that show air-trapping often measure more than 100 HU [66]. Air-trapping visible using expiratory or postexpiratory HRCT has been recognized in patients with various obstructive or airway diseases, such as emphysema [67, 68, 69], chronic airways disease [58], asthma [70, 71, 72], bronchiolitis obliterans [59,68,73,74,75,76,77,78,79,80], the cystic lung diseases associated with Langerhans histiocytosis and tuberous sclerosis [81], and bronchiectasis [68, 82]. It has also proven valuable in demonstrating the presence of bronchiolitis in patients with primarily infiltrative diseases such as hypersensitivity pneumonitis [83, 84], sarcoidosis [85, 86], and pneumonia.

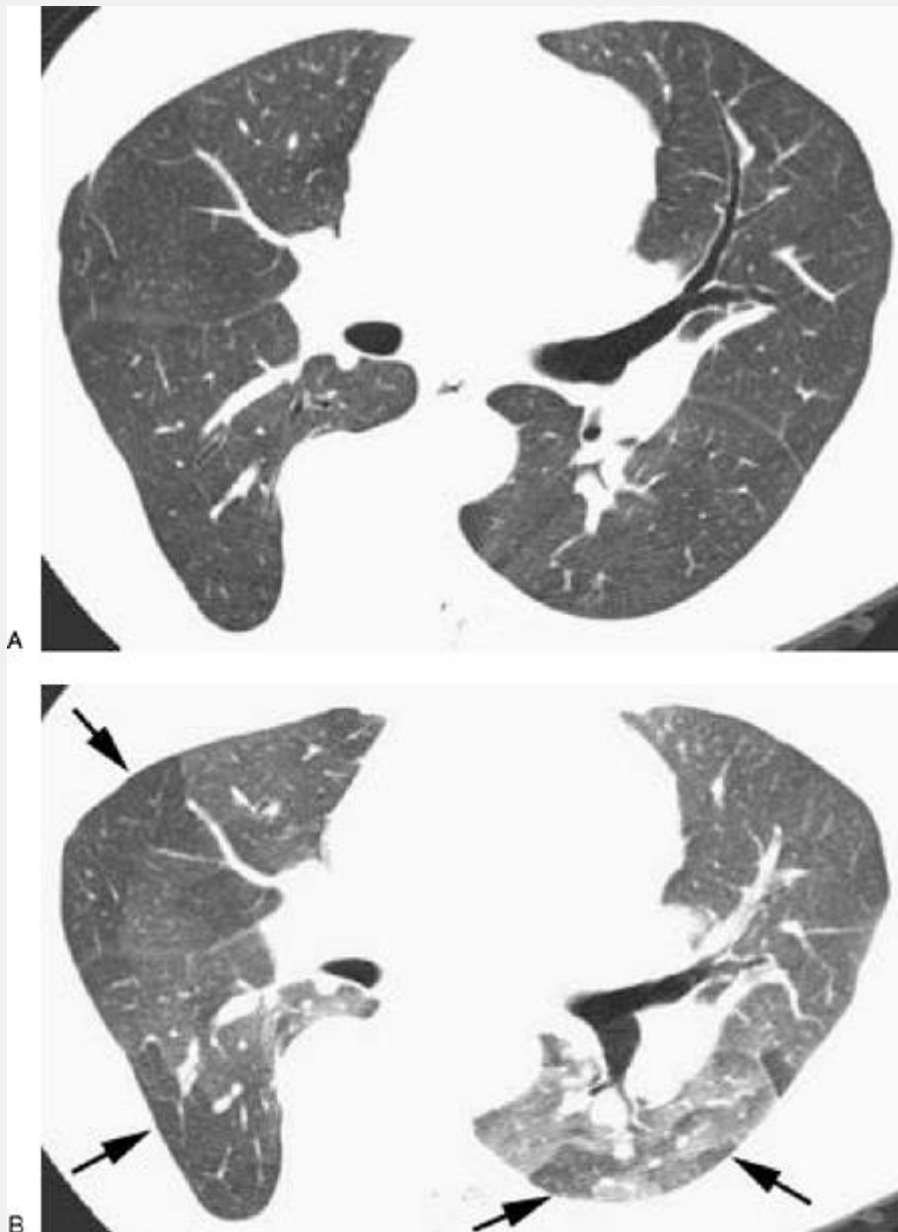


FIG. 1-28. Expiratory air-trapping in a patient with idiopathic scoliosis and normal inspiratory scans. A: An inspiratory scan shows homogeneous lung attenuation without evidence of airways disease. B: Routine expiratory scan shows patchy air-trapping (arrows) indicative of small airways disease.

Some investigators obtain expiratory scans routinely in all patients who have HRCT, whereas others limit their use to patients with inspiratory scan abnormalities or suspected obstructive lung disease [55]. We recommend the routine use of expiratory scans in a patient's initial HRCT evaluation. The functional cause of respiratory disability is not always known before HRCT. Furthermore, even in patients with a known restrictive abnormality on pulmonary function tests, expiratory HRCT may show air-trapping, a finding of potential value in differential diagnosis. Limiting expiratory HRCT to patients with evidence of airway abnormalities on inspiratory scans will result in some missed diagnoses. Expiratory HRCT may show findings of air-trapping in the absence of inspiratory scan abnormalities (Fig. 1-28) [59]. The use of expiratory scans may be of great value in the follow-up of patients at risk of developing an obstructive abnormality. For example, expiratory scans are valuable in detecting bronchiolitis obliterans in patients being followed for lung transplantation [79, 87]. Expiratory HRCT scans may be obtained during suspended respiration after forced exhalation (postexpiratory CT), during forced exhalation (dynamic expiratory CT) [64, 68], at a user-selected respiratory level controlled during exhalation with a spirometer (spirometrically triggered expiratory CT), or during other methods [88, 89, 90, 91, 92, 93]. Generally, with these techniques, expiratory scans are obtained at selected levels. Three scans, five scans, or scans at 4-cm intervals have been used by different authors. Expiratory imaging may also be performed using spiral technique and 3D volumetric reconstruction

[94, 95]. **Although not a “high-resolution” technique, this method can be valuable in patients also having HRCT for evaluation of lung disease, particularly emphysema.**

Postexpiratory High-Resolution Computed Tomography

Postexpiratory HRCT scans, obtained during suspended respiration after a forced exhalation, are easily performed with any scanner and are most suitable for a routine examination (Fig. 1-28). The primary advantage of this technique is its simplicity. In obtaining expiratory HRCT, the patient is instructed to forcefully exhale and then hold his or her breath for the duration of the single scan. This maneuver is practiced with the patient before the scans are obtained to ensure an adequate level of expiration.

Postexpiratory scans can be performed at several predetermined levels (e.g., aortic arch, carina, and lung bases), at 2- to 4-cm intervals, or at levels appearing abnormal on the inspiratory images. Scans at two to five levels have been used by different authors [60,70,71,76,96,97]. Expiratory scans at three selected levels (aortic arch, hila, lower lobes) are generally sufficient for showing significant air-trapping when present, and are used routinely in addition to inspiratory scan series in patients with suspected airways or obstructive lung diseases. Although targeting postexpiratory scans to lung regions that appear abnormal on the inspiratory scans would seem advantageous, using preselected scans allows the same lung regions to be routinely imaged on follow-up

examinations and, in some patients, can show air-trapping when inspiratory scans are normal.

Each of the postexpiratory scans is compared to the inspiratory scan that most closely duplicates its level to detect air-trapping. Anatomic landmarks such as pulmonary vessels, bronchi, and fissures are most useful for localizing corresponding levels. Because of diaphragmatic motion occurring with expiration, attempting to localize the same scan levels by using the scout view is difficult and sometimes misleading.

Dynamic Expiratory High-Resolution Computed Tomography

Scans obtained dynamically during forced expiration can be obtained using an electron-beam scanner or a helical scanner. There is some evidence to suggest that a greater increase in lung attenuation occurs with dynamic expiratory imaging than with simple postexpiratory HRCT and that air-trapping consequently is more easily diagnosed.

Dynamic scanning with an electron-beam scanner has been termed *dynamic ultrafast HRCT* [68, 81, 98, 99]. This technique is performed using a scanner capable of obtaining a series of images with a 100-millisecond scan time [500-millisecond interscan delay, 1.5- to 3-mm collimation, 150 kV(p), 650 mA] [68, 81, 98, 100]. In general, when using this technique, a series of ten scans is performed at a single level during a 6-second period, as the patient first inspires and then forcefully exhales. Patients are instructed to breathe in deeply and then breathe out as rapidly as possible (Fig. 1-29). Images are reconstructed using a high-spatial frequency algorithm. Usually, dynamic CT scan sequences are obtained at several selected levels through

the lungs. In papers describing this technique, three levels were used (e.g., at the level of the aortic arch, carina, and lung bases), although the protocol can be varied in individual cases, with imaging limited to a specific region. During expiration, the diaphragm ascends, and the lungs move cephalad. Lung motion is most significant on scans through the lung bases. Although slightly different regions of the lung are imaged on sequential scans obtained at the same level, the effect of diaphragmatic motion on the assessment of lung attenuation has been regarded as inconsequential [64, 68, 98]. Little motion-related image degradation is visible on dynamic ultrafast HRCT scans because of the very rapid scan time used [81, 100].

Dynamic scans can also be obtained using a spiral or helical CT scanner with a gantry rotation time of 1 second or less. If images are reconstructed using half the scan circle, individual images represent a scan period of one-half second or less. Because of the continuous scanning that is possible with the helical technique, scans can be reconstructed at any point during the scan sequence, thus providing a temporal resolution equivalent or superior to that of dynamic ultrafast HRCT. However, because of the longer time required to obtain each image, some degradation of anatomic detail can be expected on individual images. In performing dynamic expiratory CT, although one or more images obtained during the rapid phases of expiration will show significant motion artifact, images near and at full expiration show little artifact and allow optimal assessment of lung attenuation (Fig. 1-30) [101].

The use of a dynamic spiral technique may be combined with a reduced mA (e.g., 40 mA) so that the sequence of images obtained represents the same radiation dose as that

associated with a single expiratory image (see Fig. 2-20). Using such a technique, continuous imaging is performed during 6 seconds, as the patient rapidly exhales. The total radiation dose for the 6-second sequence is equivalent to that of a single scan. Although image quality is reduced using the low-dose technique, images adequate for the diagnosis of air-trapping are obtained. In a group of lung transplant recipients studied using both postexpiratory HRCT and low-dose dynamic expiratory spiral HRCT [101], lung attenuation was noted to increase significantly more with the dynamic technique (204 HU versus 130 HU, $p = .0007$), and in one patient, air-trapping was diagnosed only on the dynamic images.

Using either technique, the dynamic scan sequence is viewed with attention to changes in lung attenuation and regional lung volume during the forced expiration. The images can be evaluated quantitatively or qualitatively, with measurement of lung attenuation during different phases of the respiratory maneuver, calculation of time-attenuation curves, or simple viewing of the serial scans in sequence or in cine mode. Air-trapping is considered to be present when the lung fails to increase normally in attenuation during exhalation [68, 81, 98]. The image sequence can be analyzed quantitatively as well as

P.38

P.39

qualitatively. The mean HU attenuation for a specific region of interest in the lung can be measured and plotted for each scan, producing a time-attenuation curve graphically

demonstrating the changes in lung attenuation that have occurred during a single expiration and inspiration (Fig. 1-29B) [81]. This use of dynamic expiratory HRCT is discussed further in Chapters 2 and 3.

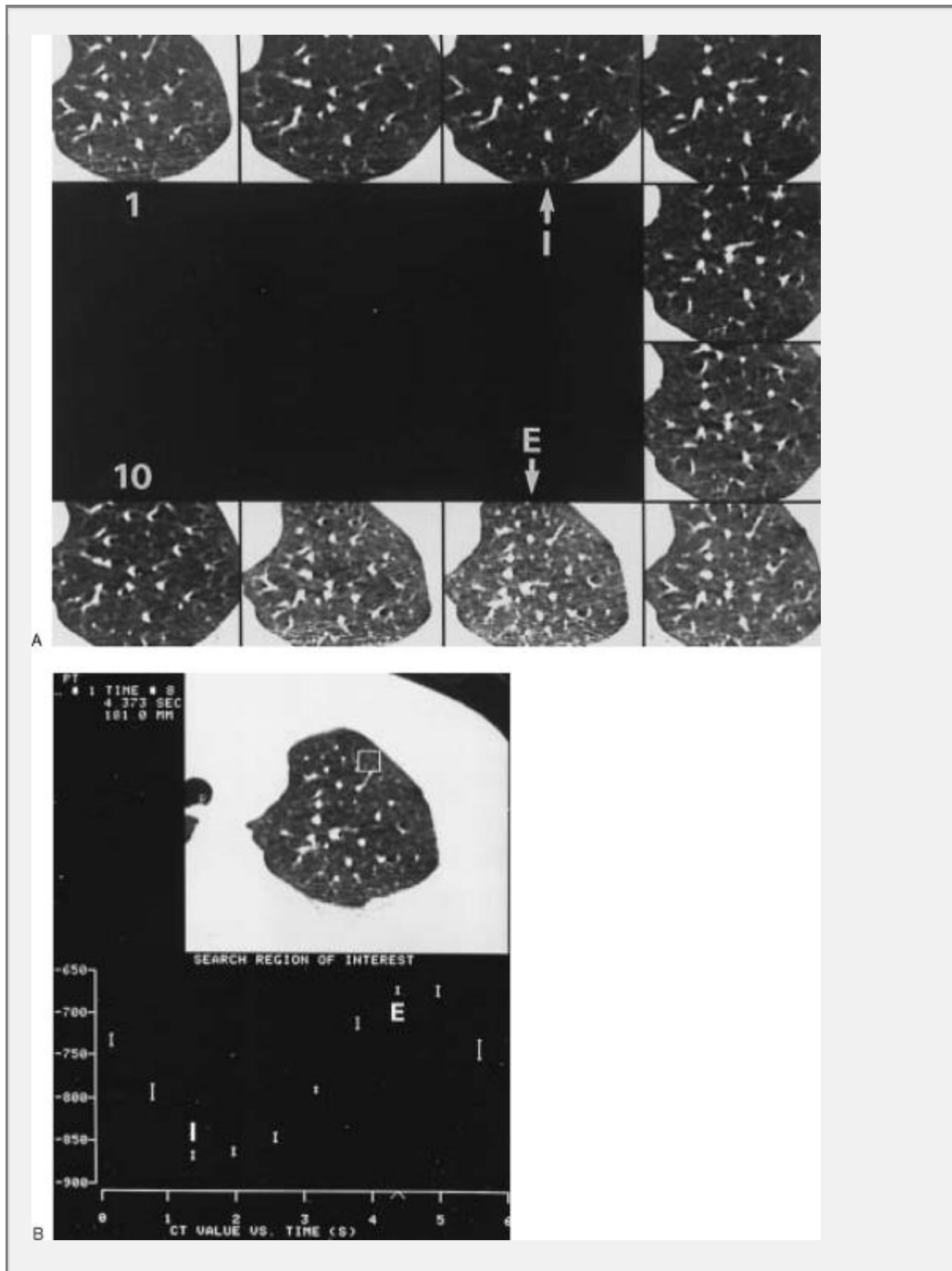


FIG. 1-29. Dynamic expiratory HRCT in a normal subject obtained using an electron-beam scanner. A: The ten-image dynamic ultrafast HRCT sequence acquired during a single forced vital capacity maneuver is shown, with the field of view limited to the left upper lobe. These ten 100-millisecond images were obtained at 600-millisecond intervals. They are shown in sequence, in a clockwise fashion, from the left upper corner (1) to the lower left corner (10). Images at full inspiration (I) and full expiration (E) are visible. Note the increase in lung attenuation and decrease in lung volume that occur as the subject exhales. As in most normal subjects, lung attenuation increase on expiration is relatively homogeneous. B: A time-attenuation curve is produced by measuring the mean lung attenuation (HU) for a specific region of interest (ROI). In this subject, for an ROI in the anterior lung, attenuation decreases to approximately -870 HU at maximum inspiration (I) and increases in attenuation to -670 HU at maximum expiration (E) for an overall attenuation increase of approximately 200 HU. Each point on the time-attenuation curve represents one image from the dynamic sequence. (From Webb WR, Stern EJ, Kanth N, et al. Dynamic pulmonary CT: findings in normal adult men. *Radiology* 1993;186:117, with permission.)

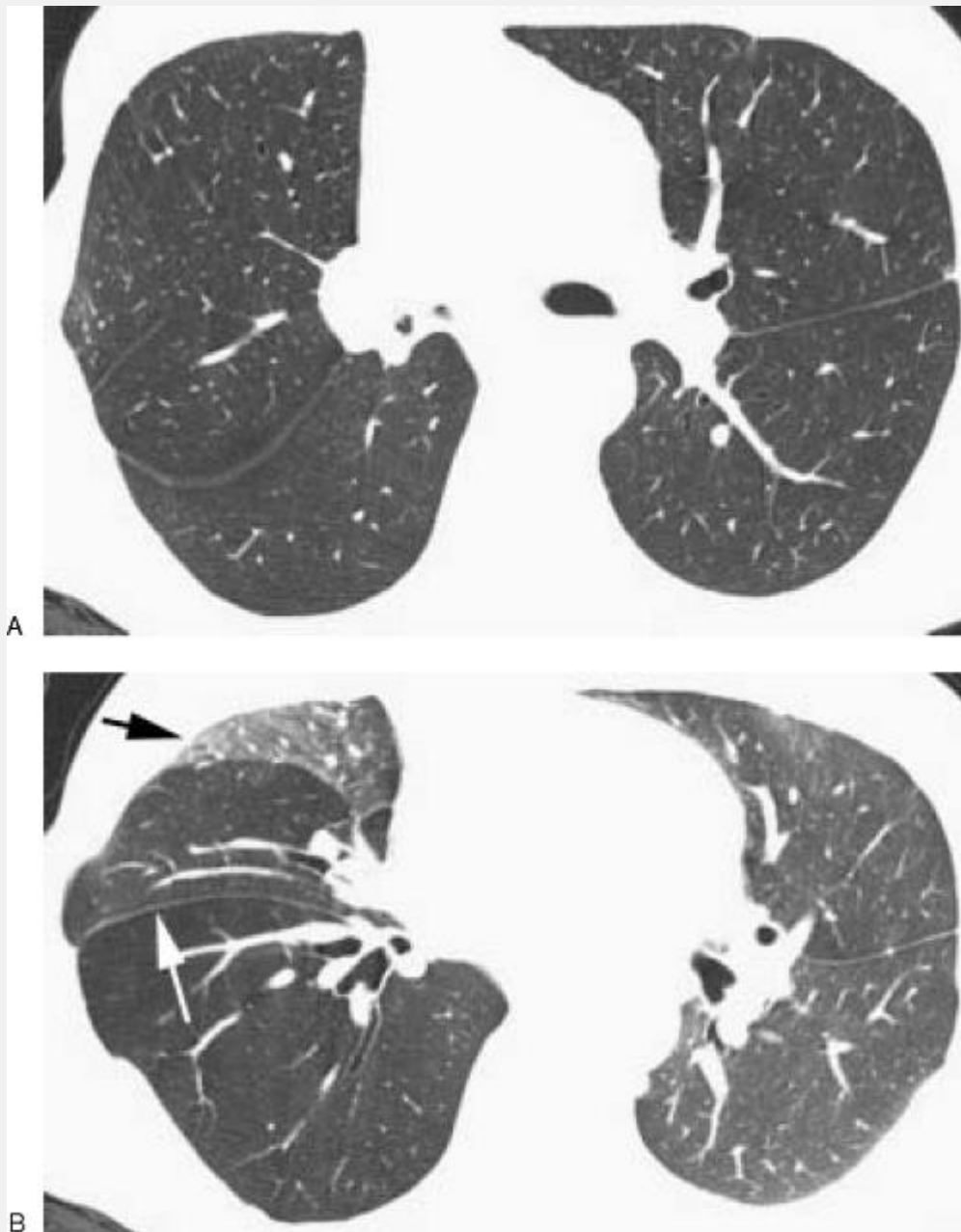


FIG. 1-30. Dynamic expiratory HRCT obtained using a spiral scanner. A: In a patient with bilateral lung transplantation, inspiratory HRCT shows stenosis of the bronchus intermedius. The lungs appear normal. B: On an image from the expiratory phase, there is marked air-trapping in right middle and lower lobes. Note that the right major fissure (white arrow) is bowed forward in comparison to the left

major fissure and the inspiratory scan. The right upper lobe (black arrow) and left lung increase normally in attenuation.

Spirometrically Triggered Expiratory High-Resolution Computed Tomography

Spirometrically triggered expiratory HRCT is a technique by which expiratory scanning can be done at specific, reproducible, user-selected lung volumes [88,89,90,93]. With this technique, the patient breathes through a small hand-held spirometer while positioned on the CT table. Before scanning, a spirometric measurement of the vital capacity is obtained, and trigger level (e.g., 90% of vital capacity) is chosen. During exhalation, the spirometer and associated microcomputer measure the volume of gas expired and trigger CT after a specific volume is reached. When the trigger signal is generated, air flow is inhibited by closure of a valve attached to the spirometer, and a scanning starts. Two or three different levels in the chest are typically selected and evaluated with respect to lung attenuation at specific lung volumes. Using this method, quantitative assessment of CT images with respect to lung attenuation can be performed with excellent precision [88, 89]. This technique may also be used with a spiral scanner or an electron beam scanner [91]. Spirometrically gated or controlled imaging may be particularly valuable in pediatric patients [91]; with inhibition of respiration, respiratory motion artifacts may be avoided. Motion-free inspiratory and expiratory imaging can also be obtained in pediatric

patients by using a positive-pressure ventilation device and controlled pauses in spontaneous respiration [92].

P.40

Three-Dimensional Expiratory Computed Tomography

The use of helical CT performed with thick collimation (7 to 8 mm) at inspiration and expiration, with 3D reconstruction of the CT data, has also been used to assess lung volume and the extent of emphysema. However, in patients having an HRCT study for diagnosis of a diffuse lung disease, obtaining selected expiratory HRCT scans is generally simpler and preferable to obtaining a spiral CT examination for the diagnosis of air-trapping.

The method of assessing lung attenuation or lung volume using spiral CT has varied with the investigator. Kauczor et al. [94] used helical CT (slice thickness, 8 mm; pitch, 2; increment, 8 mm) with two-dimensional (2D) and 3D postprocessing to assess lung volume at deep inspiration and expiration. 2D and 3D techniques were found to correlate with lung volumes. In another study, 3D volumetric reconstructions of total lung volume at inspiration and at expiration and quantitation of regions of low attenuation (lung attenuation measuring less than -896 HU on inspiratory CT and -790 HU on expiratory CT) were correlated with pulmonary function test results [95]; in this study, an excellent correlation was found between the volume of low-attenuation lung and pulmonary function test findings of obstruction, such as the ratio of forced

expiratory volume in 1 sec (FEV1) to the forced vital capacity.

The use of multidetector-row volumetric HRCT during inspiration and expiration may also be used for the global assessment of lung attenuation, with the advantage that it would also provide anatomic detail.

Recommended High-Resolution Computed Tomography Protocols

HRCT may be obtained in a number of different clinical settings, and to some extent the manner in which the examination is obtained is varied according to the diseases suspected. The following protocols are provided as guides, but these may be varied in individual cases.

Suspected Emphysema, Airways, or Obstructive Disease

In patients suspected of having airways or obstructive disease on the basis of clinical, pulmonary function, or plain radiographic findings, HRCT should be obtained at full inspiration, at 1-cm intervals from lung apices to bases, and with the patient supine (Table 1-2); prone scans are not usually needed. This protocol has been recommended specifically for studying patients with suspected bronchiectasis [102]. Scans after expiration obtained at three or more levels are recommended to detect air-trapping. Gantry angulation may be appropriate in selected cases when bronchiectasis is suspected, but it is not recommended as routine [40, 41]. Multidetector-row spiral HRCT, using 1- to 1.25-mm detector width would be ideal for assessing this type of abnormality. The assessment of airways disease is discussed in further detail in Chapter 8.

TABLE 1-2. *Scan protocols: suspected emphysema, airways disease, or obstructive lung disease*

Full inspiration

Supine scans with 1-cm spacing from lung apices to bases

Expiratory scans at three or more levels

Options: Gantry angulation for airways disease

Spiral CT (3-mm collimation; pitch, 1.7-2.0) for airways disease

Multidetector-row spiral HRCT

In patients with emphysema being evaluated for lung transplantation or volume-reduction surgery, obtaining a routine CT with thick collimation for the detection of lung nodules suspicious for carcinoma is also important. HRCT and volumetric imaging may be combined by using multidetector-row spiral HRCT.

Suspected Fibrotic or Restrictive Disease, or Unknown Lung Disease

In patients suspected of having a fibrotic or restrictive lung disease on the basis of clinical, pulmonary function, or plain radiographic findings, or in patients with an unknown type of respiratory disability, it is also appropriate to obtain HRCT scans at 1-cm intervals with the patient supine. If the chest radiograph appears normal or subtle lung disease is present, or if chest radiographs are unavailable for review,

additional prone scans should be obtained, or the scans should be monitored for the presence of problematic dependent opacity (Table 1-3). If the plain radiograph shows a distinct abnormality, prone scans likely will not be needed.

TABLE 1-3. Scan protocols: suspected restrictive or fibrotic lung disease, or diffuse lung disease of unknown type

Chest radiograph abnormal

Full inspiration.

Supine scans with 1-cm spacing from lung apices to bases.

Expiratory scans at three or more levels (initial examination only).

Chest radiograph normal or minimally abnormal; chest radiograph unavailable

Option 1

Full inspiration.

Scans with 2-cm spacing in both prone and supine positions from lung apices to bases.

Expiratory scans at three or more levels (initial evaluation only).

Option 2

Full inspiration.

Supine scans with 1-cm spacing from lung apices to bases.

Check scans for “dependent density” and obtain

prone scans at appropriate levels if present.

Expiratory scans at three or more levels (initial evaluation only).

P. 41

Prone scans at 2-cm intervals, in combination with the supine scans, are recommended when obtaining prone scans routinely; they obviate the need for reviewing plain radiographs or monitoring scans. Scans at 2-cm intervals, in both supine and prone positions, have proven to be a useful protocol for prone and supine imaging and provide the same number of images to review as obtained when scanning a patient with obstructive disease [29] (Table 1-3). In patients having their initial diagnostic evaluation, obtaining expiratory scans at three or more levels is recommended. In a patient with an unknown lung disease, airway obstruction may be the cause of the patient's disability. Furthermore, in a patient with a restrictive or fibrotic disease, the presence of air-trapping visible on expiratory images may be helpful in differential diagnosis [60].

In patients with restrictive disease who are having follow-up HRCT examinations, inspiratory images may be obtained at fewer levels (e.g., at three levels) than are appropriate for

the initial examination [33], and expiratory scans are not usually necessary.

Hemoptysis

In patients who present with hemoptysis possibly related to airway abnormalities or an endobronchial lesion, it has been recommended that CT be obtained through the hila using 5-mm collimation with or without spiral technique to allow evaluation of the central bronchi, with HRCT at 1-cm intervals through the remainder of the lung parenchyma to look for bronchiectasis or other airway abnormalities (Table 1-4) [103, 104]. Multidetector-row HRCT would also be appropriate in the assessment of patients with hemoptysis, allowing the assessment of both large and small airways disease. Scans may be reconstructed using narrow detector width or by combining detectors to produce thicker scans (see Chapter 8).

Suspected Pulmonary Vascular Disease

Some patients may have symptoms or signs (e.g., hypoxemia, pulmonary hypertension) that may result from lung disease (e.g., emphysema), pulmonary vascular disease (e.g., chronic pulmonary embolism, vasculitis), or a combination of these [105, 106, 107, 108, 109]. In such patients, combining HRCT with a contrast-enhanced spiral CT may be necessary for diagnosis. The HRCT study is used to detect findings of lung disease or small vessel disease, and the contrast-enhanced spiral CT is used to detect large vessel abnormalities and vascular obstruction.

TABLE 1-4. *Scan protocols:*

hemoptysis

Full inspiration

Supine scans with contiguous 5-mm collimation through the hila

HRCT with 1-cm spacing at other levels

Expiratory scans at three or more levels (initial evaluation only)

Option: Multidetector-row HRCT

TABLE 1-5. Scan protocols: suspected pulmonary vascular disease

Full inspiration

HRCT with 1-cm spacing

Expiratory scans at three or more levels (initial evaluation only)

Contrast-enhanced spiral CT

Option: Contrast-enhanced multidetector-row HRCT

HRCT obtained at 1-cm intervals in the supine position with expiratory scans would be appropriate (Table 1-5). The spiral CT technique used would depend on the indications. For the diagnosis of chronic pulmonary embolism, although the precise technique varies with the investigator and is beyond the scope of this book, the use of 3-mm collimation

and a pitch of 1.7 to 2 during contrast infusion is most appropriate for a single detector-row spiral scanner [110, 111, 112, 113]. The use of contrast-enhanced multidetector-row HRCT with 1.25-mm detector width and a pitch of 6 would be ideal for this indication, allowing the detailed assessment of both large and small vessel abnormalities and associated lung disease (Figs. 1-26 and 1-27).

Combined Diagnosis of Diffuse Lung Disease and Focal Abnormalities

Combining conventional CT with HRCT examinations may be of value in patients with a variety of diseases (Table 1-6), but it is particularly important in patients being evaluated before volume-reduction surgery for emphysema or before lung transplantation. In such patients, volumetric lung imaging may be of value in the diagnosis of lung carcinoma, which has an increased incidence in patients with emphysema or lung fibrosis, or other significant focal abnormalities [54]. In patients having single lung transplantation, identification of significant abnormalities localized to one lung may be valuable in allowing the appropriate choice of which lung to remove. Multidetector-row spiral CT would be very useful in this regard.

TABLE 1-6. Scan protocols: combined diagnosis of diffuse lung disease and focal abnormalities

Full inspiration
 HRCT with 1-cm spacing
 Prone scans if appropriate
 Expiratory scans at three or more levels (initial evaluation only)
 Spiral CT with or without contrast infusion
 Option: Multidetector-row HRCT

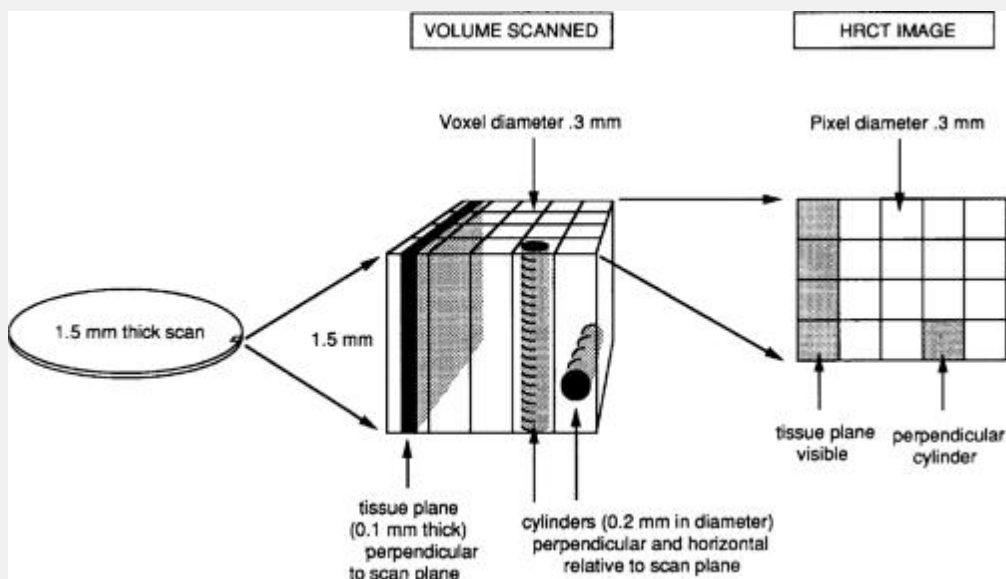


FIG. 1-31. Resolution and size or orientation of structures. The tissue plane, 1 mm thick, and the perpendicular cylinder, 0.2 mm in diameter, are visible on the HRCT scan because they extend through the thickness of the scan volume or voxel. The horizontal cylinder cannot be seen.

P. 42

Spatial Resolution

A fundamental relationship exists between pixel size and the size of structures that can be resolved by CT. For optimal matching of image display to the attainable spatial resolution of the scanner, there should be two pixels for the smallest structure resolved [12]. If a sufficiently small FOV is used with pixel sizes approximating 0.25 mm, current scanners are capable of providing a resolution of 10 to 12 line pairs per cm by using a high-resolution algorithm [11, 42].

Structures smaller than the pixel size should be difficult to resolve on HRCT; however, resolution is sometimes possible. Interlobular septa as thin as 0.1 mm and arteries with a diameter of 0.3 mm are sometimes visible on HRCT using a small FOV. The reasons such small structures are visible include the large differences in attenuation between the soft-tissue structures present in the lung and the air-filled alveoli surrounding them, and the use of a high-spatial frequency algorithm for reconstruction, which often results in some edge enhancement.

The ability of HRCT to resolve fine lung structures depends on their orientation relative to the scan plane (Fig. 1-31). Structures measuring 0.1 to 0.2 mm in thickness can be seen if they are largely oriented perpendicular to the scan plane and extend through the thickness of the scan plane or voxel (e.g., 1.5 mm) [10, 11, 114, 115]. Similarly sized structures (0.1 to 0.2 mm) that are oriented horizontally within the scan plane will not be visible because of volume averaging with the air-filled lung, which occupies most of the thickness of the voxel.

These limitations explain the visibility of various lung structures on HRCT. For example, HRCT allows us to resolve some normal interlobular septa, which represent a plane of

tissue approximately 100 to 200 μm or 0.1 to 0.2 mm in thickness, or small vessels that are oriented perpendicular to the scan plane (Fig. 1-31) [10, 114, 115], whereas vessels or septa lying in the plane of scan are usually visible as discrete structures only if they are larger or thicker than 0.3 to 0.5 mm. Bronchi or bronchioles measuring less than 2 to 3 cm in diameter and having a wall thickness of approximately 0.3 mm are usually invisible in peripheral lung because they have courses that lie roughly in the plane of scan. Bronchi or bronchioles of similar sizes are sometimes visible when oriented perpendicular to the plane of scan.

It should be kept in mind that, although soft-tissue structures can be resolved when they are thinner or smaller than the pixel size, their apparent size in the final HRCT image will be determined, at least partially, by the pixel size and the interpolation algorithm used in the workstation or camera and not by their actual dimensions. This can make the measurement of such small structures on HRCT difficult and prone to inaccuracies.

P.43

Radiation Dose

HRCT as routinely performed results in a low radiation dose as compared to conventional CT obtained with contiguous 1-cm collimation [116]. Radiation doses at the breast skin surface for patients undergoing conventional chest CT with contiguous 10-mm collimation [140 kV(p), 200 mA] are approximately 20 mGy [117].

Initially, a study of contiguous HRCT scans reported the upper limit of the radiation dose that could be expected using this technique, as measured in the center of a 16-cm plastic phantom [11]. In this study, contiguous HRCT scans resulted in a higher dose than contiguous scans with 10-mm collimation. One-and-one-half-mm scans [120 kV(p), 300 mA] resulted in a dose of 61 mGy, as compared to 55 mGy for contiguous 10-mm collimated scans obtained using the same technique. However, it is important to recognize that the measured radiation dose is affected by scatter and penumbra effects [117]. These effects are greater with contiguous scans than with spaced scans, and it must be kept in mind that HRCT is normally performed using scans spaced at 1- or 2-cm intervals.

In a more recent study [116], the radiation dose to the chest associated with spaced HRCT scans was compared to the radiation dose produced by conventional CT. In this study, using a scan technique of 120 kV(p), 200 mA, and 2 seconds, the mean skin radiation dose was 4.4 mGy for 1.5-mm HRCT scans at 10 mm-intervals, 2.1 mGy for scans at 20-mm intervals, and 36.3 mGy for conventional 10-mm scans at 10-mm intervals. Thus, HRCT scanning at 10- and 20-mm intervals, as done in clinical imaging, results in 12% and 6%, respectively, of the radiation dose associated with conventional CT. It has also been pointed out that obtaining low-dose HRCT (20 mA, 2 seconds) [20] at 20-mm intervals would result in an average skin dose comparable to that administered with chest radiography [116]. This has been confirmed by Lee et al. [21]; the effective radiation dose of low-dose HRCT obtained at three levels with 80 mA is quite similar to that of chest radiographs [118, 119].

The use of spiral CT or a multidetector-row spiral CT for volumetric HRCT examination results in a higher radiation dose than conventional HRCT. However, with multidetector-row spiral CT, a volumetric study may be obtained with a radiation dose similar to that of routine chest CT.

High-Resolution Computed Tomography Artifacts

Several confusing artifacts can be seen on HRCT. However, familiarity with their appearances should eliminate potential misdiagnoses [9, 11, 25, 120, 121].

Streak Artifacts

Fine streak artifacts that radiate from the edges of sharply margined, high-contrast structures such as bronchial walls, ribs, or vertebral bodies are common on HRCT. On HRCT, streak artifacts are often visible as fine, linear, or netlike opacities (Figs. 1-4 and 1-32) that can be seen anywhere but are most commonly found overlying the posterior lung, paralleling the pleural surface and posterior chest wall [11]. Although streak artifacts degrade the image, they do not usually mimic pathology or cause confusion in image interpretation. Streak artifacts are thinner and less dense and have a different appearance than the normal or abnormal interstitium (interlobular septa) visible in this region. Streak artifacts can result from two separate mechanisms—aliasing and correlated noise. Streak artifacts are more evident on scans obtained with low mA [20, 25].



FIG. 1-32. "**Double fissure**" artifact. The left major fissure (arrows) appears to be double. Fine streak artifacts are visible posteriorly. Pulsation artifacts are also visible adjacent to the left heart border.

Aliasing is a geometric phenomenon that occurs because of undersampling of spatial information and is related to detector spacing and scan collimation [12]. As it is independent of radiation dose, increasing scan technique is of no value in reducing this type of artifact.

Correlated noise has a similar appearance and is most notable in the paravertebral regions, adjacent to the highly attenuating vertebral bodies [12]. This type of artifact is

strongly related to radiation dose and can be minimized by increasing kV(p) and mA.

Motion Artifacts

Pulsation or star artifacts are commonly visible, particularly at the left lung base, adjacent to the heart (Figs. 1-6, 1-32, and 1-33). With pulsation artifacts, thin streaks radiate from the edges of vessels or other visible structures, which therefore

P.44

resemble stars, and small areas of apparent lucency may be seen between these streaks. These lucent areas, if not recognized as artifactual, may be mistaken for dilated bronchi [121].

Doubling artifacts. The major fissure, usually on the left (Figs. 1-32, 1-33, and 1-34), or other parenchymal structures such as vessels and bronchi, may be seen as double because of cardiac pulsation or respiration during the scan [25, 120]. This appearance can mimic bronchiectasis (Fig. 1-33). It results when a linear structure, such as the fissure or vessel, is in a slightly different position when scanned by the gantry from opposite directions (180 degrees apart) (Fig. 1-34). As with image noise, these artifacts are much more conspicuous when high-resolution techniques are used, simply because they are more sharply resolved.

Motion-related artifacts can be reduced by ECG gating of scan acquisition [42], by using scanners with very rapid scan times (100 milliseconds) [98], or by spirometrically controlled respiration [91, 92].

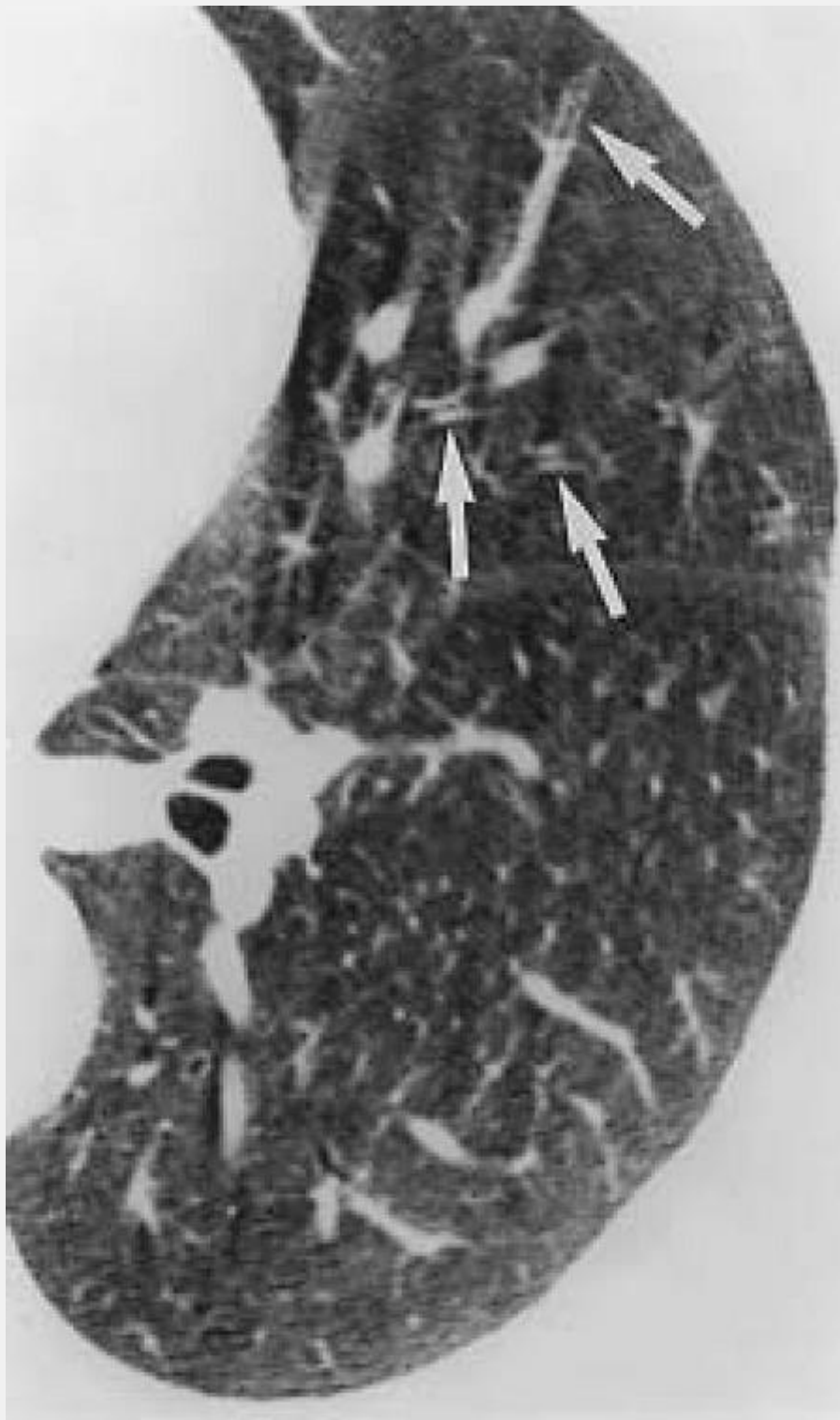
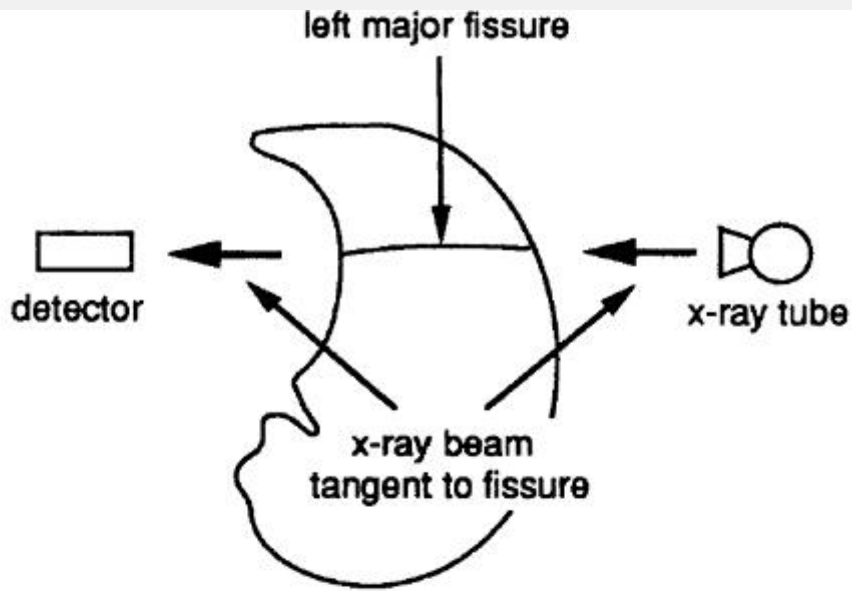
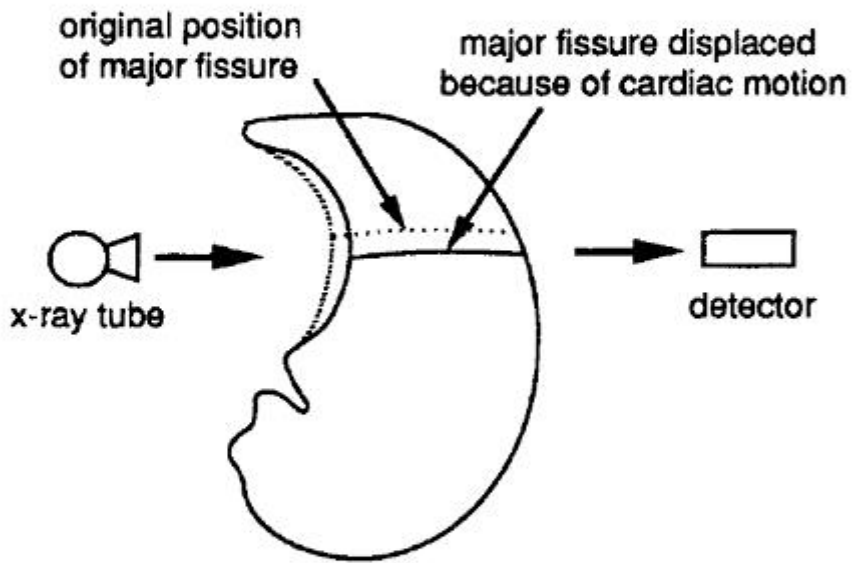


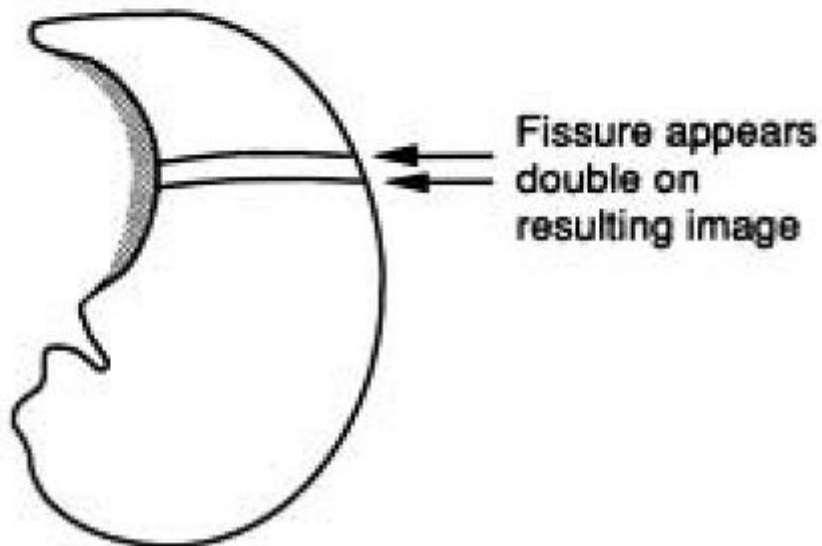
FIG. 1-33. Bronchiectasis artifact ("pseudobronchiectasis"). Several linear structures (arrows) appear double, mimicking bronchiectasis.



A



B



C

FIG. 1-34. Mechanism of "double fissure" artifact. The major fissure is seen by the scanner only when the x-ray beam is tangent to it. If the position of the fissure is slightly altered by cardiac pulsation during the period in which the gantry has rotated 180 degrees (A, B), it appears to be seen in two different locations on the resulting image (C).

References

1. Naidich DP. Pulmonary parenchymal high-resolution CT: to be or not to be. *Radiology* 1989;171:22-24.
2. Siegelman SS, Zerhouni EA, Leo FP, et al. CT of the solitary pulmonary nodule. *AJR Am J Roentgenol* 1980;135:1-13.
3. Todo G, Itoh H, Nakano Y, et al. [High-resolution CT for the evaluation of pulmonary peripheral disorders]. *Jpn J Clin Radiol* 1982;27:1319-1326.

P.45

4. Nakata H, Kimoto T, Nakayama T, et al. Diffuse peripheral lung disease: evaluation by high-resolution computed tomography. *Radiology* 1985;157:181-185.
5. Naidich DP, Zerhouni EA, Hutchins GM, et al. Computed tomography of the pulmonary parenchyma: part 1, distal air-space disease. *J Thorac Imaging* 1985;1:39-53.
6. Zerhouni EA, Naidich DP, Stitik FP, et al. Computed tomography of the pulmonary parenchyma: part 2, interstitial disease. *J Thorac Imaging* 1985;1:54-64.

7. Müller NL, Miller RR. Computed tomography of chronic diffuse infiltrative lung disease: part 1. *Am Rev Respir Dis* 1990; 142: 1206-1215.
8. Müller NL, Miller RR. Computed tomography of chronic diffuse infiltrative lung disease: part 2. *Am Rev Respir Dis* 1990; 142: 1440-1448.
9. Webb WR. High-resolution CT of the lung parenchyma. *Radiol Clin North Am* 1989; 27: 1085-1097.
10. Zerhouni E. Computed tomography of the pulmonary parenchyma: an overview. *Chest* 1989; 95: 901-907.
11. Mayo JR, Webb WR, Gould R, et al. High-resolution CT of the lungs: an optimal approach. *Radiology* 1987; 163: 507-510.
12. Mayo JR. High resolution computed tomography: technical aspects. *Radiol Clin North Am* 1991; 29: 1043-1049.
13. Murata K, Khan A, Rojas KA, et al. Optimization of computed tomography technique to demonstrate the fine structure of the lung. *Invest Radiol* 1988; 23: 170-175.
14. Webb WR, Gamsu G, Wall SD, et al. CT of a bronchial phantom: factors affecting appearance and size measurements. *Invest Radiol* 1984; 19: 394-398.
15. Mayo JR. The high-resolution computed tomography technique. *Semin Roentgenol* 1991; 26: 104-109.
16. Zwirewich CV, Terriff B, Müller NL. High-spatial-frequency (bone) algorithm improves quality of standard CT of the thorax. *AJR Am J Roentgenol* 1989; 153: 1169-1173.
17. Naidich DP, Marshall CH, Gribbin C, et al. Low-dose CT of the lungs: preliminary observations. *Radiology* 1990; 175: 729-731.
18. Murata K, Khan A, Herman PG. Pulmonary parenchymal disease: evaluation with high-resolution CT. *Radiology* 1989; 170: 629-635.

19. Remy-Jardin M, Giraud F, Remy J, et al. Pulmonary sarcoidosis: role of CT in the evaluation of disease activity and functional impairment and in prognosis assessment. *Radiology* 1994;191:675-680.
20. Zwirerich CV, Mayo JR, Müller NL. Low-dose high-resolution CT of lung parenchyma. *Radiology* 1991;180:413-417.
21. Lee KS, Primack SL, Staples CA, et al. Chronic infiltrative lung disease: comparison of diagnostic accuracies of radiography and low- and conventional-dose thin-section CT. *Radiology* 1994;191:669-673.
22. Majurin ML, Varpula M, Kurki T, et al. High-resolution CT of the lung in asbestos-exposed subjects: comparison of low-dose and high-dose HRCT. *Acta Radiol* 1994;35:473-477.
23. Majurin ML, Valavaara R, Varpula M, et al. Low-dose and conventional-dose high resolution CT of pulmonary changes in breast cancer patients treated by tangential field radiotherapy. *Eur J Radiol* 1995;20:114-119.
24. Bankier AA, Fleischmann D, Mallek R, et al. Bronchial wall thickness: appropriate window settings for thin-section CT and radiologic-anatomic correlation. *Radiology* 1996;199:831-836.
25. Primack SL, Remy-Jardin M, Remy J, et al. High-resolution CT of the lung: pitfalls in the diagnosis of infiltrative lung disease. *AJR Am J Roentgenol* 1996;167:413-418.
26. Maguire WM, Herman PG, Khan A, et al. Comparison of fixed and adjustable window width and level settings in the CT evaluation of diffuse lung disease. *J Comput Assist Tomogr* 1993;17:847-852.

27. Remy-Jardin M, Remy J, Giraud F, et al. Computed tomography assessment of ground-glass opacity: semiology and significance. *J Thorac Imaging* 1993;8:249-264.
28. Aberle DR, Gamsu G, Ray CS, et al. Asbestos-related pleural and parenchymal fibrosis: detection with high-resolution CT. *Radiology* 1988;166:729-734.
29. Volpe J, Storto ML, Lee K, et al. High-resolution CT of the lung: determination of the usefulness of CT scans obtained with the patient prone based on plain radiographic findings. *AJR Am J Roentgenol* 1997;169:369-374.
30. Mathieson JR, Mayo JR, Staples CA, et al. Chronic diffuse infiltrative lung disease: comparison of diagnostic accuracy of CT and chest radiography. *Radiology* 1989;171:111-116.
31. Swensen SJ, Aughenbaugh GL, Brown LR. High-resolution computed tomography of the lung. *Mayo Clin Proc* 1989;64:1284-1294.
32. Aberle DR, Gamsu G, Ray CS. High-resolution CT of benign asbestos-related diseases: clinical and radiographic correlation. *AJR Am J Roentgenol* 1988;151:883-891.
33. Kazerooni EA, Martinez FJ, Flint A, et al. Thin-section CT obtained at 10-mm increments versus limited three-level thin-section CT for idiopathic pulmonary fibrosis: correlation with pathologic scoring. *AJR Am J Roentgenol* 1997;169:977-983.
34. Gamsu G, Aberle DR, Lynch D. Computed tomography in the diagnosis of asbestos-related thoracic disease. *J Thorac Imaging* 1989;4:61-67.
35. Friedman AC, Fiel SB, Fisher MS, et al. Asbestos-related pleural disease and asbestosis: a comparison of CT and chest radiography. *AJR Am J Roentgenol* 1988;150:268-275.

36. Friedman AC, Fiel SB, Radecki PD, et al. Computed tomography of benign pleural and pulmonary parenchymal abnormalities related to asbestos exposure. *Semin Ultrasound CT MR* 1990; 11: 393-408.
37. Staples CA. Computed tomography in the evaluation of benign asbestos-related disorders. *Radiol Clin North Am* 1992; 30: 1191-1207.
38. Murray K, Gamsu G, Webb WR, et al. High-resolution CT sampling for detection of asbestos-related lung disease. *Acad Radiol* 1995; 2: 111-115.
39. Henschke CI. Image selection for computed tomography of the chest: a sampling approach. *Invest Radiol* 1992; 27: 908-911.
40. Remy-Jardin M, Remy J. Comparison of vertical and oblique CT in evaluation of the bronchial tree. *J Comput Assist Tomogr* 1988; 12: 956-962.
41. Grenier P, Cordeau MP, Beigelman C. High-resolution computed tomography of the airways. *J Thorac Imaging* 1993; 8: 213-229.
42. Schoepf UJ, Becker CR, Bruening RD, et al. Electrocardiographically gated thin-section CT of the lung. *Radiology* 1999; 212: 649-654.
43. Swensen SJ, Brown LR, Colby TV, et al. Lung nodule enhancement at CT: prospective findings. *Radiology* 1996; 201: 447-455.
44. Engeler CE, Tashjian JH, Engeler CM, et al. Volumetric high-resolution CT in the diagnosis of interstitial lung disease and bronchiectasis: diagnostic accuracy and radiation dose. *AJR Am J Roentgenol* 1994; 163: 31-35.
45. Bhalla M, Naidich DP, McGuinness G, et al. Diffuse lung disease: assessment with helical CT—preliminary

observations of the role of maximum and minimum intensity projection images. *Radiology* 1996;200:341-347.

46. Coakley FV, Cohen MD, Johnson MS, et al. Maximum intensity projection images in the detection of simulated pulmonary nodules by spiral CT. *Br J Radiol* 1998;71:135-140.

47. Remy-Jardin M, Remy J, Artaud D, et al. Diffuse infiltrative lung disease: clinical value of sliding-thin-slab maximum intensity projection CT scans in the detection of mild micronodular patterns. *Radiology* 1996;200:333-339.

48. Kalender WA, Seissler W, Klotz E, et al. Spiral volumetric CT with single-breath-hold technique, continuous transport, and continuous scanner rotation. *Radiology* 1990;176:181-183.

49. Vock P, Soucek M. Spiral computed tomography in the assessment of focal and diffuse lung disease. *J Thorac Imaging* 1993;8:283-290.

50. Paranjpe DV, Bergin CJ. Spiral CT of the lungs: optimal technique and resolution compared with conventional CT. *AJR Am J Roentgenol* 1994;162:561-567.

51. Heiken JP, Brink JA, Vannier MW. Spiral (helical) CT. *Radiology* 1993;189:647-656.

52. Polacin A, Kalender WA, Marchal G. Evaluation of section sensitivity profiles and image noise in spiral CT. *Radiology* 1992;185:29-35.

53. Kuriyama K, Tateishi R, Kumatani T, et al. Pleural invasion by peripheral bronchogenic carcinoma: assessment with three-dimensional helical CT. *Radiology* 1994;191:365-369.

54. Kazerooni EA, Chow LC, Whyte RI, et al. Preoperative examination of lung transplant candidates: value of chest

CT compared with chest radiography. *AJR Am J Roentgenol* 1995;165:1343-1348.

55. Arakawa H, Webb WR. Expiratory high-resolution CT scan. *Radiol Clin North Am* 1998;36:189-209.

56. Webb WR. Radiology of obstructive pulmonary disease. *AJR Am J Roentgenol* 1997;169:637-647.

57. Chen D, Webb WR, Storto ML, et al. Assessment of air trapping using postexpiratory high-resolution computed tomography. *J Thorac Imaging* 1998;13:135-143.

P.46

58. Lucidarme O, Coche E, Cluzel P, et al. Expiratory CT scans for chronic airway disease: correlation with pulmonary function test results. *AJR Am J Roentgenol* 1998;170:301-307.

59. Arakawa H, Webb WR. Air trapping on expiratory high-resolution CT scans in the absence of inspiratory scan abnormalities: correlation with pulmonary function tests and differential diagnosis. *AJR Am J Roentgenol* 1998;170:1349-1353.

60. Arakawa H, Webb WR, McCowin M, et al. Inhomogeneous lung attenuation at thin-section CT: diagnostic value of expiratory scans. *Radiology* 1998;206:89-94.

61. Vock P, Malanowski D, Tschaeppler H, et al. Computed tomographic lung density in children. *Invest Radiol* 1987;22:627-631.

62. Robinson PJ, Kreel L. Pulmonary tissue attenuation with computed tomography: comparison of inspiration and expiration scans. *J Comput Assist Tomogr* 1979;3:740-748.

63. Millar AB, Denison DM. Vertical gradients of lung density in healthy supine men. *Thorax* 1989;44:485-490.

64. Webb WR, Stern EJ, Kanth N, et al. Dynamic pulmonary CT: findings in normal adult men. *Radiology* 1993;186:117-124.
65. Verschakelen JA, Van Fraeyenhoven L, Laureys G, et al. Differences in CT density between dependent and nondependent portions of the lung: influence of lung volume. *AJR Am J Roentgenol* 1993;161:713-717.
66. Webb WR. High-resolution computed tomography of obstructive lung disease. *Radiol Clin North Am* 1994;32:745-757.
67. Knudson RJ, Standen JR, Kaltenborn WT, et al. Expiratory computed tomography for assessment of suspected pulmonary emphysema. *Chest* 1991;99:1357-1366.
68. Stern EJ, Webb WR, Gamsu G. Dynamic quantitative computed tomography: a predictor of pulmonary function in obstructive lung diseases. *Invest Radiol* 1994;29:564-569.
69. Kitahara Y, Takamoto M, Maruyama M, et al. Differential diagnosis of pulmonary emphysema using the CT index: LL%. *Nippon Kyobu Shikkan Gakkai Zasshi* 1989;27:689-695.
70. Newman KB, Lynch DA, Newman LS, et al. Quantitative computed tomography detects air trapping due to asthma. *Chest* 1994;106:105-109.
71. Park CS, Müller NL, Worthy SA, et al. Airway obstruction in asthmatic and healthy individuals: inspiratory and expiratory thin-section CT findings. *Radiology* 1997;203:361-367.
72. Lynch DA. Imaging of asthma and allergic bronchopulmonary mycosis. *Radiol Clin North Am* 1998;36:129-142.

73. Garg K, Lynch DA, Newell JD, et al. Proliferative and constrictive bronchiolitis: classification and radiologic features. *AJR Am J Roentgenol* 1994;162:803-808.
74. Padley SPG, Adler BD, Hansell DM, et al. Bronchiolitis obliterans: high-resolution CT findings and correlation with pulmonary function tests. *Clin Radiol* 1993;47:236-240.
75. Moore ADA, Godwin JD, Dietrich PA, et al. Swyer-James syndrome: CT findings in eight patients. *AJR Am J Roentgenol* 1992;158:1211-1215.
76. Marti-Bonmati L, Ruiz PF, Catala F, et al. CT findings in Swyer-James syndrome. *Radiology* 1989;172:477-480.
77. Sweatman MC, Millar AB, Strickland B, et al. Computed tomography in adult obliterative bronchiolitis. *Clin Radiol* 1990;41:116-119.
78. Aquino SL, Webb WR, Golden J. Bronchiolitis obliterans associated with rheumatoid arthritis: findings on HRCT and dynamic expiratory CT. *J Comput Assist Tomogr* 1994;18:555-558.
79. Leung AN, Fisher K, Valentine V, et al. Bronchiolitis obliterans after lung transplantation: detection using expiratory HRCT. *Chest* 1998;113:365-370.
80. Yang CF, Wu MT, Chiang AA, et al. Correlation of high-resolution CT and pulmonary function in bronchiolitis obliterans: a study based on 24 patients associated with consumption of sauropus androgynus. *AJR Am J Roentgenol* 1997;168:1045-1050.
81. Stern EJ, Webb WR, Golden JA, et al. Cystic lung disease associated with eosinophilic granuloma and tuberous sclerosis: air trapping at dynamic ultrafast high-resolution CT. *Radiology* 1992;182:325-329.

82. Hansell DM, Wells AU, Rubens MB, et al. Bronchiectasis: functional significance of areas of decreased attenuation at expiratory CT. *Radiology* 1994;193:369-374.
83. Hansell DM, Wells AU, Padley SP, et al. Hypersensitivity pneumonitis: correlation of individual CT patterns with functional abnormalities. *Radiology* 1996;199:123-128.
84. Small JH, Flower CD, Traill ZC, et al. Air-trapping in extrinsic allergic alveolitis on computed tomography. *Clin Radiol* 1996;51:684-688.
85. Hansell DM, Milne DG, Wilsher ML, et al. Pulmonary sarcoidosis: morphologic associations of airflow obstruction at thin-section CT. *Radiology* 1998;209:697-704.
86. Gleeson FV, Traill ZC, Hansell DM. Evidence of expiratory CT scans of small-airway obstruction in sarcoidosis. *AJR Am J Roentgenol* 1996;166:1052-1054.
87. Worthy SA, Park CS, Kim JS, et al. Bronchiolitis obliterans after lung transplantation: high resolution CT findings in 15 patients. *AJR Am J Roentgenol* 1997;169:673-677.
88. Kalender WA, Rienmuller R, Seissler W, et al. Measurement of pulmonary parenchymal attenuation: use of spirometric gating with quantitative CT. *Radiology* 1990;175:265-268.
89. Kalender WA, Fichte H, Bautz W, et al. Semiautomatic evaluation procedures for quantitative CT of the lung. *J Comput Assist Tomogr* 1991;15:248-255.
90. Lamers RJ, Thelissen GR, Kessels AG, et al. Chronic obstructive pulmonary diseases. evaluation with spirometrically controlled CT lung densitometry. *Radiology* 1994;193:109-113.
91. Robinson TE, Leung AN, Moss RB, et al. Standardized high-resolution CT of the lung using a spirometer-triggered

- electron beam CT scanner. *AJR Am J Roentgenol* 1999;172:1636-1638.
92. Long FR, Castile RG, Brody AS, et al. Lungs in infants and young children: improved thin-section CT with a noninvasive controlled-ventilation technique—initial experience. *Radiology* 1999;212:588-593.
93. Beinert T, Behr J, Mehnert F, et al. Spirometrically controlled quantitative CT for assessing diffuse parenchymal lung disease. *J Comput Assist Tomogr* 1995;19:924-931.
94. Kauczor HU, Heussel CP, Fischer B, et al. Assessment of lung volumes using helical CT at inspiration and expiration: comparison with pulmonary function tests. *AJR Am J Roentgenol* 1998;171:1091-1095.
95. Mergo PJ, Williams WF, Gonzalez-Rothi R, et al. Three-dimensional volumetric assessment of abnormally low attenuation of the lung from routine helical CT: inspiratory and expiratory quantification. *AJR Am J Roentgenol* 1998;170:1355-1360.
96. Lee ES, Gotway MB, Reddy GP, et al. Expiratory high-resolution CT: accuracy for the diagnosis of early bronchiolitis obliterans following lung transplantation. *Radiology* (in press).
97. Lee KW, Chung SY, Yang I, et al. Correlation of aging and smoking with air trapping at thin-section CT of the lung in asymptomatic subjects. *Radiology* 2000;214:831-836.
98. Stern EJ, Webb WR. Dynamic imaging of lung morphology with ultrafast high-resolution computed tomography. *J Thorac Imaging* 1993;8:273-282.
99. Stern EJ, Webb WR, Warnock ML, et al. Bronchopulmonary sequestration: dynamic, ultrafast, high-resolution CT evidence of air trapping. *AJR Am J Roentgenol* 1991;157:947-949.

100. Lynch DA, Brasch RC, Hardy KA, et al. Pediatric pulmonary disease: assessment with high-resolution ultrafast CT. *Radiology* 1990; 176:243-248.
101. Gotway MB, Lee ES, Reddy GP, et al. Low-dose, dynamic expiratory high-resolution CT using a spiral scanner. *J Thorac Imaging* (in press).
102. Grenier P, Maurice F, Musset D, et al. Bronchiectasis: assessment by thin-section CT. *Radiology* 1986;161:95-99.
103. Naidich DP, Funt S, Ettenger NA, et al. Hemoptysis: CT-bronchoscopic correlations in 58 cases. *Radiology* 1990;177:357-362.
104. Set PAK, Flower CDR, Smith IE, et al. Hemoptysis: comparative study of the role of CT and fiberoptic bronchoscopy. *Radiology* 1993;189:677-680.
105. Bergin CJ, Rios G, King MA, et al. Accuracy of high-resolution CT in identifying chronic pulmonary thromboembolic disease. *AJR Am J Roentgenol* 1996;166:1371-1377.
106. King MA, Ysrael M, Bergin CJ. Chronic thromboembolic pulmonary hypertension: CT findings. *AJR Am J Roentgenol* 1998;170:955-960.
107. Lee KN, Lee HJ, Shin WW, et al. Hypoxemia and liver cirrhosis (hepatopulmonary syndrome) in eight patients: comparison of the central and peripheral pulmonary vasculature. *Radiology* 1999;211:549-553.
108. Sherrick AD, Swensen SJ, Hartman TE. Mosaic pattern of lung attenuation on CT scans: frequency among patients with pulmonary artery hypertension of different causes. *AJR Am J Roentgenol* 1997;169:79-82.

109. Connolly B, Manson D, Eberhard A, et al. CT appearance of pulmonary vasculitis in children. *AJR Am J Roentgenol* 1996; 167:901-904.
110. Drucker EA, Rivitz SM, Shepard JA, et al. Acute pulmonary embolism: assessment of helical CT for diagnosis. *Radiology* 1998; 209:235-241.
111. Mayo JR, Remy-Jardin M, Müller NL, et al. Pulmonary embolism: prospective comparison of spiral CT with ventilation-perfusion scintigraphy. *Radiology* 1997; 205:447-452.
112. Remy-Jardin M, Remy J, Artaud D, et al. Spiral CT of pulmonary embolism: technical considerations and interpretive pitfalls. *J Thorac Imaging* 1997; 12:103-117.
113. Rubin GD, Goodman LR, Lipchik RJ, et al. Helical CT for the detection of acute pulmonary embolism: experts debate. *J Thorac Imaging* 1997; 12:81-102.
114. Webb WR, Stein MG, Finkbeiner WE, et al. Normal and diseased isolated lungs: high-resolution CT. *Radiology* 1988; 166:81-87.
115. Murata K, Itoh H, Todo G, et al. Centrilobular lesions of the lung: demonstration by high-resolution CT and pathologic correlation. *Radiology* 1986; 161:641-645.
116. Mayo JR, Jackson SA, Müller NL. High-resolution CT of the chest: radiation dose. *AJR Am J Roentgenol* 1993; 160:479-481.
117. Evans SH, Davis R, Cooke J, et al. A comparison of radiation doses to the breast in computed tomographic chest examinations for two scanning protocols. *Clin Radiol* 1989; 40:45-46.
118. Reuter FG, Conway BJ, McCrohan ML, et al. Average radiation exposure values for three diagnostic radiographic examinations. *Radiology* 1990; 177:341-345.

119. Müller NL. Clinical value of high-resolution CT in chronic diffuse lung disease. *AJR Am J Roentgenol* 1991;157:1163-1170.
120. Mayo JR, Müller NL, Henkelman RM. The double-fissure sign: a motion artifact on thin-section CT scans. *Radiology* 1987;165:580-581.
121. Tarver RD, Conces DJ, Godwin JD. Motion artifacts on CT simulate bronchiectasis. *AJR Am J Roentgenol* 1988;151:1117-1119.

Authors: Webb, W. Richard; Muller, Nestor L.; Naidich, David P.

Title: *High-Resolution CT of the Lung, 3rd Edition*

Copyright ©2001 Lippincott Williams & Wilkins

> Table of Contents > Chapter 2 - Normal Lung Anatomy

Chapter 2

Normal Lung Anatomy

The accurate interpretation of high-resolution computed tomography (HRCT) images requires a detailed understanding of normal lung anatomy and of the pathologic alterations in normal lung anatomy occurring in the presence of disease [1,2,3,4]. In this chapter, only those aspects of lung anatomy that are important in using and interpreting HRCT are reviewed.

Lung Interstitium

The lung is supported by a network of connective tissue fibers called the lung interstitium. Although the lung interstitium is not generally visible on HRCT in normal patients, interstitial thickening is often recognizable. For the purpose of interpretation of HRCT and identification of abnormal findings, the interstitium can be thought of as having several components (Fig. 2-1) [5].

The peribronchovascular interstitium is a system of fibers that invests bronchi and pulmonary arteries (Fig. 2-1). In the perihilar regions, the peribronchovascular interstitium forms a strong connective tissue sheath that surrounds large bronchi and arteries [6]. The more peripheral continuum of this interstitial fiber system, which is associated with small centrilobular bronchioles and arteries, may be termed the centrilobular interstitium (Fig. 2-1).

Taken together, the peribronchovascular interstitium and

centrilobular interstitium correspond to the “axial fiber system” described by Weibel, which extends peripherally from the pulmonary hila to the level of the alveolar ducts and sacs [5].

The subpleural interstitium is located beneath the visceral pleura; it envelops the lung in a fibrous sac from which connective tissue septa penetrate into the lung parenchyma (Fig. 2-1). These septa include the interlobular septa, which are described in detail below. The subpleural interstitium and interlobular septa are parts of the “peripheral fiber system” described by Weibel [5].

The intralobular interstitium is a network of thin fibers that forms a fine connective tissue mesh in the walls of alveoli and thus bridges the gap between the centrilobular interstitium in the center of lobules and the interlobular septa and subpleural interstitium in the lobular periphery (Fig. 2-1). Together, the intralobular interstitium, peribronchovascular interstitium, centrilobular interstitium, subpleural interstitium, and interlobular septa form a continuous fiber skeleton for the lung (Fig. 2-1). The intralobular interstitium corresponds to the “septal fibers” described by Weibel [5].

Large Bronchi and Arteries

Within the lung parenchyma, the bronchi and pulmonary artery branches are closely associated and branch in parallel. As indicated in the previous section, they are encased by the peribronchovascular interstitium, which extends from the pulmonary hila into the peripheral lung. Because some lung diseases produce thickening of the peribronchovascular interstitium in the central or perihilar lung, in relation to large bronchi and pulmonary vessels it is

important to be aware of the normal HRCT appearances of the perihilar bronchi and pulmonary vessels. When imaged at an angle to their longitudinal axis, central pulmonary arteries normally appear as rounded or elliptic opacities on HRCT, accompanied by uniformly thin-walled bronchi of similar shape (Fig. 2-2). When imaged along their axis, bronchi and vessels should appear roughly cylindrical or show slight tapering as they branch, depending on the length of the segment that is visible; tapering of a vessel or bronchus is most easily seen when a long segment is visible.

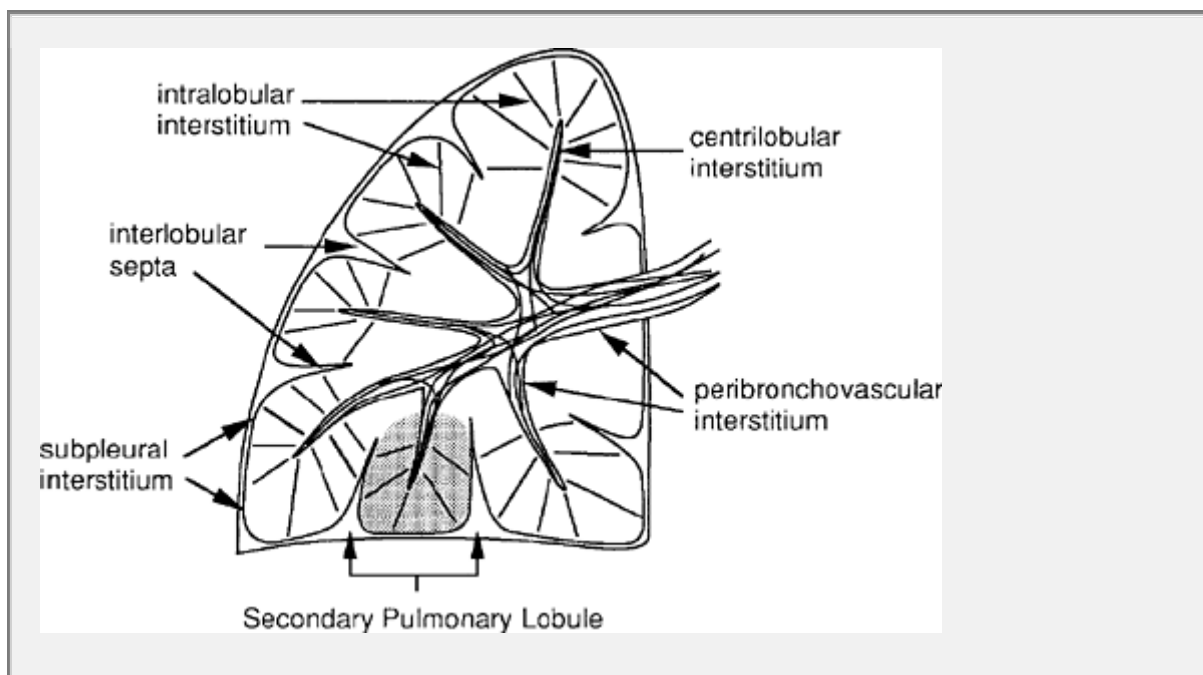


FIG. 2-1. Components of the lung interstitium. Taken together, the peribronchovascular interstitium and centrilobular interstitium correspond to the “axial fiber system” described by Weibel [5]. The subpleural interstitium and interlobular septa correspond to Weibel's “peripheral fiber system.” The intralobular interstitium is roughly equivalent to the “septal fibers” described by Weibel.

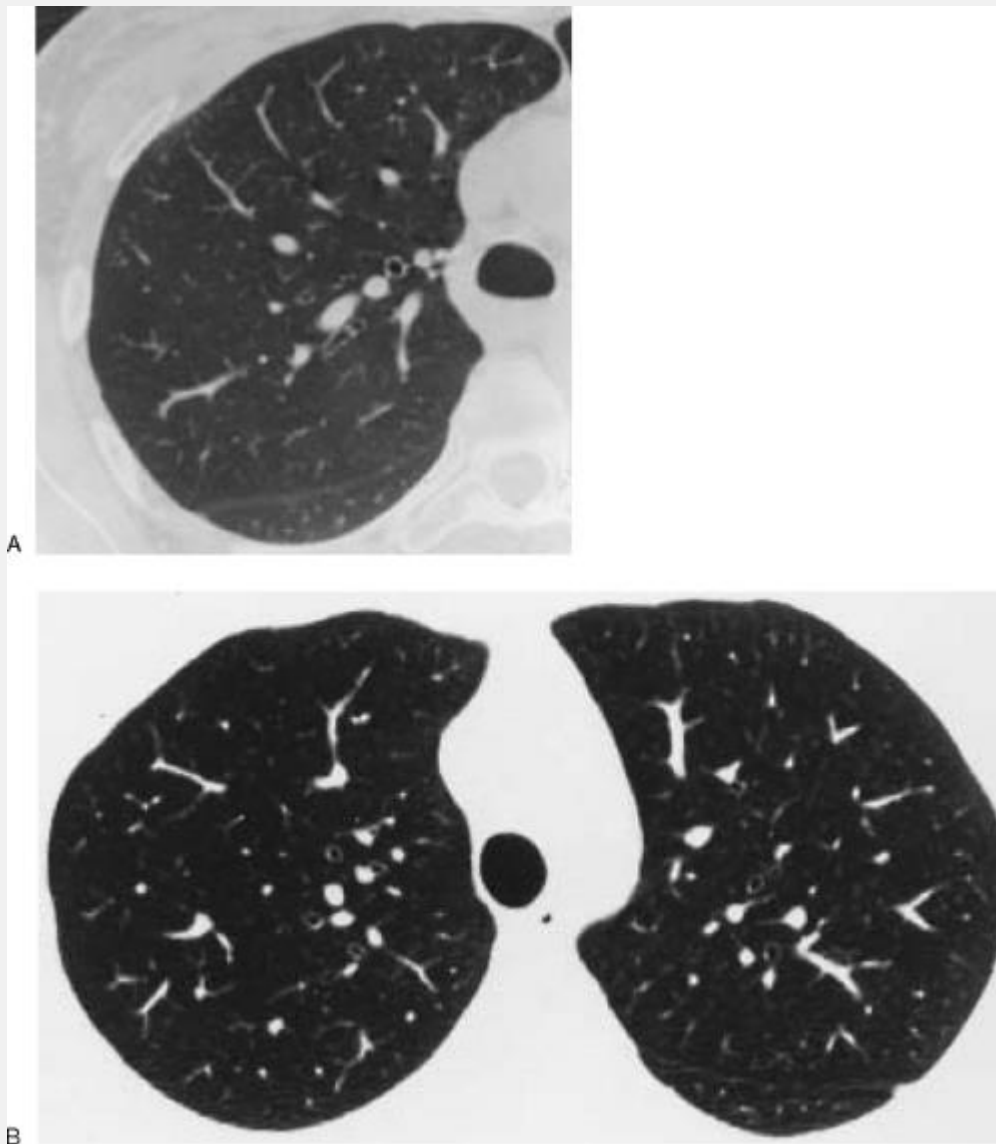


FIG. 2-2. Normal appearances of large bronchi and arteries photographed with window settings of $-600/2,000$ HU (A) and $-700/1,000$ HU (B). The diameters of vessels and their neighboring bronchi are approximately equal. The outer walls of bronchi and pulmonary vessels are smooth and sharply defined. Bronchi are usually invisible within the peripheral 2 cm of lung, despite the fact that vessels are well seen in this region.

TABLE 2-1. *Relation of airway diameter to wall thickness*

Airway	Diameter (mm)	Wall thickness (mm)
Lobular and segmental bronchi	5-8	1.5
Subsegmental bronchi/bronchiole	1.5-3.0	0.2-0.3
Lobular bronchiole	1	0.15
Terminal bronchiole	0.7	0.1
Acinar bronchiole	0.5	0.05

Modified from Weibel ER. High resolution computed tomography of the pulmonary parenchyma: anatomical background. Presented at: Fleischner Society Symposium on Chest Disease; 1990; Scottsdale, AZ.

P.50

P.51

The diameter of an artery and its neighboring bronchus should be approximately equal, although vessels may appear slightly larger than their accompanying bronchi, particularly in dependent lung regions. Although the presence of bronchi larger than their adjacent arteries is often assumed to indicate bronchial dilatation, or bronchiectasis, bronchi may appear larger than adjacent arteries in a significant number of normal subjects. In an HRCT study of normal subjects, Lynch et al. [7] compared the internal diameters of lobular, segmental, subsegmental, and smaller bronchi to those of adjacent artery branches. Nineteen percent of bronchi had an internal bronchial diameter longer than the artery diameter, and 59% of normal subjects showed at least one such bronchus. Furthermore, a bronchus may appear larger than the adjacent artery branches if the scan traverses an undivided bronchus near its branch point, and its accompanying artery has already branched. In this situation, two artery branches may be seen to lie adjacent to the "dilated" bronchus.

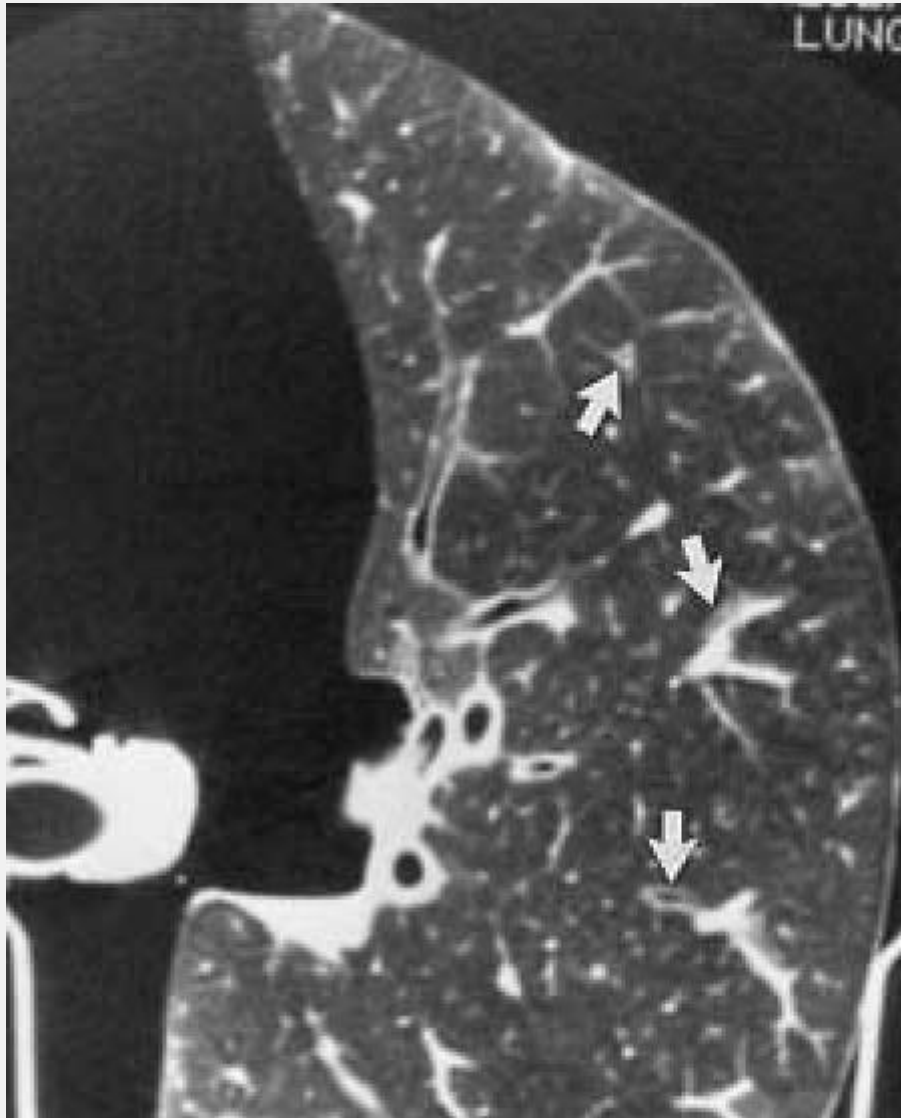


FIG. 2-3. Normal appearances of large bronchi and arteries. In an isolated lung, the smallest bronchi visible (arrows) measures 2 to 3 mm in diameter. Bronchi and bronchioles are not visible within the peripheral 1 cm of lung, although the artery branches that accompany these bronchi are **sharply seen.** (Note: The "isolated" lungs illustrated in this volume are fresh lungs obtained at autopsy and scanned while inflated with air at a pressure of approximately 30 cm of water [10].)

The outer walls of visible pulmonary artery branches form a smooth and sharply defined interface with the surrounding lung, whether they are seen in cross section or along their length. The walls of large bronchi, outlined by lung on one side and air in the bronchial lumen on the other, should appear smooth and of uniform thickness. Thickening of the peribronchial and perivascular interstitiums can result in irregularity of the interface between arteries and bronchi and the adjacent lung [4,6,8].

Assessment of bronchial wall thickness on HRCT is quite subjective and is dependent on the window settings used [7]. Also, because the apparent thickness of the bronchial wall represents not only the wall itself, but the surrounding peribronchovascular interstitium as well, peribronchovascular interstitial thickening can result in apparent bronchial wall thickening (so-called peribronchial cuffing) on HRCT.

The wall thickness of conducting bronchi and bronchioles is approximately proportional to their diameter, at least for bronchi distal to the segmental level. In general, the thickness of the wall of a bronchus or bronchiole less than 5 mm in diameter should measure from one-sixth to one-tenth of its diameter (Table 2-1) [9]; however, precise measurement of the wall thickness of small bronchi or bronchioles is difficult, as wall thickness approximates pixel size.

Because bronchi taper and become thinner-walled as they branch, they become more difficult to see as they become more peripheral. Bronchi less than 2 mm in diameter are not normally visible on HRCT, and bronchioles within 2 cm of the pleural surface tend to be inconspicuous (Figs. 2-2 and

2-3) [10,11]. It is rare for normal bronchioles to be visible within 1 cm of the pleural surface [12,13].

Secondary Pulmonary Lobule

The secondary pulmonary lobule as defined by Miller refers to the smallest unit of lung structure marginated by connective tissue septa [9,14]. Secondary lobules are easily visible on the surface of the lung because of these septa (Fig. 2-4) [9,15]. The terms secondary pulmonary lobule, secondary lobule, and pulmonary lobule are often used interchangeably, and are used as synonyms in this book. The term primary pulmonary lobule has also been used by Miller to describe a much smaller lung unit associated with a single alveolar duct [16,17], but this designation is not in common use.

Secondary pulmonary lobules are irregularly polyhedral in shape and somewhat variable in size, measuring approximately

P.52

1 to 2.5 cm in diameter in most locations (Fig. 2-5) [5,9,15,18,19]. In one study, the average diameter of pulmonary lobules measured in several adults ranged from 11 to 17 mm [19]. Each secondary lobule is supplied by a small bronchiole and pulmonary artery, and is variably marginated, in different lung regions, by connective tissue interlobular septa containing pulmonary vein and lymphatic branches [16].

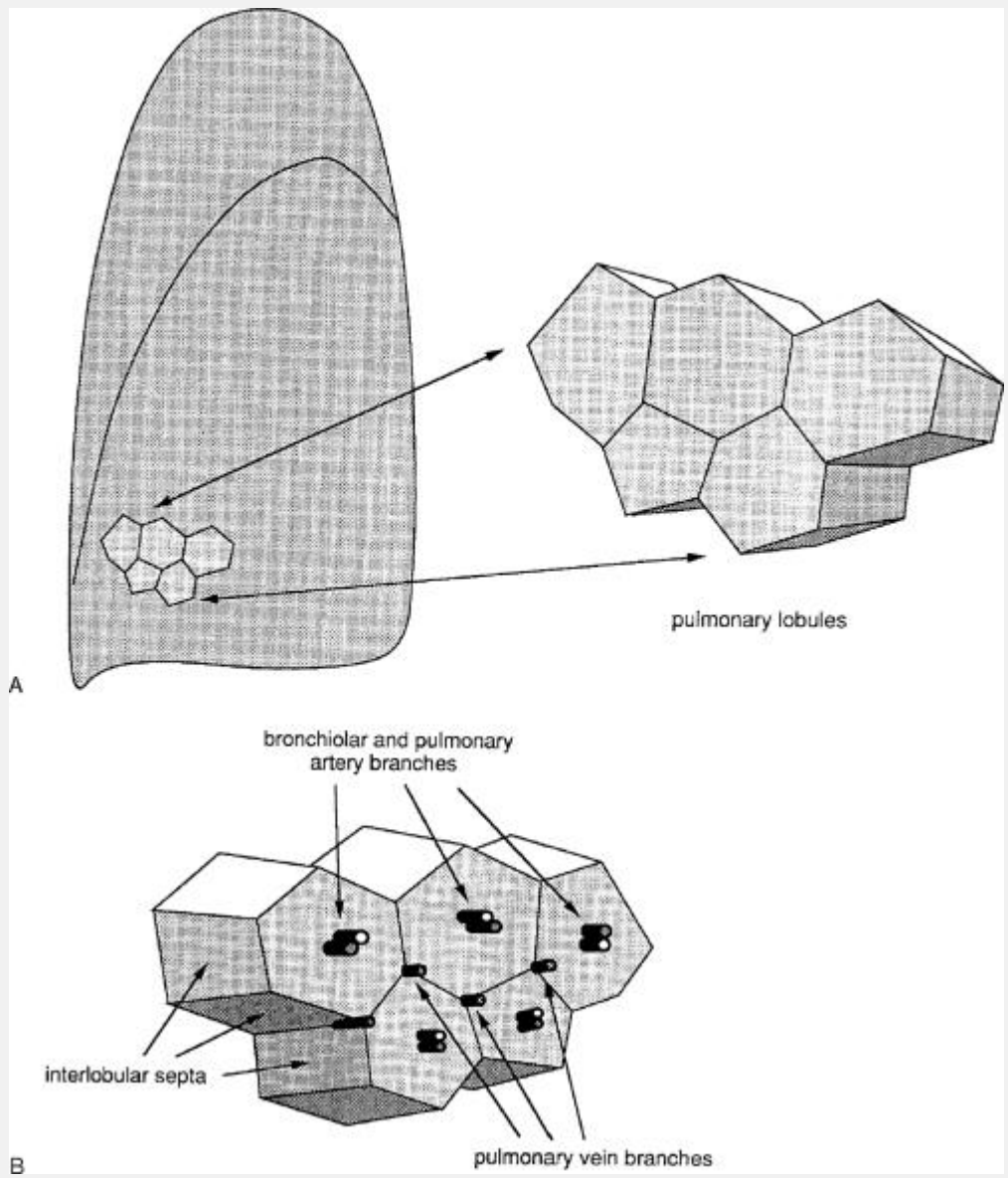


FIG. 2-4. Pulmonary lobular anatomy. A: Pulmonary lobules that are irregularly polyhedral or conical in shape are often visible on the surface of the lung, as shown in this diagram of five lobules visible on the posterior surface of the left lung. B: Lobules are supplied by small bronchiolar and pulmonary artery branches, which are central in location, and are variably margined by connective tissue interlobular septa that contain pulmonary vein and lymphatic branches.

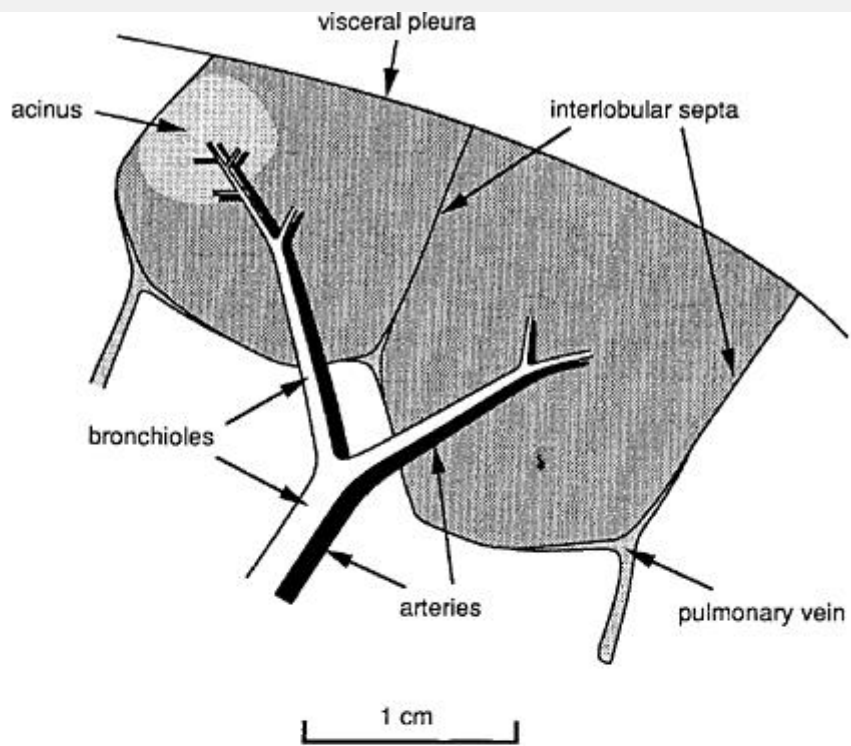
Secondary pulmonary lobules are made up of a limited number of pulmonary acini, usually a dozen or fewer, although the reported number varies considerably in different studies (Fig. 2-5A) [20,21]; in a study by Nishimura and Itoh [22], the number of acini counted in lobules of varying sizes ranged from three to 24. A pulmonary acinus is defined as the portion of the lung parenchyma distal to a terminal bronchiole and supplied by a first-order respiratory bronchiole or bronchioles [23]. Because respiratory bronchioles are the largest airways that have alveoli in their walls, an acinus is the largest lung unit in which all airways participate in gas exchange. Acini are usually described as ranging from 6 to 10 mm in diameter [19,24].

As indicated at the beginning of this section, Miller has defined the secondary lobule as the smallest lung unit marginated by connective tissue septa. Reid has suggested an alternate definition of the secondary pulmonary lobule, based on the branching pattern of peripheral bronchioles, rather than the presence and location of connective tissue septa (Fig. 2-6) [16,21,23]. On bronchograms, small bronchioles can be seen to arise at intervals of 5 to 10 mm from larger airways

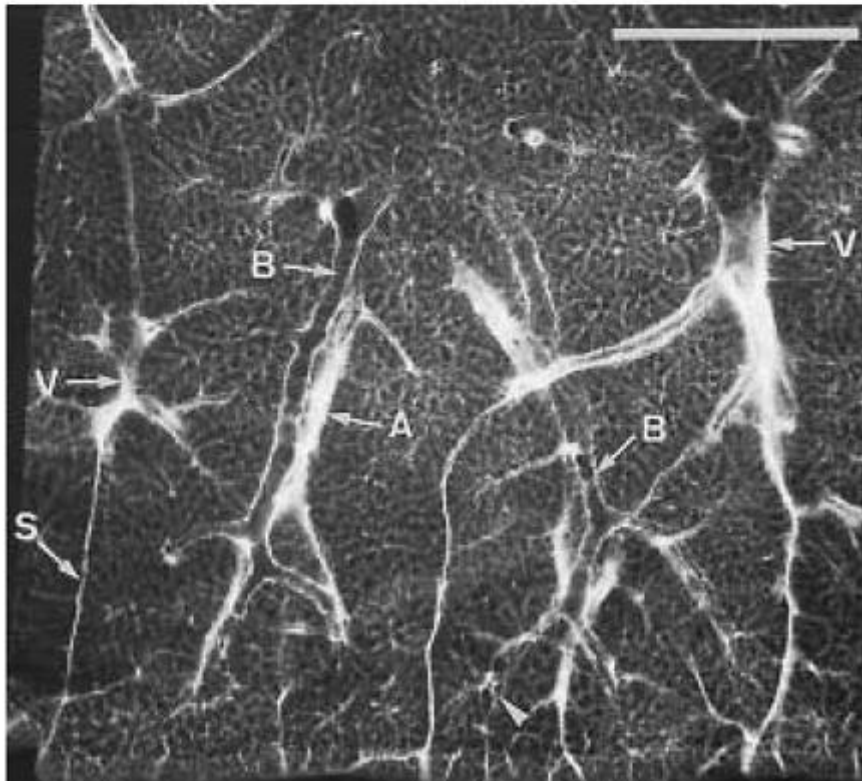
P.53

(the so-called centimeter pattern of branching); these small bronchioles then show branching at approximately 2-mm **intervals (the "millimeter pattern")** [23]. Airways showing the millimeter pattern of branching are considered by Reid to be intralobular, with each branch corresponding to a terminal bronchiole [21]. Lobules are considered to be the **lung units supplied by 3 to 5 "millimeter pattern"**

bronchioles. Although Reid's criteria delineate lung units of approximately equal size, about 1 cm in diameter and containing 3 to 5 acini, it should be noted that this definition does not necessarily describe lung units equivalent to secondary lobules as defined by Miller and marginated by interlobular septa (Fig. 2-6) [21,22], although a small Miller's lobule can be the same as a Reid's lobule. Miller's definition is most applicable to the interpretation of HRCT and is widely accepted by pathologists, because interlobular septa are visible on histologic sections [22]. In this book, we use the term secondary pulmonary lobule to refer to a lobule as defined by Miller.



A



B

FIG. 2-5. A: Anatomy of the secondary pulmonary lobule, as defined by Miller. Two adjacent lobules are shown in this

diagram. B: Radiographic anatomy of the secondary pulmonary lobule. Radiograph of a 1-mm lung slice taken from the lower lobe. Two well-defined secondary pulmonary lobules are visible. Lobules are margined by thin interlobular septa (S) containing pulmonary vein (V) branches. Bronchioles (B) and pulmonary arteries (A) are centrilobular. Bar = 1 cm. (Reprinted from Itoh H, Murata K, et al. Diffuse lung disease: pathologic basis for the high-resolution computed tomography findings. J Thorac Imaging 1993;8:176, with permission.)

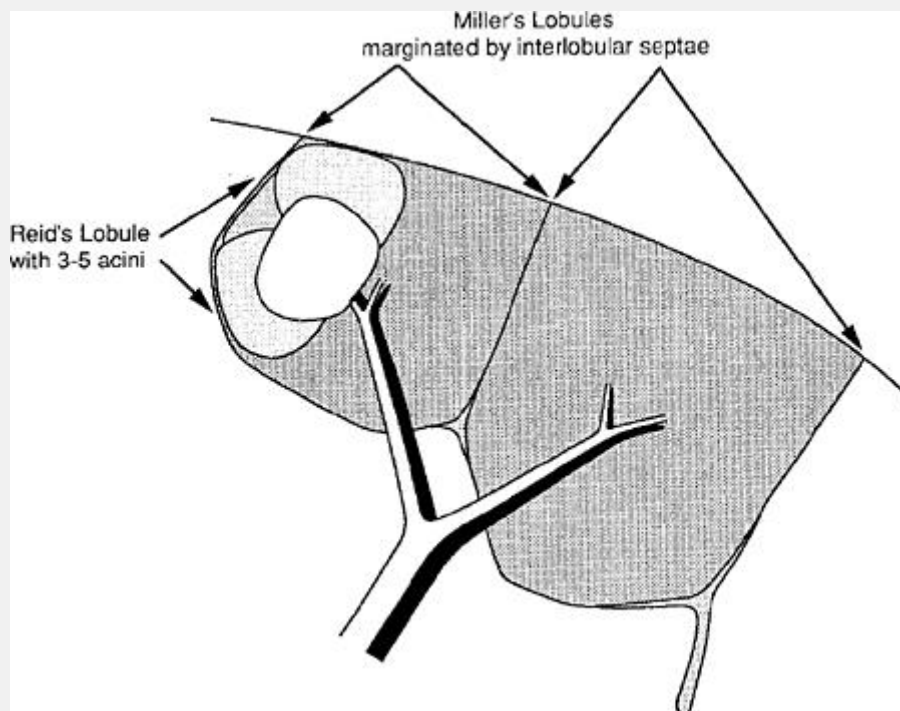


FIG. 2-6. Relative size and relationships of "Miller's lobule" and "Reid's lobule."

Anatomy of the Secondary Lobule and Its Components

An understanding of secondary lobular anatomy and the appearances of lobular structures is key to the interpretation of HRCT. HRCT can show many features of the secondary pulmonary lobule in normal and abnormal lungs, and many lung diseases, particularly interstitial diseases, produce characteristic changes in lobular structures [3,4,8,10,11,25,26]. Heitzman has been instrumental in emphasizing the importance of the secondary pulmonary lobule in the radiologic diagnosis of lung disease [15,16,27].

As discussed in Chapter 1, the visibility of normal lobular structures on HRCT is related to their size and orientation relative to the plane of scan, although size is most important (Fig. 2-7). Generally, the smallest structures visible on HRCT range from 0.3 to 0.5 mm in thickness; thinner structures, measuring 0.1 to 0.2 mm, are occasionally seen.

For the purposes of the interpretation of HRCT, the secondary lobule is most appropriately conceptualized as having three principal parts or components:

- Interlobular septa and contiguous subpleural interstitium
- Centrilobular structures
- Lobular parenchyma and acini

Interlobular Septa

Anatomically, secondary lobules are marginated by connective tissue interlobular septa, which extend inward

from the pleural surface (Figs. 2-4 and 2-5). These septa are part of the peripheral interstitial fiber system described by Weibel (Fig. 2-1) [5], which extends over the surface of the lung beneath the visceral pleura. Pulmonary veins and lymphatics lie within the connective tissue interlobular septa that marginate the lobule.

It should be emphasized that not all interlobular septa are equally well defined. The interlobular septa are thickest and most numerous in the apical, anterior, and lateral aspects of the upper lobes, the anterior and lateral aspects of the middle lobe and lingula, the anterior and diaphragmatic surfaces of the lower lobes, and along the mediastinal pleural surfaces [28]; thus, secondary lobules are best defined in these regions. Septa measure approximately 100 μm (0.1 mm) in thickness in a subpleural location [3,5,10,11]. Within the central lung, interlobular septa are thinner and less well defined than peripherally, and lobules are more difficult to identify in this location.

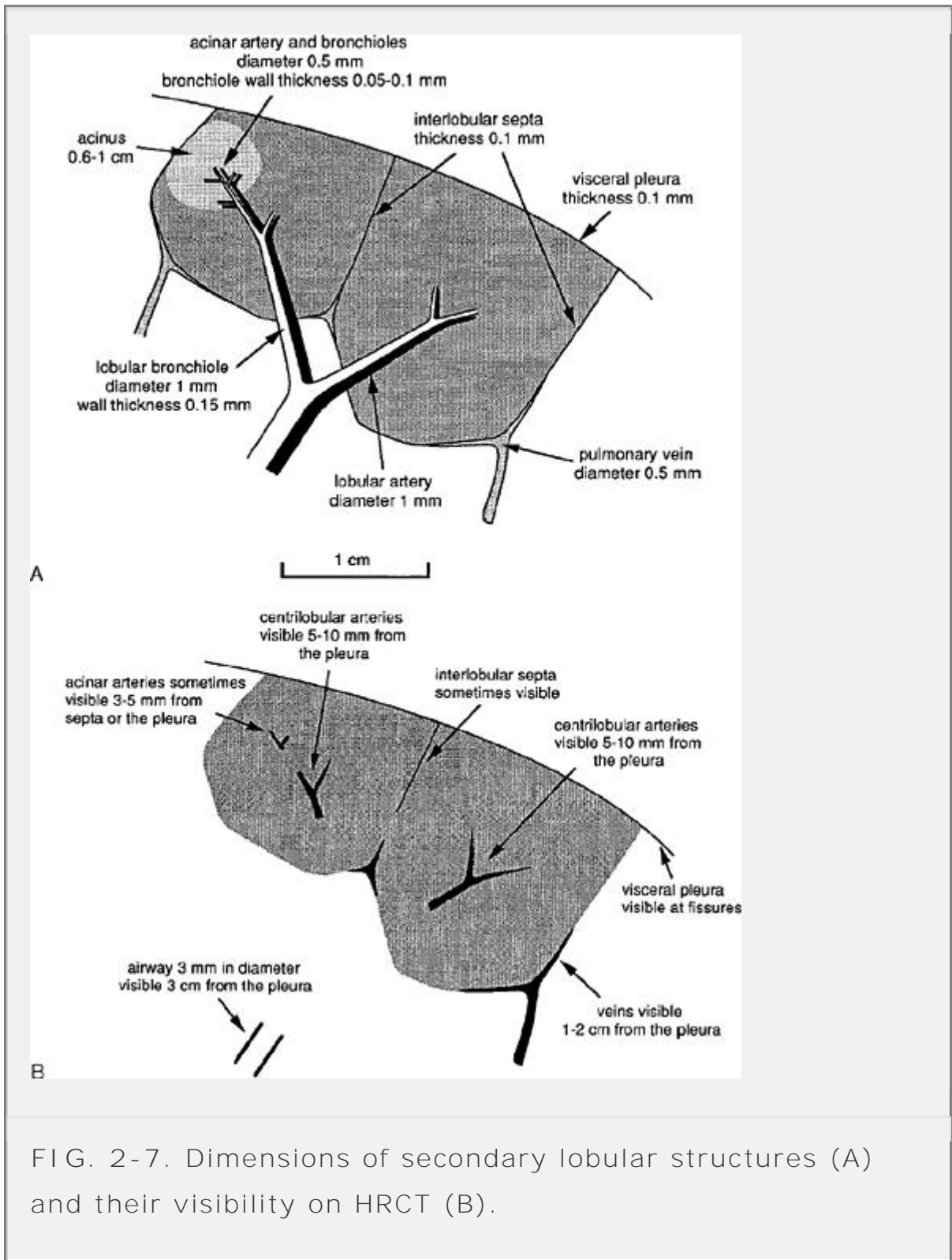
Peripherally, interlobular septa measuring 100 μm or 0.1 mm in thickness are at the lower limit of HRCT resolution [11], but nonetheless they are often visible on HRCT scans performed in vitro [10]. On in vitro HRCT, interlobular septa are often visible as very thin, straight lines of uniform thickness that are usually 1 to 2.5 cm in length and perpendicular to the pleural surface (Figs. 2-7 and 2-8). Several septa in continuity can be seen as a linear opacity measuring up to 4 cm in length (Fig. 2-9) [10].

On clinical scans in normal patients, interlobular septa are less commonly seen and are seen less well than they are in studies of isolated lungs. A few septa are often visible in the lung periphery in normal subjects, but they tend to be inconspicuous (Fig. 2-10); normal septa are most often seen

anteriorly and along the mediastinal pleural surfaces [4,29]. When visible, they are usually seen extending to the pleural surface. In the central lung, septa are thinner than they are peripherally and are infrequently seen in normal subjects (Fig. 2-9); often, interlobular septa that are clearly defined in this region are abnormally thickened. Occasionally, when interlobular septa are not clearly

P.55

visible, their locations can be inferred by locating septal pulmonary vein branches, approximately 0.5 mm in diameter. Veins can sometimes be seen as linear (Fig. 2-10B), arcuate, or branching structures (Fig. 2-10C-E), or as a row or chain of dots surrounding centrilobular arteries and approximately 5 to 10 mm from them. Pulmonary veins may also be identified by their pattern of branching; it is common for small veins to arise at nearly right angles to a much larger main branch.



Centrilobular Region and Centrilobular Structures

The central portion of the lobule, referred to as the centrilobular region or lobular core [16], contains the

pulmonary artery and bronchiolar branches that supply the lobule, as well as some supporting connective tissue (the centrilobular interstitium described previously)

[3,5,9,10,11]. It is difficult to precisely define lobules in relation to the bronchial or arterial trees; lobules do not arise at a specific branching generation or from a specific type of bronchiole or artery [9].

Branching of the lobular bronchiole and artery is irregularly dichotomous [22]. When they divide, they generally divide into two branches. Most often, they divide into two branches of different sizes, (one branch being nearly the same size as the one it arose from, and the other being smaller) (Fig. 2-5B). Thus, on bronchograms, arteriograms, or HRCT, there often appears to be a single dominant bronchiole or artery in the center of the lobule, which gives off smaller branches at intervals along its length.

The HRCT appearances and visibility of centrilobular structures are determined primarily by their size (Fig. 2-7).

Secondary

P.56

lobules are supplied by arteries and bronchioles measuring approximately 1 mm in diameter, whereas intralobular terminal bronchioles and arteries measure approximately 0.7 mm in diameter, and acinar bronchioles and arteries range from 0.3 to 0.5 mm in diameter. Arteries of this size can be easily resolved using the HRCT technique [10,11].

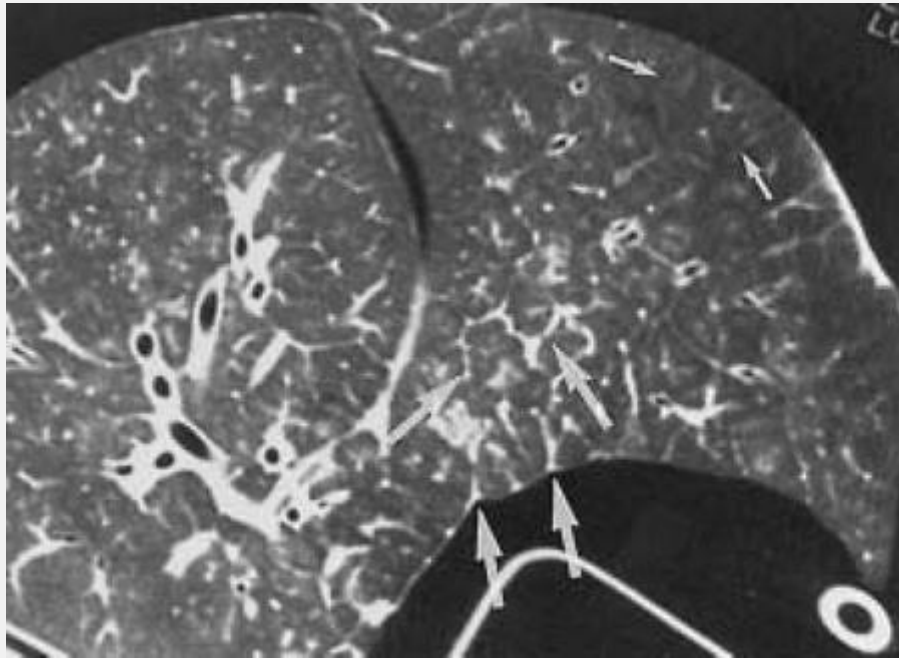


FIG. 2-8. Interlobular septa in an isolated lung. Some thin, normal interlobular septa (small arrows) are faintly visible in the peripheral lung. Interlobular septa along the mediastinal pleural surface (large arrows) are slightly thickened by edema fluid and are more easily seen. Note that a very thin line is visible at the pleural surfaces and in the lung fissure, similar in appearance and thickness to the normal interlobular septa. This line represents the subpleural interstitial compartment and visceral pleura. (From Webb WR, Stein MG, et al. Normal and diseased isolated lungs: high-resolution CT. *Radiology* 1988;166:81, with permission.)

On clinical scans, a linear, branching, or dotlike opacity frequently seen within the center of a lobule, or within a centimeter of the pleural surface, represents the intralobular artery branch or its divisions (Figs. 2-10C-E, 2-11, and 2-12) [3,10,11]. The smallest arteries resolved extend to within 3 to 5 mm of the pleural surface or lobular

margin and are as small as 0.2 mm in diameter [3,10,11]. The visible centrilobular arteries are not seen to extend to the pleural surface in the absence of atelectasis (Fig. 2-13). Regarding the visibility of bronchioles in the lungs of normal patients, it is necessary to consider bronchiolar wall thickness rather than bronchiolar diameter. For a 1-mm bronchiole supplying a secondary lobule, the thickness of its wall measures approximately 0.15 mm; this is at the lower limit of HRCT resolution. The wall of a terminal bronchiole measures only 0.1 mm in thickness, and that of an acinar bronchiole only 0.05 mm, both of which are below the resolution of HRCT technique for a tubular structure (Fig. 2-7). In one in vitro study, only bronchioles having a diameter of 2 mm or more or having a wall thickness of more than 100

P.57

μm (0.1 mm) were visible using HRCT [11]; and resolution is certainly less than this on clinical scans. It is important to remember that on clinical HRCT, intralobular bronchioles are not normally visible, and bronchi or bronchioles are rarely seen within 1 cm of the pleural surface (Figs. 2-11 and 2-12) [12,13].

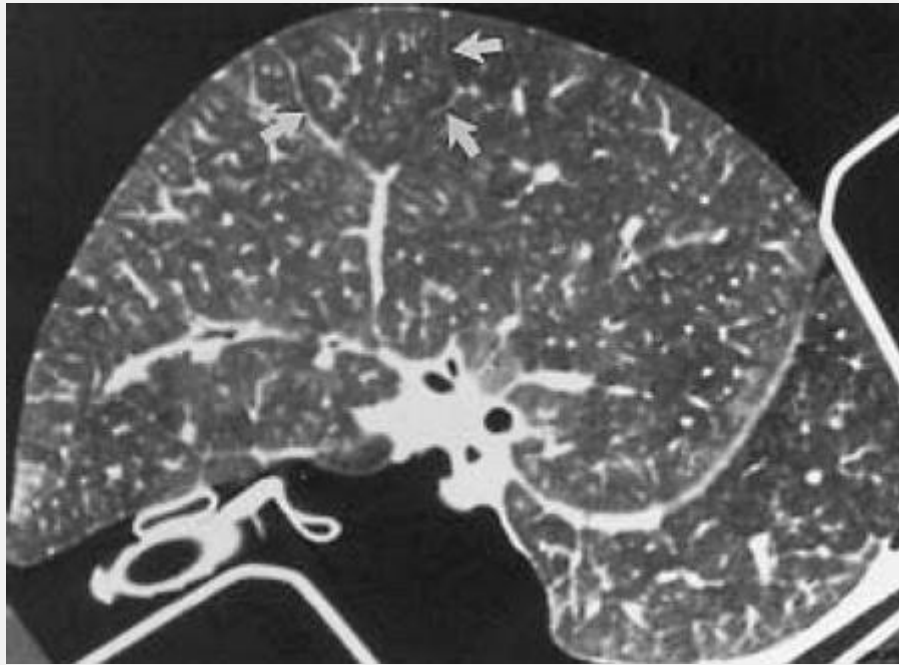


FIG. 2-9. Interlobular septa in continuity in an isolated lung. On HRCT, long interlobular septa (arrows) can be seen marginating several secondary lobules. The septa in this lung are slightly thickened by fluid. Septa are well seen peripherally, but note that the septa and, therefore, secondary lobules are less well defined in the central lung. (From Webb WR, Stein MG, et al. Normal and diseased isolated lungs: high-resolution CT. *Radiology* 1988;166:81, with permission.)

Lobular (Lung) Parenchyma

The substance of the secondary lobule, surrounding the lobular core and contained within the interlobular septa, consists of functioning lung parenchyma—namely, alveoli and the associated pulmonary capillary bed—supplied by small airways and branches of the pulmonary arteries and veins. This parenchyma is supported by a connective tissue stroma, a fine network of very thin fibers within the alveolar

septa called the intralobular interstitium (Fig. 2-1) [5,9], which is normally invisible. On HRCT, the lobular parenchyma should be of greater opacity than air (Fig. 2-14), but this difference may vary with window settings (see Chapter 1). Some small intralobular vascular branches are often visible.

It should be emphasized that all three interstitial fiber systems described by Weibel (axial, peripheral, and septal) are represented at the level of the pulmonary lobule (Fig. 2-1), and abnormalities in any can produce recognizable lobular abnormalities on HRCT [10]. Axial (centrilobular) fibers surround the artery and bronchiole in the lobular core, peripheral fibers making up the interlobular septa marginate the lobule, and septal fibers (the intralobular interstitium) extend throughout the substance of the lobule in relation to the alveolar walls.

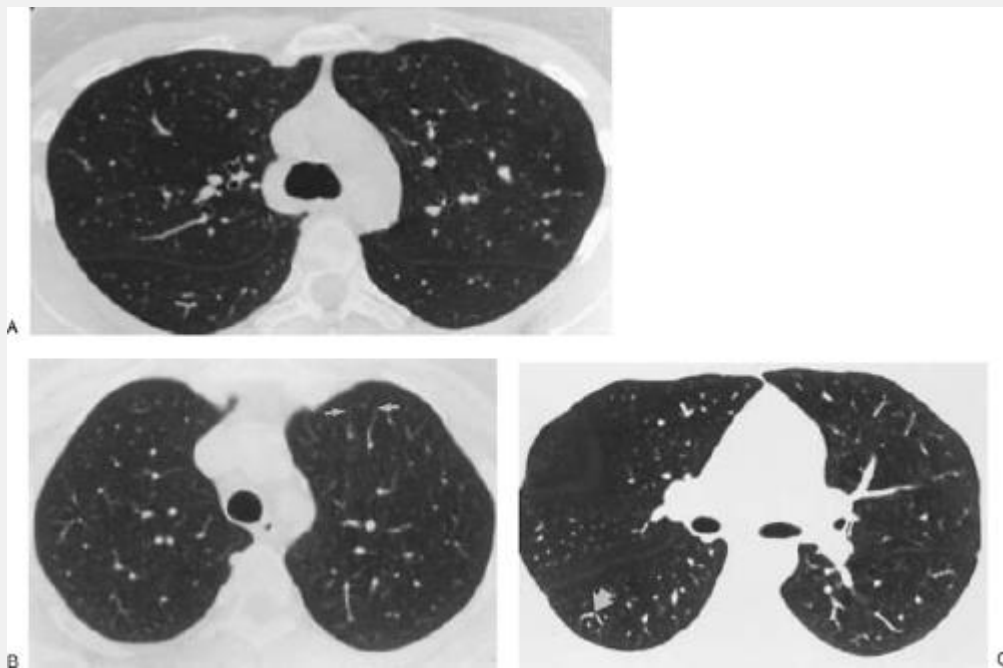


FIG. 2-10. Normal HRCT in different subjects. A: HRCT in a normal subject; window mean/width: 600/2,000 HU.

Interlobular septa are inconspicuous, and those few that are visible are very thin. The major fissures appear as thin, sharply defined lines. B: Two pulmonary vein branches (arrows) marginate a pulmonary lobule in the anterior lung, but the interlobular septa surrounding this lobule are very thin and difficult to see. The centrilobular artery lies equidistant between the veins. C: HRCT in a normal subject (-700/1,000 HU) shows few interlobular septa. A venous arcade (arrow) is visible in the lower lobe, with the centrilobular artery visible as a dot centered in the arcade. D: HRCT through the upper lobes in a normal subject (-700/1,000 HU). Normal interlobular septa (black arrows) are visible. The centrilobular artery (white arrow) is centered between them. E: In the same patient as D, a scan through the lower lobes shows normal pulmonary vein branches (black arrows) marginating pulmonary lobules. The centrilobular artery branches (white arrow) are visible as a rounded dot between the veins.

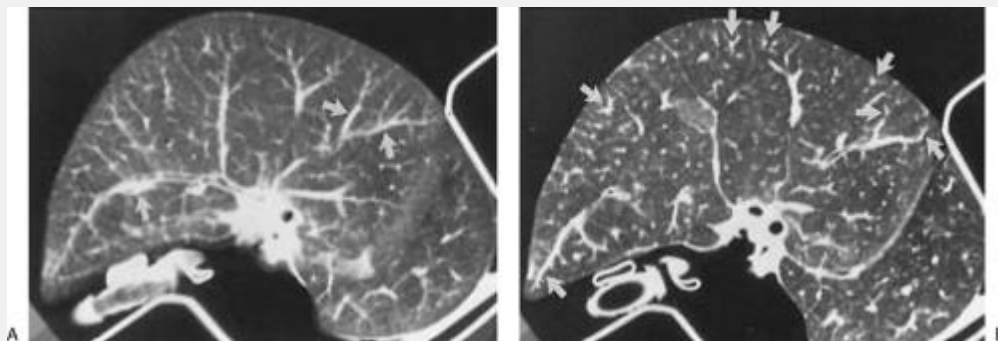


FIG. 2-11. Centrilobular anatomy in an isolated lung. A: On

a CT scan obtained with 1-cm collimation, pulmonary artery branches (arrows) with their accompanying bronchi can be identified. B: On an HRCT scan at the same level, interlobular septa can be seen marginating one or more lobules (Fig. 2-9). Pulmonary artery branches (arrows) can be seen extending into the centers of pulmonary lobules, but intralobular bronchioles are not visible. The last visible branching point of pulmonary arteries is approximately 1 cm from the pleural surface. Bronchi are invisible within 2 or 3 cm of the pleural surface. (From Webb WR, Stein MG, et al. Normal and diseased isolated lungs: high-resolution CT. Radiology 1988;166:81, with permission.)

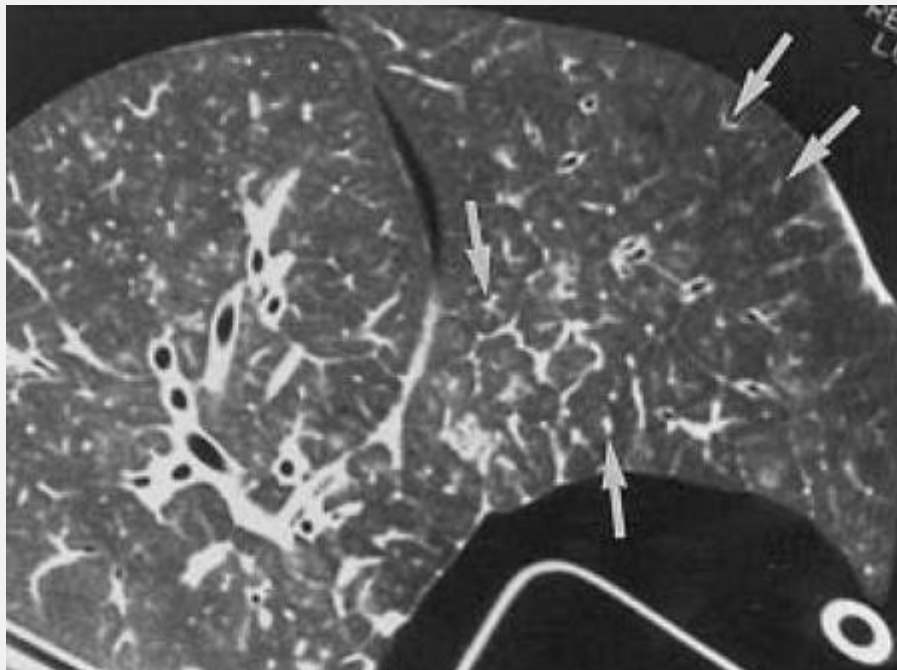


FIG. 2-12. Centrilobular anatomy in an isolated lung. Lobular core anatomy in an isolated lung. Branching pulmonary arteries (arrows) are visible within 1 cm of the pleural surface, but intralobular bronchioles are invisible. In

the central lung, centrilobular arteries appear dotlike or as a branching structure. (From Webb WR, Stein MG, et al. Normal and diseased isolated lungs: high-resolution CT. Radiology 1988;166:81, with permission.)

P.58

P.59

Pulmonary Acinus

Pulmonary acini are not normally visible on HRCT [22]. As with lobules, acini vary in size. They are usually described as ranging from 6 to 10 mm in diameter and have been measured as averaging 7 to 8 mm in diameter in adults [19,24]. As indicated above, secondary pulmonary lobules defined by the presence of connective tissue interlobular septa usually consist of a dozen or fewer pulmonary acini (Fig. 2-5A) [9,19,20,24].

First-order respiratory bronchioles and the acinar artery branch measure approximately 0.5 mm in diameter (Fig. 2-7A); thus, intralobular acinar arteries are large enough to be seen on HRCT in some normal subjects [5,9,19,24].

Murata [11] has shown that pulmonary artery branches as small as 0.2 mm, associated with a respiratory bronchiole and thus acinar in nature, are visible on HRCT and extend to within 3 to 5 mm of the lobular margins or pleural surface (Fig. 2-7).

Lobular Anatomy and the Concept of Cortical and Medullary Lung

At least partially based on differences in lobular anatomy, it has been suggested that the lung can be divided into a peripheral cortex and a central medulla [16,30]. Although these terms are not in general use, the concept of cortical and medullary lung regions is useful in highlighting differences in lung anatomy and the varying appearances of secondary pulmonary lobules in the peripheral and central lung regions [31]. It also serves to emphasize some anatomic (and perhaps physiologic) differences between the peripheral and central lung that are useful in predicting the HRCT distribution of some lung diseases [32].

Peripheral or Cortical Lung

Cortical lung can be conceived of as consisting of two or three rows or tiers of well-organized and well-defined secondary pulmonary lobules, which together form a layer 3 to 4 cm in thickness at the lung periphery and along the lung surfaces adjacent to fissures (Fig. 2-15) [16,30]. The pulmonary lobules in the lung cortex are relatively large in size and are marginated by interlobular septa that are thicker and better defined than in other parts of the lung; thus, cortical lobules tend to be better defined than those in the central or medullary lung. Bronchi and pulmonary vessels in the lung cortex are relatively small; although cortical arteries and veins are visible on HRCT, bronchi and bronchioles are uncommonly visible. This contrasts with the anatomy of medullary lung, in which large vessels and bronchi are visible.

Lobules in the lung cortex tend to be relatively uniform in appearance and can be conceived of as being similar to the stones in a Roman arch: all of similar size and shape (Fig. 2-15) [30]. They can appear cuboid or be shaped like a truncated cone or pyramid [16]. However, it should be remembered that the size, shape, and appearance of pulmonary lobules as seen on HRCT are significantly affected by the orientation of the scan plane relative to the central and longitudinal axes of the lobules. A single scan typically traverses different parts of adjacent lobules (Figs. 2-8 and 2-9), resulting in widely varying appearances of the lobules, despite the fact that they are all of similar size and shape.

Central or Medullary Lung

Pulmonary lobules in the central or medullary lung are smaller and more irregular in shape than in the cortical lung and are marginated by interlobular septa that are thinner and less well defined. When visible, medullary lobules may appear hexagonal or polygonal in shape, but well-defined lobules are uncommonly seen in normals. In contrast with the peripheral lung, perihilar vessels and bronchi in the lung medulla are large and easily seen on HRCT.

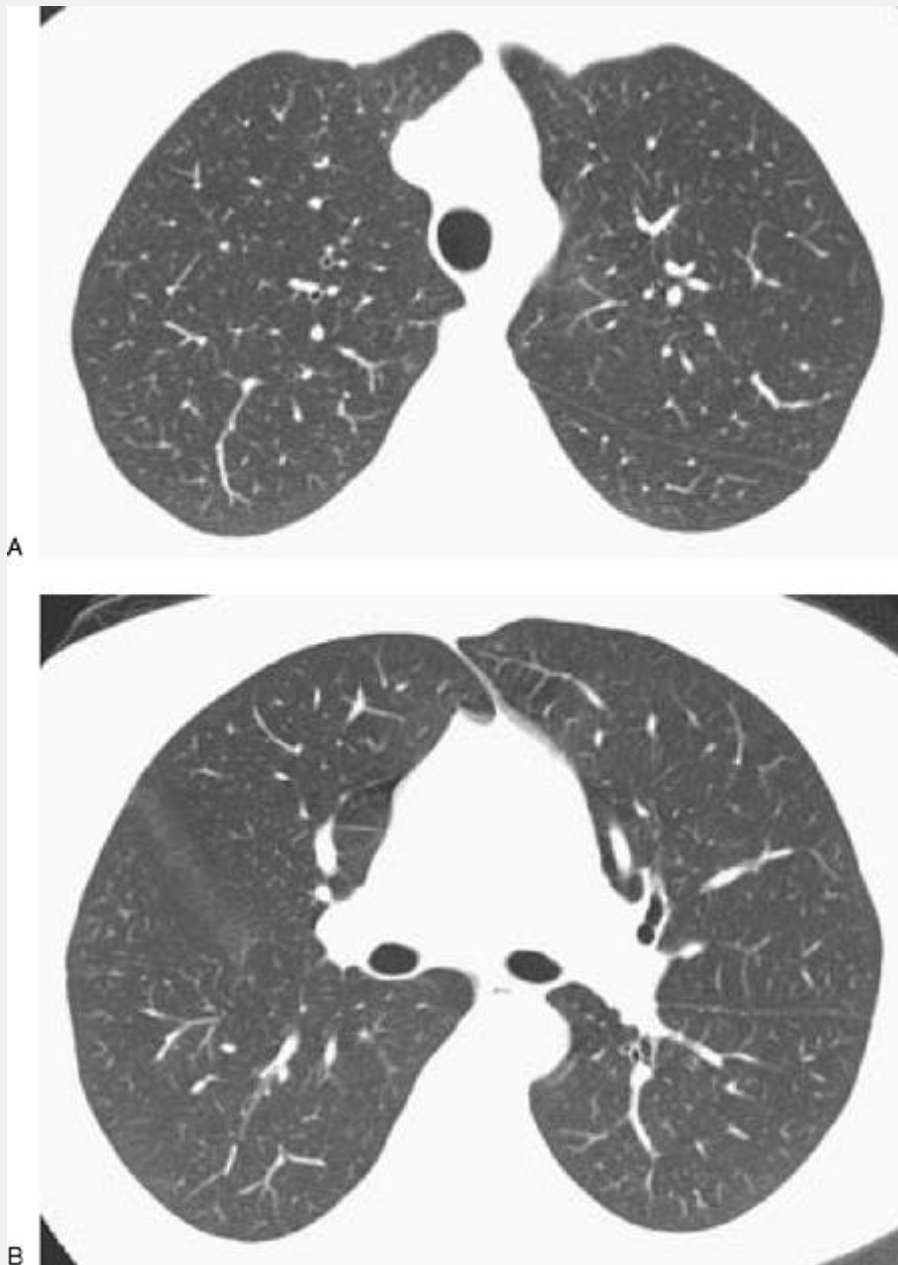


FIG. 2-13. Normal lobular anatomy. HRCT (-700/1,000 HU) at two levels (A, B) in a normal subject shows artery branches extending to within 1 cm of the pleural surface. The arteries do not reach the pleura.

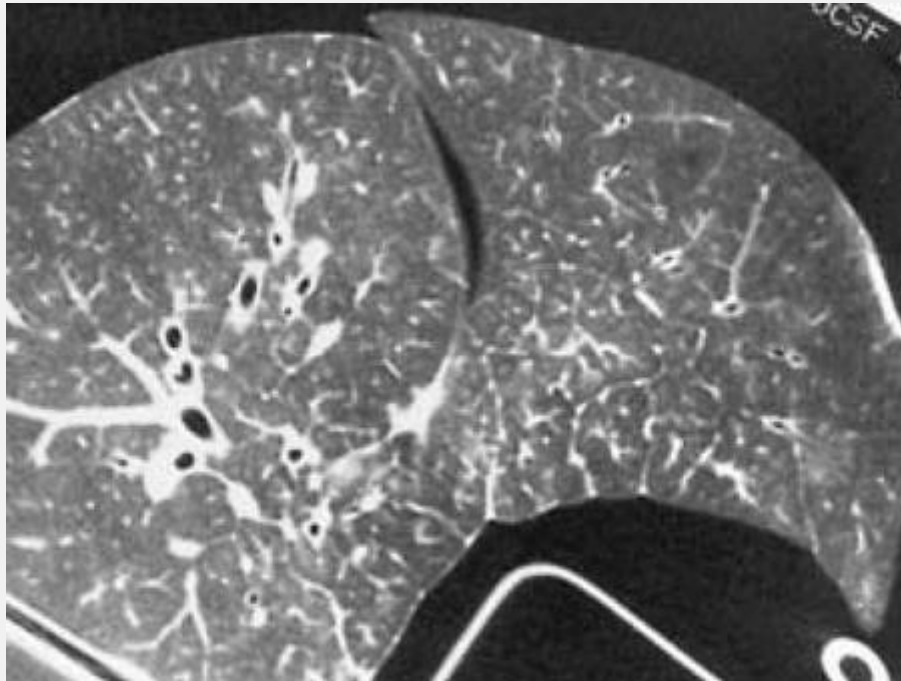


FIG. 2-14. Normal appearance of the lobular parenchyma. The lung parenchyma should appear to be homogeneously denser than air in the bronchi or, as in this isolated lung, denser than room air surrounding the specimen. The relative opacities of lung and air depend on the window settings.

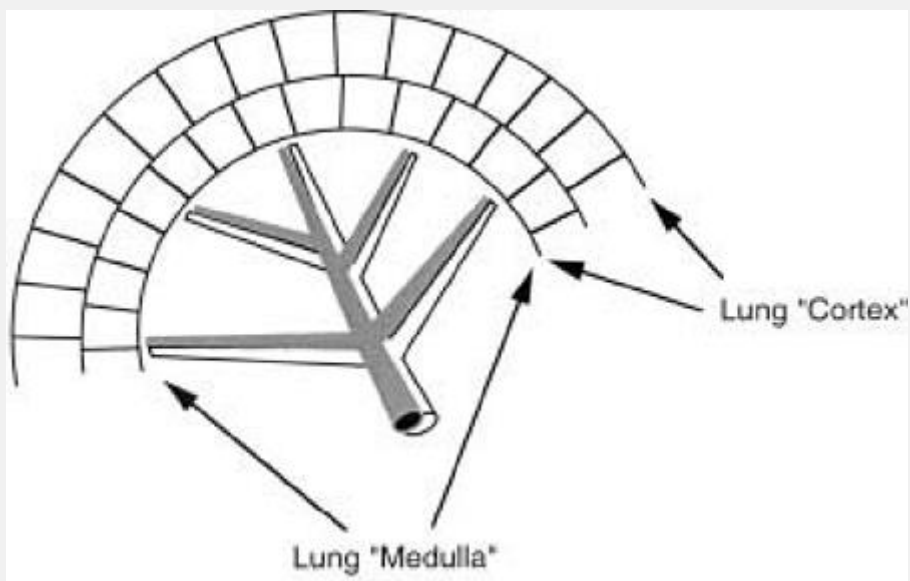


FIG. 2-15. Corticomedullary differentiation in the lung. The lung cortex is composed of one or two rows or tiers of well-organized and well-defined secondary pulmonary lobules 3 to 4 cm in thickness. The pulmonary lobules in the lung cortex tend to be well defined and relatively large, and can be conceived of as being similar to the stones in a Roman arch: all of similar size and shape. The cortical airways and vessels are small, usually less than 2 to 3 mm in diameter.

P.60

P.61

Subpleural Interstitium and Pleural Surfaces

Diffuse infiltrative lung diseases involving the subpleural interstitium or pleura can result in abnormalities visible at the pleural surfaces.

Subpleural Interstitium and Visceral Pleura

The visceral pleura consists of a single layer of flattened mesothelial cells that is subtended by layers of fibroelastic connective tissue; it measures 0.1 to 0.2 mm in thickness [33,34]. The connective tissue component of the visceral pleura is generally referred to on HRCT as the **subpleural interstitium, and is part of the "peripheral" interstitial fiber network** described by Weibel (Fig. 2-1) [5]. The subpleural interstitium contains small vessels, which are involved in

the formation of pleural fluid, and lymphatic branches. Interstitial lung diseases that affect the interlobular septa or result in lung fibrosis often result in abnormalities of the subpleural interstitium.

Abnormalities of the subpleural interstitium can be recognized over the costal surfaces of the lung, but are more easily seen in relation to the major fissures, at which two layers of the visceral pleura and subpleural interstitium come in contact. In contrast to conventional CT, in which the obliquely oriented major fissures are usually seen as broad bands of increased or decreased opacity, these fissures are consistently visualized on HRCT as continuous, smooth, and very thin linear opacities. Normal fissures are P.62

less than 1 mm thick, smooth in contour, uniform in thickness, and sharply defined (Figs. 2-2A, 2-10A, and 2-13). The visceral pleura and subpleural interstitium along the costal surfaces of lung are not visible on HRCT in normal subjects.

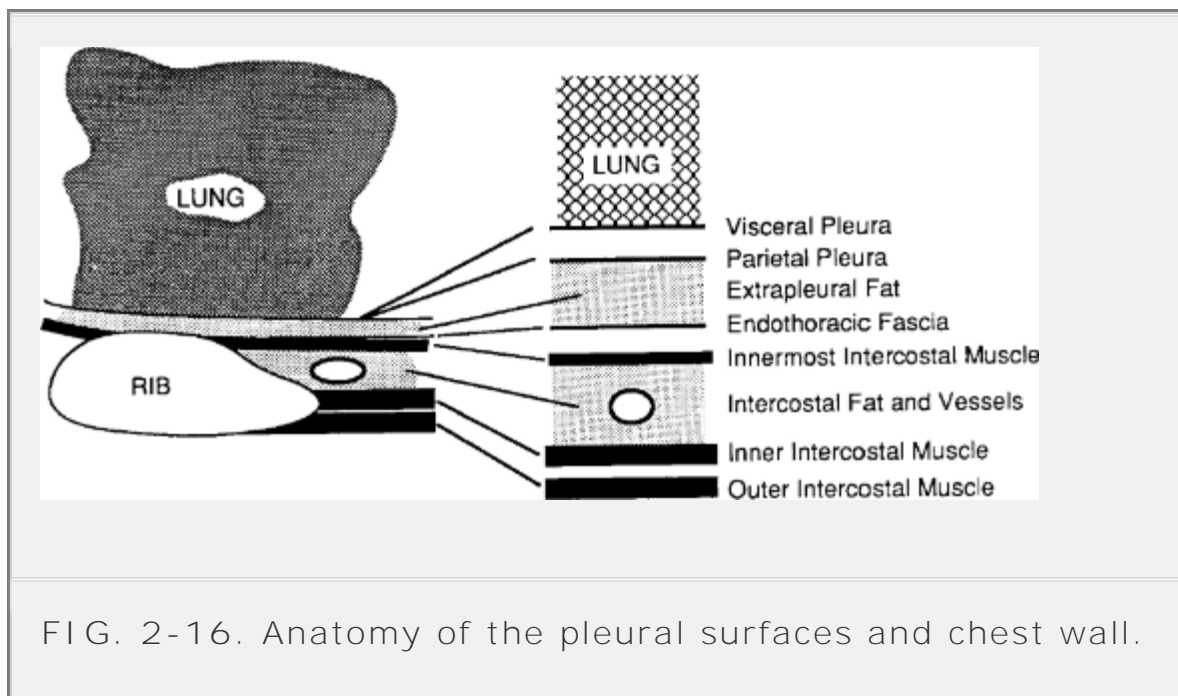


FIG. 2-16. Anatomy of the pleural surfaces and chest wall.

Parietal Pleura

The parietal pleura, as with the visceral pleura, consists of a mesothelial cell membrane in association with a thin layer of connective tissue. The parietal pleura is somewhat thinner than the visceral pleura, measuring approximately 0.1 mm [33,34]. External to the parietal pleura is a thin layer of loose areolar connective tissue or extrapleural fat, which separates the pleura from the fibroelastic endothoracic fascia and lines the thoracic cavity (Fig. 2-16); the endothoracic fascia is approximately 0.25 mm thick [34,35]. External to the endothoracic fascia are the innermost intercostal muscles and ribs. The innermost intercostal muscles pass between adjacent ribs but do not extend into the paravertebral regions.

As stated in Chapter 1, window level/width settings of 50/350 Hounsfield units (HU) are best for evaluating the parietal pleura and adjacent chest wall. Images at a level of -600 HU with an extended window width of 2,000 HU are also useful in evaluating the relationship of peripheral parenchymal abnormalities to the pleural surfaces [3,36]. On HRCT in normal patients, the innermost intercostal muscles are often visible as 1- to 2-mm-thick stripes (the intercostal stripes) of soft-tissue opacity at the lung-chest wall interface, passing between adjacent rib segments in the anterolateral, lateral, and posterolateral thorax (Fig. 2-17). The parietal pleura is too thin to see on HRCT along the costal pleural surfaces, even in combination with the visceral pleura and endothoracic fascia [37]. However, in the paravertebral regions, the innermost intercostal muscle is anatomically absent, and a very thin line (the

paravertebral line) is sometimes visible at the interface between lung and paravertebral fat or rib (Fig. 2-18) [37]. This line probably represents the combined thickness (0.2 to 0.4 mm) of the normal pleural layers and endothoracic fascia.

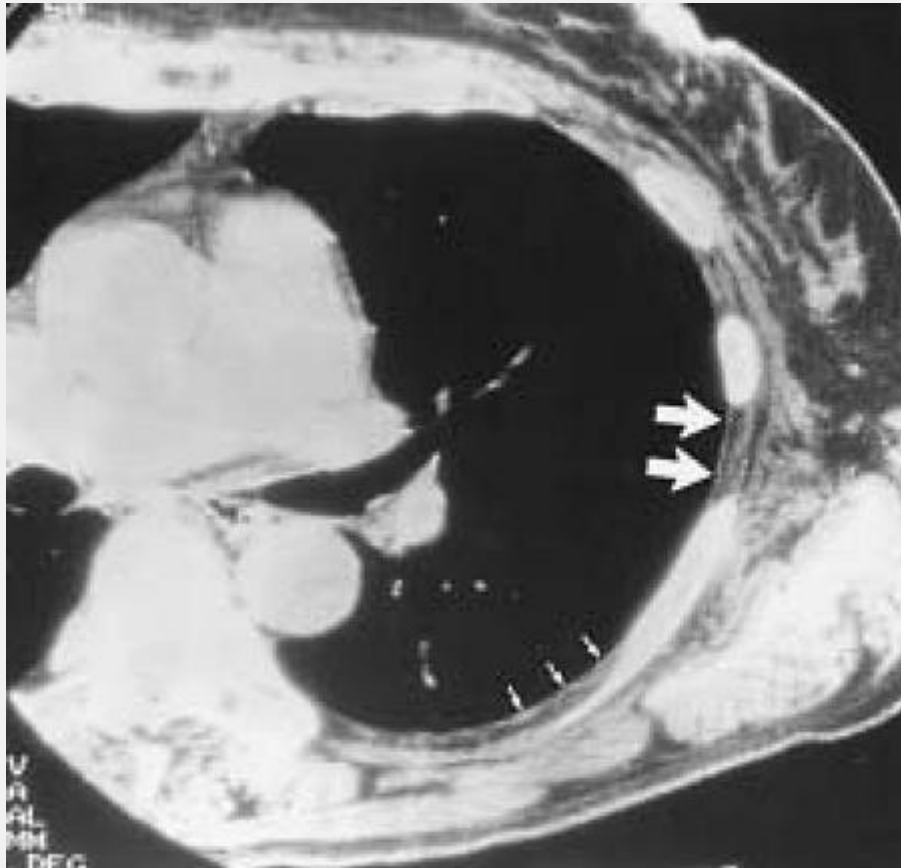


FIG. 2-17. Normal intercostal stripe. On high-resolution CT in a normal subject, the intercostal stripe is visible as a thin white line (large arrows). Although it represents the combined thickness of visceral and parietal pleurae, the fluid-filled pleural space, endothoracic fascia, and innermost intercostal muscle, it primarily represents the innermost intercostal muscle. The intercostal stripe is seen as separate from the more external layers of the intercostal muscles

because of a layer of intercostal fat. Posteriorly, the intercostal stripe (small arrows) is visible anterior to the lower edge of a rib.

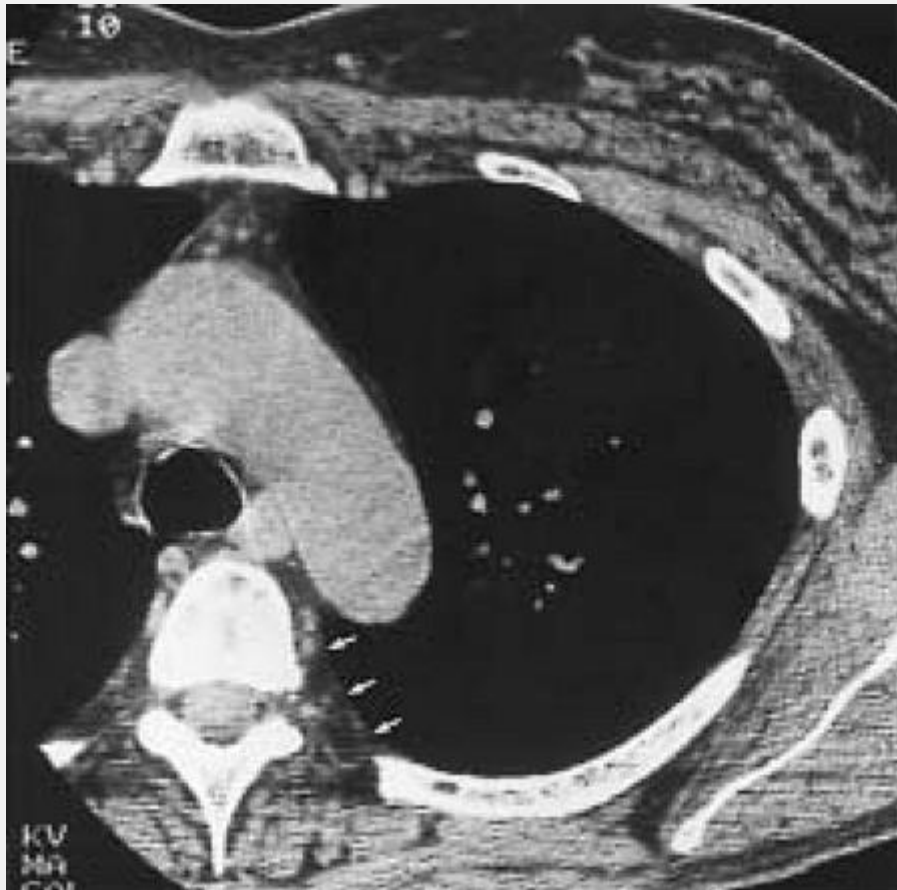


FIG. 2-18. The paravertebral line. In the paravertebral regions (arrows), the innermost intercostal muscle is absent, and, at most, a very thin line (the paravertebral line) is present at the lung-chest wall interface. As in this case, a distinct line may not be seen.

High-Resolution Computed Tomography Measurement of Lung Attenuation

Generally speaking, lung attenuation appears relatively homogeneous on HRCT scans obtained at full inspiration. Measurements of lung attenuation in normal subjects usually range from -700 to -900 HU, corresponding to lung densities of approximately 0.300 to 0.100 g per mL, respectively [38,39]. In a study by Lamers et al. [40], with HRCT obtained using spirometric control of lung volume, the mean lung attenuation measured in 20 healthy subjects at 90% of vital capacity was -859 HU [standard deviation (SD), 39] in the upper lung zones and -847 (SD, 34) in the lower lung zones. A mean lung density of -866 ± 16 HU (range -983 to -824 HU) was found by Gevenois et al. [41] in a study of 42 healthy subjects (21 men, 21 women) from 23 to 71 years of age. In this study, no significant correlation between mean lung density and age was found, but a significant correlation between the total lung capacity, expressed as absolute values and mean lung density was found. A study by Chen et al. [42] of 13 patients with normal pulmonary function tests showed an average lung attenuation of -814 ± 24 HU on HRCT when the entire cross section of lung was used for measurement and an attenuation of -829 ± 21 HU (range, -858 to -770 HU) using three small regions of interest placed in anterior, middle, and posterior lung regions.

An attenuation gradient is normally present, with the most dependent lung regions being the densest, and the least dependent lung regions being the least dense. This gradient is largely caused by regional differences in blood and gas volume that, in turn, are determined by gravity, mechanical stresses on the lung, and intrapleural pressures [36,38]. Differences in attenuation between anterior and posterior lung have been measured in supine patients, and values

generally range from 50 to 100 HU [38,43,44], although gradients of more than 200 HU have been reported [43]. The anteroposterior attenuation gradient was found to be nearly linear and was present regardless of whether the subject was supine or prone [43].

Genereux measured anteroposterior attenuation gradients at three levels (aortic arch, carina, and above the right hemidiaphragm) in normal subjects [44]. An anteroposterior attenuation gradient was found at all levels, although the gradient was larger at the lung bases than in the upper lung; the anteroposterior gradient averaged 36 HU at the aortic arch, 65 HU at the carina, and 88 HU at the lung bases. The attenuation gradient was even larger if only cortical lung was considered. Within cortical lung, the attenuation differences at the three levels studied were 45, 81, and 113 HU, respectively.

Vock et al. [38] analyzed CT-measured pulmonary attenuation in children. In general, lung attenuation in children is greater than in adults [38,43], but anteroposterior attenuation gradients were similar to those found in adults, averaging 56 HU at the subcarinal level. Although most authors have reported that normal anteroposterior lung attenuation gradients are linear, with attenuation increasing gradually from anterior to posterior lung, the lingula and superior segments of the lower lobes can appear relatively lucent in many normal subjects [45]; focal lucency in these segments should be considered a normal finding. Although the reason is unclear, these slender segments may be less well ventilated than adjacent lung and therefore less well perfused, or some air-trapping may be present.

Normal Expiratory High-Resolution Computed Tomography

Expiratory HRCT is generally performed to detect air-trapping in patients with a small airway obstruction or emphysema. On expiratory HRCT, changes in the lung attenuation, cross-sectional area [46], and appearance of airways are typical [47]. Air-trapping of limited extent may also be seen in normals.

Lung Attenuation Changes

Lung parenchyma normally increases in CT attenuation as lung volume is reduced during expiration. This change can generally be recognized on HRCT as an increase in lung opacity (Figs. 2-19, 2-20, and 2-21; see Figs. 1-28, 1-29 1-30) [8,38,43,48,49,50]. Robinson and Kreel [49] found significant inverse correlations between lung volumes determined spirometrically and CT-measured lung attenuation, for the whole

P.64

lung ($r = -0.680$, $p > .0005$) and for anterior, middle, and posterior lung zones considered individually.

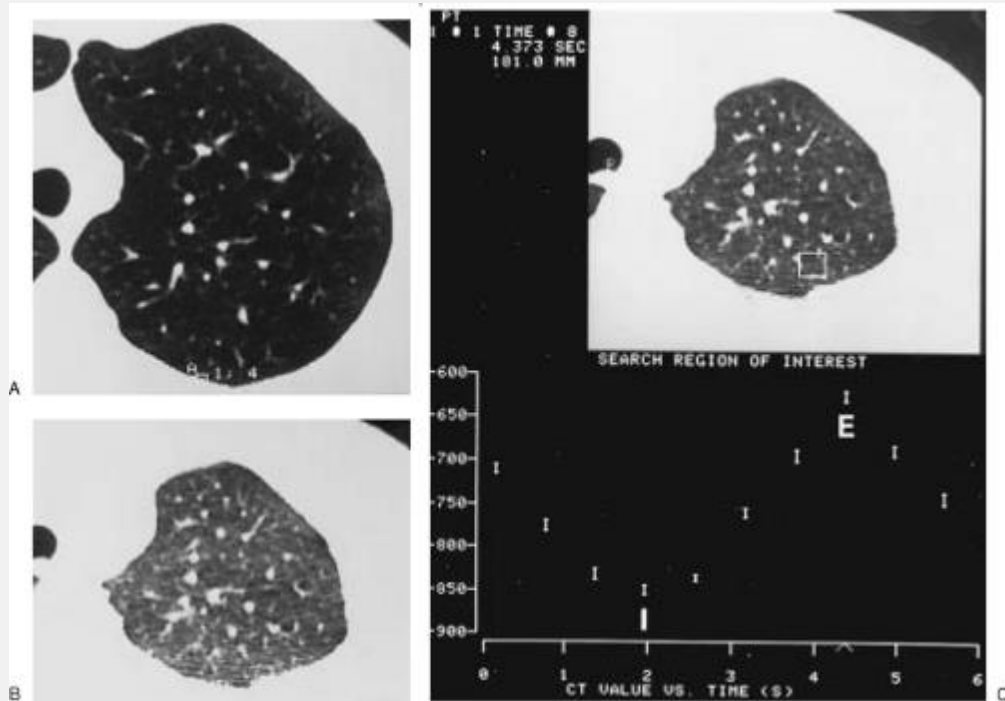


FIG. 2-19. Normal dynamic expiratory HRCT. Inspiratory (A) and expiratory (B) images from a sequence of ten scans obtained during forced expiration in a normal subject. Lung attenuation increases and cross-sectional lung area decreases on the expiratory scan. C: A region of interest has been positioned in the posterior lung, and a time-attenuation curve calculated for this region of interest shows an increase in attenuation from -850 HU to -625 HU from maximal inspiration (I) to maximal expiration (E). Each point on the time density curve represents one image from the dynamic sequence.

The mean attenuation change between full inspiration and expiration ranges from 80 to 300 HU regardless of the expiratory technique used [8,38,40,45,50]. In a study of young, normal volunteers, an increase in lung attenuation averaging 200 HU was consistently seen during forced expiration, but the increase was variable and ranged from

84 to 372 HU [45]. In a study by Chen et al. [42] of patients with normal pulmonary function tests, the average lung attenuation increase on postexpiratory HRCT was 144 ± 47 HU (range, 85 to 235 HU) when three small regions of interest placed in different lung regions were used for measurement and 149 ± 54 HU when the entire cross section of lung was used for measurement. Average lung attenuation on postexpiratory HRCT was $-685 \text{ HU} \pm 51$ (range, -763 to -580 HU) using three regions of interest and -665 ± 80 HU for the entire cross section of lung [42]. According to Kalender et al., using spirometrically triggered CT [51], a 10% change in vital capacity resulted, on average, in a change of approximately 16 HU, and estimates of lung attenuation at 0% and 100% of vital capacity were -730 HU and -895 HU, respectively. In a study by Lamers et al. [40], with HRCT obtained using spirometric control of lung volume, the mean lung attenuation in 20 healthy subjects measured in the upper lung zones at 90% of vital capacity was -859 HU (SD, 39), whereas at 10% of vital capacity, it was -786 HU (SD, 39). In the lower lung zones, lung attenuation increased from -847 HU (SD, 34) at 90% of vital capacity to -767 HU (SD, 56) at 10% of vital capacity. In a study of spirometrically gated HRCT [52] at 20%, 50%, and 80% of vital capacity, mean lung attenuation measured -747, -816, and -855 HU, respectively. Millar et al. [48] calculated the physical density of lung at full inspiration and expiration, based on the assumption that physical density had

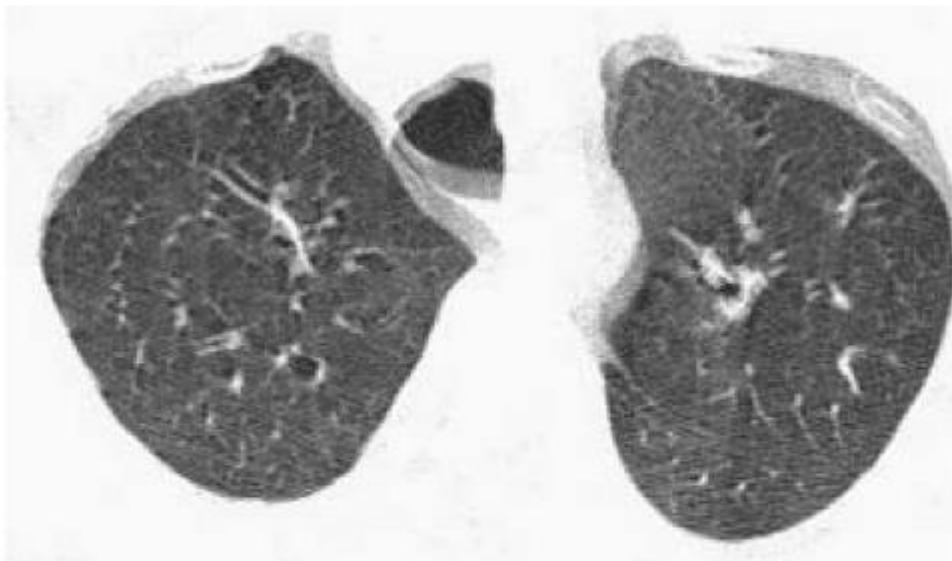
P.65

linear relation to radiographic density (physical density = 1 - CT attenuation in HU/1,000) [53]. Using this method,

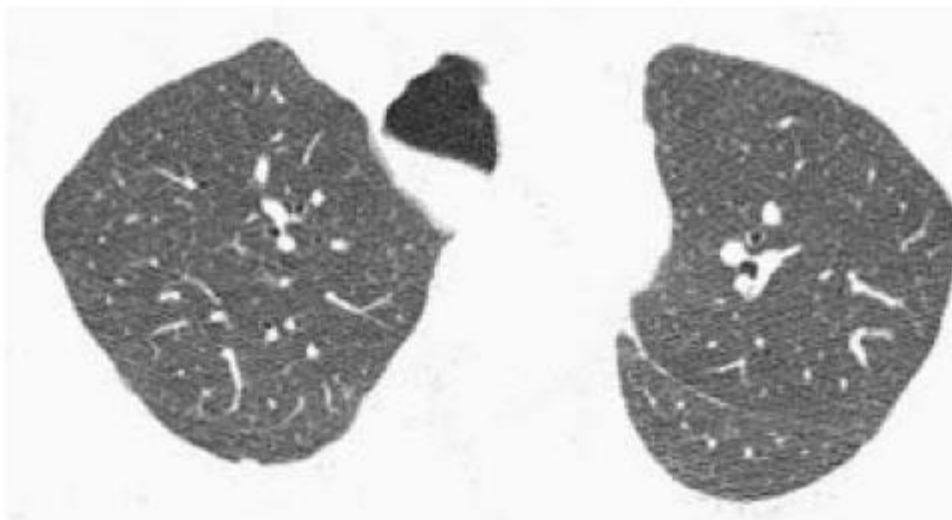
peripheral lung tissue density was measured as 0.0715 g per cm³ (SD, 0.017) at full inspiration and 0.272 g per cm³ (SD, 0.067) at end expiration. Using dynamic expiratory HRCT, a greater increase in lung attenuation may be seen than with static imaging.



A



B



C

FIG. 2-20. Dynamic inspiratory (A) and expiratory (B-C) HRCT in a normal subject, obtained with low (40) mA. On the inspiratory scan (A), lungs appear homogeneous in attenuation. Lung attenuation measured -875 HU in the posterior right lung. During rapid expiration (B), image quality is degraded by respiratory motion. On a scan at maximum expiration (C), lung decreases in volume and increases in attenuation. Posterior dependent lung increases in attenuation to a greater degree than anterior nondependent lung, now measuring -750 HU. Note some anterior bowing of the posterior tracheal membrane, typical of expiratory images.

In children, the CT attenuation of lung parenchyma is higher than in adults and decreases with age [38,43]. Attenuation increases seen with expiration are similar to those found
P.66

in adults. Ringertz et al. [54], using ultrafast CT, measured the CT attenuation of children younger than 2.5 years during quiet respiration; the average CT lung attenuation was -551 (SD, 106) on inspiration and -435 HU (SD, 103) on expiration. Vock et al. [38] measured the lung attenuation changes in children ranging in age from 9 to 18 years. Mean lung attenuation at full inspiration and full expiration measured -804 HU and -646 HU, respectively. The anteroposterior attenuation differences were similar to those seen in adults, averaging 56 HU at the subcarinal level, and increased with maximal expiration and increased during expiration [38].

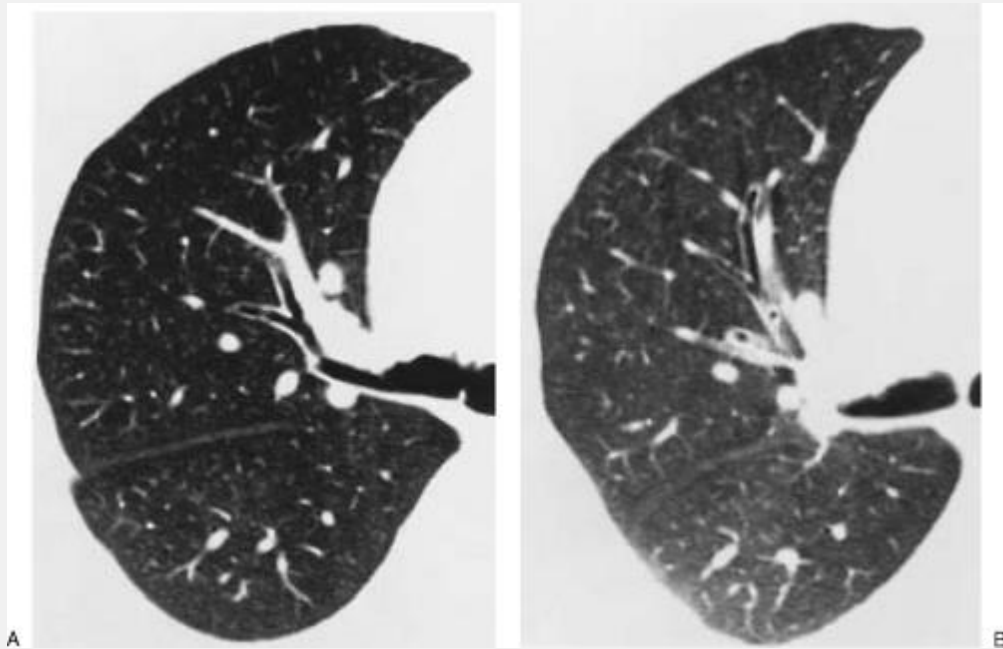


FIG. 2-21. Inspiratory (A) and postexpiratory (B) HRCT in a normal subject. On the expiratory scan, lung increases in attenuation. Posterior dependent lung increases in attenuation to a greater degree than anterior nondependent lung.

Usually, dependent lung regions show a greater increase in lung attenuation during expiration than do nondependent lung regions irrespective of the patient's position [8,43,45,49,50,55]. As a result, the anteroposterior attenuation gradients normally seen on inspiration are significantly greater on expiratory scans (Fig. 2-21) [38,49,50]; the increase in the anterior-to-posterior attenuation gradient after expiration has been reported to range from 47 to 130 HU in different studies [8,38,45,50]. Furthermore, the expiratory lung attenuation increase in dependent lung regions is greater in the lower lung zones than in the middle and upper zones, probably due to greater diaphragmatic movement or greater basal blood volume

[45]. The sum of these changes may be recognizable as increased attenuation or dependent density on supine scans at low lung volume. Although using measurements of attenuation gradients on inspiration and expiration has been investigated as a method of diagnosing lung disease [8,48,56], this technique has not assumed a clinical role.

Normal Air-Trapping

In many normal subjects, areas of air-trapping are visible on expiratory scans (Figs. 2-22 and 2-23); in these regions, lung does not increase normally in attenuation and appears relatively lucent. This appearance is most typically seen in the superior segments of the lower lobes or in the anterior middle lobe or lingula, or it involves individual pulmonary lobules, particularly in the lower lobes [45,57]; it is limited to a small proportion of lung volume. In a study by Chen et al. [42], focal areas of air-trapping, including the superior segments of the lower lobes, were visible in 61% of patients having normal pulmonary function tests. In a study by Lee et al. [57], air-trapping was seen in 52% of 82 asymptomatic subjects with normal pulmonary function tests. The frequency of air-trapping increased with age ($p < .05$), being seen in 23% of patients aged 21 to 30 years, 41% of those aged 31 to 40 years, 50% aged 41 to 50 years, 65% aged 51 to 60 years, and 76% of those older than 61 years. In another study, discounting the superior segments and air-trapping involving less than two contiguous or five noncontiguous pulmonary lobules, air-trapping was not seen on expiratory

P.67

scans in ten healthy nonsmokers, although it was visible in

40% of patients with suspected chronic airways disease who had normal pulmonary function tests [58]. Normal air-trapping is discussed in greater detail in Chapter 3.

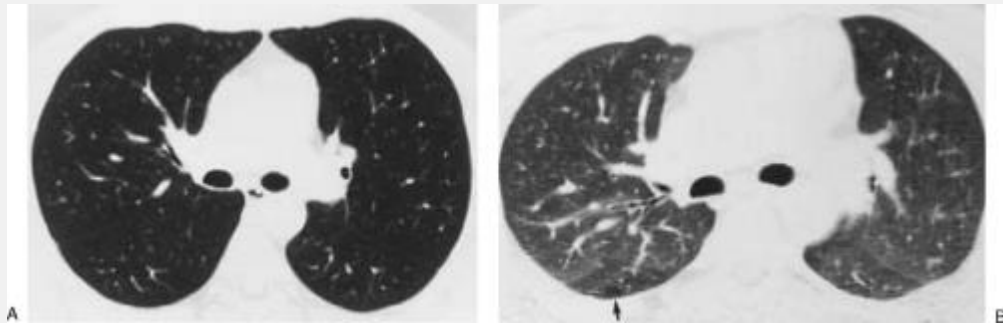


FIG. 2-22. Inspiratory (A) and postexpiratory (B) HRCT in a normal subject. On the expiratory scan, there is relative lucency in the superior segments of the lower lobes, posterior to the major fissures. This appearance is normal. Also, focal air-trapping is present in a single lobule (arrow) in the posterior right lung. Note slight anterior bowing of the posterior right bronchus intermedius. This may be seen in some patients on expiration.

Changes in Cross-Sectional Lung Area

The reduction in cross-sectional lung area occurring with expiration has been assessed in several studies and usually ranges from 40% to 50%. In a study of dynamic expiratory HRCT, Webb et al. [45] determined the percent decrease in lung cross-sectional area from full inspiration to full expiration in ten normal volunteers. The area change ranged from 14.8% to 61.3% for all subjects, subject positions, and lung regions. The greatest percentage decrease in cross-

sectional area during exhalation occurred in the upper lung zones. This value averaged 51.3% (SD, 6.7) in the supine position and 43.1% (SD, 10.2) in the prone position. The percentage decrease in lung cross-sectional area was least at the lung bases, averaging 30.9% (SD, 7.5) in the supine position and 25.2% (SD, 5) in the prone position. The average area changes for the midlung regions were intermediate between those of upper and lower lung zones, measuring 38.9% (SD, 7.4) in the supine position and 36.7% (SD, 5.3) in the prone position. Similarly, in a study by Lucidarme et al. [58], cross-sectional lung area decreased by an average of 43% (range, 34% to 57%) in a group of ten normal volunteers. Mitchell et al. [46] measured lung area on inspiratory and end expiratory scans at the level of the carina in 78 normal subjects. The percentage change in area from inspiration to expiration averaged 55% (SD, 8.7%).

Changes in cross-sectional lung area during expiration can be related to changes in lung attenuation as shown on HRCT. Simply stated, attenuation increases at the same time that cross-sectional lung area decreases during expiration (Fig. 2-19). For example, Robinson and Kreel [49] found a significant inverse correlation between the expiratory change in cross-sectional lung area measured on CT and changes in CT-measured lung attenuation ($r = -0.793$, $p > .0005$). In a study using dynamic expiratory HRCT [45], a correlation between cross-sectional lung area and lung attenuation was found for each of three lung regions evaluated (upper lung, $r = 0.51$, $p = .03$; midlung, $r = 0.58$, $p = .01$; lower lung, $r = 0.51$, $p = .05$). The lower lung zone showed a greater attenuation increase for a given area change; this phenomenon likely reflects the much-

greater effect of diaphragmatic elevation on basal lung attenuation than occurs in the upper lungs.



FIG. 2-23. Dynamic expiratory HRCT in a normal subject showing air-trapping in the anterior lingula (arrows) and relative lucency posterior to the left major fissure. Pulmonary lobules in the lung medulla are smaller and less well defined than in the periphery. However, vessels and bronchi in the lung medulla are large and easily seen on HRCT. Note anterior bowing of the posterior wall of the right bronchus.

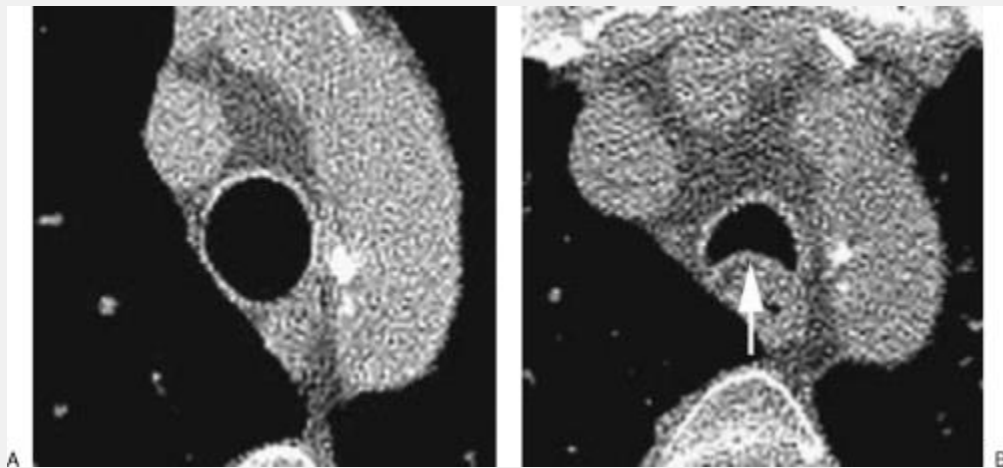


FIG. 2-24. Normal HRCT appearances of the trachea on inspiratory (A) and expiratory (B) scans. A: On an inspiratory scan shown at a tissue window setting, the trachea appears elliptic. B: After forced expiration, there is marked anterior bowing of the posterior tracheal membrane (arrow) resulting in a decreased anteroposterior diameter. There is little side-to-side narrowing of the tracheal lumen.

P.68

Changes in Airway Morphology

The intrathoracic trachea shows significant changes in cross-sectional area, anteroposterior diameter, and transverse diameter from full inspiration to full expiration (Figs. 2-20 and 2-24). In a study using ultrafast dynamic CT in ten healthy men [56], the mean cross-sectional area of the trachea decreased 35% during forced vital capacity maneuver (range, 11% to 61%; SD, 18). The anteroposterior diameter decreased from a mean of 19.6 mm (range, 16.1 to 23.2 mm; SD, 2.3) to 13.3 mm (range,

8.3 to 18.0 mm; SD, 3.5), for a mean decrease of 32%. This change is largely due to an invagination of the posterior tracheal membrane, a finding that is useful in confirming that an adequate expiration has occurred on expiratory CT (Fig. 2-24). The transverse diameter shows less change with expiration; in this study, it decreased from a mean of 19.4 mm (range, 15.2 to 25.3 mm; SD, 2.7) to a mean of 16.9 mm (range, 12.3 to 20.5 mm; SD, 2.6), for a mean decrease of 13%. The change of cross-sectional area correlated strongly with the changes in the anteroposterior and transverse diameters of the trachea ($r = 0.88, 0.92$; $p = .0018, .0002$, respectively). The shape of the normal trachea is round or elliptic on inspiration and horseshoe-shaped during and at the end of a full expiration, as the posterior tracheal membrane bows anteriorly.

Morphologic changes in the appearances of bronchi during respiration have not been studied systematically. In our experience, the cross-sectional area of main and lobular bronchi appears slightly reduced on full expiration; some invagination of the posterior wall of the right main bronchus or bronchus intermedius sometimes occurs during forced expiration (Figs. 2-22 and 2-23). Because slightly different levels are usually imaged on the inspiratory and expiratory scans, comparing individual bronchi or specific bronchial levels is often difficult.

References

1. Müller NL, Miller RR. Computed tomography of chronic diffuse infiltrative lung disease: part 1. *Am Rev Respir Dis* 1990; 142:1206-1215.

2. Müller NL, Miller RR. Computed tomography of chronic diffuse infiltrative lung disease: part 2. *Am Rev Respir Dis* 1990;142:1440-1448.
3. Webb WR. High-resolution CT of the lung parenchyma. *Radiol Clin North Am* 1989;27:1085-1097.
4. Zerhouni E. Computed tomography of the pulmonary parenchyma: an overview. *Chest* 1989;95:901-907.
5. Weibel ER. Looking into the lung: What can it tell us? *AJR Am J Roentgenol* 1979;133:1021-1031.
6. Murata K, Takahashi M, Mori M, et al. Peribronchovascular interstitium of the pulmonary hilum: normal and abnormal findings on thin-section electron-beam CT. *AJR Am J Roentgenol* 1996;166:309-312.
7. Lynch DA, Newell JD, Tschomper BA, et al. Uncomplicated asthma in adults: comparison of CT appearance of the lungs in asthmatic and healthy subjects. *Radiology* 1993;188:829-833.
8. Zerhouni EA, Naidich DP, Stitik FP, et al. Computed tomography of the pulmonary parenchyma: part 2. Interstitial disease. *J Thorac Imaging* 1985;1:54-64.
9. Weibel ER, Taylor CR. Design and structure of the human lung. In: Fishman AP, ed. *Pulmonary diseases and disorders*. New York: McGraw-Hill, 1988:11-60.
10. Webb WR, Stein MG, Finkbeiner WE, et al. Normal and diseased isolated lungs: high-resolution CT. *Radiology* 1988;166:81-87.
11. Murata K, Itoh H, Todo G, et al. Centrilobular lesions of the lung: demonstration by high-resolution CT and pathologic correlation. *Radiology* 1986;161:641-645.
12. Kim JS, Müller NL, Park CS, et al. Cylindrical bronchiectasis: diagnostic findings on thin-section CT. *AJR Am J Roentgenol* 1997;168:751-754.

13. Kang EY, Miller RR, Müller NL. Bronchiectasis: comparison of preoperative thin-section CT and pathologic findings in resected specimens. *Radiology* 1995;195:649-654.
14. Miller WS. The lung. Springfield, IL: Charles C Thomas Publisher, 1947:39-42.
15. Heitzman ER, Markarian B, Berger I, et al. The secondary pulmonary lobule: a practical concept for interpretation of radiographs: II. Application of the anatomic concept to an understanding of roentgen pattern of in disease states. *Radiology* 1969;93:514-520.
16. Heitzman ER, Markarian B, Berger I, et al. The secondary pulmonary lobule: a practical concept for interpretation of radiographs: I. Roentgen anatomy of the normal secondary pulmonary lobule. *Radiology* 1969;93:508-513.
17. Miller WS. The lung. Springfield, IL: Charles C Thomas Publisher, 1947:203.
18. Raskin SP. The pulmonary acinus: historical notes. *Radiology* 1982;144:31-34.
19. Osborne DR, Effmann EL, Hedlund LW. Postnatal growth and size of the pulmonary acinus and secondary lobule in man. *AJR Am J Roentgenol* 1983;140:449-454.
20. Weibel ER. High resolution computed tomography of the pulmonary parenchyma: anatomical background. Presented at: Fleischner Society Symposium on Chest Disease; 1990. Scottsdale, AZ.

21. Reid L. The secondary pulmonary lobule in the adult human lung, with special reference to its appearance in bronchograms. *Thorax* 1958;13:110-115.
22. Itoh H, Murata K, Konishi J, et al. Diffuse lung disease: pathologic basis for the high-resolution computed tomography findings. *J Thorac Imaging* 1993;8:176-188.
23. Reid L, Simon G. The peripheral pattern in the normal bronchogram and its relation to peripheral pulmonary anatomy. *Thorax* 1958;13:103-109.
24. Gamsu G, Thurlbeck WM, Fraser RG, et al. Peripheral bronchographic morphology in the normal human lung. *Invest Radiol* 1971;6:161-170.
25. Bergin C, Roggli V, Coblenz C, et al. The secondary pulmonary lobule: normal and abnormal CT appearances. *AJR Am J Roentgenol* 1988;151:21-25.
26. Hruban RH, Meziane MA, Zerhouni EA, et al. High resolution computed tomography of inflation fixed lungs: pathologic-radiologic correlation of centrilobular emphysema. *Am Rev Respir Dis* 1987;136:935-940.
27. Heitzman ER. Subsegmental anatomy of the lung. In: *The lung: radiologic-pathologic correlations*, 2nd ed. St. Louis: Mosby, 1984:42-49.
28. Reid L, Rubino M. The connective tissue septa in the foetal human lung. *Thorax* 1959;14:3-13.
29. Aberle DR, Gamsu G, Ray CS, et al. Asbestos-related pleural and parenchymal fibrosis: detection with high-resolution CT. *Radiology* 1988;166:729-734.
30. Fleischner FG. The butterfly pattern of pulmonary edema. In: *Frontiers of pulmonary radiology*. New York: Grune & Stratton, 1969:360-379.

31. Genereux GP. The Fleischner lecture: computed tomography of diffuse pulmonary disease. *J Thorac Imaging* 1989; 4: 50-87.
32. Gurney JW. Cross-sectional physiology of the lung. *Radiology* 1991; 178: 1-10.
33. Agostoni E, Miserocchi G, Bonanni MV. Thickness and pressure of the pleural liquid in some mammals. *Respir Phys* 1969; 6: 245-256.
34. Bernaudin J-F, Fleury J. Anatomy of the blood and lymphatic circulation of the pleural serosa. In: The pleura in health and disease. New York: Marcel Dekker, 1985: 101-124.
35. Policard A, Galy P. La Plevre. Paris: Masson, 1942: 23-33.
36. Murata K, Khan A, Herman PG. Pulmonary parenchymal disease: evaluation with high-resolution CT. *Radiology* 1989; 170: 629-635.
37. Im JG, Webb WR, Rosen A. Costal pleura: appearances at high-resolution CT. *Radiology* 1989; 171: 125-131.
38. Vock P, Malanowski D, Tschaeppler H, et al. Computed tomographic lung density in children. *Invest Radiol* 1987; 22: 627-631.
39. Millar AB, Denison DM. Vertical gradients of lung density in supine subjects with fibrosing alveolitis or pulmonary emphysema. *Thorax* 1990; 45: 602-605.
40. Lamers RJ, Thelissen GR, Kessels AG, et al. Chronic obstructive pulmonary diseases. evaluation with spirometrically controlled CT lung densitometry. *Radiology* 1994; 193: 109-113.
41. Gevenois PA, Scillia P, de Maertelaer V, et al. The effects of age, sex, lung size, and hyperinflation on CT lung densitometry. *AJR Am J Roentgenol* 1996; 167: 1169-1173.

42. Chen D, Webb WR, Storto ML, et al. Assessment of air trapping using postexpiratory high-resolution computed tomography. *J Thorac Imaging* 1998;13:135-143.
43. Rosenblum LJ, Mauceri RA, Wellenstein DE, et al. Density patterns in the normal lung as determined by computed tomography. *Radiology* 1980;137:409-416.
44. Genereux GP. Computed tomography and the lung: review of anatomic and densitometric features with their clinical application. *J Can Assoc Radiol* 1985;36:88-102.
45. Webb WR, Stern EJ, Kanth N, et al. Dynamic pulmonary CT: findings in normal adult men. *Radiology* 1993;186:117-124.
46. Mitchell AW, Wells AU, Hansell DM. Changes in cross-sectional area of the lungs on end expiratory computed tomography in normal individuals. *Clin Radiol* 1996;51:804-806.
47. Arakawa H, Webb WR. Expiratory high-resolution CT scan. *Radiol Clin North Am* 1998;36:189-209.
48. Millar AB, Denison DM. Vertical gradients of lung density in healthy supine men. *Thorax* 1989;44:485-490.
49. Robinson PJ, Kreef L. Pulmonary tissue attenuation with computed tomography: comparison of inspiration and expiration scans. *J Comput Assist Tomogr* 1979;3:740-748.
50. Verschakelen JA, Van Fraeyenhoven L, Laureys G, et al. Differences in CT density between dependent and nondependent portions of the lung: influence of lung volume. *AJR Am J Roentgenol* 1993; 161:713-717.
51. Kalender WA, Rienmuller R, Seissler W, et al. Measurement of pulmonary parenchymal attenuation: use of spirometric gating with quantitative CT. *Radiology* 1990;175:265-268.

52. Beinert T, Behr J, Mehnert F, et al. Spirometrically controlled quantitative CT for assessing diffuse parenchymal lung disease. *J Comput Assist Tomogr* 1995;19:924-931.
53. Denison DM, Morgan MDL, Millar AB. Estimation of regional gas and tissue volumes of the lung in supine man using computed tomography. *Thorax* 1986;41:620-628.
54. Ringertz HG, Brasch RC, Gooding CA, et al. Quantitative density-time measurements in the lungs of children with suspected airway obstruction using ultrafast CT. *Pediatr Radiol* 1989; 19:366-370.
55. Stern EJ, Webb WR. Dynamic imaging of lung morphology with ultrafast high-resolution computed tomography. *J Thorac Imaging* 1993;8:273-282.
56. Stern EJ, Graham CM, Webb WR, et al. Normal trachea during forced expiration: dynamic CT measurements. *Radiology* 1993;187:27-31.
57. Lee KW, Chung SY, Yang I, et al. Correlation of aging and smoking with air trapping at thin-section CT of the lung in asymptomatic subjects. *Radiology* 2000;214:831-836.
58. Lucidarme O, Coche E, Cluzel P, et al. Expiratory CT scans for chronic airway disease: correlation with pulmonary function test results. *AJR Am J Roentgenol* 1998;170:301-307.

Authors: Webb, W. Richard; Muller, Nestor L.; Naidich, David P.

Title: *High-Resolution CT of the Lung, 3rd Edition*

Copyright ©2001 Lippincott Williams & Wilkins

> Table of Contents > Chapter 3 - High-Resolution Computed Tomography Findings of Lung Disease

Chapter 3

High-Resolution Computed Tomography Findings of Lung Disease

The detection and diagnosis of diffuse lung disease using high-resolution computed tomography (HRCT) are based on the recognition of specific abnormal findings [1,2,3,4]. In this chapter, we review a number of HRCT findings of value in the differential diagnosis of diffuse lung disease.

First, a word about terminology. In the past, different terms have been used by authors to describe similar or identical HRCT abnormalities, which has led to confusion and difficulty in comparing one study to another [5]. In this book, whenever possible, we name and define HRCT findings on the basis of their specific corresponding anatomic abnormalities, as there is a close correlation in many instances between these findings and pathologic or histologic lung abnormalities. Furthermore, the terms used comply with those recommended by the Nomenclature Committee of the Fleischner Society [6]. Nonspecific, descriptive, or nonanatomic terms have been avoided, unless the HRCT findings themselves are nonspecific and cannot be related to particular anatomic abnormalities, or unless a descriptive term is particularly helpful in understanding and recognizing the specific abnormal

finding. Several of these colorful terms have become indispensable parts of the HRCT lexicon. For easy reference, an illustrated glossary of many of these terms is provided at the end of this book.

P.72

Generally, HRCT findings of lung disease can be classified into four large categories based on their appearances. These are (i) linear and reticular opacities, (ii) nodules and nodular opacities, (iii) increased lung opacity, and (iv) abnormalities associated with decreased lung opacity, including cystic lesions, emphysema, and airway abnormalities.

Linear and Reticular Opacities

Thickening of the interstitial fiber network of the lung by fluid or fibrous tissue, or because of interstitial infiltration by cells or other material, primarily results in an increase in linear or reticular lung opacities as seen on HRCT. Linear or reticular opacities may be manifested by the interface sign, peribronchovascular interstitial thickening, interlobular septal thickening, parenchymal bands, subpleural interstitial thickening, intralobular interstitial thickening, honeycombing, irregular linear opacities, and subpleural lines (Fig. 3-1).

Interface Sign

The presence of irregular interfaces between the aerated lung parenchyma and bronchi, vessels, or visceral pleural surfaces has been termed the *interface sign* by Zerhouni et al. [4,7] (Fig. 3-2). The interface sign is nonspecific, and is commonly seen in patients with an interstitial abnormality,

regardless of its cause. In the original description of the interface sign, this finding was visible in 89% of patients with interstitial lung disease [7].

The interface sign is generally associated with an increase in lung reticulation; the presence of thin linear opacities contacting the bronchi, vessels, or pleural surfaces is responsible for their having an irregular or spiculated appearance on HRCT. These linear opacities represent thickened interlobular septa, thickened intralobular interstitial fibers, or irregular scars (Fig. 3-1). The interface sign is most frequently visible in patients with fibrotic lung disease, and Nishimura et al. [8] reported the presence of irregular pleural surfaces and irregular vessel margins in 94% and 98%, respectively, of patients with idiopathic pulmonary fibrosis. In virtually all cases showing the interface sign, other, more specific, abnormal findings will also be visible on HRCT.

Peribronchovascular Interstitial Thickening

Central bronchi and pulmonary arteries are surrounded and enveloped by a strong connective tissue sheath, termed the *peribronchovascular interstitium*, extending from the level of the pulmonary hila into the peripheral lung. In the lung periphery, the peribronchovascular interstitium surrounds centrilobular arteries and bronchioles, and, more distally, supports the alveolar ducts and alveoli (see Fig. 2-1) [9]. The peribronchovascular interstitium is also termed the *axial interstitium* by Weibel [10]. Thickening of the perihilar peribronchovascular interstitium occurs in many diseases that cause a generalized interstitial abnormality [3,11,12,13]. Peribronchovascular interstitial thickening is

common in patients with lymphangitic spread of carcinoma [11,12,14]; lymphoma [15]; leukemia [16]; lymphoproliferative disease such as lymphocytic interstitial pneumonia (LIP) [17,18,19]; interstitial pulmonary edema; diseases that result in a perilymphatic distribution of nodules (e.g., sarcoidosis) [20]; and in many diseases that result in pulmonary fibrosis, particularly sarcoidosis, which has a propensity to involve the peribronchovascular interstitium (Table 3-1) [21]. Peribronchovascular interstitial thickening has also been reported in as many as 65% of patients with nonspecific interstitial pneumonia (NSIP) [22] and 19% of patients with chronic hypersensitivity pneumonitis [23].

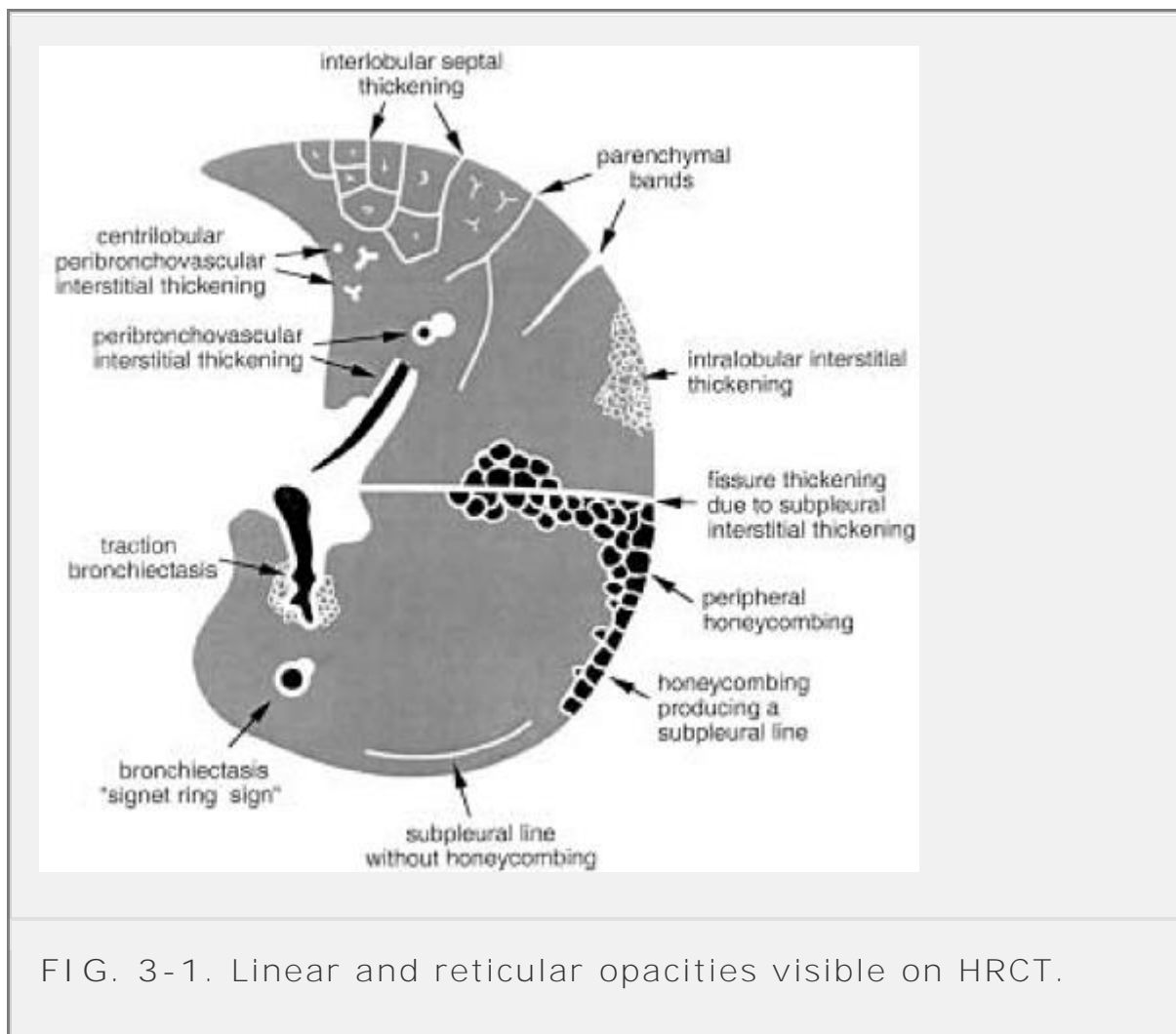


FIG. 3-1. Linear and reticular opacities visible on HRCT.

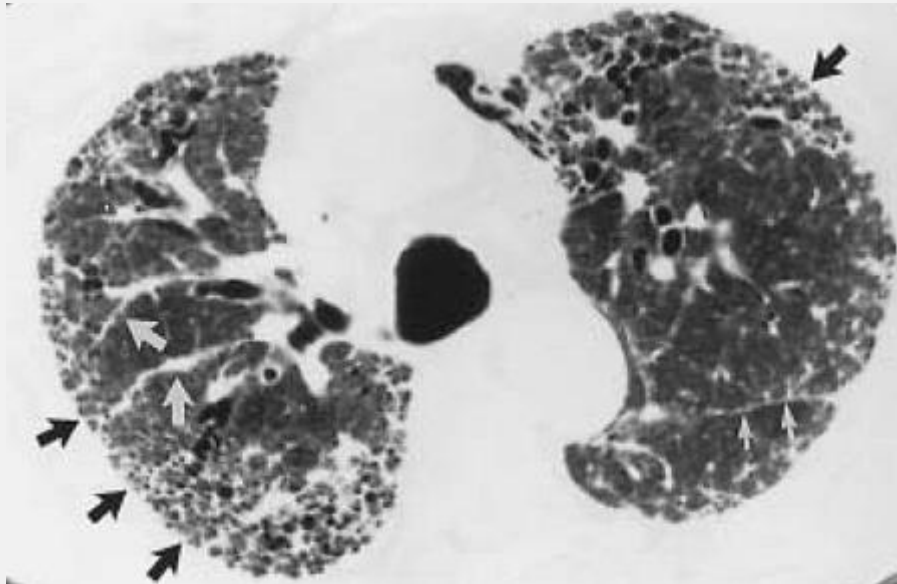


FIG. 3-2. The interface sign. In this patient with idiopathic pulmonary fibrosis and honeycombing, irregular interfaces are visible between the aerated lung parenchyma and structures such as vessels (*large white arrows*), fissures (*small white arrows*), and the visceral pleural surfaces (*black arrows*). This finding is commonly seen in patients with an interstitial abnormality, regardless of its cause, but is most frequent in patients with abnormal reticular opacities and fibrosis.

P.73

Because the thickened peribronchovascular interstitium cannot be distinguished from the underlying opacity of the bronchial wall or pulmonary artery, this abnormality is usually perceived on HRCT as an increase in bronchial wall thickness or an increase in diameter of pulmonary artery branches (Fig. 3-3) [11]. Apparent bronchial wall thickening is the easier of these two findings to recognize. This finding

is exactly equivalent to “peribronchial cuffing” seen on plain chest radiographs in patients with an interstitial abnormality. In patients with pulmonary interstitial emphysema, air is commonly seen within the peribronchovascular interstitium, outlining vessels and bronchi (Fig. 3-3D) [24,25,26].

Thickening of the peribronchovascular interstitium can appear smooth, nodular, or irregular in different diseases (Fig. 3-3) (Table 3-1) [9]. Smooth peribronchovascular interstitial thickening is most typical of patients with lymphangitic spread of carcinoma or lymphoma (Fig. 3-4) and interstitial pulmonary edema [27,28] but can be seen in patients with fibrotic lung disease as well. Nodular thickening of the peribronchovascular interstitium is particularly common in sarcoidosis (Fig. 3-5) and lymphangitic spread of carcinoma. The presence of irregular peribronchovascular interstitial thickening, as an example of the interface sign, is most frequently seen in patients with peribronchovascular and adjacent lung fibrosis. Extensive peribronchovascular fibrosis can also result in the presence of large conglomerate masses of fibrous tissue (Fig. 3-6). This can occur in patients with sarcoidosis [20], silicosis, tuberculosis, and talcosis and is discussed in greater detail in the section Conglomerate Nodules or Masses in Diffuse Lung Disease.

TABLE 3-1. *Differential diagnosis of peribronchovascular interstitial thickening*

Diagnosis	Comments
Lymphangitic carcinomatosis, lymphoma, leukemia	Common; smooth or nodular; may be the only abnormality
Lymphoproliferative disease (e.g., lymphocytic interstitial pneumonia)	Smooth or nodular; other abnormalities typically present
Pulmonary edema	Common; smooth
Sarcoidosis	Common; usually nodular or irregular; conglomerate masses of fibrous tissue with bronchiectasis typical in end stage
Idiopathic pulmonary fibrosis or other cause of usual interstitial pneumonia	Common; often irregular; associated with traction bronchiectasis; other findings of fibrosis predominate
Nonspecific interstitial pneumonia	With findings of ground-glass opacity and reticulation
Silicosis/coal worker's	Conglomerate masses

pneumoconiosis, talcosis	
Hypersensitivity pneumonitis (chronic)	Sometimes visible; often irregular; associated with traction bronchiectasis

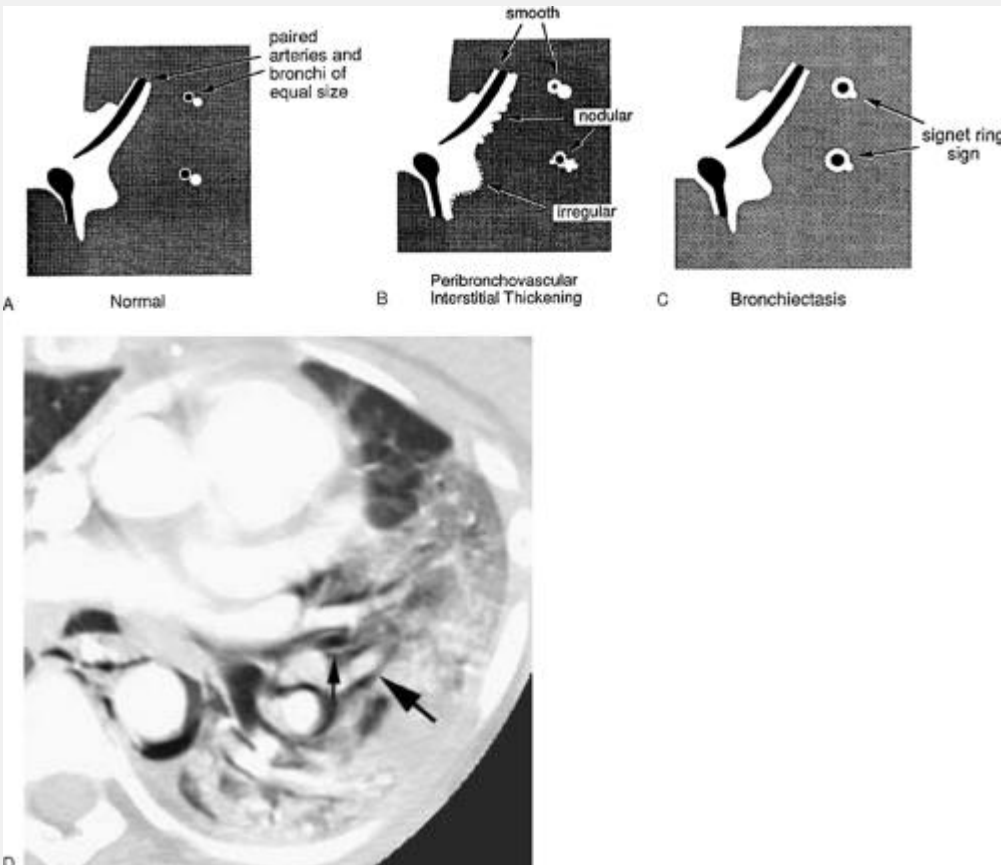


FIG. 3-3. Differentiation of peribronchovascular interstitial thickening and bronchiectasis. A: In a normal subject, bronchi are uniformly thin-walled and appear approximately equal in diameter to adjacent pulmonary arteries. B: In the

presence of peribronchovascular interstitial thickening, there appears to be an increase in bronchial wall thickness and a corresponding increase in diameter of pulmonary artery branches. The contours of the bronchi and vessels can appear smooth, nodular, or irregular in different diseases. C: In bronchiectasis, bronchi are usually thick-walled and appear larger than adjacent pulmonary arteries. This can result in the so-called signet ring sign. D: CT with 3-mm collimation in a patient with pulmonary interstitial emphysema. Air is visible within the peribronchovascular interstitial sheath, outlining pulmonary arteries (*large black arrow*) and bronchi (*small black arrow*). Air also surrounds pulmonary veins.



FIG. 3-4. Peribronchovascular interstitial thickening. In a patient with unilateral lymphangitic spread of carcinoma involving the left lung, there is smooth thickening of the

peribronchovascular interstitium manifested by peribronchial cuffing (*arrows*); this appearance is easily contrasted with that of normal bronchi in the right lung. Note that the left-sided pulmonary artery branches appear similar in diameter to the cuffed bronchi because the thickened interstitium surrounds them as well. Small intrapulmonary vessels on the left also appear more prominent than those on the normal side because of perivascular interstitial thickening. Interlobular septal thickening and subpleural nodules are also visible on the left. Subpleural interstitial thickening results in nodular thickening of the left major fissure.



FIG. 3-5. Nodular peribronchovascular interstitial thickening in a patient with sarcoidosis. Numerous small nodules surround central bronchi and vessels.

P.74

P.75

Peribronchovascular interstitial thickening is easy to diagnose if it is of a marked degree, in which bronchial walls appear several millimeters thick or bronchovascular structures show evidence of the interface sign or nodules. However, the diagnosis of minimal peribronchovascular thickening can be difficult and quite subjective, particularly if the abnormality is diffuse and symmetric. Although the thickness of the wall of a normal bronchus should measure from one-sixth to one-tenth of its diameter [29], there are no reliable criteria as to what represents the upper limit of normal for the combined thickness of bronchial wall and the surrounding interstitium [30]. Furthermore, these measurements vary depending on the lung window chosen, and too low a window mean can make normal bronchi or vessels appear abnormal (see Fig. 1-13). However, in many patients with peribronchovascular interstitial thickening, and particularly in patients with lymphangitic spread of carcinoma and sarcoidosis, this abnormality is unilateral or patchy, sparing some areas of lung. In such patients, normal and abnormal lung regions easily can be contrasted (Fig. 3-4). As a rule, bronchial walls in corresponding regions of one or both lungs should be similar in thickness.

In patients with lung fibrosis and peribronchovascular interstitial thickening, bronchial dilatation is commonly present and results from traction by fibrous tissue on the bronchi walls. This is termed *traction bronchiectasis* (Figs. 3-1 and 3-6); it typically results in irregular bronchial dilatation that appears varicose or corkscrewed [31,32]. Traction bronchiectasis usually involves the segmental and subsegmental bronchi and is most commonly visible in the perihilar regions in patients with significant lung fibrosis [20,33]. It can also affect small peripheral bronchi or bronchioles, an occurrence termed *traction bronchiolectasis*. Bronchial wall thickening occurring in patients with true bronchiectasis produces an abnormality that closely mimics the HRCT appearance of peribronchovascular interstitial thickening. However, airway diseases and interstitial diseases can usually be distinguished on the basis of symptoms or pulmonary function abnormalities, and confusion between these two is not often a problem in clinical diagnosis. In addition, several HRCT findings allow these two entities to be differentiated (Fig. 3-3). First, peribronchovascular interstitial thickening is often associated with other findings of interstitial disease, such as septal thickening, honeycombing, or the interface sign, whereas bronchiectasis usually is not. Second, in patients with bronchiectasis, the abnormal thick-walled and dilated bronchi often appear much larger than the adjacent pulmonary artery branches (Fig. 3-7). This results in the appearance of large ring shadows, each associated with a small, rounded opacity, a finding that has been termed the *signet ring sign*, and is considered to be diagnostic of bronchiectasis [34,35,36,37,38]. In patients with peribronchovascular interstitial thickening, on the other

hand, the size relationship between the bronchus and artery is maintained, and they appear to be of approximately equal size. The diagnosis and appearances of bronchiectasis is discussed in greater detail in the section Bronchiectasis and in Chapter 8.

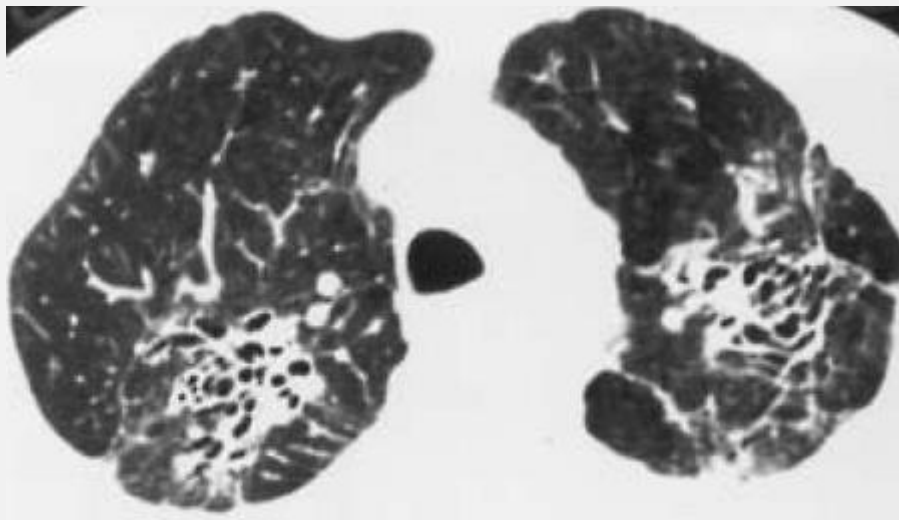


FIG. 3-6. Peribronchovascular interstitial thickening in end-stage sarcoidosis, with conglomerate masses of fibrous tissue surrounding central vessels and bronchi. Bronchi appear dilated and thick walled because of surrounding fibrosis and traction bronchiectasis. Note that vessels and bronchi appear to be of similar diameter.



FIG. 3-7. Bronchiectasis with the signet ring sign. Thick-walled and dilated bronchi (large arrows) appear larger than the adjacent pulmonary artery branches (small arrows). This appearance is termed the signet ring sign and is typical of bronchiectasis.

Diseases that cause peribronchovascular interstitial thickening often result in prominence of the centrilobular artery, which normally appears as a dot, Y-shaped, or X-shaped branching opacity. This finding reflects thickening of the intralobular component of the peribronchovascular interstitium, also termed the *centrilobular interstitium* (see 2-1) [3,7,12,39]. On HRCT, a linear, branching, or dotlike centrilobular opacity may be seen (Fig. 3-1).

Thickening of the centrilobular interstitium is usually associated with interlobular septal thickening or intralobular interstitial thickening (Fig. 3-1) but sometimes occurs as an isolated abnormality. Centrilobular interstitial thickening is common in patients with lymphangitic spread of carcinoma or lymphoma [11,12] and interstitial pulmonary edema [28,40]. In patients with lung fibrosis, centrilobular interstitial thickening is common but almost always associated with honeycombing or intralobular lines.

Interlobular Septal Thickening

On HRCT, numerous clearly visible interlobular septa almost always indicate the presence of an interstitial abnormality; only a few septa should be visible in normal patients. Septal thickening can be seen in the presence of interstitial fluid, cellular infiltration, or fibrosis.

Within the peripheral lung, thickened septa 1 to 2 cm in length may outline part of or an entire lobule and are usually seen extending to the pleural surface, being roughly perpendicular to the pleura (Figs. 3-1, 3-8, and 3-9) [3,4,11,12,39,41,42,43]. Lobules at the pleural surface may have a variety of appearances, but they are often longer than they are wide, resembling a cone or truncated cone. Within the central lung, thickened septa outline lobules that

are 1 to 2.5 cm in diameter and appear polygonal, or sometimes hexagonal, in shape (Figs. 3-8 and 3-9). Lobules delineated by thickened septa commonly contain a visible dotlike or branching centrilobular pulmonary artery. The characteristic relationship of the interlobular septa and centrilobular artery is often of value in identifying each of these structures.

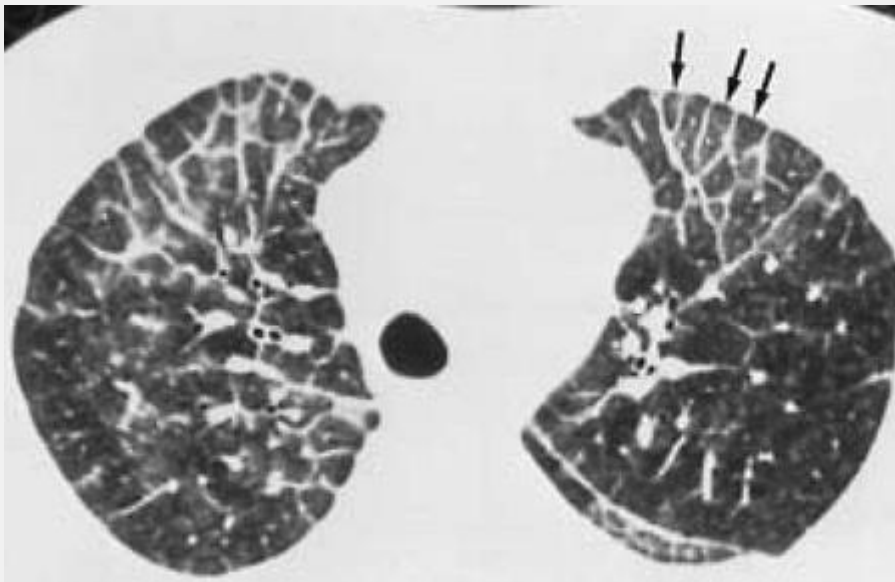


FIG. 3-8. Interlobular septal thickening in a patient with lymphangitic spread of carcinoma. Diffuse interlobular septal thickening outlines numerous pulmonary lobules. Those visible in the peripheral lung may appear to be of various sizes and shapes, depending at least partially on the relationship of the lobule to the plane of scan. However, many lobules are conical in shape (*arrows*). In the more central lung, lobules appear more hexagonal or polygonal. The branching or dotlike intralobular vessel is often visible. The septal thickening in this case is primarily smooth in contour, although nodularity is seen in several regions, particularly adjacent to the left major fissure. Long septa

that marginate several lobules have been termed *parenchymal bands*. The presence of multiple thickened septa form "peripheral" or "polygonal arcades."

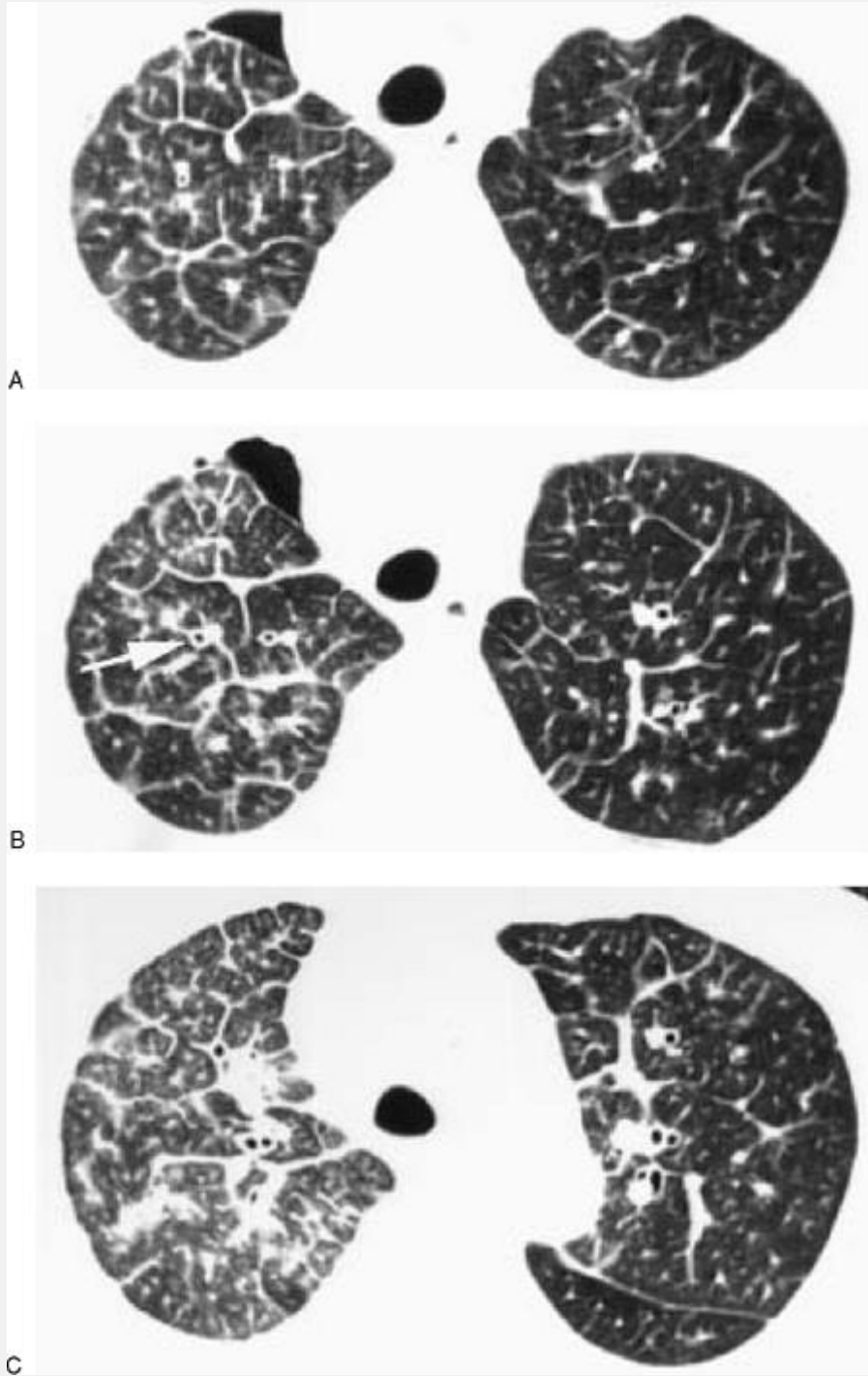


FIG. 3-9. A-C: Interlobular septal thickening in a patient with lymphangitic spread of breast carcinoma. Diffuse, smooth interlobular septal thickening outlines numerous pulmonary lobules, primarily in the right lung. In addition to septal thickening, there is increased prominence of the peribronchovascular interstitium most easily recognized as bronchial wall thickening (*arrow*, B). A small pneumothorax is visible on the right because of a recent thoracentesis.

P.77

Thickened interlobular septa also may be described using the terms *septal lines* or *septal thickening* (Figs. 3-8, 3-9, 3-10) [6], and are preferred to terms such as *peripheral lines*, *short lines*, and *interlobular lines* [12,39,44].

Similarly, although thickened septa outlining one or more pulmonary lobules have been described as producing a **"large reticular pattern"** [4,7] or **"polygons"** [45], and, if they can be seen contacting the pleural surface, as **"peripheral arcades"** or **"polygonal arcades"** [12], the terms *interlobular septal thickening*, *septal thickening*, and *septal lines* are considered more appropriate in describing these appearances [5,6].

Thickening of the interlobular septa is commonly seen in patients with interstitial lung disease. When visible as a predominant feature, however, it has a limited differential diagnosis (Table 3-2). Septal thickening can be smooth, nodular, or irregular in contour in different pathologic processes [46]. Smooth septal thickening is seen in patients with pulmonary edema or hemorrhage (Fig. 3-10) [28,47,48], lymphangitic spread of carcinoma (Figs. 3-8 and

3-9) [11,12,49], lymphoma, leukemia, interstitial infiltration associated with amyloidosis [50], and some pneumonias, and in a small percentage of patients with pulmonary fibrosis. Smooth septal thickening may also be seen in association with ground-glass opacity, a pattern termed *crazy-paving*; this pattern is typical of alveolar proteinosis (Fig. 3-11) but has a long differential diagnosis which is reviewed elsewhere [51,52,53,54,55]. **Nodular or "beaded"** septal thickening occurs in lymphangitic spread of carcinoma or lymphoma (Figs. 3-12 and 3-13) [11,12,49], sarcoidosis, silicosis or coal worker's pneumoconiosis (CWP) [20,21,56,57,58], LIP [17,18,19], and amyloidosis [50,59]. In patients who have interstitial fibrosis, septal thickening visible on HRCT is often irregular in appearance (Figs. 3-14, 3-15, 3-16) [32]. A simple algorithm (Algorithm 1) based on the recognition of these findings may be used for diagnosis.



FIG. 3-10. Interlobular septal thickening resulting from pulmonary edema. Prone HRCT shows thickening of numerous interlobular septa in the dependent lung and over the pleural surfaces. Septa within the dependent lung are thickest. Centrilobular arteries appear prominent within

most of the lobules surrounded by thickened septa, a finding that reflects thickening of the centrilobular interstitium. Peribronchovascular interstitial thickening is also present.

P.78

Pulmonary disease occurring predominantly in relation to interlobular septa and the periphery of lobules has been termed *perilobular* [60,61]. Johkoh et al. [55,61] have emphasized that a perilobular distribution of disease may reflect abnormalities of the peripheral alveoli and subpleural interstitium in addition to thickening of interlobular septa. Although interlobular septal thickening can be seen on HRCT in association with fibrosis and honeycombing [44], it is not usually a predominant feature [8,42,62]. Generally speaking, in the presence of significant fibrosis and honeycombing, distortion of lung architecture makes the recognition of thickened septa difficult (Fig. 3-15). Among **patients with pulmonary fibrosis and “end-stage” lung disease**, the presence of interlobular septal thickening on HRCT is most frequent in patients with sarcoidosis (Fig. 3-16) (56% of patients) and is less common in those with usual interstitial pneumonia (UIP) of various causes (Fig. 3-17), asbestosis, and hypersensitivity pneumonitis [62]. The frequency of septal thickening and fibrosis in patients with sarcoidosis reflects the tendency of active sarcoid granulomas to involve the interlobular septa. In patients with idiopathic pulmonary fibrosis (IPF) or UIP of another cause, the appearance of irregular septal thickening correlates with the presence of fibrosis predominantly affecting the periphery of the secondary lobule [8].

TABLE 3-2. *Differential diagnosis of interlobular septal thickening*

Diagnosis	Comments
Lymphangitic carcinomatosis, lymphoma, leukemia	Common; predominant finding in most; usually smooth; sometimes nodular
Lymphoproliferative disease (e.g., lymphocytic interstitial pneumonia)	Smooth or nodular; other abnormalities (i.e., nodules) typically present
Pulmonary edema	Common; predominant finding in most; smooth; ground-glass opacity can be present
Pulmonary hemorrhage	Smooth; associated with ground-glass opacity
Pneumonia (e.g., viral, <i>Pneumocystis carinii</i>)	Smooth; associated with ground-glass opacity
Sarcoidosis	Common; usually nodular or irregular; conglomerate masses of fibrous tissue

	with bronchiectasis typical in end stage
Idiopathic pulmonary fibrosis or other cause of usual interstitial pneumonia	Sometimes visible but not common; appears irregular; intralobular thickening and honeycombing usually predominate
Nonspecific interstitial pneumonia	With findings of ground-glass opacity and reticulation
Silicosis/coal worker's pneumoconiosis; talcosis	Occasionally visible; nodular when active; irregular in end-stage disease
Asbestosis	Sometimes visible; irregular
Hypersensitivity pneumonitis (chronic)	Uncommon; irregular reticular opacities and honeycombing usually predominate
Amyloidosis	Smooth or nodular

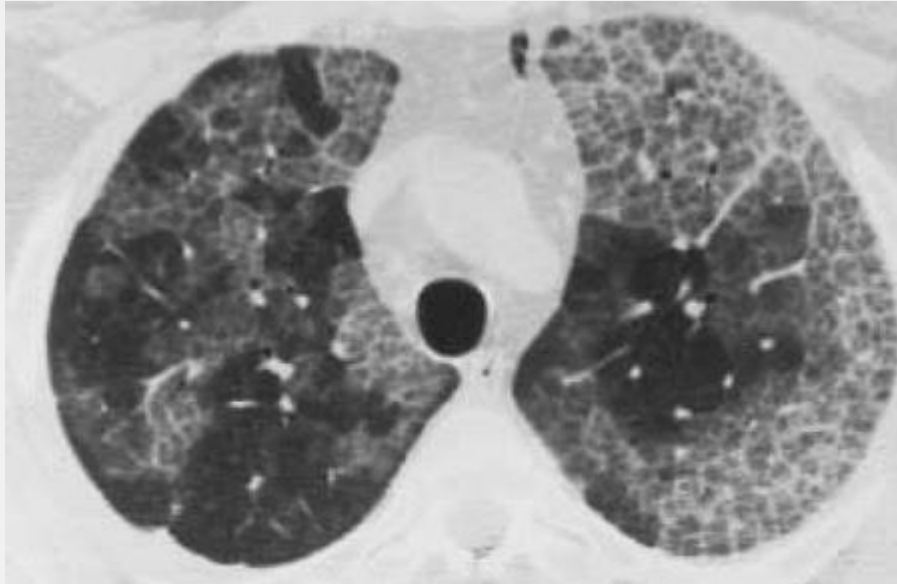


FIG. 3-11. Interlobular septal thickening in alveolar proteinosis. Thickened septa are associated with ground-glass opacity. This appearance is typical of alveolar proteinosis.

P.79

Parenchymal Bands

The term *parenchymal band* has been used to describe a nontapering, reticular opacity, usually several millimeters in thickness and from 2 to 5 cm in length, seen in patients with atelectasis, pulmonary fibrosis, or other causes of interstitial thickening (Figs. 3-1, 3-16, and 3-18) [6,39,63]. A parenchymal band is often peripheral and generally contacts the pleural surface, which may be thickened and retracted inward.

In some patients, these bands represent contiguous thickened interlobular septa and have the same significance and differential diagnosis as septal thickening [44]. When

parenchymal bands can be identified as thickened septa (Figs. 3-16 and 3-18), the use of a separate term to describe this finding is unjustified; the term *septal thickening* should suffice.

However, parenchymal bands visible on HRCT can also represent areas of peribronchovascular fibrosis, coarse scars, or atelectasis associated with lung infiltration or pleural fibrosis (Figs. 3-19, 3-20, 3-21) [44,64]. These nonseptal bands are often several millimeters thick and irregular in contour and are associated with significant distortion of adjacent lung parenchyma and bronchovascular structures [65].

Parenchymal bands have been reported as most common in patients with asbestos-related lung and pleural disease (Fig. 3-21), sarcoidosis with interstitial fibrosis (Figs. 3-16 and 3-18) [20], silicosis associated with progressive massive fibrosis and conglomerate masses, and tuberculosis (Table 3-3). In patients with asbestos exposure, multiple parenchymal bands are common; in one study [39], multiple parenchymal bands were seen in 66% of asbestos-exposed patients. In patients with asbestos-related disease, parenchymal bands can reflect thickened interlobular septa, indicating pulmonary fibrosis, or, more often, areas of atelectasis and focal scarring occurring in association with pleural plaques. In asbestos-exposed patients, parenchymal bands are frequently associated with areas of thickened pleura and have a basal predominance [39,64].

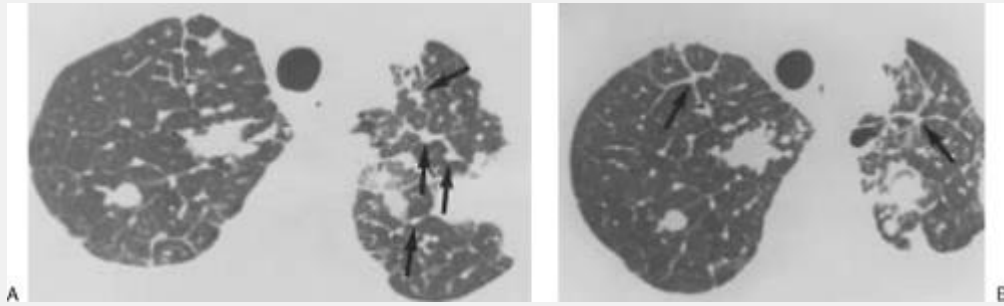


FIG. 3-12. "Beaded" or nodular septal thickening with lymphangitic spread of carcinoma. A, B: Generalized septal thickening is associated with some nodularity (arrows); this has been termed the beaded septum sign. Septa are well defined. Several large nodules are also visible in the lung. This is a common appearance in patients with lymphangitic spread of carcinoma.

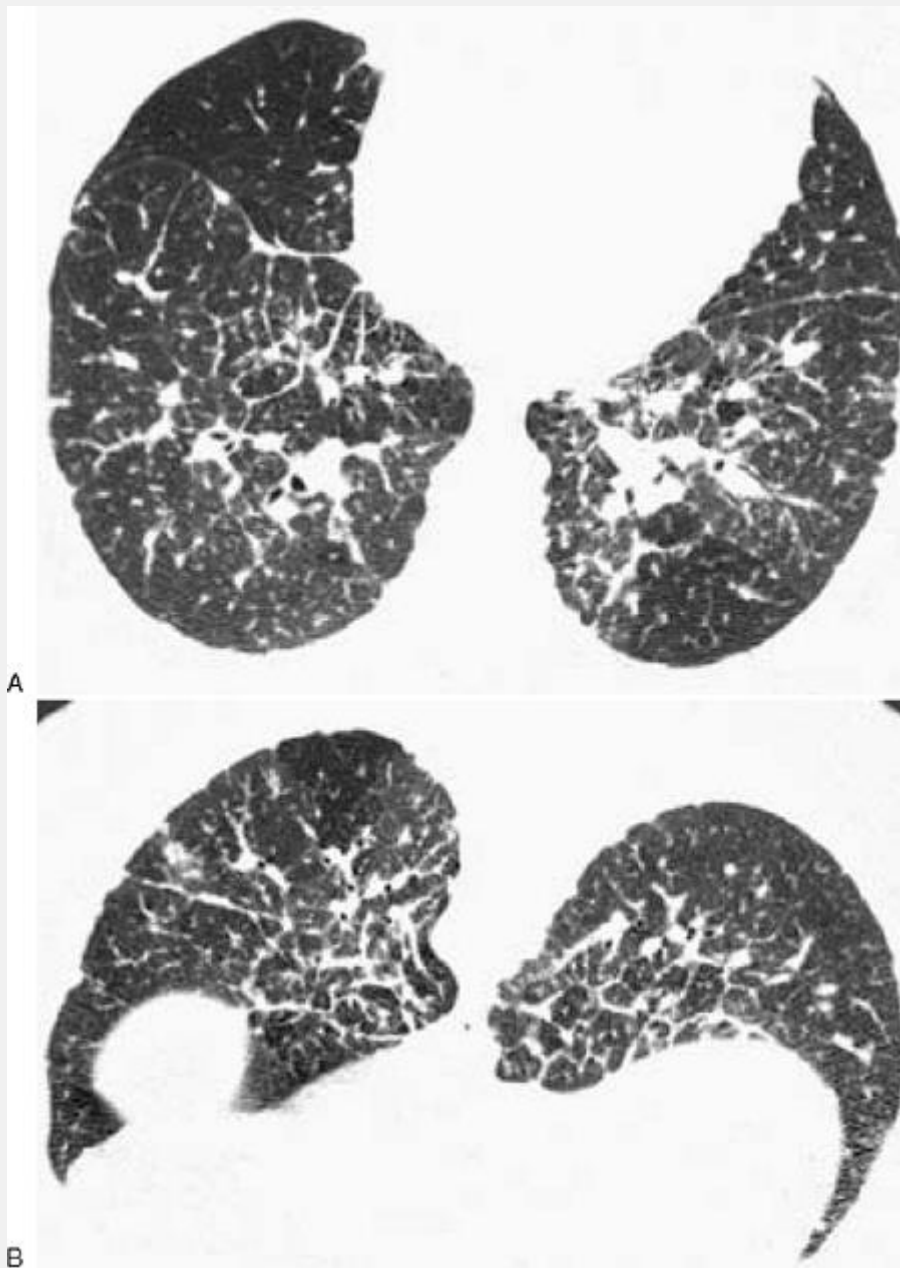


FIG. 3-13. Nodular septal thickening in a patient with sarcoidosis. Septal thickening at the lung bases is associated with a distinct nodularity on supine (A) and prone (B) scans. In patients with sarcoidosis, this appearance correlates with the presence of septal granulomas.

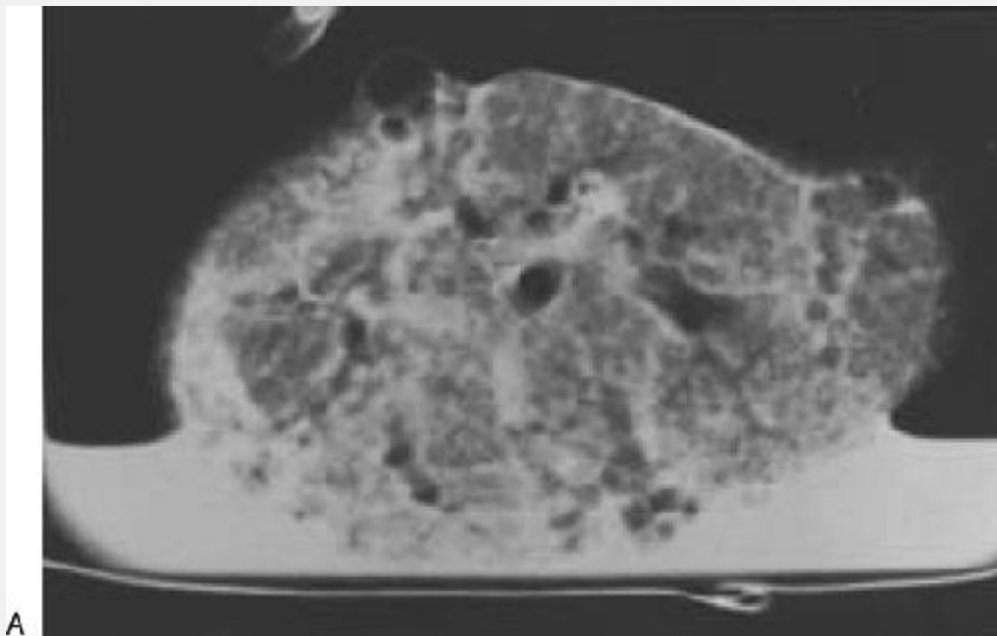


FIG. 3-14. Pulmonary fibrosis in an isolated inflated lung specimen. Scans performed with 1-cm collimation and conventional technique (A) and with HRCT technique (B). On the HRCT scan, a lobule at the lung surface is well shown. It is margined with irregularly thickened interlobular septa (*small arrows*). Intralobular interstitial thickening is visible as a fine network of lines. The intralobular bronchiole is also visible (*white arrow*). The subpleural interstitium is thickened. These findings are not clearly shown with conventional technique. (B from Webb WR. HRCT of the lung parenchyma. *Radiol Clin North Am* 1989;27:1085, with permission.)

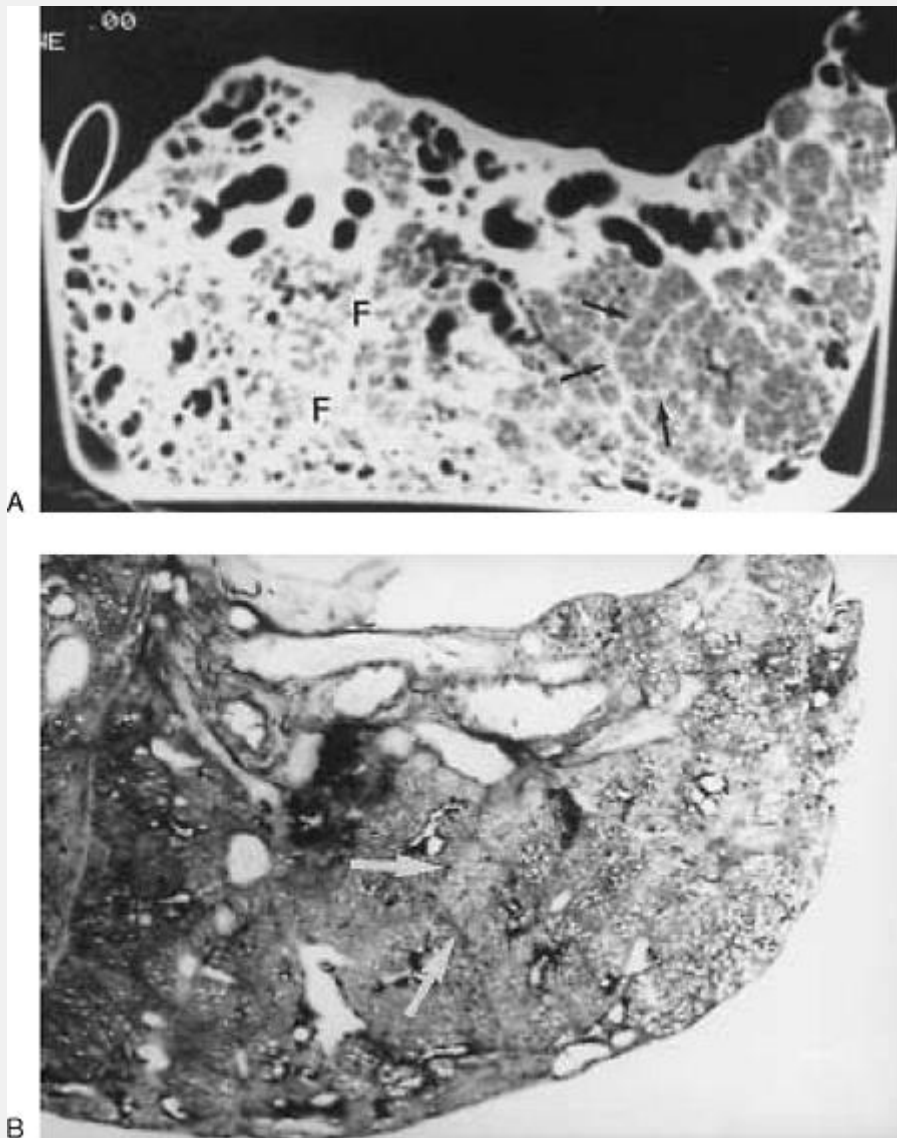


FIG. 3-15. HRCT of pulmonary fibrosis in an isolated inflated lung. The HRCT (A) and the corresponding lung section (B) are shown for comparison. Typical HRCT findings of fibrosis include interlobular septal thickening that is irregular in contour (*arrows*) and subpleural interstitial thickening shown at the lung surfaces and adjacent to the major fissure (F). (From Webb WR, Stein MG, et al. Normal and diseased isolated lungs: HRCT. *Radiology* 1988;166:81, with permission.)

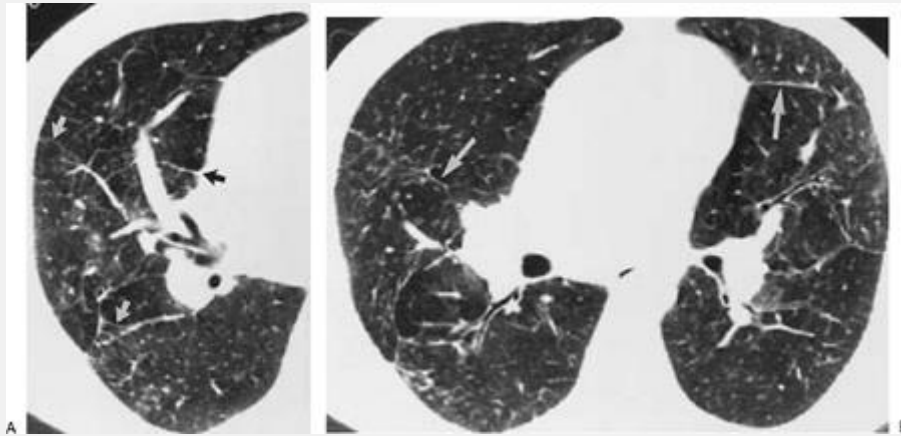


FIG. 3-16. Interlobular septal thickening and parenchymal bands in a patient with end-stage sarcoidosis. A: Septa (*arrows*) appear irregular in contour, a finding usually associated with fibrosis. B: Longer lines (*arrows*) are parenchymal bands. As in this patient, these often represent several contiguous thickened septa. Lung distortion is also present, indicative of fibrosis.

P.80

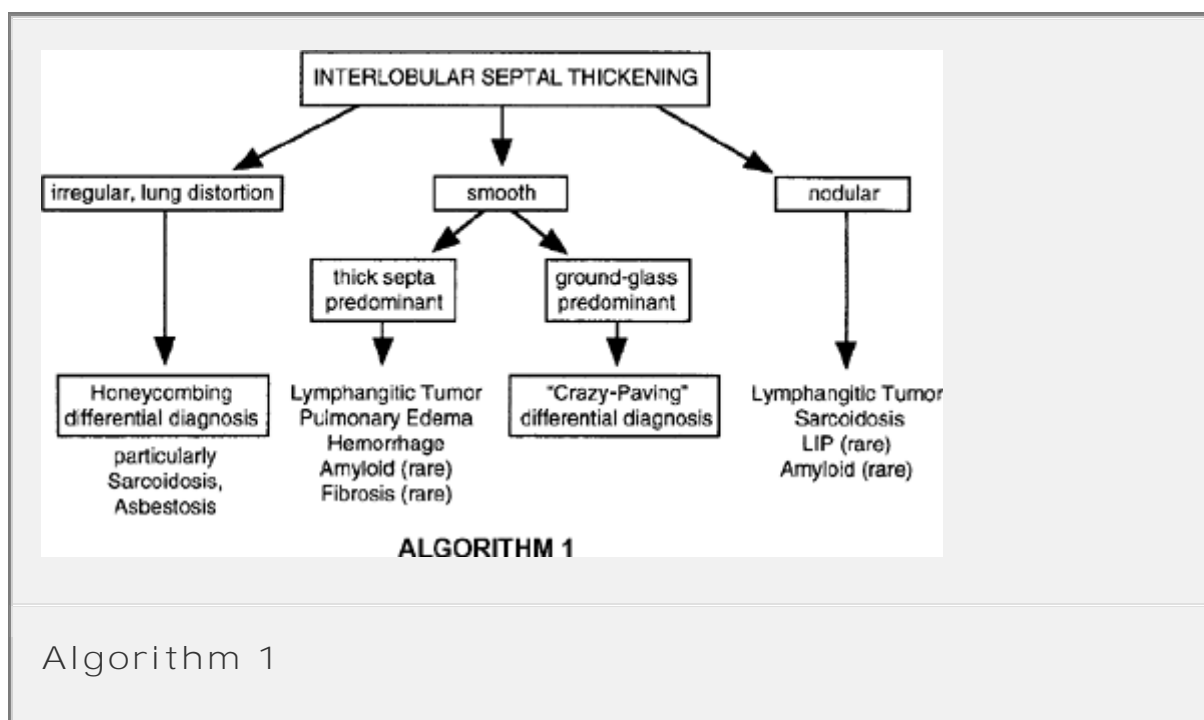
P.81

P.82

Subpleural Interstitial Thickening

Usually, thickening of the interlobular septa within the peripheral lung is associated with thickening of the subpleural interstitium [3,4]; both the septa and the

subpleural interstitium are part of the peripheral interstitial fiber system described by Weibel (see 2-1) [10]. Subpleural interstitial thickening can be difficult to recognize in locations where the lung contacts the chest wall or mediastinum but is easy to see adjacent to the major fissures (Figs. 3-1, 3-4, 3-8, and 3-22). Because two layers of the subpleural interstitium are seen adjacent to each other in this location, any subpleural abnormality appears twice as abnormal as it does elsewhere. Thus, thickening of the fissure visible on HRCT often represents subpleural interstitial thickening. If the thickening is smooth, it may be difficult to distinguish from fissural fluid. If the interface sign is present and the thickening is irregular in appearance (Fig. 3-22) [4,7], or if the thickening is nodular (Figs. 3-4 and 3-8), an interstitial abnormality is more easily diagnosed.



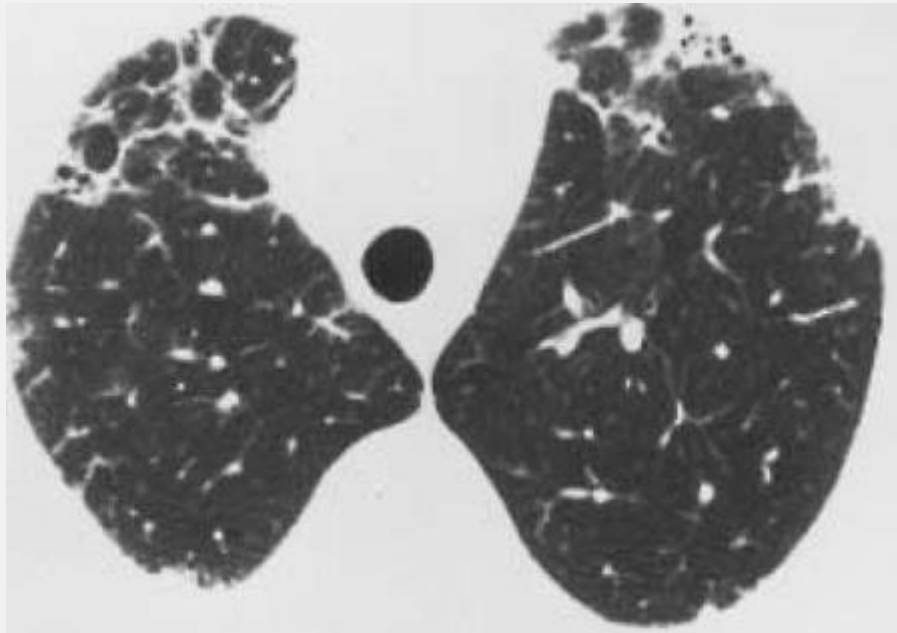


FIG. 3-17. Interlobular septal thickening in a patient with rheumatoid lung disease. Numerous irregularly thickened septa are visible in the anterior right lung.

P.83

In general, the differential diagnosis of subpleural interstitial thickening is the same as that of interlobular septal thickening, although subpleural interstitial thickening is more common than septal thickening in patients with IPF or UIP of any cause (Table 3-2). The presence of subpleural **interstitial fibrosis with irregular or “rugged” pleural** surfaces has been reported by Nishimura et al. [8] as a common finding in IPF, correlating with the presence of fibrosis predominantly affecting the lobular periphery; this finding was present in 94% of the cases of IPF that he studied. A subpleural predominance of fibrosis can also be

seen in patients with collagen-vascular diseases and drug-related fibrosis [66].

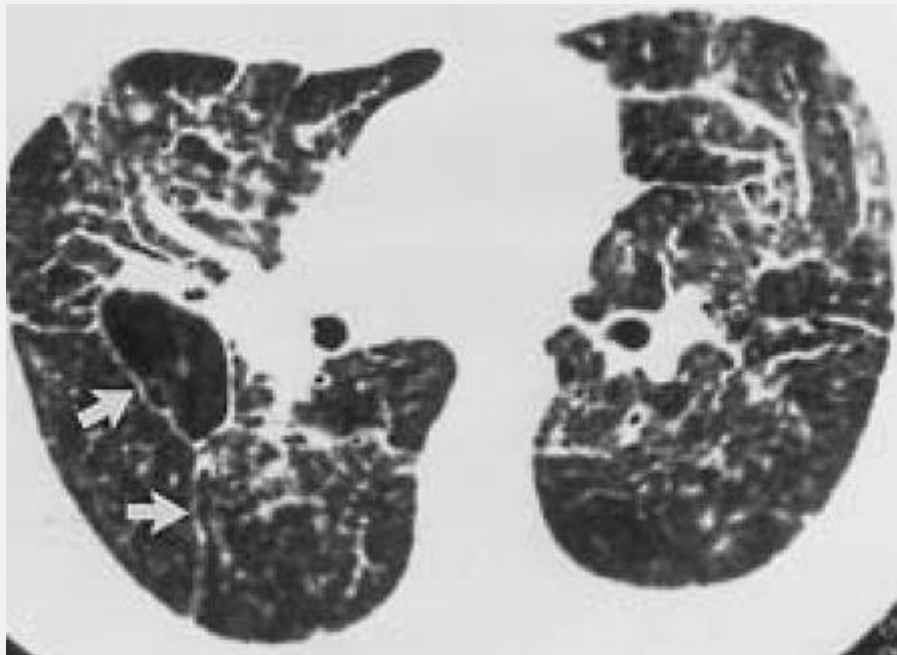


FIG. 3-18. Pulmonary fibrosis and parenchymal bands in a patient with sarcoidosis. Irregular septal thickening is present with distortion of lung architecture. Long confluent septa or parenchymal bands (*arrows*) are present bilaterally. Peribronchovascular interstitial thickening also results in prominence of the bronchi and pulmonary vessels. The pleural surfaces and the walls of vessels and bronchi appear irregular.

Nodular thickening of the subpleural interstitium can also be seen (Fig. 3-4), and it has the same differential diagnosis as nodular septal thickening [57]. Remy-Jardin et al. [57] have reported the appearance of *subpleural micronodules*, defined as 7 mm or less in diameter, on HRCT in patients with sarcoidosis, CWP, lymphangitic spread of carcinoma, and LIP, and in a small percentage of normal subjects.

Subpleural nodules are described further in the section Perilymphatic Distribution.

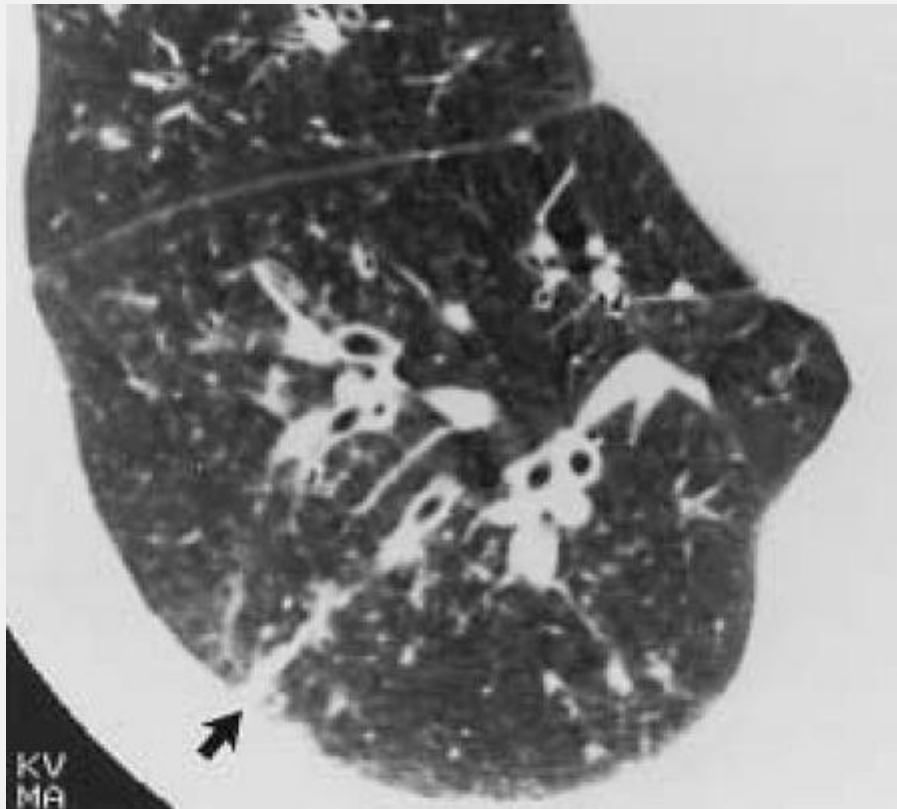


FIG. 3-19. Thick parenchymal band (arrow) represents a coarse scar in the peripheral lung. Also note thickening of the bronchial walls because of peribronchovascular fibrosis.

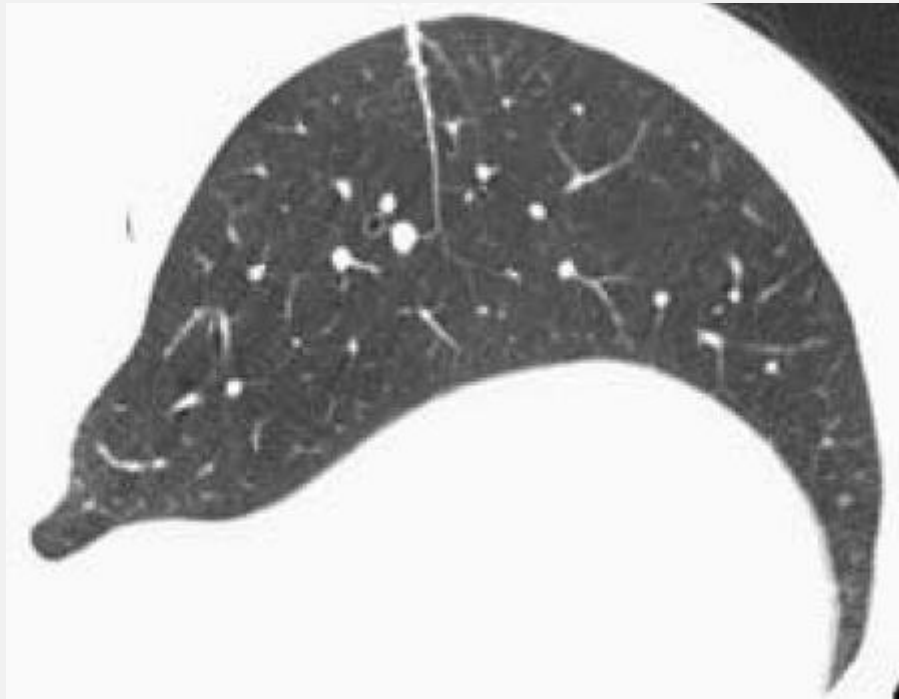


FIG. 3-20. Parenchymal band in a patient with otherwise normal lungs. This likely represents an isolated scar.

P.84

Intralobular Interstitial Thickening

Thickening of the intralobular interstitium (see 2-1) results in a fine reticular pattern as seen on HRCT, with the lines of opacity separated by a few millimeters [32]. Lung regions showing this finding characteristically have a fine lace- or netlike appearance that is easy to recognize (Figs. 3-1 and 3-23, 3-24, 3-25 3-26). This appearance is nonspecific and may be associated with interstitial fibrosis or diffuse interstitial infiltration in the absence of fibrosis. The presence of intralobular interstitial thickening can also be described using the term *intralobular lines* [6]. This finding

is responsible for the "small reticular pattern" described by Zerhouni [7].

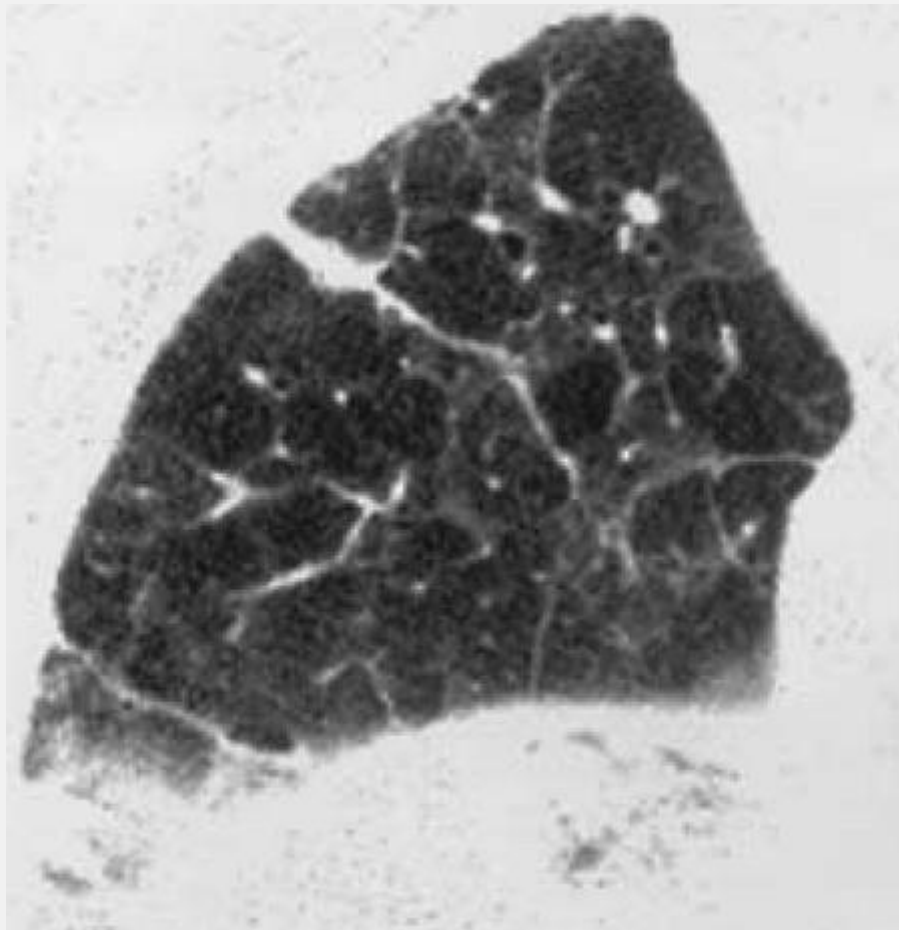


FIG. 3-21. Parenchymal bands in a patient with asbestosis. A prone scan shows both thick and thin bands. Most correspond to thickened septa.

TABLE 3-3. *Differential diagnosis of parenchymal bands*

Diagnosis	Comments
Asbestosis	Multiple parenchymal bands common; smooth; associated with thickened pleura
Sarcoidosis	Common; associated with septal thickening
Silicosis/coal worker's pneumoconiosis	In association with progressive massive fibrosis and emphysema
Tuberculosis	Associated with scarring

In patients with intralobular interstitial thickening resulting from fibrosis, intralobular bronchioles may be visible in the peripheral lung. This results from a combination of their dilatation (i.e., traction bronchiolectasis) and thickening of the peribronchiolar interstitium that surrounds them (Figs. 3-1, 3-23, and 3-24) [8,32]. Traction bronchiectasis, dilatation of large bronchi occurring because of fibrosis, may also be seen (Figs. 3-27 and 3-28). Interlobular septal thickening may or may not be present in patients who have intralobular interstitial thickening; when thickened septa are visible, they usually appear irregular. The pleural surfaces also appear irregular in the presence of intralobular interstitial thickening.

Intralobular interstitial thickening as perceived on HRCT reflects thickening of the distal peribronchovascular

interstitial tissues and the intralobular interstitium. As an isolated finding, it is most commonly seen in patients with pulmonary fibrosis (Figs. 3-23, 3-24, 3-25, 3-26, 3-27, 3-28) (Table 3-4). In patients who have IPF or other causes of UIP, such as rheumatoid arthritis, scleroderma, or other collagen-vascular diseases, fibrosis tends to predominantly involve alveoli in the periphery of acini, resulting in a **“peripheral acinar distribution” of interstitial fibrosis** [8,66]; this histologic finding correlates with the presence of intralobular lines on HRCT. In addition, the HRCT pattern of intralobular interstitial thickening can reflect the presence of very small honeycomb cysts or dilated bronchioles associated with surrounding lung fibrosis. Nishimura et al. [8] reviewed 46 cases of IPF with UIP, correlating findings on CT with appearances of lung histology from open biopsy specimens or autopsy. Visibility of centrilobular bronchioles in association with a fine reticulation or increased lung attenuation was found in 96% of cases, indicating the presence of bronchiolar dilatation, fibrosis, and **“microscopic” honeycombing, with dilated bronchioles or** small cysts measuring approximately 1 mm in diameter [8]. Intralobular lines, resulting in a fine reticular pattern, can also be seen in patients with NSIP [22,67,68,69]. In this entity, the appearance of intralobular lines or irregular linear opacities correlated with the presence of interstitial fibrosis and was often associated with bronchial or bronchiolar dilatation (traction bronchiectasis or bronchiolectasis) [22]. In a study of HRCT appearances of various idiopathic interstitial pneumonias, intralobular lines were visible in 97% of patients with UIP, 93% of patients with NSIP, 78% of patients with desquamative interstitial pneumonia (DIP), 71% of patients with bronchiolitis

obliterans organizing pneumonia (BOOP), and 70% of patients with acute interstitial pneumonia (AIP) [67].

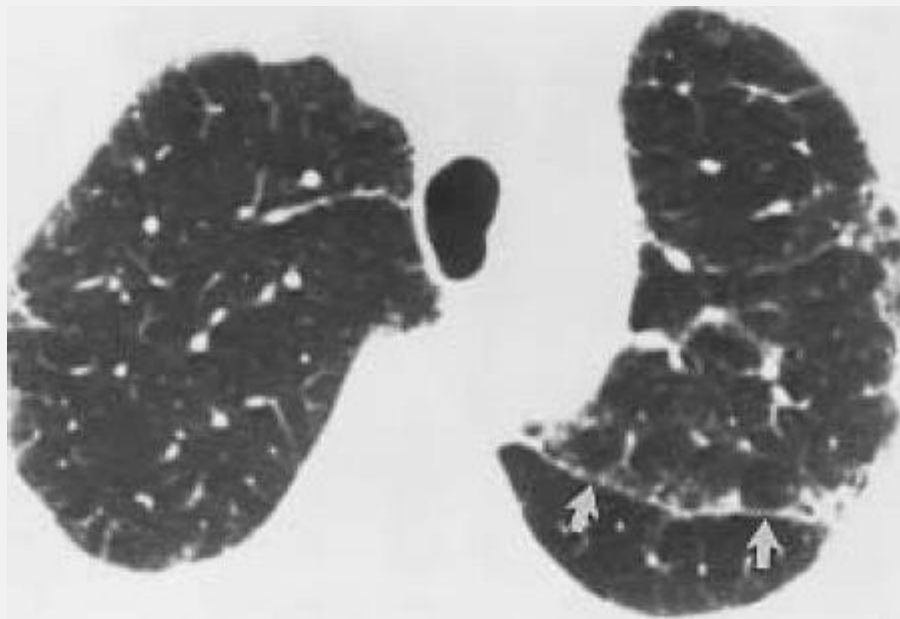


FIG. 3-22. Subpleural interstitial thickening in a patient with pulmonary fibrosis. Apparent thickening of the left major fissure (arrows) reflects irregular thickening of the subpleural interstitium. This finding is easiest to recognize adjacent to the fissures.

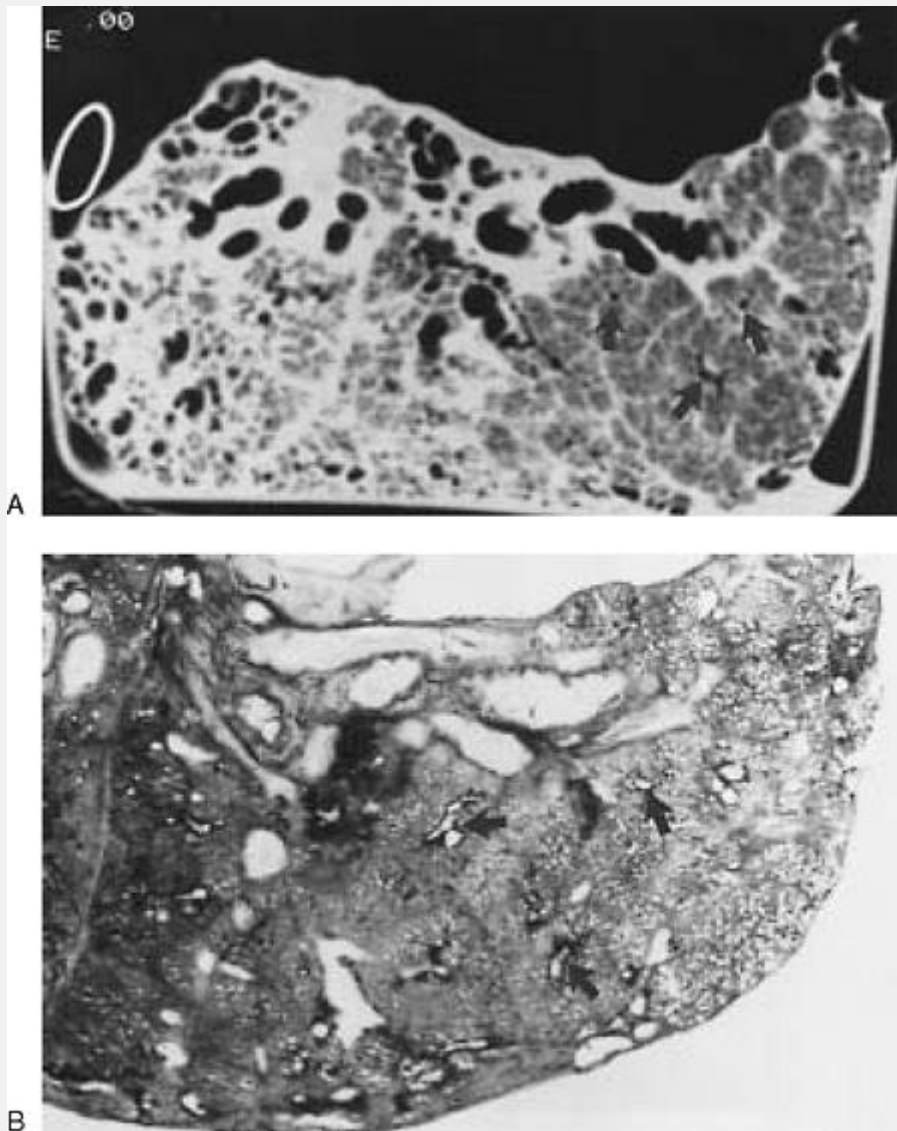


FIG. 3-23. Intralobular interstitial thickening in an isolated lung with pulmonary fibrosis. This is the same specimen as shown in Figure 3-15. A fine network of lines within visible lobules produces a "spider-web" or "netlike" appearance (A). This abnormality contributes to the appearance of irregular interfaces (the "interface sign") at the edges of various structures such as arteries and bronchi. Intralobular bronchioles (*arrows*, A and B) are visible because of a combination of increased attenuation of surrounding lung, thickening of the peribronchiolar interstitium, and dilatation

of the bronchiole that occur as a result of fibrosis. (From Webb WR, Stein MG, et al. Normal and diseased isolated lungs: HRCT. *Radiology* 1988;166:81, with permission.)

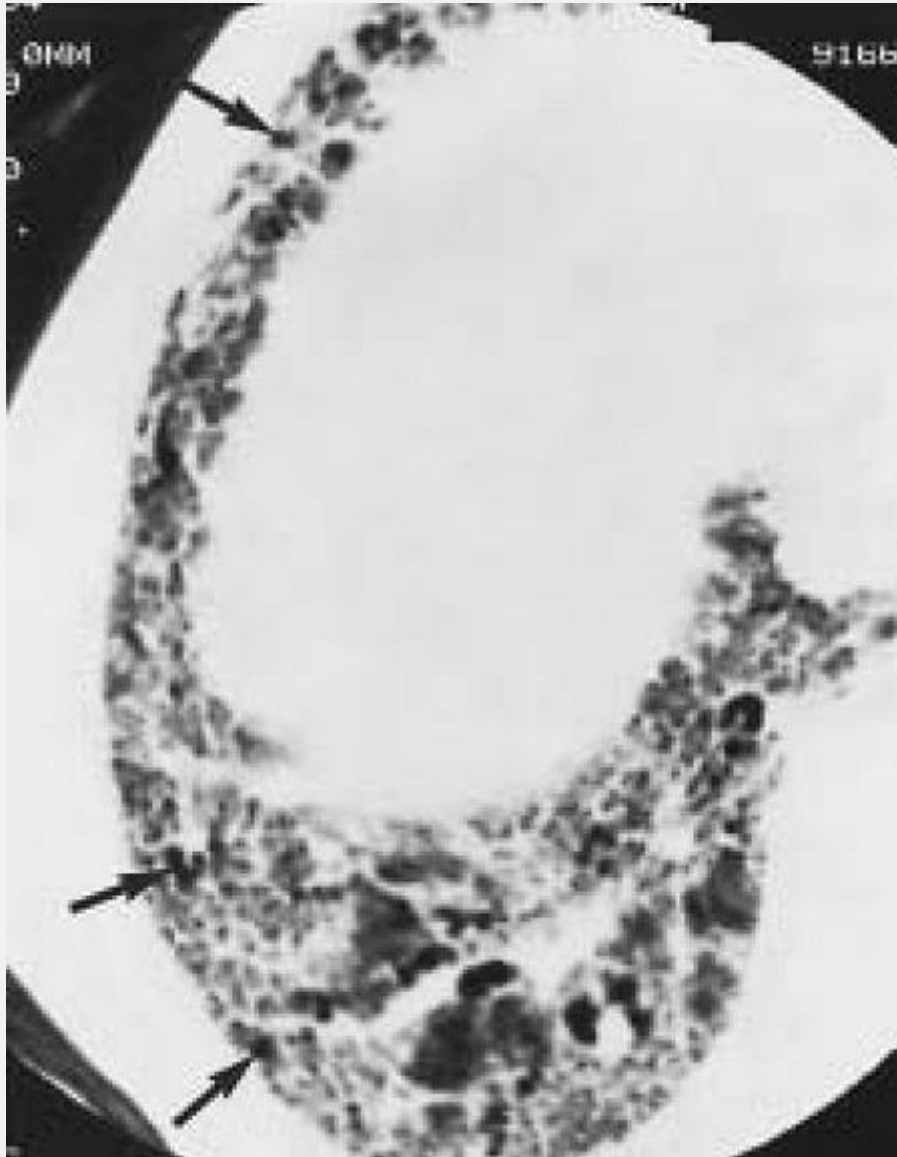


FIG. 3-24. Intralobular interstitial thickening in a patient with idiopathic pulmonary fibrosis. A fine network of lines is visible. Intralobular bronchioles (arrows) are visible throughout the peripheral lung as a result of fibrosis and traction bronchiolectasis.

P.85

P.86

Intralobular interstitial thickening can also be seen in the absence of significant fibrosis in patients with a variety of infiltrative lung diseases. When this is the case, traction bronchiectasis or other manifestations of fibrosis are absent. Intralobular interstitial thickening may be seen in association with interlobular septal thickening in patients with diseases such as lymphangitic spread of carcinoma [11] and pulmonary edema (Algorithm 2). The differential diagnosis of this is identical to that of interlobular septal thickening. Intralobular lines may also be seen in patients with ground-glass opacity or the pattern of crazy-paving, in association with diseases such as pulmonary hemorrhage, some pneumonias (e.g., *Pneumocystis carinii*, cytomegalovirus), and alveolar proteinosis (Fig. 3-11).

Honeycombing

Extensive interstitial and alveolar fibrosis that results in alveolar disruption and bronchiolectasis produces the classic and characteristic appearance of *honeycombing* or *honeycomb lung*. Pathologically, honeycombing is defined by the presence of small air-containing cystic spaces, generally lined by bronchiolar epithelium and having thickened walls composed of dense fibrous tissue. Honeycombing indicates the presence of end-stage lung and can be seen in many diseases leading to end-stage pulmonary fibrosis (Table 3-5) [62,70].

Honeycombing produces a characteristic cystic appearance on HRCT that allows a confident diagnosis of lung fibrosis [32,42]. On HRCT, the cystic spaces of honeycombing usually average 1 cm in diameter, although they can range from several millimeters to several centimeters in size; they are characterized by clearly definable walls 1 to 3 mm in thickness [32,42] (Figs. 3-1, 3-2, 3-29, and 3-30). The cysts are air-filled and appear lucent in comparison to normal lung parenchyma. Adjacent honeycomb cysts typically share walls. Although there is some overlap between the appearances of fine honeycombing and intralobular interstitial thickening, if the spaces between the lines (i.e., the cysts) appear to be air-filled (i.e., black), rather than having the density of lung parenchyma, honeycombing is present. Honeycombing has been described **by Zerhouni and associates as producing an “intermediate reticular pattern” to distinguish it from the larger pattern** seen with interlobular septal thickening and the smaller pattern visible with intralobular interstitial thickening [7].

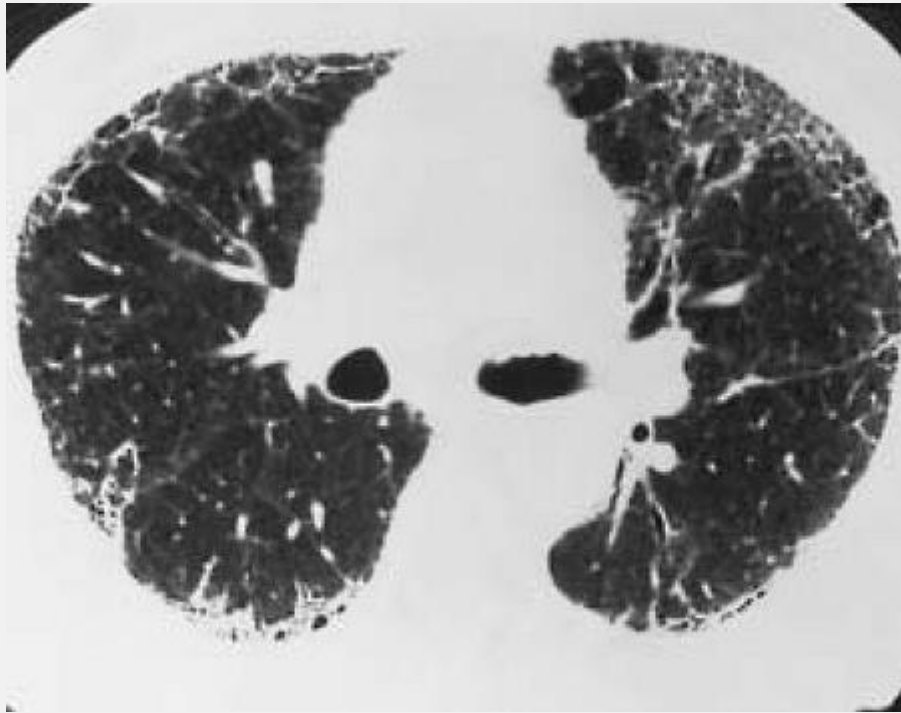


FIG. 3-25. Intralobular interstitial thickening in a patient with idiopathic pulmonary fibrosis. A fine network of lines in the anterior left lung reflects intralobular interstitial thickening.

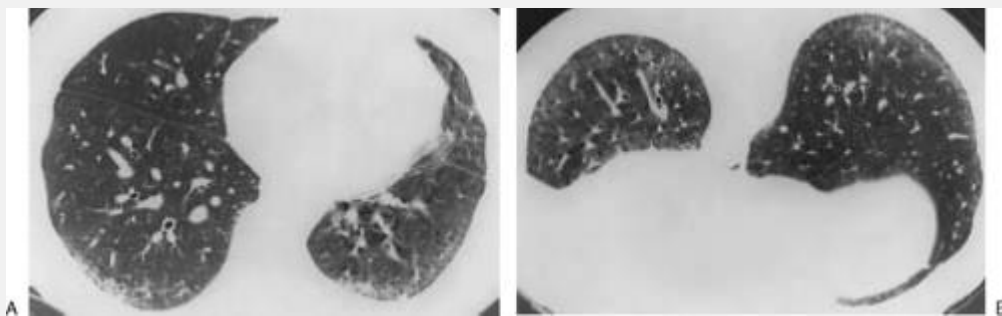


FIG. 3-26. Intralobular interstitial thickening in a patient with idiopathic pulmonary fibrosis. A: On a supine scan, an

ill-defined increase in opacity is visible posteriorly. This would be difficult to diagnose as abnormal with certainty on this scan alone. B: In the prone position, a very fine reticular or weblike pattern is visible posteriorly in the peripheral lung, along with a few thickened septa. This appearance is typical of intralobular interstitial thickening. The peripheral distribution is characteristic of idiopathic pulmonary fibrosis.

P.87

Honeycomb cysts often predominate in the peripheral and subpleural lung regions regardless of their cause, and perihilar lung can appear normal despite the presence of extensive peripheral abnormalities (Figs. 3-30, 3-31, 3-32, 3-33). Subpleural honeycomb cysts typically occur in several contiguous layers (Figs. 3-31, 3-32, 3-33). This finding can allow honeycombing to be distinguished from subpleural emphysema (paraseptal emphysema); in paraseptal emphysema, subpleural cysts usually occur in a single layer. Lung consolidation in a patient with emphysema can mimic the appearance of honeycombing.

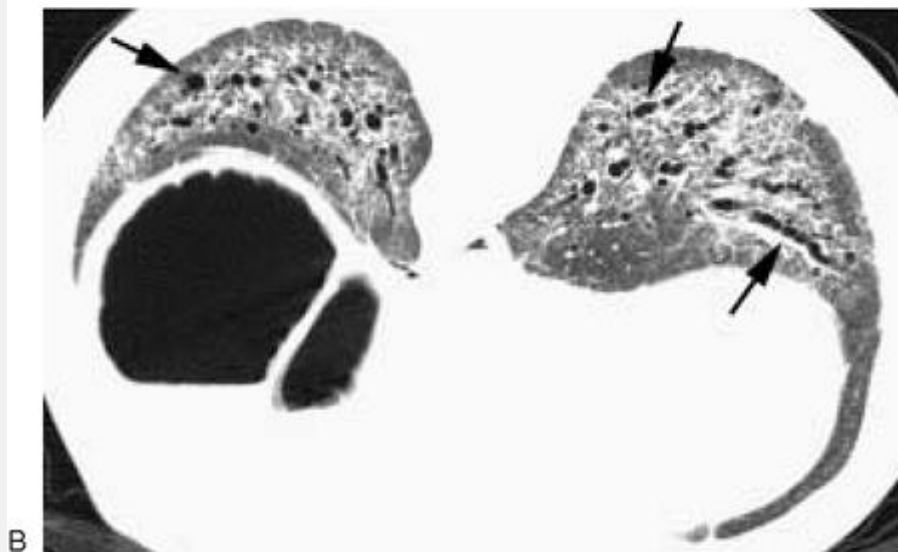
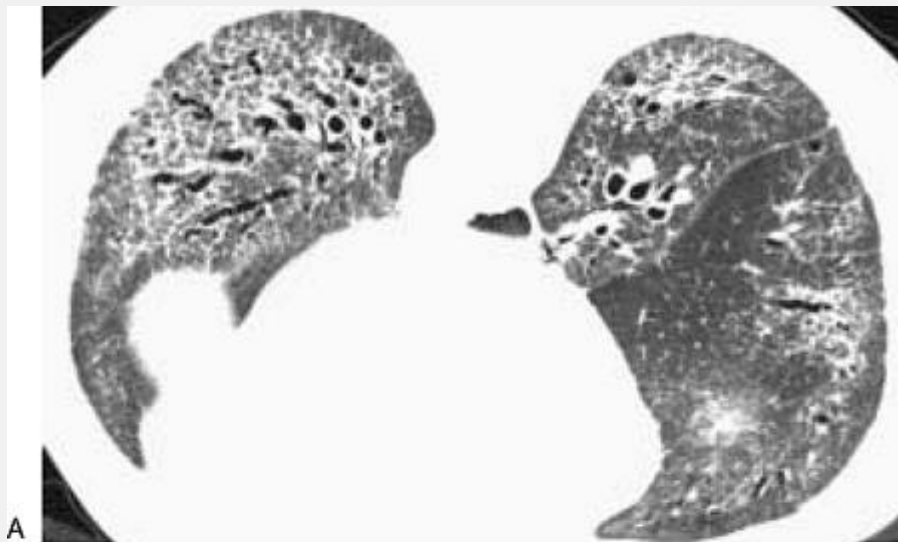
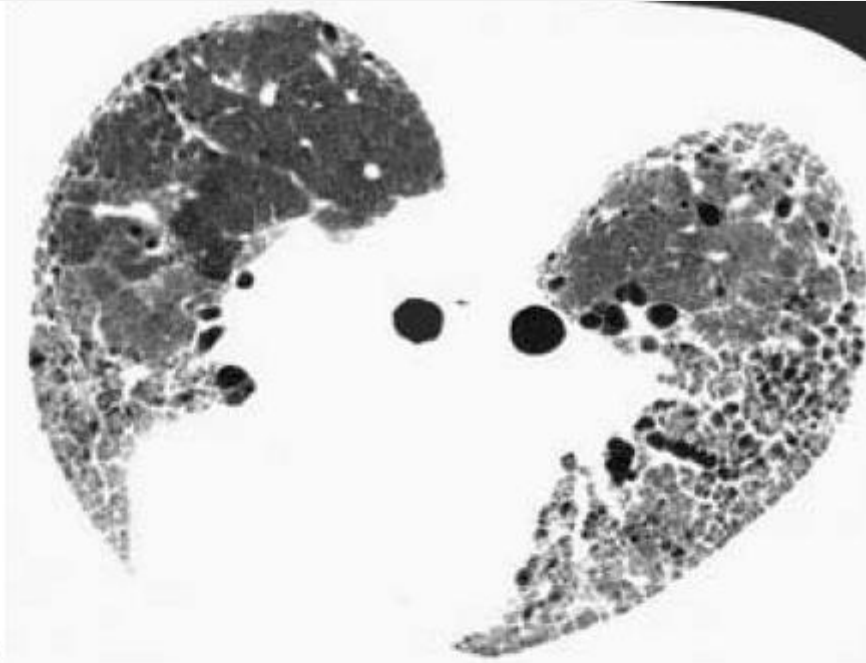
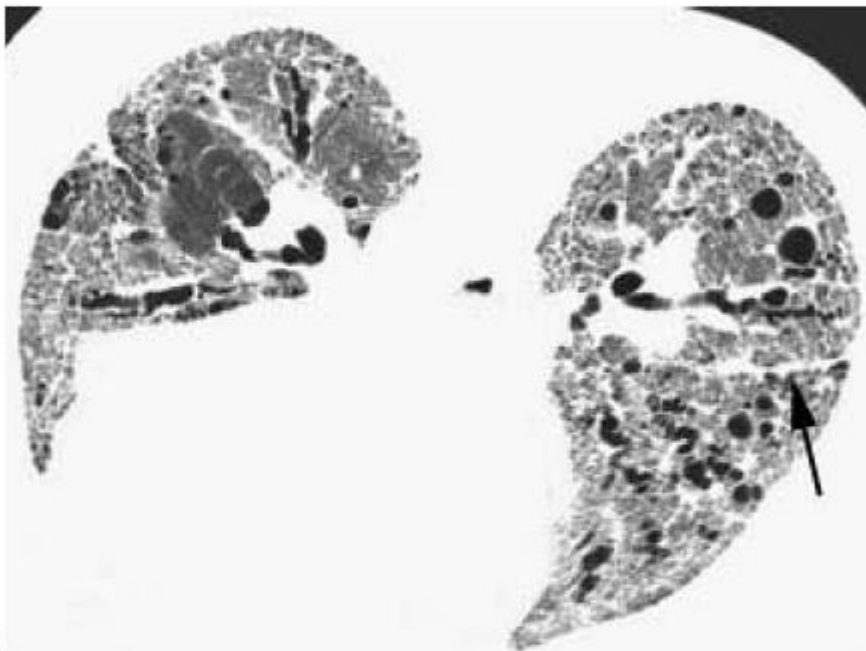


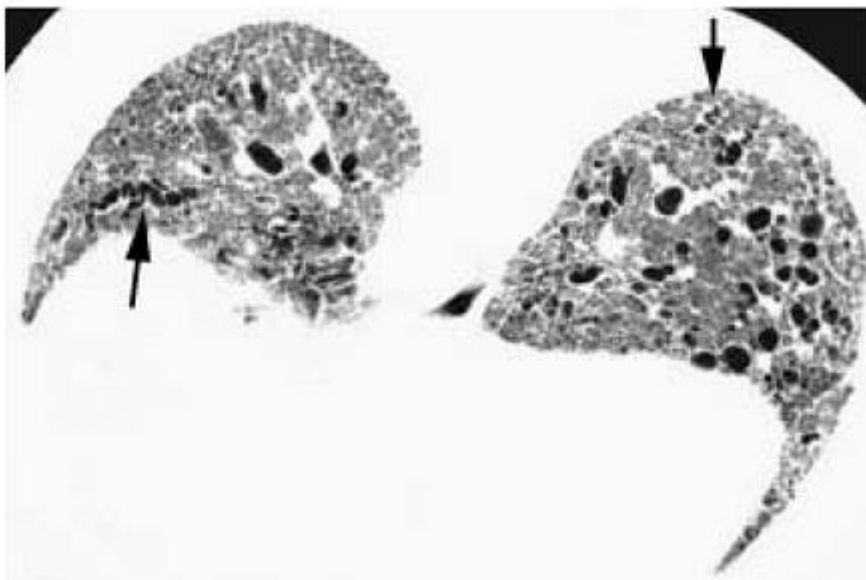
FIG. 3-27. Prone scans in a patient with idiopathic pulmonary fibrosis. A: Abnormal reticulation represents intralobular interstitial thickening. B: At a lower level, traction bronchiectasis and bronchiolectasis (arrows) are easily seen.



A



B



C

FIG. 3-28. Prone scans in a patient with idiopathic pulmonary fibrosis. A: Abnormal reticulation representing intralobular interstitial thickening predominates in the subpleural lung. B: At a lower level, fibrosis is more extensive. Traction bronchiectasis and bronchiolectasis are predominant features. Also note irregular thickening of the major fissure (*large arrow*) and irregular interlobular septal thickening. C: Typically, traction bronchiectasis and bronchiolectasis are characterized by an irregular, varicose, or corkscrew appearance (*arrows*).

TABLE 3-4. *Differential diagnosis of intralobular interstitial thickening*

Diagnosis	Comments
Idiopathic pulmonary fibrosis or other cause of usual interstitial pneumonia	Common (97%); often associated with honeycombing
Hypersensitivity pneumonitis (chronic)	Common; associated with other findings of fibrosis
Asbestosis	Common; associated with other findings of fibrosis

Nonspecific interstitial pneumonia	Common (93%); ground-glass opacity commonly visible
Other idiopathic interstitial pneumonia (i.e., desquamative interstitial pneumonia, bronchiolitis obliterans organizing pneumonia, acute interstitial pneumonia)	Common (70%); other findings (i.e., ground-glass opacity, consolidation also present)
Lymphangitic carcinomatosis; lymphoma; leukemia	Smooth or nodular; associated with septal thickening
Pulmonary edema	Smooth; associated with septal thickening and ground-glass opacity
Pulmonary hemorrhage	Smooth; associated with septal thickening and ground-glass opacity
Pneumonia (e.g., viral, Pneumocystis carinii)	Smooth; associated with septal thickening and ground-glass opacity

Alveolar proteinosis	Smooth; associated with septal thickening and ground-glass opacity
----------------------	--

P.88

P.89

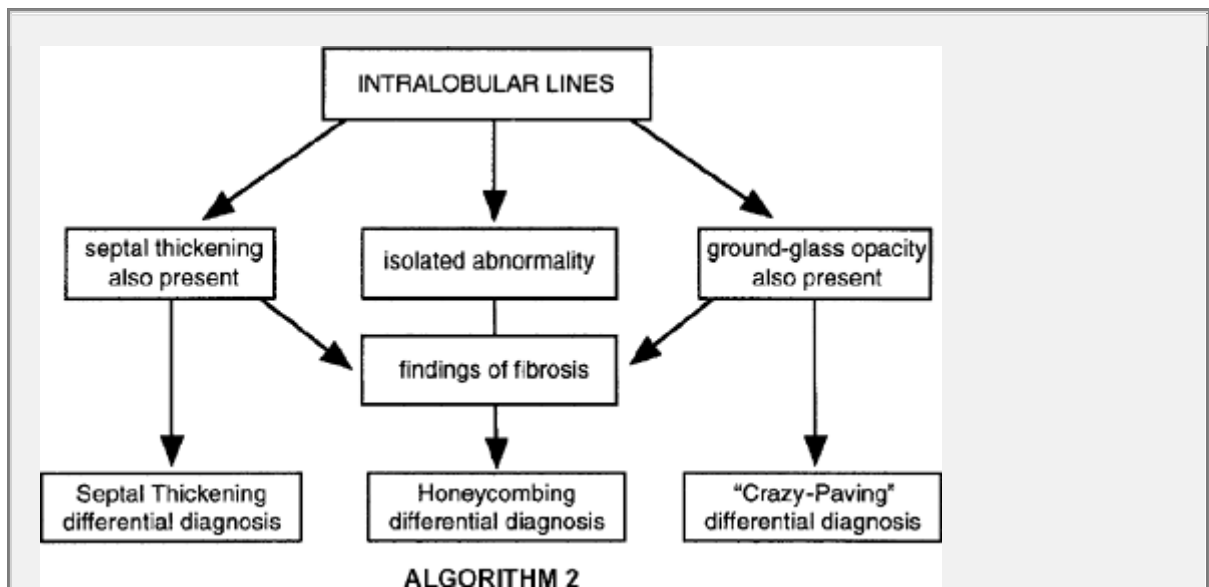
Honeycombing is often associated with other findings of lung fibrosis, such as architectural distortion, intralobular interstitial thickening, traction bronchiectasis, traction bronchiolectasis, irregular subpleural interstitial thickening, and irregular linear opacities (Fig. 3-29). On the other hand, significant interlobular septal thickening is not commonly visible in association with honeycombing, except in patients with sarcoidosis [62]. In patients with HRCT findings of septal thickening, the presence of honeycombing distinguishes fibrosis from other causes of reticulation, such as pulmonary edema or lymphangitic spread of carcinoma. The visible presence of honeycombing on HRCT is indicative of significant lung fibrosis and in most cases should lead to a diagnosis of UIP and a consideration of its most common causes, including IPF (Fig. 3-32); collagen-vascular diseases, most notably rheumatoid arthritis (Fig. 3-33) and

scleroderma; asbestosis; and drug-related fibrosis.

However, other diseases may also result in honeycombing that is visible on HRCT. In a survey of patients with end-stage lung [62], subpleural honeycombing was present in 96% of patients with UIP associated with IPF or rheumatoid arthritis, in 100% of asbestosis patients, in 44% of those with sarcoidosis, and in 75% of those with hypersensitivity pneumonitis (Table 3-5). Honeycombing is relatively uncommon in patients with NSIP [22,68,69]. In a study of HRCT appearances of proven cases of idiopathic interstitial pneumonias, honeycombing was visible in 71% of patients with UIP, 39% of patients with DIP, 30% of patients with AIP, 26% of patients with NSIP, and 13% of patients with BOOP [67].

The distribution of honeycombing is of some value in differential diagnosis (Algorithm 3). Honeycombing in patients with IPF and asbestosis is usually most severe in the subpleural lung regions and at the lung bases. The honeycombing in chronic hypersensitivity pneumonitis may be most marked in the subpleural lung regions, but is more often patchy in distribution, and tends to be most severe in the midlung zones with relative sparing of the lung bases [23,62]. Honeycombing in sarcoidosis may have an upper lobe predominance. In patients who have pulmonary fibrosis resulting from adult respiratory distress syndrome (ARDS) [71], findings of fibrosis on follow-up HRCT had a striking anterior distribution (see 6-76). This distribution of reticular opacities and lung fibrosis is unusual in other diseases. Lung fibrosis limited to anterior lung regions probably reflects the fact that patients with ARDS typically develop posterior lung atelectasis and consolidation during the acute phase of their disease; it is thought that consolidation

protects the posterior lung regions from the effects of mechanical ventilation, including high ventilatory pressures and high oxygen tension [71].



Algorithm 2

TABLE 3-5. *Differential diagnosis of honeycombing*

Diagnosis	Comments
Idiopathic pulmonary fibrosis or other cause of usual interstitial pneumonia such as collagen-vascular disease	Common (70%); peripheral, basal, and subpleural predominance
Asbestosis	Common in advanced disease; peripheral, basal, and subpleural

	predominance
Hypersensitivity pneumonitis (chronic)	Common in advanced disease; may be peripheral, patchy, or diffuse; midlung predominance common
Sarcoidosis	A few percent of cases; may be peripheral or patchy; upper lung predominance common
Nonspecific interstitial pneumonia	Uncommon (10-20%); other findings usually predominate
Other idiopathic interstitial pneumonia (i.e., desquamative interstitial pneumonia, bronchiolitis obliterans organizing pneumonia, acute interstitial pneumonia)	Uncommon (10-20%); other findings usually predominate
Silicosis/coal worker's pneumoconiosis	Uncommon

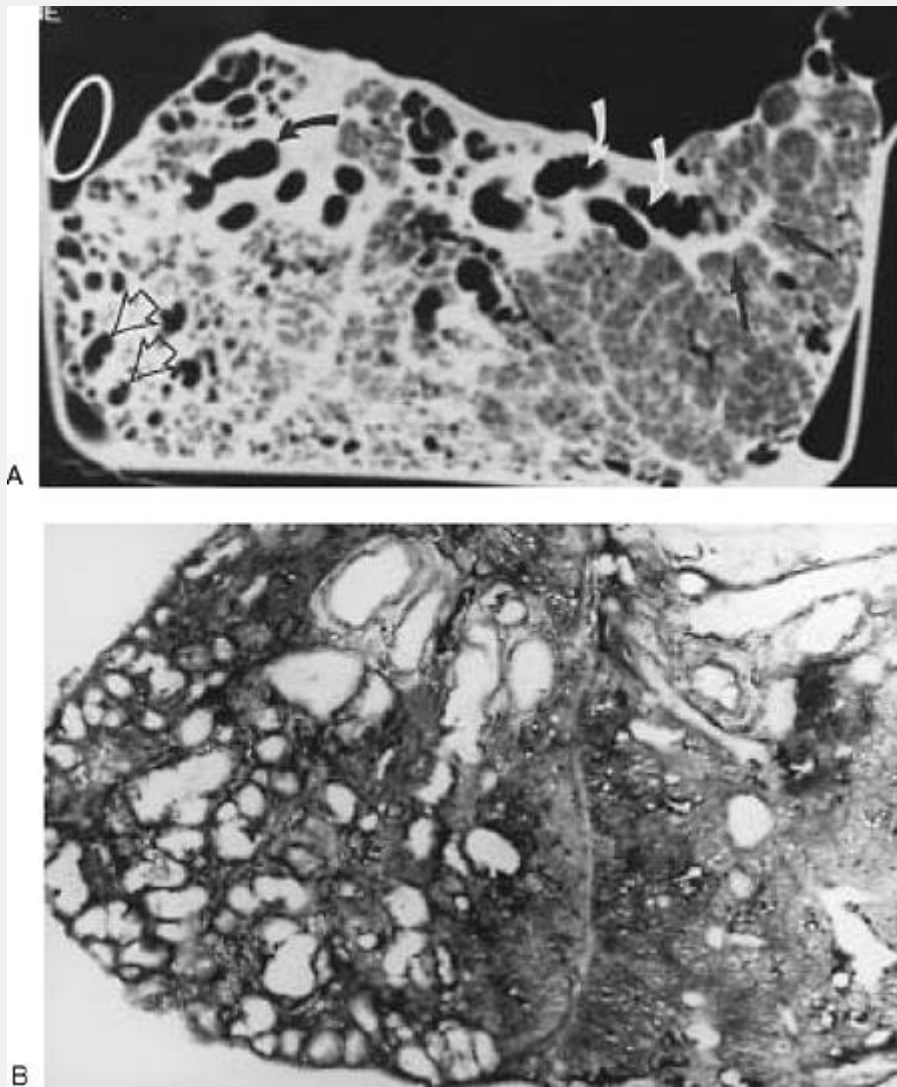


FIG. 3-29. Honeycombing and traction bronchiectasis in the patient with pulmonary fibrosis shown in Figs. 3-15 and 3-23. Large honeycomb cysts present in the posterior lung result in cystic spaces ranging up to several centimeters in diameter (*open arrows, A*). They are characterized by thick, clearly definable, fibrous walls, and are easily identified in the corresponding lung section (B). Traction bronchiectasis (*curved arrows, A*) also reflects extensive fibrosis, and is often seen in patients with honeycombing. The edges of pulmonary vessels (*solid arrows, A*) appear irregular

because of surrounding fibrosis. (From Webb WR, Stein MG, et al. Normal and diseased isolated lungs: HRCT. *Radiology* 1988;166:81, with permission.)

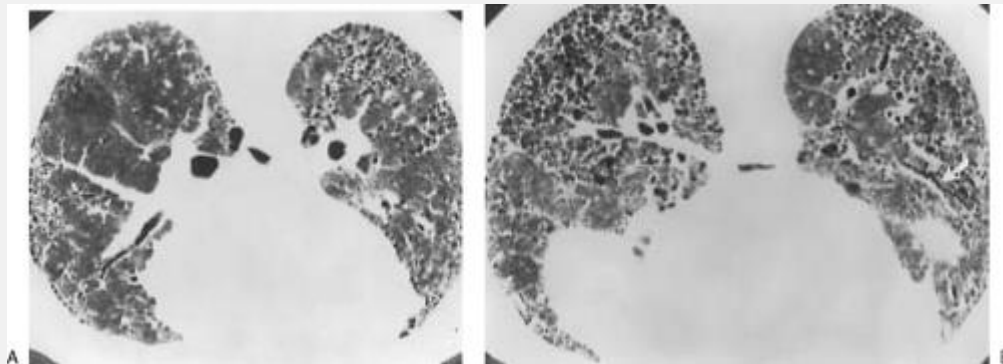


FIG. 3-30. Honeycombing in a patient with idiopathic pulmonary fibrosis (A, B; prone HRCT). Honeycombing results in cysts of varying sizes, which have a peripheral predominance. The cysts have thick and clearly definable walls. In areas of honeycombing, lobular anatomy cannot be resolved because of architectural distortion. In less abnormal areas, some septal thickening can be seen. Vessels and bronchi have irregular interfaces, and bronchial irregularity (*arrow*) indicates traction bronchiectasis (B). Findings of honeycombing are more severe at the lung bases (B).

P.90

P.91

In the majority of patients who present with clinical features of UIP, the presence of a predominantly subpleural and basal distribution of fibrosis on HRCT can be sufficiently characteristic to obviate biopsy, especially in patients in whom HRCT shows no evidence suggesting disease activity [72,73]. HRCT findings, including the presence of honeycombing with a subpleural and basal predominance, have been shown to be highly accurate in making this diagnosis [62,74,75,76,77,78,79,80]; a confident first-choice diagnosis of UIP was made in 77% to 89% of cases in these studies. However, a definite diagnosis of UIP cannot be made using HRCT. In a study by Johkoh et al. [67] of 129 patients with idiopathic interstitial pneumonia, admittedly including atypical cases requiring biopsy for diagnosis, a combination of honeycombing with a basal predominance was found in 59% of patients with UIP, 26% of patients with DIP, 22% of patients with NSIP, and 4% of patients with BOOP.

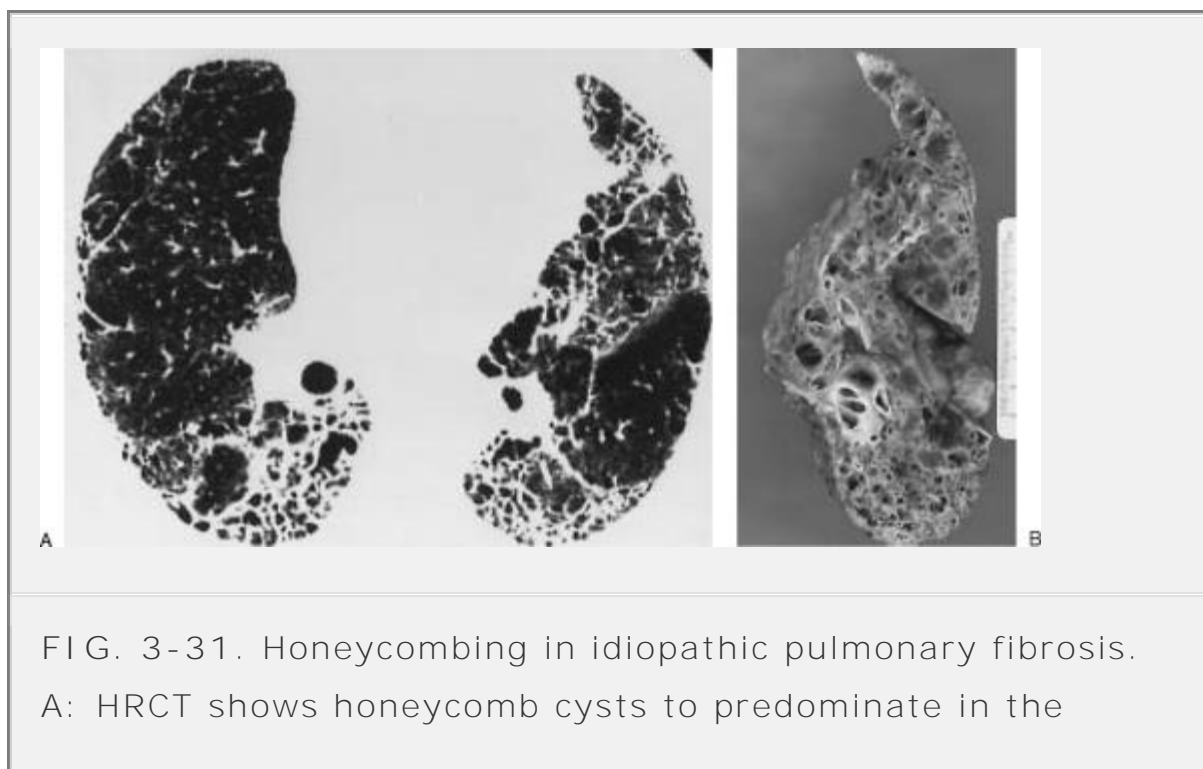
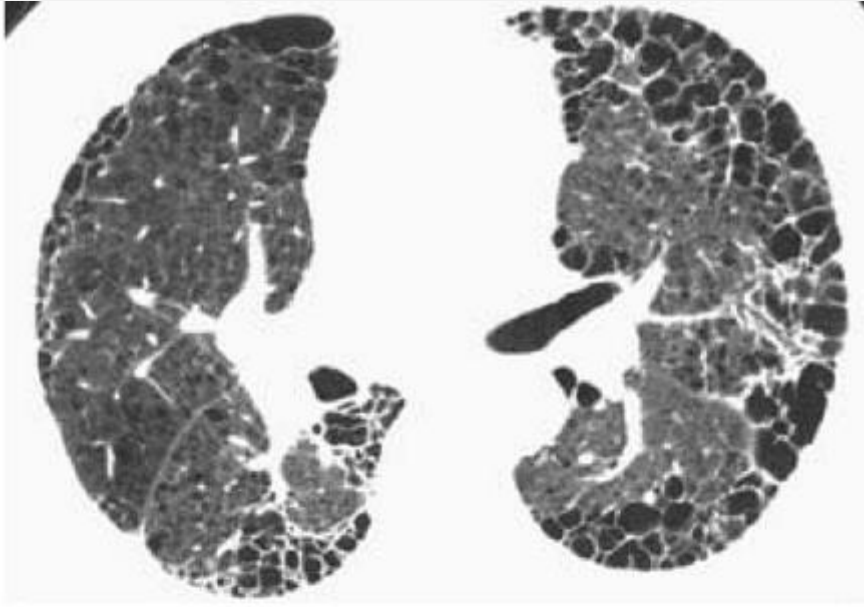


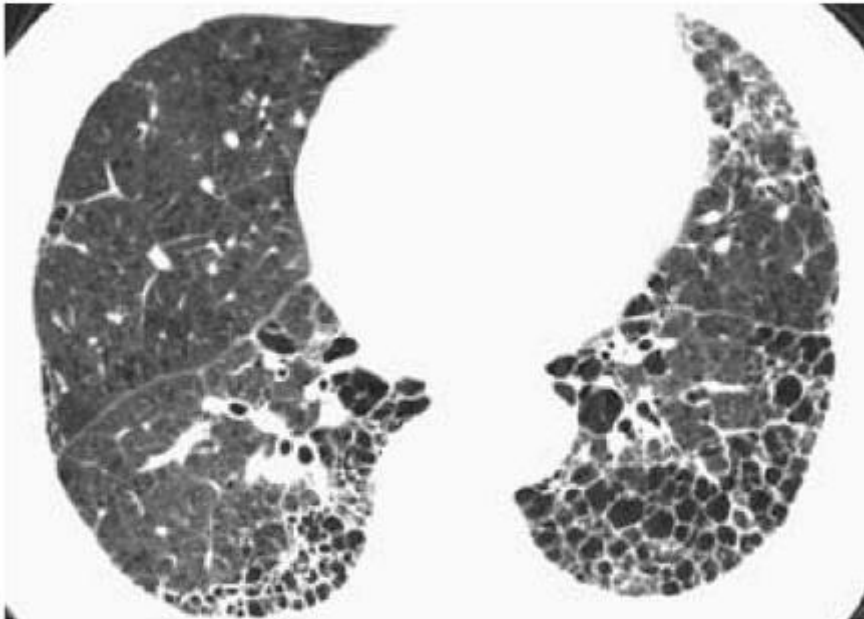
FIG. 3-31. Honeycombing in idiopathic pulmonary fibrosis. A: HRCT shows honeycomb cysts to predominate in the

peripheral and subpleural regions. Note that the cysts occur in several layers. B: The resected left lung in this patient sectioned at the level of the HRCT shown in A, shows the honeycomb cysts, which are most extensive in the posterior and peripheral lung.

A



B



C

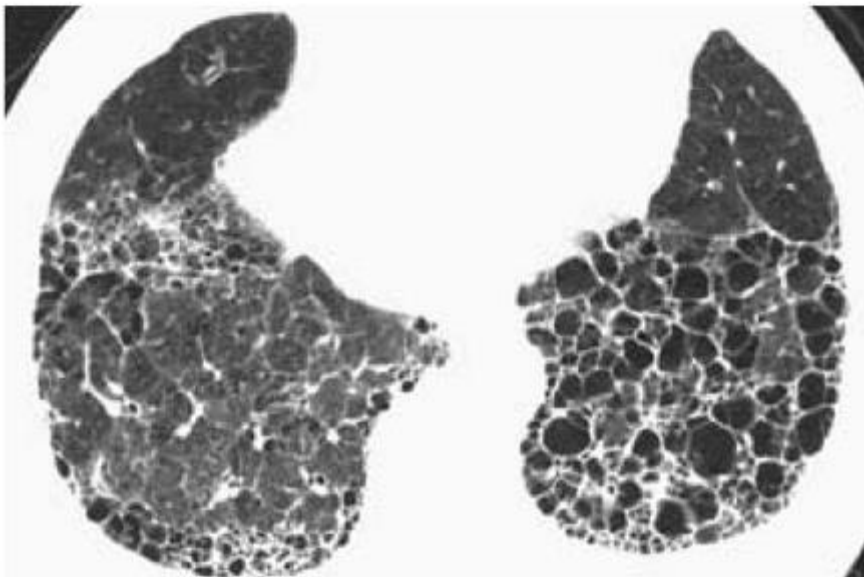
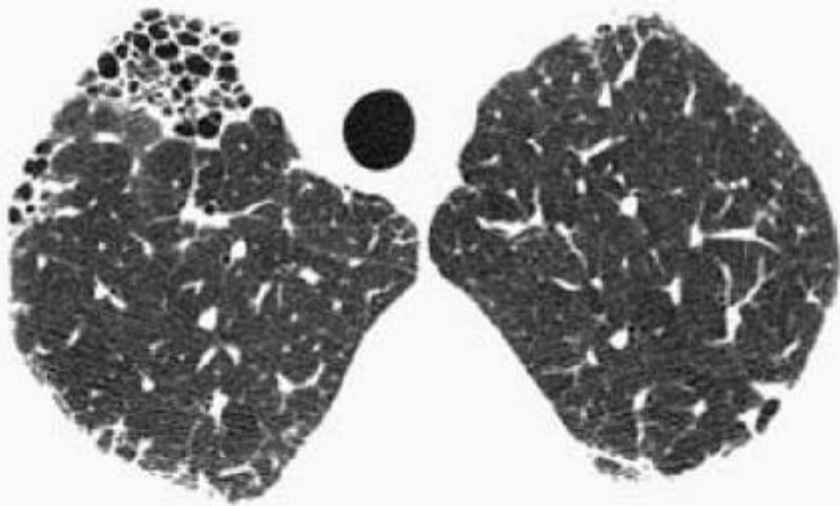
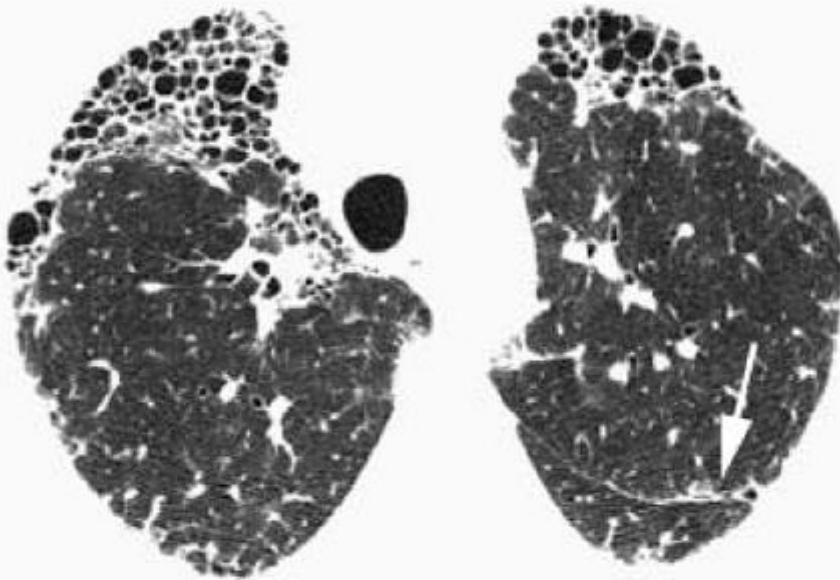


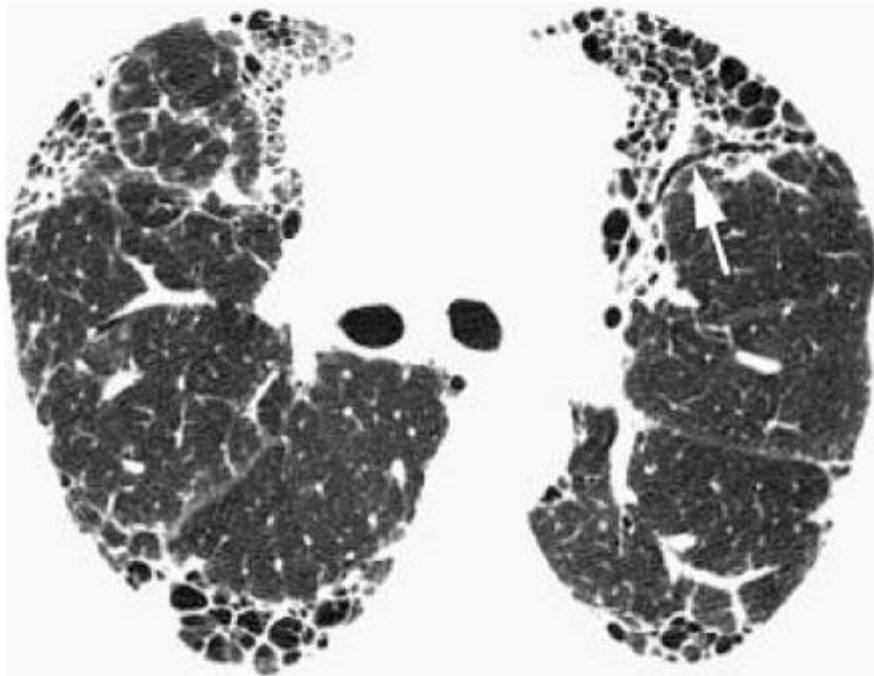
FIG. 3-32. A-C: Honeycombing in idiopathic pulmonary fibrosis. HRCT shows honeycomb cysts with a distinct predominance in the peripheral and subpleural regions. The cysts occur in several layers at the pleural surface, and the largest cysts are slightly larger than 1 cm in diameter. A basal predominance is also noted, and this is typical of idiopathic pulmonary fibrosis and most other causes of honeycombing. As in this case, some asymmetry is not uncommon.



A

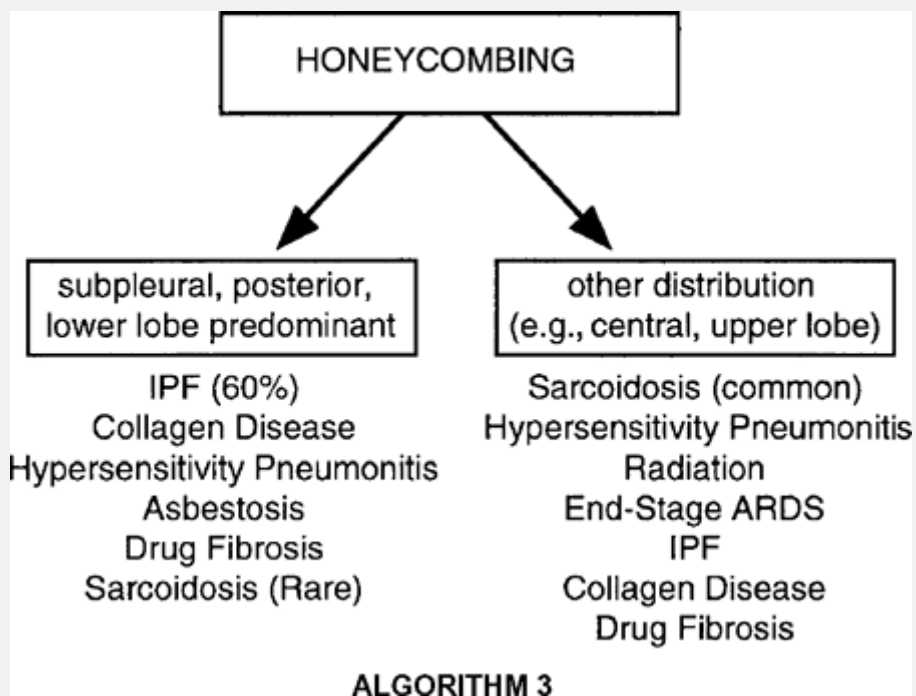


B



C

FIG. 3-33. A-C: Honeycombing in rheumatoid lung disease. HRCT shows honeycomb cysts with a distinct subpleural predominance. The cysts are generally smaller than 1 cm in diameter and share walls. Other findings of fibrosis include irregular thickening of the left major fissure (*arrow*, B), and traction bronchiectasis (*arrow*, C).



ALGORITHM 3

P. 92

P. 93

P. 94

Irregular Linear Opacities

Irregular linear opacities 1- to 3-mm thick that cannot be characterized as representing parenchymal bands, peribronchovascular interstitial thickening, interlobular septal thickening, intralobular lines, or honeycombing are often visible in patients with interstitial disease, usually representing irregular areas of fibrosis (Fig. 3-34) [6]. These are nonspecific and may be seen in a variety of diseases, including UIP and NSIP [22,67,68,69]. In patients who have UIP and its various causes, irregular linear opacities may be seen instead of honeycombing; in patients with NSIP, they are more common than honeycombing.

Subpleural Lines

A curvilinear opacity a few millimeters or less in thickness, less than 1 cm from the pleural surface and paralleling the pleura, is termed a *subpleural line* [6]. It is a nonspecific indicator of atelectasis, fibrosis, or inflammation. It was first described in patients with asbestosis [81], and was termed a *subpleural curvilinear shadow*. It was originally suggested that a subpleural line reflects the presence of fibrosis associated with honeycombing [81], and in some patients, a confluence of honeycomb cysts can result in a somewhat irregular subpleural line (Figs. 3-35, 3-36, 3-37). A subpleural line is much more common in patients who have asbestosis than in those who have IPF or other causes of UIP [75]. Indeed, the presence of a subpleural line in nondependent lung has been reported in as many as 41% of patients with clinical findings of asbestosis [39]. However, the presence of this finding is nonspecific and can be seen in a variety of lung diseases (Fig. 3-1). The presence of a subpleural line has also been reported as common in

patients with scleroderma who have interstitial disease [82,83].

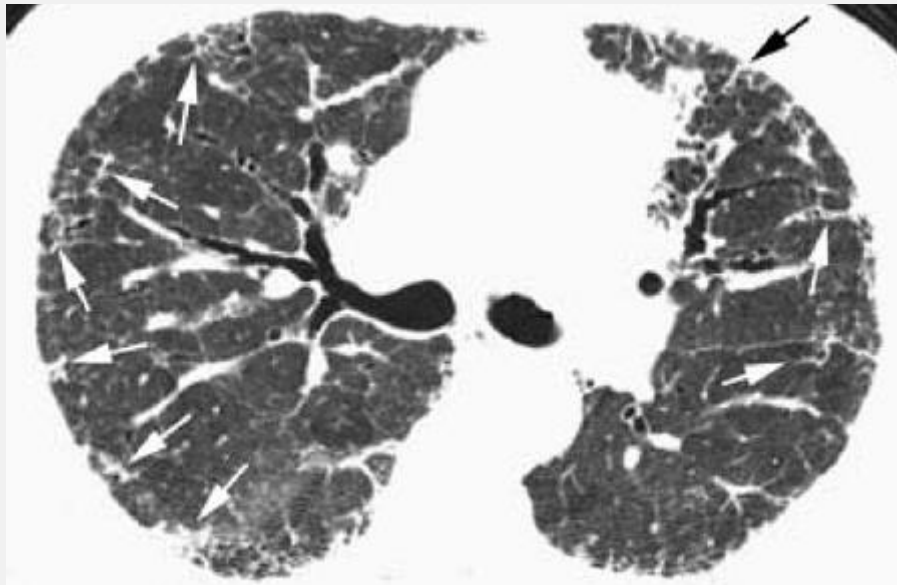


FIG. 3-34. Irregular linear opacities (*arrows*) in a patient with pulmonary fibrosis related to treatment with methotrexate. Irregular lines may be seen in various diseases resulting in fibrosis. These are nonspecific, but in a subpleural location as in this patient are suggestive of usual interstitial pneumonia or nonspecific interstitial pneumonia.

P.95

A subpleural line also has been reported to occur as a result of the confluence of peribronchiolar interstitial abnormalities in patients with asbestosis, representing early fibrosis with associated alveolar flattening and collapse [44]. In these patients, honeycombing was not present. Also, in patients with asbestos exposure, a subpleural line may be seen adjacent to focal pleural thickening or plaques. These most likely represent focal atelectasis.

A subpleural line can also be seen in normal patients as a result of atelectasis within the dependent lung (e.g., the posterior lung when the patient is positioned supine) (Fig. 3-38); the presence of dependent atelectasis has been confirmed experimentally [84]. Also, a thicker, less-well-defined subpleural opacity, a so-called dependent density [39], can also be seen in normal subjects as a result of volume loss. Such normal posterior lines or opacities are transient and disappear in the prone position. In a study by Aberle and associates [39] of patients with asbestos exposure, neither transient subpleural lines nor transient dependent densities correlated with the clinical suspicion of pulmonary fibrosis.

In patients with early interstitial lung disease, there may be a greater tendency for atelectasis to develop in the peripheral lung, resulting in the appearance of a subpleural line. As such, the presence of this abnormality could reflect an increased closing volume (i.e., an increased tendency for the lung to collapse) that is known to occur as a result of early interstitial lung disease. In the presence of appropriate treatment, such a finding might disappear (Fig. 3-39). The association of platelike atelectasis at the **junction of "cortical" and "medullary" lung regions, air-trapping** in the lung peripheral to the atelectasis, and decreased compliance of lung because of interstitial infiltration was first reported by Kubota et al. [85]. In addition, in some patients with asbestos exposure, a subpleural line may be seen adjacent to pleural plaques, representing focal atelectasis.

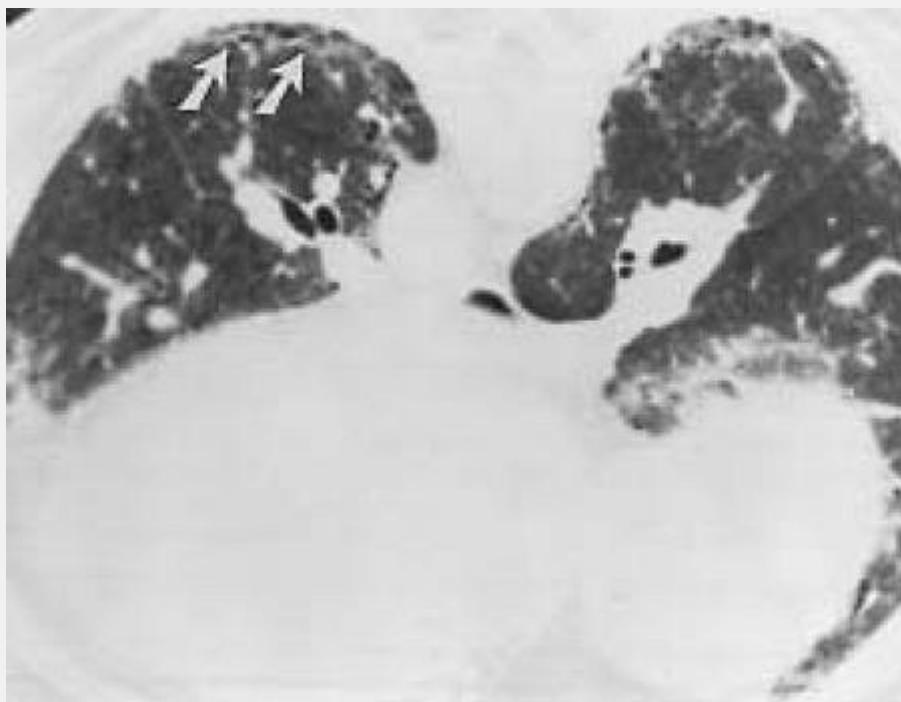


FIG. 3-35. Subpleural line in a patient with asbestosis. An ill-defined subpleural line (arrows) on a prone scan reflects subpleural fibrosis and honeycombing. Other findings of pulmonary fibrosis are also present.



FIG. 3-36. Subpleural line (arrows) in a patient with rheumatoid lung disease and fibrosis, shown on a prone

scan. Small honeycomb cysts are associated.



FIG. 3-37. Bilateral subpleural lines (arrows) in a patient with early idiopathic pulmonary fibrosis.



FIG. 3-38. Dependent atelectasis resulting in a posterior subpleural line. An ill-defined subpleural line is present

posteriorly. No other findings of fibrosis are present, and this line disappeared in the prone position.

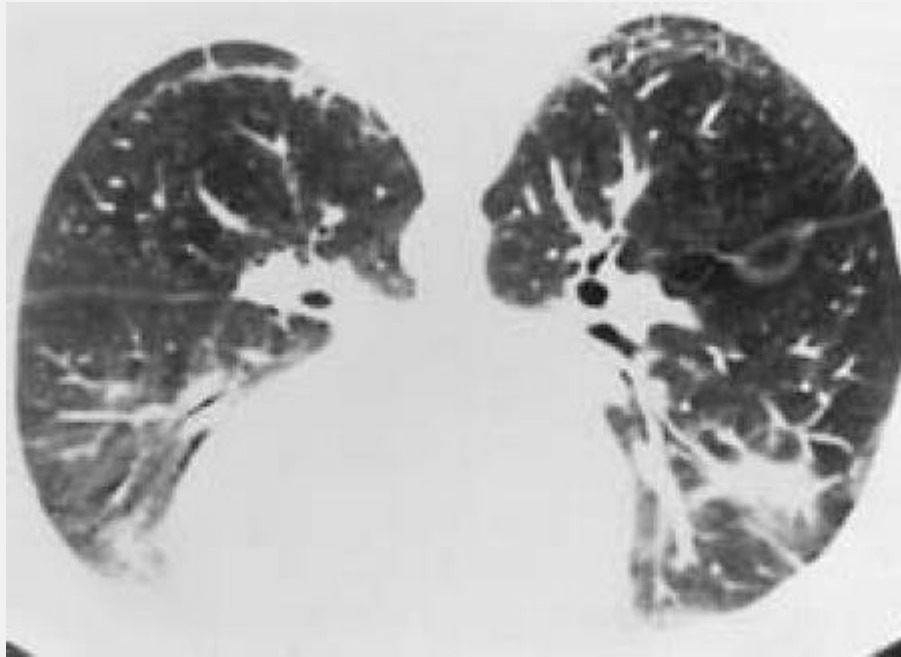


FIG. 3-39. Subpleural line that resolved after treatment in a patient with idiopathic pulmonary fibrosis. In the prone position, bilateral nontransient subpleural lines appear to represent fibrosis. Several small lucencies peripheral to them appear to represent areas of lung destruction or honeycombing. However, all of these findings cleared after treatment with steroids. This appearance may reflect atelectasis and air-trapping within the peripheral lung, occurring as a result of an increased closing volume (i.e., an increased tendency for lung collapse).

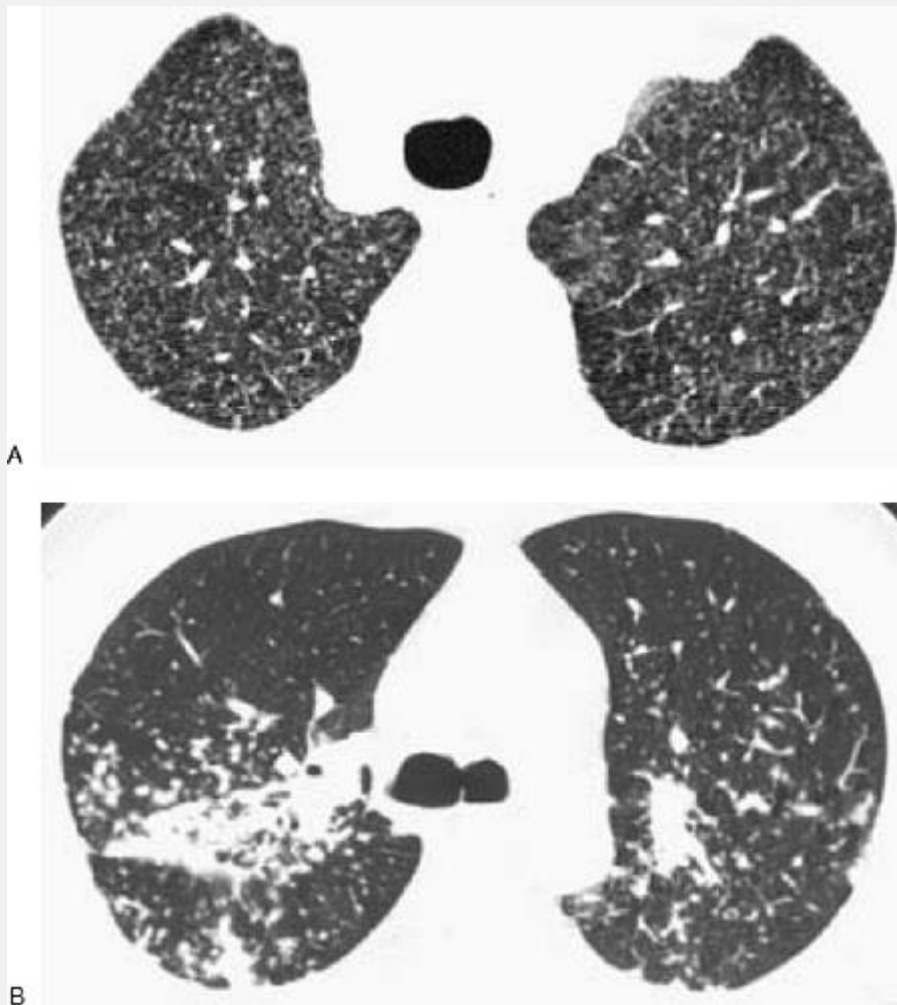


FIG. 3-40. Interstitial nodules. A: Very small nodules are easily visible in a patient with miliary tuberculosis. B: In a patient with sarcoidosis, nodules a few millimeters in diameter are sharply margined and of soft-tissue attenuation. In regions of confluence, the nodules obscure vessels.

P.96

P.97

Nodules and Nodular Opacities

The term *nodule* is defined as a rounded opacity, at least moderately well-defined, and no more than 3 cm in diameter [6]. An approach to the HRCT assessment and differential diagnosis of multiple nodular opacities is based on a consideration of their size (small or large), appearance (well-defined or ill-defined), attenuation (soft-tissue or ground-glass opacity), and distribution.

Small Nodules

In this book, the term *small nodule* is used to define a rounded opacity smaller than 1 cm in diameter, whereas *large nodule* is used to refer to nodules 1 cm or larger in diameter. Some authors have used *micronodule* to describe nodules that are either smaller than 3 mm [77] or smaller than 7 mm in diameter [57,86]. The Nomenclature Committee of the Fleischner Society [6] recommends that **“micronodule” be used to refer to nodules no larger than 7 mm in diameter.** It is not clear that a distinction between a small nodule and a micronodule is of value in differential diagnosis [77].

Differences in the appearances of nodules that are predominantly interstitial or predominantly airspace in origin have been emphasized by several authors. Nodules considered to be interstitial are usually well-defined despite their small size (Fig. 3-40). Nodules as small as 1 to 2 mm in diameter can be detected on HRCT in patients with interstitial diseases such as miliary tuberculosis (Fig. 3-40A) [43,87,88,89], sarcoidosis (Fig. 3-40B) [13,21,56,60,90,91], Langerhans histiocytosis [92,93], silicosis and CWP [57,58,76,94,95], and metastatic tumor [4,49,96]. Interstitial nodules usually appear to be of soft-

tissue attenuation and obscure the edges of vessels or other structures that they touch (Fig. 3-40B) [97,98,99,100,101]. Airspace nodules, on the other hand, are more likely to be ill-defined [3,43,102,103,104]; they can be of homogeneous soft-tissue attenuation (Figs. 3-41 and 3-42) or hazy and less dense than adjacent vessels (so-called ground-glass opacity) (Fig. 3-43). A cluster or rosette of small nodules can also be seen in patients who have airspace disease [102]. Airspace nodules have also been termed *acinar nodules* because they approximate the size of acini, but these nodules are not acinar histologically and instead tend to be centrilobular and peribronchiolar [103]; *ill-defined nodule* or *airspace nodule* is a preferable term.

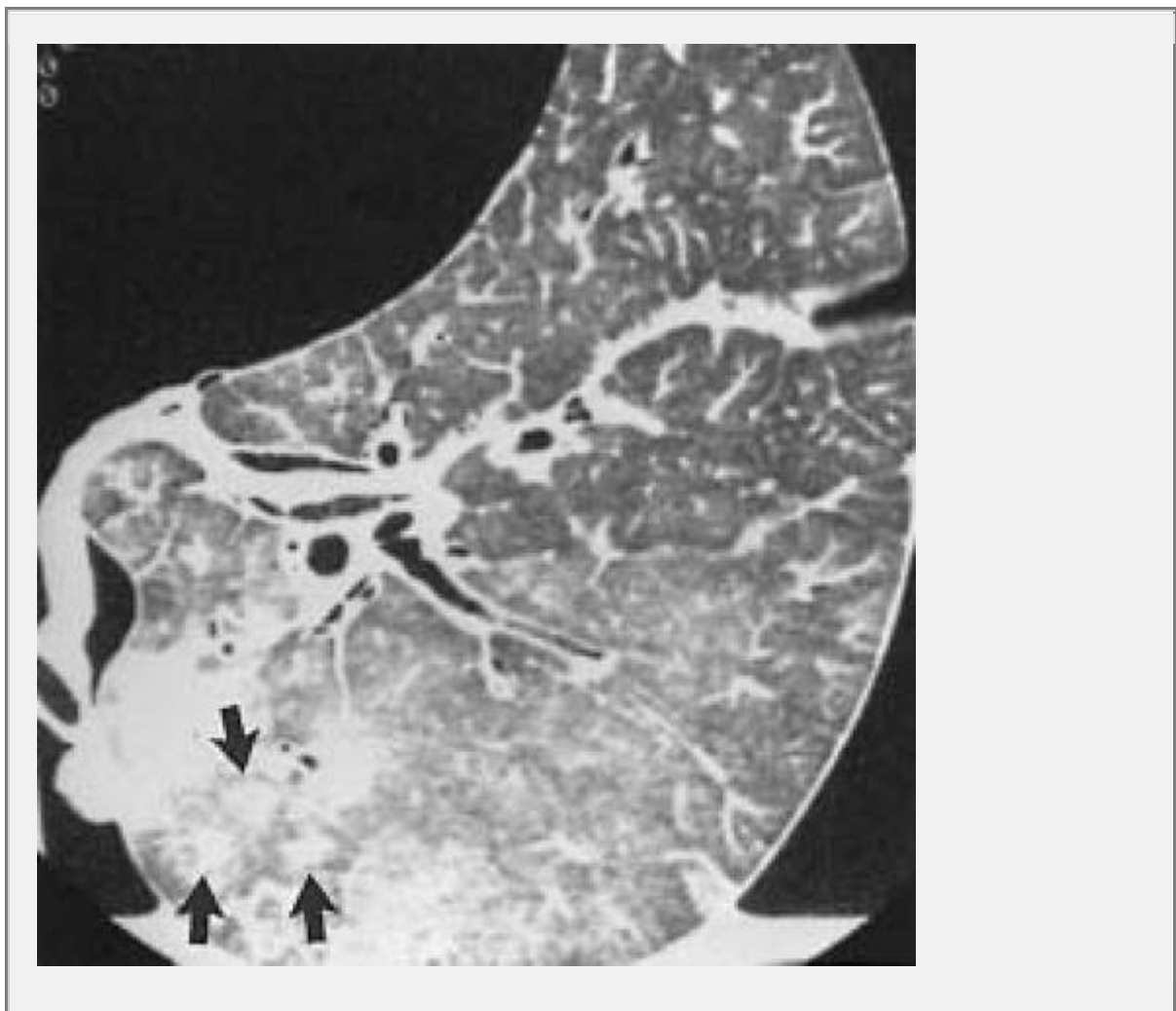


FIG. 3-41. Airspace nodules in an isolated lung. In this patient, centrilobular nodules (arrows) representing airspace pulmonary edema are visible in the posterior lung. These are larger and less well defined than interstitial nodules. (From Webb WR. HRCT of the lung parenchyma. *Radiol Clin North Am* 1989;27:1085, with permission.)



FIG. 3-42. Airspace nodules in a patient with a lobular pneumonia. The nodules are of soft-tissue opacity and

obscure vessels. They are centrilobular in location and spare the subpleural lung peripherally and adjacent to the fissures. The small lucency seen within several of the nodules may reflect the centrilobular bronchiole. (From Webb WR. HRCT of the lung parenchyma. Radiol Clin North Am 1989;27:1085, with permission.)

P.98

Despite these differences in appearance, a distinction between interstitial and airspace nodules on the basis of HRCT findings can be quite difficult, and, in fact, is somewhat arbitrary, because many nodular diseases affect both the interstitial and alveolar compartments histologically.

The distribution or location of small nodules is generally of more value in differential diagnosis than their appearance, although both are usually taken into account (Table 3-6). In different conditions, small nodules can appear perilymphatic in distribution, randomly distributed, or predominantly centrilobular. Although there may be some overlap between these appearances, in most cases, a predominant distribution of nodules is evident on HRCT [105,106].

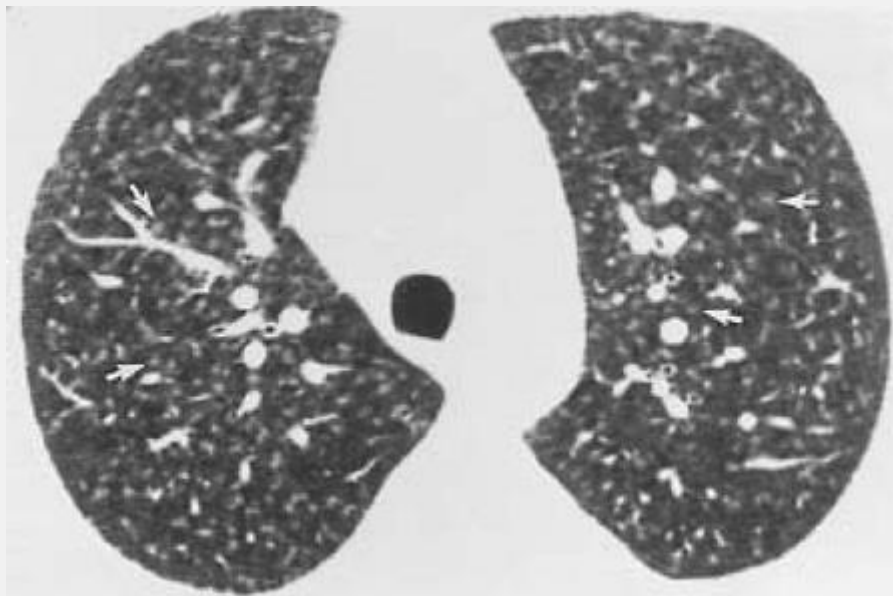


FIG. 3-43. Airspace nodules in bronchiolitis obliterans organizing pneumonia. Small, ill-defined ground-glass opacity nodules (arrows) are visible diffusely. Some can be seen to be centrilobular.

TABLE 3-6. *Differential diagnosis and characteristics of small nodules*

Disease	Distribution	Size (mm)	Appearance	Comments
Sarcoidosis	PL, occ R	≥1	W/ID, ST ± CALC	Subpleural, peribronchovascular; often patchy

				and asymmetric
Silicosis	PL, CL	≥ 1	WD, ST \pm CALC	CL, subpleural, symmetric; posterior upper lobe predominance
Lymphangitic carcinoma	PL	≥ 1	WD, ST	Septal, peribronchovascular; may be patchy or unilateral
Amyloidosis	PL	≥ 1	WD, ST \pm CALC	Predominantly septal, subpleural
Lymphocytic interstitial pneumonia	PL, CL	1-5	W/ID, ST, or GGO	May mimic lymphangitic spread when PL or hypersensitivity when CL; cysts may also be

				present
Miliary infection	R	1-5	WD, ST	Diffuse and uniform involvement
Hematogenous metastases	R	≥ 1	WD, ST	May overlap with appearance of lymphangitic spread
Endobronchial spread of infection (e.g., tuberculosis)	CL	≥ 3	W/ID, ST	Tree-in-bud common; patchy or diffuse; may be confluent
Viral pneumonia (e.g., cytomegalovirus)	CL	≥ 3	ID, GGO	Nodules of similar size surrounding small vessels
Airway disease (e.g.,	CL	≥ 3	W/ID, ST	Tree-in-bud common; patchy;

cystic fibrosis)				bronchiectasis common
Panbronchiolitis	CL	≥ 3	W/ID, ST	Tree-in-bud common; bronchiectasis common
Allergic bronchopulmonary aspergillosis	CL	≥ 3	W/ID, ST	Tree-in-bud common; bronchiectasis common
Hypersensitivity pneumonitis	CL	≥ 3	ID, GGO	Nodules of similar size surrounding small vessels
Langerhans histiocytosis	CL, occ R	≥ 3	WD, ST	Cysts may also be present
Bronchiolitis obliterans organizing pneumonia	CL	≥ 3	W/ID, ST, or GGO	Patchy or diffuse; peripheral predominance; consolidation

Bronchiolitis obliterans	CL	≥ 3	ID, GGO	Nodules uncommon; tree-in-bud rare
Respiratory bronchiolitis	CL	≥ 3	ID, GGO	Patchy GGO also common
Asbestosis	CL	2-3	W/ID, ST, or GGO	Early finding; basal, subpleural predominance; also reticular opacities
Follicular bronchiolitis	CL	≥ 1	WD, ST	Manifestation of collagen diseases, acquired immunodeficiency syndrome; branching appearance common

Endobronchial spread of tumor	CL	≥3	WD, ST	Patchy or diffuse; consolidation may be present; tree-in-bud rare
Edema, hemorrhage	CL	≥3	ID, GGO	± Septal thickening
Vasculitis	CL	≥3	ID, GGO	Talcosis; collagen disease
Metastatic calcification	CL	≥3	ID, GGO, or CALC	± Visible CALC on tissue window scans; upper lobe predominance

CALC, calcification; CL, centrilobular; GGO, ground-glass opacity; ID, ill defined; occ, occasionally; PL, perilymphatic; R, random; ST, soft-tissue attenuation; WD, well defined; W/ID, well or ill defined.

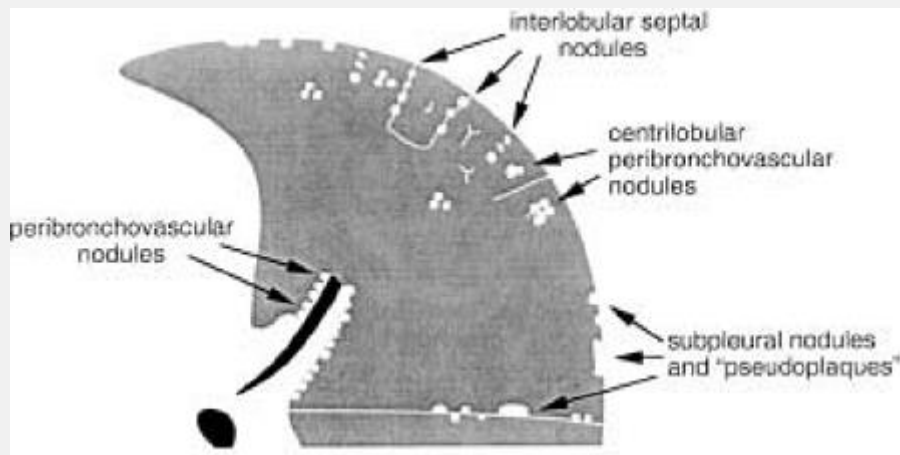


FIG. 3-44. Appearance of small nodules with a perilymphatic distribution. Nodules predominate in relation to the perihilar peribronchovascular interstitium, centrilobular interstitium, interlobular septa, and subpleural regions. Conglomerate subpleural nodules can form pseudoplaques.

P.99

P.100

Perilymphatic Distribution

Several diseases are characteristically associated with nodules occurring predominantly in relation to pulmonary lymphatics. These diseases have been termed *lymphatic* or *perilymphatic* [57,66] (Table 3-6). In patients with a perilymphatic distribution, both histologically and on HRCT, nodules predominate in relation to (i) the perihilar peribronchovascular interstitium, (ii) the interlobular septa,

(iii) the subpleural regions, and (iv) the centrilobular interstitium. This pattern is most typical in patients with sarcoidosis, silicosis and CWP, and lymphangitic spread of carcinoma (Fig. 3-44) [20].

Subpleural nodules are usually seen in patients with a perilymphatic distribution of nodules. These are most easily recognized in relation to the fissures, where they can be easily distinguished from pulmonary vessels (Figs. 3-45, 3-46, 3-47). Subpleural nodules have been reported in approximately 80% of patients with silicosis or CWP, and at least 50% of patients with sarcoidosis, and are also common with lymphangitic spread of carcinoma [57]. Confluent subpleural nodules can result in the appearance of *pseudoplaques*: linear areas of subpleural opacity several millimeters in thickness that mimic the appearance of asbestos-related parietal pleural plaques (Figs. 3-44, 3-46, and 3-47). The presence of pseudoplaques in these diseases correlates significantly with the profusion of subpleural nodules [57].

Although sarcoidosis, silicosis and CWP, and lymphangitic spread of carcinoma all have a perilymphatic distribution of nodules, these diseases usually show different patterns of involvement of the perilymphatic interstitium. HRCT findings allow their differentiation in most cases.

Sarcoidosis

In nearly all patients with sarcoidosis, HRCT shows nodules ranging in size from several millimeters to 1 cm or more in diameter [20,21,56]. The nodules often appear sharply defined despite their small size, but they can be ill-defined (Figs. 3-40B and 3-45, 3-46, 3-47 and 3-48). Nodules are most frequently seen in relationship to the perihilar

peribronchovascular interstitium (Fig. 3-5), the subpleural interstitium, and small vessels; histologically small clusters of granulomas are visible in these locations (Figs. 3-45, 3-46, 3-47) [21,56,97]. A preponderance of nodules in relation to the major fissures and central bronchi and vessels is very typical of sarcoidosis. Nodules recognizable as centrilobular or septal in location are less frequently seen on HRCT (Figs. 3-13 and 3-45) [107], but they also correlate with typical histologic abnormalities. Large nodules measuring from 1 to 4 cm in diameter are seen in 15% to 25% of patients (Figs. 3-47 and 3-48) [21,98,99] and represent masses of granulomatous lesions, each granuloma being less than 0.4 millimeters in diameter [97]. These large nodules tend to have irregular margins (Fig. 3-48). Nodules can cavitate, but this is uncommon; Grenier et al. [77] reported this finding in only 3% of cases. Occasionally, nodules visible on HRCT represent nodular areas of fibrosis rather than active granulomas [56]. An upper-lobe predominance of nodules is common in sarcoidosis [57]. The lung is characteristically involved in a patchy fashion, with groups of granulomas occurring in some regions of lung, whereas other regions appear normal (Fig. 3-47). Asymmetry is very common.

Silicosis

Silicosis and CWP are associated with the presence of small, well-defined nodules, usually measuring from 2 to 5 mm in diameter, which predominantly appear centrilobular and subpleural in location on HRCT (Fig. 3-49) [57,58,94,95,100]. These correlate with areas of fibrosis surrounding centrilobular respiratory bronchioles and involving the subpleural interstitium caused by the

accumulation of particulate material in these regions [57,95]. Parenchymal nodules are visible in 80% of patients with CWP, whereas subpleural nodules are seen in 87% [57,58]. Nodules occurring in relation to the peribronchovascular interstitium and thickened interlobular septa are less frequent and less conspicuous than in patients with sarcoidosis or lymphangitic spread of tumor. Also, nodules appear more evenly distributed than in patients with sarcoidosis; they are present diffusely, bilaterally, and symmetrically, but in patients with mild silicosis

P.101

or CWP are usually visible only in the upper lobes. A posterior predominance of nodules is often present [58,94]. In patients who have silicosis, the nodules can calcify.

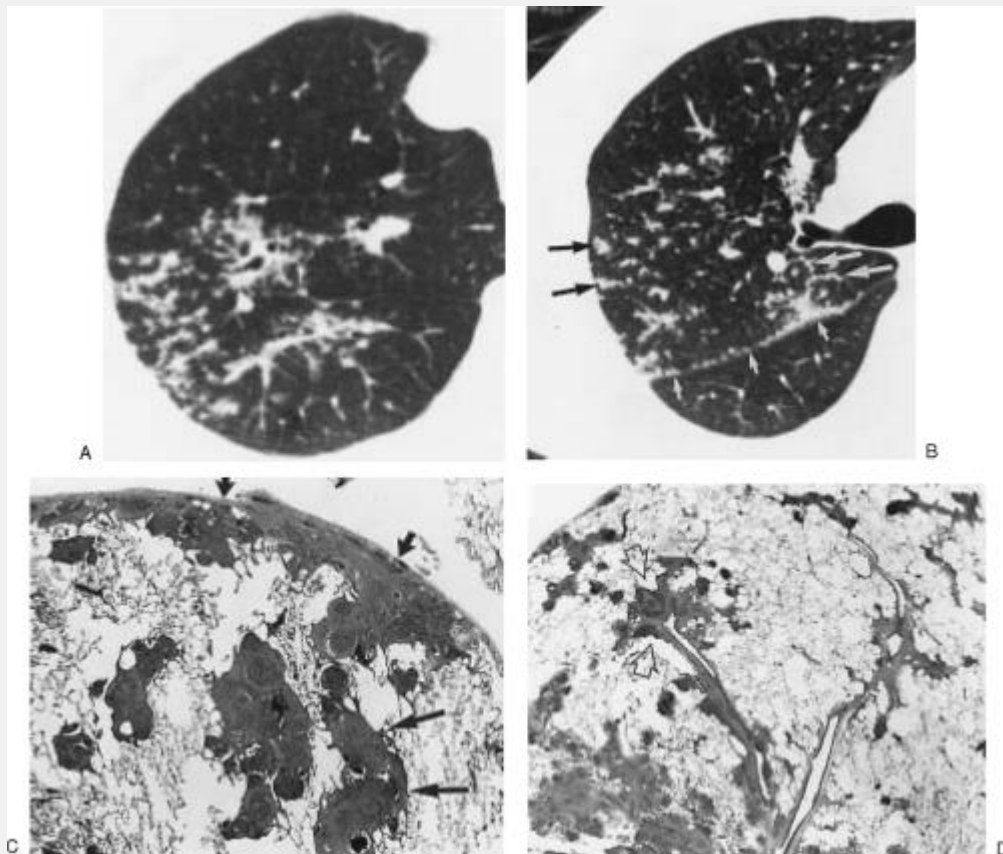


FIG. 3-45. Sarcoidosis showing a perilymphatic distribution on HRCT and open lung biopsy. A: HRCT through the upper lobe shows small nodules in relation to the peribronchovascular regions and small vessels. Vessels and bronchi show a nodular appearance. B: At a lower level, small nodules are seen in the subpleural regions along the fissure (*small white arrows*), in the centrilobular regions (*black arrows*), and interlobular septa (*long white arrows*). C, D: Open lung biopsy shows that the small nodules correspond to groups of granulomas that are subpleural (C, *short arrows*), septal (C, *long arrows*), and centrilobular and peribronchiolar (D, *open arrows*).

Lymphangitic Spread of Tumor

In patients with lymphangitic spread of tumor, when nodules are visible, they are most often visible within the thickened peribronchovascular interstitium and interlobular septa (Figs. 3-12 and 3-50, 3-51 and 3-52) [7,11,12,14,49,76]. Peribronchovascular and subpleural nodules are typically not as profuse as in patients with sarcoidosis. Septal thickening results in the appearance of a **"beaded" septum** (Figs. 3-12 and 3-50, 3-51 and 3-52) [13,49,101]. In an HRCT study of postmortem lung specimens [49], 19 of 22 cases with interstitial pulmonary metastases showed the appearance of **"beaded" or nodular septal thickening on HRCT. The beaded septa** corresponded directly to the presence of tumor growing in pulmonary capillaries, lymphatics, and septal interstitium. In this study [49], beaded septa were not noted in any of the specimens of patients with pulmonary edema, fibrosis, or in normal lungs. In patients with lymphangitic carcinomatosis, the abnormalities may be unilateral, patchy, bilateral, or symmetric.

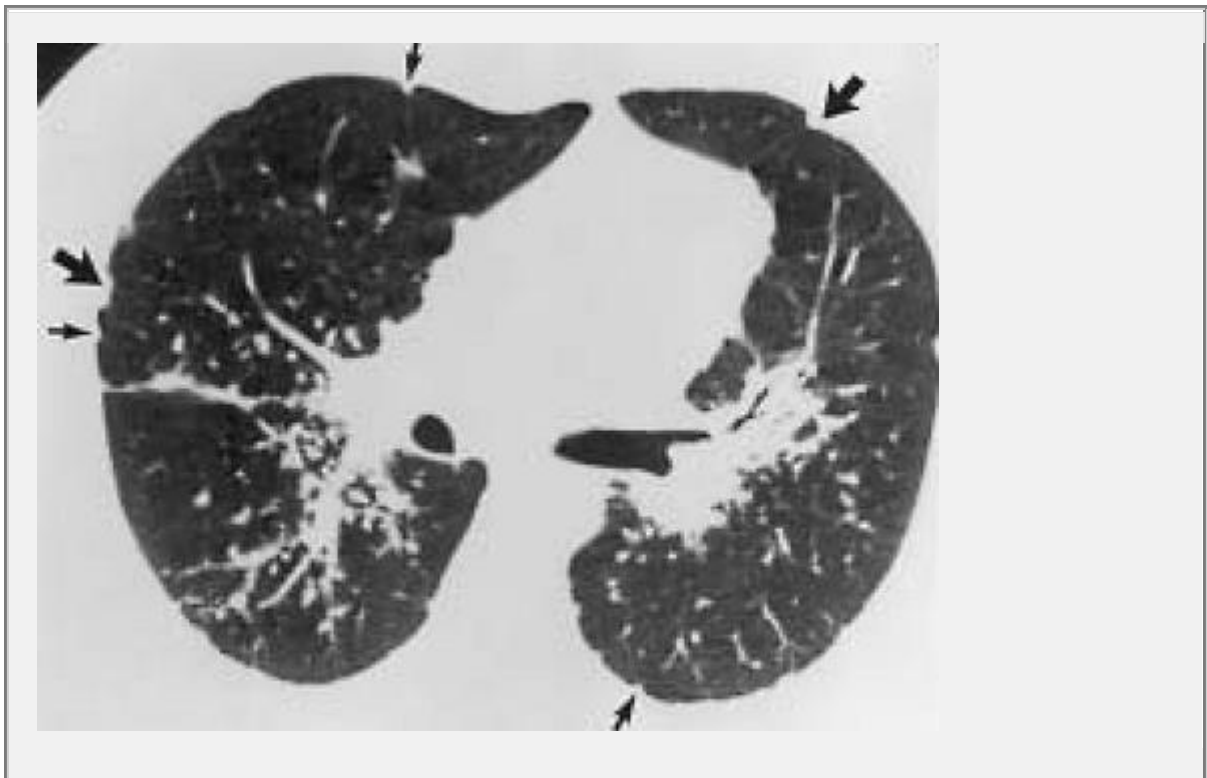


FIG. 3-46. Sarcoidosis with a perilymphatic distribution of nodules. Numerous small nodules are seen in relation to the perihilar, bronchovascular interstitium. Bronchial walls appear irregularly thickened. Subpleural nodules (*small arrows*) are also seen bordering the costal pleural surfaces and right major fissure. This appearance is virtually diagnostic of sarcoidosis. Clusters of subpleural granulomas (*large arrows*) have been termed *pseudoplaques*.

P.102

A perilymphatic distribution of nodules also may be seen in other diseases, but these are uncommon. In patients with *diffuse amyloidosis*, interstitial thickening with nodularity visible in relation to vessels, bronchi, interlobular septa, and the subpleural interstitium has been reported (Fig. 3-53; see Fig. 5-59) [50,106]. In smokers, a few small subpleural and centrilobular nodules can be seen, probably related to the presence of fibrosis and accumulated particulate material in the peribronchial regions and at the bases of interlobular septa, and related to pathways of lymphatic drainage [108,109]. LIP, occurring primarily in patients with dysproteinemia; autoimmune disease, particularly Sjögren's syndrome; multicentric Castleman's disease; and in patients with acquired immunodeficiency syndrome (AIDS), can result in the presence of lymphocytic and plasma cell infiltrates in relation to the peribronchovascular interstitium and interlobular septa, and in the subpleural and centrilobular regions [110,111,112,113]. On HRCT, LIP may result in a variety of appearances [17,19, 114], but in some patients, it closely

mimics the appearance of lymphangitic spread of carcinoma, with subpleural, peribronchovascular, and septal nodules (Fig. 3-54).

Random Distribution

Small nodules that appear randomly distributed in relation to structures of the secondary lobule and lung are often seen in patients with miliary tuberculosis (Fig. 3-55) [88,89], miliary fungal infections, and hematogenous metastases [66] (Table 3-6). As with a perilymphatic distribution, the nodules can be seen in relation to the pleural surfaces, small vessels, and interlobular septa but do not appear to have a consistent or predominant relationship to any of these. On HRCT, a uniform distribution of nodules throughout the lung, without respect for anatomic structures, is most typical. Lung involvement tends to be bilateral and symmetric; a patchy distribution of nodules, as is often seen in patients with a perilymphatic pattern, is atypical.

In miliary tuberculosis (Fig. 3-55) or fungal infections (Fig. 3-56), the nodules tend to be well-defined and up to several millimeters in diameter [89]. Hematogenous metastases also tend to be well-defined (Fig. 3-57) [115]. As with miliary tuberculosis, the nodules can be seen in relation to small vessels in some locations, a fact that likely reflects their mode of dissemination. Although random in distribution, they have a recognized tendency to predominate in the lung periphery and at the lung bases [115]. An appearance of small well-defined and ill-defined random nodules has also been reported with varicella-zoster pneumonia [116].

In a study correlating HRCT and pathologic findings in patients with metastatic tumor [115], nodules less than 3 mm in diameter had no consistent relationship to lobular structures. Eleven percent of nodules were seen in relation to the centrilobular pulmonary arteries, 21% were related to interlobular septa, and 68% were located in-between. On examination of specimen radiographs and pathology, a similar distribution was noted. Nodules resulting from hematogenous metastasis are characteristically well-defined. Some overlap between a random pattern and a perilymphatic pattern may be seen in patients with metastatic tumor.

When numerous, nodules in patients with sarcoidosis (Fig. 3-58), Langerhans histiocytosis (Fig. 3-59), or silicosis may appear to be randomly and diffusely distributed [66] and may be difficult to distinguish from the nodules of miliary infection or metastases.

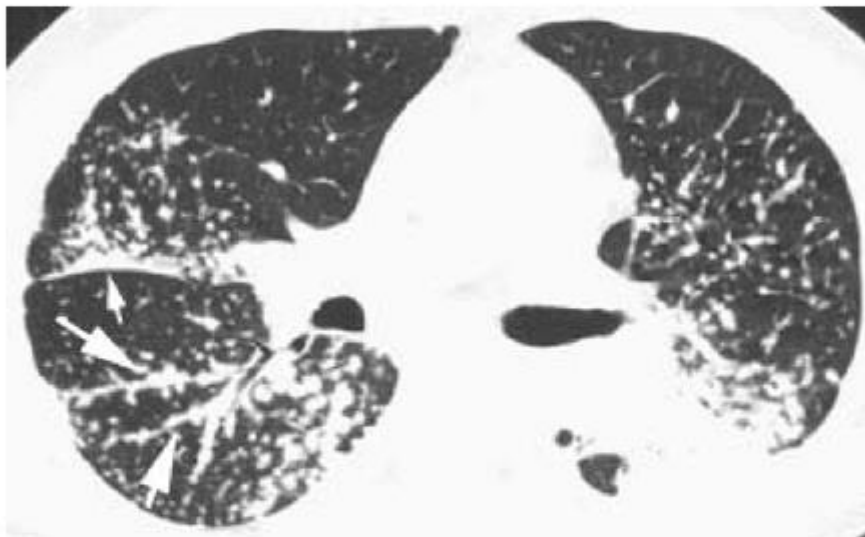
Centrilobular Distribution

Nodules limited to the centrilobular regions can also be seen (Fig. 3-60). Centrilobular nodules can reflect the presence of either interstitial or airspace abnormalities, and the histologic correlations reported to occur in association with centrilobular nodules vary with the disease entity [107]. Centrilobular nodules may be dense and of homogeneous opacity, or of ground-glass opacity (Figs. 3-61 and 3-62), and may range from a few millimeters to a centimeter in size. Either a single centrilobular nodule or a centrilobular rosette of nodules may be visible [43,102,103]. Although they are often ill-defined, this is not always the case. Because of the similar size of secondary lobules, centrilobular nodules often appear to be evenly spaced.

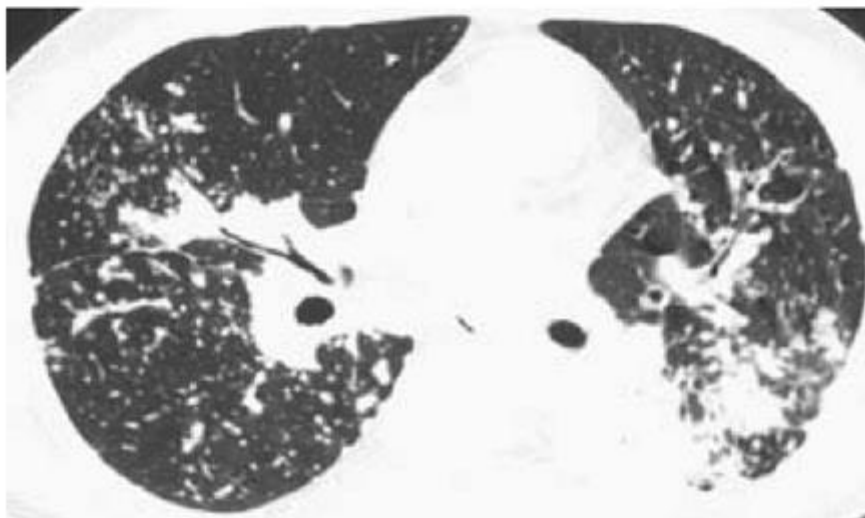
They may appear patchy or diffuse in different diseases. The **finding of "tree-in-bud," representing impaction of** centrilobular bronchioles by fluid, mucus, or pus and often appearing as a branching opacity in the peripheral lung (Fig. 3-63), may be present in patients with a centrilobular distribution of nodules. Tree-in-bud almost always indicates the presence of bronchiolar infection. The appearance and significance of tree-in-bud are discussed in detail later.



A



B



C

FIG. 3-47. A-C: HRCT at three levels in a patient with

sarcoidosis and a typical perilymphatic distribution of nodules. Numerous nodules are predominant in relation to the major fissure (*small arrows*) and perihilar bronchovascular interstitium (*large arrows*). Subpleural nodules and pseudoplaques are also seen bordering the costal pleural surfaces. Confluence of granulomas in the left lower lobe (B and C) results in consolidation or large masses. As in this patient, lung involvement in patients with sarcoidosis is often patchy, with some areas appearing relatively normal.

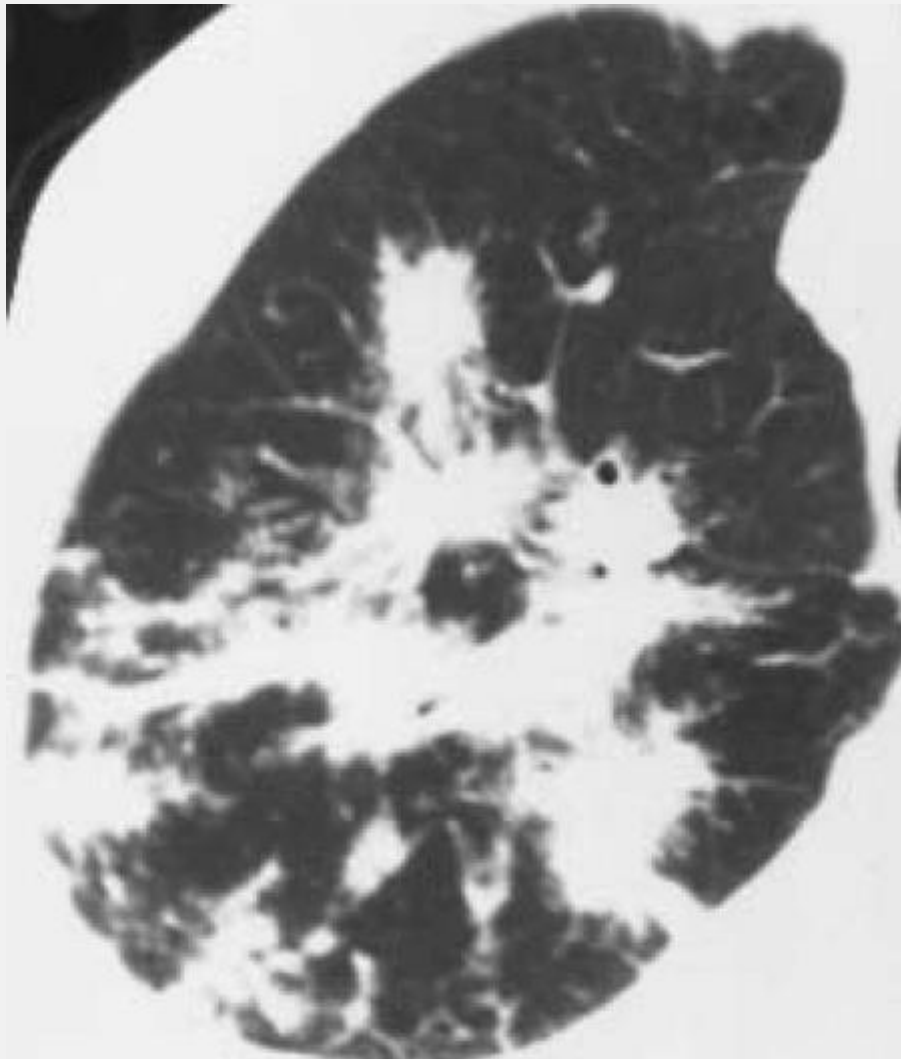


FIG. 3-48. Large peribronchovascular nodules in a patient with sarcoidosis, representing clusters of granulomas. These have irregular margins. Small nodules are also visible.

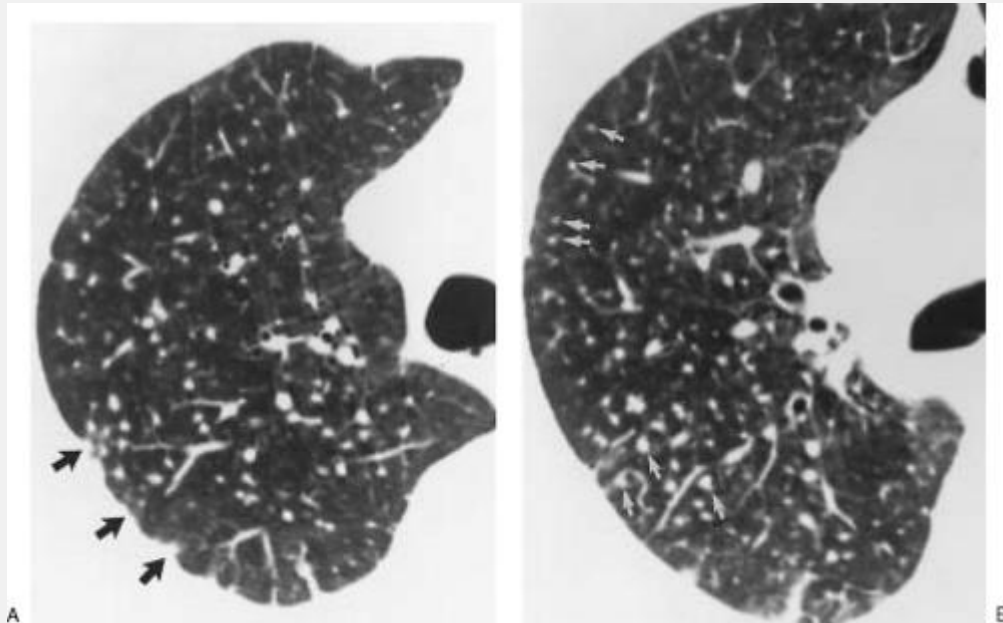


FIG. 3-49. A, B: Perilymphatic nodules in a patient with silicosis. Nodules predominate in the subpleural (A, black arrows) and centrilobular (B, white arrows) regions. In patients with silicosis, peribronchovascular nodules are less frequent than in sarcoidosis, and the nodules appear more evenly distributed. The nodules often predominate posteriorly and in the upper lobes in patients with this disease. (Courtesy of Raymond Glyn Thomas, M.D., The Rand Mutual Hospital, Johannesburg, South Africa.)

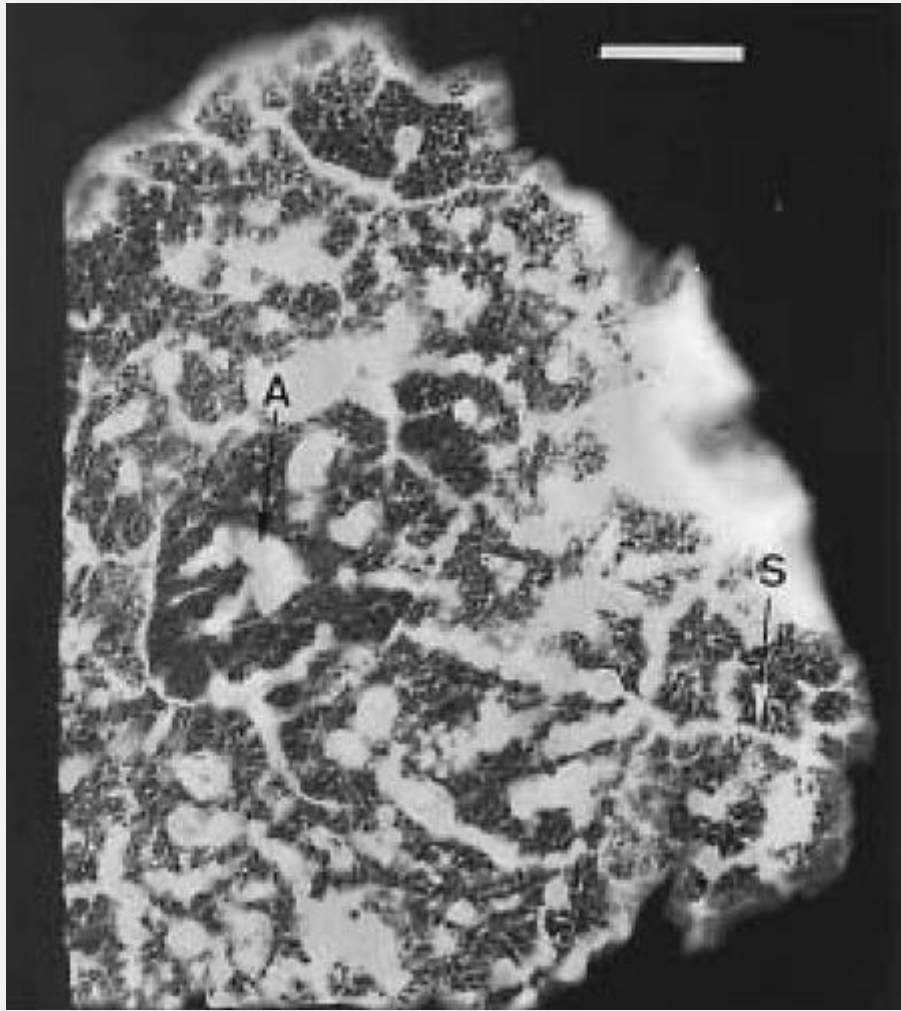


FIG. 3-50. Radiograph of a 1-mm-thick lung slice in a patient with lymphangitic spread of tumor. Note the nodular thickening of interlobular septa (S), and the centrilobular interstitium surrounding arteries (A). Bar = 1 cm. (Courtesy of Harumi Itoh, M.D., Chest Disease Research Institute, Kyoto University, Kyoto, Japan.)

P.103

P.104

Centrilobular nodules are usually separated from the pleural surfaces, fissures, and interlobular septa by a distance of several millimeters. In the lung periphery, the nodules are usually centered 5 to 10 mm from the pleural surface, a fact that reflects their centrilobular origin (Figs. 3-61 and 3-62). They are not usually seen occurring in relation to interlobular septa or the pleural surfaces, as do random or perilymphatic nodules, and the subpleural lung is typically spared. This difference can be particularly valuable in distinguishing diffuse centrilobular nodules from diffuse random nodules. Although centrilobular nodules, when large, may touch the pleural surface, they do not appear to arise at the pleural surface.

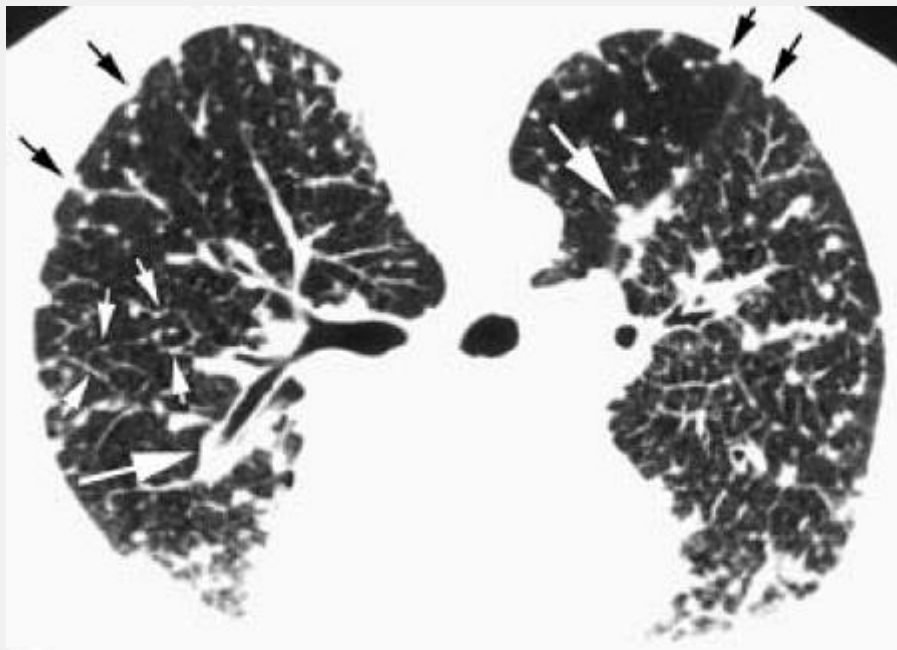


FIG. 3-51. Lymphangitic spread of carcinoma. A prone HRCT shows peribronchovascular nodules (*large white*

arrows) giving a nodular appearance to pulmonary artery branches, nodular interlobular septal thickening (*small white arrows*), and subpleural nodules (*black arrows*).

The term *centrilobular nodule* is best thought of as indicating that the nodule is related to *centrilobular structures*, such as small vessels, even if they cannot be precisely localized to the lobular core (Figs. 3-41, 3-42 and 3-43, 3-61, and 3-62). Indeed, in some cases, centrilobular nodules can be correctly identified by noting their association with small pulmonary artery branches. It is typical for centrilobular nodules to appear perivascular on HRCT, surrounding or obscuring the smallest visible pulmonary arteries (Fig. 3-62). In occasional cases, the air-filled centrilobular bronchiole can be recognized as a rounded lucency within a centrilobular nodule (Figs. 3-42, 3-64, and 3-65).

As indicated above, centrilobular nodules can be seen in patients having a perilymphatic distribution of disease. Pulmonary lymphatics are located in the peribronchovascular interstitial compartment in the centrilobular region. However, in patients with a perilymphatic distribution, nodules will also be seen in other locations (i.e., subpleural regions or interlobular septa). Sarcoid granulomas are typically distributed along lymphatics in the peribronchovascular interstitial space both in the perihilar regions and lobular core (Fig. 3-45) [56,57,60]. In some cases, centrilobular clusters of granulomas are a predominant feature of the disease, but nodules involving the subpleural regions are also present in most cases. Small centrilobular nodules are also characteristic of both silicosis and CWP [58,95]. In patients

with silicosis, early lesions are centrilobular and peribronchiolar; the

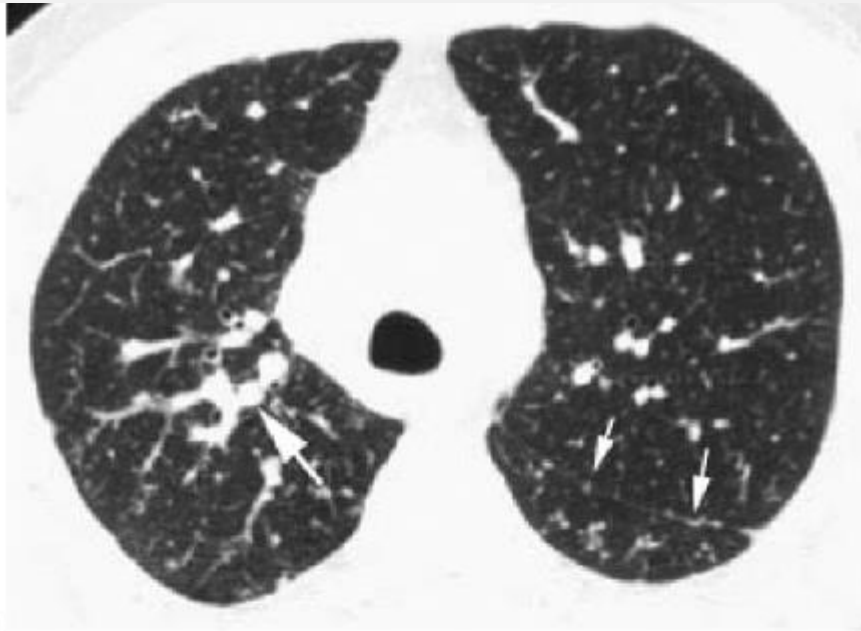
P.106

nodules are a few millimeters in diameter and consist of layers of lamellated connective tissue. Subpleural nodules are also typically present (Fig. 3-49). The characteristic lesion of CWP is the so-called coal macule, which consists of a focal accumulation of coal dust surrounded by a small amount of fibrous tissue, occurring in a centrilobular, peribronchiolar location. In patients with lymphangitic spread of carcinoma, although interlobular septal thickening is usually a predominant feature of the disease, centrilobular peribronchovascular interstitial thickening or nodules are commonly seen (Fig. 3-50) [107]. Other findings include thickening of the peribronchovascular interstitium in the perihilar lung. LIP or follicular bronchiolitis in AIDS patients can result in the presence of ill-defined centrilobular opacities. LIP is associated with a lymphocytic and plasma cell infiltrate in relation to lymphatics; it may predominate in the centrilobular regions or mimic the appearance of lymphangitic spread of carcinoma.

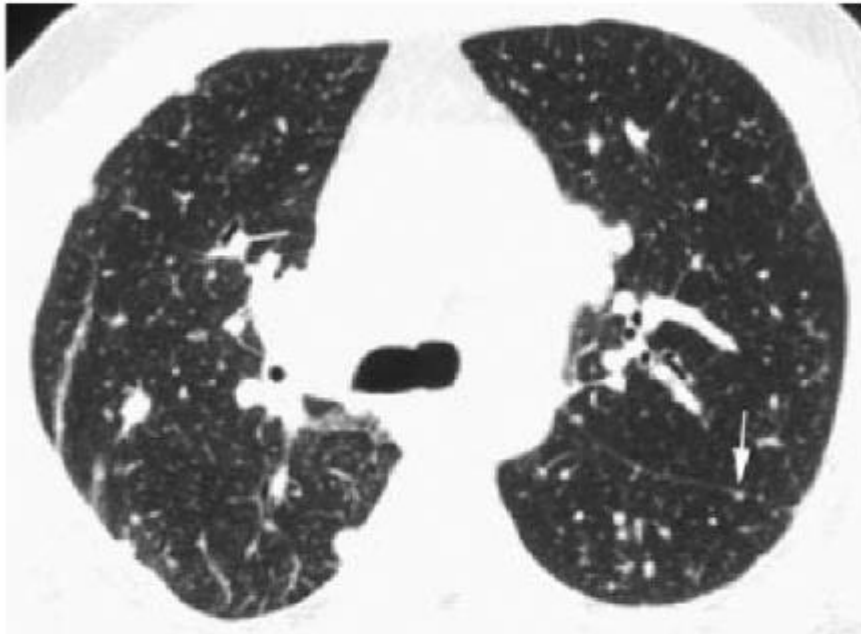
Nodules limited to centrilobular regions (i.e., a centrilobular distribution) can be seen in patients with a variety of diseases that primarily affect centrilobular bronchioles or arteries and result in inflammation, infiltration, or fibrosis of the surrounding interstitium and alveoli (Table 3-6) [66,107]. The differential diagnosis of this appearance is long. Diseases

P.107

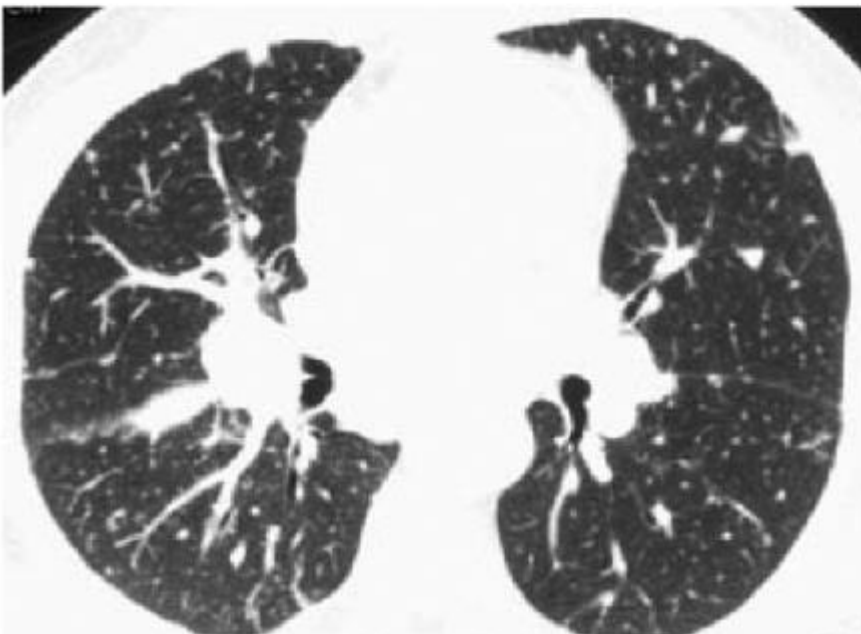
resulting in this appearance may be classified as bronchiolar and peribronchiolar or vascular and perivascular.



A



B



C

FIG. 3-52. Lymphangitic spread of thyroid carcinoma. HRCT at three levels (A-C) shows subpleural nodules along the fissures (*small arrows*) and peribronchovascular nodules (*large arrow*) resulting in a nodular appearance of pulmonary artery branches. Interlobular septal thickening is inconspicuous in this patient. Subpleural nodules are easy to see in the periphery. Note the presence of right hilar lymph node enlargement.

Bronchiolar and Peribronchiolar Diseases

Bronchiolar diseases secondarily involving the peribronchiolar interstitium or alveoli, or both, are the most frequent causes of centrilobular opacities seen on HRCT. Their histologic correlates and HRCT appearances vary with the nature of the disease. The differential diagnosis of airway diseases associated with centrilobular abnormalities includes the following entities:

Endobronchial Spread of Tuberculosis, Nontuberculous Mycobacteria, and Other Granulomatous Infections.

Bronchogenic dissemination of infection can occur in patients with active tuberculosis and nontuberculous mycobacterial disease (Figs. 3-66, 3-67, 3-68, 3-69) [43,60,65,103,117,118]. Nodules, or clusters of nodules, that reflect peribronchiolar consolidation or granuloma formation are common, visible on HRCT in as many as 97% of patients with active tuberculosis, and are also common in patients with nontuberculous mycobacterial infection [118,119]. Bronchioles filled with infected material can also result in the appearance of a tree-in-bud (Fig. 3-66) [65]. Fungal infections may result

in similar findings [120]. Specifically, *Aspergillus bronchiolitis* and bronchopneumonia (airway invasive aspergillosis) are characterized by patchy consolidation, centrilobular nodules, and the finding of a tree-in-bud (see Figs. 5-88 and 5-89) [121,122].

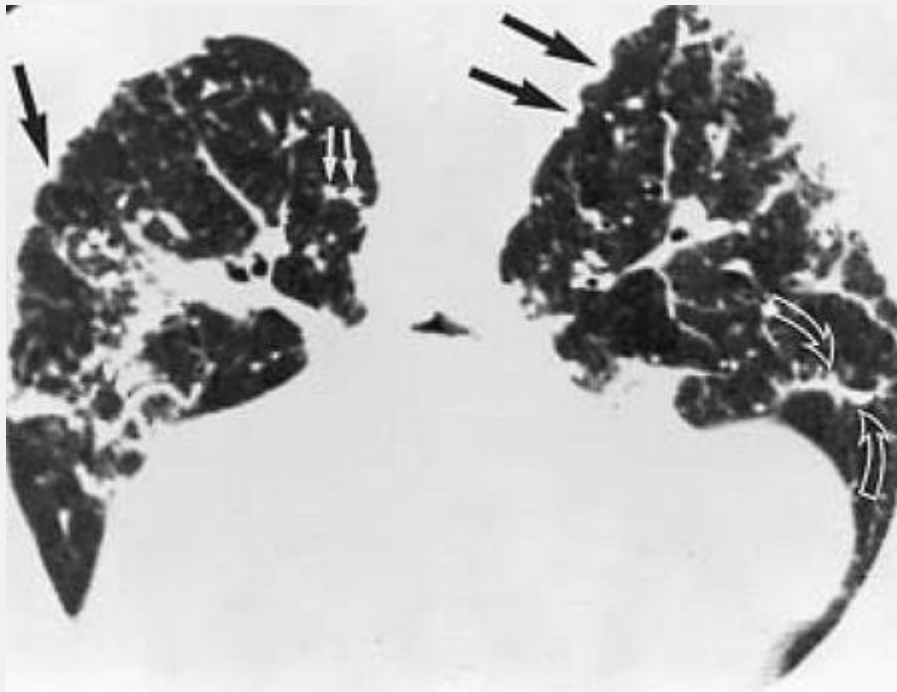


FIG. 3-53. Amyloidosis with perilymphatic nodules. Small subpleural nodules (*large arrows*) and interlobular septal nodules (*small arrows*) were found on biopsy to represent small nodular deposits of amyloid. Nodules are also seen along the right major fissure (*open arrows*).

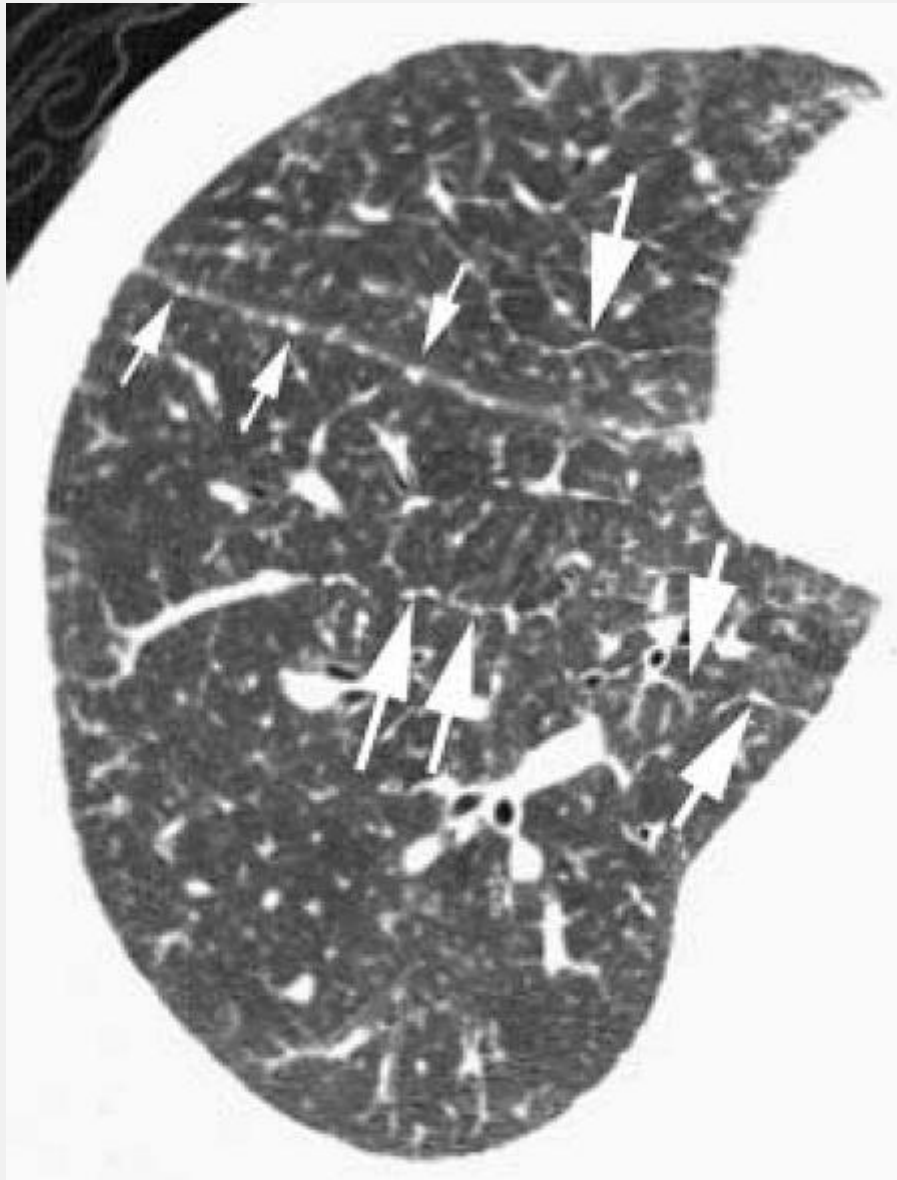


FIG. 3-54. Perilymphatic nodules in an acquired immunodeficiency syndrome patient with lymphocytic interstitial pneumonia. Small subpleural nodules (small arrows) are visible along the major fissure. Nodules within interlobular septa (large arrows) are also visible.

Bronchopneumonia. Bronchopneumonia resulting from various organisms, most commonly bacteria, is associated with the presence of bronchial and peribronchiolar inflammatory exudates, which also involve surrounding

alveoli. HRCT findings are quite similar to those of endobronchial spread of tuberculosis (Figs. 3-42, 3-64, 3-65, 3-70, and 3-71) [3,60,102]. Viral infections and *P. carinii* pneumonia can also result in the appearance of centrilobular nodules (see Fig. 6-52).

Infectious Bronchiolitis. Infectious bronchiolitis is seen most often in children, and presents with fever, dyspnea, and wheezing. It is often due to respiratory syncytial virus, although other viruses and bacteria, particularly mycoplasma, may be involved. Centrilobular nodules or tree-in-bud may be visible [123].

Cystic Fibrosis. In patients with cystic fibrosis, thick-walled, mucus- or pus-filled bronchioles are seen as rounded or branching centrilobular opacities (i.e., tree-in-bud), usually in association with central bronchiectasis (Figs. 3-63 and 3-72) [60,124,125]. The centrilobular bronchiolar abnormalities can be an early finding and can be patchy in distribution.

Bronchiectasis. Findings similar to those of cystic fibrosis can be seen in patients with chronic bronchiectasis of any cause, including congenital immunodeficiency states, ciliary dysmotility syndrome, and the syndrome of yellow nails and lymphedema (Figs. 3-73 and 3-74).

Panbronchiolitis. In patients with Asian panbronchiolitis, aggregates of histiocytes, lymphocytes, and plasma cells infiltrate the walls of respiratory bronchioles and extend into the peribronchiolar tissues. HRCT can show (i) prominent branching centrilobular opacities representing dilated bronchioles with inflammatory bronchiolar wall thickening and abundant intraluminal secretions, (ii) bronchiolar dilatation that tends to occur late in the disease process [126,127,128] and is typically proximal to the

nodular peribronchiolar opacities, and (iii) centrilobular nodules that reflect bronchiolar and peribronchiolar inflammation and fibrosis (Fig. 3-75) [127].

Asthma and Allergic Bronchopulmonary Aspergillosis.

Patients with asthma and allergic bronchopulmonary aspergillosis may develop mucoid impaction of centrilobular bronchioles visible as centrilobular opacities. These are more common in patients with allergic bronchopulmonary aspergillosis (93%) than in those who have asthma (28%) [129].

Hypersensitivity Pneumonitis. An immunologic response to a variety of inhaled allergens in sensitized persons, subacute hypersensitivity pneumonitis (extrinsic allergic alveolitis) is characterized by a peribronchiolar and perivascular lymphocytic and plasma cell infiltrate with formation of poorly defined granulomas [130]. There may be associated plugs of granulation tissue within bronchiolar lumens (bronchiolitis obliterans). Centrilobular nodules of ground-glass opacity seen on HRCT are typical (Figs. 3-61 and 3-62), reflecting the histologic abnormality [130,131,132,133].

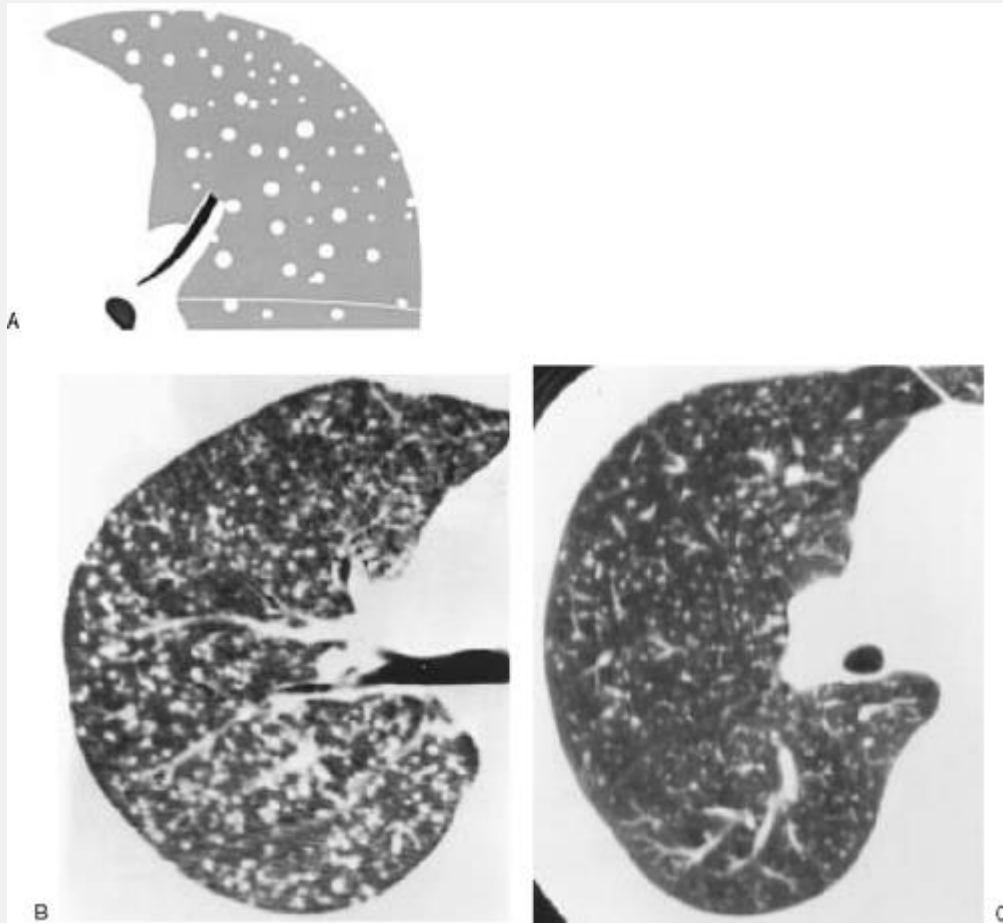


FIG. 3-55. A: Appearance of small nodules with a random distribution. Although some nodules can be seen in relation to interlobular septa, vessels, or the pleural surfaces, nodules do not appear to have a consistent or predominant relationship to any of these structures. A uniform distribution is most typical. B: Miliary tuberculosis with small nodules. Nodules a few millimeters in diameter have a random distribution and appear widely and evenly distributed throughout the lung. Some nodules can be seen in relation to small vessels, the pleural surfaces, and the interlobar fissure, but the nodules do not predominate in relation to these structures. (From Im JG, Itoh H, et al. Pulmonary tuberculosis: CT findings—early active disease

and sequential change with antituberculous therapy.

Radiology 1993;186:653, with permission.) C: In another patient with miliary tuberculosis, the nodules are smaller than those shown in B. The nodules are widely dispersed. (Courtesy of Shin-Ho Kook, M.D., Koryo General Hospital, Seoul, South Korea.)

P.109

Langerhans Histiocytosis. Initially, granulomas form in the peribronchiolar tissues and adjacent alveolar interstitium. Mononuclear Langerhans cells are present in the early stages of the disease; later, the cellular response diminishes and fibrosis dominates. Centrilobular nodules on HRCT reflect the peribronchiolar abnormality (Fig. 3-59) [93]. Later in the course of the disease, cavitation of nodules, cyst formation, and centrilobular bronchiolectasis can be seen.

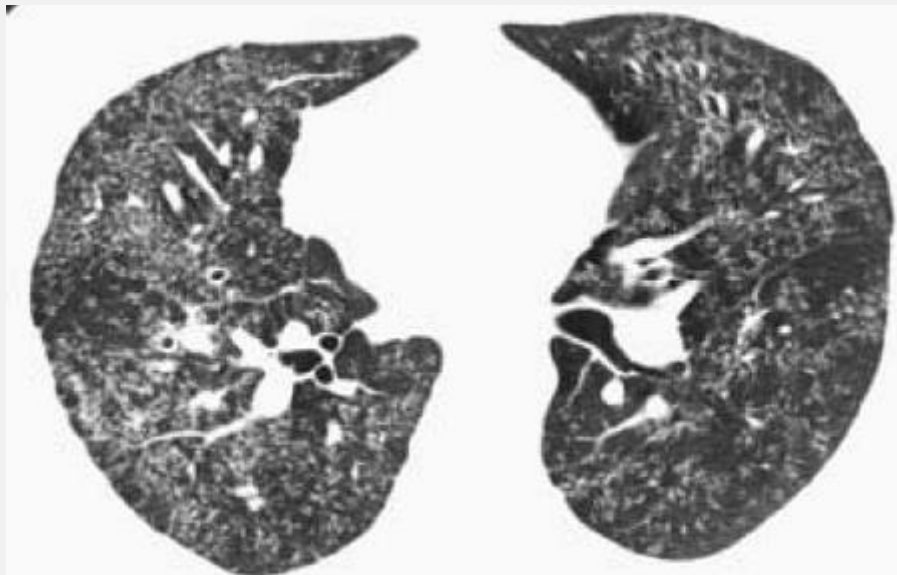


FIG. 3-56. Miliary coccidioidomycosis with numerous very small nodules that have a random distribution.

Bronchiolitis Obliterans Organizing Pneumonia BOOP, also known as *cryptogenic organizing pneumonia* (COP) or simply *organizing pneumonia*, is characterized by the presence of inflammatory cells lining the walls of the terminal and respiratory bronchioles with plugs of granulation tissue within airway lumen and organizing pneumonia. Because the organizing pneumonia is distributed in the peribronchiolar airspaces, centrilobular opacities can be present in patients P.110

with BOOP (Figs. 3-76 and 3-77). Frank consolidation or larger areas of ground-glass opacity, however, are more common [134,135]. Tree-in-bud may occasionally be seen [123].

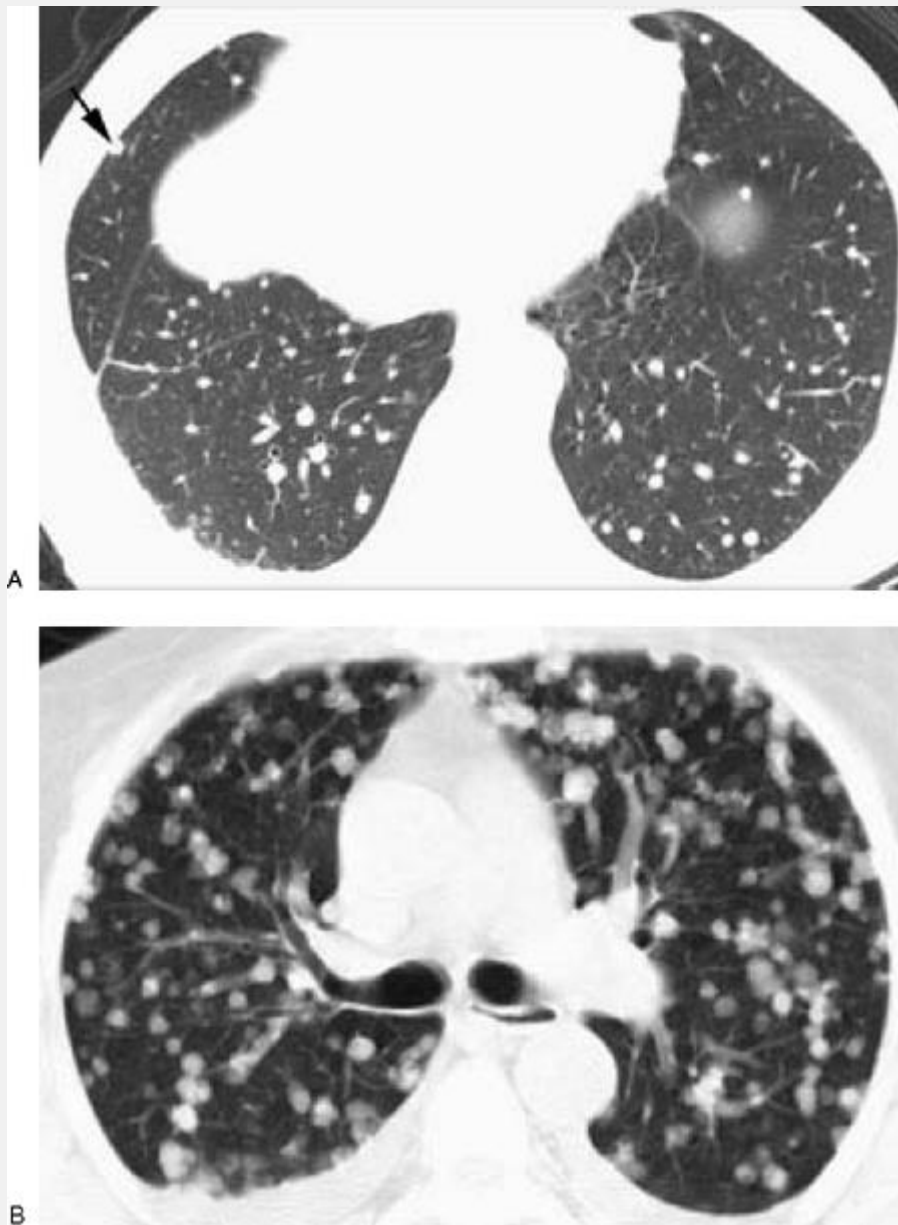


FIG. 3-57. Hematogenous metastases from a rectal carcinoma. A: HRCT obtained in a patient with an abnormal chest radiograph and no known tumor. Multiple small, well-defined nodules are visible, with involvement of the peripheral pleural surfaces (*arrow*). The overall pattern of distribution is random. B: Spiral CT obtained 6 months later following diagnosis of the patient's tumor shows progression of the metastases. A random distribution, with diffuse and

uniform lung involvement is well demonstrated.

Bronchiolitis Obliterans. Bronchiolitis obliterans, also known as *constrictive bronchiolitis*, is characterized primarily by concentric bronchiolar and peribronchiolar fibrosis and luminal narrowing or obliteration. In an acute phase, ill-defined centrilobular nodules may sometimes be seen, reflecting peribronchiolar inflammation [107,136,137]. In the later obliterative stage, centrilobular opacities occasionally may be seen, but they are not a common feature of this disease [60]. Airway obstruction with air-trapping is much more frequent.

Respiratory Bronchiolitis. Respiratory bronchiolitis is thought to represent a nonspecific reaction to inhaled irritants, usually in association with cigarette smoking; it is almost always seen in smokers. Inflammation of the respiratory bronchioles, with filling of the bronchioles by brown-pigmented macrophages, plasma cells, and lymphocytes is present histologically. In symptomatic patients, macrophages and inflammatory cells extend into the peribronchiolar airspaces and alveolar walls. When associated with symptoms, the term *respiratory bronchiolitis-interstitial lung disease* is used. HRCT findings in symptomatic patients include multifocal ground-glass opacities with a centrilobular distribution that reflects the peribronchiolar nature of this disease (see Figs. 6-34 and 6-35) [109,138,139,140]. Patchy opacities can also be seen. Distinct centrilobular opacities may be seen in patients who use inhalational drugs—for example, so-called crack lung.



FIG. 3-58. Diffuse sarcoidosis with a random distribution of nodules. Very small nodules are seen in relation to the major fissure, but the overall distribution is diffuse and uniform. Findings typical of sarcoidosis, such as a patchy distribution or a predominance of nodules in relation to peribronchovascular regions, are not seen. (Courtesy of Luigia Storto, Chieti, Italy.)

Cigarette Smoking. A few small subpleural and centrilobular nodules can be seen in subjects who smoke or have a history of smoking. Ill-defined centrilobular nodules have been reported in as many as 12% to 27% of smokers studied using HRCT, reflecting the presence of bronchiolectasis and peribronchiolar fibrosis [108,109], although in our experience, this is not a common finding.

Aspiration. Aspiration of a variety of materials, including gastric contents, water, or blood, associated with a variable inflammatory response may result in ill-defined centrilobular opacities [136,137].

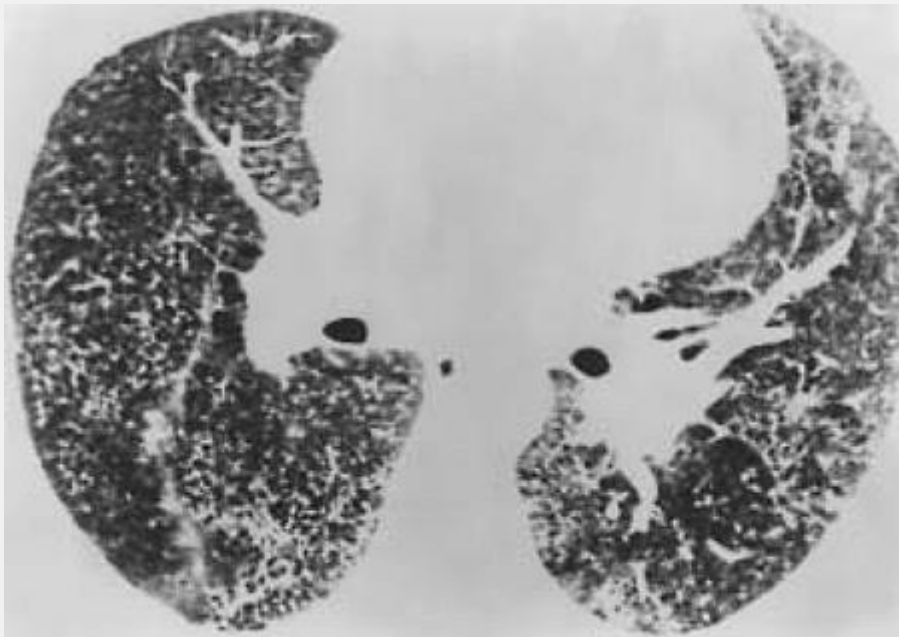


FIG. 3-59. Langerhans histiocytosis with small nodules. Small nodules, best seen in the paravertebral regions, are numerous and have a random distribution.

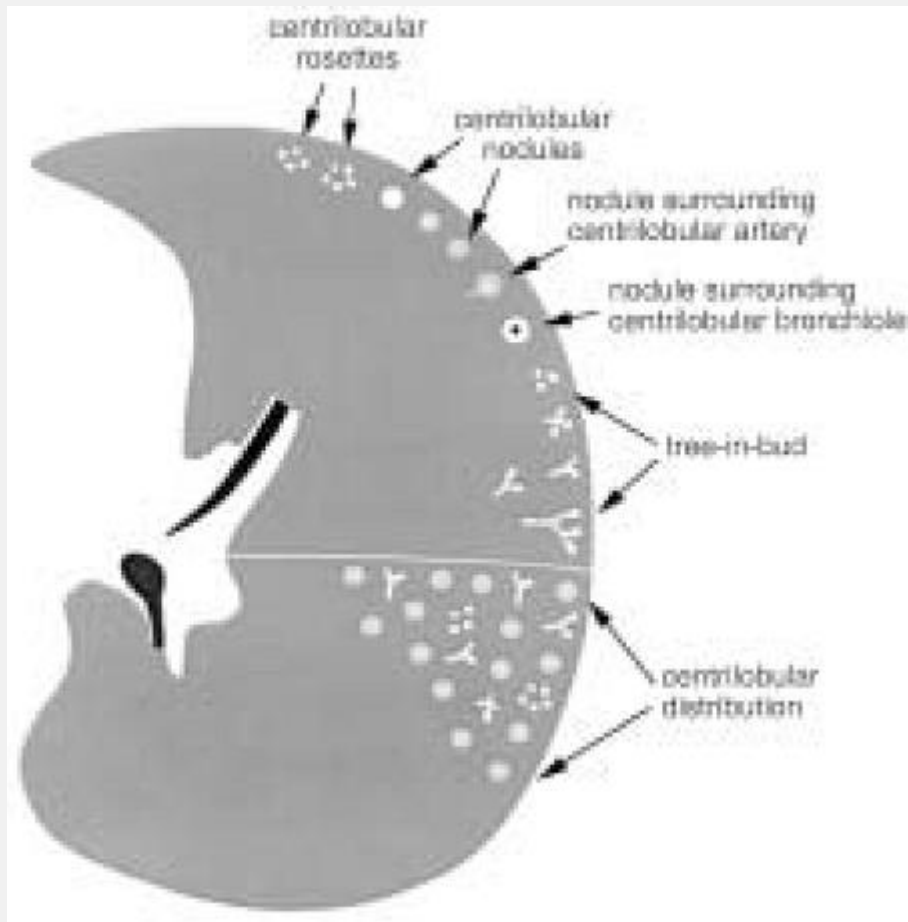


FIG. 3-60. HRCT appearances of centrilobular nodules. Centrilobular nodules are usually separated from the interlobular septa and pleural surfaces by a distance of several millimeters; in the lung periphery, the nodules are usually centered 5 to 10 mm from the pleural surface. Also, centrilobular nodules may be associated with small pulmonary artery branches. Because of the similar size of secondary lobules, centrilobular nodules often appear to be evenly spaced. Although they are often ill defined, this is not always the case. Either a single centrilobular nodule or a centrilobular rosette of nodules may be seen. In occasional cases, the air-filled centrilobular bronchiole can be recognized as a rounded lucency within a centrilobular

nodule. Tree-in-bud may be seen in patients with a centrilobular distribution, representing impaction of centrilobular bronchioles.

Asbestosis. In patients with early asbestosis, the histologic abnormality is nearly identical to that seen in patients
P.112

P.113

with respiratory bronchiolitis, but asbestos fibers can be identified in the peribronchiolar tissues. Fiber deposition in the respiratory bronchioles results in a peribronchiolar cellular response and fibrosis that eventually extends to involve the contiguous airspaces and alveolar interstitium. Ill-defined centrilobular opacities have been reported on HRCT in as many as half of patients with early asbestosis (see Figs. 4-46 and 4-47) [141]. Nodules predominate posteriorly and at the lung bases, probably due to the gravitational effects of fiber deposition [44,141]. Other inhaled inorganic materials can result in similar histologic and imaging abnormalities.

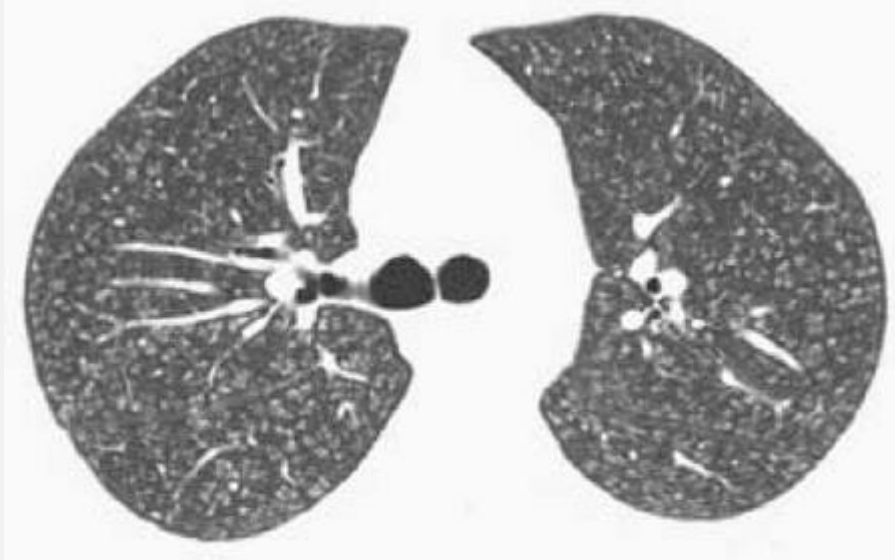


FIG. 3-61. Ill-defined centrilobular nodules and rosettes in a patient with hypersensitivity pneumonitis. The nodules are separated from the pleural surfaces and fissures by a distance of several millimeters. As is typical, the nodules often appear to be evenly spaced and, in this case, are diffusely distributed. This is a common appearance in hypersensitivity pneumonitis.



FIG. 3-62. Centrilobular nodules of ground-glass opacity in a patient with hypersensitivity pneumonitis. The ill-defined opacities are visible in relation to small vascular branches throughout the lung. The most peripheral nodules are centered 5 to 10 mm from the pleural surface. The subpleural lung region appears spared.

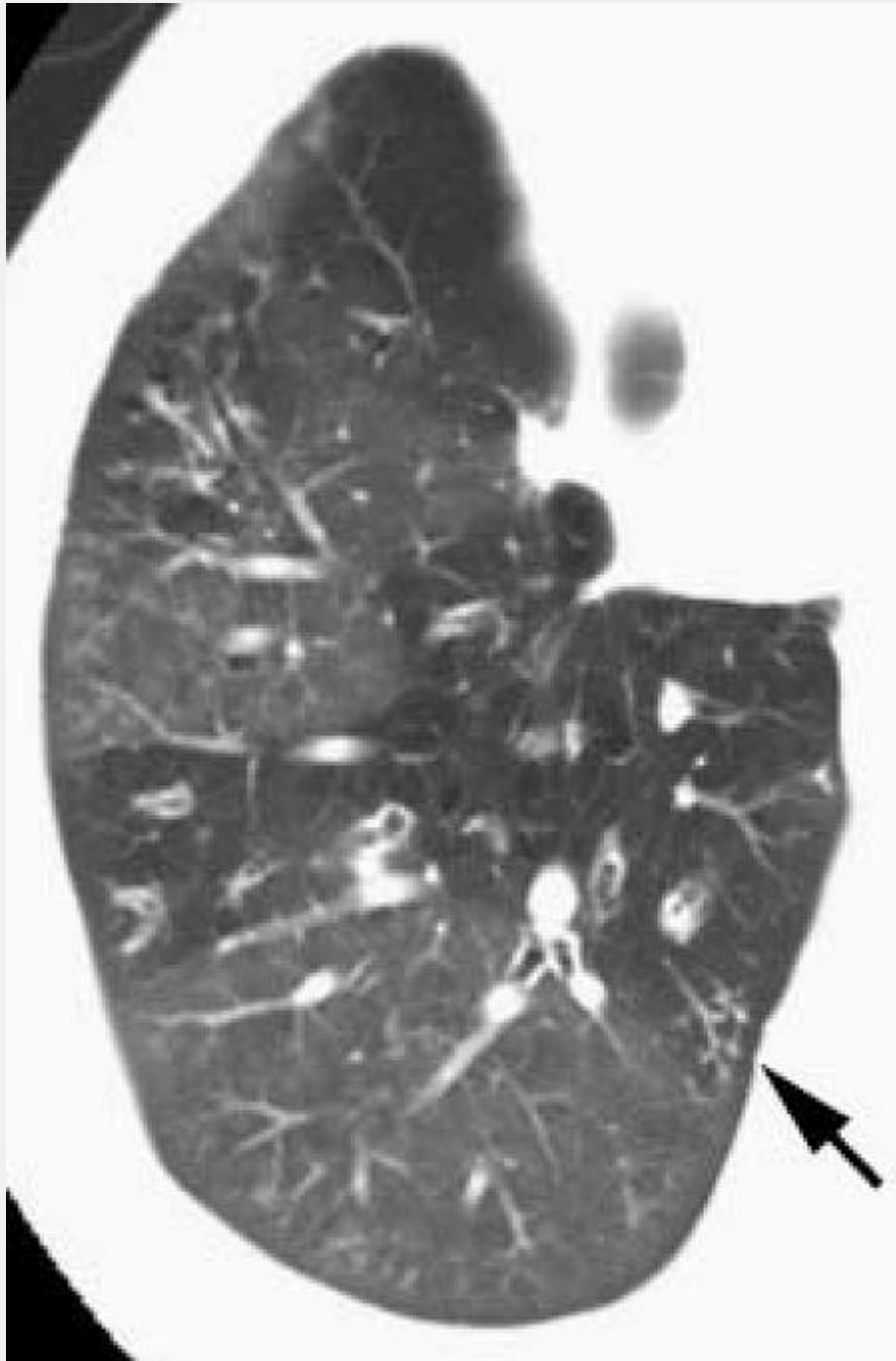


FIG. 3-63. Centrilobular tree-in-bud (arrow) in a patient with cystic fibrosis and chronic airway infection. Also note bronchial wall thickening and inhomogeneous lung attenuation due to airways obstruction and air-trapping with mosaic perfusion.

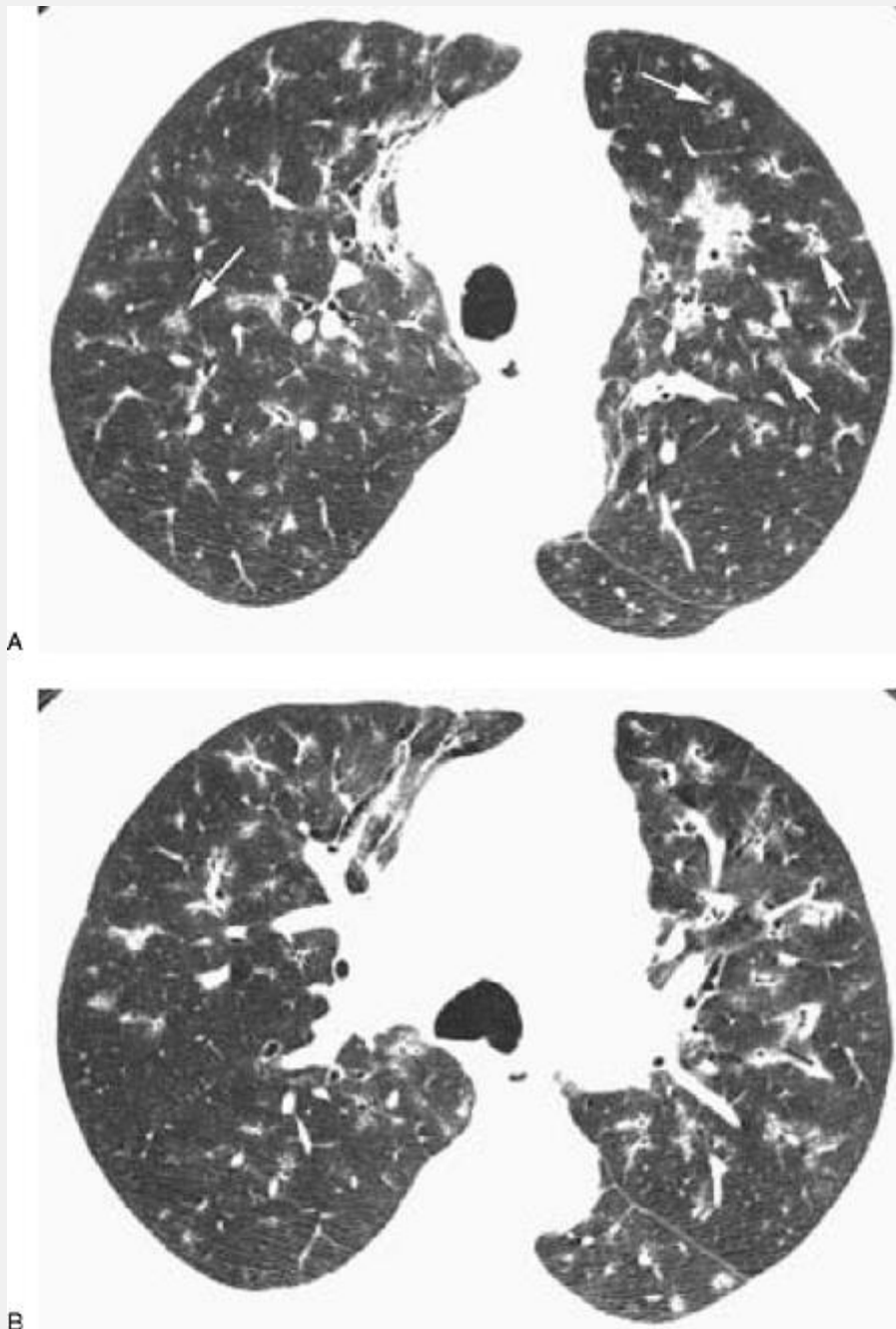


FIG. 3-64. A, B: Ill-defined centrilobular nodules in a patient with chronic airways disease and bronchopneumonia. A number of the ill-defined nodules surround an air-filled bronchus or bronchiole (arrows).

Follicular Bronchiolitis. This entity, defined as lymphoid hyperplasia of bronchus-associated lymphoid tissue, is

characterized by hyperplastic lymphoid follicles along the walls of centrilobular bronchioles. It may be seen in patients with collagen-vascular diseases, particularly rheumatoid arthritis or AIDS, and is related histologically to LIP. Small, well-defined centrilobular nodules, often smaller than 3 mm in diameter, are invariably seen, and large airway abnormalities and peribronchial nodules may also be present (see Figs. 4-21 and 5-14) [120,142,143,144].

Endobronchial Spread of Neoplasm. Centrilobular nodules can be seen in bronchioloalveolar carcinoma (see Fig. 5-11) P.114

or tracheobronchial papillomatosis (Fig. 3-78) when endobronchial spread of tumor occurs [145,146]. These can be well-defined or ill-defined. Large airway papillomas or cystic lesions may also be visible in patients with tracheobronchial papillomatosis.

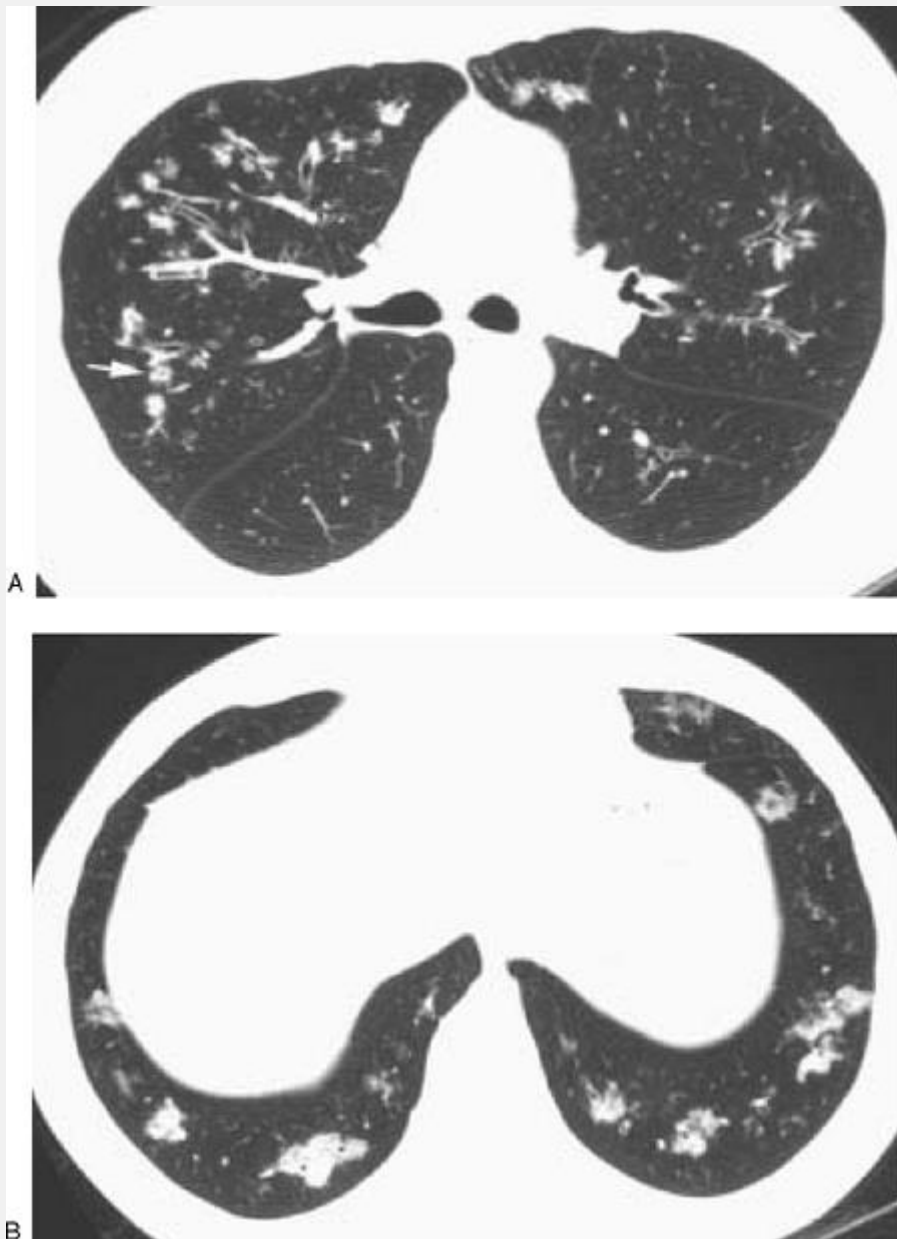


FIG. 3-65. Centrilobular nodules in a patient with bronchopneumonia. A: Scattered ill-defined nodules represent peribronchiolar consolidation and may contain a visible bronchiole (*arrow*). B: At the lung bases, consolidated lobules surround air-filled bronchioles in several locations. Bronchopneumonia is also termed *lobular pneumonia* because of this appearance.

Vascular and Perivascular Diseases

Vascular pathology, either localized to the walls of arteries or to perivascular tissues, can cause centrilobular abnormality. Because airways are not involved, bronchiolectasis and tree-in-bud are absent, although if the cellular response extends into the peribronchiolovascular interstitium, apparent bronchiolar wall thickening may result.

Pulmonary Edema. Mild cases of edema may show hazy, ill-defined centrilobular opacities (see Figs. 6-71 and 6-72) [28,40,103]. Increased prominence of the centrilobular artery resulting from perivascular interstitial thickening is also commonly visible (Figs. 3-10 and 3-41). Septal thickening is variably associated, but in some patients, centrilobular opacities predominate. Pleural effusion may also be present.

Vasculitis. Processes resulting in a vascular and perivascular inflammatory response, including vasculitis and reaction to injected substances, such as talc [95,107,147], can result in ill-defined centrilobular opacities on HRCT. Connolly et al. [148] reported hazy or fluffy centrilobular, perivascular opacities in eight children with vasculitis,

P.115

P.116

including five with Wegener's granulomatosis, one with systemic lupus erythematosus, one with scleroderma-polymyositis overlap syndrome, and one with Churg-Strauss syndrome. In these eight children, centrilobular opacities were associated with the onset of active disease or with an

exacerbation of preexisting disease. In four of five patients, this abnormality disappeared on treatment.

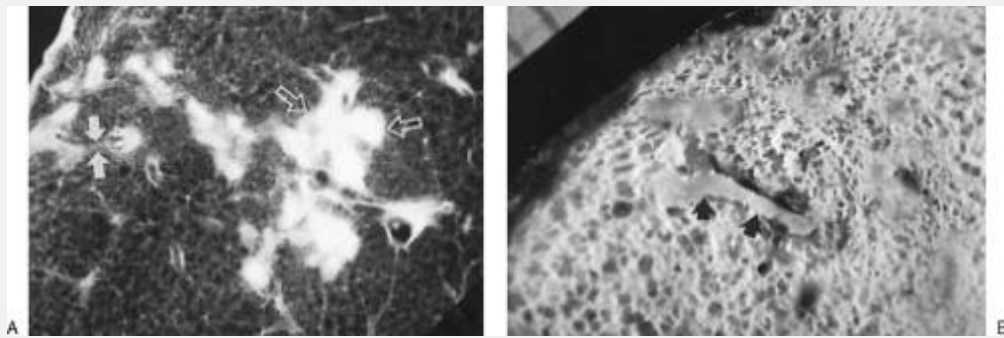


FIG. 3-66. Centrilobular nodules and tree-in-bud in a patient with tuberculosis. A: Radiograph of a resected lung in a patient with endobronchial spread of tuberculosis, shows a branching centrilobular opacity (*solid arrows*), and rosettes of small nodular opacities producing a tree-in-bud appearance (*open arrows*). B: On pathologic examination, the branching centrilobular opacity represents caseous material filling bronchioles and alveolar ducts (*arrows*). (From Im JG, Itoh H, et al. Pulmonary tuberculosis: CT findings—early active disease and sequential change with antituberculous therapy. *Radiology* 1993;186:653, with permission.)

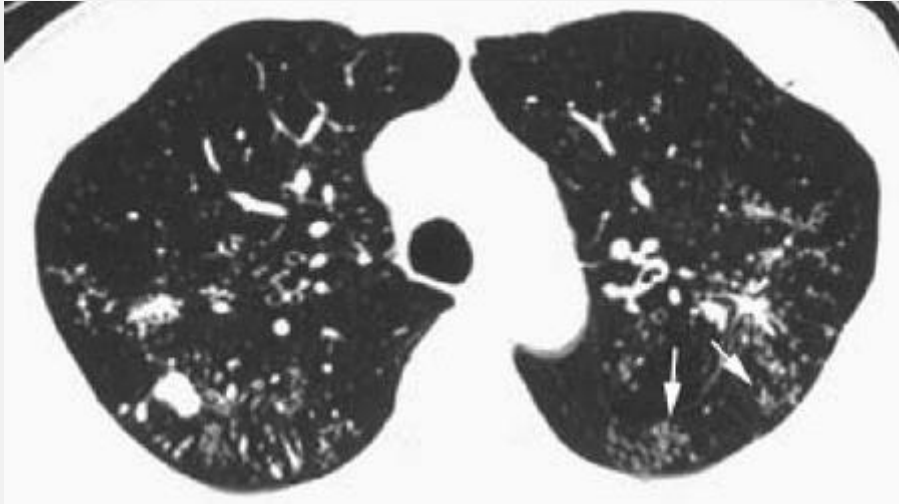


FIG. 3-67. Centrilobular nodules and rosettes in a patient with endobronchial spread of tuberculosis. Multiple small nodules occurring in clusters (*arrows*) are common in patients with this disease. The nodules, being centrilobular, spare the pleural surfaces.

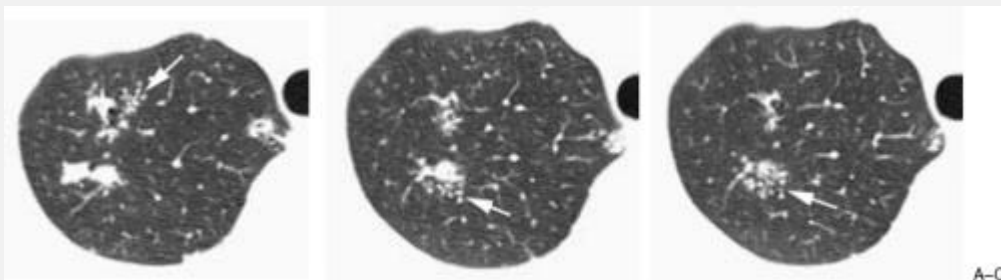


FIG. 3-68. A-C: Centrilobular rosettes and tree-in-bud in a patient with endobronchial spread of tuberculosis. Multiple small nodules occurring in clusters and the appearance of tree-in-bud (*arrows*) are seen in association with several

larger nodules in the right lung apex. The appearance of tree-in-bud almost always indicates infection. *Mycobacterium tuberculosis* was found in this patient's sputum.

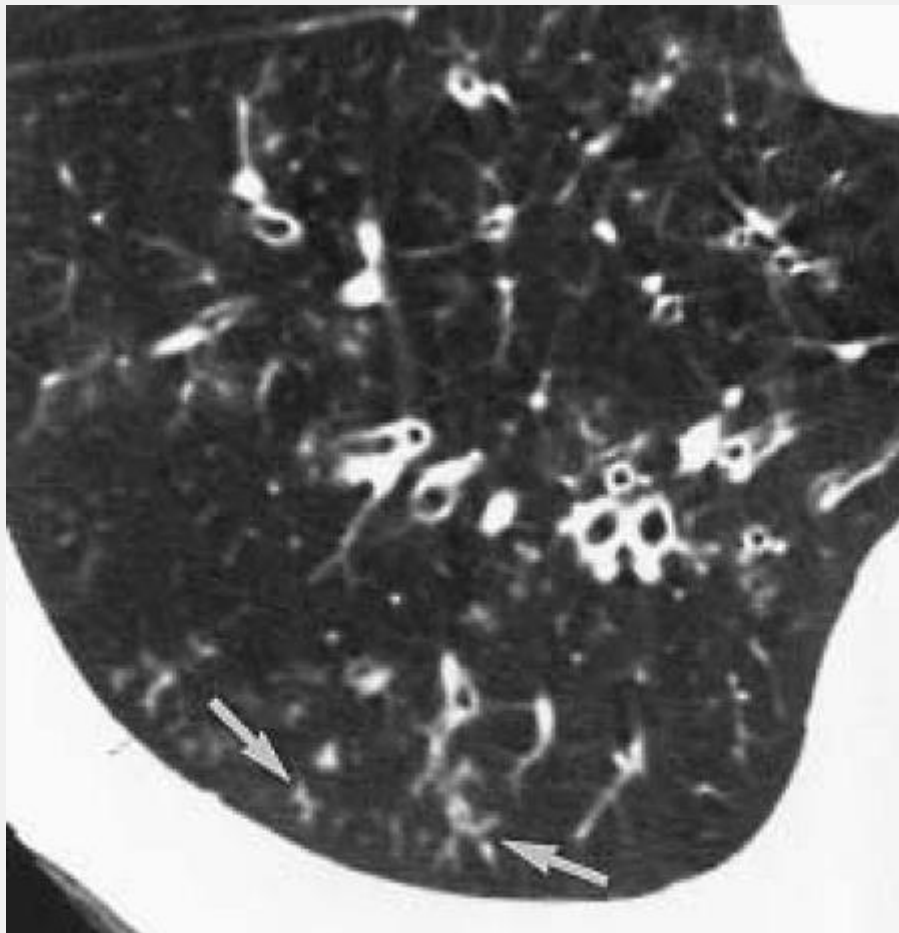


FIG. 3-69. Nontuberculous mycobacterial infection with endobronchial spread. Coned view of the right lower lobe in a patient with chronic obstructive lung disease and *Mycobacterium avium-intracellulare* complex infection on sputum cultures. Central bronchi are dilated and thick walled; centrilobular bronchioles are also dilated, and have a tree-in-bud appearance (*arrows*). (From Gruden JF, Webb WR, et al. Centrilobular opacities in the lung on HRCT:

diagnostic considerations and pathologic correlation. *AJR Am J Roentgenol* 1994;162:569, with permission.)



FIG. 3-70. Bronchopneumonia. HRCT shows a right lower lobe bronchopneumonia with ill-defined centrilobular

nodules and bronchiolar dilatation. Lower lobe bronchi also appear thick walled.

Pulmonary Hemorrhage. Ill-defined centrilobular nodules may occasionally be seen in patients with acute pulmonary hemorrhage [149]. In children with idiopathic pulmonary hemorrhage, also known as *idiopathic pulmonary hemosiderosis*, recurrent episodes of pulmonary hemorrhage may result in ill-defined centrilobular nodules [121]. This finding may be related to deposition of hemosiderin-laden macrophages in relation to small vessels and bronchioles.

Metastatic Calcification. Metastatic calcification is described in detail in the section Metastatic Calcification. Calcium deposits typically involve the interstitium and alveolar septa in a centrilobular perivascular distribution. Ill-defined nodules of ground-glass opacity or obvious calcifications may be seen. These may be lobular or centrilobular (Fig. 3-106) [150,151].

Pulmonary Hypertension. Cholesterol granulomas may be seen in a centrilobular location in patients with pulmonary hypertension. In one study, histopathologic evidence of cholesterol granulomas was found in five (25%) of 20 patients with severe pulmonary hypertension [152]. In three of these five patients, the granulomas manifested on HRCT as small centrilobular nodules. These may also occur in patients with endogenous lipoid pneumonia and alveolar proteinosis. In patients with pulmonary hypertension and capillary hemangiomatosis, ill-defined centrilobular nodules may also be seen (see Fig. 9-9) [153].

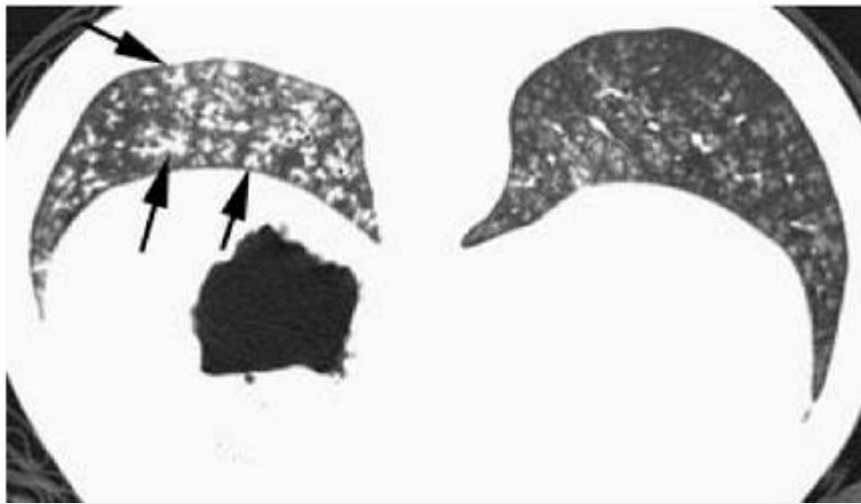
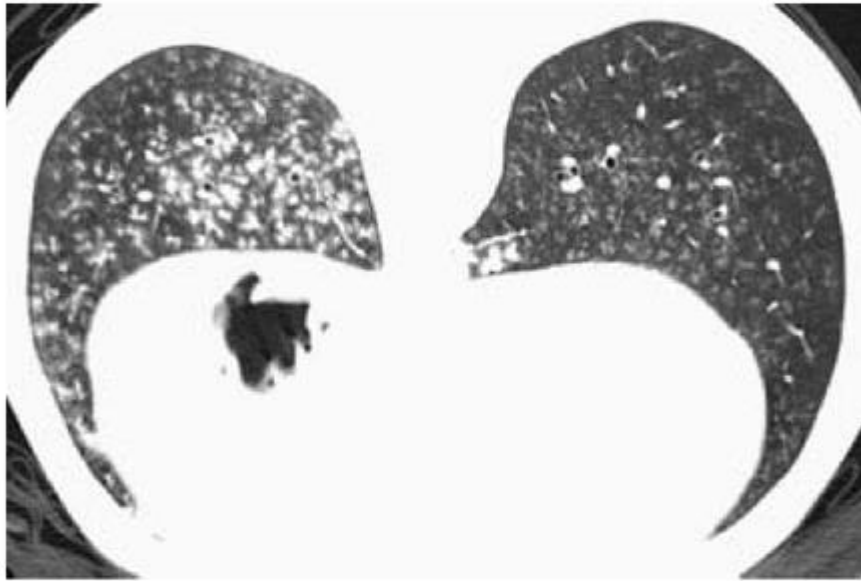


FIG. 3-71. Supine (A) and prone (B and C) HRCT in a patient with bronchopneumonia due to *Haemophilus influenzae*. Ill-defined centrilobular nodules are visible bilaterally, with a predominance on the left. An appearance of tree-in-bud is visible in many locations (*arrows*, C).

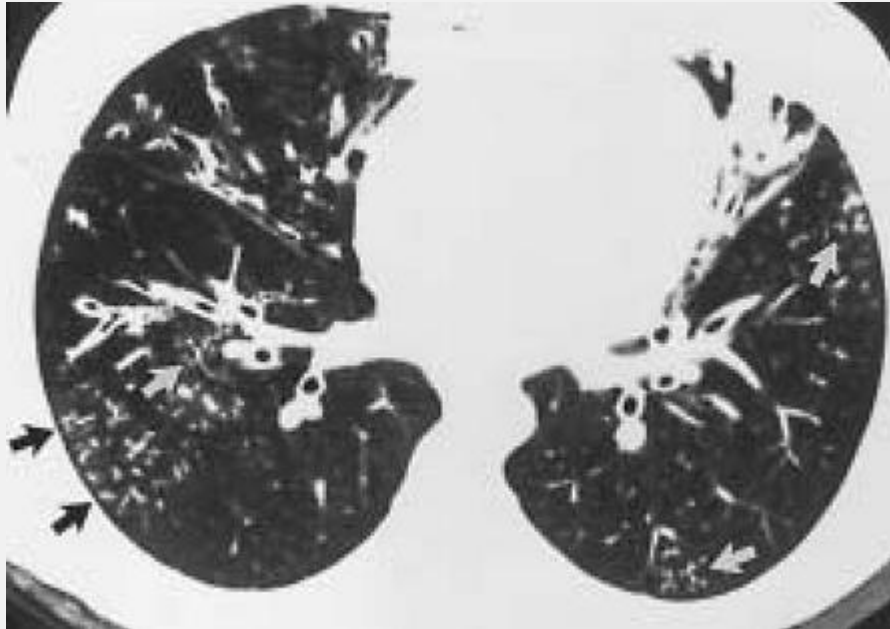


FIG. 3-72. Centrilobular bronchiolar abnormality with tree-in-bud in a patient with cystic fibrosis. Fluid, mucus, or pus-filled centrilobular bronchioles result in a tree-in-bud appearance in several lung regions (*arrows*). These are associated with findings of bronchiectasis.

P.117

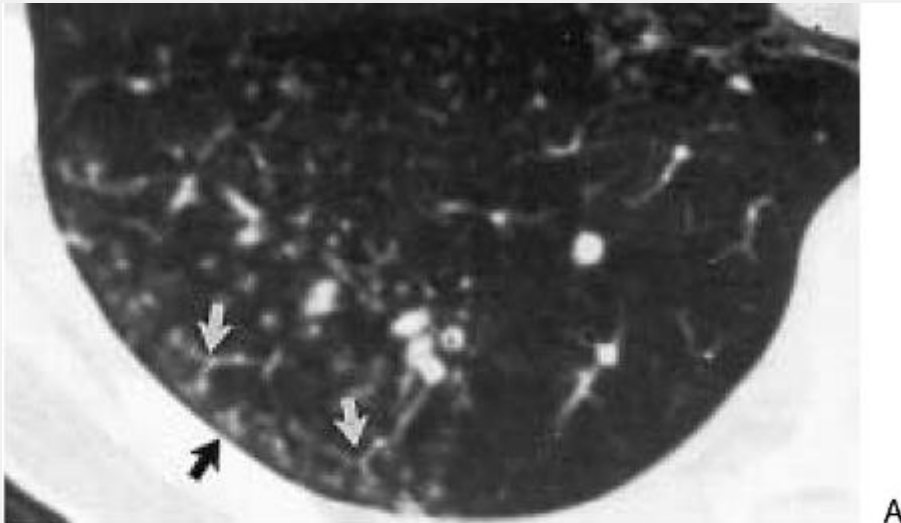
P.118

Centrilobular Distribution with Tree-in-Bud

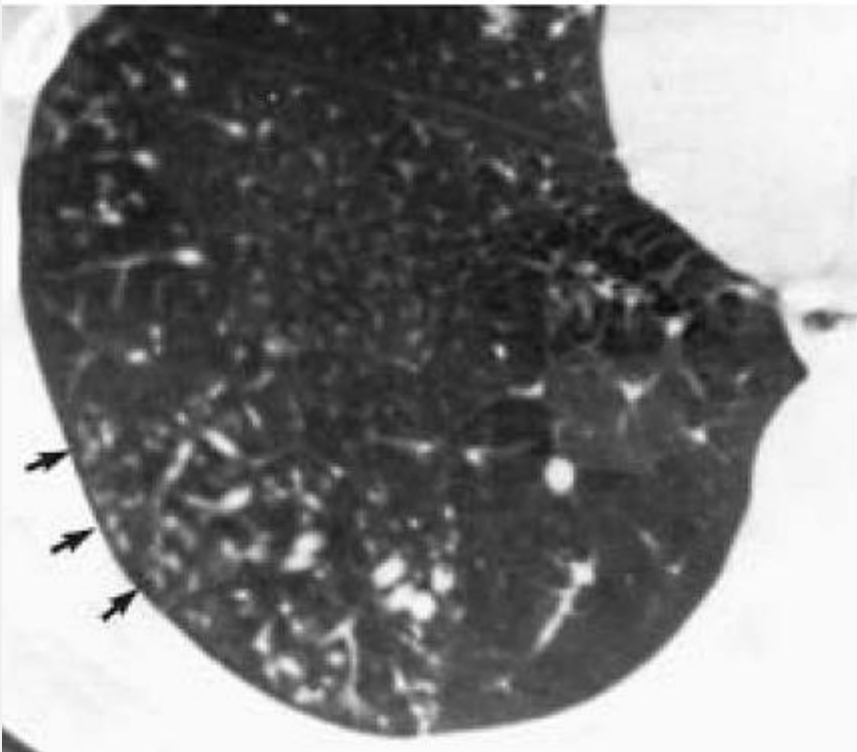
A centrilobular distribution of nodular opacities may be associated with an important finding, termed *tree-in-bud*, which is of great value in differential diagnosis (Table 3-6) [65,107,136,137,154]. The finding of tree-in-bud reflects the presence of dilated centrilobular bronchioles, their lumina impacted with mucus, fluid, or pus, and often associated with peribronchiolar inflammation. Because of the branching pattern of the dilated bronchiole and the presence of ill-defined nodules of peribronchiolar inflammation, its appearance has been likened to a budding or fruiting tree [65,126], or the children's toy jacks [154] (Figs. 3-60, 3-63, 3-66, 3-68, 3-69, 3-71, 3-72, 3-73, 3-74, 3-75, 3-79, and 3-80). The term *budding tree* has also been used to describe the appearance of small airway filling on bronchography [155].

On HRCT, the finding of tree-in-bud is usually easy to recognize, but several different appearances may be seen alone or in combination. In the lung periphery, tree-in-bud may be associated with a typical branching appearance, with the most peripheral branches or nodular opacities being several millimeters from the pleural surface. Tree-in-bud may also appear as a centrilobular cluster of nodules, depending on the relationship of the bronchiole to the plane of scan. If the centrilobular bronchiole is sectioned across its axis, as is typical in the costophrenic angles, the impacted bronchiole may appear to be a single, well-defined, centrilobular nodule a few millimeters in diameter. Abnormal bronchioles producing a tree-in-bud pattern can usually be distinguished from normal centrilobular vessels

by their more irregular appearance, a lack of tapering, and a knobby or bulbous appearance at the tips of small branches (Figs. 3-79 and 3-80). Normal centrilobular arteries are considerably thinner than the branching bronchioles seen in patients with this finding, and are much less conspicuous. Furthermore, because tree-in-bud is often patchy in distribution, it is easy to contrast its appearance with that of adjacent normal lung regions.



A



B

FIG. 3-73. A, B: Centrilobular bronchiolar abnormality and tree-in-bud in a patient with yellow nails and lymphedema syndrome and chronic bronchial sepsis. A tree-in-bud appearance and small well-defined centrilobular nodules (*arrows*) are visible in the posterior right lower lobe. These reflect the presence of pus-filled centrilobular bronchioles.

This appearance is easily contrasted with the appearance of normal lung more medially.

Tree-in-bud is not usually the only abnormal finding visible on HRCT. Bronchiolar dilatation and wall thickening can sometimes be seen in association with tree-in-bud if the dilated bronchioles are air-filled; normal bronchioles should not be visible in the peripheral 1 cm of lung. Tree-in-bud may also be associated with ill-defined centrilobular nodules representing areas of inflammation (Fig. 3-71). Large airway abnormalities with wall thickening or bronchiectasis are also often present (Fig. 3-72) [107]. For example, in a study by Aquino et al. [137], 26 (96%) of 27 patients showing tree-in-bud on HRCT also showed bronchiectasis or bronchial wall thickening.

The finding of tree-in-bud is indicative of small airways disease. Furthermore, a tree-in-bud appearance is associated

P.119

P.120

with airway infection in the large majority of cases, although it may also be seen in patients with mucoid impaction of centrilobular bronchioles in absence of infection and in some patients with bronchiolar wall infiltration [142]. In a study by Aquino et al. [137], 25% of patients with bronchiectasis and 18% of patients with infectious bronchitis showed tree-in-bud, but this finding was not visible in patients with other diseases involving the airways, such as emphysema, respiratory bronchiolitis,

bronchiolitis obliterans, BOOP, or hypersensitivity pneumonitis. Similarly, in patients with active tuberculosis, a tree-in-bud appearance was visible in 72% of patients in one study [65], correlating with the presence of solid caseous material within terminal and respiratory bronchioles (Fig. 3-66). In patients with Asian panbronchiolitis, prominent, branching centrilobular opacities represent dilated bronchioles with inflammatory bronchiolar wall thickening and abundant intraluminal secretions (Fig. 3-75) [126,127].

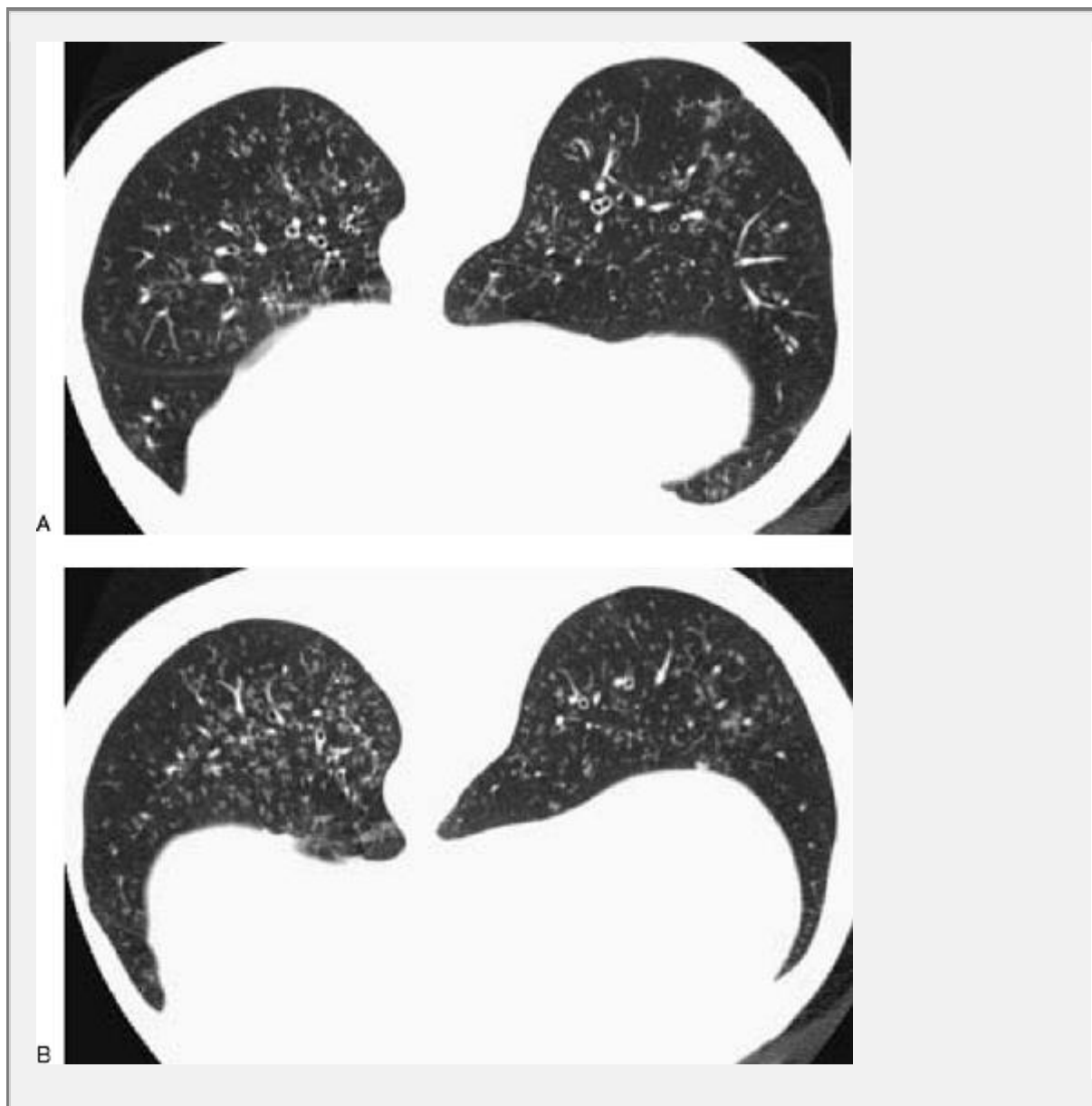


FIG. 3-74. A, B: Prone scans in a patient with chronic bronchiectasis and small airway infection. Small centrilobular nodules, rosettes, and tree-in-bud are visible throughout the lower lobes.

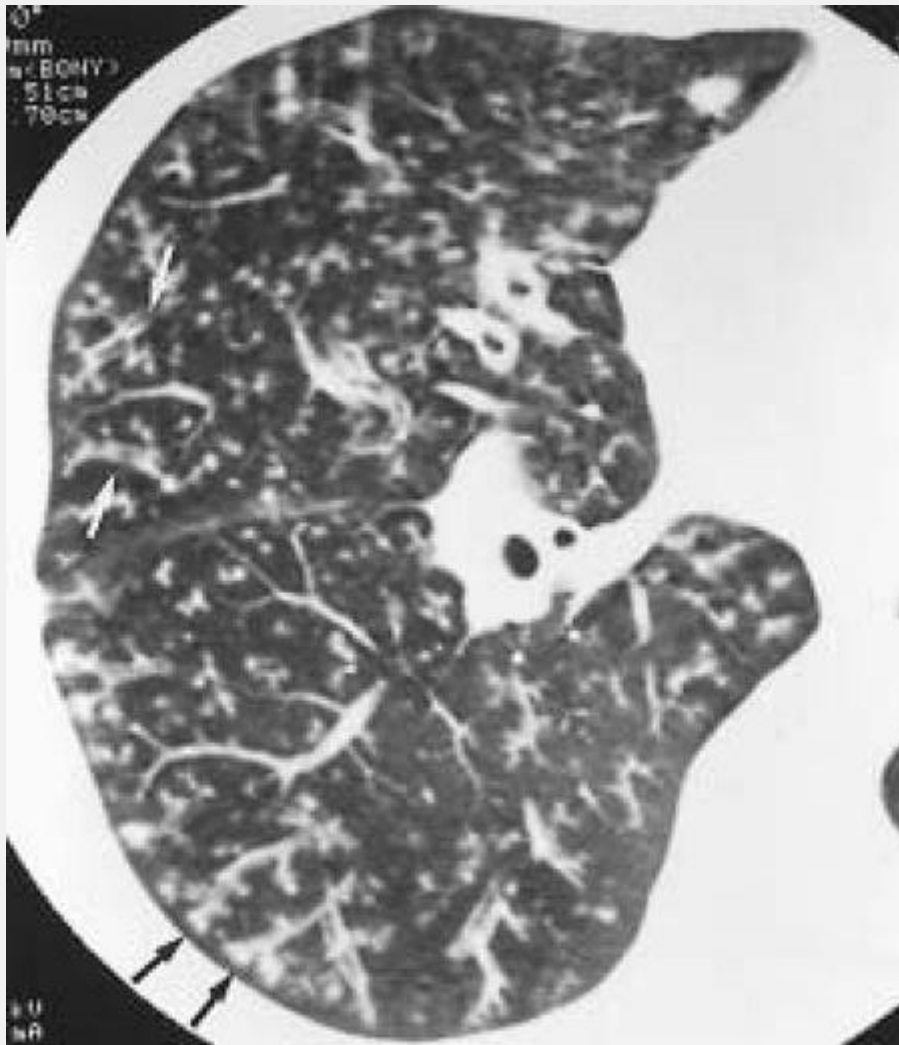


FIG. 3-75. Bronchiolar abnormalities in Asian panbronchiolitis. Dilated and thick-walled bronchioles (*white arrows*) are seen in association with a tree-in-bud appearance (*black arrows*) and multiple centrilobular nodules. These findings correlate pathologically with the presence of dilated bronchioles, inflammatory bronchiolar

wall thickening, abundant intraluminal secretions, and peribronchiolar inflammation. (Courtesy of Harumi Itoh, M.D., Chest Disease Research Institute, Kyoto University, Kyoto, Japan.)

Thus, in patients with a centrilobular distribution of nodules, if tree-in-bud can be recognized, the differential diagnosis is limited. Among the larger group of diseases causing centrilobular nodules listed in the previous paragraph, tree-in-bud may be seen in patients with endobronchial spread of tuberculosis [65] or nontuberculous mycobacteria [107], bronchopneumonia, infectious bronchiolitis [123], cystic fibrosis [124], bronchiectasis of any cause [107,136,137], and Asian panbronchiolitis [126,127]. It may also be seen in airway diseases that result in the accumulation of mucus within small bronchi, such as asthma or allergic bronchopulmonary aspergillosis [136], but this finding is less frequent. It is rarely seen in patients with constrictive bronchiolitis, presumably related to impaction of bronchioles [136]. An appearance resembling tree-in-bud has been reported in patients with follicular bronchiolitis, an entity in which hyperplasia of lymphoid follicles occurs in relation to centrilobular airways; it is seen in association with collagen-vascular disease or AIDS [142]. Bronchioloalveolar carcinoma may occasionally show tree-in-bud, although nodules are more typical [146]. In some patients with sarcoidosis, nodules occurring in relation to centrilobular arteries may mimic the appearance of tree-in-bud, although other typical features of sarcoidosis are usually present [107,136].

Algorithmic Approach to Nodule Localization and Diagnosis

A simple algorithm may be used to help localize small nodules as perilymphatic, random, or centrilobular and classify them for the purposes of differential diagnosis (Algorithm 4) [156]. Distinguishing these three distributions is most easily accomplished by looking first for pleural nodules and nodules arising in relation to the fissures.

If subpleural nodules are absent, the pattern is centrilobular. Keep in mind that large centrilobular nodules may touch the pleura but do not appear to arise from it; nodules a few millimeters in diameter that touch the pleura are not centrilobular. If a centrilobular distribution is present, the finding of tree-in-bud should be sought. The differential diagnosis of centrilobular nodules unassociated with tree-in-bud is long and includes airway abnormalities and vascular abnormalities. If tree-in-bud is present, then nearly all cases will represent airway disease, which is infectious in nature.

If numerous subpleural or fissural nodules are present, then the pattern is either perilymphatic or random. These two patterns are distinguished by looking at the distribution of other nodules. If they are patchy in distribution, and particularly if a distinct predominance is noted relative to the peribronchovascular interstitium, interlobular septa, or subpleural regions, then the nodules are perilymphatic. If the nodules are distributed in a diffuse and uniform manner, the pattern is random.

The presence of a few subpleural nodules is nonspecific and may be seen regardless of the pattern. A few subpleural nodules that look different than the other visible nodules

(i.e., smaller, denser, or better defined) are likely unrelated to the patient's disease and should be ignored, whereas subpleural nodules that appear similar to other visible nodules are of potential significance in differential diagnosis. If a few subpleural nodules are visible, a determination of the

P.121

P.122

distribution and differential diagnosis should generally be based on other findings, such as tree-in-bud (i.e., centrilobular airways disease), patchy distribution (i.e., perilymphatic or centrilobular disease), predominant involvement of the peribronchovascular interstitium or interlobular septa (i.e., perilymphatic), or nodules of ground-glass opacity (centrilobular).

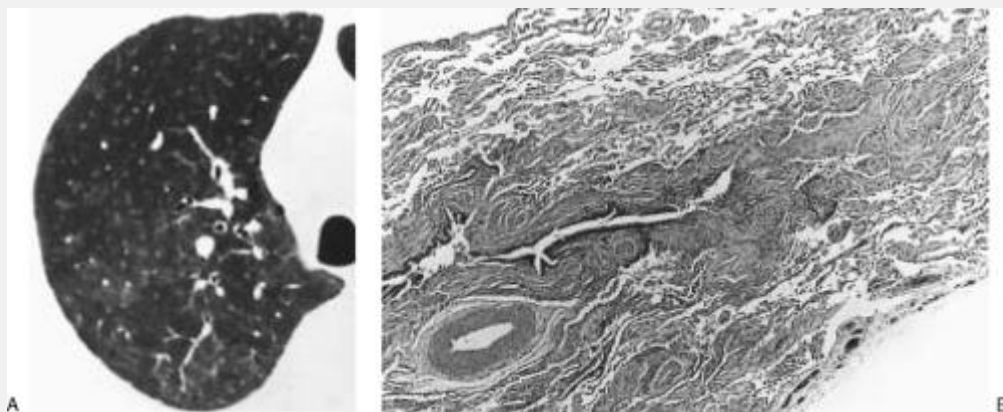


FIG. 3-76. Bronchiolitis obliterans organizing pneumonia (BOOP) with ill-defined centrilobular nodules. A: Multifocal areas of ill-defined opacity are present in the right upper

lobe. Note that small pulmonary artery branches are partially obscured by the centrilobular opacities. B: Open lung biopsy showed features of BOOP. Bronchioles are compressed and occluded by granulation tissue; organizing pneumonia and loose connective tissue are also present, surrounding the bronchioles. (From Gruden JF, Webb WR, et al. Centrilobular opacities in the lung on HRCT: diagnostic considerations and pathologic correlation. *AJR Am J Roentgenol* 1994;162:569, with permission.)

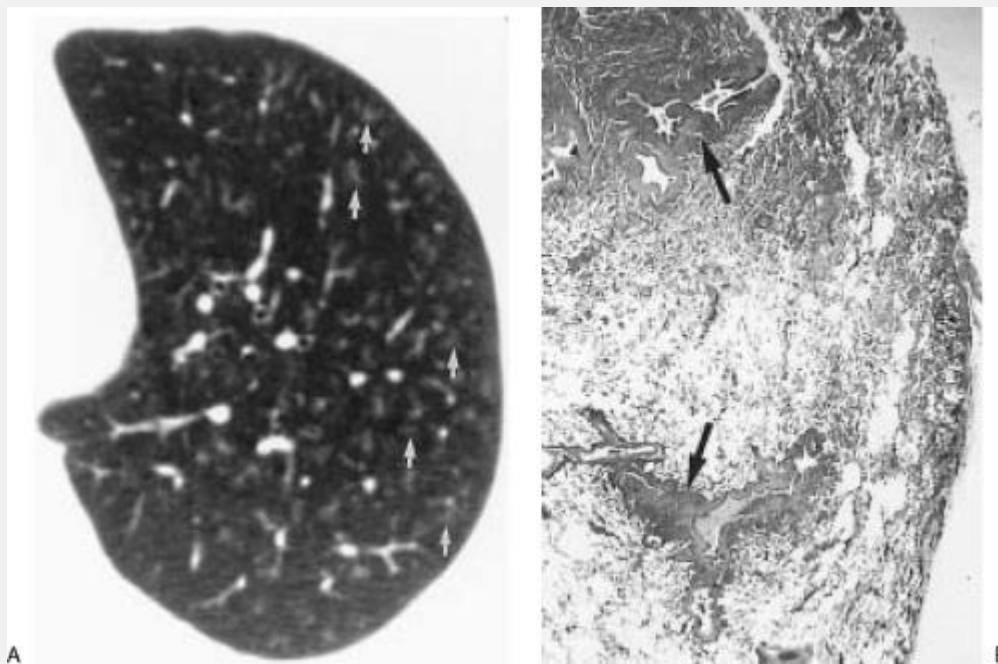


FIG. 3-77. Bronchiolitis obliterans organizing pneumonia with centrilobular opacities. A: Ill-defined nodular opacities (*arrows*) are scattered throughout the left upper lobe in this patient who had received an allogenic bone marrow transplant several years previously. Their centrilobular location can be inferred in that they surround small artery branches. B: Open lung biopsy shows bronchioles (*arrows*)

partially occluded by plugs of granulation tissue. Inflammation surrounding the bronchioles probably accounts for the opacities seen on HRCT. (From Gruden JF, Webb WR, et al. Centrilobular opacities in the lung on HRCT: diagnostic considerations and pathologic correlation. *AJR Am J Roentgenol* 1994;162:569, with permission.)

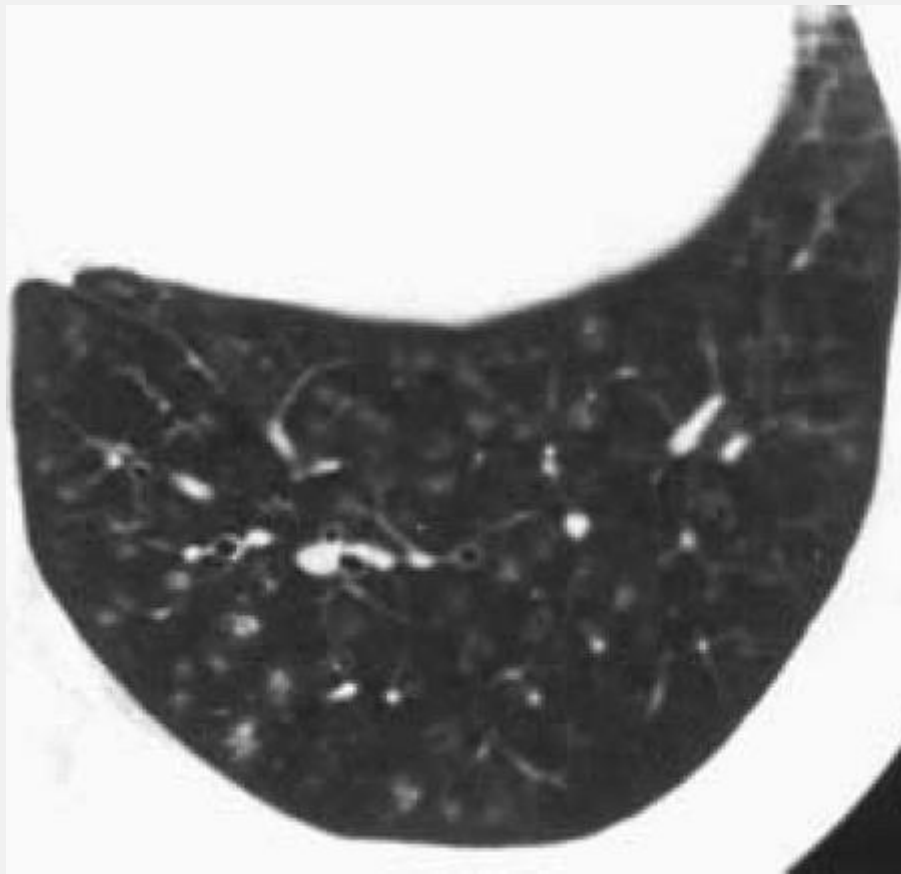


FIG. 3-78. Endobronchial spread of tracheobronchial papillomatosis. Multiple small, ill-defined, centrilobular nodules are present in the posterior left lower lobe. Many appear to be approximately 1 cm from the pleural surface or are related to small vessels.

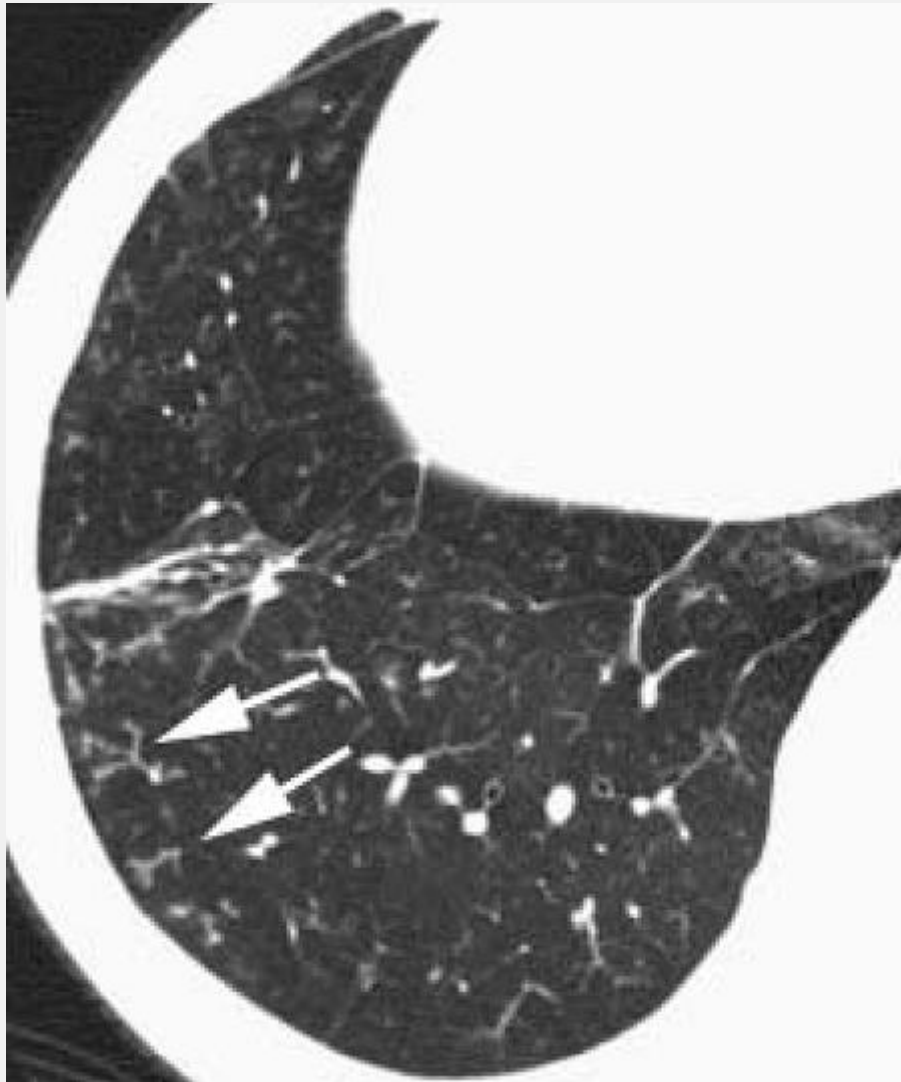


FIG. 3-79. Tree-in-bud in a patient with airway infection. Branching, impacted, pus-filled bronchioles (arrows) are visible in the peripheral lung. A parenchymal band seen more anteriorly represents focal atelectasis.

Accuracy of High-Resolution Computed Tomography in Nodule Localization

HRCT is accurate in localizing nodules according to their anatomic distribution, thus limiting the differential diagnosis. In a study by Gruden et al. [105], the interobserver variability

P.123

P.124

and accuracy of the algorithm described (i.e., Algorithm 4) was assessed; four experienced chest radiologists independently evaluated HRCT images in 58 patients with nodular lung disease [105]. Nodules were classified as perilymphatic, random, centrilobular, or associated with tree-in-bud and small airways disease. The observers were correct in 218 (94%) of 232 localizations in the 58 cases. Three of four observers agreed in 56 (97%) of 58 cases, and all four observers agreed in 79% (46 of 58) of the cases. The most noteworthy source of error and of disagreement between observers was the confusion of perilymphatic and small airways disease-associated nodules in a small number of cases.

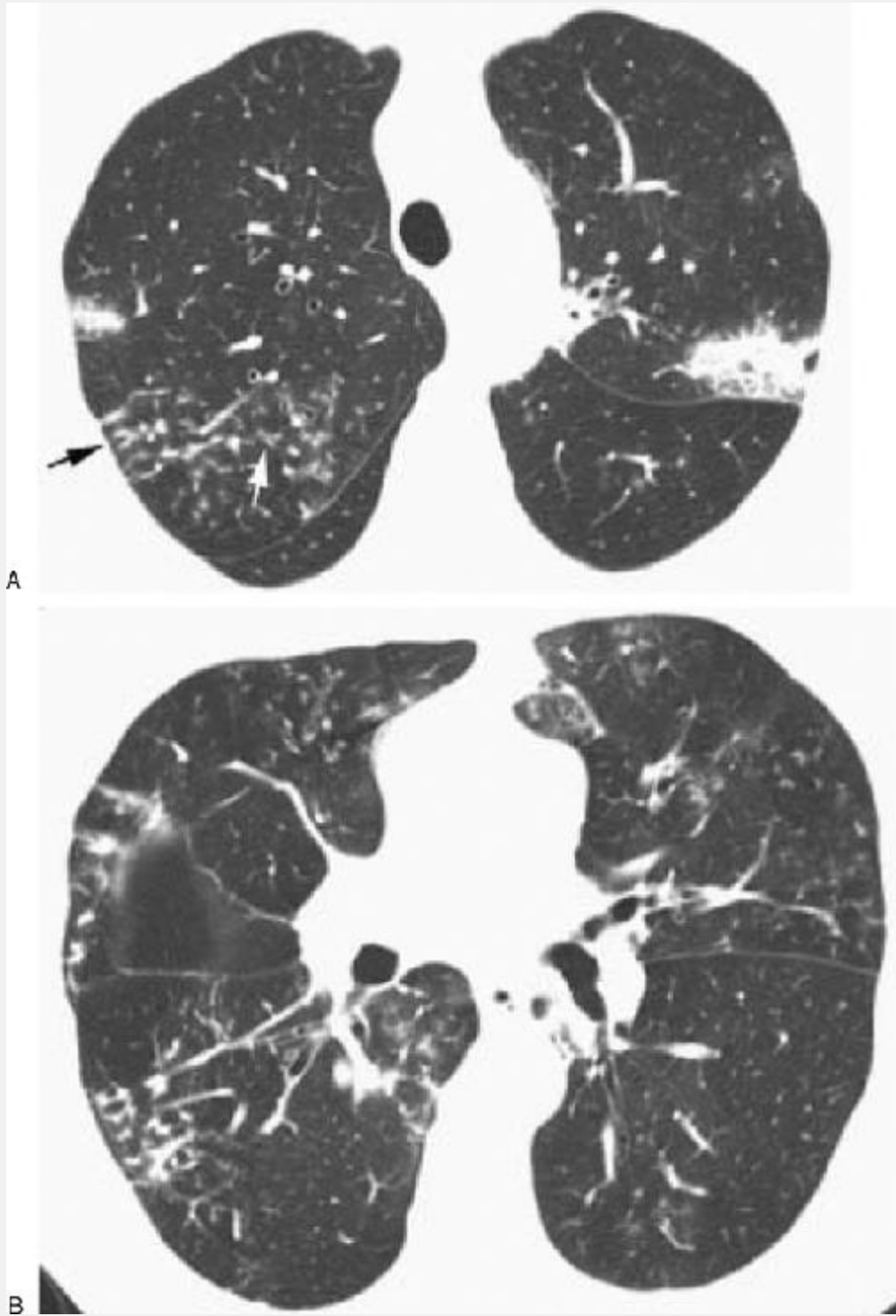
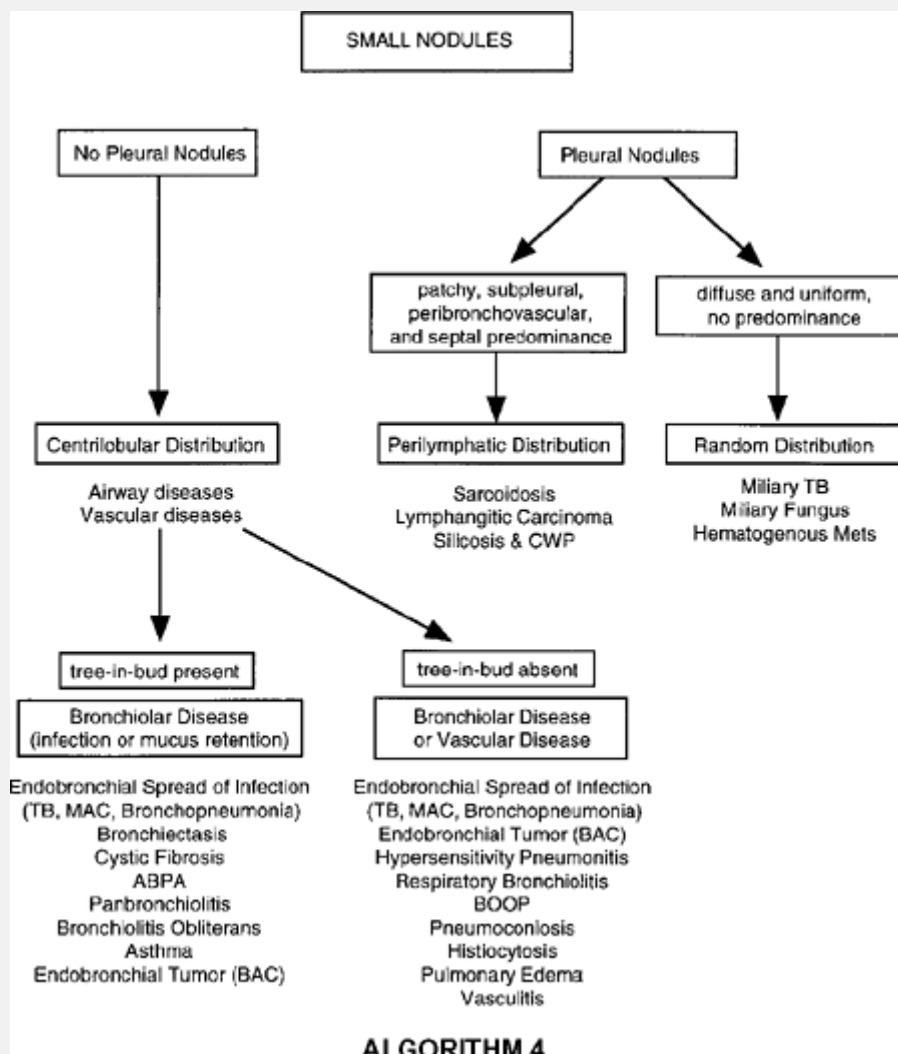


FIG. 3-80. Tree-in-bud in a patient with *Mycobacterium avium* complex infection. A: In addition to patchy consolidation, branching centrilobular structures (*arrows*) in the right lung are typical of tree-in-bud, and strongly

suggest the presence of infection. Tree-in-bud can be distinguished from normal branching arteries because of their more irregular appearance, lack of tapering, and a knobby or bulbous appearance. B: At a lower level, centrilobular nodules and tree-in-bud are visible in several locations.



ALGORITHM 4

TABLE 3-7. *Differential diagnosis of*

large nodules and masses

Diagnosis	Comments
Sarcoidosis	Common; upper lobe and peribronchovascular predominance; confluent masses of granulomas (active disease) or fibrous tissue (end-stage disease)
Silicosis/coal worker's pneumoconiosis	Common in advanced disease; upper lobe; associated with surrounding emphysema
Talcosis	Conglomerate masses of fibrous tissue; upper lobe and perihilar predominance; high-attenuation common
Langerhans histiocytosis	Large nodules in 20%
Metastatic carcinoma	Peripheral and basal predominance common
Diffuse bronchioloalveolar carcinoma	Large nodules in 30%; ill defined; basal predominance

Lymphoma	Commonly contain air bronchograms
Lymphoproliferative disease	Large nodules common; air bronchograms; often peribronchovascular or subpleural
Bronchiolitis obliterans organizing pneumonia	Uncommon
Wegener's granulomatosis	Common manifestation; cavitation common
Churg-Strauss syndrome	Cavitation may be present
Amyloidosis	Smooth or lobulated; cavitation in 20%
Infection	Fungal infection in immunosuppressed patient
Rounded atelectasis	Associated with asbestos pleural disease

In another study [106], HRCT findings were compared to those from pathologic examination in 40 consecutive patients with diffuse micronodular lung disease. HRCT scans

were analyzed with particular attention to the location of nodules (i.e., centrilobular, perilymphatic, and random) and their zonal distribution. HRCT scans showed centrilobular nodules in patients with diffuse panbronchiolitis (n = 4), infectious bronchiolitis (n = 4), hypersensitivity pneumonitis (n = 3), endobronchial spread of tuberculosis (n = 3), pneumoconiosis (n = 1), primary lymphoma of the lung (n = 1), and foreign body-induced necrotizing vasculitis (n = 1). They demonstrated perilymphatic nodules in patients with pneumoconiosis (n = 5), sarcoidosis (n = 2), and amyloidosis (n = 2). HRCT demonstrated micronodules of random distribution in the patients with miliary tuberculosis (n = 9) and pulmonary metastasis (n = 5). An upper- and middle-zonal predominance was seen in patients with sarcoidosis and in two of six patients with pneumoconiosis.

Large Nodules and Masses

The term *large nodule* is used in this book to refer to rounded opacities that are 1 cm or more in diameter. The term *mass* is generally used to describe nodular lesions larger than 3 cm in diameter [6,157]. Nodules approximating 1 cm may be seen in many small nodular lung diseases and are nonspecific. Furthermore, in patients with small nodular diseases, larger nodules or masses may sometimes be seen, representing conglomerate masses; these are common in sarcoidosis, silicosis, and talcosis (Table 3-7). Some diffuse lung diseases result in large nodules as a primary manifestation of the disease (Table 3-7).

Conglomerate Nodules or Masses in Diffuse Lung Disease

In patients who have diseases characterized by small nodules, conglomeration or confluence of nodules can result in large nodular or masslike opacities [90].

Sarcoidosis

Sarcoidosis may be associated with the presence of confluent nodules larger than 1 cm in diameter in half of all sarcoidosis patients [77]. In our experience, these predominate in the upper lobes and the peribronchovascular regions (Figs. 3-48 and 3-81). These nodules or masses are often irregular in shape, surround central bronchi and vessels, and can show small, discrete nodules at their periphery (Fig. 3-81). In patients with end-stage sarcoidosis, it is not uncommon to see conglomerate masses in the upper lobes associated with

P.125

central crowding of vessels and bronchi as a result of peribronchovascular fibrosis (Figs. 3-6 and 3-82). Traction bronchiectasis is often visible within the masses of fibrous tissue, and posterior displacement of upper lobe bronchi is commonly present. Adjacent areas of emphysema or bullae are visible in some cases. Similar upper lobe masses associated with bronchiectasis have been reported in patients with tuberculosis and are most frequent after treatment [65].

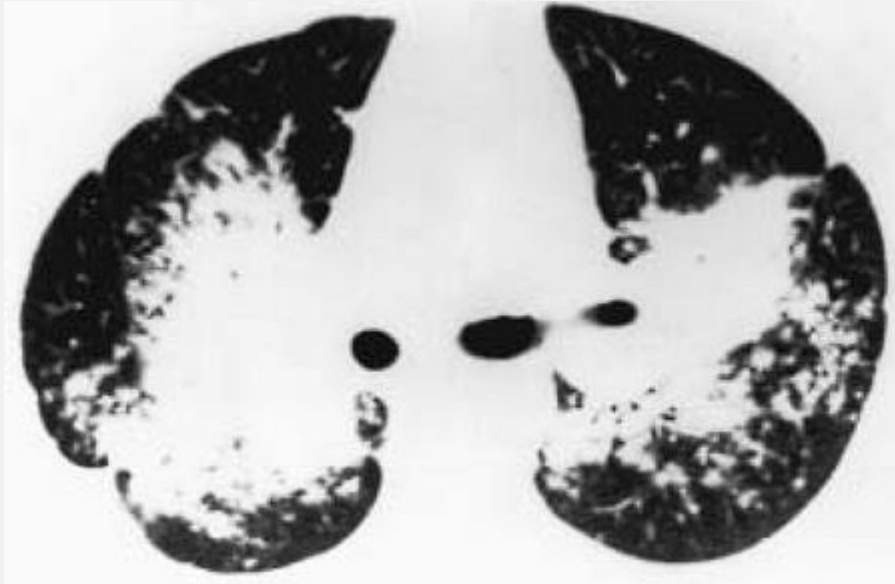


FIG. 3-81. Conglomerate masses of nodules in a patient with sarcoidosis. These masses, which surround central bronchi and vessels, show small discrete nodules at their margins.

Silicosis

Patients who have silicosis and coal workers who have complicated pneumoconiosis or progressive massive fibrosis also show conglomerate masses in the upper lobes, but these are typically of homogeneous opacity and tend to be unassociated with visible traction bronchiectasis, as seen in sarcoidosis (Fig. 3-83) [58,94]. Also, areas of emphysema peripheral to the conglomerate masses are common. This finding is present in as many as 48% of patients with CWP [58].

Talcosis

An appearance of progressive massive fibrosis very similar to that occurring in patients with silicosis or sarcoidosis can be seen in intravenous drug users who develop talcosis from

injection of talc-containing substances [147]. The fibrotic masses can show high attenuation at soft-tissue windows, indicating the presence of talc (see Fig. 5-58). A perihilar and upper lobe predominance has been reported.

Langerhans Histiocytosis

Large nodules have been seen in as many as 24% of patients with Langerhans histiocytosis, although masses are not generally seen in this disease [77].

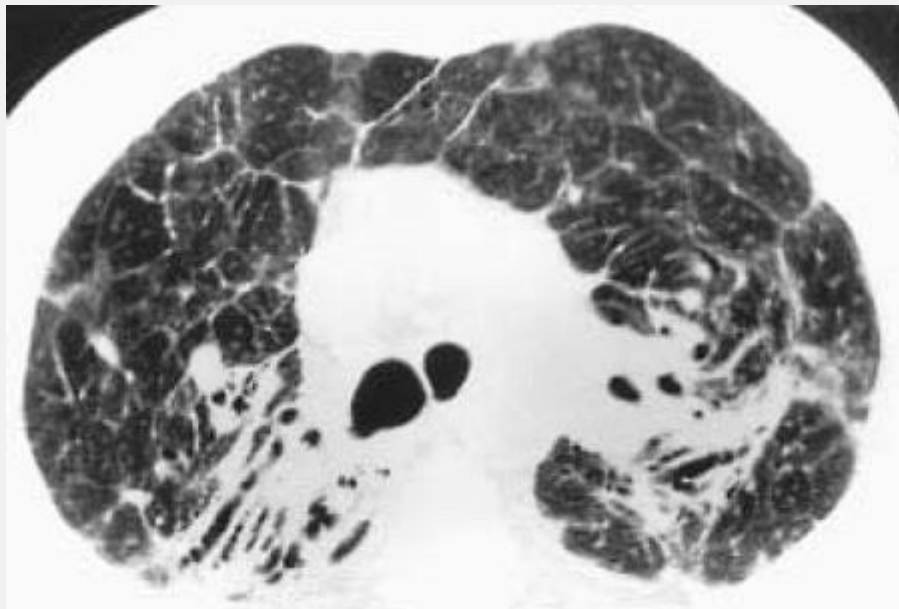


FIG. 3-82. Sarcoidosis with peribronchovascular fibrosis associated with traction bronchiectasis. Volume loss, interlobular septal thickening, and parenchymal bands are also evident.

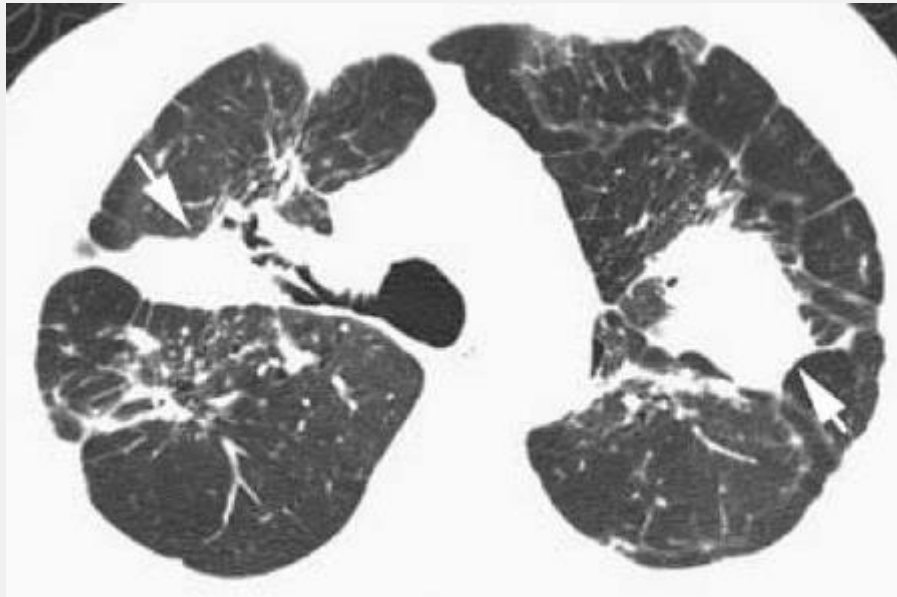


FIG. 3-83. Conglomerate masses of fibrosis in silicosis. Central areas of peribronchovascular fibrosis (*arrows*) are associated with small nodules, typical of silicosis, and distortion of lung architecture.

P.126

Large Nodules in Diffuse Infiltrative Lung Diseases

Several subacute or chronic infiltrative lung diseases may be characterized by large nodules as the primary manifestation of disease.

Metastatic Carcinoma

Metastatic carcinoma commonly results in large nodules or masses [146,158,159]. They may be well-defined or ill-defined, and they typically have a peripheral and basal predominance. Large nodules or masses may sometimes be seen in patients with neoplasms being assessed using HRCT,

but spiral CT is more appropriate if large nodules are visible on chest radiographs. Primary lung cancer presenting as a large solitary nodule or mass may sometimes be associated with other findings evaluated using HRCT, such as lymphangitic spread of carcinoma.

Diffuse Bronchioloalveolar Carcinoma

Diffuse bronchioloalveolar carcinoma shows a pattern of multiple nodules, up to 3 cm in size, in approximately 30% of cases [146]. Half of the cases have a peripheral or lower lobe predominance. Nodules are most often ill-defined or associated with a halo sign. Cavitation of nodules is sometimes present.

Lymphoma

Lymphoma involving the lung most commonly results in airspace consolidation (66% of cases) and large nodules (41% of cases) [114], often ill-defined and sometimes containing air bronchograms [160]. In most instances, spiral CT, rather than HRCT, is most appropriate in evaluation of a patient with lymphoma [15,161].

Lymphoproliferative Disorders

Lymphoproliferative disorders, often associated with the Epstein-Barr virus, may range from benign lymphoid hyperplasia to high-grade lymphoma and occur in immunosuppressed patients (e.g., those with AIDS, congenital immune deficiency, or receiving immunosuppressive therapy). The most common CT manifestation consists of multiple nodules, 2 to 4 cm in diameter, frequently in a predominantly peribronchovascular or subpleural distribution [162]. In a review of 246 patients who had lung transplantation [163], nine patients (4%) were diagnosed with posttransplantation lymphoproliferative

disorders. The most common abnormality visible on CT was the presence of multiple, well-defined pulmonary nodules ranging up to 3 cm in diameter. These nodules, when multiple, had basilar and peripheral predominance. Other abnormal features included hilar or mediastinal adenopathy. Three patients had nodules with a surrounding area of ground-glass opacity ("halo sign").

Bronchiolitis Obliterans Organizing Pneumonia

Multiple large nodules or masses are an uncommon manifestation of BOOP, but may be seen (see Fig. 6-30) [164]. Akira et al. [164] reviewed the HRCT scans and clinical records of 59 consecutive patients with histologically proven BOOP; 12 patients had multiple large nodules or masses. Of 60 lesions found in the 12 patients, 53 (88%) had an irregular margin, 27 (45%) had an air bronchogram, 23 (38%) had a pleural tail, and 21 (35%) had a spiculated margin. Ancillary findings included focal thickening of the interlobular septa in five (42%) of the 12 patients, pleural thickening in four (33%) patients, and parenchymal bands in three (25%) patients.

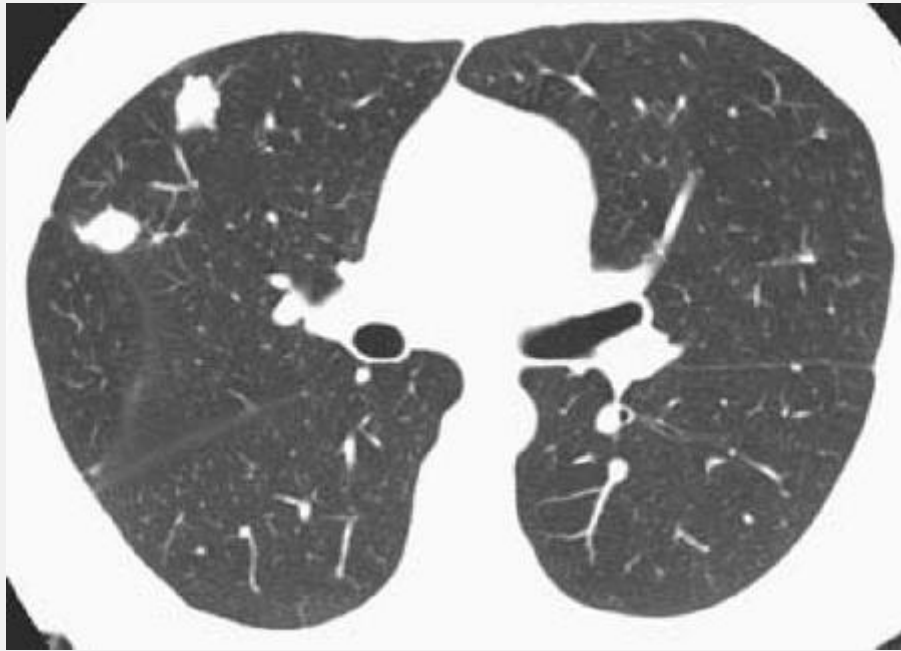


FIG. 3-84. Large lung nodules in Wegener's granulomatosis. These are nonspecific in appearance.

P.127

Wegener's Granulomatosis

Wegener's granulomatosis is typically manifested by multiple nodules that are usually limited in number, range in size from a few millimeters to 10 cm in diameter, have no zonal predominance, and have a random distribution (Fig. 3-84) [165,166,167]. Masses may also appear peribronchial or peribronchovascular in distribution [168]. In a study of ten patients [167], CT scans revealed multiple pulmonary nodules in seven patients and a single nodule in one. The nodules ranged in diameter from 2 mm to 7 cm, and most had irregular margins. Ill-defined centrilobular nodules, likely reflecting the presence of vasculitis, have also been reported [148]. Cavitation of nodules is common, being

present in all nodules larger than 2 cm in one study [167]; the cavity walls are often thick and irregular or shaggy, although thin-walled cavities may also be seen. Consolidation may also be associated, usually related to pulmonary hemorrhage.

Churg-Strauss Syndrome

Churg-Strauss syndrome is most often characterized by parenchymal opacification (consolidation or ground-glass attenuation), but pulmonary nodules may be present with or without cavitation [169].

Amyloidosis

Large pulmonary nodules are common in patients with localized amyloidosis [170], ranging in size from 8 mm to 3 cm [59]. Nodules may be solitary (60% of cases) or multiple, with a smooth or lobular contour, and are often subpleural or peripheral. Calcification may occur (20% of cases) [59].

Infections

Infections, particularly in immunosuppressed patients and usually representing a fungus, may be manifested by multiple large nodules or masses. Nodules are often ill-defined and may be associated with cavitation, air bronchograms, or a surrounding halo of ground-glass **opacity (i.e., the "halo sign")**. In a study of immunosuppressed patients with fever, large nodules shown on CT predicted the presence of a fungal infection [171]. Invasive aspergillosis is most common in neutropenic patients, typically showing scattered nodules that are often associated with vessels, the halo sign, and cavitation during later stages of the infection [172]. Although the halo sign can be associated with a variety of infectious processes,

including tuberculosis [173], candidiasis, *Legionella pneumoniae*, cytomegalovirus, or herpes simplex [174] in a neutropenic patient, it should suggest invasive aspergillosis [175].

Rounded Atelectasis

Rounded atelectasis represents a focal, collapsed, and often folded region of lung [64,176,177,178]. It almost always occurs in association with ipsilateral pleural disease and typically contacts the pleural surface. Rounded atelectasis occurs most commonly in the paravertebral regions of the posterior lung and may be bilateral. Bending or bowing of adjacent bronchi and arteries toward the area of atelectasis because of volume loss or folding of lung is characteristic. This appearance has been likened to a comet tail. Air bronchograms within the mass can sometimes be seen. In the presence of pleural disease and these typical findings, the diagnosis can usually be suggested. Focal fibrotic masses, usually irregular in shape, have been described as occurring

P.128

in the peripheral lung in relation to pleural abnormalities in patients with asbestos exposure [64]. These represent focal areas of scarring or rounded atelectasis (Fig. 3-85).

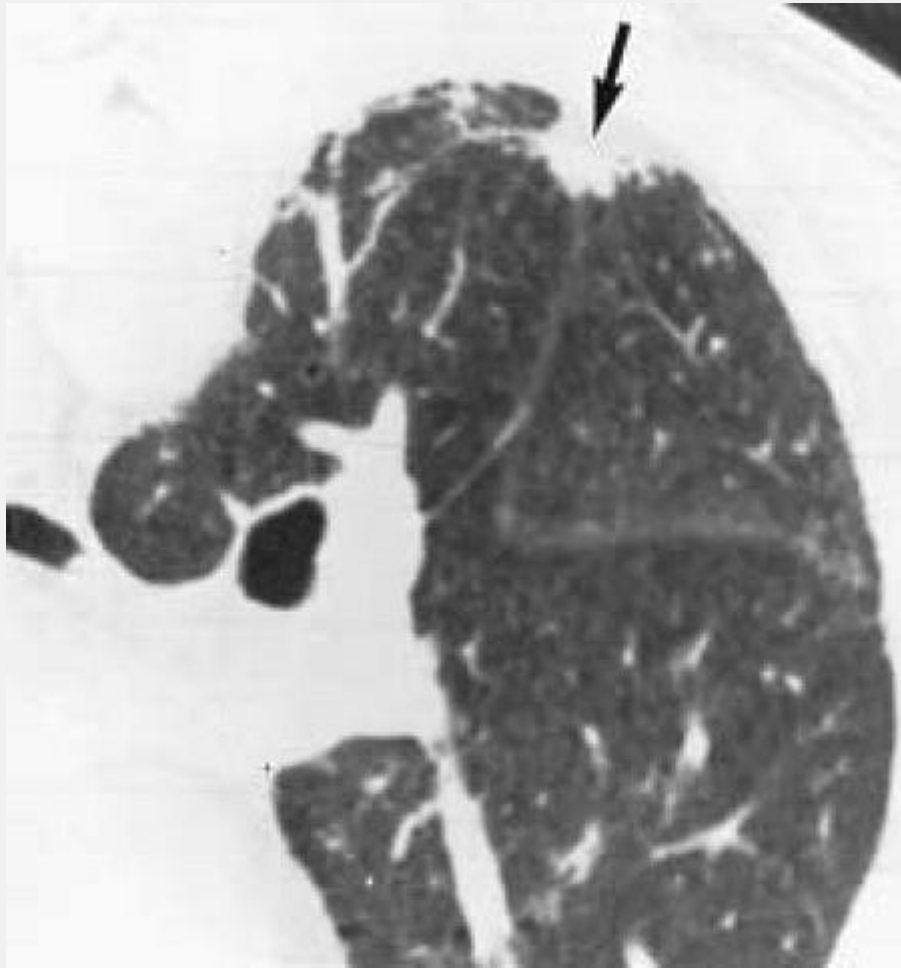


FIG. 3-85. Peripheral fibrotic mass in a patient with pulmonary fibrosis. The focal fibrotic mass (arrow) is irregular in shape and associated with other findings of fibrosis.

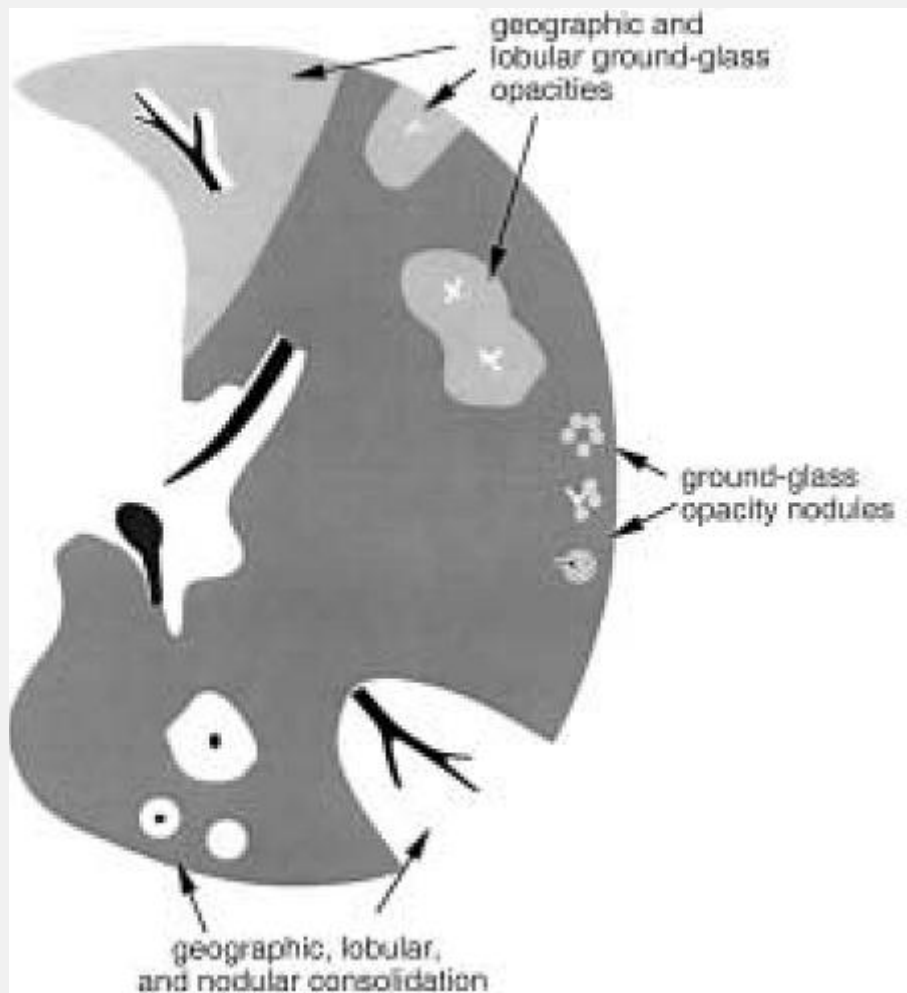


FIG. 3-86. HRCT appearances of increased lung opacity. Ground-glass opacity does not result in obscuration of underlying vessels, whereas consolidation does. Both can be associated with air bronchograms and can be nodular, lobular, or patchy and geographic.

Increased Lung Opacity

Increased lung opacity, or parenchymal opacification, is a common finding on HRCT in patients with chronic lung disease. Increased lung opacity is generally described as being ground-glass opacity or consolidation [5,6,157] (Fig. 3-86). Lung calcification may also result in increased attenuation.

Ground-Glass Opacity

Ground-glass opacity, or *ground-glass attenuation*, is a nonspecific term referring to the presence on HRCT of a hazy increase in lung opacity that is not associated with obscuration of underlying vessels (Figs. 3-86 and 3-87); if vessels are obscured, the term *consolidation* is generally used [5,6,157]. This finding can reflect the presence of a number of diseases and can be seen in patients with minimal airspace disease (Fig. 3-88), interstitial thickening (Fig. 3-89), or both [3,73,135,179,180,181,182,183]. Ground-glass opacity results from the volume averaging of morphologic abnormalities too small to be clearly resolved by HRCT [73,181,182,183]. It can reflect the presence of **minimal thickening of the "septal" or alveolar interstitium**, thickening of alveolar walls, or the presence of cells or fluid partially filling the alveolar spaces. Ground-glass opacity has been seen in patients with histologic findings of mild or early interstitial inflammation or infiltration [72,135]. Also, when a small amount of fluid is present within the alveoli, as can occur in the early stages of an airspace filling disease, the fluid tends to layer against the alveolar walls and is indistinguishable on HRCT from alveolar wall thickening [102]. In a study comparing the results of lung biopsy with HRCT in 22 patients who showed ground-glass opacity, 14%

P.129

had diseases primarily affecting airspaces, 32% had a mixed interstitial and airspace abnormality, and 54% had a primarily interstitial abnormality [135]. The term *ground-glass opacity* may also be used to refer to increased lung

density resulting from increased capillary blood volume, although this is better termed *mosaic perfusion* if the etiology of the lung attenuation abnormality is known [6]. The appearance of mosaic perfusion is described below.



FIG. 3-87. Ground-glass opacity in a 16-year-old boy with Goodpasture's syndrome and pulmonary hemorrhage.

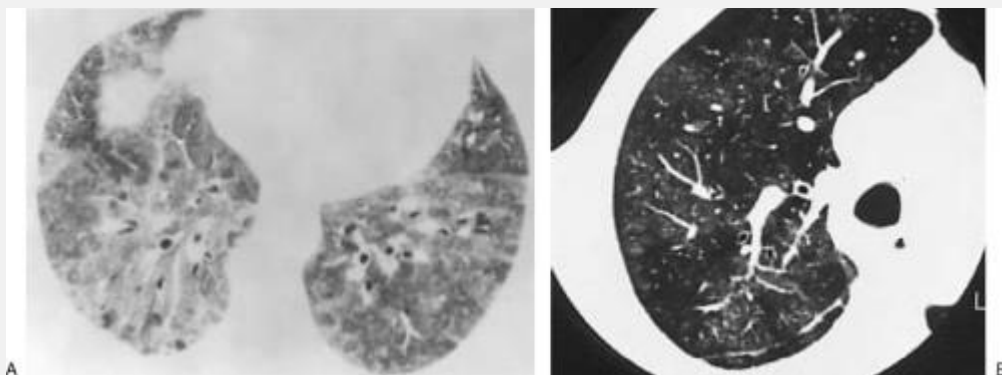


FIG. 3-88. Pneumocystis carinii pneumonia with ground-

glass opacity. A: In one patient, ground-glass opacity is extensive but patchy in distribution. B: In another patient, who had a normal chest radiograph, minimal patchy ground-glass opacity is visible.

Ground-glass opacity is difficult to recognize if it is of minimal severity and diffuse in distribution, involving all of the lung to an equal degree. However, this abnormality is almost always patchy in distribution, affecting some lung regions whereas others appear to be spared; this **“geographic” appearance of the lung parenchyma makes it** easier to detect and diagnose with confidence (Figs. 3-89, 3-90, 3-91). In some patients, entire lobules may appear abnormally dense, whereas adjacent lobules appear normal. In others, the abnormal ground-glass opacities are centrilobular and peribronchiolar in location (Fig. 3-62), resulting in the appearance of ill-defined centrilobular nodules [3,43,102,104,130,184]. Ground-glass opacity can involve individual segments and lobes, can involve nonsegmental regions of lung (Fig. 3-92), or may be diffuse (Fig. 3-93). The presence of air-filled bronchi that appear **“too black” within an area of lung can also be a clue as to** the presence of ground-glass opacity (Figs. 3-92 and 3-93A); this dark bronchus appearance is essentially that of an air bronchogram.

Significance and Differential Diagnosis of Ground-Glass Opacity

Ground-glass opacity is a highly significant finding, as it often indicates the presence of an ongoing, active, and potentially treatable process. In patients with acute symptoms, the association of ground-glass opacity with

active disease is very high. For example, in patients with AIDS and acute respiratory distress, ground-glass opacity visible on HRCT accurately predicts the presence of *P. carinii* pneumonia [156].

In patients who have subacute or chronic symptoms, ground-glass opacity also indicates the likelihood of active disease, although in this setting fibrosis may also result in this finding. Of the 22 patients with ground-glass opacity studied by Leung et al. [135], 18 (82%) were considered to have active or potentially reversible disease on lung biopsy. In a similar study by Remy-Jardin et al. [72], HRCT findings were correlated with histology at 37 biopsy sites in 26 patients. In 24 (65%) of the 37 biopsies, they found that ground-glass opacity corresponded to the presence of inflammation that exceeded or was equal to fibrosis in degree. In eight biopsies (22%), inflammation was present but fibrosis predominated, whereas in the remaining five (13%), fibrosis was the sole histologic finding. Because of its association with active lung disease, the presence of ground-glass opacity often leads to further diagnostic evaluation, including lung biopsy, depending on the clinical status of the patient. Also, when a lung biopsy is performed, areas of ground-glass opacity can be targeted by the surgeon or bronchoscopist. Because such areas are most likely to be active, they are most likely to yield diagnostic material.

Because ground-glass opacity can reflect the presence of either fibrosis or inflammation, one should be careful to diagnose an active process only when ground-glass opacity is unassociated with HRCT findings of fibrosis or is the predominant finding (Figs. 3-90, 3-91, 3-92, 3-93, 3-94). If ground-glass opacity is seen only in lung regions that also

show significant HRCT findings of fibrosis, such as traction bronchiectasis

P.130

or honeycombing, it is most likely that fibrosis will be the predominant histologic abnormality (Figs. 3-89 and 3-95). For example, in a study by Remy-Jardin et al. [72], patients showing traction bronchiectasis or bronchiolectasis on HRCT in regions of ground-glass opacity all had fibrosis on lung biopsy. On the other hand, in patients without traction bronchiectasis in areas of ground-glass opacity, 92% were found to have active inflammatory disease on lung biopsy.

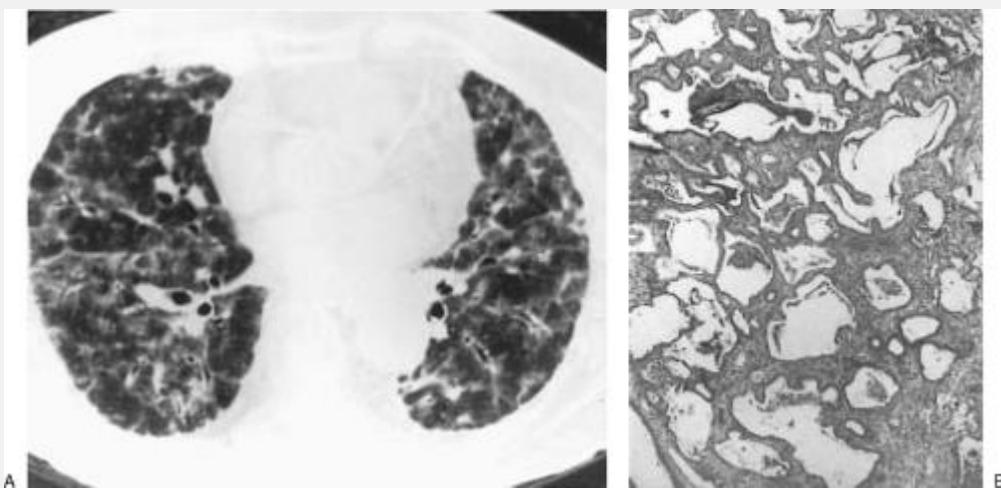


FIG. 3-89. Ground-glass opacity associated with interstitial fibrosis. A: HRCT shows patchy areas of ground-glass opacity. B: Biopsy specimen shows the abnormality to consist of alveolar wall thickening and fibrosis, with little airspace abnormality. (From Leung AN, Miller RR, et al. Parenchymal opacification in chronic infiltrative lung diseases: CT-pathologic correlation. *Radiology* 1993; 188:209, with permission.)

A large number of diseases can be associated with ground-glass opacity on HRCT. In many, this reflects the presence of similar histologic reactions in the early or active stages of disease, with inflammatory exudates involving the alveolar septa and alveolar spaces, although this pattern can be the result of a variety of pathologic processes.

When considering the differential diagnosis of ground-glass opacity, it is important to know whether the patient's symptoms are acute, subacute, or chronic (Table 3-8).

Among those causes of ground-glass opacity typically having an acute presentation are AIP (see Figs. 6-40, 6-41, 6-42 and 6-43) [185] or other causes of diffuse alveolar damage (Fig. 3-92), or the adult respiratory distress syndrome (ARDS); pulmonary edema of various causes (see Figs. 6-73 and 6-74) [27,28]; pulmonary hemorrhage (Fig. 3-87) [149]; pneumonias of all types, but particularly *P. carinii* pneumonia (Figs. 3-88 and 3-93) [27,156,186,187,188] (Fig. 3-58), viral pneumonias (e.g., cytomegalovirus) (see Fig. 6-62) [189], and mycoplasma pneumonia (see Fig. 6-65) [190]; acute eosinophilic pneumonia [191]; and early radiation pneumonitis [33,184,192].

The most common causes of ground-glass opacity in patients having subacute or chronic symptoms (Table 3-8) include interstitial pneumonias such as NSIP or UIP (Fig. 3-94),

P.131

either idiopathic or associated with specific diseases, such as scleroderma or other collagen-vascular diseases [22,69,72,135,143]; DIP [193]; respiratory bronchiolitis interstitial lung disease (RB-ILD) (see Figs. 6-34 and 6-35) [109,138,139]; hypersensitivity pneumonitis (Figs. 3-90 and

3-91) [72,130,131,132]; BOOP (Fig. 3-100) [72,135]; chronic eosinophilic pneumonia [55]; Churg-Strauss syndrome [169]; lipoid pneumonia [194]; bronchioloalveolar carcinoma [195]; sarcoidosis (see Figs. 5-40 and 5-41) [56,72,90,135,196]; and alveolar proteinosis (Figs. 3-11 and 3-96) [51,52,53,19].

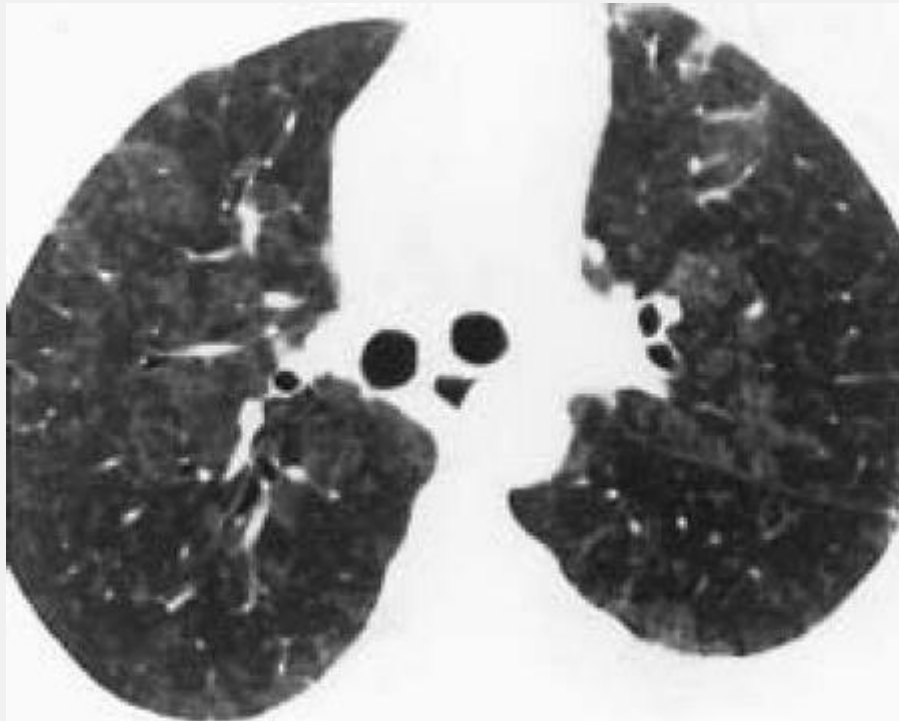


FIG. 3-90. Patchy areas of subtle ground-glass opacity in a patient with hypersensitivity pneumonitis.

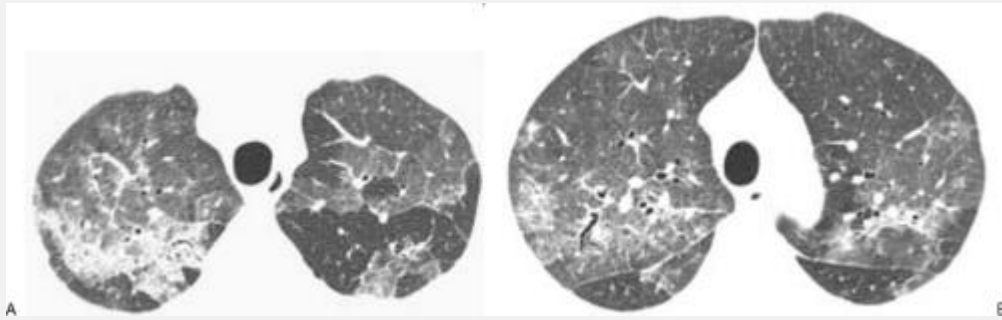


FIG. 3-91. A, B: Patchy ground-glass opacity associated with hypersensitivity pneumonitis. Abnormalities had an upper lobe predominance.

In patients with ground-glass opacity, the nature of the histologic abnormalities associated with this finding varies according to the typical histologic features of the disease; no specific histology is associated with this finding (Table 3-9) [97,109,130,135,198,199]. In patients with UIP due to IPF, NSIP, scleroderma, or other collagen-vascular diseases, a number of studies have correlated the presence of ground-glass opacity on HRCT with biopsy results, response to treatment, and patient survival [8,73,143,179,182,183,193,200,201,202]. In histologic studies of patients with interstitial pneumonia, ground-glass opacity has been shown to be associated with the presence of alveolar wall or intraalveolar inflammation in most. For example, in a study of scleroderma patients by Wells et al. [182], increased opacity on HRCT correlated with predominant inflammation on biopsy in four of seven cases, whereas reticulation on HRCT indicated fibrosis in 12 of 13 [182]. In another study, of 14 patients with IPF and ground-

glass opacity on HRCT, 12 had inflammation on biopsy [135]. In patients with UIP, ground-glass opacity is associated with alveolar septal inflammation, varying numbers of intraalveolar histiocytes, and varying degrees of fibrosis;

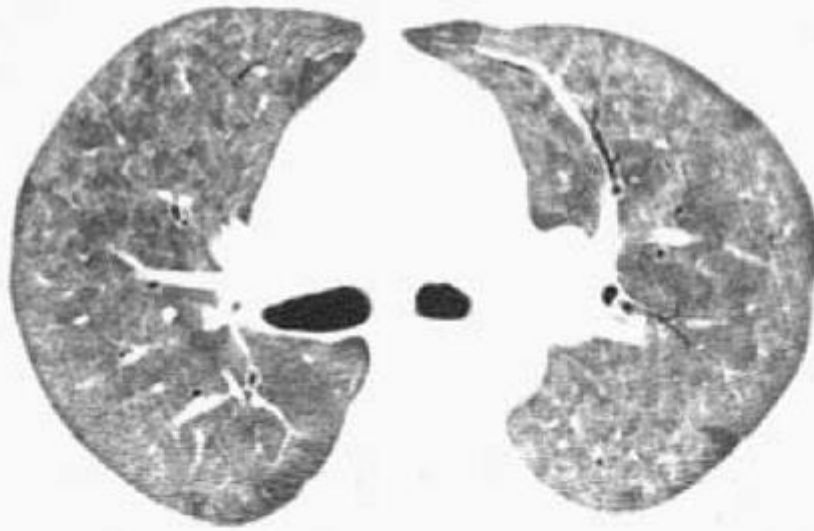
P.132

P.133

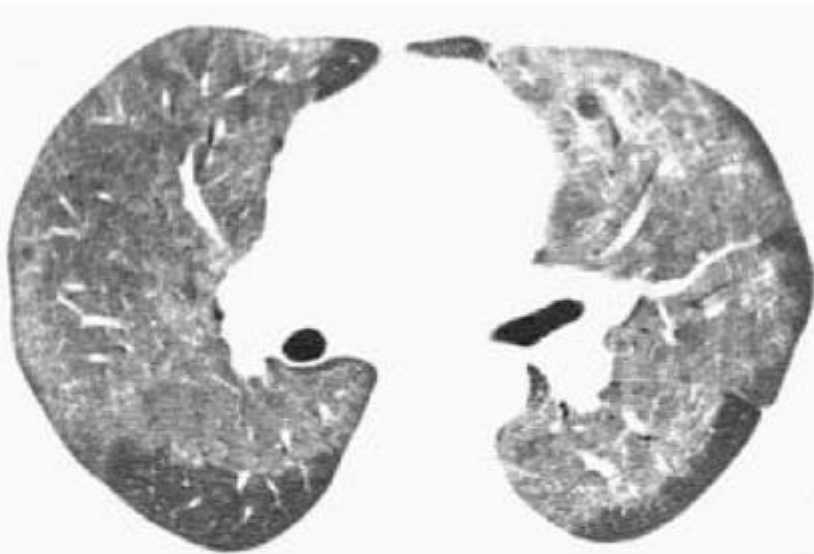
ground-glass opacity in patients with DIP largely reflects the presence of macrophages within alveoli [8,135,182,193].



FIG. 3-92. Extensive perihilar ground-glass opacity associated with acute lung injury and diffuse alveolar damage related to smoking cocaine. This abnormality was transient and cleared within 2 weeks.



A



B



C

FIG. 3-93. A-C: HRCT at three levels in a patient with *Pneumocystis carinii* pneumonia associated with acquired immunodeficiency syndrome. Diffuse ground-glass opacity predominates in the upper lobes and perihilar regions (A). In the lower lobes (C), ground-glass opacity is more patchy in distribution.



FIG. 3-94. Patchy ground-glass opacity in a patient with nonspecific interstitial pneumonia. A posterior and subpleural predominance is present. Findings of fibrosis, such as traction bronchiectasis, are absent.

Crazy-Paving Pattern

In some patients with ground-glass opacity visible on HRCT, superimposition of a reticular pattern results in an appearance termed *crazy-paving* [51]. This pattern was first recognized in patients with pulmonary alveolar proteinosis (PAP) (Figs. 3-11 and 3-96) [51] and is quite typical of PAP, but may also be seen in patients with a variety of other diseases [54,55]. In patients with crazy-paving, ground-

glass opacity may reflect the presence of airspace or interstitial abnormalities; the reticular opacities may represent interlobular septal thickening, thickening of the intralobular interstitium, irregular areas of fibrosis, or a preponderance of an airspace-filling process at the periphery of lobules or acini [55].

The differential diagnosis of crazy-paving includes diseases considered to be primarily airspace or interstitial and mixed (Table 3-10) [54,55]. These include PAP (Fig. 3-96) [51,53]; pulmonary edema [28]; pulmonary hemorrhage (Fig. 3-97) [149]; ARDS [54]; AIP; diffuse alveolar damage; pneumonias due to *P. carinii* (Fig. 3-98), virus (e.g., cytomegalovirus) (Fig. 3-99), mycoplasma, bacteria, and tuberculosis; BOOP (Fig. 3-100); chronic eosinophilic pneumonia; acute eosinophilic pneumonia [191]; Churg-Strauss syndrome [169], radiation pneumonitis [33], or drug-related pneumonitis; bronchioloalveolar carcinoma (Fig. 3-101) [195]; and lipoid pneumonia [194]. Clearly, the differential diagnosis of a crazy-paving pattern must be based on a consideration of clinical as well as HRCT findings, and knowledge of whether symptoms are acute or chronic (Table 3-10).

In the study by Johkoh et al. [55] of 46 patients showing the crazy-paving pattern on HRCT, the most common causes included ARDS (n = 8), bacterial pneumonia (n = 7),

P.134

AIP (n = 5), and, despite its rarity, alveolar proteinosis (n = 5). Of these common causes of crazy-paving, it is worth noting that only PAP presents with subacute or chronic symptoms, and ARDS, bacterial pneumonia, and AIP are not commonly studied using HRCT in clinical practice. Also, the

highest prevalences of crazy-paving in this study were seen in PAP (100%), diffuse alveolar damage (67%), AIP (31%), and ARDS (21%) [55].

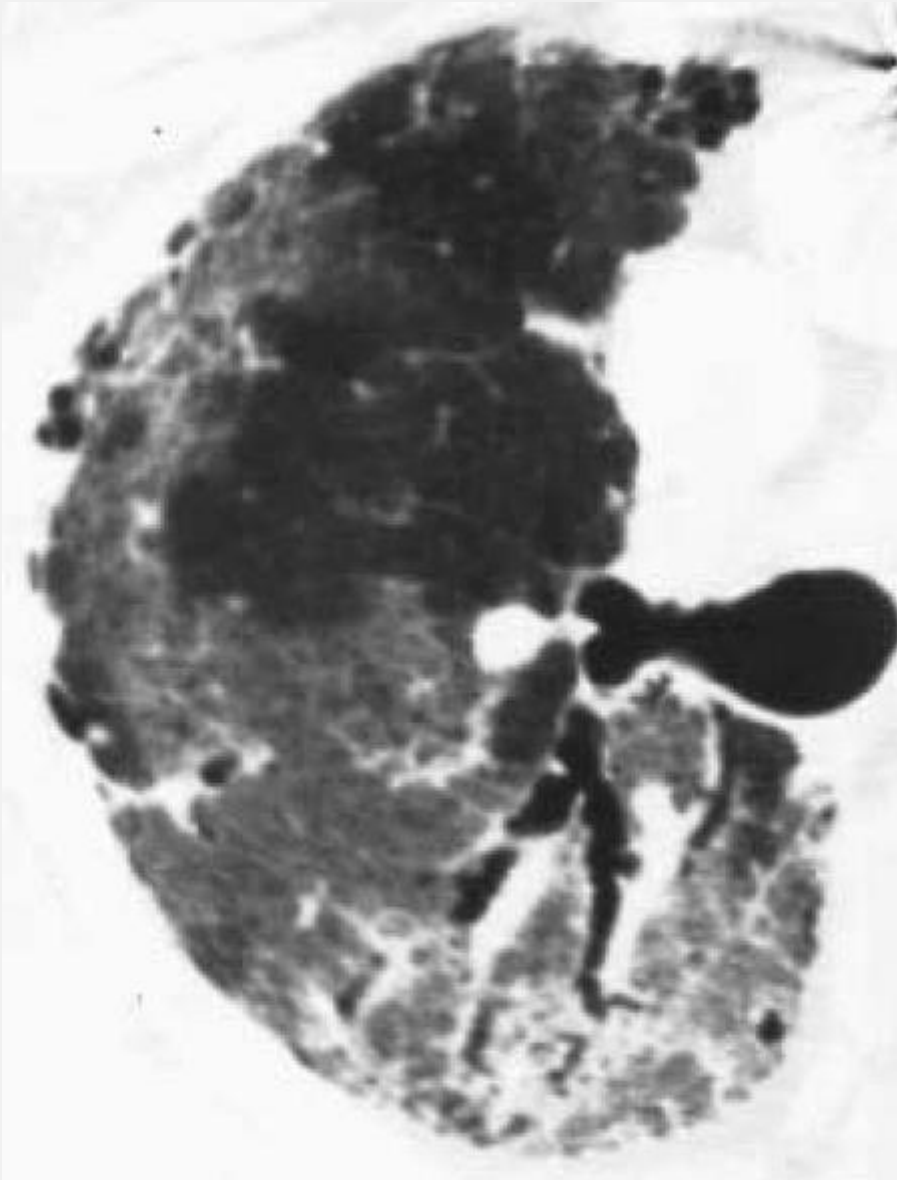


FIG. 3-95. Ground-glass opacity with a peripheral and posterior predominance in a patient with idiopathic pulmonary fibrosis. In addition to the increased lung opacity, there is evidence of increased reticulation, traction bronchiectasis, and some subpleural honeycombing. These findings indicate the presence of fibrosis. End-stage fibrosis

was found on biopsy, without evidence of active disease.

TABLE 3-8. *Differential diagnosis of ground-glass opacity*

Diagnosis	Course	Comments
Acute interstitial pneumonia; adult respiratory distress syndrome	Acute	Always present; consolidation common; patchy or diffuse
Pulmonary edema	Acute	Diffuse or centrilobular; septal thickening sometimes present
Pulmonary hemorrhage	Acute	Patchy or diffuse; septal thickening sometimes present
Pneumonia (e.g., Pneumocystis carinii, viral, Mycoplasma pneumonias)	Acute	Common; diffuse or patchy; centrilobular nodules; consolidation or septal thickening may also be

		present
Acute eosinophilic pneumonia	Acute	Diffuse; respiratory failure common
Radiation pneumonitis	Acute	Extent usually corresponds to radiation ports
Nonspecific interstitial pneumonia	Subacute, chronic	Common; patchy; subpleural; reticular opacities often associated; multiple causes including collagen diseases
Usual interstitial pneumonia and idiopathic pulmonary fibrosis	Subacute, chronic	Common in association with findings of fibrosis; uncommon as an isolated finding; subpleural and basal predominance
Desquamative	Subacute,	Always present;

interstitial pneumonia	chronic	diffuse or patchy; findings of fibrosis less common than in usual interstitial pneumonia
Respiratory bronchiolitis interstitial lung disease	Subacute, chronic	Always present; patchy and localized; may be centrilobular; fibrosis uncommon
Hypersensitivity pneumonitis	Subacute, chronic	Very common; patchy or nodular; can be centrilobular; consolidation and air-trapping may also be present
Bronchiolitis obliterans organizing pneumonia	Subacute, chronic	Common; consolidation may also be present; often predominant in peripheral regions; can be nodular
Chronic eosinophilic	Subacute,	Consolidation more

pneumonia	chronic	common; patchy or nodular; peripheral predominance
Churg-Strauss syndrome	Subacute, chronic	Consolidation also present; nodular
Bronchioloalveolar carcinoma (diffuse)	Subacute, chronic	Diffuse, patchy, or centrilobular; consolidation common
Lipoid pneumonia	Subacute, chronic	Patchy or lobular; low-attenuation consolidation may be present
Sarcoidosis	Subacute, chronic	Uncommon manifestation due to confluence of very small granulomas
Alveolar proteinosis	Subacute, chronic	Very common; patchy or diffuse; septal thickening common; fibrosis rare

In a prospective study of patients showing this pattern [54], a variety of causes of crazy-paving were identified. These included *P. carinii* pneumonia, alveolar proteinosis, UIP, pulmonary hemorrhage, acute radiation pneumonitis, ARDS, and drug-induced pneumonitis. Of these, *P. carinii* pneumonia was most common.

Algorithmic Approach to the Diagnosis of Ground-Glass Opacity

If ground-glass opacity is associated with significant reticulation, the reticular pattern should be identified (Algorithm 5). If honeycombing or traction bronchiectasis is present in areas of increased attenuation, fibrosis is very likely present, and the differential diagnosis is that of honeycombing. If the reticular pattern is that of interlobular septal thickening, crazy-paving is present (Table 3-10). If the only reticular pattern present is that of intralobular interstitial thickening, fibrosis is likely present if opacities are peripheral and subpleural (i.e., as in IPF), but the pattern is nonspecific. Ground-glass opacity unassociated with reticulation, as with crazy-paving, likely represents active disease. In this situation, a specific diagnosis is difficult to make, but the differential diagnosis is based, at least to some extent, on the distribution of abnormalities, and, as indicated above, the presence of acute, subacute, or chronic symptoms. Ground-glass opacity with a patchy or peripheral distribution is most likely due to active interstitial pneumonia (NSIP, UIP, and DIP), eosinophilic pneumonia, hypersensitivity pneumonitis, BOOP, alveolar proteinosis, sarcoidosis, pulmonary edema, or hemorrhage. The differential diagnosis of a centrilobular nodular

distribution of ground-glass opacity includes hypersensitivity pneumonitis, P.135

BOOP, LIP, cytomegalovirus and *P. carinii* pneumonia, and vasculitis. Diffuse and extensive ground-glass opacity may be seen with hypersensitivity pneumonitis, *P. carinii* pneumonia, cytomegalovirus pneumonia, pulmonary edema, pulmonary hemorrhage, ARDS, and AIP.



FIG. 3-96. Geographic ground-glass opacities in association with interlobular septal thickening, characteristic of alveolar proteinosis. This pattern, characterized by the association of ground-glass opacity and interlobular septal thickening or reticulation, is termed crazy-paving.

Pitfalls in the Diagnosis of Ground-Glass Opacity

There are several potential pitfalls in the recognition and diagnosis of ground-glass opacity. First, it is important to keep in mind that because ground-glass opacity reflects the volume averaging of subtle morphologic abnormalities, the thicker the collimation used for scanning, the more likely volume averaging will occur, regardless of the nature of the anatomic abnormality present. Thus, ground-glass opacity should be diagnosed only on scans obtained with thin collimation.

The diagnosis of ground-glass opacity is largely subjective and based on a qualitative assessment of lung attenuation [181]. The use of lung attenuation measurements to determine the presence of increased lung density in patients with ground-glass opacity is difficult because of the variations in attenuation measurements that are known to be associated with gravitational density gradients in the lung, the level of inspiration, and fluctuations that occur as a result of patient size, position, chest wall thickness, and kilovolt peak [kV(p)]. Using consistent window settings for the interpretation of HRCT is very important. Using too low a window mean in conjunction with a relatively narrow window width can give the appearance of a diffuse ground-glass abnormality [181]. In addition, using a wider window width than one is accustomed to without changing window mean can give the impression of increased lung attenuation. In assessing the attenuation of lung parenchyma, it is often helpful to compare its appearance to that of air in the trachea or bronchi; if tracheal air appears gray instead of **black, then increased attenuation or "grayness" of the lung parenchyma may not be significant.**

Also, as previously indicated, increased lung opacity is commonly seen in the dependent lung on HRCT largely as a

result of volume loss in the dependent lung parenchyma; this is so-called dependent density [39]. This can result in a stripe of ground-glass opacity several centimeters thick in the posterior lung of supine patients; prone scans allow this transient finding to be distinguished from a true abnormality. Similarly, on expiration, because of a reduction of the amount of air within alveoli, lung regions increase in attenuation and can mimic the appearance of ground-glass opacity resulting from lung disease.

TABLE 3-9. Histologic abnormalities associated with ground-glass opacity [22,97,109,130,135,138,198,199]

Diagnosis	Histologic findings
Usual interstitial pneumonia	Alveolar septal inflammation; intraalveolar cellular infiltrate; fibrosis
Nonspecific interstitial pneumonia	Alveolar septal inflammation; intraalveolar cellular infiltrate; fibrosis
Desquamative interstitial pneumonia	Alveolar macrophages; interstitial inflammatory infiltrate; mild fibrosis
Respiratory	Pigment-containing alveolar

bronchiolitis	macrophages
Acute interstitial pneumonia	Interstitial inflammatory exudate; edema; diffuse alveolar damage with hyaline membranes
Hypersensitivity pneumonitis	Alveolitis; interstitial infiltrates; poorly defined granulomas; cellular bronchiolitis
Bronchiolitis obliterans organizing pneumonia	Alveolar septal inflammation; alveolar cellular desquamation
Eosinophilic pneumonia	Eosinophilic interstitial infiltrate; alveolar eosinophils and histiocytes
Pneumocystis carinii pneumonia	Alveolar inflammatory exudate; alveolar septal thickening
Sarcoidosis	Largely due to numerous small granulomas; alveolitis less important
Alveolar proteinosis	Intraalveolar lipoproteinaceous

material

TABLE 3-10. *Differential diagnosis of crazy-paving*

Diagnosis	Course	Comments
Acute interstitial pneumonia; adult respiratory distress syndrome	Acute	Consolidation common; patchy or diffuse
Pulmonary edema	Acute	Common
Pulmonary hemorrhage	Acute	Patchy or diffuse
Pneumonia (e.g., <i>Pneumocystis carinii</i> , viral, <i>Mycoplasma</i> , bacterial)	Acute	Common; diffuse or patchy; centrilobular nodules;

pneumonias)		consolidation
Acute eosinophilic pneumonia	Acute	Rare
Radiation pneumonitis	Acute	Extent usually corresponds to radiation ports
Alveolar proteinosis	Subacute, chronic	Always present; patchy or diffuse; geographic
Nonspecific interstitial pneumonia	Subacute, chronic	Patchy; subpleural
Usual interstitial pneumonia and idiopathic pulmonary fibrosis	Subacute, chronic	Uncommon cause; subpleural
Hypersensitivity pneumonitis	Subacute, chronic	Very common; patchy or nodular; can be centrilobular; consolidation and air-trapping may also be present

Bronchiolitis obliterans organizing pneumonia	Subacute, chronic	Common; consolidation may also be present; often predominant in peripheral regions; can be nodular
Chronic eosinophilic pneumonia	Subacute, chronic	Consolidation more common; patchy; peripheral predominance
Churg-Strauss syndrome	Subacute, chronic	Consolidation also present; nodular
Lipoid pneumonia	Subacute, chronic	Patchy or lobular; low-attenuation consolidation may be present
Bronchioloalveolar carcinoma (diffuse)	Subacute, chronic	Diffuse, patchy, or centrilobular; consolidation nodules common

Furthermore, in patients who have emphysema or other causes of lung hyperlucency, such as airways obstruction and air-trapping, normal lung regions can appear relatively dense, thus mimicking the appearance of ground-glass opacity. This pitfall can usually be avoided if consistent window settings are used for interpretation of scans, and the interpreter is accustomed to the appearances of normal lung, lung of increased attenuation, and lung of decreased attenuation. Also, dark bronchi or air bronchograms will not be seen within the relatively dense, normal lung regions, as they are in patients with true ground-glass opacity. The use of expiratory HRCT can also be of value in distinguishing the presence of heterogeneous lung attenuation resulting from emphysema or air-trapping from that representing ground-glass opacity. This is described further in the section Inhomogeneous Lung Opacity.

Consolidation

Increased lung attenuation with obscuration of underlying pulmonary vessels is referred to as *consolidation* (Figs. 3-86 and 3-102, 3-103, 3-104) [5,157]; air bronchograms may be present. HRCT has little to add to the diagnosis of patients with clear-cut evidence of consolidation visible on chest radiographs. However, HRCT can allow the detection of consolidation before it becomes diagnosable radiographically. Some evidence of consolidation can be seen in patients with a variety of diffuse lung diseases. By definition, diseases that produce consolidation are characterized by a replacement of alveolar air by fluid, cells, tissue, or some other substance [102,157,197]. Most

are associated with airspace filling, but diseases that produce an extensive, confluent interstitial abnormality, such as UIP or sarcoidosis, can also result in this finding [20,135]. Airspace nodules or focal areas of ground-glass opacity are often seen in association with areas of frank consolidation. Patients who show consolidation in association with another pattern, such as small nodules, should be diagnosed using the other pattern. In such patients, consolidation probably represents confluent disease.

Areas of consolidation are common in patients with diffuse lung disease regardless of the diagnosis and generally may be discounted. The differential diagnosis of consolidation overlaps that listed for ground-glass opacity (Table 3-8), and, in fact, many of the diseases listed in Table 3-8 can show a mixture of both findings. Consolidation representing the predominant abnormality has a limited differential diagnosis (Table 3-11). The differential diagnosis of consolidation includes pneumonia of different causes including *P. carinii* pneumonia [102,187], BOOP (Fig. 3-102) [134,203], eosinophilic pneumonia (Figs. 3-103 and 3-104) [204], hypersensitivity pneumonitis [132], radiation pneumonitis [33,184, 192,205,206], bronchioloalveolar carcinoma and lymphoma [102,135,146], UIP [135,179], alveolar proteinosis [52], AIP [185], sarcoidosis [98], drug reactions [207], pulmonary edema, and ARDS [102].

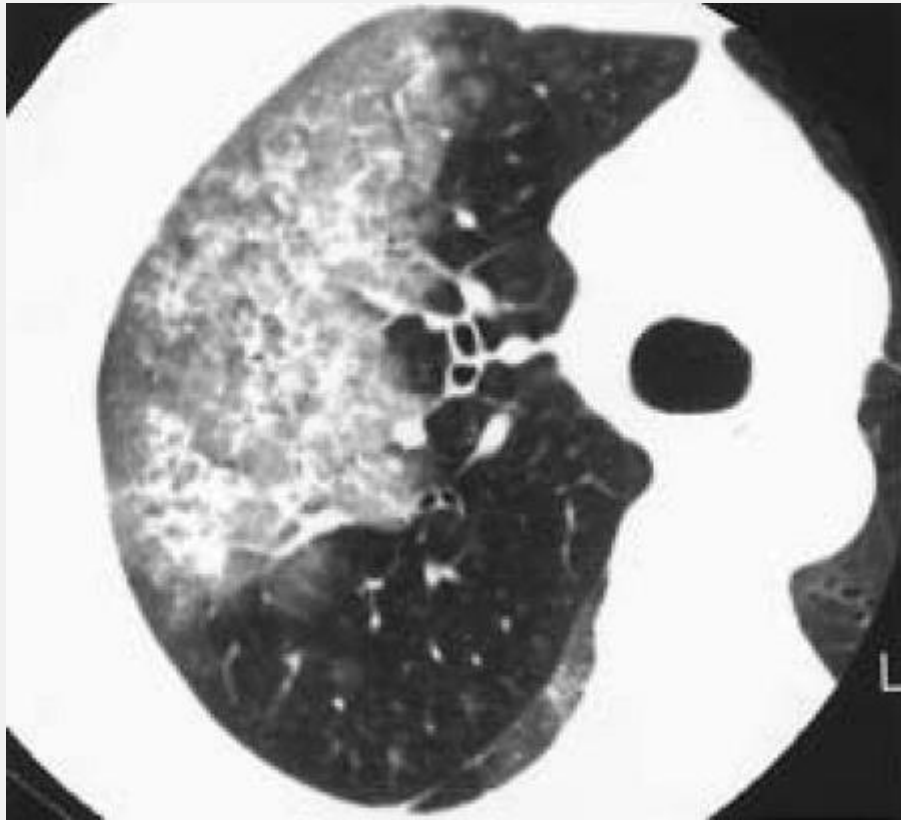


FIG. 3-97. Ground-glass opacity in a patient with pulmonary hemorrhage. Vessels are visible within the area of opacity, as are areas of reticulation. The reticular opacities appear to represent thickening of the intralobular interstitium.

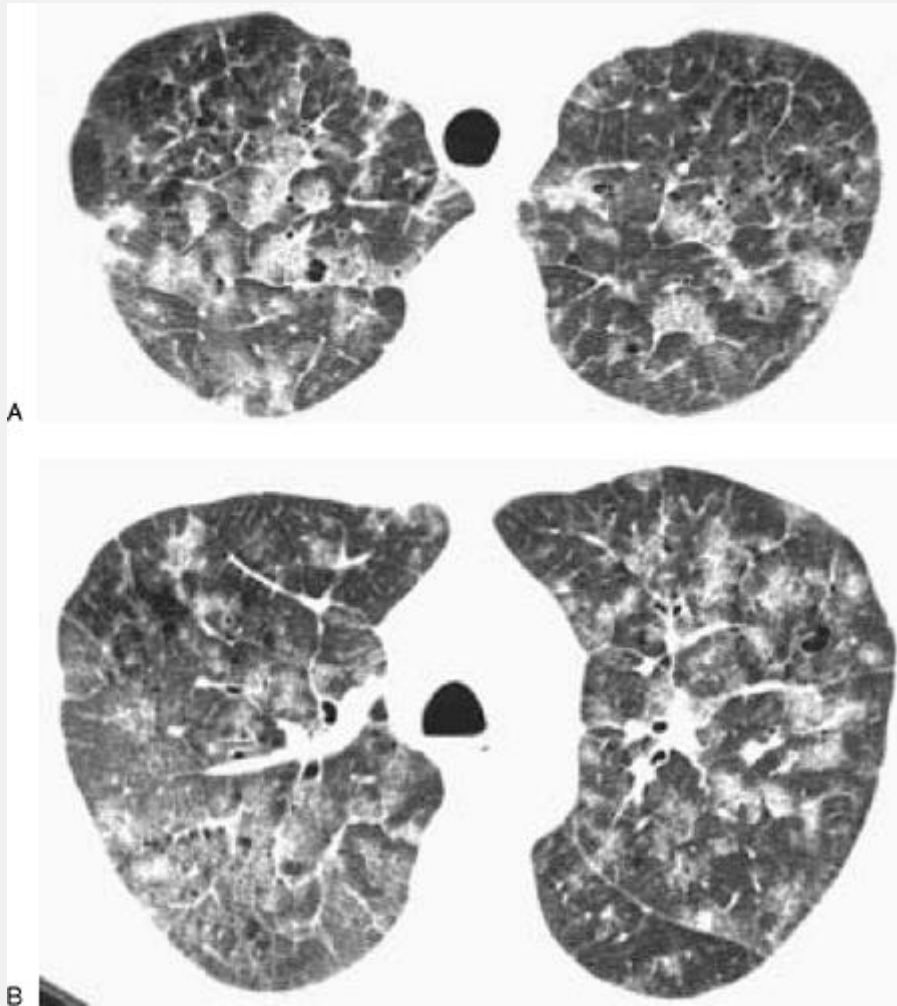


FIG. 3-98. A, B: *Pneumocystis carinii* pneumonia in an immunosuppressed patient with leukemia. Patchy areas of ground-glass opacity are associated with distinct interlobular septal thickening.

P.137

Lung diseases causing consolidation can have widely differing appearances and distributions depending on the nature of the pathologic process responsible (Algorithm 6). Lobular consolidation is often due to infection, although consolidation due to bronchioloalveolar carcinoma and

alveolar proteinosis can also have a lobular predominance. Diffuse consolidation is most typical of pneumonia, bronchioloalveolar carcinoma, ARDS, AIP, pulmonary edema, and pulmonary hemorrhage. A subpleural distribution is most suggestive of eosinophilic pneumonia and BOOP but may also be seen with UIP and NSIP. Chronic lung diseases that result in consolidation often involve the lung in a patchy fashion. Patchy consolidation can show a nonanatomic and nonsegmental distribution, but can also be panlobular (Fig. 3-65B) or can appear nodular and centrilobular on HRCT [3,60,65,102]. Eosinophilic pneumonia, BOOP, bronchioloalveolar carcinoma, and bronchopneumonia may show this appearance. A *panlobular distribution*—that is, uniform involvement of secondary pulmonary lobules by the pathologic process [60]—is typical of diseases producing airspace consolidation, such as bronchopneumonia or lobular pneumonia (Fig. 3-65) [65], but it can be seen in a variety of diffuse interstitial diseases characterized by ground-glass opacity and is nonspecific.

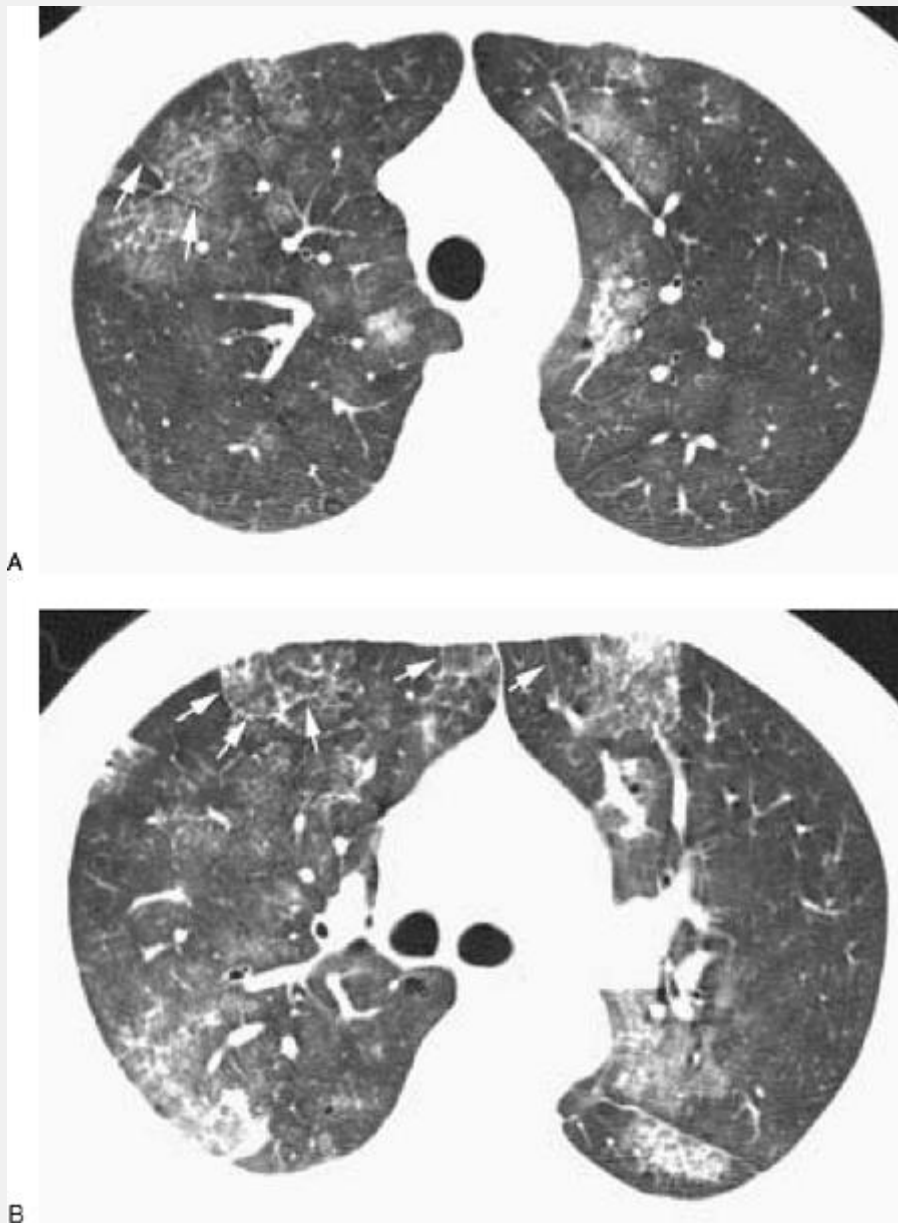


FIG. 3-99. A, B: Pneumonia due to respiratory syncytial virus. HRCT at two levels shows patchy ground-glass opacity associated with some interlobular septal thickening (*arrows*).

Lung Calcification and Lung Attenuation Greater than Soft Tissue

Multifocal lung calcification, often associated with lung nodules, has been reported in association with infectious granulomatous diseases such as tuberculosis [65], sarcoidosis (Fig. 3-105) [57], silicosis [57,58], amyloidosis [50], and fat embolism associated with ARDS [208]. Diffuse and dense lung calcification can be seen in the presence of metastatic calcification, disseminated pulmonary ossification, or alveolar microlithiasis. Increased attenuation can be seen in patients with talcosis [147] associated with fibrotic masses, although this may represent the injected material rather than calcification. Diffuse, increased lung attenuation in the absence of calcification can be seen as a result of amiodarone lung toxicity.

Disseminated pulmonary ossification is a rare condition in which very small deposits of mature bone form within the lung parenchyma [209]. It can be associated with chronic heart disease, such as mitral stenosis, or chronic interstitial fibrosis, such as IPF or asbestosis, or be related to drugs. Such calcification is usually invisible on chest radiographs and on HRCT.

Metastatic Calcification

Deposition of calcium within the lung parenchyma (metastatic calcification) can occur due to hypercalcemia in patients

P.139

with abnormal calcium and phosphate metabolism and is most common in patients with chronic renal failure and

secondary hyperparathyroidism (Fig. 3-106) [150,151,210]. Metastatic calcification is typically interstitial, involving the alveolar septa, bronchioles, and arteries, and can be associated with secondary lung fibrosis. Plain radiographs are relatively insensitive in detecting this calcification, whereas HRCT can show calcification in the absence of radiographic findings. Calcifications can be focal, centrilobular, or diffuse (Fig. 3-106). Ground-glass opacities with a centrilobular distribution have been reported in association with metastatic calcification [150].

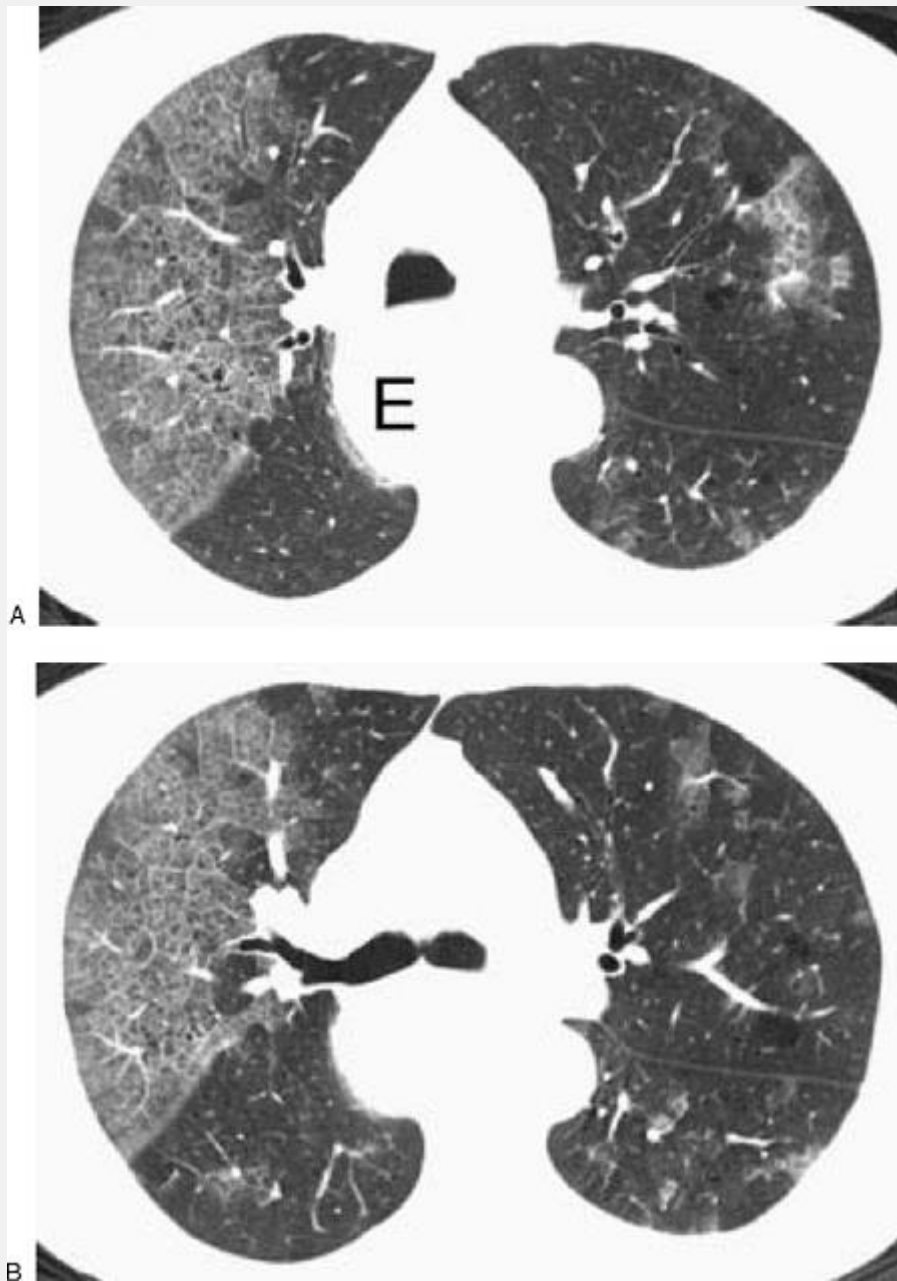


FIG. 3-100. A, B: Patchy areas of ground-glass opacity and interlobular septal thickening (crazy-paving) in a patient with bronchiolitis obliterans organizing pneumonia associated with aspiration. Note the presence of a dilated fluid-filled esophagus (E).

Hartman et al. [151] reviewed the chest radiographs and CT and HRCT scans of seven patients with hypercalcemia and

biopsy-proven metastatic calcification. In five patients, the radiographic findings were nonspecific, consisting of poorly defined nodular opacities and patchy areas of parenchymal consolidation, whereas in two patients calcified nodules were visible. CT and HRCT findings consisted of numerous fluffy and poorly defined nodules measuring 3 to 10 mm in diameter. The nodules primarily involved the upper lobes in three patients, were diffuse in three, and were predominant in the lower lung zones in one. Areas of ground-glass opacity were present in three of the seven patients, and patchy areas of consolidation were present in two. Calcification of some or all of the nodules was seen on CT in four of the seven patients.

P.140

Six of the seven patients also had evidence of calcification in the vessels of the chest wall, and one had calcification of the left atrial wall.

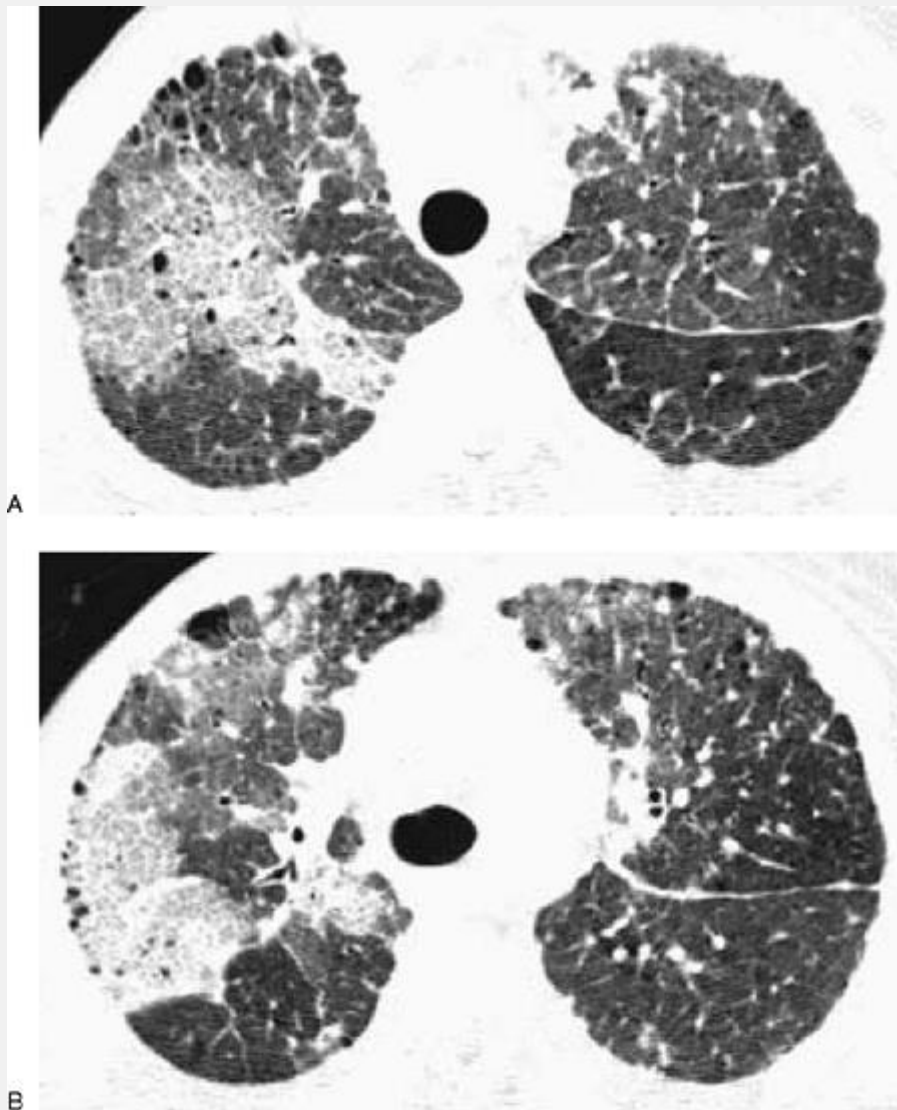


FIG. 3-101. A, B: Patchy areas of ground-glass opacity and interlobular septal thickening in a patient with diffuse bronchioloalveolar carcinoma. Nodules within the left lung and nodular thickening of the subpleural interstitium adjacent to the left major fissure also reflect tumor spread. Focal lucencies within the upper lobes are caused by underlying emphysema.

Alveolar Microlithiasis

The HRCT appearances of several patients with pulmonary alveolar microlithiasis have been reported, corresponding

closely to pathologic findings in this disease [211,212,213]. Alveolar microlithiasis is characterized by widespread intraalveolar calcifications, representing so-called microliths or calcospheres. HRCT shows a posterior and lower lobe predominance of the calcifications, with a high concentration in the subpleural parenchyma and in association with bronchi and vessels (Fig. 3-107). A perilobular and centrilobular distribution of the calcifications may be seen, or calcifications may be associated with interlobular septa. Intraparenchymal cysts or paraseptal emphysema may be associated [211,212]. In children or patients with early disease, ground-glass opacity or reticulation may be the predominant finding, with calcification being inconspicuous [213].

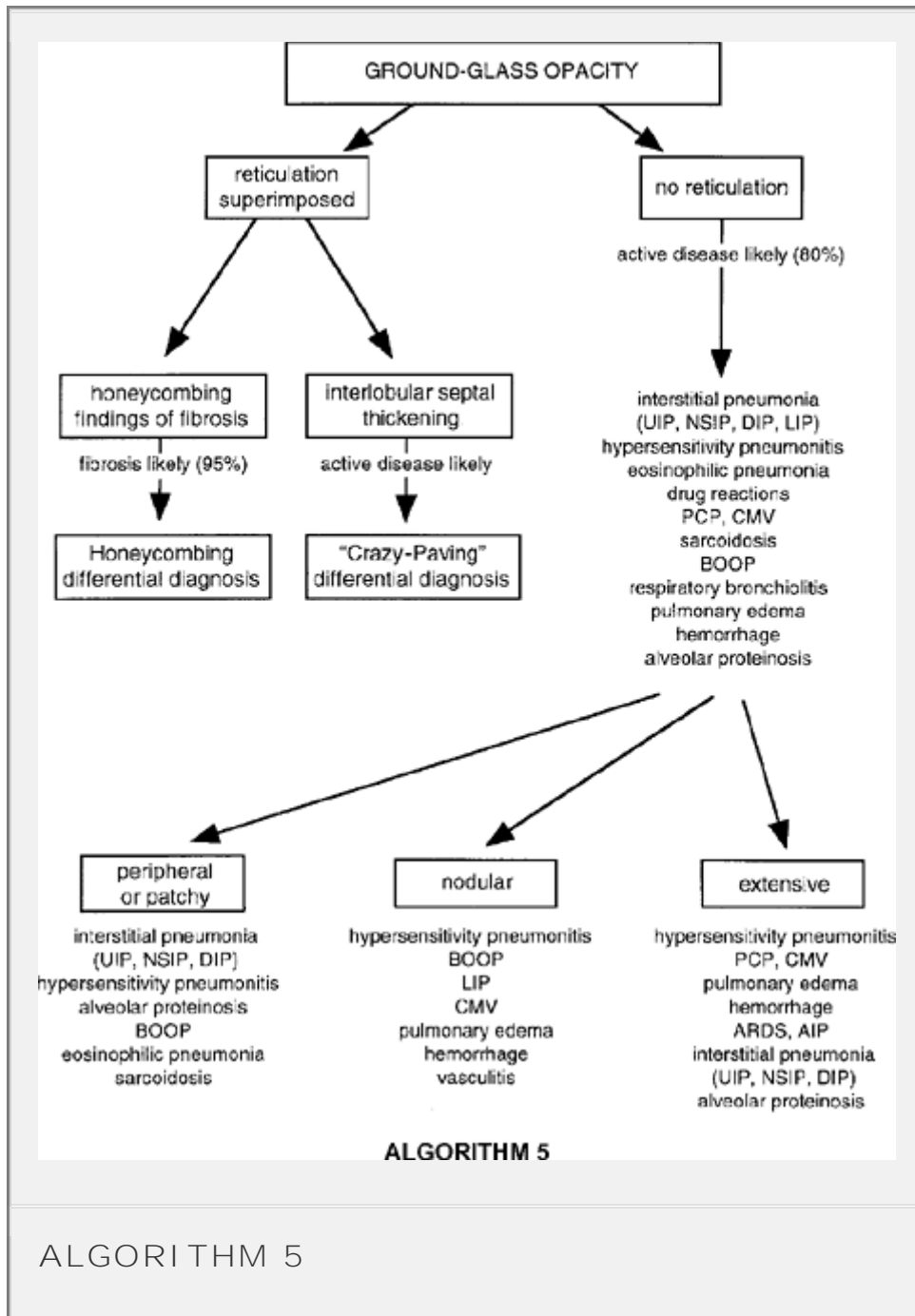
Amiodarone Pulmonary Toxicity

Amiodarone is a triiodinated drug used to treat refractory tachyarrhythmias. It accumulates in lung, largely within macrophages and type-2 pneumocytes, where it forms lamellar inclusion bodies and has a very long half-life. In some patients, accumulation of the drug results in pulmonary toxicity with interstitial pneumonia and fibrosis, although the mechanisms of disease are unclear. CT in patients with amiodarone can show high-attenuation areas of consolidation or high-attenuation nodules or masses, sometimes in association with an abnormal reticulation or ground-glass opacity (Fig. 3-108) [207,214]. High-attenuation consolidation or masses

P.141

were seen in 8 of 11 patients in one series [214], correlating with the presence of numerous foamy

macrophages in the interstitium and alveolar spaces. Unconsolidated lung parenchyma does not appear abnormally dense. Because the drug also accumulates in the liver and spleen, these also appear abnormally dense on scans obtained through the lung bases.



Heavy Metal Pneumoconiosis

Inhalation of radiodense material, such as iron oxide, tin, and barium, may result in dense pulmonary lesions. The

HRCT appearance of dense lung lesions secondary to inhaled iron oxide has been reported in welders [215].

TABLE 3-11. *Differential diagnosis of consolidation*

Diagnosis	Course	Comments
Pneumonia (e.g., bacterial, Pneumocystis carinii, viral, Mycoplasma pneumonias)	Acute	Patchy, nodular, lobular, or diffuse depending on the organism
Acute interstitial pneumonia; acute respiratory distress syndrome	Acute	Patchy or diffuse
Pulmonary edema	Acute	Diffuse
Pulmonary hemorrhage	Acute	Patchy or diffuse
Acute eosinophilic pneumonia	Acute	Diffuse
Radiation pneumonitis	Acute	Extent usually corresponds to

		radiation ports
Bronchiolitis obliterans organizing pneumonia	Subacute, chronic	Common; peripheral; can be masslike
Chronic eosinophilic pneumonia	Subacute, chronic	Patchy or nodular; peripheral
Churg-Strauss syndrome	Subacute, chronic	Consolidation also present; nodular
Bronchioloalveolar carcinoma (diffuse)	Subacute, chronic	Diffuse, patchy, or nodular
Lymphoma	Subacute, chronic	Diffuse, patchy, or nodular
Nonspecific interstitial pneumonia	Subacute, chronic	Patchy; subpleural
Usual interstitial pneumonia and idiopathic pulmonary fibrosis	Subacute, chronic	Subpleural and basal predominance

Hypersensitivity pneumonitis	Subacute, chronic	Patchy; ground-glass opacity more common
Lipoid pneumonia	Subacute, chronic	Patchy or lobular; low-attenuation consolidation
Sarcoidosis	Subacute, chronic	Confluence of very small granulomas
Alveolar proteinosis	Subacute, chronic	Ground-glass opacity more common

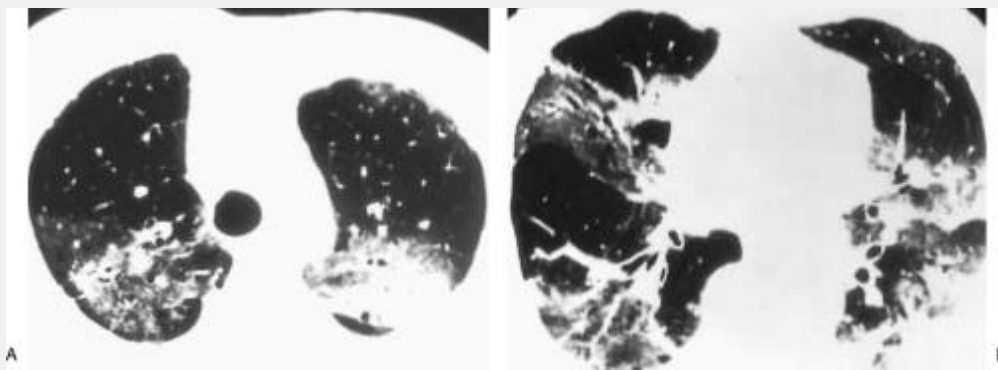


FIG. 3-102. A, B: Bronchiolitis obliterans organizing pneumonia with patchy areas of consolidation and ground-

glass opacity. A peripheral distribution is typical.

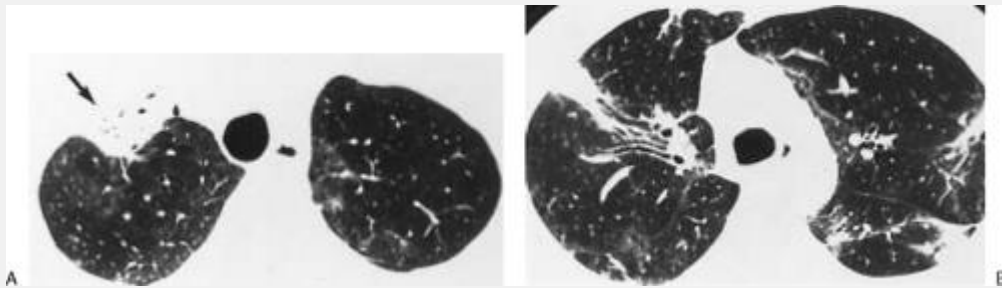
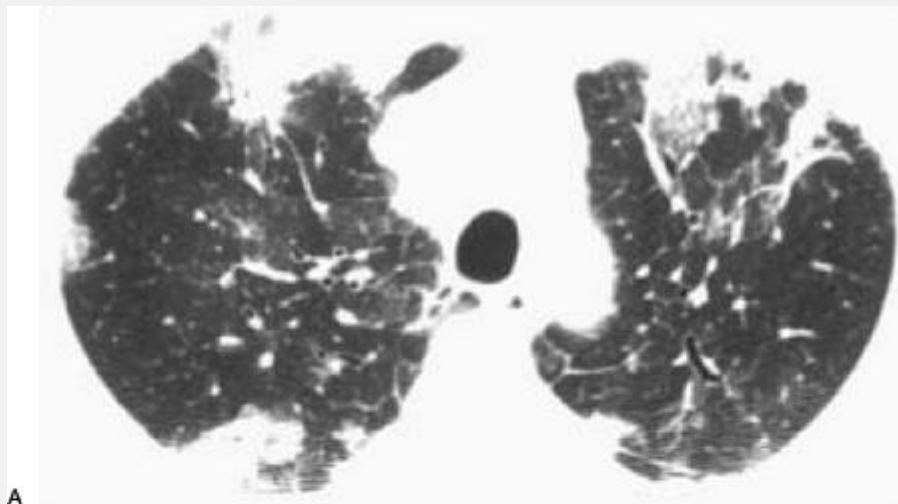
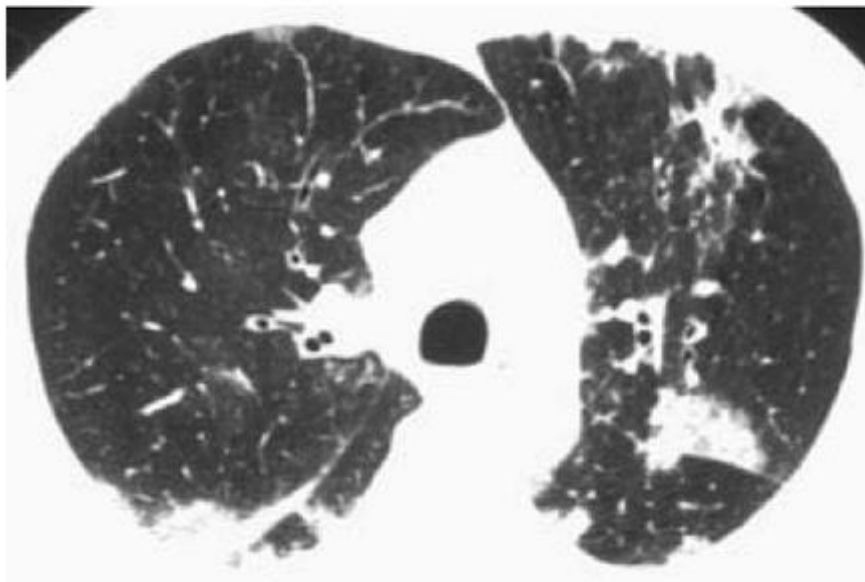


FIG. 3-103. Eosinophilic pneumonia with focal areas of consolidation and ground-glass opacity. As in patients with bronchiolitis obliterans organizing pneumonia, a peripheral distribution is typical. Note the presence of air bronchograms and obscuration of vessels in the apical opacity (arrow).

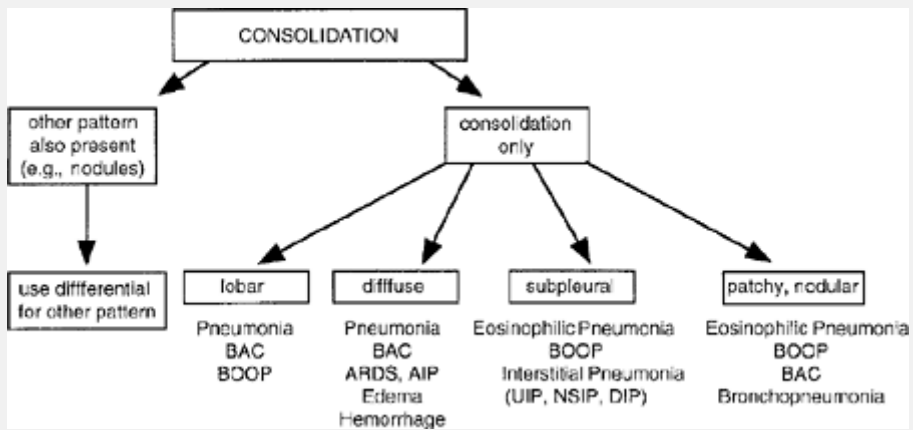


A



B

FIG. 3-104. A, B: Eosinophilic pneumonia with focal areas of consolidation having a peripheral and subpleural distribution.



ALGORITHM 6

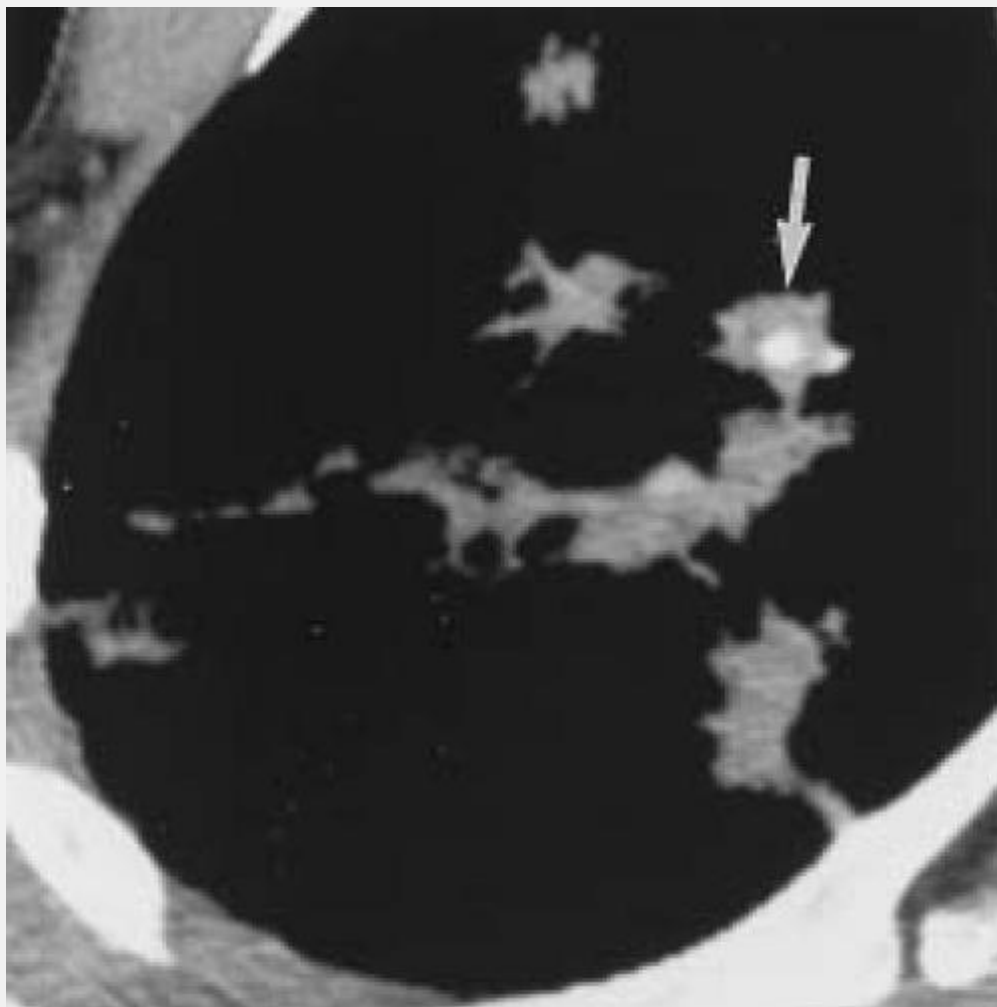


FIG. 3-105. Calcification (arrow) within nodular lung disease in a patient with sarcoidosis.

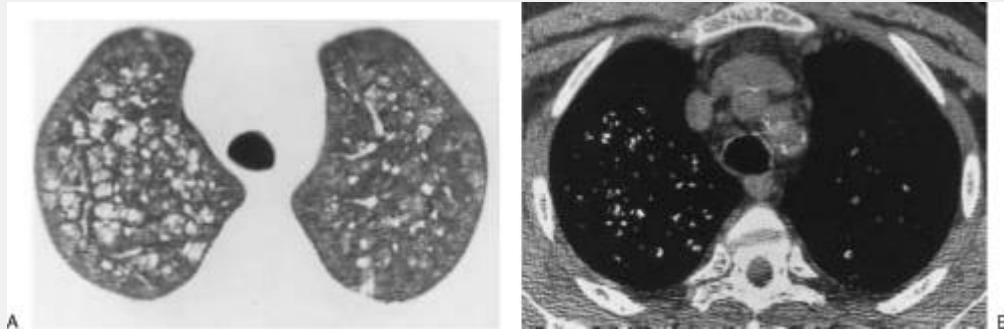


FIG. 3-106. A 42-year-old man with chronic renal failure and metastatic calcification. A: HRCT shows nodular areas of opacity that appear centrilobular, as well as some ground-glass opacities. B: Soft-tissue window scan shows multiple areas of calcification within these opacities.

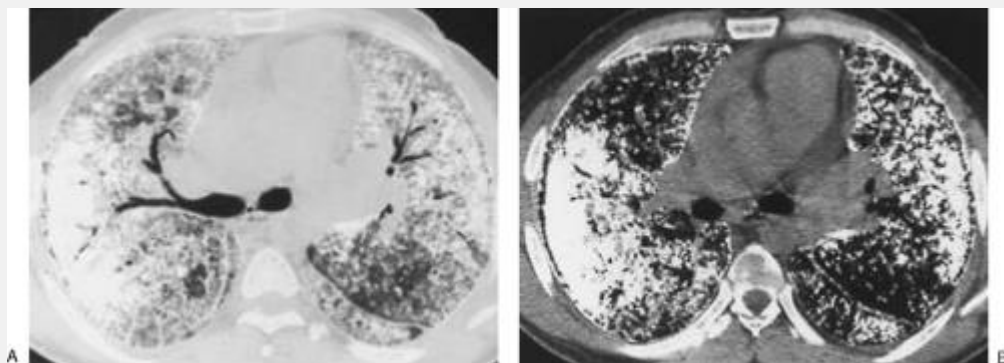


FIG. 3-107. HRCT in a patient with alveolar microlithiasis,

with lung (A) and soft-tissue (B) windows. Calcifications that are very small and diffuse show a subpleural predominance. (Courtesy of Joseph Cherian, M.D., Al-Sabah Hospital, Kuwait.)

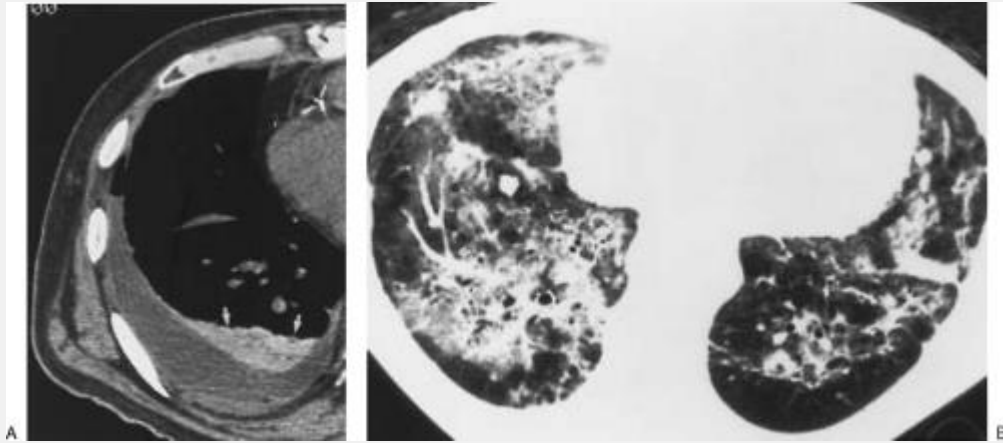


FIG. 3-108. HRCT in pulmonary amiodarone toxicity. A: On an unenhanced HRCT, a focal area of dense lung consolidation is present in the posterior lung. A pleural effusion is also visible, due to cardiac decompensation. B: In another patient with amiodarone toxicity, a lung window scan shows areas of ground-glass opacity, consolidation, nodular opacities, and abnormal reticulation. The high attenuation cannot be appreciated with this window setting.

P.142

P.143

P.144

Decreased Lung Opacity, Cysts, and Airway Abnormalities

A variety of abnormalities result in decreased lung attenuation or air-filled cystic lesions on HRCT. These include honeycombing, lung cysts, emphysema, bullae, pneumatoceles, cavitary nodules, bronchiectasis, mosaic perfusion, and air-trapping due to airways disease (Fig. 3-109). In most cases, these can be readily distinguished on the basis of HRCT findings [216].

Honeycombing

In patients with interstitial fibrosis, alveolar disruption, dilatation of alveolar ducts, and bronchiolar dilatation result in the formation of honeycomb cysts [8,217]. These cysts

P.146

P.147

have fibrous walls and are lined by bronchiolar epithelium. On HRCT, honeycombing is characterized by the presence of air-filled, cystic spaces, several millimeters to several centimeters in diameter, which often predominate in a peripheral and subpleural location, occur in several layers, and are characterized by clearly definable walls 1- to 3-mm in thickness [32,42] (Figs. 3-29, 3-31, 3-32, and 3-110, 3-

111, 3-112). In contradistinction to the lung cysts seen in patients with lymphangiomyomatosis (LAM), Langerhans histiocytosis and LIP, and the lucencies seen in patients with centrilobular emphysema, honeycomb cysts tend to share walls. The presence of honeycombing on HRCT indicates the presence of severe fibrosis.

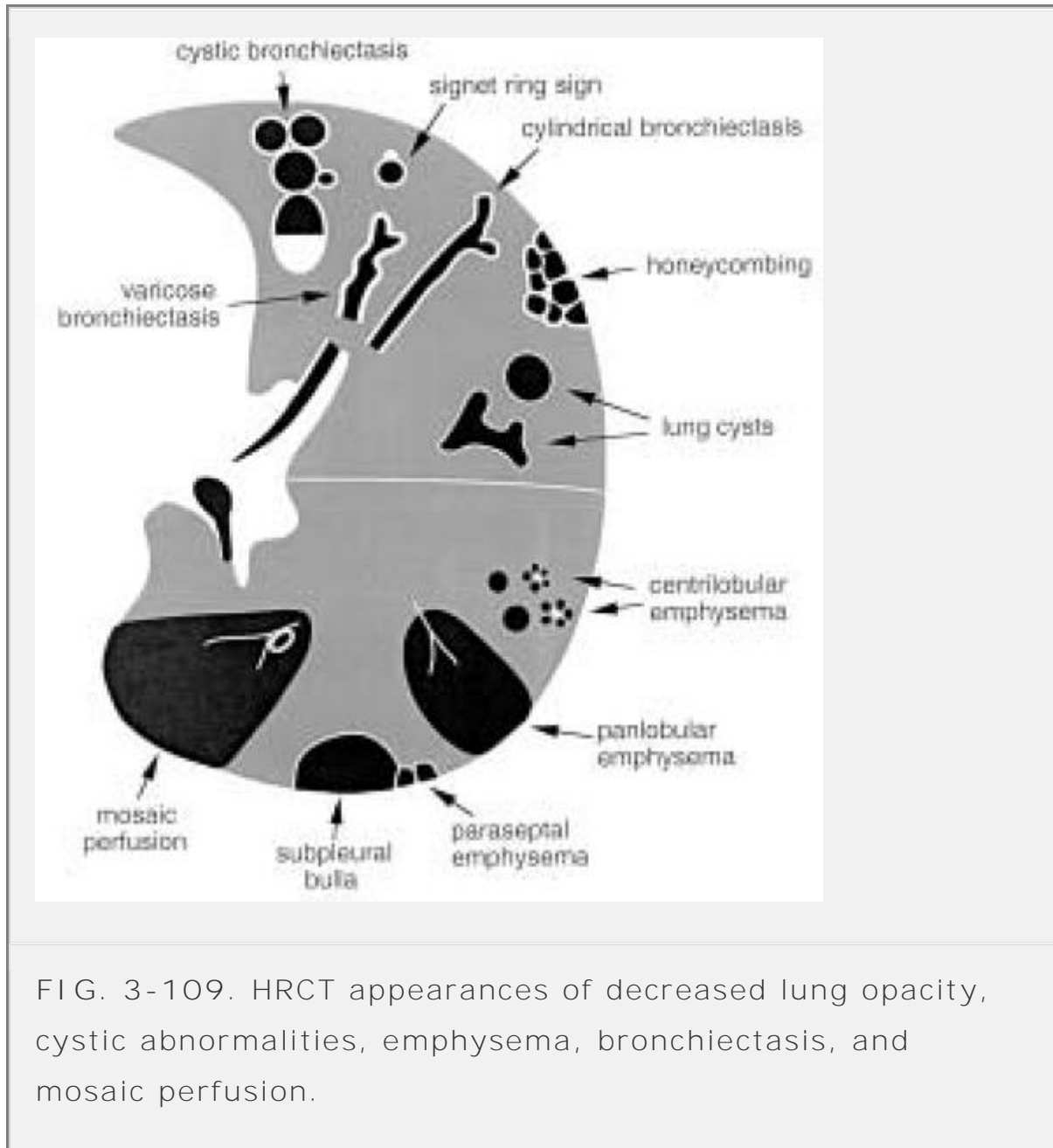


FIG. 3-109. HRCT appearances of decreased lung opacity, cystic abnormalities, emphysema, bronchiectasis, and mosaic perfusion.

Large cystic spaces, several centimeters in diameter, can be associated with honeycombing, mimicking the appearance of bullae (Figs. 3-111 and 3-112). These large cysts tend to

predominate in the upper lobes, but they may be seen at the lung bases as well. They often have a subpleural predominance. These large honeycomb cysts decrease in size on expiratory scans [218,219].

Lung Cysts

On HRCT, the term *lung cyst* is used to refer to a well-defined, rounded, and circumscribed lesion, with a wall that may be uniform or varied in thickness but which is usually thin (less than 3 mm thick) [216]. It usually contains air but may also contain liquid, semisolid, or solid material [6,216]. Lung cysts are also defined as having a wall composed of one of a variety of cellular elements, usually fibrous or epithelial in nature [157]. For example, in patients with end-stage pulmonary fibrosis, honeycomb cysts are lined by bronchiolar epithelium; on the other hand, in patients with LAM, the cysts are lined by abnormal spindle cells resembling smooth muscle. This term is not usually used to describe airspaces in patients with emphysema. The term *cystic airspace* may be used to describe a peripheral air-containing lesion surrounded by a wall of variable thickness, that may be thin, as in LAM or thick as in honeycombing [6].



A



B

FIG. 3-110. Honeycombing in a patient with idiopathic pulmonary fibrosis. A, B: On HRCT, honeycombing cysts have clearly definable walls a few millimeters in thickness. In areas of honeycombing, lobular anatomy cannot be

resolved because of architectural distortion. Bronchial irregularity and traction bronchiectasis (*arrows, B*) are often present in patients with severe fibrosis and may be difficult to distinguish from honeycombing.

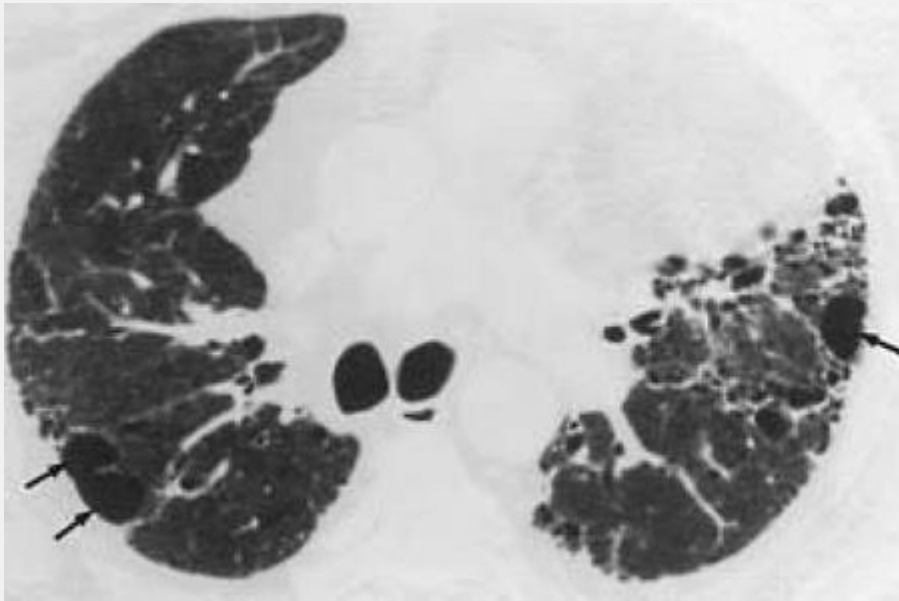


FIG. 3-111. Honeycombing with large lung cysts. In a patient with idiopathic pulmonary fibrosis, peripheral honeycombing, traction bronchiectasis, and several large lung cysts (*arrows*) are visible.

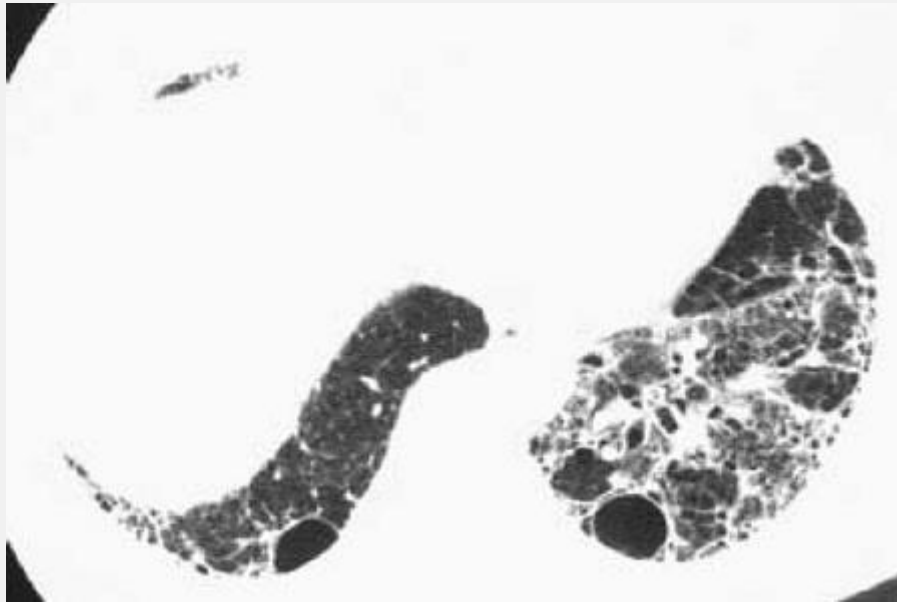


FIG. 3-112. Idiopathic pulmonary fibrosis with asymmetric honeycombing and large lung cysts. Peripheral honeycombing and irregular reticular opacities are associated with large lung cysts. These are predominantly subpleural in location.

TABLE 3-12. *Differential diagnosis of cystic lung disease*

Diagnosis	Comments
Lymphangiomyomatosis (LAM)	Cysts usually round and relatively uniform in size and shape; diffuse lung involvement; almost exclusively in women

Langerhans histiocytosis	Cysts have unusual shapes; larger and more numerous in lung apices; costophrenic angles usually spared; small nodules may be present
Lymphocytic interstitial pneumonitis	Less numerous than in LAM or histiocytosis; nodules may be associated
Bullae	Subpleural distribution in most cases; single layer at the pleural surface; centrilobular emphysema may be present
Pneumatocoles	Scattered; patchy distribution; limited in number; findings of pneumonia
Honeycombing	Subpleural predominance; multiple layers at the pleural surface; cysts share walls; findings of fibrosis
Cystic bronchiectasis	Clustered or perihilar distribution; air-fluid levels may be present

LAM, Langerhans histiocytosis, and LIP often produce multiple lung cysts, whose appearance on HRCT is usually quite distinct from that of honeycombing (Table 3-12) [17,18,92,93,220,221,222,223,224,225]. The cysts have a thin but easily discernible wall in most instances, ranging up to a few millimeters in thickness (Figs. 3-113, 3-114, 3-115, 3-116, 3-117, 3-118). Associated findings of fibrosis are usually absent or much less conspicuous than they are in patients with honeycombing and end-stage lung disease. In LAM, Langerhans histiocytosis, and LIP, the cysts are usually interspersed within areas of normal-appearing lung. In patients with Langerhans histiocytosis, the cysts can have bizarre shapes because of the fusion of several cysts, or perhaps because they represent ectatic and thick-walled bronchi (Figs. 3-113, 3-114, 3-115). Although confluent cysts can also be seen with LAM, they are less common; in patients with LAM, cysts generally appear rounder and more uniform in size than those seen with histiocytosis (Figs. 3-116, 3-117, 3-118). Multiple thin-walled lung cysts are also seen in patients with LIP (see Figs. 5-19 and 5-61) [17,18,225]. In one study of 22 patients with LIP, cystic air-spaces were seen in 15; other findings included small subpleural nodules, centrilobular nodules, interlobular septal thickening, and ground-glass attenuation [17].

As described above, the term *lung cyst* refers to a specific type of cystic space within the lung parenchyma. If possible, lung cysts should be distinguished from other air-containing spaces, such as emphysematous bullae, blebs, and

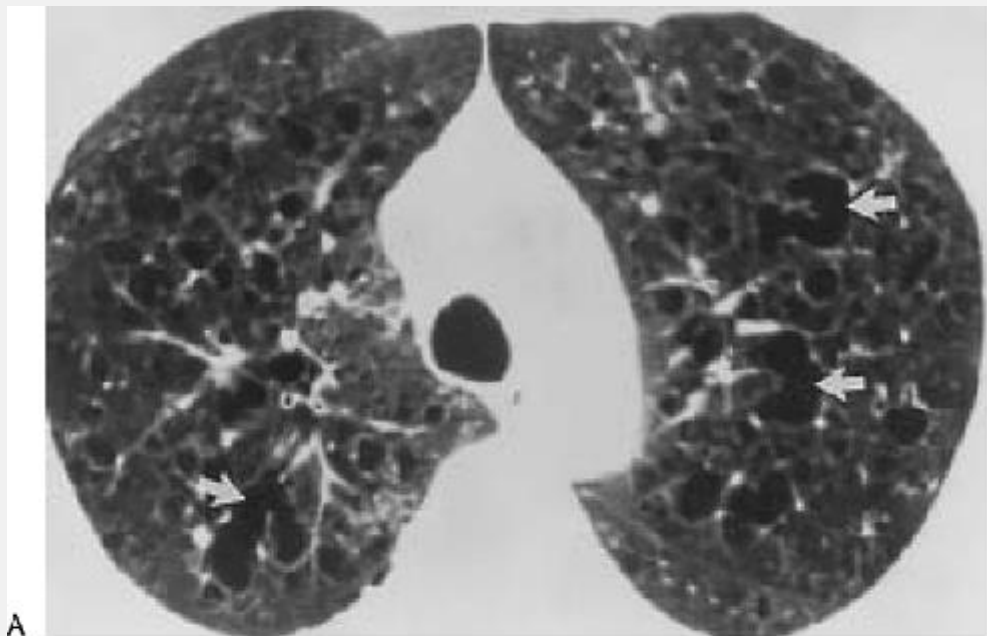
pneumatocoeles, which are described in the paragraphs that follow.

Emphysema

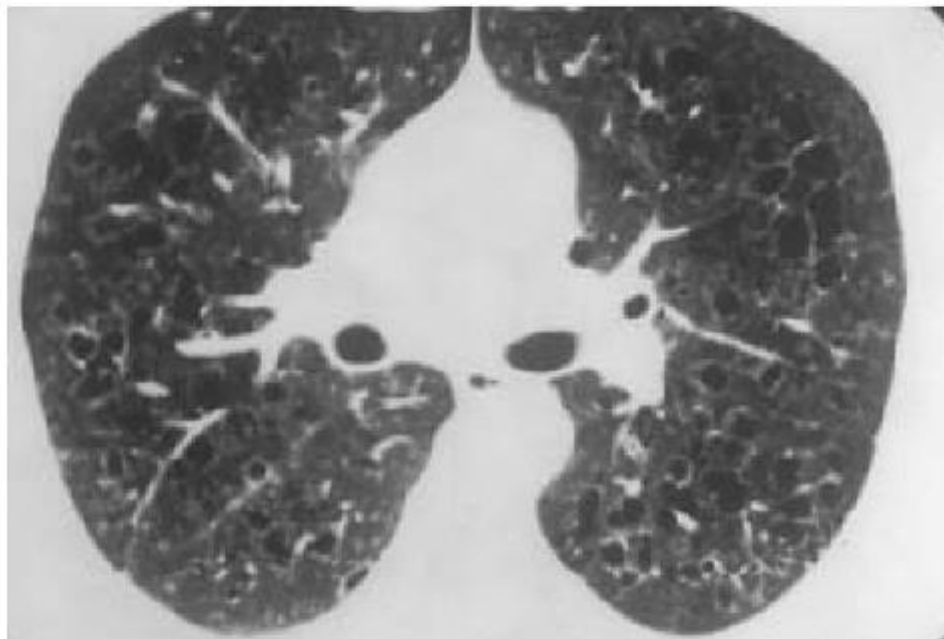
Emphysema is defined as a permanent, abnormal enlargement of airspaces distal to the terminal bronchiole and accompanied by the destruction of the walls of the involved airspaces [216]. Emphysema can be accurately diagnosed using HRCT [32,43,96,226,227,228] and results in focal areas of very low attenuation that can be easily contrasted

P.149

with surrounding higher-attenuation normal lung parenchyma if sufficiently low-window means [-600 to -800 Hounsfield units (HU)] are used (Figs. 3-119, 3-120, 3-121, 3-122 and 3-123 and 3-125, 3-126, 3-127, 3-128 and 3-129). Although some types of emphysema can have walls visible on HRCT, these are usually inconspicuous.



A



B

FIG. 3-113. Langerhans histiocytosis with lung cysts. HRCT at two levels show numerous thin-walled lung cysts. The cysts are larger and most numerous in the upper lobes (A) than in the lower (B), as is characteristic of this disease. Some cysts (*arrows*) are confluent, branching, or irregular in shape. Note that the intervening lung appears normal. The peripheral predominance commonly seen with

honeycombing is absent.

In many patients, it is possible to classify the type of emphysema on the basis of its HRCT appearance [32,43]. *Centrilobular* (proximal or centriacinar) *emphysema* is characterized on HRCT by the presence of multiple small lucencies that predominate in the upper lobes and, in some subjects or regions, may appear centrilobular (Figs. 3-109 and 3-119, 3-120, 3-121, 3-122 and 3-123). Even if the centrilobular location of these lucencies is not visible, a spotty distribution is typical of centrilobular emphysema (Figs. 3-121, 3-122, 3-123). In most cases, the areas of low attenuation seen on HRCT in patients with centrilobular emphysema lack a visible wall, although very thin walls are occasionally visible and are related to areas of fibrosis (Fig. 3-122). In severe cases, the areas of centrilobular emphysema may become confluent.

Panlobular (*panacinar*) *emphysema* typically results in an overall decrease in lung attenuation and a reduction in size of pulmonary vessels, without the focal areas of lucency typically seen in patients with centrilobular emphysema (Fig. 3-124). Areas of panlobular emphysema typically lack visible walls. This form of emphysema has been aptly described as a diffuse simplification of lung architecture. Severe or confluent centrilobular emphysema can mimic this appearance (Figs. 3-125 and 3-126).

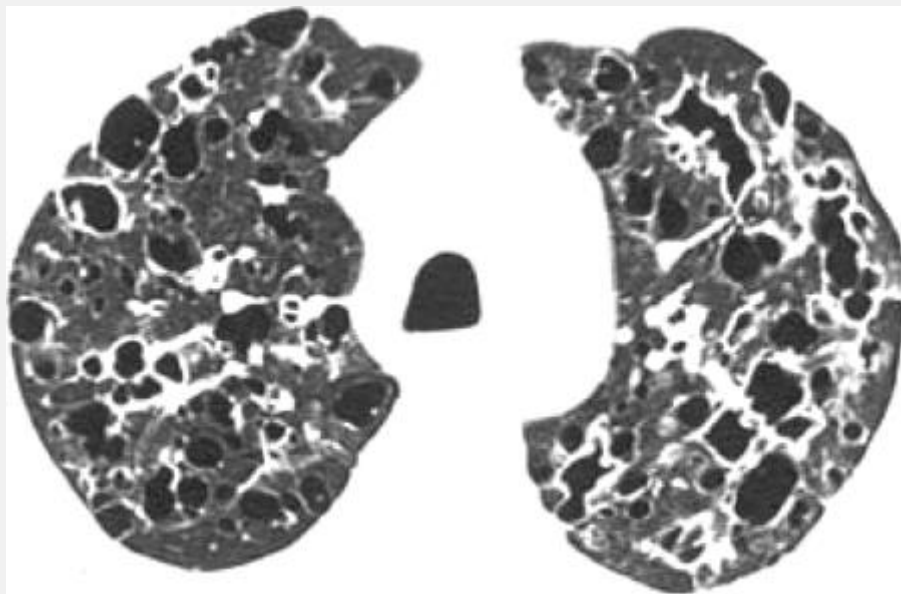


FIG. 3-114. HRCT in a man with Langerhans histiocytosis. The cysts vary in size, and many are irregular in shape. These findings are typical of this disease. (Courtesy of Marcia McCowin, San Francisco, CA.)

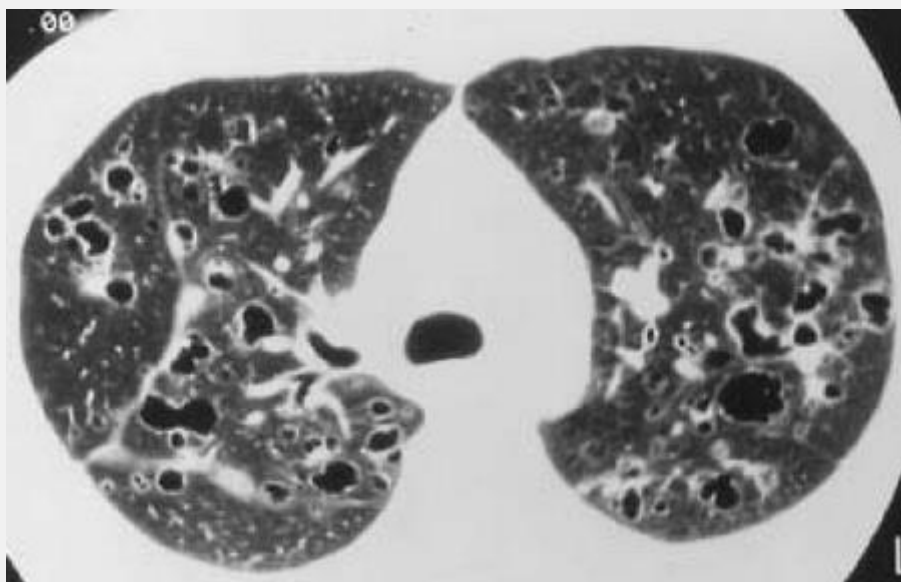


FIG. 3-115. HRCT in a patient with cystic lung disease typical of Langerhans histiocytosis. Multiple lung cysts,

many bifurcating or complex, are interspersed within normal-appearing lung. (Courtesy of Shin-Ho Kook, M.D., Koryo General Hospital, Seoul, Korea.)

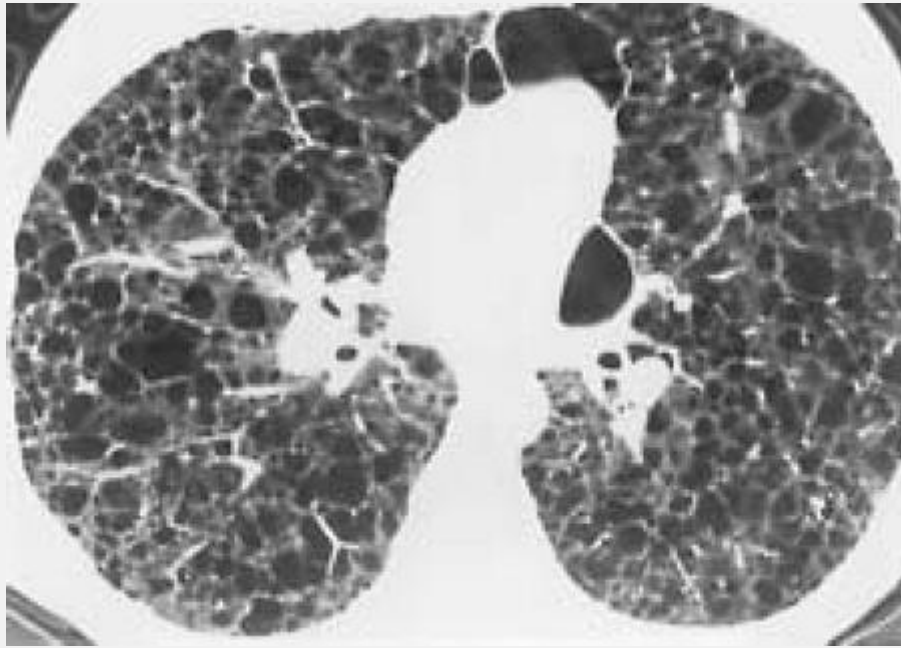


FIG. 3-116. HRCT in a patient with tuberous sclerosis and lymphangiomyomatosis. Cystic airspaces have clearly defined walls measuring up to 2 mm in thickness.

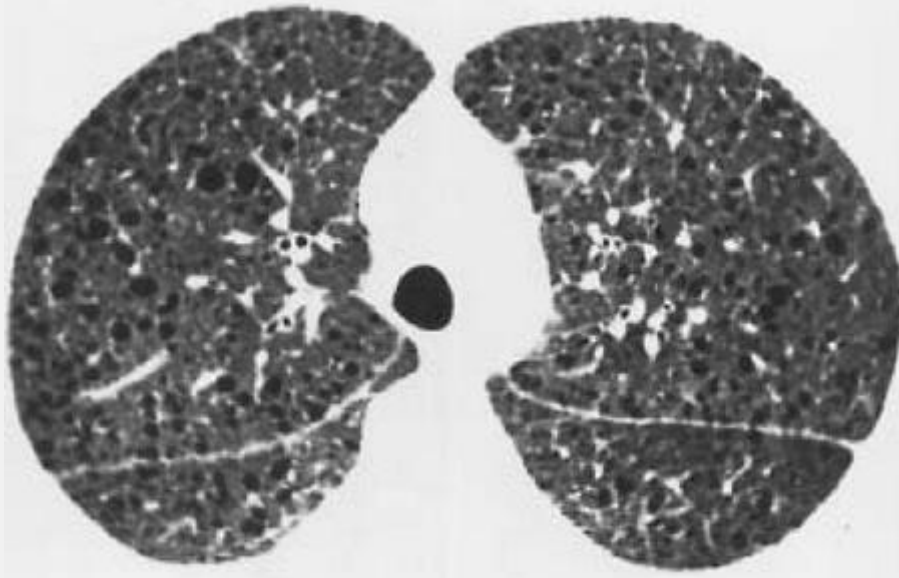


FIG. 3-117. HRCT in a woman with lymphangiomyomatosis. Cysts are rounder and more regular in size than those seen in patients with Langerhans histiocytosis.



FIG. 3-118. HRCT in a young woman with lymphangiomyomatosis associated with tuberous sclerosis. Cysts are round and very thin walled. Intervening lung

parenchyma appears normal.

P.150

P.151

Paraseptal (distal acinar) emphysema results in the presence of subpleural lucencies, which often share very thin walls that are visible on HRCT; paraseptal emphysema can be seen as an isolated abnormality but is often associated with centrilobular emphysema (Figs. 3-127, 3-128, 3-129).

Irregular airspace enlargement, previously known as *irregular* or *cicatricial emphysema*, can be seen in association with fibrosis, as in patients with silicosis and progressive massive fibrosis or sarcoidosis (see Fig. 5-47) [95,229].

Bullous emphysema does not represent a specific histologic entity but represents emphysema characterized primarily by large bullae (Fig. 3-129) [230]. It is often associated with centrilobular and paraseptal emphysema. These types of emphysema and their HRCT appearances are further described in Chapter 7.

Paraseptal Emphysema versus Honeycombing

The appearance of paraseptal emphysema may mimic that of honeycombing in some cases, although a careful consideration of anatomic findings usually allows them to be distinguished. In patients with paraseptal emphysema,

areas of lung destruction are typically margined by thin linear opacities extending to the pleural surface. These linear opacities often correspond to interlobular septa, sometimes thickened by minimal fibrosis (Figs. 3-109 and 3-127, 3-128 and 3-129). Areas of paraseptal emphysema usually occur in a single layer at the pleural surface, predominate in the upper lobes, and may be associated with other findings of emphysema such as large subpleural bullae, but are typically unassociated with significant fibrosis. Honeycomb cysts are usually

P.152

smaller, occur in several layers in the subpleural lung, tend to predominate at the lung bases, and are associated with disruption of lobular architecture and other findings of fibrosis, such as traction bronchiectasis. In occasional patients, emphysema and honeycombing coexist. In such cases, emphysema usually predominates in the upper lobes and central or subpleural lung, whereas honeycombing predominates at the bases and in the subpleural lung regions (Fig. 3-130). The HRCT appearance, however, may be confusing.

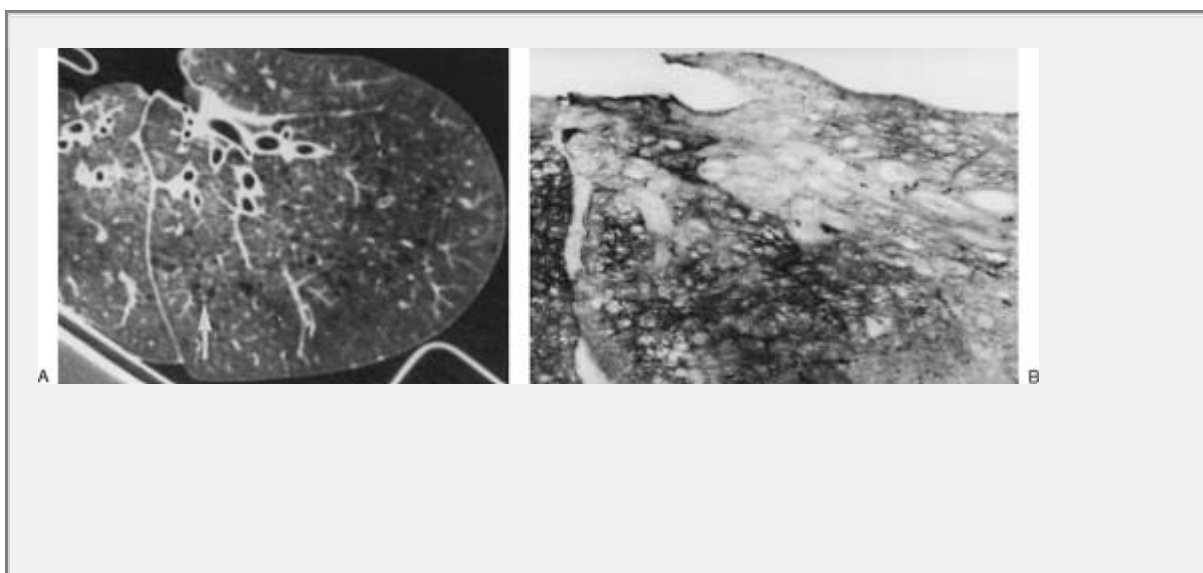


FIG. 3-119. Isolated inflated lung from a patient with centrilobular emphysema. A: Small lucencies without identifiable walls are present. Some lucencies are seen to cluster around a centrilobular artery (arrow). This appearance is typical of centrilobular emphysema. B: On the corresponding lung section, the small centrilobular foci of destruction are clearly seen. (From Webb WR, Stein MG, et al. Normal and diseased isolated lungs: HRCT. *Radiology* 1988;166:81, with permission.)

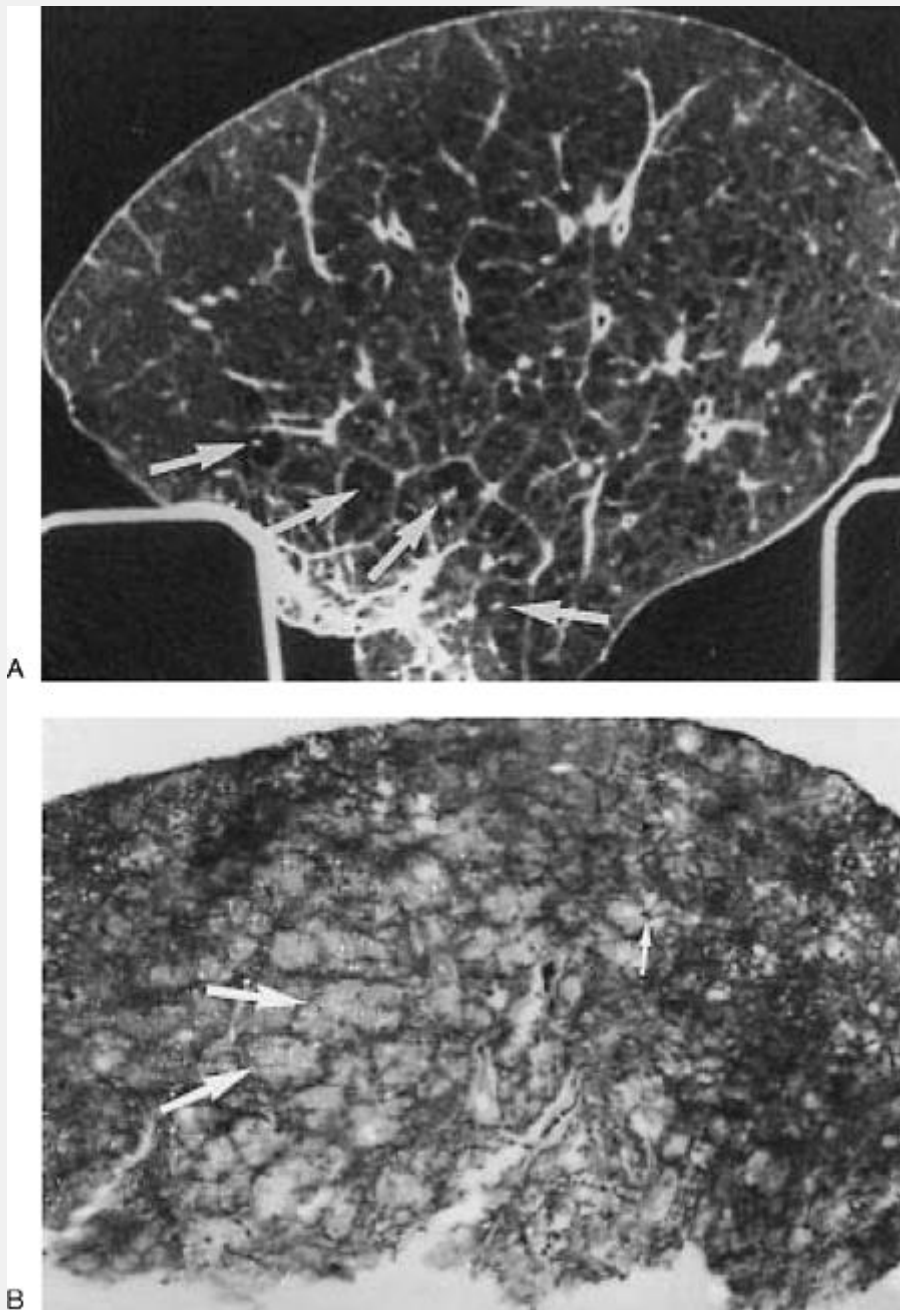


FIG. 3-120. Centrilobular emphysema in an isolated lung. A: More severe, but patchy, emphysema is visible on the HRCT. The areas of destruction cluster about the centrilobular arteries (*arrows*). (From Webb WR, Stein MG, et al. Normal and diseased isolated lungs: HRCT. *Radiology* 1988;166:81, with permission.) B: On the pathologic

specimen, some lobules (*large arrows*) show extensive destruction. In some, the centrilobular artery remains visible (*small arrow*) within the area of emphysema.

Centrilobular Emphysema versus Lung Cysts

In many patients with centrilobular emphysema, the focal areas of lucency that characterize this condition lack visible walls; lung cysts, on the other hand, have walls recognizable on HRCT. However, in some patients with centrilobular emphysema, areas of lung destruction show very thin walls on HRCT, mimicking the appearance of lung cysts. These walls likely reflect the presence of minimal lung fibrosis or compressed adjacent lung parenchyma and are usually less well-defined than those seen in patients with cystic lung disease. Also, lung cysts often appear larger than areas of centrilobular emphysema, which usually range from several millimeters to 1 cm. In patients with centrilobular emphysema, lucencies can often be seen involving only one part of an otherwise normal-appearing secondary lobule (Fig. 3-109); this appearance is diagnostic.

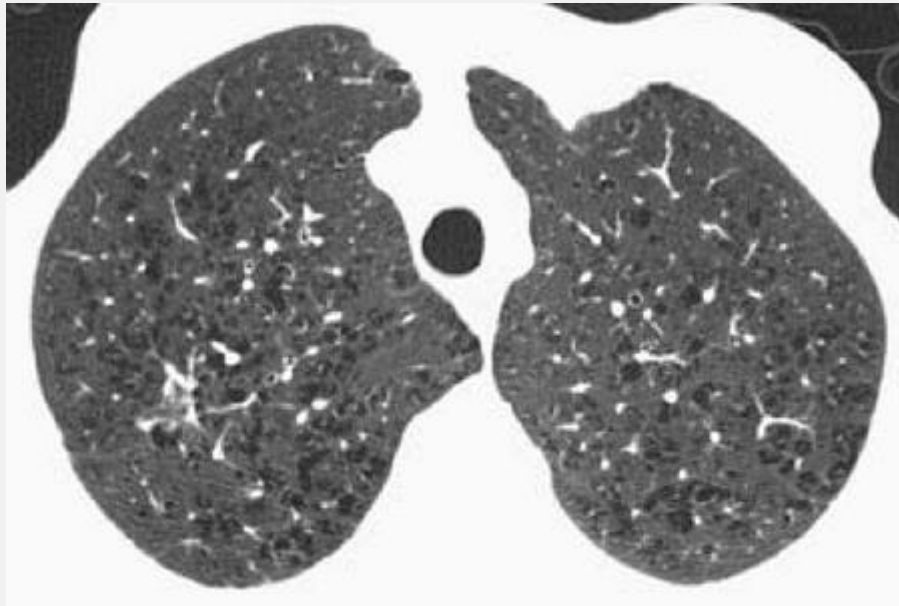


FIG. 3-121. Centrilobular emphysema on HRCT. Spotty areas of lucency predominate in the upper lobes. This appearance is typical and diagnostic. The small areas of emphysema lack visible walls.

P.153

Bullae and Blebs

Emphysematous bullae are well seen using HRCT. A *bulla* has been defined as a sharply demarcated area of emphysema measuring 1 cm or more in diameter and possessing a thin epithelialized wall that is usually no thicker than 1 mm (Figs. 3-128 and 3-129) [6,157]. Although it is not always possible to distinguish a bulla from a lung cyst, bullae are uncommon as isolated findings, except in the lung apices, and are usually associated with evidence of extensive centrilobular or paraseptal emphysema. Subpleural bullae are often associated with

areas of paraseptal emphysema. When emphysema is associated with predominant bullae, it may be termed *bullous emphysema* [230].

On HRCT, bullae show a distinct wall that usually appears approximately 1-mm thick. Bullae can range up to 20 cm in diameter but are usually between 2 and 8 cm in diameter. Bullae can be seen in a subpleural location or within the lung parenchyma, but subpleural bullae appear more frequently. In patients with bullous emphysema, bullae are often asymmetric, with one lung being involved to a greater degree [230].

The term *bleb* is used pathologically to refer to a gas-containing space within the visceral pleura [157].

Radiographically, this term is sometimes used to describe a focal thin-walled lucency contiguous with the pleura, usually at the lung apex. However, the distinction between bleb and bulla is of little practical significance and is seldom justified. The term *bulla* is preferred [157].

Pneumatocele

Pneumatocele is defined as a thin-walled, gas-filled space within the lung, usually occurring in association with acute pneumonia and almost invariably transient [157].

Pneumatocele has an appearance similar to lung cyst or bulla on HRCT and cannot be distinguished on the basis of HRCT findings. The association of such an abnormality with acute pneumonia, particularly resulting from *P. carinii* or *Staphylococcus*, would suggest the presence of a pneumatocele, but a spectrum of cystic abnormalities can be seen in such patients (Figs. 3-131 and 3-132) [231,232,233]. The association of lung cysts or bullae with *P. carinii* pneumonia is discussed in Chapter 6.

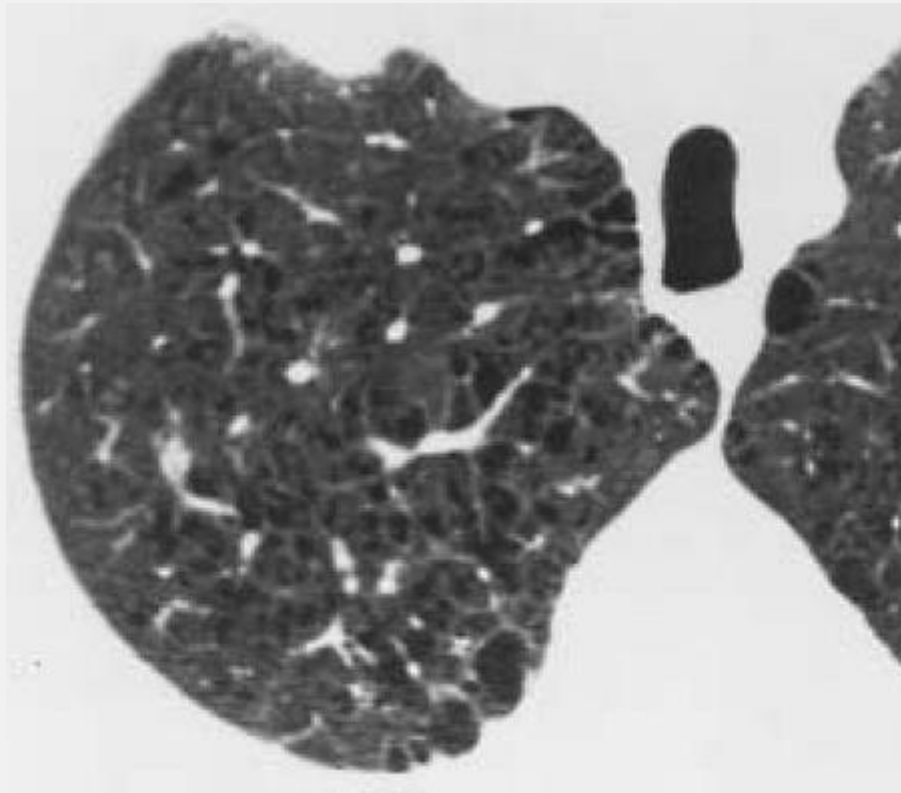
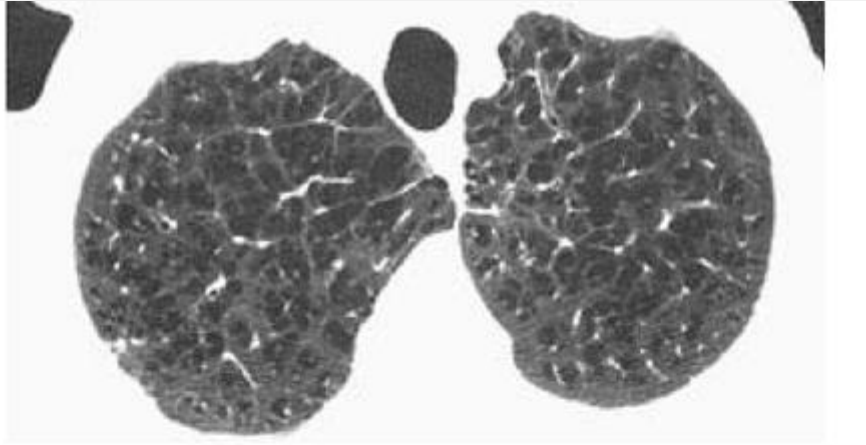
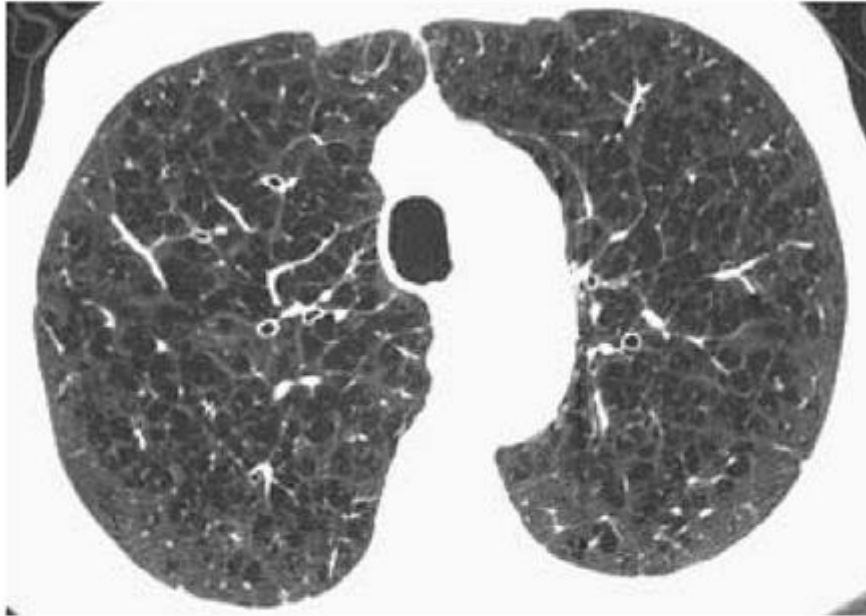


FIG. 3-122. Centrilobular emphysema on HRCT. Spotty areas of lucency predominate in the upper lobes. This appearance is typical and diagnostic. Some of the areas of emphysema have very thin walls, likely reflecting the presence of associated fibrosis.



A



B



C

FIG. 3-123. A-C: Centrilobular emphysema on HRCT showing an upper lobe predominance. Spotty areas of lucency predominate in the upper lobes (A), and some are centrilobular in location, surrounding small vessels. At lower levels (B and C), lucencies are smaller in size and more normal lung is visible.

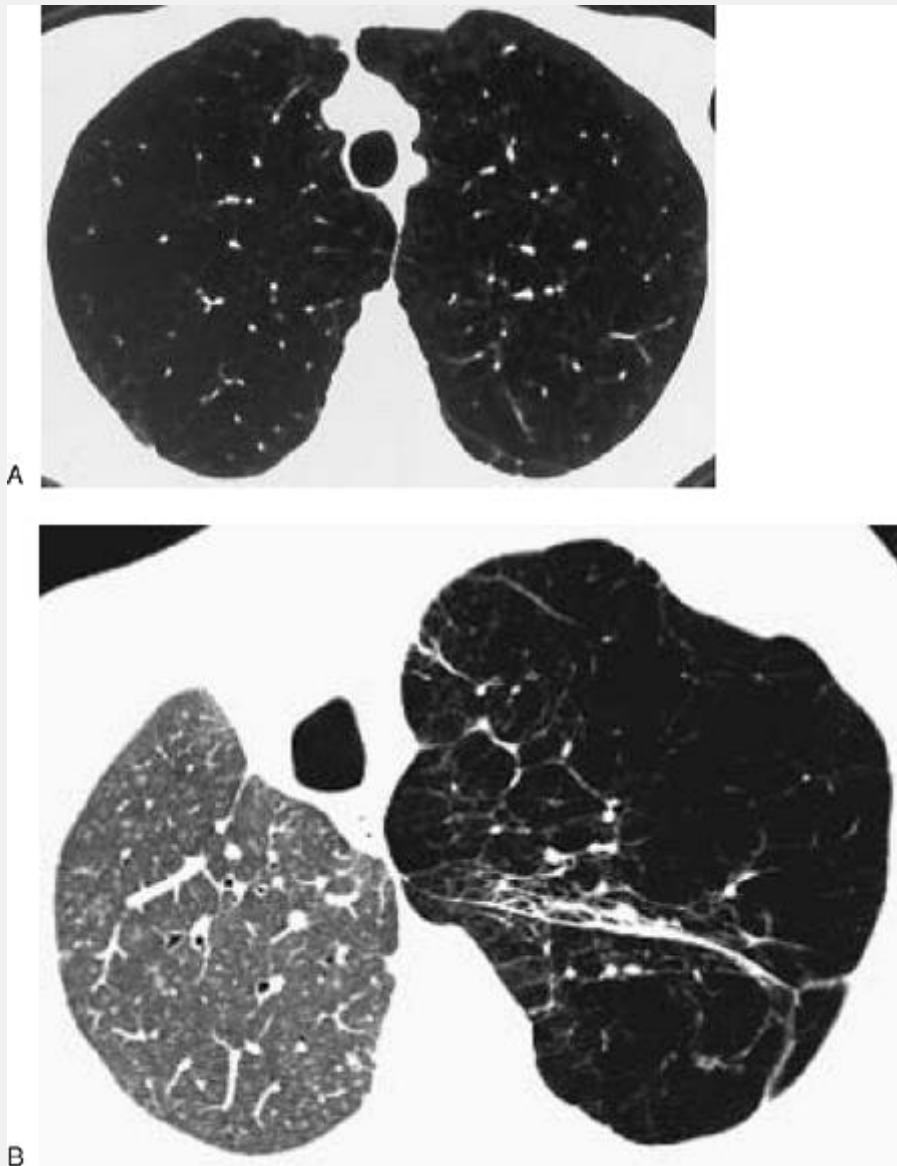


FIG. 3-124. Panlobular emphysema in two patients. A: On HRCT, lung volumes are increased, the lungs appear lucent,

and the size of pulmonary vessels is diminished. Focal lucencies, as seen in patients with centrilobular emphysema, are not visible. B: Panlobular emphysema in a patient who has had a right lung transplantation. The right lung is normal in appearance and attenuation. The emphysematous left lung is abnormally lucent, increased in volume, and contains fewer and smaller visible vessels.

P.154

P.155

Cavitary Nodules

Cavitary nodules have thicker and more irregular walls than lung cysts, but there is some overlap between these appearances (Figs. 3-133 and 3-134). In patients with diffuse lung diseases, such nodules have been reported in Langerhans histiocytosis [92,93], tuberculosis [65], fungal infections, and sarcoidosis [97], but they could also be seen in patients with such disorders as rheumatoid lung disease, septic embolism, pneumonia, metastatic tumor, tracheobronchial papillomatosis (Fig. 3-134), and Wegener's granulomatosis. Also, some nodular opacities that have central lucencies may represent dilated bronchioles surrounded by areas of consolidation or interstitial thickening [92].

Bronchiectasis

Bronchiectasis is generally defined as localized, irreversible bronchial dilatation, often with thickening of the bronchial

wall [6,234]. Generally speaking, a bronchus is considered to be dilated if its internal diameter is greater than that of its accompanying artery (Figs. 3-7, 3-109, and 3-135). However, this appearance is sometimes seen in normals [235]. Also, a bronchus may normally appear larger than its adjacent artery if the scan traverses an undivided bronchus near its branch point, and its accompanying artery has already branched. In this situation, two artery branches **may be seen to lie adjacent to the "dilated" bronchus** (Fig. 3-135). The presence of bronchial wall thickening in addition to an increase in bronchial diameter can be helpful in diagnosing true bronchiectasis.

Although bronchiectasis usually results from chronic infection, airway obstruction by tumor, stricture, impacted material, or inherited abnormalities can also play a significant role. Bronchiectasis has been classified into three types, depending on the morphology of the abnormal bronchi, although these distinctions are of little clinical value [216]. The HRCT diagnosis of bronchiectasis is described in detail in Chapter 8.

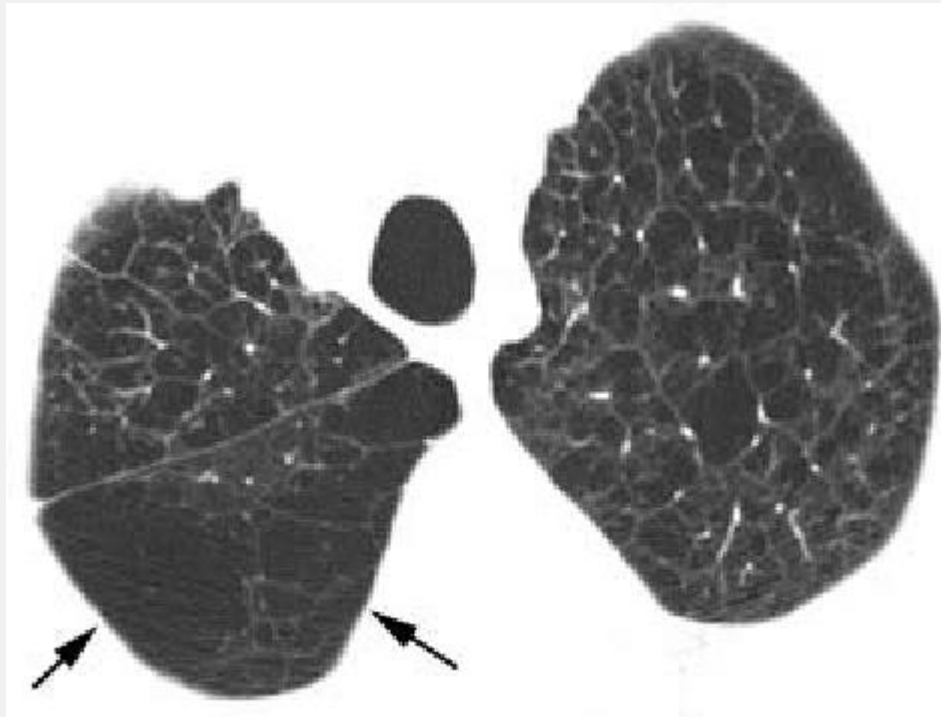


FIG. 3-125. Confluent centrilobular emphysema. Areas of centrilobular emphysema have coalesced in the posterior right lung (*arrows*), resulting in an area of very low attenuation that mimics the appearance of panlobular emphysema. Mild interlobular septal thickening is also visible, usually indicative of some associated fibrosis.

P.156

Cylindrical bronchiectasis, the mildest form of this disease, is characterized on HRCT by the presence of thick-walled bronchi that extend into the lung periphery and fail to show normal tapering. On HRCT, bronchi are not normally visible in the peripheral 1 cm of lung, but in patients with bronchiectasis, bronchial wall thickening, peribronchial fibrosis, and dilatation of the bronchial lumen, they can be seen in the lung periphery (Figs. 3-7, 3-109, 3-135, and 3-

136) [236,237]. Depending on their orientation relative to the scan plane they can simulate tram tracks or can show the signet ring sign, in which the dilated, thick-walled bronchus and its accompanying pulmonary artery branch are seen adjacent to each other [34]. Ectatic bronchi containing fluid or mucus appear as tubular opacities.

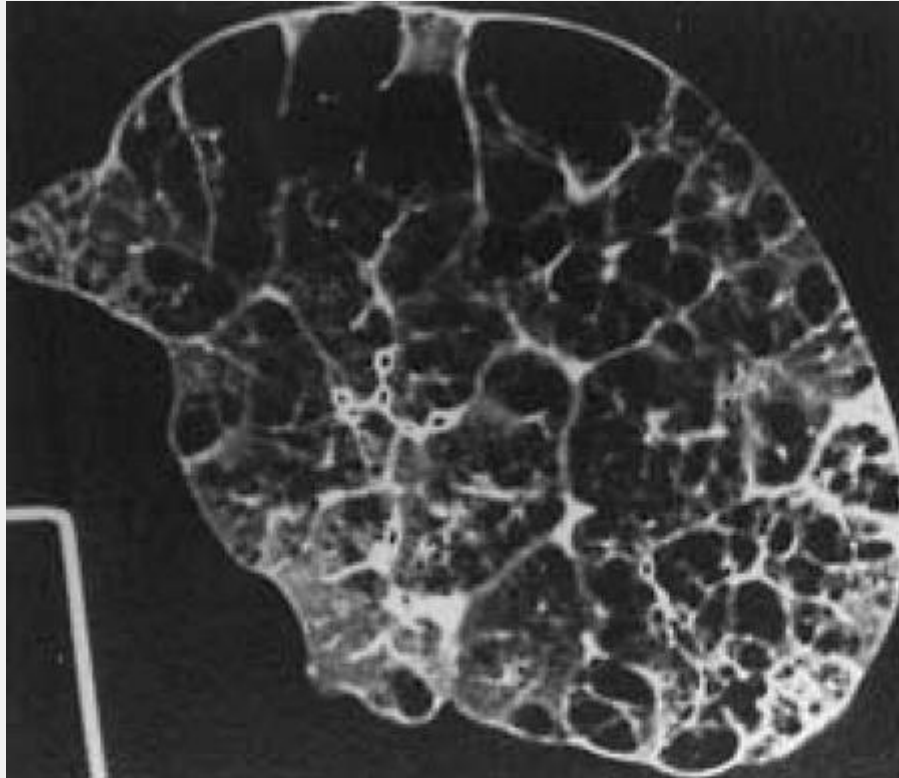


FIG. 3-126. Confluent centrilobular emphysema in an isolated lung. On HRCT, areas of centrilobular emphysema have coalesced to form peripheral bulla. These are margined by residual normal septa. Because of its peripheral location, this may be termed paraseptal emphysema.

Varicose bronchiectasis is similar in appearance to cylindrical bronchiectasis; however, with varicose bronchiectasis the bronchial walls are more irregular and can assume a beaded appearance (Figs. 3-109, 3-137, and

3-138). The term string of pearls has been used to describe varicose bronchiectasis. Traction bronchiectasis often appears varicose.



FIG. 3-127. Centrilobular and paraseptal emphysema. Small isolated areas of destruction are present within the central upper lobes and adjacent to the mediastinal pleura. Some of the paramediastinal cysts (arrows) have visible walls, as is characteristic of paraseptal emphysema.

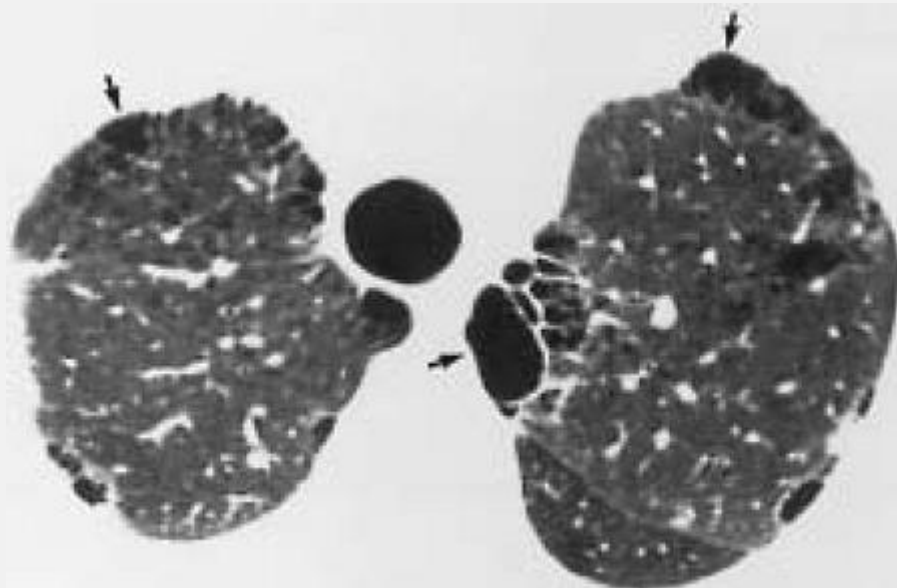


FIG. 3-128. HRCT in a patient with paraseptal and centrilobular emphysema. The larger areas of subpleural emphysema (arrows) are most appropriately termed bullae.

P.157

Cystic bronchiectasis most often appears as a group or cluster of air-filled cysts, but cysts can also be fluid-filled, giving the appearance of a cluster of grapes. Cystic bronchiectasis is often patchy in distribution, allowing it to be distinguished from a cystic lung disease such as LAM (Figs. 3-109 and 3-139). Also, air-fluid levels, which may be present in the dependent portions of the cystic dilated bronchi, are a very specific sign of bronchiectasis and are not usually seen in patients with lung cysts.

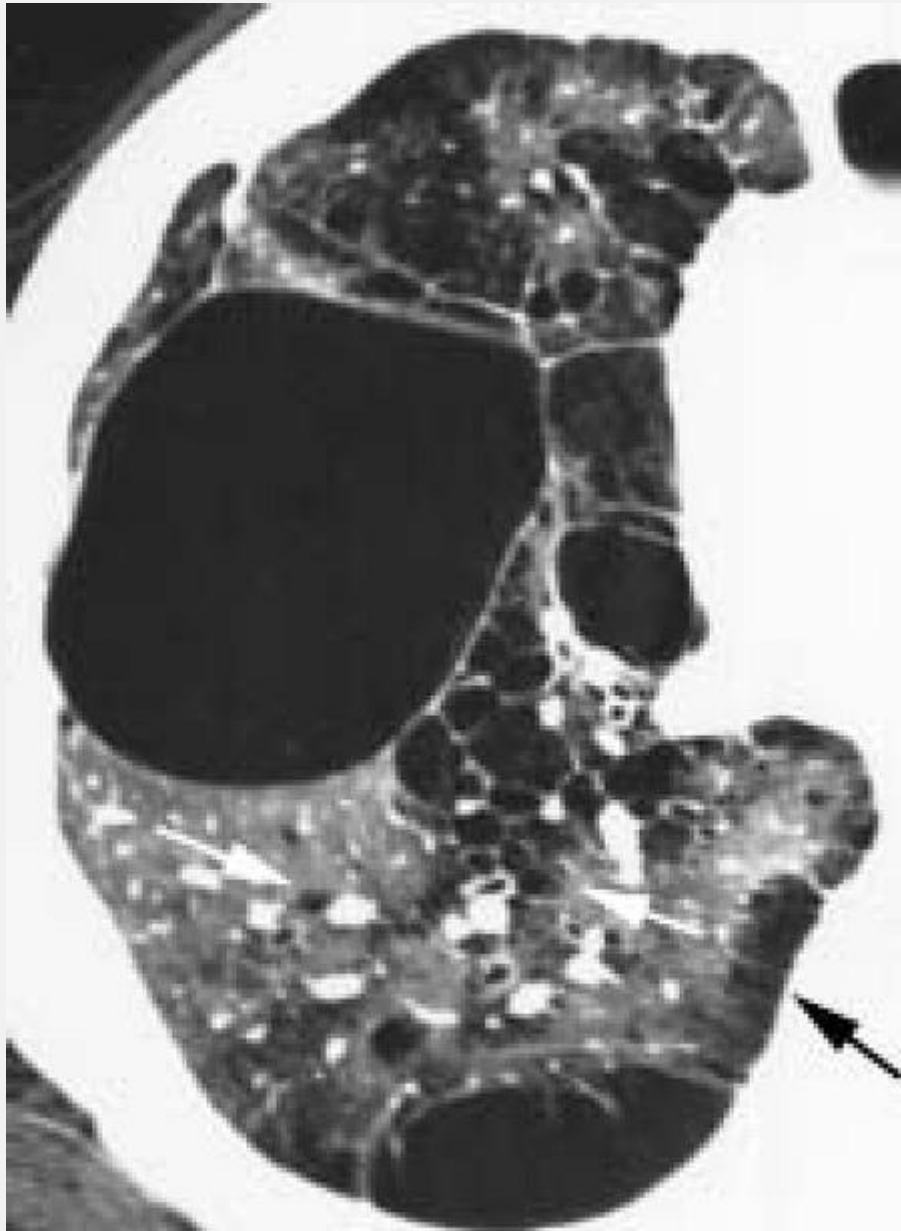


FIG. 3-129. HRCT in a patient with paraseptal and centrilobular emphysema associated with large bullae. Small lucencies lacking walls in the central lung (white arrows) represent centrilobular emphysema. Subpleural lucencies (black arrow) reflect associated paraseptal emphysema. Large bullae are also subpleural in location.

Traction Bronchiectasis

In patients with lung fibrosis and distortion of lung architecture, traction bronchiectasis is commonly present (Figs. 3-28, 3-29, 3-82, and 3-140). In this condition, traction by fibrous tissue on the walls of bronchi results in irregular bronchial dilatation, or bronchiectasis, which is typically varicose in appearance [31,32]. Traction bronchiectasis usually involves the segmental and subsegmental bronchi and can also affect small peripheral bronchi or bronchioles. Dilatation of intralobular bronchioles because of surrounding fibrosis is termed *traction bronchiolectasis*. In patients with honeycombing, bronchiolar dilatation contributes to the cystic appearance seen on HRCT [8].

The increased transpulmonary pressure and elastic recoil associated with advanced pulmonary fibrosis, along with local distortion of airways by fibrotic tissue, contribute to the varicose dilatation of airways seen in these conditions. Because of peribronchial interstitial thickening, bronchial walls can appear to measure up to several millimeters in thickness. Traction bronchiectasis is usually most marked in areas of lung that show the most severe fibrosis. It is commonly seen in association with honeycombing, as is bronchiolectasis. Muroid impaction or air-fluid levels are characteristically absent.

Mosaic Perfusion

Lung density and attenuation are partially determined by the amount of blood present in lung tissue. On HRCT, inhomogeneous lung opacity can result from regional differences in lung perfusion in patients with airways disease or pulmonary vascular disease [124,125,238]. Because this phenomenon is often patchy or mosaic in

distribution, with adjacent areas of lung being of differing attenuation, it has been termed *mosaic perfusion* [5] or *mosaic oligemia* [239], although the former term is most appropriate [6]. Areas of relatively decreased lung opacity seen on HRCT can be of varying sizes and sometimes appear to correspond to lobules, segments, lobes, or an entire lung (Figs. 3-63, 3-109, 3-138, and 3-141, 3-142, 3-143, 3-144 and 3-145). In almost all cases, mosaic perfusion is seen in association with diseases causing regional decreases in lung perfusion. However, differences in attenuation between normal and abnormal lung regions recognizable on HRCT are accentuated by compensatory increased perfusion of normal or relatively normal lung areas.

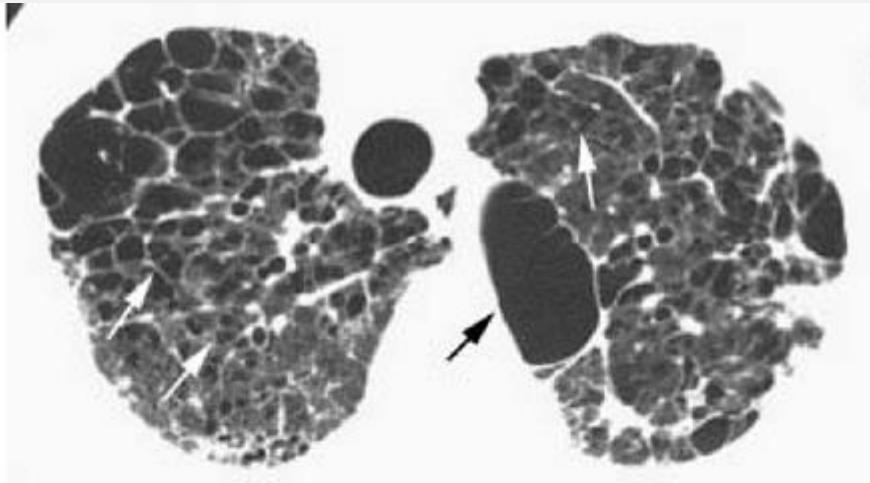
Mosaic perfusion is most frequent in patients with airways diseases that result in focal air-trapping or poor ventilation of lung parenchyma (Figs. 3-141, 3-142, 3-143, 3-144) [124,125,238]; in these patients, areas of poorly ventilated lung are poorly perfused because of reflex vasoconstriction or because of a permanent reduction in the pulmonary capillary bed. In our experience, this finding has been most common in patients with bronchiolitis obliterans (constrictive bronchiolitis) (Figs. 3-142, 3-143, 3-144) or other diseases associated with small airways obstruction such as cystic fibrosis or bronchiectasis of any cause

P.158

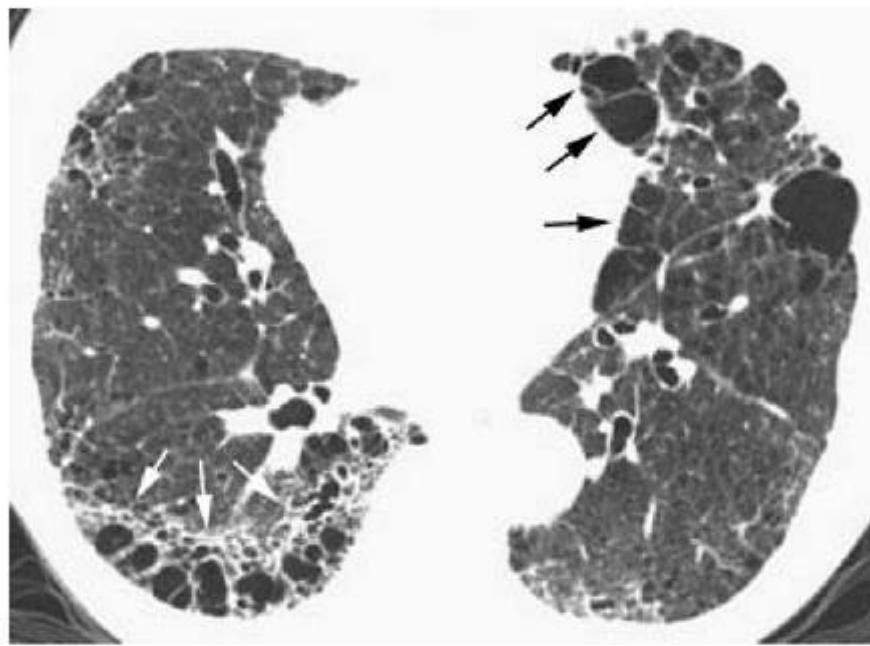
P.159

(Figs. 3-63 and 3-141), but it can also be seen as a result of large bronchial obstruction [240,241,242]. Mosaic perfusion has also been reported in association with

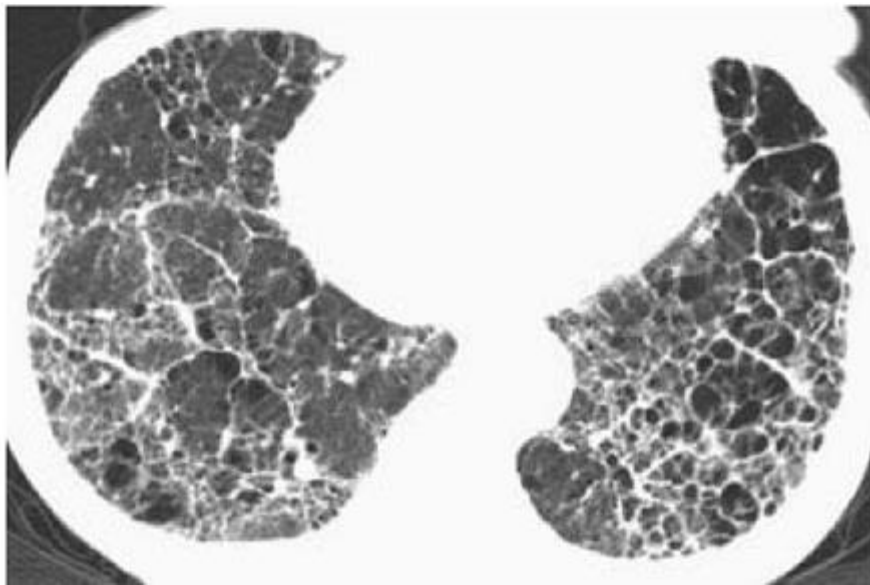
pulmonary vascular obstruction such as that caused by chronic pulmonary embolism [239,243,244].



A



B



C

FIG. 3-130. HRCT at three levels in a patient with combined honeycombing and centrilobular and paraseptal emphysema. A: In the upper lobes, clear-cut areas of centrilobular emphysema (*white arrows*) can be seen, with subpleural bullae due to paraseptal emphysema (*black arrow*). B: At a lower level, findings of both emphysema and fibrosis are visible. Areas of paraseptal emphysema are visible anteriorly (*black arrows*) whereas honeycombing and traction bronchiectasis are visible in the posterior lung (*white arrows*). Paraseptal emphysema occurs in a single layer whereas honeycomb cysts occur in multiple layers. C: Near the lung bases, findings of honeycombing and fibrosis predominate.

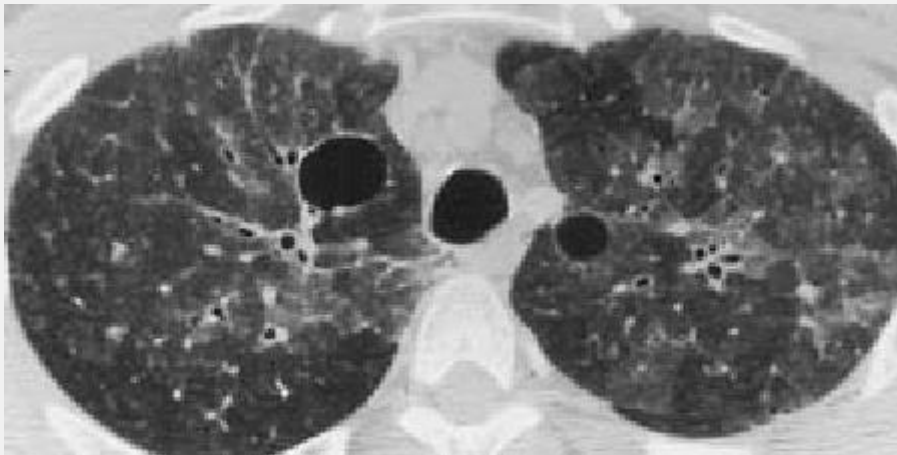


FIG. 3-131. HRCT in a patient with *Pneumocystis carinii* pneumonia shows ground-glass opacity and focal lung cysts representing pneumatoceles.

Regardless of its cause, when mosaic perfusion is present, pulmonary vessels in the areas of decreased opacity often appear smaller than vessels in relatively dense areas of lung [125,244] (Figs. 3-141, 3-142, 3-143, 3-144, 3-145). This

discrepancy reflects differences in regional blood flow and can be quite

P.160

P.161

helpful in distinguishing mosaic perfusion from ground-glass opacity, which can otherwise have a similar patchy appearance. In patients with ground-glass opacity, vessels usually appear equal in size throughout the lung. For example, in a series of 48 patients with mosaic perfusion primarily due to airways disease, Im et al. [245] observed smaller vessels in areas of low attenuation in 93.8% of cases. It must be pointed out, however, that decreased vessel size may be subtle and difficult to observe in some patients with mosaic perfusion. In a blinded study by Arakawa et al. [246] of patients with inhomogeneous lung opacity of various causes, only 68% of patients with airways or vascular disease were thought to show small vessels in areas of low attenuation.

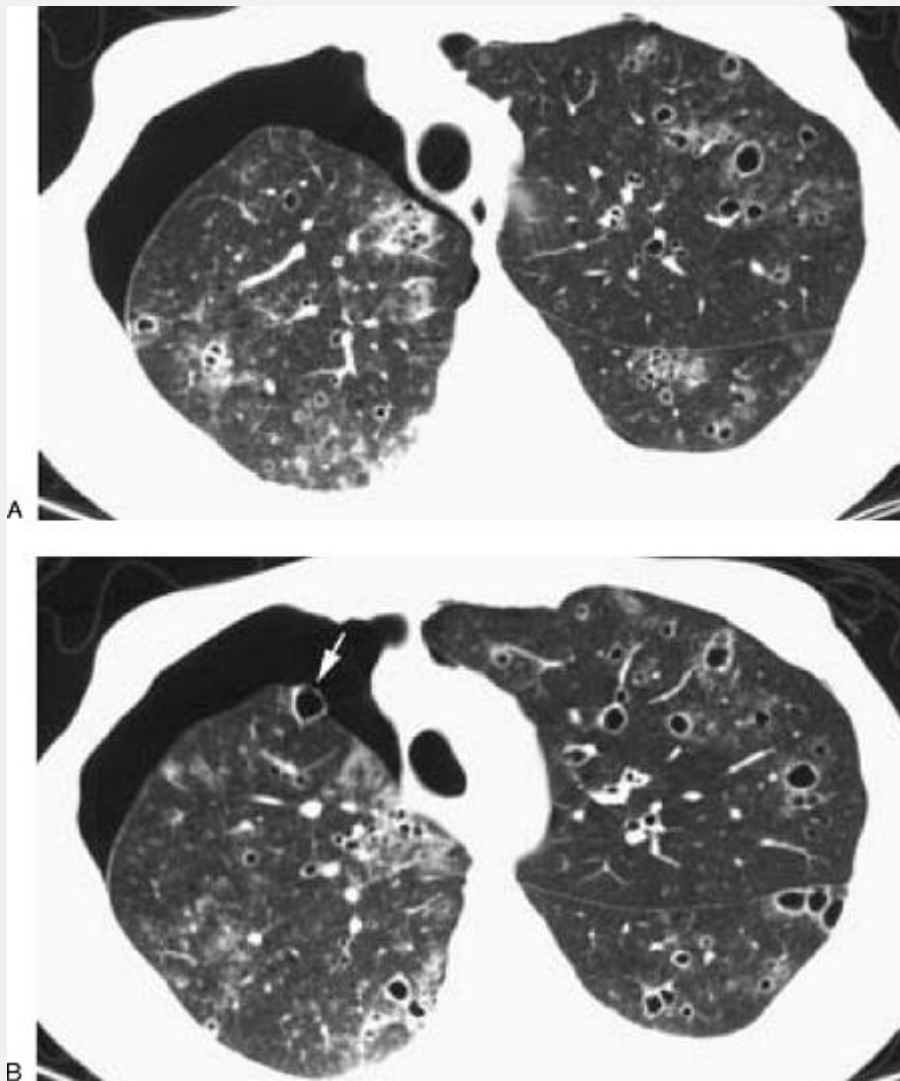


FIG. 3-132. HRCT at two levels in an acquired immunodeficiency syndrome patient with recurrent *Pneumocystis carinii* pneumonia associated with pneumatocoeles and pneumothorax. A: Patchy areas of ground-glass opacity are associated with a number of small cystic spaces representing pneumatocoeles. A moderate pneumothorax is present on the right, and a small pneumothorax is visible on the left. B: At a lower level, one of the cystic lesions (*arrow*) in the right lung is visible protruding into the air-filled pleural space. The rupture of

such a lesion likely accounts for the pneumothorax.

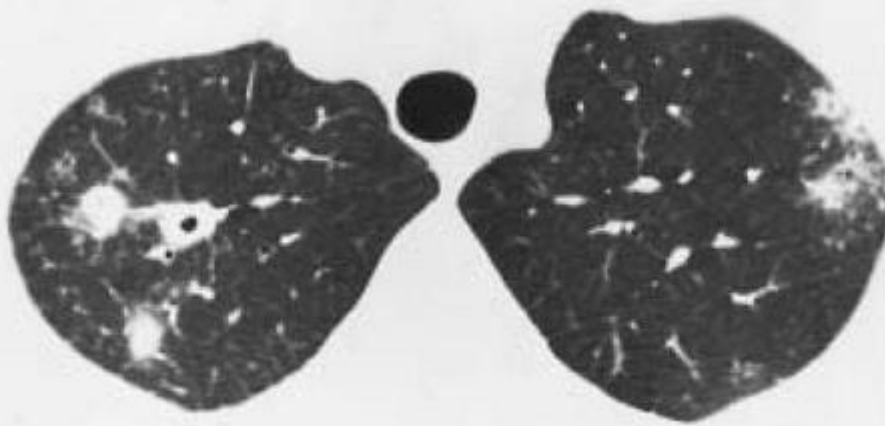
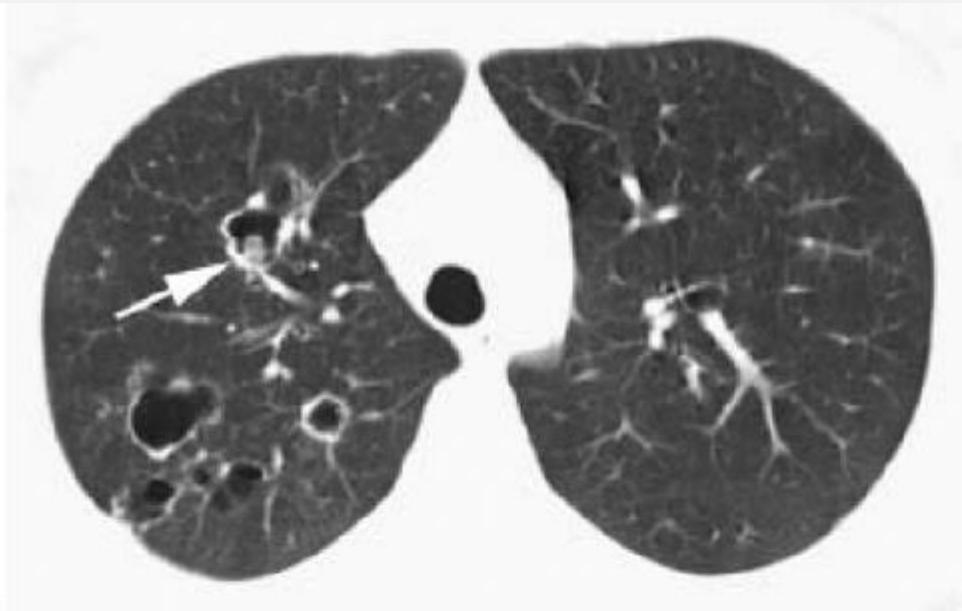
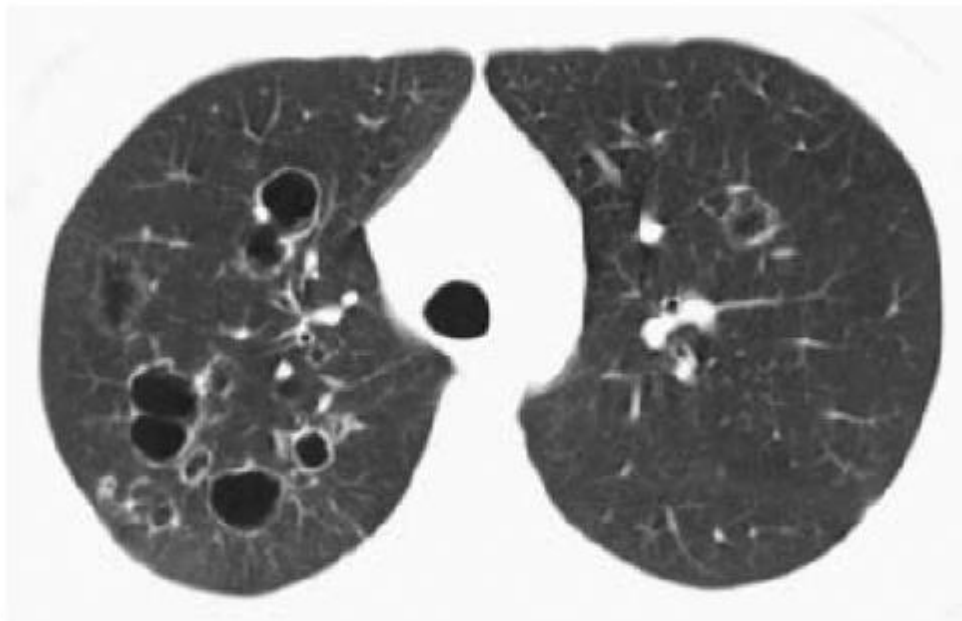


FIG. 3-133. Cavitary nodules in an acquired immunodeficiency syndrome patient with a fungal pneumonia. Nodules appear both solid and cavitary. The cavitated nodule in the right upper lobe is thick-walled.



A



B



C

FIG. 3-134. A-C: Cavitory nodules or cysts in a patient with tracheobronchial papillomatosis. Thin-walled cystic lesions are visible, with a predominance in the right lung. Associated nodules may be seen within cysts (*arrow, A*) or within lung parenchyma (*arrow, C*).

Mosaic Perfusion Due to Airways Disease

In patients with mosaic perfusion resulting from airways disease, abnormal dilated or thick-walled airways (i.e., bronchiectasis) may be visible in the relatively lucent lung regions, thus suggesting the proper diagnosis [125,242,246]. In one study [247], abnormal airways were seen in 70% of patients with airways disease and mosaic lung attenuation (Figs. 3-141, 3-142, and 3-144). Mosaic perfusion can be seen in a variety of airways diseases including bronchiectasis, cystic fibrosis, and constrictive bronchiolitis. In patients with mosaic perfusion secondary to airways disease, lobular areas of low attenuation are common. Air-trapping on expiratory

P.162

scans, described in the section below, is often helpful in confirming the diagnosis.

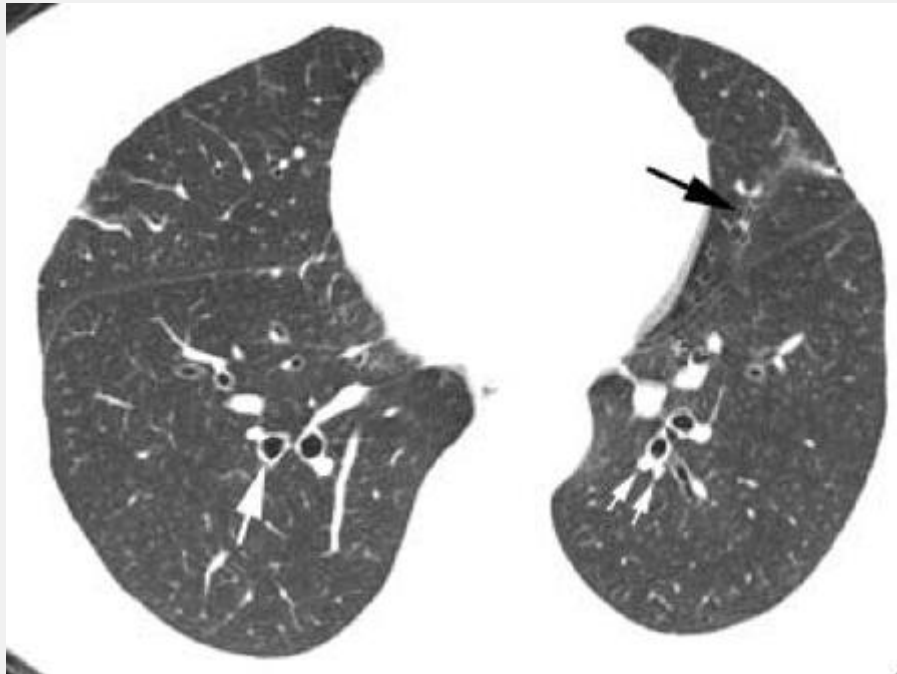


FIG. 3-135. Bronchiectasis and pseudobronchiectasis. Bronchiectasis is considered to be present if the internal diameter of a bronchus is greater than that of its accompanying artery (i.e., the signet ring sign) (*large white arrow*). In the left lower lobe, a bronchus appears to be dilated because its adjacent artery has divided into two branches (*small white arrows*). In the left upper lobe (*black arrow*), a cardiac pulsation or "doubling" artifact results in the appearance of bronchiectasis.

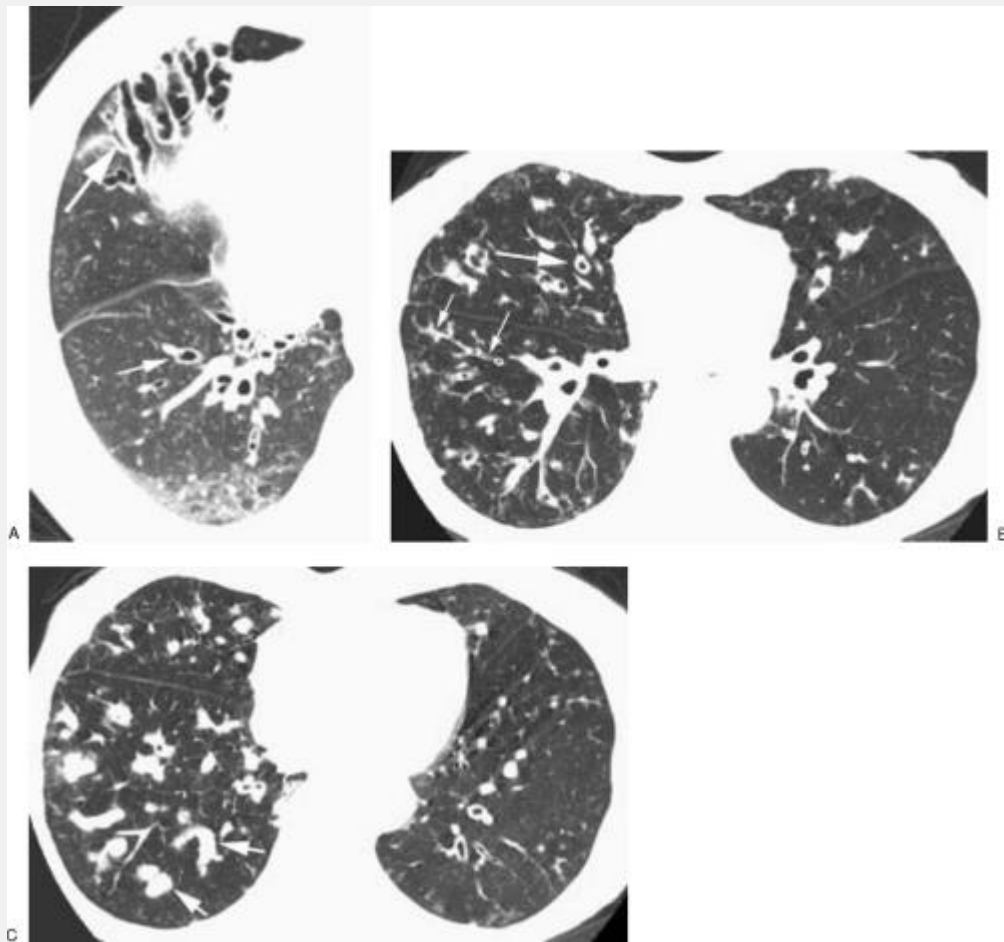


FIG. 3-136. Cylindrical bronchiectasis in two patients. A: Dilated bronchi in the anterior lung are seen extending to the pleural surface. Bronchi are not normally visible in the peripheral 1 cm of lung. The dilated bronchi appear largely cylindrical (*large arrow*). The signet ring sign (*small arrow*) is visible posteriorly. Note that bronchial walls are thickened. B: Cylindrical bronchiectasis in another patient is associated with the signet ring sign (*large arrow*). A smaller bronchus is thick-walled and is contiguous with a tree-in-bud in the more peripheral lung (*small arrows*). C: At a lower level in the patient shown in B, mucous plugging of dilated bronchi in the lower lobes (*arrows*) has a nodular appearance.

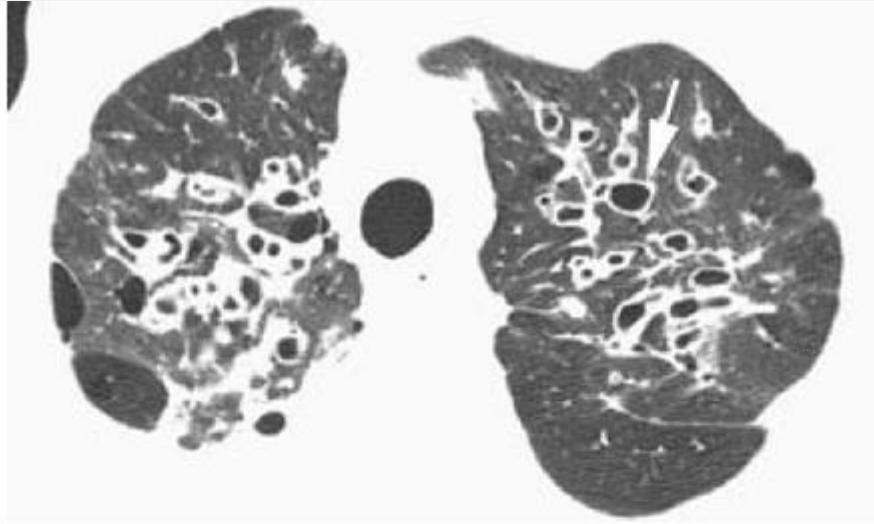
Mosaic Perfusion Due to Vascular Disease

Inhomogeneous lung attenuation is common in patients with chronic pulmonary embolism (CPE), and decreased vessel size in less opaque regions is often visible (Fig. 3-145). In a study of pulmonary parenchymal abnormalities in 75 patients with CPE, 58 patients (77.3%) showed mosaic perfusion with normal or dilated arteries in areas of hyperattenuation [244]; areas of relatively increased attenuation averaged -727 HU, whereas areas of decreased attenuation averaged -868 HU. In another study of patients with pulmonary hypertension due to CPE, pulmonary hypertension of other causes, and a variety of other pulmonary diseases, HRCT was thought to show mosaic perfusion in all patients with CPE [248]. Considerably more variation in vessel size in different lung regions was also visible in the patients with CPE. Overall, HRCT had a sensitivity

P.163

P.164

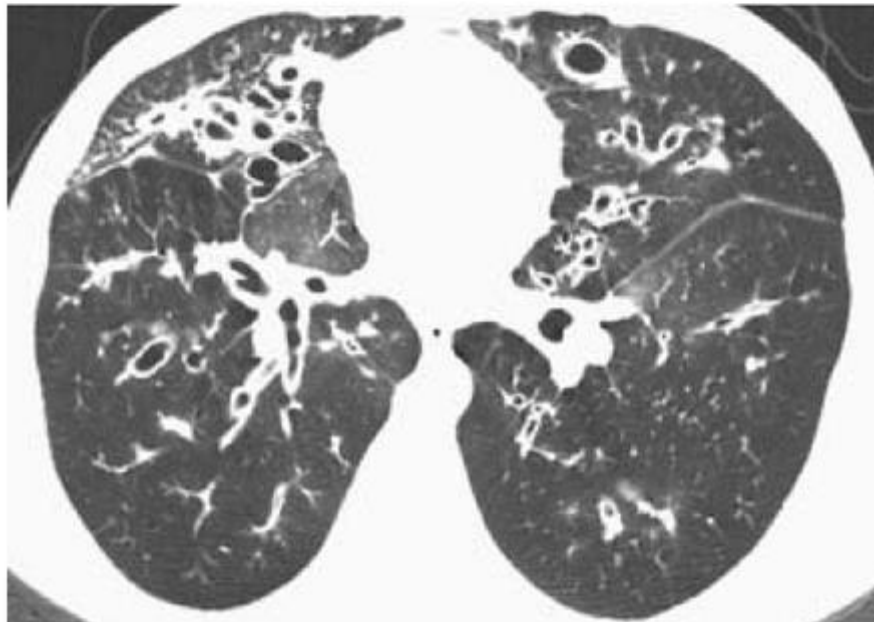
of 94% to 100% and a specificity of 96% to 98% in diagnosing CPE [248].



A



B



C

FIG. 3-137. Bronchiectasis in a patient with cystic fibrosis. A: In the upper lung, multiple dilated thick-walled bronchi are present. The signet ring sign is visible (*arrow*). B: Irregular or varicose bronchiectasis is visible in the anterior right lung (*large white arrow*). Mucous plugging of bronchi is also visible (*small white arrows*), as is tree-in-bud (*black arrows*). C: Multiple dilated bronchi with examples of the signet ring sign are also visible at the lung bases.

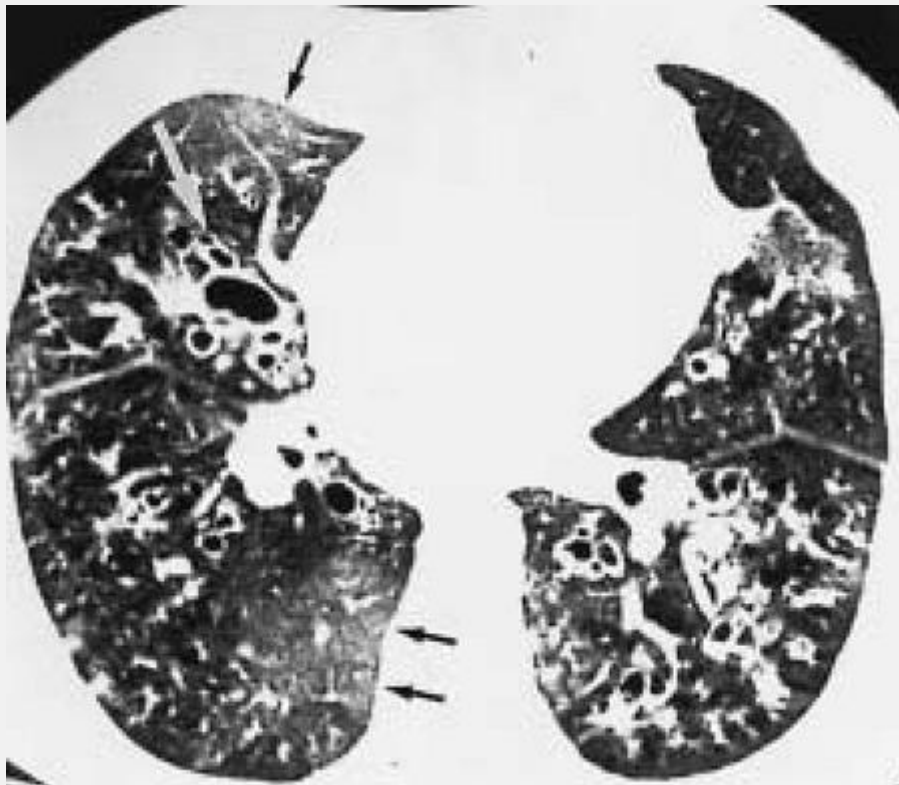


FIG. 3-138. HRCT in a patient with varicose bronchiectasis resulting from allergic bronchopulmonary aspergillosis. Irregular bronchial dilatation (*white arrow*) is visible in the anterior right lung. Dilatation of small bronchioles in the peripheral lung is visible, as is tree-in-bud. Patchy lung opacity, with focal regions of decreased and increased

attenuation (*black arrows*), reflects mosaic perfusion.

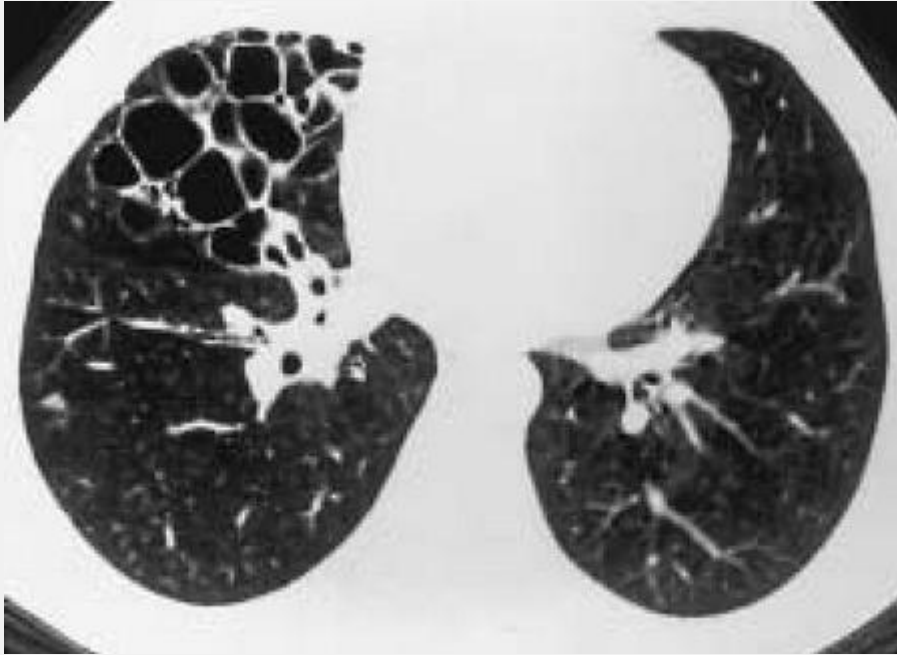


FIG. 3-139. Cystic bronchiectasis involving the right middle lobe. The focal distribution allows distinction of this entity from cystic lung disease, such as in lymphangiomyomatosis.

The frequency with which a mosaic pattern of lung opacity is seen on CT in patients with various causes of pulmonary artery hypertension (PAH) has also been studied [249]. Twenty-one patients had PAH caused by lung disease; 17 patients, caused by cardiac disease; and 23 patients, caused by vascular disease. Of the 23 patients with PAH caused by vascular disease, 17 patients (74%) had a mosaic pattern of lung attenuation; 12 of these had CPE. Of the 21 patients with PAH caused by lung disease, one patient (5%) had a mosaic pattern of lung attenuation. Among the 17 patients with PAH caused by cardiac disease, two patients (12%) had a mosaic pattern of lung attenuation [249]. Thus, a mosaic pattern of lung attenuation was seen

significantly more often in patients with PAH caused by vascular disease than in patients with PAH caused by cardiac or lung disease.

In patients with vascular disease as a cause of mosaic perfusion, areas of low attenuation are usually larger than lobules. In patients with mosaic perfusion occurring in association with CPE, enlargement of the main pulmonary arteries may be visible because of pulmonary hypertension (see Chapter 9).

Algorithmic Approach to the Diagnosis of Decreased Lung Opacity

The following series of algorithms may be used to help conceptualize the diagnosis of focal or diffuse lung lucencies.

Decreased lung opacity may be caused by (i) lung destruction, resulting in discrete cystic airspaces not containing recognizable vessels, or (ii) reduction in lung attenuation, or inhomogeneous lung attenuation, without the presence of discrete air-filled spaces or loss of visible vessels (Algorithm 7A). The presence of air-filled cystic spaces or focal lung destruction may indicate the presence of honeycombing,

P.165

emphysema, cystic bronchiectasis, lung cysts, or pneumatoceles. A reduction in lung attenuation or patchy inhomogeneous lung attenuation may be seen in patients with panlobular emphysema, airways disease, vascular disease, or mixed airway and infiltrative disease.

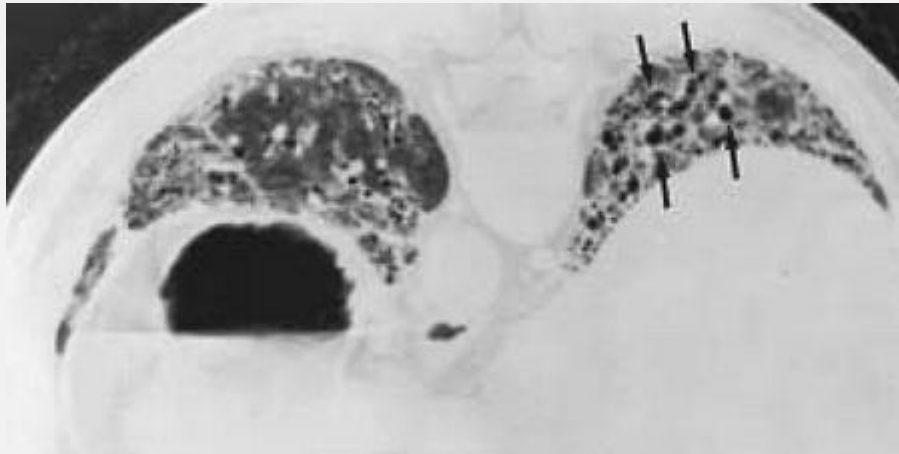
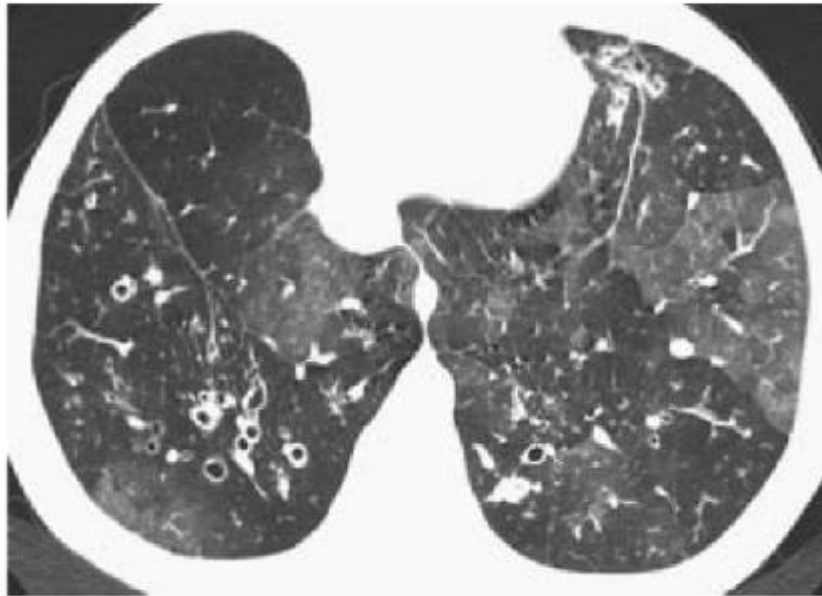


FIG. 3-140. Traction bronchiectasis in a patient with idiopathic pulmonary fibrosis. Dilated bronchi (arrows) are visible in the posterior lung base.

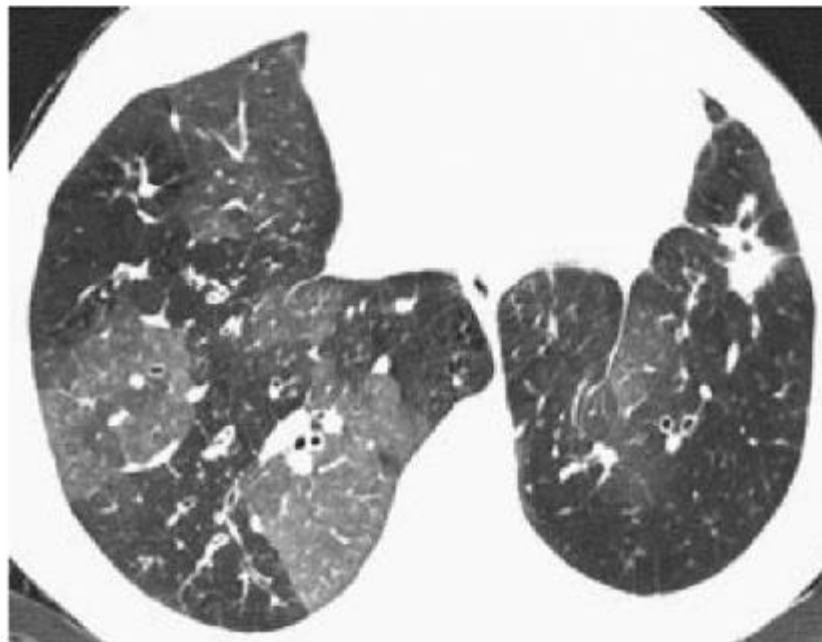
Air-filled cystic spaces first may be classified as subpleural or intraparenchymal for the purposes of differential diagnosis (Algorithm 7B). Air-filled cystic spaces in the subpleural regions may represent paraseptal emphysema or honeycombing. Both have distinct walls. Paraseptal emphysema is usually distinguishable from honeycombing because the cystic spaces occur in a single layer, whereas honeycomb cysts usually occur in multiple layers. Areas of paraseptal emphysema also can be larger (bullae) than typical honeycomb cysts. Paraseptal emphysema tends to have an upper lobe predominance and may be associated with centrilobular emphysema, whereas honeycombing usually has a lower lobe predominance and is associated with findings of fibrosis.



A



B



C

FIG. 3-141. A-C: Mosaic perfusion in three patients with cystic fibrosis. In each patient, vessels appear larger in relatively dense lung regions, a finding of great value in making the diagnosis of mosaic perfusion. The relatively dense lung regions are normally perfused or overperfused because of shunting of blood away from the abnormal areas. Also note that abnormal airways (i.e., bronchiectasis, bronchial wall thickening, tree-in-bud) are often visible in relatively lucent lung regions. These areas are poorly ventilated and poorly perfused.

P.166

Intraparenchymal cystic airspaces (i.e., those not occurring primarily at the pleural surface) can represent centrilobular emphysema, lung cysts, dilated bronchi, or pneumatoceles (Algorithm 7C). In patients with centrilobular emphysema, areas of lucency do not usually have recognizable walls, have an upper lobe distribution in most patients, are relatively small (less than 1 cm in diameter), have a spotty distribution, and may sometimes be seen surrounding a centrilobular artery. Cystic bronchiectasis may result in clustered or scattered thin-walled cystic airspaces. The correct diagnosis may be suggested if air-fluid levels or other findings of bronchiectasis are visible. The term *lung cyst* is used to describe a thin-walled, well-defined and circumscribed air-containing lesion that is 1 cm or larger in diameter. Langerhans histiocytosis and LAM result in multiple lung cysts [92,93,220,221,222,223,224]. The cysts have a thin but easily discernible wall, ranging up to a few millimeters in thickness. Associated findings of fibrosis are

usually absent or much less conspicuous than they are in patients with honeycombing. In these diseases, the cysts are usually interspersed within areas of normal-appearing lung. In patients with histiocytosis, the cysts can have bizarre shapes, typically have an upper lobe predominance, and may occur in men. LAM is associated with rounder and more uniformly shaped cysts, is diffusely distributed from apex to base, and exclusively occurs in women. Cysts are rarely seen in patients with LIP associated with Sjögren's syndrome, AIDS, or other systemic diseases; cystic airspaces in LIP have thin walls, measure 1 to 30 mm in diameter, and are typically less numerous than with histiocytosis and LAM [17,225,250]. Cysts representing pneumatoceles can be seen in patients with infection, particularly *P. carinii* pneumonia; pneumatoceles are often scattered and patchy in distribution and limited in number, and findings of pneumonia or a history of pneumonia may be present.

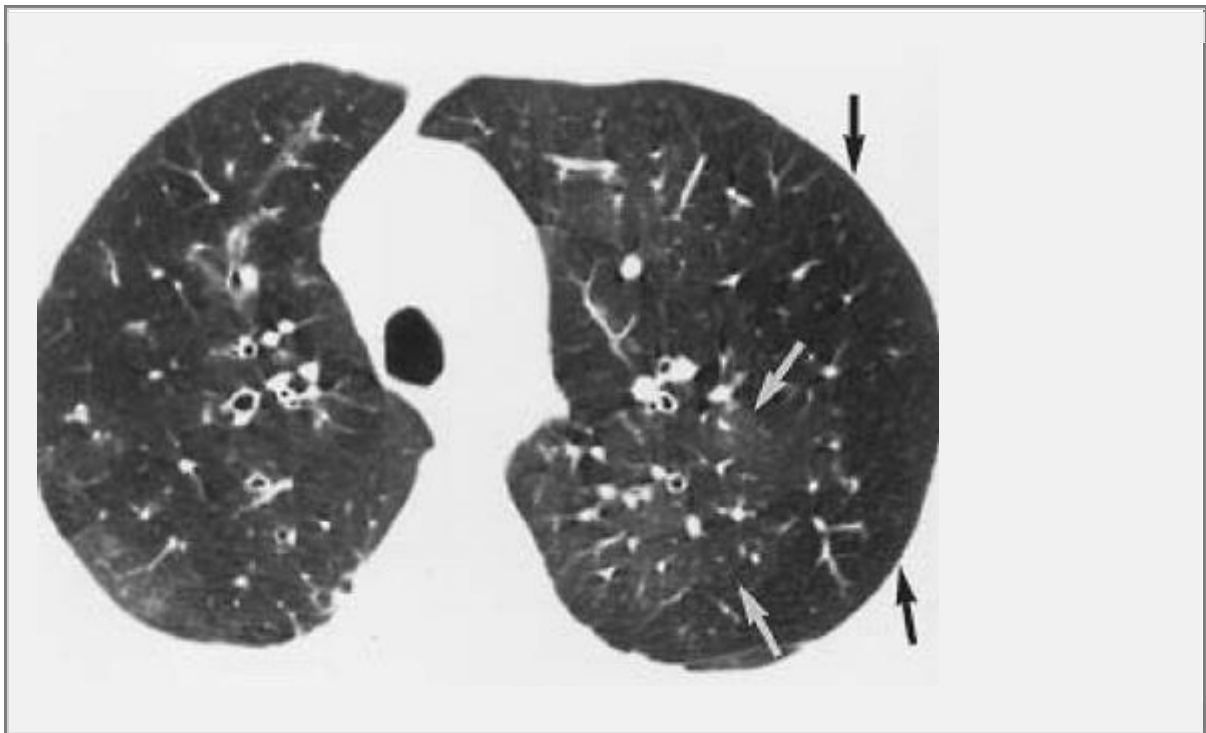


FIG. 3-142. HRCT in a patient with bronchiolitis obliterans related to rheumatoid arthritis. Bronchiectasis is visible, along with patchy lung attenuation, a finding that reflects mosaic perfusion. Note that the pulmonary vessels in the lucent-appearing peripheral left lung (*black arrows*) are smaller than vessels in the denser medial left lung (*white arrows*).

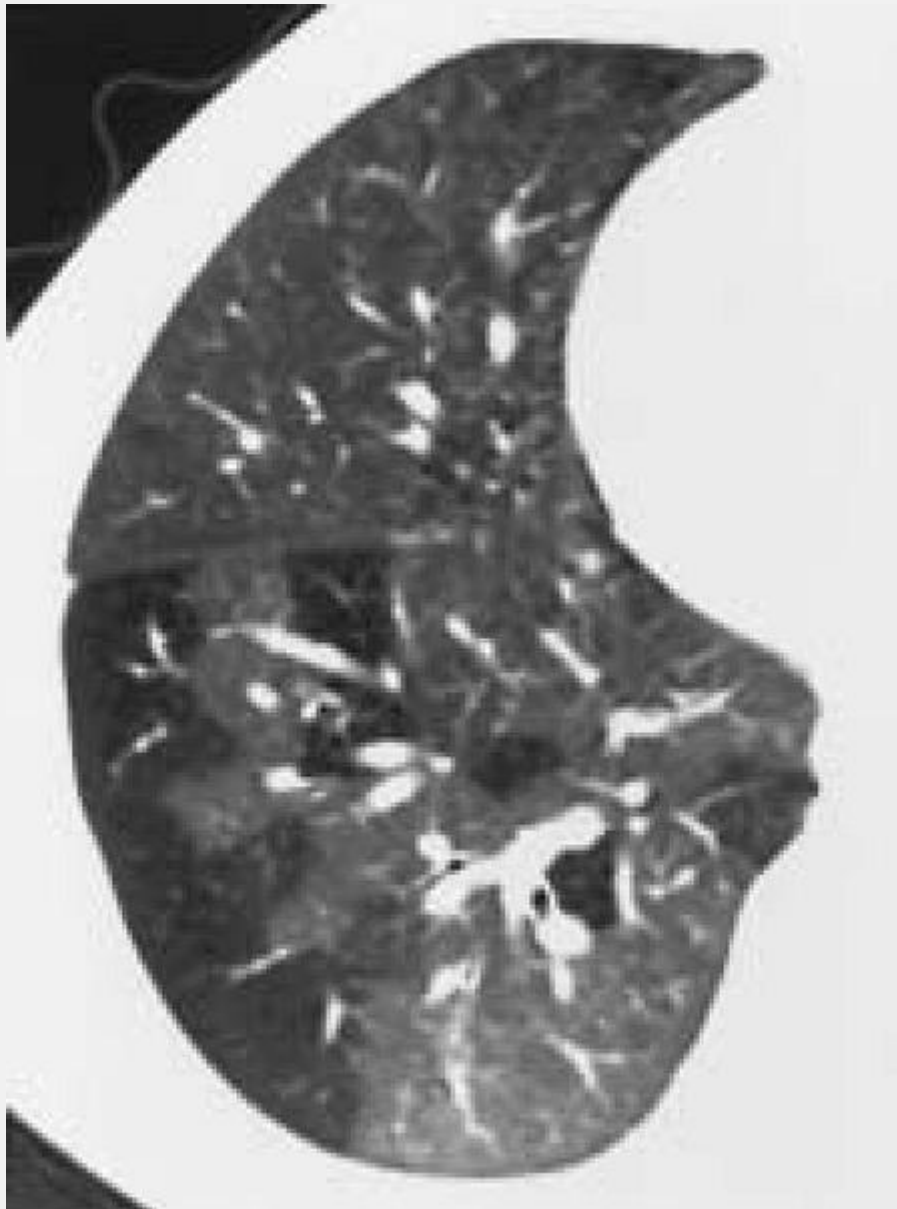


FIG. 3-143. HRCT in a 9-year-old boy with postinfectious bronchiolitis obliterans. Patchy areas of mosaic perfusion are visible, with decreased vascular size within the lucent regions.

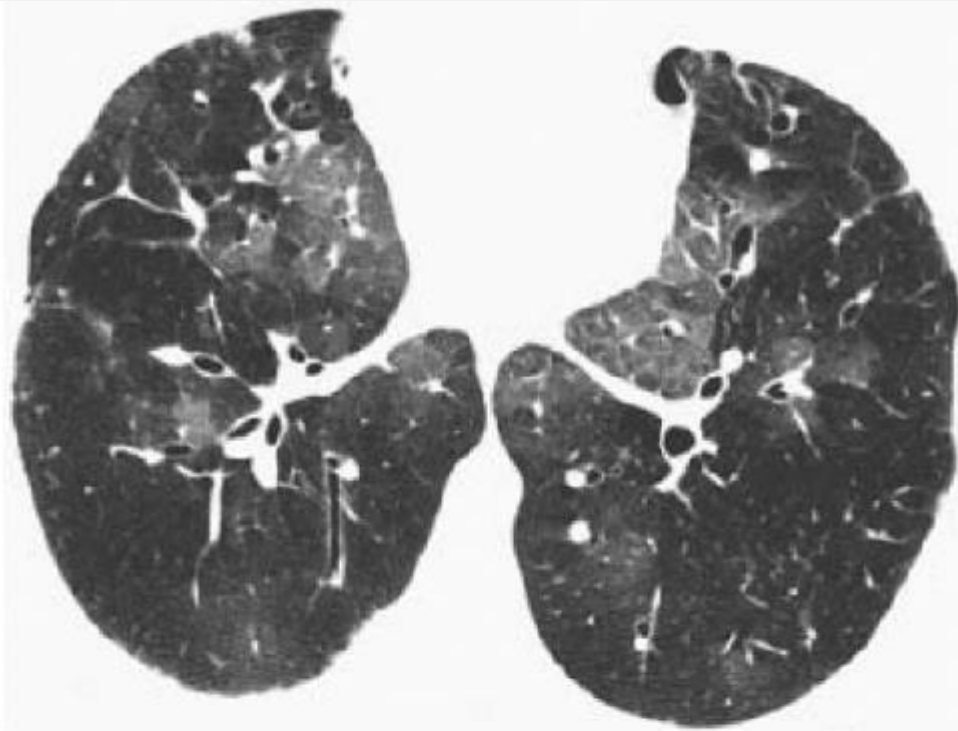
P.167

Decreased lung attenuation in the absence of cystic airspaces, when diffuse, can reflect panlobular emphysema or diffuse airways disease with air-trapping (Algorithm 7D). [124,238]. Patchy, decreased lung opacity often reflects “**mosaic perfusion**” [239]; it most often is caused by airway and obstructive diseases, such as cystic fibrosis or bronchiolitis obliterans, but can also be seen with vascular diseases such as CPE. Mosaic perfusion may be recognized by the presence of decreased vessel size in areas of lucency. The presence of vascular disease as a cause may be suggested if findings of pulmonary hypertension or chronic pulmonary embolism is present. Similarly, if large or small airway abnormalities are visible, then obstructive disease is the likely cause (Algorithm 7D). Because inhomogeneous lung attenuation resulting from subtle ground-glass opacity may also mimic mosaic perfusion, the presence of infiltrative disease must also be considered in patients with an appearance suggesting mosaic perfusion.

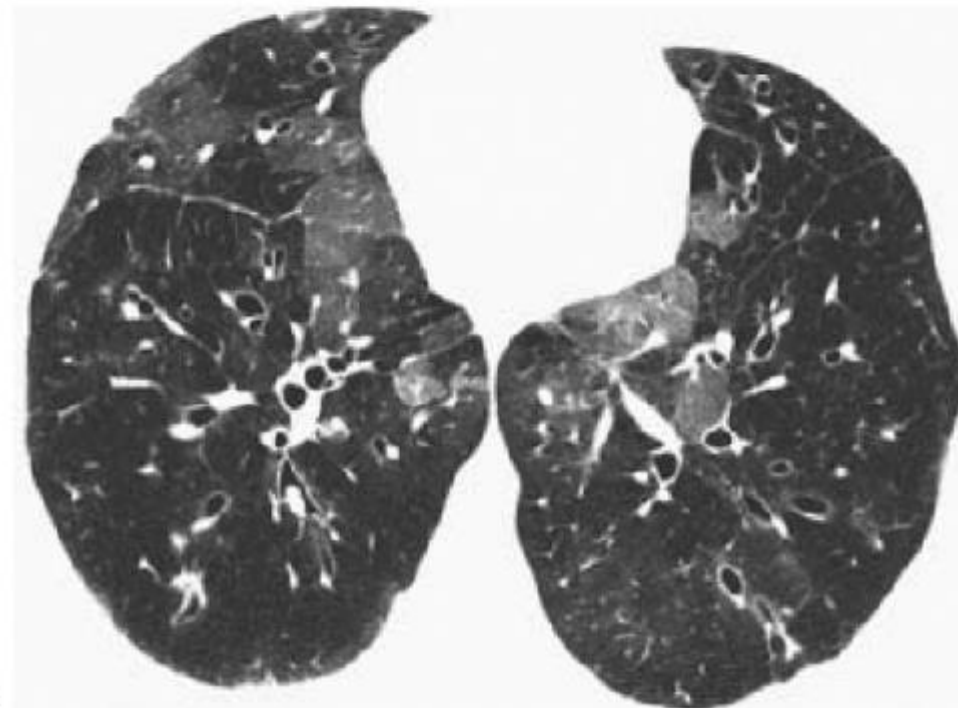
Inhomogeneous Lung Opacity:

*Differentiation of Mosaic Perfusion
from Ground-Glass Opacity*

The presence of inhomogeneous lung attenuation on HRCT is a common finding; in one study, inhomogeneous lung opacity was the predominant HRCT abnormality in 19% of scans reviewed [246]. This appearance can be a diagnostic dilemma, resulting from (i) ground-glass opacity, (ii) mosaic perfusion resulting from airways obstruction and reflex vasoconstriction, (iii) mosaic perfusion resulting from vascular obstruction, or (iv) a combination of these (i.e., mixed disease). Because the finding of inhomogeneous lung opacity may be nonspecific, it has been referred to as the *mosaic pattern* [251]. However, most cases of inhomogeneous opacity can be correctly classified as one of these based on HRCT findings [246,247].



A



B

FIG. 3-144. A, B: HRCT in a bone marrow transplant recipient with bronchiolitis obliterans. Patchy areas of mosaic perfusion are visible, associated with findings of bronchiectasis. In patients with bronchiolitis obliterans,

bronchiectasis is commonly visible.

P.168

On inspiratory scans, it is often possible to distinguish among ground-glass opacity, mosaic perfusion caused by airways disease, and mosaic perfusion caused by vascular disease (Algorithm 8). In two studies [246,247], an accurate distinction was possible in more than 80% of cases based on HRCT findings. The use of expiratory scanning, described in the next section, can also be very helpful in the diagnosis of inhomogeneous lung opacity.

The most important finding in making the diagnosis of mosaic perfusion is that of reduced vessel size in lucent lung regions. If reduced vessel size is visible, a confident diagnosis of mosaic perfusion can usually be made. Also, in patients with mosaic perfusion, some lung regions may appear too lucent to be normal, but this is somewhat subjective and based on experience with the window settings used for scan viewing.

In patients with mosaic perfusion resulting from airways disease, abnormal dilated or thick-walled airways (i.e., bronchiectasis) may be visible in the relatively lucent lung regions, suggesting the proper diagnosis; this is visible in approximately 70% of cases and is very helpful in suggesting the correct diagnosis [241,252,253,254,255]. Furthermore, lobular areas of lucency are common in patients with airways disease. In a study by Im et al. [245] of 48 consecutive patients with lobular areas of low attenuation seen on HRCT, 46 (95%) had symptoms related to respiratory disease, such as productive cough (n = 25)

and hemoptysis (n = 18). Only two patients with this appearance, one with chronic pulmonary embolism and one with Takayasu's arteritis combined with bronchiectasis, had pulmonary vascular disease.

In patients with vascular obstruction (e.g., chronic pulmonary embolism) as a cause of mosaic perfusion, dilatation of central pulmonary arteries may be present as a result of pulmonary hypertension, lobular areas of lucency are typically absent, and larger areas of low attenuation are usually visible.

Ground-glass opacity may be accurately diagnosed as the cause of inhomogeneous lung opacity if it is associated with other findings of infiltrative disease such as consolidation, reticular opacities (i.e., the crazy-paving pattern), or nodules. Also, a pattern in which the areas of higher attenuation are centrilobular almost always represents ground-glass opacity with a centrilobular distribution. This pattern is not seen with mosaic perfusion resulting from airways disease; it is uncommonly the result of vascular disease with mosaic perfusion. Ground-glass opacity may also result in very ill-defined and poorly margined areas of increased opacity, lacking the sharply margined and geographic appearance sometimes seen in patients with mosaic perfusion. Ground-glass opacity can often be diagnosed simply because lung looks too dense, although this is quite subjective and depends on using consistent window settings and being familiar with the appearance of normal lung parenchyma.

Mixed Disease and the Head-Cheese Sign

In occasional patients, inspiratory scans show a patchy pattern of variable lung attenuation, representing the combination of ground-glass opacity (or consolidation), normal lung, and reduced lung attenuation as a result of mosaic perfusion. This combination of mixed densities, including the presence of mosaic perfusion, often gives the lung a geographic appearance and has been termed the head-cheese sign because of its resemblance to the variegated appearance of a sausage made from parts of the head of a hog (Fig. 3-146) [256]. If you can be sure that both ground-glass opacity or consolidation and mosaic perfusion are visible (rather than one or the other), the head-cheese sign is present. Air-trapping is commonly visible on expiratory scans (Fig. 3-158).

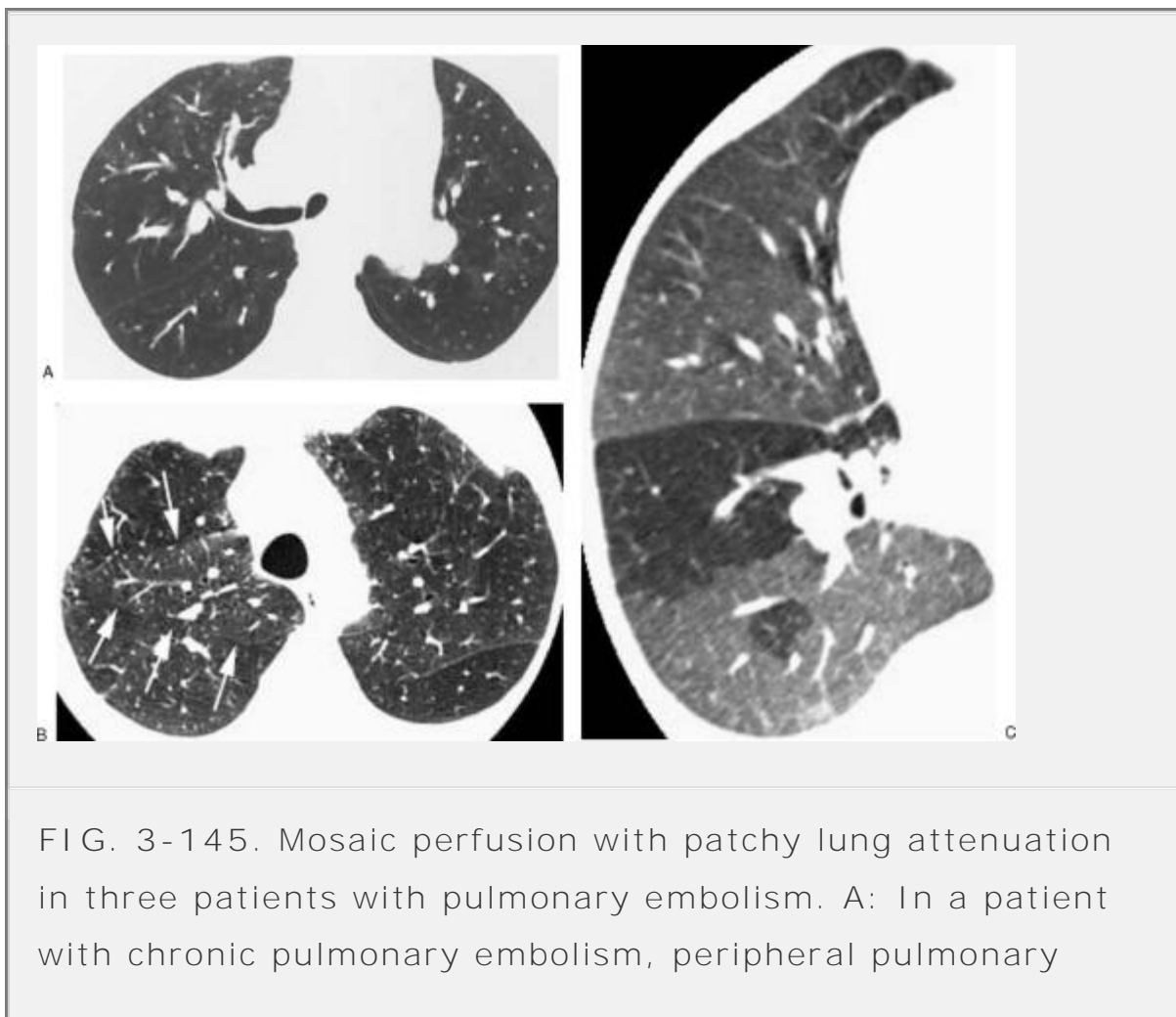
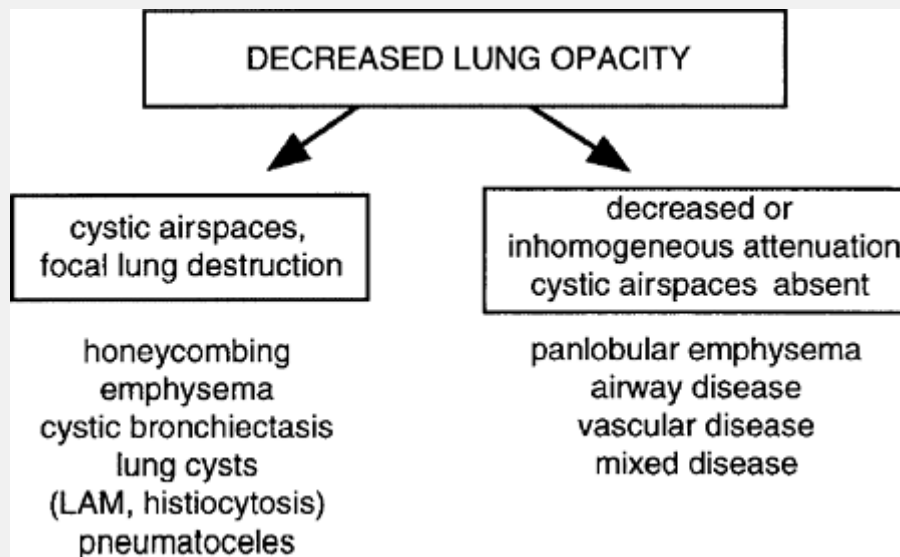
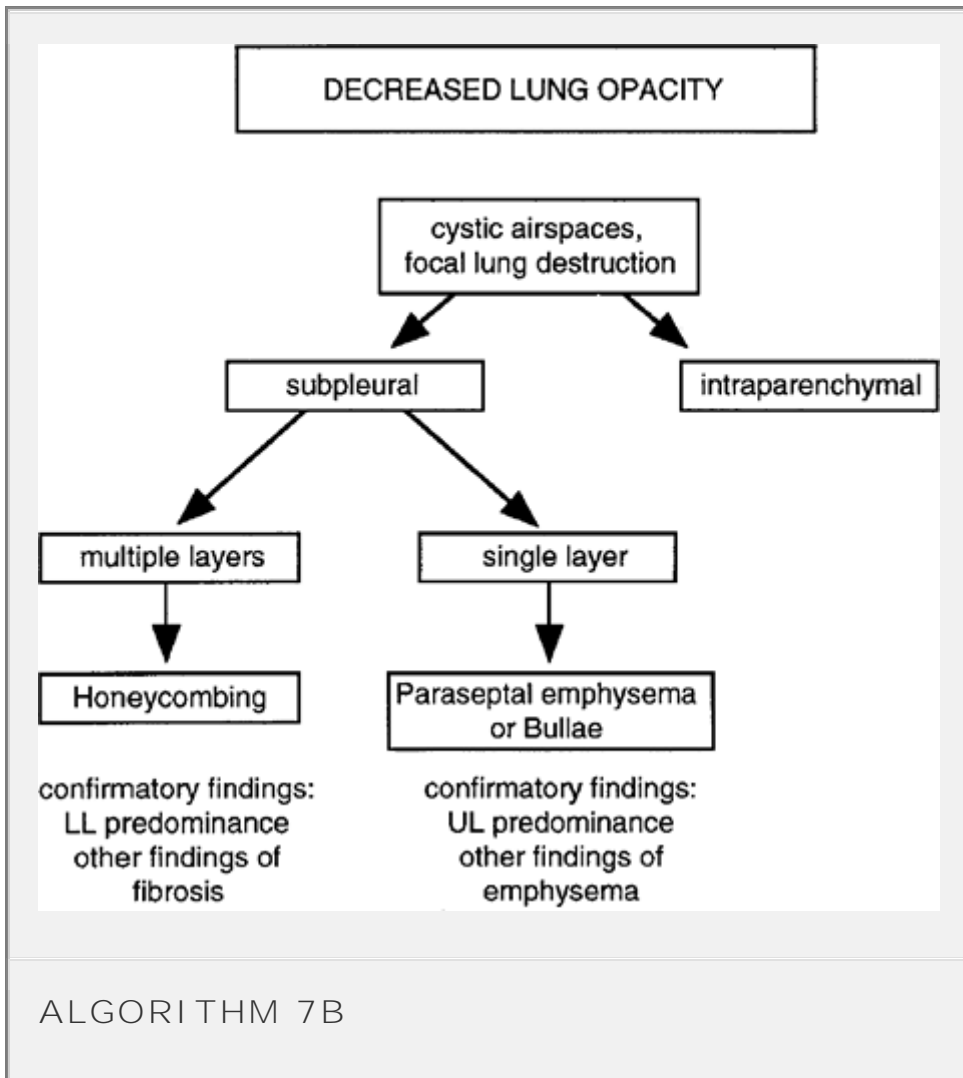


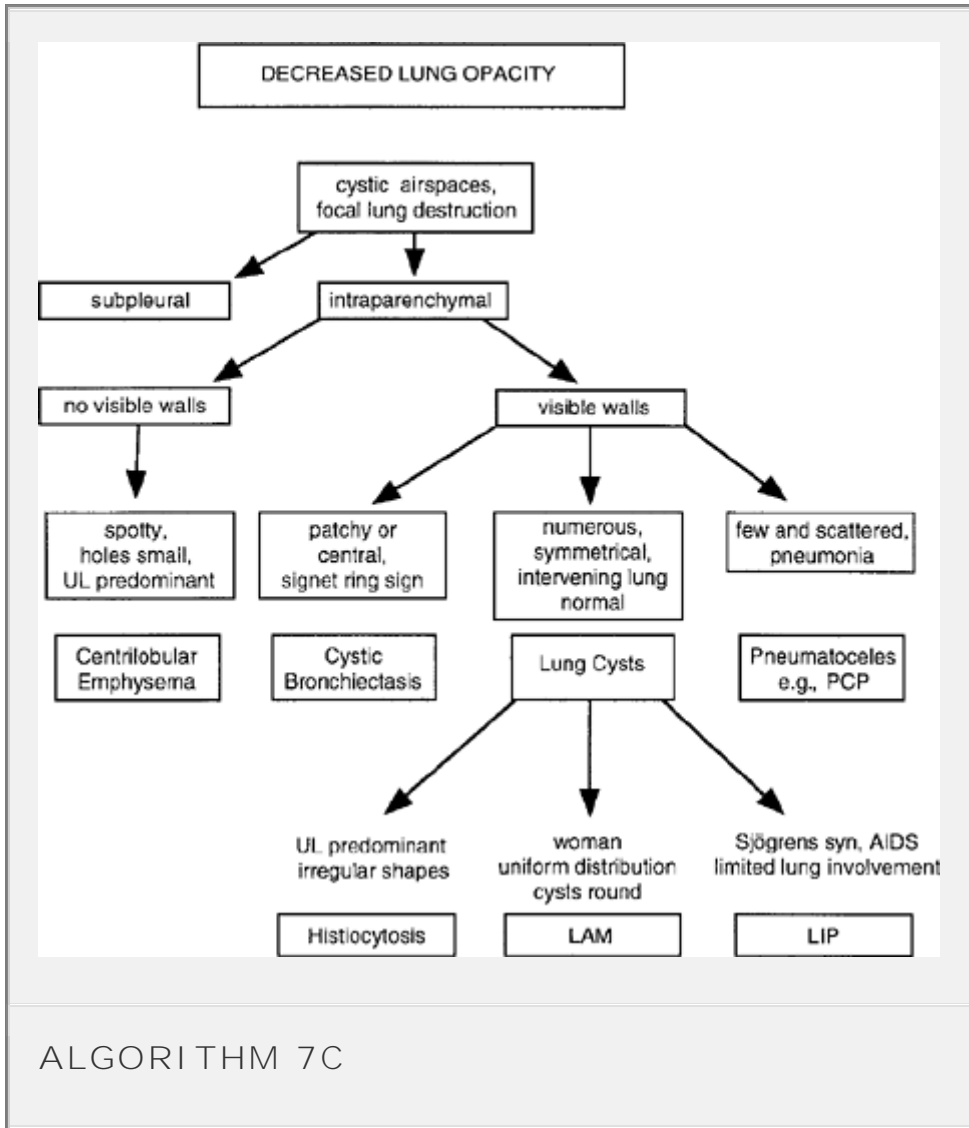
FIG. 3-145. Mosaic perfusion with patchy lung attenuation in three patients with pulmonary embolism. A: In a patient with chronic pulmonary embolism, peripheral pulmonary

vessels are largest in the relatively dense anterior right upper lobe. The main pulmonary artery appears enlarged. B: In a patient with acute pulmonary embolism, vessels appear larger in a wedge-shaped area of the relatively dense right upper lobe (*arrows*). C: Multidetector-row HRCT through the right lower lobe in a patient with chronic pulmonary thromboembolism shows areas of reduced attenuation caused by vascular obstruction.

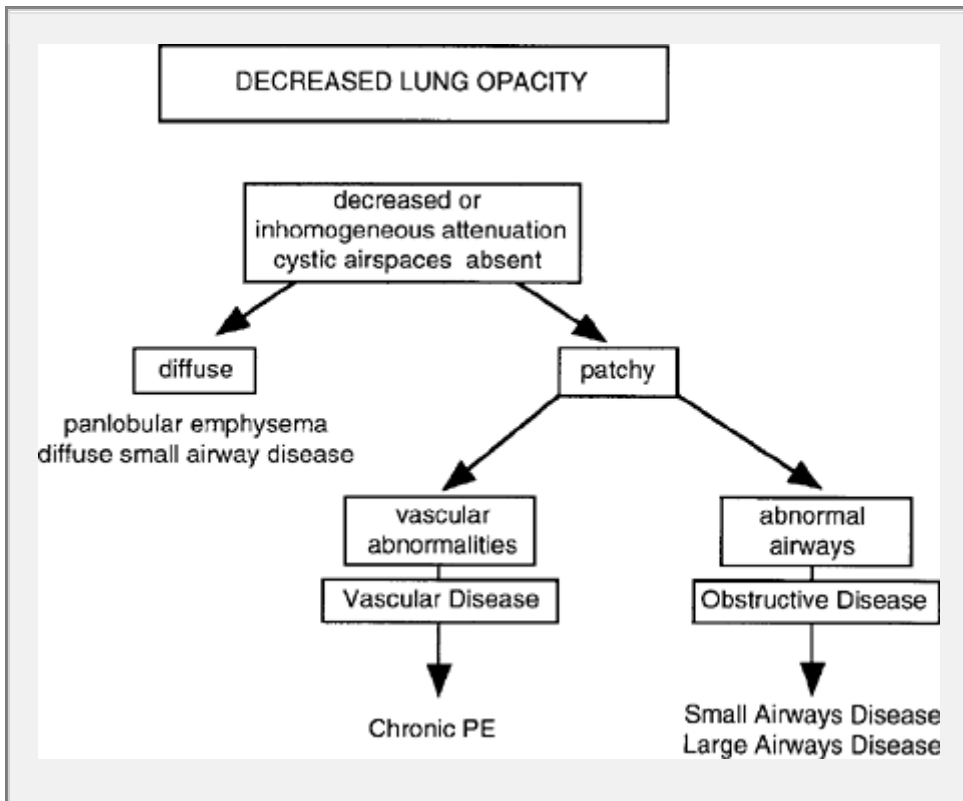


ALGORITHM 7A

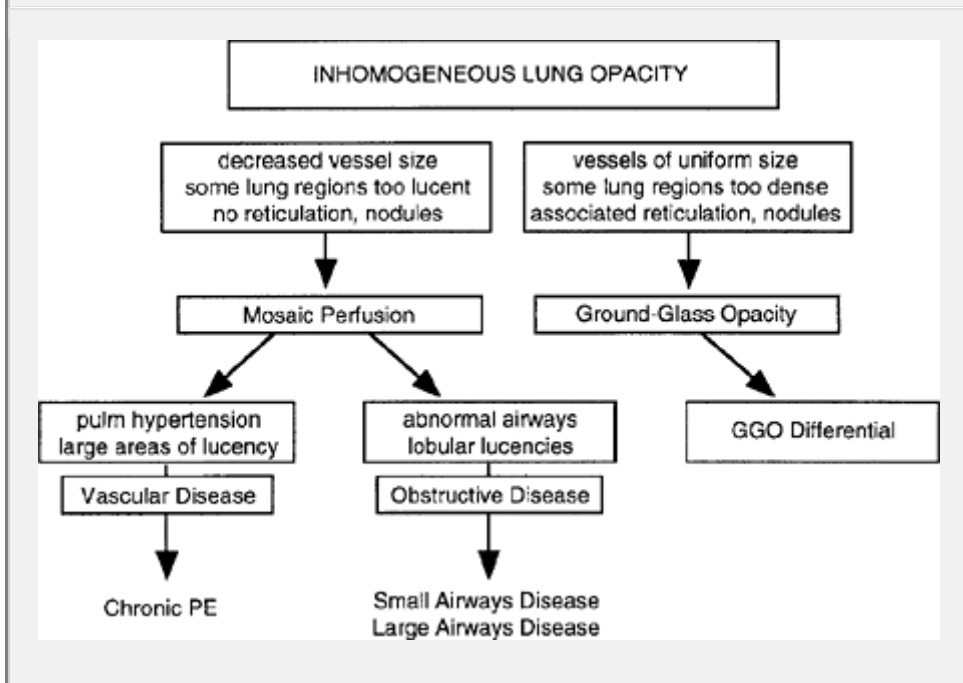




ALGORITHM 7C



ALGORITHM 7D



ALGORITHM 8

P.170

P.171

The head-cheese sign is usually indicative of mixed infiltrative and obstructive disease, usually associated with bronchiolitis. In patients with this appearance, the presence of ground-glass opacity or consolidation is caused by lung infiltration, whereas the presence of mosaic perfusion with decreased vessel size is usually caused by small airway obstruction.

The most common causes of this pattern are hypersensitivity pneumonitis, sarcoidosis, and, in our experience, atypical infections with associated bronchiolitis. Each of these diseases results in infiltrative abnormalities and may be associated with airway abnormalities.

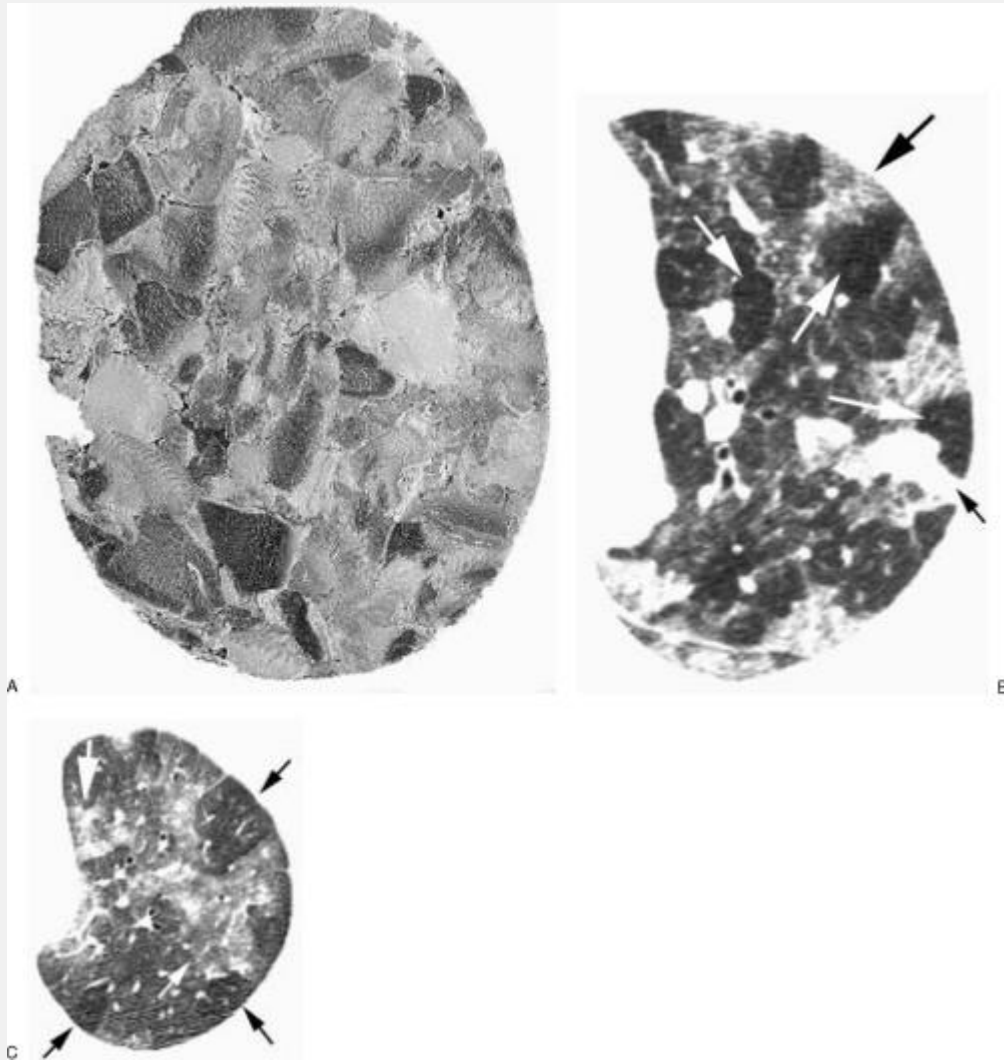


FIG. 3-146. Head cheese and the head-cheese sign. A: A slice of head cheese shows a variegated appearance, consisting of chunks of different meats from the head of a hog. Some appear dark, some appear light, and some are gray. B: In a patient with *Mycoplasma pneumoniae* associated with lung infiltration and bronchiolitis, the head-cheese sign is associated with consolidation (*small black arrow*), ground-glass opacity (*large black arrow*), and lobular areas of mosaic perfusion (*white arrows*). Note the pulmonary arteries are small or invisible in the regions of mosaic perfusion. C: In a patient with hypersensitivity pneumonitis

showing the head-cheese sign, areas of varying attenuation are visible, including consolidation (*large white arrow*), ground-glass opacity (*small white arrow*), normal lung, and areas of reduced attenuation due to mosaic perfusion (*black arrows*).

P.172

Expiratory High-Resolution Computed Tomography

Obtaining HRCT scans at selected levels after expiration may be useful in (i) the diagnosis of air-trapping in patients with obstructive lung disease [246,254,255], (ii) the diagnosis of airways disease unassociated with distinct morphologic abnormalities on inspiratory images [257], (iii) distinguishing mosaic perfusion from ground-glass opacity [246,247], and (iv) allowing the diagnosis of mixed infiltrative and obstructive diseases [246,258,259].

Diagnosis of Air-Trapping in Obstructive Lung Disease

Expiratory HRCT scans have proved useful in the evaluation of patients with a variety of lung diseases characterized by obstruction of airflow [241,242]. Air-trapping visible using expiratory or postexpiratory HRCT techniques has been recognized in patients with emphysema [253,260,261], chronic airways disease [255], asthma [262,263,264], bronchiolitis obliterans [238,253,257,265,266,267,268,269,270,271], the cystic lung diseases associated with Langerhans histiocytosis and

tuberous sclerosis [272], bronchiectasis [253,273], and airways disease related to AIDS [274]. Expiratory HRCT also has proved valuable in demonstrating the presence of bronchiolitis in patients with primarily infiltrative diseases such as hypersensitivity pneumonitis [259,275], sarcoidosis [258,276], and pneumonia.

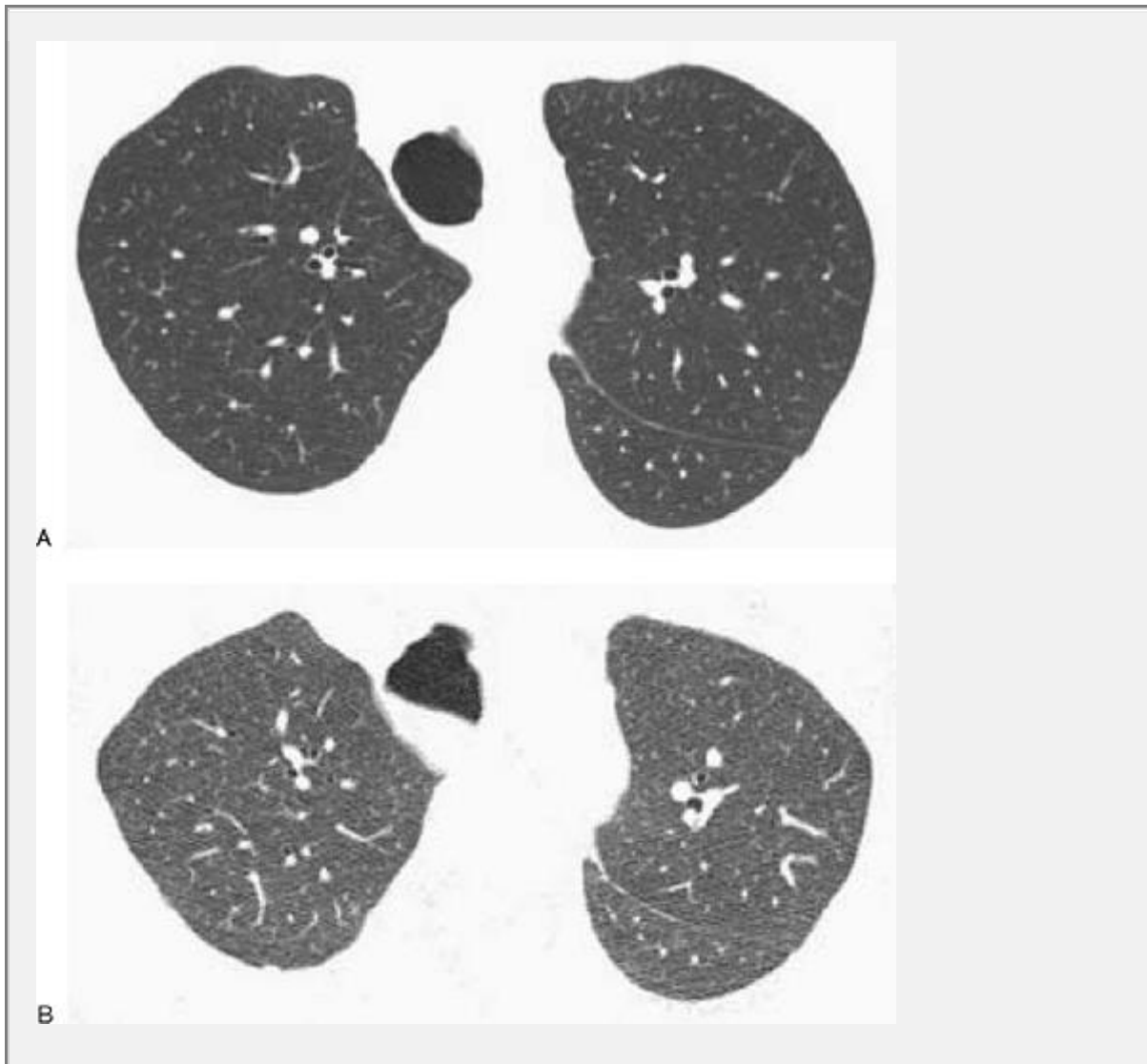


FIG. 3-147. Normal postexpiratory HRCT. Inspiratory image (A) shows homogeneous lung attenuation. B: After expiration, there has been a significant reduction in lung volume associated with an increase in lung attenuation. Lung attenuation remains homogeneous. Note flattening of

the posterior tracheal membrane.

P.173

It must be recognized that limited air-trapping can be seen in normal subjects, particularly in the superior segments of the lower lobes or in isolated secondary lobules. Abnormal air-trapping differs from this occurrence to an extent.

Expiratory CT techniques and normal findings are described in Chapters 1 and 2.

Lung Attenuation Abnormalities

In normal subjects, lung increases significantly in attenuation during expiration (see Fig. 2-19, 2-20, 2-21; Fig. 3-147). In the presence of airway obstruction and air-trapping, lung remains lucent on expiration and shows little change in a cross-sectional area. Areas of air-trapping are seen as relatively low in attenuation on expiratory scans. On expiratory HRCT, the diagnosis of air-trapping is easiest to make when the abnormality is patchy in distribution, and normal lung regions can be contrasted with abnormal, lucent lung regions (Figs. 3-148, 3-149, 3-150, 3-151, 3-152, 3-153) [125,242]. Areas of air-trapping can be patchy and nonanatomic, can correspond to individual secondary pulmonary lobules, segments, and lobes, or may involve an entire lung [252,277]. Air-trapping in a lobe or lung is usually associated with large airway or generalized small airway abnormalities, whereas lobular or segmental air-trapping is associated with diseases that produce small airway abnormalities [252]. Pulmonary vessels within the low-attenuation areas of air-trapping often appear small

relative to vessels in the more opaque normal lung regions [252].

In patients with airways disease or emphysema who have a diffuse abnormality, expiratory inhomogeneities in lung attenuation may not be visible, but air-trapping can be detected by measuring the lung attenuation change occurring with expiration [241,252,253,254,255]. Areas of air-trapping show significantly less attenuation increase than seen in normal lung [269]. The normal mean attenuation difference between full inspiration and expiration usually ranges from 80 to 300 HU. On dynamic scans, a lung attenuation change of less than 70 or 80 HU between full inspiration and full exhalation may be regarded as abnormal (Fig. 3-153). On simple postexpiratory scans, a lung attenuation change of less than 70 HU sometimes may be seen. Lung attenuation change is most simply measured using small (1 to 2 cm) regions of interest on both inspiratory and expiratory scans [254]. Measuring the change in overall lung attenuation from inspiration to expiration may be used in patients with diffuse air-trapping [254] but is clearly less sensitive in patients with patchy disease.



FIG. 3-148. Dynamic inspiratory (A) and expiratory (B) HRCT in a patient with postinfectious bronchiolitis obliterans. On expiration, marked inhomogeneity in lung attenuation is noted, with focal air-trapping in the left upper lobe (*asterisk*). Note the relatively small size of pulmonary vessels in the region of air-trapping. A region of interest placed in the area of air-trapping shows a paradoxical decrease in lung attenuation of 30 HU during expiration.

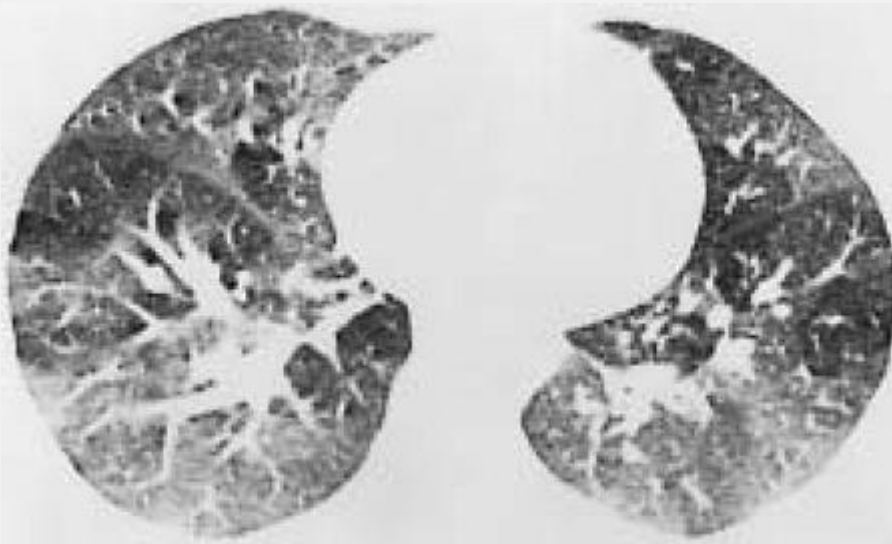


FIG. 3-149. Dynamic expiratory HRCT in a patient with asthma. On expiration, marked inhomogeneity in lung attenuation is noted, with multifocal regions of air-trapping. (From Webb WR. High-resolution computed tomography of obstructive lung disease. Radiol Clin North Am 1994;32:745, with permission.)

P.174

A second method is to compare equivalent areas in each lung on expiratory scans. In healthy subjects, the mean

difference in attenuation change between symmetric regions of the right and left lungs during exhalation was measured as $36 \text{ HU} \pm 14$ [278]. From this, a right-left difference in attenuation increase during exhalation exceeding 78 HU [more than three standard deviations greater than the mean] can be considered abnormal. This method is especially useful when air-trapping is unilateral.

Occasionally, lung attenuation decreases during expiration in regions of air-trapping; a decrease of attenuation by as much as -258 HU has been reported during dynamic expiration [253]. Although there is no definite explanation for this phenomenon, several suggestions have been made [253]. The most likely is that during exhalation, lung units trapping air compress small pulmonary vessels, squeezing blood out of the lung and decreasing lung perfusion.

Another possible explanation is so-called pendelluft, in which air may pass from a normally ventilated lung unit to a partially obstructed lung unit during rapid expiration, resulting in an increased gas volume [252].

Although measurement of lung attenuation can be used to diagnose air-trapping except in patients with diffuse air-trapping (e.g., emphysema, large bronchial obstruction), the extent of air-trapping rather than overall lung attenuation better predicts pulmonary function test findings of obstruction [252,253].

Pixel Index

The *pixel index* (PI) is defined as the percentage of pixels in both lungs on a single scan that show an attenuation lower than a predetermined threshold value (usually -900 HU to -950 HU) (Fig. 3-154) [260,262,279]. Although the inspiratory PI has wide normal range, the expiratory PI is

relatively constant. The normal PI at full inspiration ranges from 0.6 to as much as 58.0 when the threshold is -900 HU [280], although the mean value ranges from 10 to 25 depending on the level scanned and on the CT scan collimation (Fig. 3-154) [262]. In a study of 42 healthy subjects (21 men, 21 women) aged 23 to 71 years, the inspiratory PI measured using -950 HU ranged from 1.2 to 22.3 (mean, 7.8) [279]. At full expiration, with a threshold value of -900 HU, the normal range of PI is rather small with a mean of less than 1.04 (SD, 1.3) [262]. Thus, in normals, the area of lung having an attenuation of less than -900 HU at full expiration in normals can generally be regarded as less than a few percent.

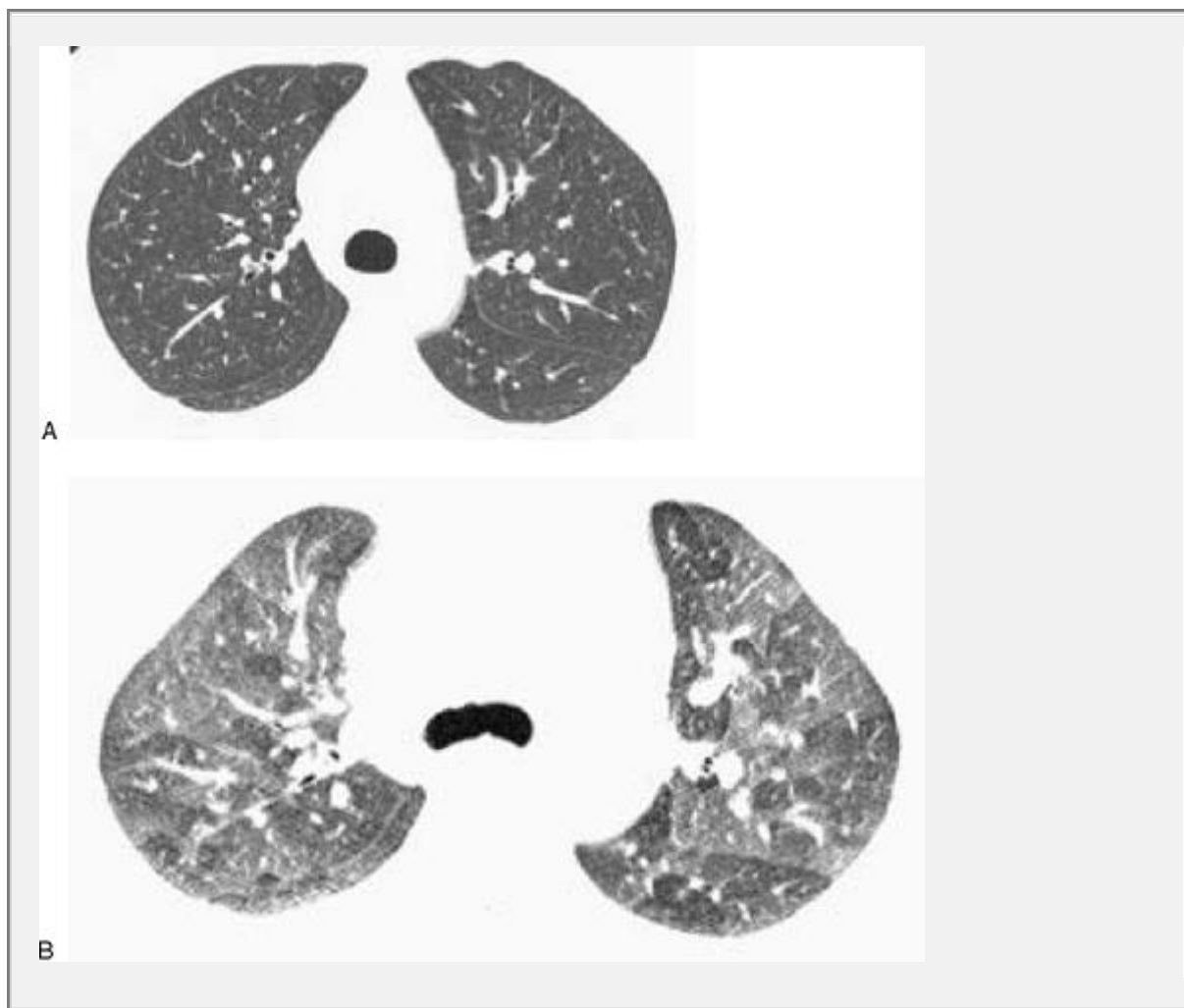


FIG. 3-150. Expiratory air-trapping in a patient with bronchiolitis obliterans. A: Inspiratory scan is normal. B: Postexpiratory scan shows patchy lung attenuation with the relatively lucent regions representing regions of air-trapping. Normally ventilated areas increase significantly in attenuation on expiration.

P.175

The expiratory PI can be used to quantitatively assess the area of low attenuation lung in patients with air-trapping or emphysema (Fig. 3-155). For example, in one study [260], 64 patients underwent both inspiratory and expiratory CT correlated with pulmonary physiology. There were 28 patients with an inspiratory PI of more than 40, and 14 of these had an expiratory PI of more than 15. This group showed markedly abnormal pulmonary function test values suggestive of emphysema, whereas other patients showed preserved lung function. Also, an expiratory PI over 15 accurately reflected and quantitated the degree of emphysema estimated by various pulmonary function tests. The expiratory PI has also been used to quantitatively discriminate asthmatic patients from normal subjects. In one study of both asthmatic and normal subjects [262], both inspiratory and expiratory PI were obtained at two levels (at the transverse aorta and just superior to the diaphragm) and compared with pulmonary function tests. Using collimations of 10 mm and 1.5 mm, the expiratory PI at a level immediately superior to the diaphragm was significantly higher in asthmatic subjects (4.45 and 10.03 for the two collimations, respectively) than in normal

subjects (0.16 and 1.04, respectively) and provided the best separation between the groups [262].

Air-Trapping Score

The extent of air-trapping present on expiratory scans can be measured using a semiquantitative scoring system, which estimates the percentage of lung that appears abnormal on each scan [253,254,255,273,278,281,282]. Such systems have the advantage of being simple, quick, and easy to perform at the time of image interpretation. Furthermore, in one study [281], a simple 5-point scoring system was found to be associated with better interobserver agreement than a more detailed scoring system.

For example, in the scoring system proposed by Webb et al. [278] and Stern et al. [253], estimates of air-trapping are made at three levels scanned using expiratory technique (at the aortic arch, carina, and 5 cm below the carina). At each level and for each lung, a 5-point scale is used to estimate the extent of air-trapping visible subjectively: 0 = no air-trapping; 1 = 1% to 25% of cross-sectional area of lung affected; 2 = 26% to 50% of affected lung; 3 = 51% to 75% of affected lung; 4 = 76% to 100% of affected lung. The air-trapping score is the sum of these numbers for the three levels studied and ranges from 0 to 24. In several studies using this method, significant differences were found in the extent of air-trapping in normal patients and those with airway obstruction [254], and significant correlations were found between the extent of air-trapping and pulmonary function test measures of airway obstruction [246,253,254].

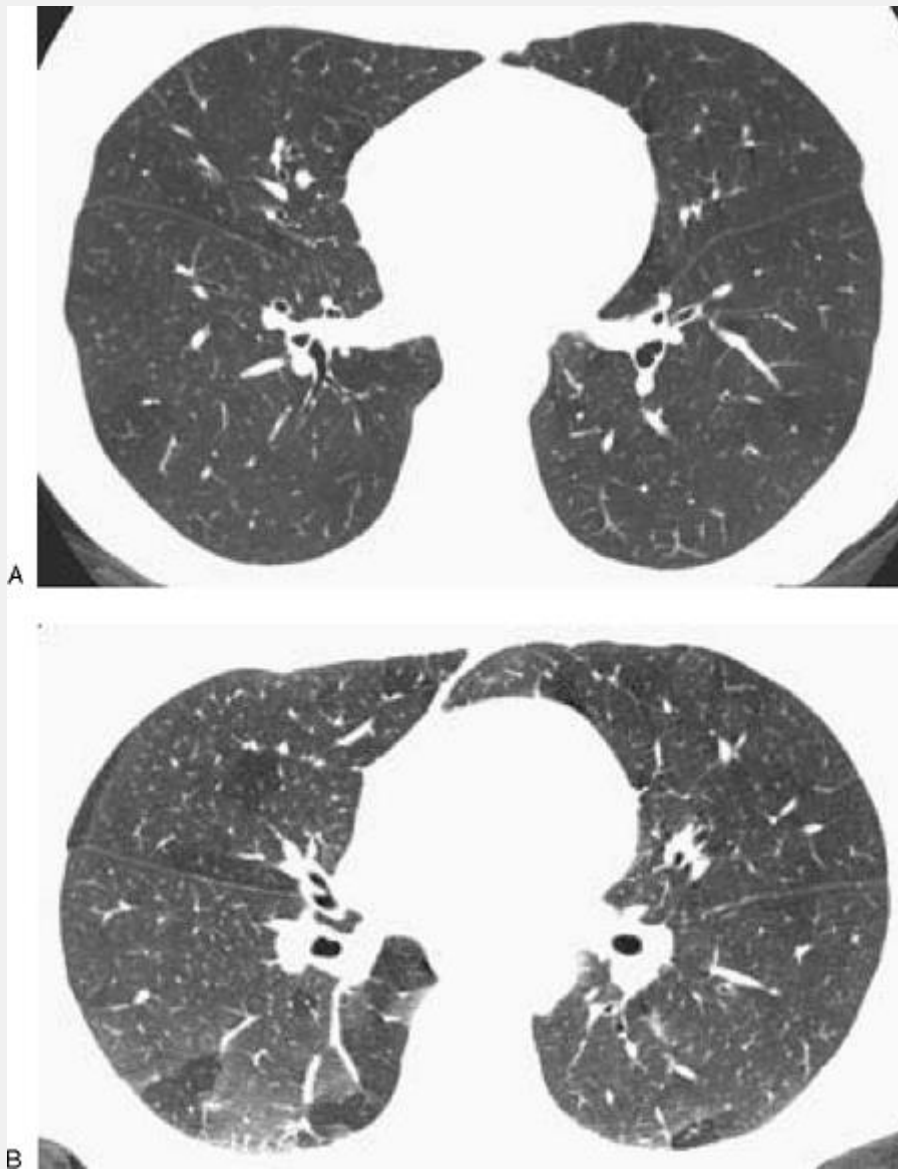


FIG. 3-151. Postexpiratory air-trapping in a patient with asthma. A: An inspiratory scan is normal. B: Routine postexpiratory scan obtained during suspended respiration after a forced exhalation scan shows patchy air-trapping.

P.176

Other methods of visually scoring the extent of air-trapping on expiratory scans have been used and validated

[255,273]. Lucidarme et al. [255] and Lee et al. [282] used a grid superimposed on the expiratory HRCT image and counted the number of squares containing lucent lung and the number encompassing the entire lung. The air-trapping score represented the ratio of air-trapping squares to the total number of squares overlying lung and approximated the cross-sectional percent of abnormal lung. Excellent interobserver agreement was achieved using this method [255].

In patients studied using postexpiratory HRCT, correlations between the air-trapping score and various pulmonary function test findings of obstruction range from approximately $r = -0.4$ to $r = -0.6$ [246,254,282]; correlations are generally best when normal and abnormal patients are grouped together and when patients with emphysema are included among those with airway obstruction [254]. Thus, in a study by Chen et al. [254], considering only patients with obstructive disease, air-trapping score correlated significantly with forced expiratory volume in 1 second (FEV_1) ($r = -0.78$), FEV_1 /forced vital capacity (FVC) ($r = -0.64$), FVC ($r = -0.61$), and forced expiratory flow (FEF) at 25% to 75% of vital capacity ($r = -0.65$); when both normal and abnormal patients were considered together, correlations were higher, with r values measuring -0.89 , -0.74 , -0.77 , and -0.81 , respectively. In a study by Lucidarme et al. [255] of 74 patients with suspected chronic airway disease, expiratory air-trapping was seen in 18 of 35 (51%) patients with severe airway obstruction ($FEV_1/FVC < 80\%$), in 21 of 29 (72%) patients with predominantly small airway obstruction (abnormal flow-volume curve and $FEV_1/FVC \geq 80\%$), and in four of ten (40%) patients with normal PFT results. Air-trapping scores

were 27%, 12%, and 8% for these groups, respectively, with significant negative correlations with FEV₁ ($r = -0.45$), FEV₁/FVC ($r = -0.31$), and FEF at 25% of vital capacity ($r = -0.57$). Lee et al. [282] studied 47 asymptomatic subjects using PFT and expiratory HRCT; in all, PFT were considered to be normal. In this study, the air-trapping grade correlated with FEV₁/FVC ($r = -0.44$) In a study of 70 patients with chronic purulent sputum production [273], the air-trapping score defined at a lobular level significantly correlated with values of FEV₁ and FEV₁/FVC.

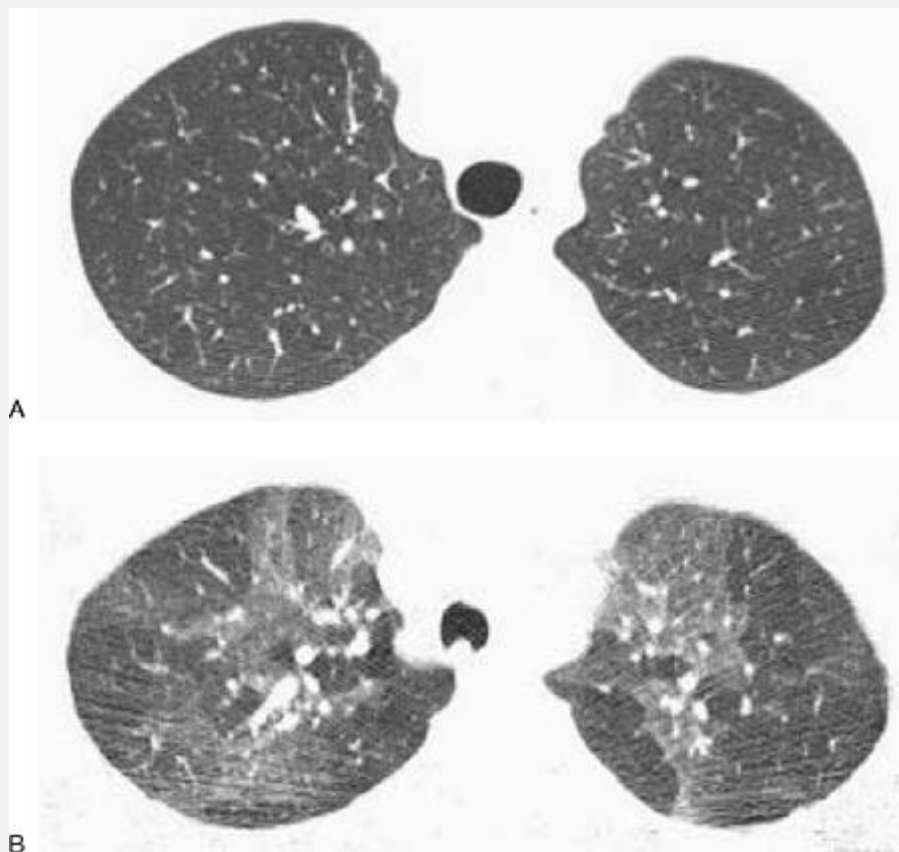


FIG. 3-152. Postexpiratory air-trapping in a patient with bronchiolitis obliterans related to smoke inhalation. A: An inspiratory scan is normal. B: A low-dose dynamic expiratory scan shows patchy air-trapping. Note anterior

bowing of the posterior tracheal membrane, a good indication of forceful exhalation.

P.177

Air-trapping can also be seen in normal subjects, although its extent is limited. Air-trapping in one or more secondary pulmonary lobules is not uncommon. Also, focal areas of relative lucency can be seen in normal subjects on expiratory scans in the superior segments of the lower lobes and in the lingula or middle lobe [252,278]. It is postulated that the slender segments may be less well ventilated than adjacent lung, having a tendency to trap air during exhalation [252]. In their study of ten young normal subjects, Webb et al. [278] found that, although air-trapping was present in four patients, the air-trapping score never exceeded a total of 2 (i.e., 25%) at any one level. In subsequent experience with patients having normal PFT, an air-trapping score of up to 6/24 (i.e., 25%) has been found when the superior segments are included in analysis [254]. In a study by Lucidarme et al. [255] of ten normal nonsmokers, excluding the superior segments of the lower lobes and isolated pulmonary lobules, no air-trapping was visible. In a study by Lee et al. [282], an air-trapping score equivalent to less than 5% of lung was seen in 32% of asymptomatic patients, and an air-trapping score of between 5% and 25% was seen in an additional 20%. In this study, although all patients were considered normal, an air-trapping extent between 5% and 25% was more frequent in smokers (33%) than nonsmokers (14%) [282].

Lung Area Changes

Robinson and Kreel have shown that a significant correlation exists between changes in cross-sectional lung area measured using CT and lung volume ($r = 0.569$) [283]. The percentage decrease in lung cross-sectional area that occurred during exhalation also correlates with the attenuation increase [278,283]. In a study using dynamic ultrafast HRCT [278], a significant correlation between cross-sectional lung area and lung attenuation was found for each of three lung regions evaluated (upper lung: $r = 0.51$, $p = .03$, midlung: $r = 0.58$, $p = .01$; lower lung: $r = 0.51$, $p = .05$).

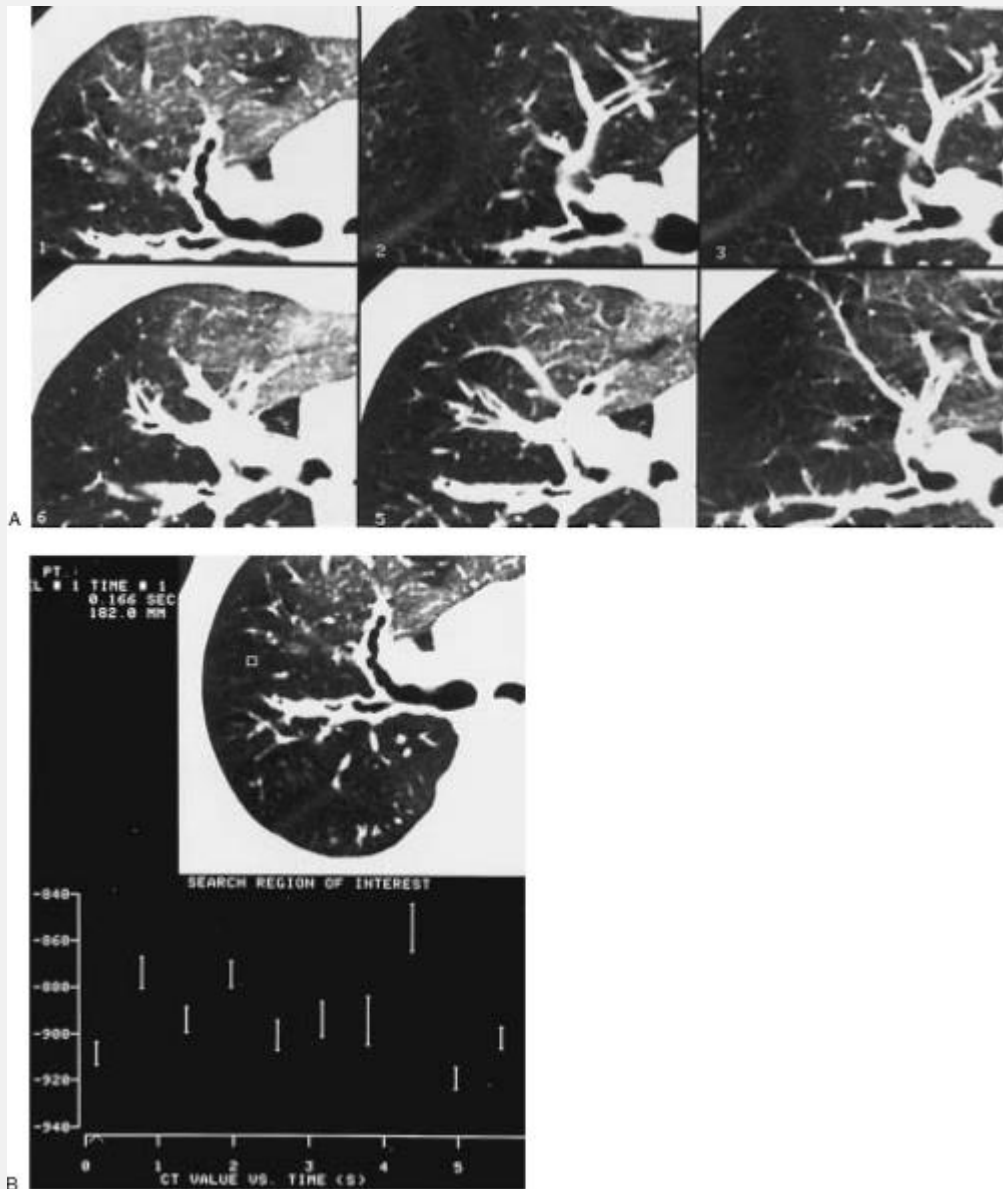


FIG. 3-153. Dynamic expiratory HRCT in a patient with cystic fibrosis obtained using an electron-beam scanner. A: Six dynamic images from a sequence of ten, through the right upper lobe region, shown sequentially in a clockwise fashion from the upper left to lower left. On inspiration (*top middle*), lung opacity appears homogeneous. On expiration (*lower left corner*), a part of the anterior segment shows a normal increase in opacity, whereas the remainder of the upper lobe remains lucent. B: Time-attenuation curve

measured in a lucent region of the upper lobe shows little change in attenuation during expiration.

P.178

Usually, areas of air-trapping show little or no area and volume change during exhalation and can help to identify areas of air-trapping. In one study of nine cases of Swyer-James syndrome [238], expiratory CT scans in areas of abnormal lung showed no significant lung volume change, and mediastinal shift toward the normal lung was also seen.

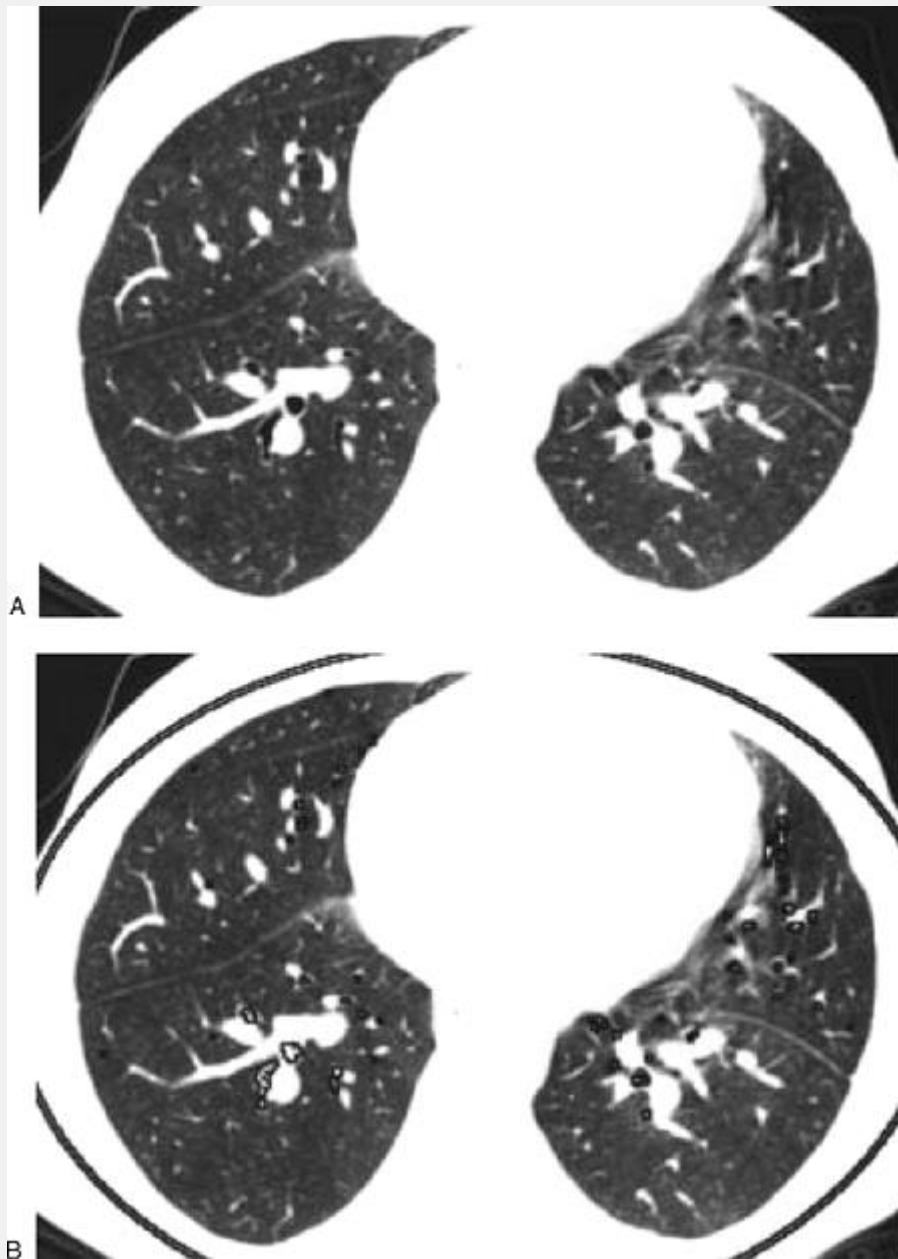


FIG. 3-154. Pixel index measured in a patient with bilateral lung transplantation and normal lung function. An expiratory scan (A) and scan with pixels measuring less than -900 HU (highlighted) (B) are shown. The low attenuation pixels shown in B represent 0.6% of lung area (pixel index, 0.6). This is normal. (From Arakawa H, Webb WR. Expiratory HRCT scan. *Radiol Clin North Am* 1998;36:189, with

permission.)

P.179

In a study by Lucidarme et al. [255] of 74 patients with suspected chronic airway disease and ten normal subjects, an area-reduction score was measured, representing the reduction in cross-sectional lung area from inspiration to expiration. Area-reduction scores were 18%, 30%, and 35%, respectively, for groups of patients with severe airway obstruction ($FEV_1/FVC < 80\%$), predominantly small airways obstruction (abnormal flow-volume curve and $FEV_1/FVC \geq 80\%$), and normal PFT results. In the normal subjects, the area-reduction score was 43%. Area-reduction score correlated significantly with all PFT indexes ($r = 0.35$ to 0.66) except total lung capacity.

Diagnosis of Air-Trapping in Patients with Normal Inspiratory Scans

In some patients, inhomogeneous lung attenuation is visible on expiratory scans in the presence of normal inspiratory scans, indicating the presence of obstructive disease (Figs. 3-149, 3-150, 3-151, 3-152). In one study [257], HRCT in 273 consecutive patients with suspected diffuse lung disease was reviewed. Forty-five patients showed air-trapping on expiratory HRCT scans. Of these 45 patients, inspiratory HRCT scans showed abnormal findings in 36 (bronchiectasis, bronchiolitis obliterans, asthma, chronic bronchitis, and cystic fibrosis). In the remaining nine patients, inspiratory HRCT showed normal findings; conditions in these nine patients included bronchiolitis obliterans ($n = 5$), asthma (n

= 3), and chronic bronchitis (n = 1). Results of pulmonary function tests in patients with air-trapping and normal findings on inspiratory scans were intermediate, falling between those of patients with normal findings on inspiratory and expiratory HRCT scans and those of patients with air-trapping and abnormal findings on inspiratory scans. This appearance can also be seen in patients with hypersensitivity pneumonitis.

P.180

Inhomogeneous Lung Opacity: Differentiation of Mosaic Perfusion from Ground-Glass Opacity

As indicated above, the presence of inhomogeneous lung attenuation on inspiratory scans is a common finding [246]. This appearance may result from ground-glass opacity, mosaic perfusion resulting from airways obstruction and reflex vasoconstriction, mosaic perfusion resulting from vascular obstruction, or a combination of these.

Expiratory HRCT scans may be useful in the diagnosis of inhomogeneous opacity and can usually allow the differentiation of mosaic perfusion resulting from airways obstruction from other abnormalities when the inspiratory scans are inconclusive (Algorithm 9). In patients with ground-glass opacity, expiratory HRCT typically shows a proportional increase in attenuation in areas of both increased and decreased opacity (Fig. 3-156). In patients with mosaic perfusion resulting from airways disease, attenuation differences are accentuated on expiration (Fig.

3-157); relatively dense areas increase in attenuation, whereas lower attenuation regions remain lucent (i.e., air-trapping is present) [125,252,272,278].

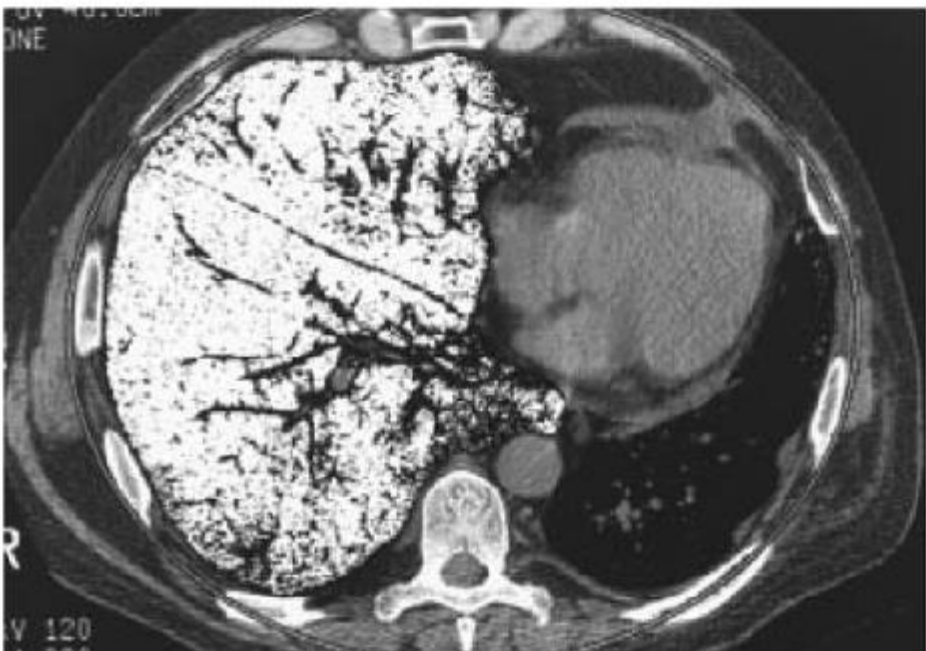
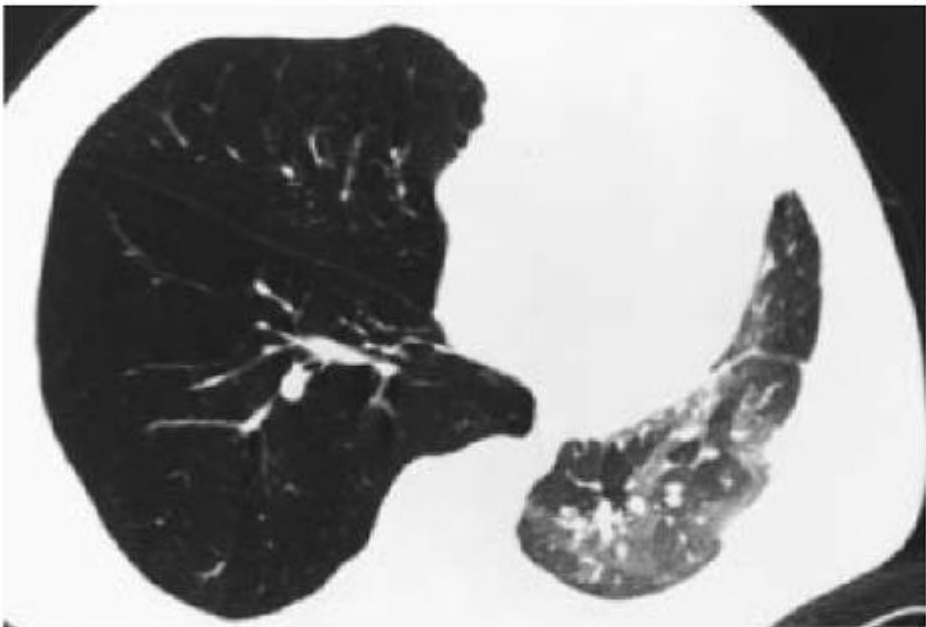
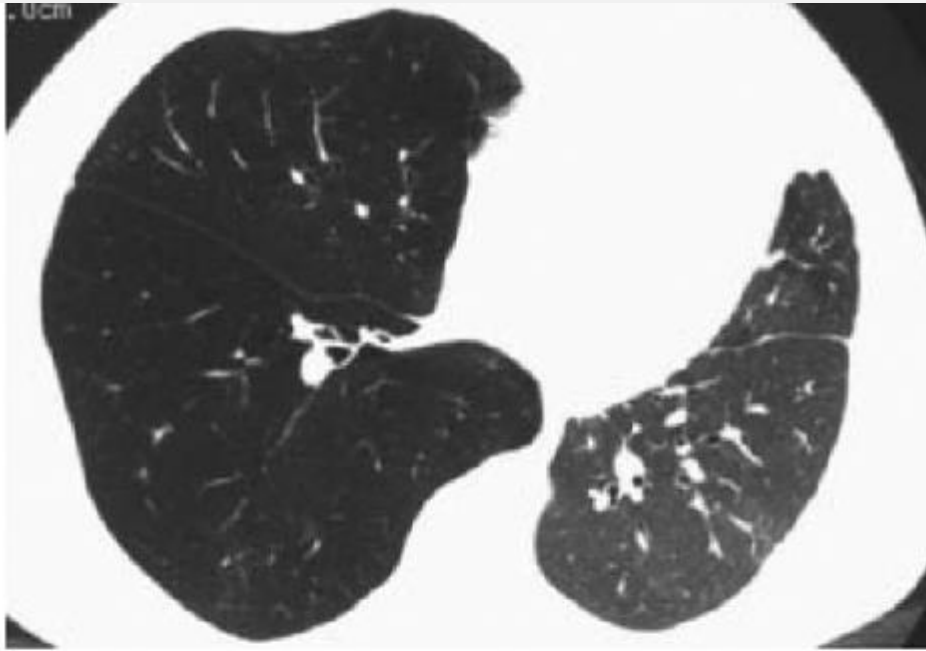


FIG. 3-155. Inspiratory and postexpiratory images in a patient with left lung transplantation for panlobular emphysema. A: Inspiratory HRCT shows extensive right-sided emphysema. B: On a postexpiratory HRCT, measured using a region of interest, there was little or no attenuation increase in the right lung. As compared to the inspiratory image, patchy air-trapping on the left is visible as inhomogeneous opacity. This finding suggests small airway obstruction and is consistent with constrictive bronchiolitis. This was confirmed on transbronchoscopic biopsy. C: Pixels having a value of less than -900 HU in the post-expiratory image have been highlighted. The pixel index for the emphysematous right lung measures 72 and is markedly abnormal. The pixel index for the left lung measures 0.7, and is within normal limits. (From Arakawa H, Webb WR. Expiratory HRCT scan. *Radiol Clin North Am* 1998;36:189, with permission.)

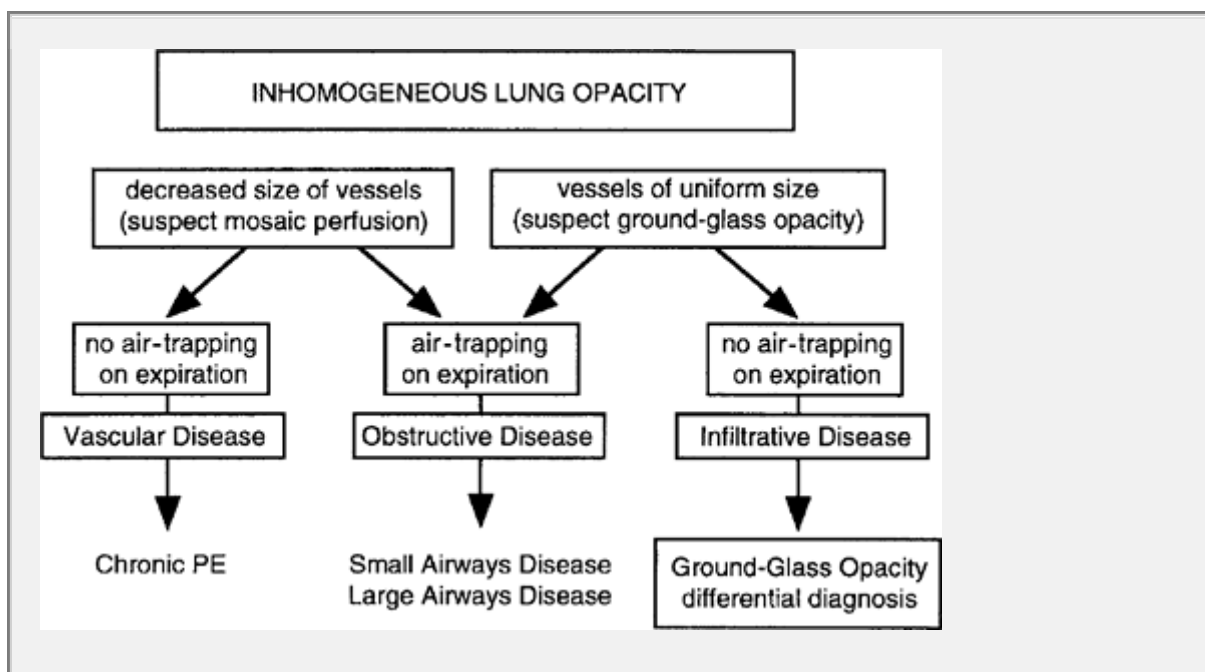
P.181

In a study by Arakawa et al. [246] of patients showing inhomogeneous opacity as their predominant HRCT abnormality, the accuracy of HRCT in correctly diagnosing the type of disease present increased from 81% to 89% in patients with ground-glass opacity and from 84% to 100% in diagnosing airways disease when expiratory scans were included in the analysis [246]. Some patients who appear to show ground-glass opacity on inspiratory scans and show air-trapping on expiratory scans thus may be correctly diagnosed as having obstructive disease (Algorithm 9).

In patients with mosaic perfusion resulting from vascular disease, expiratory HRCT findings mimic those seen in patients with ground-glass opacity; both low-attenuation and high-attenuation regions increase in attenuation on expiration. In patients with mosaic perfusion due to vascular disease, air-trapping is not usually seen. However, in a study of patients with inhomogeneous lung attenuation of various causes [247], air-trapping was thought to be present on expiratory scans in some patients with vascular disease when scans were viewed blindly.

Mixed Disease

In patients with mixed infiltrative and airways disease, inspiratory scans may show a patchy pattern of variable lung attenuation, representing the combination of ground-glass opacity (or consolidation), normal lung, and reduced lung attenuation as a result of mosaic perfusion. This combination of mixed densities has been termed the *head-cheese sign* (Fig. 3-146) [256] and is most typical of hypersensitivity pneumonitis (Fig. 3-158), sarcoidosis, and atypical infections with associated bronchiolitis (Fig. 3-159).



ALGORITHM 9

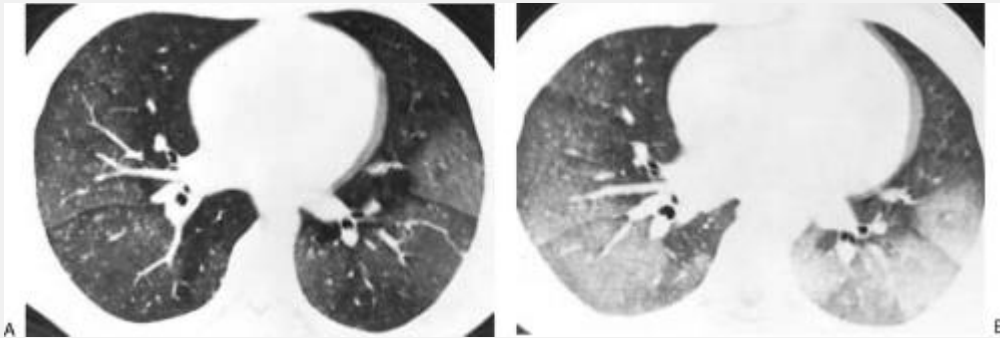


FIG. 3-156. Inspiratory and postexpiratory HRCT in a patient with pulmonary hemorrhage and ground-glass opacity. A: Patchy differences in lung opacity are visible on the inspiratory scan. This appearance mimics mosaic perfusion. B: On a postexpiratory scan, proportional increases in lung opacity are seen throughout the lungs. Lung attenuation increased by 150 to 200 HU on the expiratory scan in all lung regions.

P.182

In some patients with mixed infiltrative and obstructive diseases, ground-glass opacity may be seen on the inspiratory scans without clear-cut findings of mosaic perfusion. However, in such cases, the presence of air-trapping on expiratory images may allow the correct diagnosis of mixed infiltrative and obstructive disease [246]. The combination of ground-glass opacity or consolidation on inspiratory scans and air-trapping on

expiratory scans should also be considered indicative of a mixed abnormality (Fig. 3-158) [246].

In a study by Chung et al. [256], 14 of 400 consecutive patients having HRCT with routine expiratory images showed findings of infiltrative lung disease on inspiratory scans and significant air-trapping on expiratory scans. These 14 patients included six with hypersensitivity pneumonitis, five with sarcoidosis, two with atypical infections, and one with pulmonary edema. Ten patients showed ground-glass opacity on inspiratory scans, whereas four patients with sarcoidosis showed nodules. Mosaic perfusion was seen in ten patients. Pulmonary function tests demonstrated a mixed pattern in five patients, an obstructive pattern in four patients, and a restrictive pattern in three patients.

FEV₁/FVC correlated significantly with the extent of air-trapping score ($r = 0.58$, $p = .05$). The extent of infiltrative abnormalities correlated significantly with FVC ($r = -0.77$, $p = .003$) and diffusing capacity (DLco) ($r = -0.75$, $p = .01$).



FIG. 3-157. Inspiratory and postexpiratory HRCT in a patient with bronchiolitis obliterans. A: Inspiratory scan shows subtle differences in opacity in different lung regions,

representing mosaic perfusion. B: Postexpiratory HRCT shows a marked accentuation in attenuation inhomogeneities due to air-trapping. Regions of lucency increased in attenuation by approximately 50 HU on expiration. Although some areas of air-trapping appear patchy and nonanatomic (asterisk), others appear subsegmental or lobular (arrows).

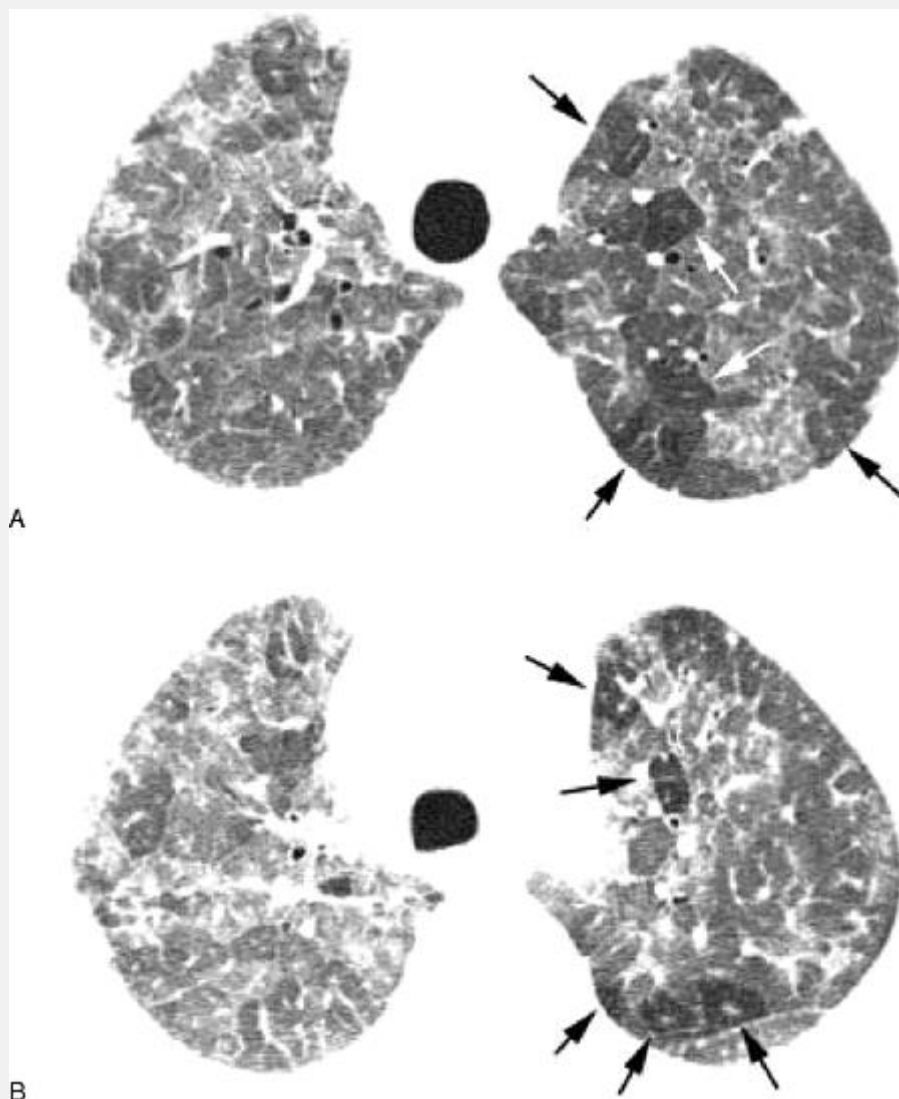


FIG. 3-158. Hypersensitivity pneumonitis with the head-cheese sign. A: An inspiratory scan shows inhomogeneous

lung attenuation consisting of ground-glass opacity and lobular areas of lucency (*arrows*) due to mosaic perfusion. B: Expiratory scan shows air-trapping in the lucent regions (*arrows*). These areas show little or no change in attenuation on the expiratory scans.

P.183

Air-trapping in association with ground-glass opacity is a common HRCT finding in both the subacute and chronic stages of hypersensitivity pneumonitis [259]. In a series of 22 patients with hypersensitivity pneumonitis, HRCT scans with a limited number of expiratory images were correlated with pulmonary function tests [259]. Areas of decreased attenuation, mosaic perfusion, and air-trapping were seen in 19 patients and were the most frequent findings. In addition, the extent of decreased attenuation correlated well with severity of functional index of air-trapping as indicated by increased residual volume ($r = 0.58$, $p < .01$).

In patients with sarcoidosis, HRCT commonly shows findings of mosaic perfusion and air-trapping in addition to findings of infiltrative disease [258,276]. Hansell et al. [258] attempted to determine the relationship between the obstructive defects of pulmonary sarcoidosis and HRCT patterns of disease in 45 patients. The most prevalent CT patterns were decreased lung attenuation on expiratory scans ($n = 40$), a reticular pattern ($n = 37$), and a nodular pattern ($n = 36$). A reticular pattern was the main determinant of functional impairment, particularly airflow obstruction, as shown by inverse relationships with FEV_1 and FEV_1/FVC , among others. Decreased attenuation on

expiratory scans was also significantly related to measures of airway obstruction, although correlations were weaker.

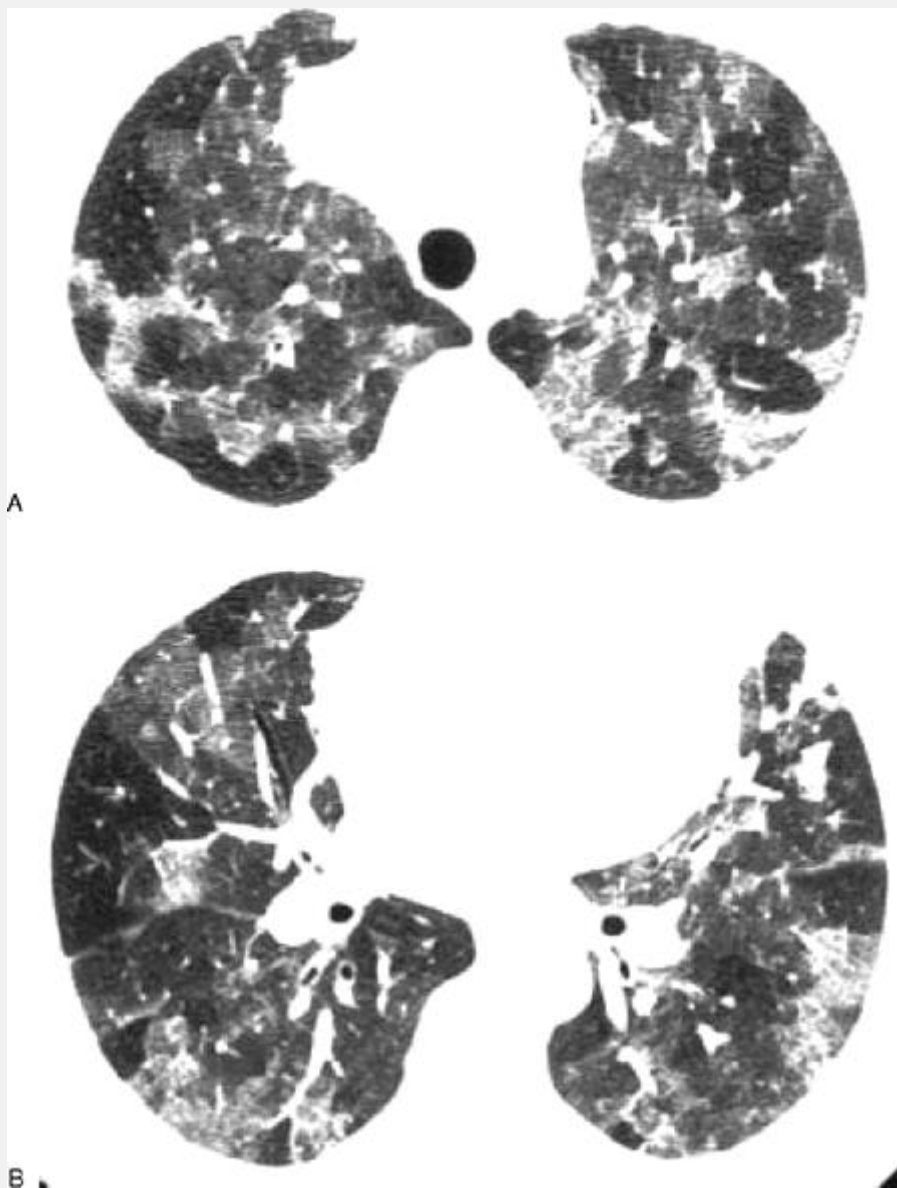


FIG. 3-159. A, B: *Mycoplasma pneumoniae* pneumonia with the head-cheese sign. Inspiratory images show inhomogeneous lung attenuation consisting of ground-glass opacity and multiple lobular areas of lucency due to mosaic perfusion, and secondary to bronchiolitis. Air-trapping was present on expiratory scans.

Distribution of Parenchymal Abnormalities in the Diagnosis of Lung Disease

When attempting to reach a diagnosis or differential diagnosis of lung disease using HRCT, the overall distribution of pulmonary abnormalities should be considered along with their morphology, HRCT appearance, and distribution relative to lobular structures [41,60,76,101]. Many lung diseases show specific regional distributions or preferences, a fact that is likely related to their underlying pathogenesis and pathophysiology [284]. Preferential or predominant involvement of one or more lung regions is commonly seen on HRCT, even in patients with chest radiographs showing a diffuse abnormality. For the purposes of interpreting HRCT, the regional distribution of lung abnormalities can be categorized in several ways: central lung versus peripheral lung, upper lung versus lower lung, anterior lung versus posterior lung, or unilateral versus bilateral.

An important caveat to keep in mind when reading the following section is that significant variations in classical patterns of lung involvement can be seen in individual patients. A specific diagnosis should not be excluded because of an atypical distribution of abnormalities.

Central Lung versus Peripheral Lung

Some diseases have a central, perihilar, bronchocentric, or bronchovascular distribution [9,60], whereas others favor the peripheral or subpleural parenchyma, or lung cortex

(Table 3-13). Diseases that can have a central or perihilar predominance include sarcoidosis (Fig. 3-81), silicosis (Fig. 3-83), lymphangitic spread of carcinoma [285], and large airways diseases, such as bronchiectasis, cystic fibrosis, and allergic bronchopulmonary aspergillosis (Fig. 3-138) [11,12,41,56,76,90,101]. In a study by Grenier et al. [285], a predominantly central distribution of abnormalities was visible in 16% of patients with sarcoidosis, 31% of patients with silicosis, and 8% of those with lymphangitic spread of carcinoma. In another study [76], a central or peribronchovascular predominance was seen in 70% of patients with sarcoidosis and 60% of patients with lymphangitic spread of carcinoma.

TABLE 3-13. Predominance of lung disease on HRCT: central lung versus peripheral lung

Lung disease	Findings
Central lung	
Sarcoidosis	Peribronchovascular nodules; conglomerate fibrosis with traction bronchiectasis
Silicosis	Conglomerate masses of fibrosis

Talcosis	Conglomerate masses of fibrosis
Lymphangitic spread of carcinoma	Peribronchovascular interstitial thickening or nodules
Large airways diseases	Bronchiectasis (e.g., cystic fibrosis)
Peripheral lung	
Usual interstitial pneumonitis–idiopathic pulmonary fibrosis; collagen diseases; asbestosis	Subpleural fibrosis; honeycombing; sometimes ground-glass opacity
Nonspecific interstitial pneumonia	Subpleural ground-glass opacity; reticulation
Chronic eosinophilic pneumonia	Subpleural consolidation or ground-glass opacity
Bronchiolitis obliterans organizing pneumonia	Subpleural consolidation or ground-glass opacity
Acute interstitial	Peripheral consolidation;

pneumonia	ground-glass opacity
Desquamative interstitial pneumonia	Peripheral ground-glass opacity in some
Hypersensitivity pneumonitis	Peripheral ground-glass opacity in some
Hematogenous metastases	Peripheral predominance of nodules common

P.185

A peripheral, cortical, or subpleural predominance of abnormalities has been reported in nearly all patients with eosinophilic pneumonia (Figs. 3-103 and 3-104) [204] and asbestosis [62], 81% to 94% of patients with IPF (Figs. 3-25 and 3-95) [62,76,77], and a similar high percentage of patients with scleroderma, rheumatoid lung disease (Figs. 3-17 and 3-36), or interstitial pneumonia of other causes [143,285]. Peripheral predominance of abnormalities is somewhat less common, visible in approximately half of patients with BOOP (Fig. 3-102) and DIP [62,76,134,193]. It is occasionally present in patients with hypersensitivity pneumonitis and sarcoidosis, ranging from a few percent to 18% in different studies, and in patients with AIP [185]. In patients with hematogenous metastases, nodules may have a peripheral predominance. A subpleural predominance is

also typical of amyloidosis, although this disease is quite rare.

Upper Lung versus Lower Lung

The relative extent and severity of abnormalities in the upper lungs and midlungs and at the lung bases can be determined on HRCT if scans have been obtained at several levels and if one level is compared to the others. Some diseases tend to predominate in the upper lobes, whereas others predominate in the lower lobes (Table 3-14) [286]. Diseases that have been recognized to have an upper lobe predominance on HRCT include sarcoidosis (Figs. 3-5, 3-6, and 3-81), Langerhans histiocytosis (Figs. 3-113, 3-114, 3-115), CWP and silicosis (Fig. 3-49), and centrilobular emphysema (Fig. 3-123) [21,58,76,77,90,92,93,101,285]. An upper lobe predominance of abnormalities is present in nearly equal percentages of patients with sarcoidosis (47% to 50%), Langerhans histiocytosis (57% to 62%), and silicosis (55% to 69%), whereas a lower lobe predominance is present in less than 10% of patients with these diseases [77,285]. An upper lobe predominance may be present in patients with respiratory bronchiolitis [109].

A basal distribution is most typical of lymphangitic metastasis (46%), hematogenous metastases, IPF (68%) (Fig. 3-30), collagen-vascular diseases such as rheumatoid lung disease and scleroderma (80%), and asbestosis [39,41,42,62,63,76,77,143,285]. Pulmonary fibrosis of any cause has a basal predominance in approximately 60% of cases [76,77]. Although hypersensitivity pneumonitis is believed to have an upper lobe predominance, it more often appears to be diffuse or preponderant in the mid [23,62] or lower lung zones (30%) [285].

Anterior versus Posterior

Some diseases produce their initial or most extensive abnormalities in the posterior lung (Table 3-15). The distinction between anterior and posterior, of course, is easily made on HRCT. However, it is important to recognize the value of using both prone and supine scans in this regard. Areas of increased attenuation that are limited to the posterior lung on scans obtained in the supine position can reflect normal dependent volume loss; prone scans are essential in making a confident diagnosis of early posterior lung disease. Although the percentages vary in different series, a posterior preponderance of disease is particularly common in scleroderma (60%), sarcoidosis (32% to 36%) (Fig. 3-82), silicosis (31% to 38%) (Fig. 3-49), hypersensitivity pneumonitis (23%), IPF (9% to 21%), and other causes of UIP (Figs. 3-31 and 3-36) [58,76,77,90,285]. A posterior predominance of abnormalities is also common in patients with asbestosis, lymphangitic carcinomatosis, and pulmonary edema [39,41,63,76,77,90,143,285]. In patients with pulmonary edema, the predominant abnormality is more appropriately referred to as *dependent* (Fig. 3-10) rather than *posterior*.

TABLE 3-14. *Predominance of lung disease on HRCT: upper lung versus lower lung*

Lung disease	Findings
Upper lung	
Sarcoidosis	Nodules; fibrosis; conglomerate masses
Langerhans histiocytosis	Nodules; cysts
Silicosis	Nodules; conglomerate masses
Talcosis	Conglomerate masses of fibrosis
Tuberculosis	Consolidation; nodules; cavities; scarring
Cystic fibrosis	Bronchiectasis; emphysema
Centrilobular emphysema	Focal lucencies
Respiratory bronchiolitis	Ground-glass opacity
Lower lung	
Usual interstitial	Subpleural fibrosis;

pneumonitis–idiopathic pulmonary fibrosis; collagen diseases; asbestosis	honeycombing; sometimes ground-glass opacity
Nonspecific interstitial pneumonia	Subpleural ground-glass opacity; reticulation
Lipoid pneumonia	Consolidation; ground-glass opacity
Bronchiolitis obliterans organizing pneumonia	Subpleural consolidation or ground-glass opacity
Hematogenous or lymphangitic metastases	Nodules; septal thickening

P.186

An anterior predominance of lung disease is unusual but has been reported in adult survivors of ARDS [71]. In this study, HRCT was obtained during the acute illness and at follow-up in 27 patients with ARDS. At follow-up CT, a reticular pattern was the most prevalent abnormality (85%), with a striking anterior distribution (see Fig. 6-76). This finding was related to the duration of mechanical ventilation and was inversely correlated with the extent of parenchymal opacification on scans obtained during the acute illness.

TABLE 3-15. *Predominance of lung disease on HRCT: posterior lung versus anterior lung*

Lung disease	Findings
Posterior lung	
Usual interstitial pneumonia; Nonspecific interstitial pneumonia	Fibrosis; ground-glass opacity
Asbestosis	Fibrosis
Scleroderma	Fibrosis; ground-glass opacity
Silicosis	Nodules; conglomerate masses
Sarcoidosis	Nodules; conglomerate masses
Pulmonary edema	Septal thickening; ground-glass opacity; consolidation

Adult respiratory distress syndrome (ARDS)	Ground-glass opacity; consolidation
Hypersensitivity pneumonitis	Ground-glass opacity; nodules; fibrosis
Lipoid pneumonia	Consolidation; ground-glass opacity
Anterior lung	
Post-ARDS fibrosis	Subpleural fibrosis; honeycombing; traction bronchiectasis

TABLE 3-16. *Predominance of lung disease on HRCT: unilateral or markedly asymmetric disease*

Disease	Findings
Pneumonia	Variable
Lymphangitic spread of carcinoma	Peribronchovascular interstitial thickening; nodules; septal thickening

Sarcoidosis	Peribronchovascular; subpleural; septal nodules
Bronchiectasis	Findings of bronchiectasis

P.187

Unilateral versus Bilateral

A unilateral predominance of abnormalities is most typical of lymphangitic spread of carcinoma, which is often asymmetric in distribution (Table 3-16); this was seen in nearly 40% of patients with lymphangitic spread of carcinoma in one series (Figs. 3-4 and 3-9) [76].

Asymmetry or unilateral predominance of findings is also common in patients with sarcoidosis, ranging from 9% to 21%. It is somewhat less frequent in association with silicosis (2% to 21%), pulmonary fibrosis (3% to 14%), Langerhans histiocytosis (12%), and hypersensitivity pneumonitis (5%) [76,77].

Diffuse Lung Involvement

Some diseases that appear diffuse on chest films are in fact diffuse and involve the lung uniformly from apex to base, from anterior to posterior, and from central to peripheral (Table 3-17) [76,101]. This is not to say that the disease may not be patchy in distribution with some areas much

more abnormal than others, but rather that there is no consistent pattern to the disease. Many of the diseases that are described in the previous section as showing a particular distribution can also be diffuse; these include lymphangitic spread of carcinoma, sarcoidosis, and silicosis. One disease that typically shows this uniform distribution is hypersensitivity pneumonitis [76,101,130]. LAM tends to be diffuse, whereas Langerhans histiocytosis does not [224].

TABLE 3-17. *Diffuse lung disease*

Disease	Findings
Diffuse pneumonia	Ground-glass opacity; consolidation
Lymphangitic spread of carcinoma	Peribronchovascular interstitial thickening; nodules; septal thickening
Hematogenous metastases	Nodules
Sarcoidosis	Peribronchovascular; subpleural; septal nodules
Hypersensitivity pneumonitis	Ground-glass opacity; nodules; fibrosis
Lymphangiomyomatosis	Lung cysts

Bronchiectasis	Findings of bronchiectasis
----------------	----------------------------

References

1. Müller NL, Miller RR. Computed tomography of chronic diffuse infiltrative lung disease: part 1. *Am Rev Respir Dis* 1990;142:1206-1215.
2. Müller NL, Miller RR. Computed tomography of chronic diffuse infiltrative lung disease: part 2. *Am Rev Respir Dis* 1990;142:1440-1448.
3. Webb WR. High-resolution CT of the lung parenchyma. *Radiol Clin North Am* 1989;27:1085-1097.
4. Zerhouni E. Computed tomography of the pulmonary parenchyma: an overview. *Chest* 1989;95:901-907.
5. Webb WR, Müller NL, Naidich DP. Standardized terms for high-resolution computed tomography of the lung: a proposed glossary. *J Thorac Imag* 1993;8:167-185.
6. Austin JH, Müller NL, Friedman PJ, et al. Glossary of terms for CT of the lungs: recommendations of the Nomenclature Committee of the Fleischner Society. *Radiology* 1996;200:327-331.
7. Zerhouni EA, Naidich DP, Stitik FP, et al. Computed tomography of the pulmonary parenchyma: part 2. Interstitial disease. *J Thorac Imaging* 1985;1:54-64.

8. Nishimura K, Kitaichi M, Izumi T, et al. Usual interstitial pneumonia: histologic correlation with high-resolution CT. *Radiology* 1992;182:337-342.
9. Murata K, Takahashi M, Mori M, et al. Peribronchovascular interstitium of the pulmonary hilum: normal and abnormal findings on thin-section electron-beam CT. *AJR Am J Roentgenol* 1996;166:309-312.
10. Weibel ER. Looking into the lung: what can it tell us? *AJR Am J Roentgenol* 1979;133:1021-1031.
11. Munk PL, Müller NL, Miller RR, et al. Pulmonary lymphangitic carcinomatosis: CT and pathologic findings. *Radiology* 1988;166:705-709.
12. Stein MG, Mayo J, Müller N, et al. Pulmonary lymphangitic spread of carcinoma: appearance on CT scans. *Radiology* 1987;162:371-375.
13. Bergin CJ, Müller NL. CT in the diagnosis of interstitial lung disease. *AJR Am J Roentgenol* 1985;145:505-510.
14. Johkoh T, Ikezoe J, Tomiyama N, et al. CT findings in lymphangitic carcinomatosis of the lung: correlation with histologic findings and pulmonary function tests. *AJR Am J Roentgenol* 1992;158:1217-1222.
15. Lee KS, Kim Y, Primack SL. Imaging of pulmonary lymphomas. *AJR Am J Roentgenol* 1997;168:339-345.
16. Heyneman LE, Johkoh T, Ward S, et al. Pulmonary leukemic infiltrates: high-resolution CT findings in 10 patients. *AJR Am J Roentgenol* 2000;174:517-521.
17. Johkoh T, Müller NL, Pickford HA, et al. Lymphocytic interstitial pneumonia: thin-section CT findings in 22 patients. *Radiology* 1999;212:567-572.
18. Ichikawa Y, Kinoshita M, Koga T, et al. Lung cyst formation in lymphocytic interstitial pneumonia: CT features. *J Comput Assist Tomogr* 1994;18:745-748.

19. McGuinness G, Scholes JV, Jagirdar JS, et al. Unusual lymphoproliferative disorders in nine adults with HIV or AIDS: CT and pathologic findings. *Radiology* 1995;197:59-65.
20. Traill ZC, Maskell GF, Gleeson FV. High-resolution CT findings of pulmonary sarcoidosis. *AJR Am J Roentgenol* 1997;168:1557-1660.
21. Müller NL, Kullnig P, Miller RR. The CT findings of pulmonary sarcoidosis: analysis of 25 patients. *AJR Am J Roentgenol* 1989;152:1179-1182.
22. Kim TS, Lee KS, Chung MP, et al. Nonspecific interstitial pneumonia with fibrosis: high-resolution CT and pathologic findings. *AJR Am J Roentgenol* 1998;171:1645-1650.
23. Adler BD, Padley SP, Müller NL, et al. Chronic hypersensitivity pneumonitis: high-resolution CT and radiographic features in 16 patients. *Radiology* 1992;185:91-95.
24. Wintermark M, Wicky S, Schnyder P, et al. Blunt traumatic pneumomediastinum: using CT to reveal the Macklin effect. *AJR Am J Roentgenol* 1999;172:129-130.
P.188
25. Kemper AC, Steinberg KP, Stern EJ. Pulmonary interstitial emphysema: CT findings. *AJR Am J Roentgenol* 1999;172:1642.
26. Satoh K, Kobayashi T, Kawase Y, et al. CT appearance of interstitial pulmonary emphysema. *J Thorac Imaging* 1996;11:153-154.
27. Bessis L, Callard P, Gotheil C, et al. High-resolution CT of parenchymal lung disease: precise correlation with histologic findings. *Radiographics* 1992;12:45-58.

28. Storto ML, Kee ST, Golden JA, et al. Hydrostatic pulmonary edema: high-resolution CT findings. *AJR Am J Roentgenol* 1995;165:817-820.
29. Weibel ER, Taylor CR. Design and structure of the human lung. In: Fishman AP, ed. *Pulmonary diseases and disorders*. New York: McGraw-Hill, 1988: 11-60.
30. Bankier AA, Fleischmann D, De Maertelaer V, et al. Subjective differentiation of normal and pathological bronchi on thin-section CT: impact of observer training. *Eur Respir J* 1999;13:781-786.
31. Westcott JL, Cole SR. Traction bronchiectasis in end-stage pulmonary fibrosis. *Radiology* 1986;161:665-669.
32. Webb WR, Stein MG, Finkbeiner WE, et al. Normal and diseased isolated lungs: high-resolution CT. *Radiology* 1988;166:81-87.
33. Logan PM. Thoracic manifestations of external beam radiotherapy. *AJR Am J Roentgenol* 1998;171:569-577.
34. Naidich DP, McCauley DI, Khouri NF, et al. Computed tomography of bronchiectasis. *J Comput Assist Tomogr* 1982;6:437-444.
35. Grenier P, Maurice F, Musset D, et al. Bronchiectasis: assessment by thin-section CT. *Radiology* 1986;161:95-99.
36. Munro NC, Cooke JC, Currie DC, et al. Comparison of thin section computed tomography with bronchography for identifying bronchiectatic segments in patients with chronic sputum production. *Thorax* 1990;45:135-139.
37. Grenier P, Lenoir S, Brauner M. Computed tomographic assessment of bronchiectasis. *Semin Ultrasound CT MR* 1990;11:430-441.
38. Neeld DA, Goodman LR, Gurney JW, et al. Computerized tomography in the evaluation of allergic bronchopulmonary aspergillosis. *Am Rev Respir Dis* 1990;142:1200-1206.

39. Aberle DR, Gamsu G, Ray CS, et al. Asbestos-related pleural and parenchymal fibrosis: detection with high-resolution CT. *Radiology* 1988;166:729-734.
40. Todo G, Herman PG. High-resolution computed tomography of the pig lung. *Invest Radiol* 1986;21:689-696.
41. Swensen SJ, Aughenbaugh GL, Brown LR. High-resolution computed tomography of the lung. *Mayo Clin Proc* 1989;64:1284-1294.
42. Müller NL, Miller RR, Webb WR, et al. Fibrosing alveolitis: CT-pathologic correlation. *Radiology* 1986;160:585-588.
43. Murata K, Itoh H, Todo G, et al. Centrilobular lesions of the lung: demonstration by high-resolution CT and pathologic correlation. *Radiology* 1986;161:641-645.
44. Akira M, Yamamoto S, Yokoyama K, et al. Asbestosis: high-resolution CT-pathologic correlation. *Radiology* 1990;176:389-394.
45. Bergin CJ, Coblentz CL, Chiles C, et al. Chronic lung diseases: specific diagnosis using CT. *AJR Am J Roentgenol* 1989;152:1183-1188.
46. Kang EY, Grenier P, Laurent F, et al. Interlobular septal thickening: patterns at high-resolution computed tomography. *J Thorac Imaging* 1996;11:260-264.
47. Cassart M, Genevois PA, Kramer M, et al. Pulmonary venoocclusive disease: CT findings before and after single-lung transplantation. *AJR Am J Roentgenol* 1993;160:759-760.
48. Swensen SJ, Tashjian JH, Myers JL, et al. Pulmonary venoocclusive disease: CT findings in eight patients. *AJR Am J Roentgenol* 1996;167:937-940.
49. Ren H, Hruban RH, Kuhlman JE, et al. Computed tomography of inflation-fixed lungs: the beaded septum sign

- of pulmonary metastases. *J Comput Assist Tomogr* 1989;13:411-416.
50. Graham CM, Stern EJ, Finkbeiner WE, et al. High-resolution CT appearance of diffuse alveolar septal amyloidosis. *AJR Am J Roentgenol* 1992;158:265-267.
51. Murch CR, Carr DH. Computed tomography appearances of pulmonary alveolar proteinosis. *Clin Radiol* 1989;40:240-243.
52. Godwin JD, Müller NL, Takasugi JE. Pulmonary alveolar proteinosis: CT findings. *Radiology* 1988;169:609-613.
53. Lee KN, Levin DL, Webb WR, et al. Pulmonary alveolar proteinosis: high-resolution CT, chest radiographic, and functional correlations. *Chest* 1997;111:989-995.
54. **Murayama S, Murakami J, Yabuuchi H, et al. "Crazy-paving appearance" on high resolution CT in various diseases.** *J Comput Assist Tomogr* 1999;23:749-752.
55. Johkoh T, Itoh H, Müller NL, et al. Crazy-paving appearance at thin-section CT: spectrum of disease and pathologic findings. *Radiology* 1999;211:155-160.
56. Lynch DA, Webb WR, Gamsu G, et al. Computed tomography in pulmonary sarcoidosis. *J Comput Assist Tomogr* 1989;13:405-410.
57. Remy-Jardin M, Beuscart R, Sault MC, et al. Subpleural micronodules in diffuse infiltrative lung diseases: evaluation with thin-section CT scans. *Radiology* 1990;177:133-139.
58. Remy-Jardin M, Degreeef JM, Beuscart R, et al. Coal worker's pneumoconiosis: CT assessment in exposed workers and correlation with radiographic findings. *Radiology* 1990;177:363-371.
59. Pickford HA, Swensen SJ, Utz JP. Thoracic cross-sectional imaging of amyloidosis. *AJR Am J Roentgenol* 1997;168:351-355.

60. Murata K, Khan A, Herman PG. Pulmonary parenchymal disease: evaluation with high-resolution CT. *Radiology* 1989;170:629-635.
61. Johkoh T, Müller NL, Ichikado K, et al. Perilobular pulmonary opacities: high-resolution CT findings and pathologic correlation. *J Thorac Imaging* 1999;14:172-177.
62. Primack SL, Hartman TE, Hansell DM, et al. End-stage lung disease: CT findings in 61 patients. *Radiology* 1993;189:681-686.
63. Aberle DR, Gamsu G, Ray CS. High-resolution CT of benign asbestos-related diseases: clinical and radiographic correlation. *AJR Am J Roentgenol* 1988;151:883-891.
64. Lynch DA, Gamsu G, Ray CS, et al. Asbestos-related focal lung masses: manifestations on conventional and high-resolution CT scans. *Radiology* 1988;169:603-607.
65. Im JG, Itoh H, Shim YS, et al. Pulmonary tuberculosis: CT findings—early active disease and sequential change with antituberculous therapy. *Radiology* 1993;186:653-660.
66. Colby TV, Swensen SJ. Anatomic distribution and histopathologic patterns in diffuse lung disease: correlation with HRCT. *J Thorac Imag* 1996;11:1-26.
67. Johkoh T, Müller NL, Cartier Y, et al. Idiopathic interstitial pneumonias: diagnostic accuracy of thin-section CT in 129 patients. *Radiology* 1999;211:555-560.
68. Park JS, Lee KS, Kim JS, et al. Nonspecific interstitial pneumonia with fibrosis: radiographic and CT findings in seven patients. *Radiology* 1995;195:645-648.
69. Kim EY, Lee KS, Chung MP, et al. Nonspecific interstitial pneumonia with fibrosis: serial high-resolution CT findings with functional correlation. *AJR Am J Roentgenol* 1999;173:949-953.

70. Genereux GP. The end-stage lung: pathogenesis, pathology, and radiology. *Radiology* 1975;116:279-289.
71. Desai SR, Wells AU, Rubens MB, et al. Acute respiratory distress syndrome: CT abnormalities at long-term follow-up. *Radiology* 1999;210:29-35.
72. Remy-Jardin M, Giraud F, Remy J, et al. Importance of ground-glass attenuation in chronic diffuse infiltrative lung disease: pathologic-CT correlation. *Radiology* 1993;189:693-698.
73. Wells AU, Hansell DM, Rubens MB, et al. The predictive value of appearances of thin-section computed tomography in fibrosing alveolitis. *Am Rev Respir Dis* 1993;148:1076-1082.
74. Tung KT, Wells AU, Rubens MB, et al. Accuracy of the typical computed tomographic appearances of fibrosing alveolitis. *Thorax* 1993;48:334-338.
75. Al-Jarad N, Strickland B, Pearson MC, et al. High-resolution computed tomographic assessment of asbestosis and cryptogenic fibrosing alveolitis: a comparative study. *Thorax* 1992;47:645-650.
76. Mathieson JR, Mayo JR, Staples CA, et al. Chronic diffuse infiltrative lung disease: comparison of diagnostic accuracy of CT and chest radiography. *Radiology* 1989;171:111-116.
77. Grenier P, Valeyre D, Cluzel P, et al. Chronic diffuse interstitial lung disease: diagnostic value of chest radiography and high-resolution CT. *Radiology* 1991;179:123-132.
78. Padley SPG, Hansell DM, Flower CDR, et al. Comparative accuracy of high resolution computed tomography and chest radiography in the diagnosis of chronic diffuse infiltrative lung disease. *Clin Radiol* 1991;44:222-226.

79. Nishimura K, Izumi T, Kitaichi M, et al. The diagnostic accuracy of high-resolution computed tomography in diffuse infiltrative lung diseases. *Chest* 1993;104:1149-1155.

P.189

80. Swensen SJ, Aughenbaugh GL, Myers JL. Diffuse lung disease: diagnostic accuracy of CT in patients undergoing surgical biopsy of the lung. *Radiology* 1997;205:229-234.

81. Yoshimura H, Hatakeyama M, Otsuji H, et al. Pulmonary asbestosis: CT study of subpleural curvilinear shadow. Work in progress. *Radiology* 1986;158:653-658.

82. Schurawitzki H, Stiglbauer R, Graninger W, et al. Interstitial lung disease in progressive systemic sclerosis: high-resolution CT versus radiography. *Radiology* 1990;176:755-759.

83. Swensen SJ, Aughenbaugh GL, Douglas WW, et al. High-resolution CT of the lungs: findings in various pulmonary diseases. *AJR Am J Roentgenol* 1992;158:971-979.

84. Morimoto S, Takeuchi N, Imanaka H, et al. Gravity dependent atelectasis: radiologic, physiologic and pathologic correlation in rabbits on high-frequency ventilation. *Invest Radiol* 1989;24:522-530.

85. Kubota H, Hosoya T, Kato M, et al. Plate-like atelectasis at the corticomedullary junction of the lung: CT observation and hypothesis. *Radiat Med* 1983;1:305-310.

86. Remy-Jardin M, Remy J, Deffontaines C, et al. Assessment of diffuse infiltrative lung disease: comparison of conventional CT and high-resolution CT. *Radiology* 1991;181:157-162.

87. Lee KS, Im JG. CT in adults with tuberculosis of the chest: characteristic findings and role in management. *AJR Am J Roentgenol* 1995;164:1361-1367.
88. Im JG, Itoh H, Han MC. CT of pulmonary tuberculosis. *Semin Ultrasound CT MR* 1995;16:420-434.
89. Hong SH, Im JG, Lee JS, et al. High resolution CT findings of miliary tuberculosis. *J Comput Assist Tomogr* 1998;22:220-224.
90. Brauner MW, Grenier P, Mompoin D, et al. Pulmonary sarcoidosis: evaluation with high-resolution CT. *Radiology* 1989;172:467-471.
91. Nakata H, Kimoto T, Nakayama T, et al. Diffuse peripheral lung disease: evaluation by high-resolution computed tomography. *Radiology* 1985;157:181-185.
92. Brauner MW, Grenier P, Mouelhi MM, et al. Pulmonary histiocytosis X: evaluation with high resolution CT. *Radiology* 1989;172:255-258.
93. Moore AD, Godwin JD, Müller NL, et al. Pulmonary histiocytosis X: comparison of radiographic and CT findings. *Radiology* 1989;172:249-254.
94. Bergin CJ, Müller NL, Vedal S, et al. CT in silicosis: correlation with plain films and pulmonary function tests. *AJR Am J Roentgenol* 1986;146:477-483.
95. Akira M, Higashihara T, Yokoyama K, et al. Radiographic type p pneumoconiosis: high-resolution CT. *Radiology* 1989;171:117-123.
96. Hruban RH, Meziane MA, Zerhouni EA, et al. High resolution computed tomography of inflation fixed lungs: pathologic-radiologic correlation of centrilobular emphysema. *Am Rev Respir Dis* 1987;136:935-940.

97. Nishimura K, Itoh H, Kitaichi M, et al. Pulmonary sarcoidosis: correlation of CT and histopathologic findings. *Radiology* 1993;189:105-109.
98. Brauner MW, Lenoir S, Grenier P, et al. Pulmonary sarcoidosis: CT assessment of lesion reversibility. *Radiology* 1992;182:349-354.
99. Bergin CJ, Bell DY, Coblentz CL, et al. Sarcoidosis: correlation of pulmonary parenchymal pattern at CT with results of pulmonary function tests. *Radiology* 1989;171:619-624.
100. Bégin R, Bergeron D, Samson L, et al. CT assessment of silicosis in exposed workers. *AJR Am J Roentgenol* 1987;148:509-514.
101. Bergin CJ, Müller NL. CT of interstitial lung disease: a diagnostic approach. *AJR Am J Roentgenol* 1987;148:9-15.
102. Naidich DP, Zerhouni EA, Hutchins GM, et al. Computed tomography of the pulmonary parenchyma: part 1. Distal airspace disease. *J Thorac Imaging* 1985;1:39-53.
103. Itoh H, Tokunaga S, Asamoto H, et al. Radiologic-pathologic correlations of small lung nodules with special reference to peribronchiolar nodules. *AJR Am J Roentgenol* 1978;130:223-231.
104. Murata K, Herman PG, Khan A, et al. Intralobular distribution of oleic acid-induced pulmonary edema in the pig: evaluation by high-resolution CT. *Invest Radiol* 1989;24:647-653.
105. Gruden JF, Webb WR, Naidich DP, et al. Multinodular disease: anatomic localization at thin-section CT: multireader evaluation of a simple algorithm. *Radiology* 1999;210:711-720.

106. Lee KS, Kim TS, Han J, et al. Diffuse micronodular lung disease: HRCT and pathologic findings. *J Comput Assist Tomogr* 1999;23:99-106.
107. Gruden JF, Webb WR, Warnock M. Centrilobular opacities in the lung on high-resolution CT: diagnostic considerations and pathologic correlation. *AJR Am J Roentgenol* 1994;162:569-574.
108. Remy-Jardin M, Remy J, Boulenguez C, et al. Morphologic effects of cigarette smoking on airways and pulmonary parenchyma in healthy adult volunteers: CT evaluation and correlation with pulmonary function tests. *Radiology* 1993;186:107-115.
109. Remy-Jardin M, Remy J, Gosselin B, et al. Lung parenchymal changes secondary to cigarette smoking: pathologic-CT correlations. *Radiology* 1993;186:643-651.
110. Liebow AA, Carrington CB. Diffuse pulmonary lymphoreticular infiltration associated with dysproteinemia. *Med Clin North Am* 1973;57:809-843.
111. Steimlam CV, Rosenow EC, Divertie MB, et al. Pulmonary manifestations of Sjögren's syndrome. *Chest* 1976;70:354-361.
112. Joshi VV, Oleske JM, Minnefor AB, et al. Pathologic pulmonary findings in children with the acquired immunodeficiency syndrome. *Hum Pathol* 1985;16:241-246.
113. Grieco MH, Chinoy-Acharya P. Lymphoid interstitial pneumonia associated with the acquired immune deficiency syndrome. *Am Rev Respir Dis* 1985;131:952-955.
114. Honda O, Johkoh T, Ichikado K, et al. Differential diagnosis of lymphocytic interstitial pneumonia and malignant lymphoma on high-resolution CT. *AJR Am J Roentgenol* 1999;173:71-74.

115. Murata K, Takahashi M, Mori M, et al. Pulmonary metastatic nodules: CT-pathologic correlation. *Radiology* 1992;182:331-335.
116. Kim JS, Ryu CW, Lee SI, et al. High-resolution CT findings of varicella-zoster pneumonia. *AJR Am J Roentgenol* 1999;172:113-116.
117. Lee KS, Kim YH, Kim WS, et al. Endobronchial tuberculosis: CT features. *J Comput Assist Tomogr* 1991;15:424-428.
118. Hartman TE, Swensen SJ, Williams DE. Mycobacterium avium-intracellulare complex: evaluation with CT. *Radiology* 1993;187:23-26.
119. Swensen SJ, Hartman TE, Williams DE. Computed tomography in diagnosis of Mycobacterium avium-intracellulare complex in patients with bronchiectasis. *Chest* 1994;105:49-52.
120. McGuinness G, Gruden JF, Bhalla M, et al. AIDS-related airway disease. *AJR Am J Roentgenol* 1997;168:67-77.
121. Seely JM, Effmann EL, Müller NL. High-resolution CT of pediatric lung disease: imaging findings. *AJR Am J Roentgenol* 1997;168: 1269-1275.
122. Logan PM, Primack SL, Miller RR, et al. Invasive aspergillosis of the airways: radiographic, CT, and pathologic findings. *Radiology* 1994;193:383-388.
123. Müller NL, Miller RR. Diseases of the bronchioles: CT and histopathologic findings. *Radiology* 1995;196:3-12.
124. Lynch DA, Brasch RC, Hardy KA, et al. Pediatric pulmonary disease: assessment with high-resolution ultrafast CT. *Radiology* 1990;176: 243-248.
125. Webb WR. High-resolution computed tomography of obstructive lung disease. *Rad Clin N Am* 1994;32:745-757.

126. Akira M, Kitatani F, Lee Y-S, et al. Diffuse panbronchiolitis: evaluation with high-resolution CT. *Radiology* 1988;168:433-438.
127. Nishimura K, Kitaichi M, Izumi T, et al. Diffuse panbronchiolitis: correlation of high-resolution CT and pathologic findings. *Radiology* 1992;184:779-785.
128. Akira M, Higashihara T, Sakatani M, et al. Diffuse panbronchiolitis: follow-up CT examination. *Radiology* 1993;189:559-562.
129. Ward S, Heyneman L, Lee MJ, et al. Accuracy of CT in the diagnosis of allergic bronchopulmonary aspergillosis in asthmatic patients. *AJR Am J Roentgenol* 1999;173:937-942.
130. Silver SF, Müller NL, Miller RR, et al. Hypersensitivity pneumonitis: evaluation with CT. *Radiology* 1989;173:441-445.
131. Lynch DA, Rose CS, Way D, et al. Hypersensitivity pneumonitis: sensitivity of high-resolution CT in a population-based study. *AJR Am J Roentgenol* 1992;159:469-472.
132. Akira M, Kita N, Higashihara T, et al. Summer-type hypersensitivity pneumonitis: comparison of high-resolution CT and plain radiographic findings. *AJR Am J Roentgenol* 1992;158:1223-1228.
133. Remy-Jardin M, Remy J, Wallaert B, et al. Subacute and chronic bird breeder hypersensitivity pneumonitis: sequential evaluation with CT and correlation with lung function tests and bronchoalveolar lavage. *Radiology* 1993;198:111-118.

134. Müller NL, Staples CA, Miller RR. Bronchiolitis obliterans organizing pneumonia: CT features in 14 patients. *AJR Am J Roentgenol* 1990;154:983-987.
135. Leung AN, Miller RR, Müller NL. Parenchymal opacification in chronic infiltrative lung diseases: CT-pathologic correlation. *Radiology* 1993;188:209-214.
136. Collins J, Blankenbaker D, Stern EJ. CT patterns of bronchiolar disease: what is tree-in-bud? *AJR Am J Roentgenol* 1998;171:365-370.
137. Aquino SL, Gamsu G, Webb WR, et al. Tree-in-bud pattern: frequency and significance on thin section CT. *J Comput Assist Tomogr* 1996;20:594-599.
138. Gruden JF, Webb WR. CT findings in a proved case of respiratory bronchiolitis. *AJR Am J Roentgenol* 1993;161:44-46.
139. Holt RM, Schmidt RA, Godwin JD, et al. High resolution CT in respiratory bronchiolitis-associated interstitial lung disease. *J Comput Assist Tomogr* 1993;17:46-50.
140. Heyneman LE, Ward S, Lynch DA, et al. Respiratory bronchiolitis, respiratory bronchiolitis-associated interstitial pneumonia: different entities or part of the spectrum of the same disease process? *AJR Am J Roentgenol* 1999;173:1617-1622.
141. Akira M, Yokoyama K, Yamamoto S, et al. Early asbestosis: evaluation with high-resolution CT. *Radiology* 1991;178:409-416.
142. Howling SJ, Hansell DM, Wells AU, et al. Follicular bronchiolitis: thin-section CT and histologic findings. *Radiology* 1999;212:637-642.
143. Remy-Jardin M, Remy J, Wallaert B, et al. Pulmonary involvement in progressive systemic sclerosis: sequential

- evaluation with CT, pulmonary function tests, and bronchoalveolar lavage. *Radiology* 1993;188:499-506.
144. Remy-Jardin M, Remy J, Cortet B, et al. Lung changes in rheumatoid arthritis: CT findings. *Radiology* 1994;193:375-382.
145. Gruden JF, Webb WR, Sides DM. Adult-onset disseminated tracheobronchial papillomatosis: CT features. *J Comput Assist Tomogr* 1994;18:640-642.
146. Akira M, Atagi S, Kawahara M, et al. High-resolution CT findings of diffuse bronchioloalveolar carcinoma in 38 patients. *AJR Am J Roentgenol* 1999;173:1623-1629.
147. Padley SPG, Adler BD, Staples CA, et al. Pulmonary talcosis: CT findings in three cases. *Radiology* 1993;186:125-127.
148. Connolly B, Manson D, Eberhard A, et al. CT appearance of pulmonary vasculitis in children. *AJR Am J Roentgenol* 1996;167:901-904.
149. Primack SL, Miller RR, Müller NL. Diffuse pulmonary hemorrhage: clinical, pathologic, and imaging features. *AJR Am J Roentgenol* 1995;164:295-300.
150. Johkoh T, Ikezoe J, Nagareda T, et al. Metastatic pulmonary calcification: early detection by high-resolution CT. *J Comput Assist Tomogr* 1993;17:471-473.
151. Hartman TE, Müller NL, Primack SL, et al. Metastatic pulmonary calcification in patients with hypercalcemia: findings on chest radiographs and CT scans. *AJR Am J Roentgenol* 1994;162:799-802.
152. Nolan RL, McAdams HP, Sporn TA, et al. Pulmonary cholesterol granulomas in patients with pulmonary artery hypertension: chest radiographic and CT findings. *AJR Am J Roentgenol* 1999;172:1317-1319.

153. Dufour B, Maitre S, Humbert M, et al. High-resolution CT of the chest in four patients with pulmonary capillary hemangiomas or pulmonary venoocclusive disease. *AJR Am J Roentgenol* 1998;171: 1321-1324.
154. Gruden JF, Webb WR. Identification and evaluation of centrilobular opacities on high-resolution CT. *Semin Ultrasound CT MR* 1995;16: 435-449.
155. Reid L, Simon G. The peripheral pattern in the normal bronchogram and its relation to peripheral pulmonary anatomy. *Thorax* 1958;13: 103-109.
156. Gruden JF, Huang L, Turner J, et al. High-resolution CT in the evaluation of clinically suspected *Pneumocystis carinii* pneumonia in AIDS patients with normal, equivocal, or nonspecific radiographic findings. *AJR Am J Roentgenol* 1997;169: 967-975.
157. Tuddenham WJ. Glossary of terms for thoracic radiology: recommendations of the Nomenclature Committee of the Fleischner Society. *AJR Am J Roentgenol* 1984;143: 509-517.
158. Davis SD. CT evaluation for pulmonary metastases in patients with extrathoracic malignancy. *Radiology* 1991;180: 1-12.
159. Diederich S, Semik M, Lentschig MG, et al. Helical CT of pulmonary nodules in patients with extrathoracic malignancy: CT-surgical correlation. *AJR Am J Roentgenol* 1999;172: 353-360.
160. McCulloch GL, Sinnatamby R, Stewart S, et al. High-resolution computed tomographic appearance of MALToma of the lung. *Eur Radiol* 1998;8: 1669-1673.
161. Lewis ER, Caskey CI, Fishman EK. Lymphoma of the lung: CT findings in 31 patients. *AJR Am J Roentgenol* 1991;156: 711-714.

162. Collins J, Müller NL, Leung AN, et al. Epstein-Barr-virus-associated lymphoproliferative disease of the lung: CT and histologic findings. *Radiology* 1998;208:749-759.
163. Rappaport DC, Chamberlain DW, Shepherd FA, Hutcheon MA. Lymphoproliferative disorders after lung transplantation: imaging features. *Radiology* 1998;206:519-524.
164. Akira M, Yamamoto S, Sakatani M. Bronchiolitis obliterans organizing pneumonia manifesting as multiple large nodules or masses. *AJR Am J Roentgenol* 1998;170:291-295.
165. Hoffman GS, Kerr GS, Leavitt RY, et al. Wegener granulomatosis: an analysis of 158 patients. *Ann Intern Med* 1992;116:488-498.
166. Aberle DR, Gamsu G, Lynch D. Thoracic manifestations of Wegener granulomatosis: diagnosis and course. *Radiology* 1990;174: 703-709.
167. Weir IH, Müller NL, Chiles C, et al. Wegener's granulomatosis: findings from computed tomography of the chest in 10 patients. *Can Assoc Radiol J* 1992;43:31-34.
168. Foo SS, Weisbrod GL, Herman SJ, et al. Wegener granulomatosis presenting on CT with atypical bronchovascular distribution. *J Comput Assist Tomogr* 1990;14:1004-1006.
169. Worthy SA, Müller NL, Hansell DM, et al. Churg-Strauss syndrome: the spectrum of pulmonary CT findings in 17 patients. *AJR Am J Roentgenol* 1998;170:297-300.
170. Utz JP, Swensen SJ, Gertz MA. Pulmonary amyloidosis. The Mayo Clinic experience from 1980 to 1993. *Ann Intern Med* 1996;124:407-413.

171. Mori M, Galvin JR, Barloon TJ, et al. Fungal pulmonary infections after bone marrow transplantation: evaluation with radiography and CT. *Radiology* 1991;178:721-726.
172. Kuhlman JE, Fishman EK, Burch PA, et al. Invasive pulmonary aspergillosis in acute leukemia: the contribution of CT to early diagnosis and aggressive management. *Chest* 1987;92:95-99.
173. Gaeta M, Volta S, Stroschio S, et al. **CT "halo sign" in pulmonary tuberculoma.** *J Comput Assist Tomogr* 1992;16:827-828.
174. Primack SL, Hartman TE, Lee KS, et al. Pulmonary nodules and the CT halo sign. *Radiology* 1994;190:513-515.
175. Won HJ, Lee KS, Cheon JE, et al. Invasive pulmonary aspergillosis: prediction at thin-section CT in patients with neutropenia: a prospective study. *Radiology* 1998;208:777-782.
176. Doyle TC, Lawler GA. CT features of rounded atelectasis of the lung. *AJR Am J Roentgenol* 1984;143:225-228.
177. Ren H, Hruban RH, Kuhlman JE, et al. Computed tomography of rounded atelectasis. *J Comput Assist Tomogr* 1988;12:1031-1034.
178. McHugh K, Blaquiere RM. CT features of rounded atelectasis. *AJR Am J Roentgenol* 1989;153:257-260.
179. Müller NL, Staples CA, Miller RR, et al. Disease activity in idiopathic pulmonary fibrosis: CT and pathologic correlation. *Radiology* 1987;165:731-734.
180. Engeler CE, Tashjian JH, Trenkner SW, et al. Ground-glass opacity of the lung parenchyma: a guide to analysis with high-resolution CT. *AJR Am J Roentgenol* 1993;160:249-251.

181. Remy-Jardin M, Remy J, Giraud F, et al. Computed tomography assessment of ground-glass opacity: semiology and significance. *J Thorac Imag* 1993;8:249-264.
182. Wells AU, Hansell DM, Corrin B, et al. High resolution computed tomography as a predictor of lung histology in systemic sclerosis. *Thorax* 1992;47:508-512.
183. Wells AU, Rubens MB, du Bois RM, et al. Serial CT in fibrosing alveolitis: prognostic significance of the initial pattern. *AJR Am J Roentgenol* 1993;161:1159-1165.
184. Ikezoe J, Takashima S, Morimoto S, et al. CT appearance of acute radiation-induced injury in the lung. *AJR Am J Roentgenol* 1988;150:765-770.
185. Primack SL, Hartman TE, Ikezoe J, et al. Acute interstitial pneumonia: radiographic and CT findings in nine patients. *Radiology* 1993;188:817-820.
186. Bergin CJ, Wirth RL, Berry GJ, et al. *Pneumocystis carinii* pneumonia: CT and HRCT observations. *J Comput Assist Tomogr* 1990;14:756-759.

P.191

187. Moskovic E, Miller R, Pearson M. High resolution computed tomography of *Pneumocystis carinii* pneumonia in AIDS. *Clin Radiol* 1990;42:239-243.
188. Graham NJ, Müller NL, Miller RR, et al. Intrathoracic complications following allogeneic bone marrow transplantation: CT findings. *Radiology* 1991;181:153-156.
189. McGuinness G, Scholes JV, Garay SM, et al. Cytomegalovirus pneumonitis: spectrum of parenchymal CT findings with pathologic correlation in 21 AIDS patients. *Radiology* 1994;192:451-459.

190. Reittner P, Müller NL, Heyneman L, et al. Mycoplasma pneumoniae pneumonia: radiographic and high-resolution CT features in 28 patients. *AJR Am J Roentgenol* 1999;174:37-41.
191. Cheon JE, Lee KS, Jung GS, et al. Acute eosinophilic pneumonia: radiographic and CT findings in six patients. *AJR Am J Roentgenol* 1996;167:1195-1199.
192. Ikezoe J, Morimoto S, Takashima S, et al. Acute radiation-induced pulmonary injury: computed tomographic evaluation. *Semin Ultrasound CT MR* 1990;11:409-416.
193. Hartman TE, Primack SL, Swensen SJ, et al. Desquamative interstitial pneumonia: thin-section CT findings in 22 patients. *Radiology* 1993;187:787-790.
194. Franquet T, Giménez A, Bordes R, et al. The crazy-paving pattern in exogenous lipoid pneumonia: CT-pathologic correlation. *AJR Am J Roentgenol* 1998;170:315-317.
195. Tan RT, Kuzo RS. High-resolution CT findings of mucinous bronchioloalveolar carcinoma: a case of pseudopulmonary alveolar proteinosis. *AJR Am J Roentgenol* 1997;168:99-100.
196. Murdoch J, Müller NL. Pulmonary sarcoidosis: changes on follow-up CT examinations. *AJR Am J Roentgenol* 1992;159:473-477.
197. Hommeyer SH, Godwin JD, Takasugi JE. Computed tomography of airspace disease. *Radiol Clin North Am* 1991;29:1065-1084.
198. Nishimura K, Itoh H. High-resolution computed tomographic features of bronchiolitis obliterans organizing pneumonia. *Chest* 1992;102:26S-31S.

199. Müller NL, Miller RR. Ground-glass attenuation, nodules, alveolitis, and sarcoid granulomas (editorial). *Radiology* 1993;189:31-32.
200. Lee JS, Im JG, Ahn JM, et al. Fibrosing alveolitis: prognostic implication of ground-glass attenuation at high-resolution CT. *Radiology* 1992;184:415-454.
201. Akira M, Sakatani M, Ueda E. Idiopathic pulmonary fibrosis: progression of honeycombing at thin-section CT. *Radiology* 1993;189:687-691.
202. Terriff BA, Kwan SY, Chan-Yeung MM, et al. Fibrosing alveolitis: chest radiography and CT as predictors of clinical and functional impairment at follow-up in 26 patients. *Radiology* 1992;184:445-449.
203. Bouchardy LM, Kuhlman JE, Ball WC, et al. CT findings in bronchiolitis obliterans organizing pneumonia (BOOP) with radiographic, clinical, and histologic correlation. *J Comput Assist Tomogr* 1993;17:352-357.
204. Mayo JR, Müller NL, Road J, et al. Chronic eosinophilic pneumonia: CT findings in six cases. *AJR Am J Roentgenol* 1989;153:727-730.
205. Bourgouin P, Cousineau G, Lemire P, et al. Differentiation of radiation-induced fibrosis from recurrent pulmonary neoplasm by CT. *Can Assoc Radiol J* 1987;38:23-26.
206. Libshitz HI, Shuman LS. Radiation-induced pulmonary change: CT findings. *J Comput Assist Tomogr* 1984;8:15-19.
207. Kuhlman JE. The role of chest computed tomography in the diagnosis of drug-related reactions. *J Thorac Imaging* 1991;6(1):52-61.
208. Hamrick-Turner J, Abbitt PL, et al. Diffuse lung calcification following fat emboli and adult respiratory

distress syndromes: CT findings. *J Thorac Imag* 1994;9:47-50.

209. Gevenois PA, Abehsera M, Knoop C, et al. Disseminated pulmonary ossification in end-stage pulmonary fibrosis: CT demonstration. *AJR Am J Roentgenol* 1994;162:1303-1304.

210. Kuhlman JE, Ren H, Hutchins GM, Fishman EK. Fulminant pulmonary calcification complicating renal transplantation: CT demonstration. *Radiology* 1989;173:459-460.

211. Cluzel P, Grenier P, Bernadac P, et al. Pulmonary alveolar microlithiasis: CT findings. *J Comput Assist Tomogr* 1991;15:938-942.

212. Korn MA, Schurawitzki H, Klepetko W, et al. Pulmonary alveolar microlithiasis: findings on high-resolution CT. *AJR Am J Roentgenol* 1992;158:981-982.

213. Helbich TH, Wojnarovsky C, Wunderbaldinger P, et al. Pulmonary alveolar microlithiasis in children: radiographic and high-resolution CT findings. *AJR Am J Roentgenol* 1997;168:63-65.

214. Kuhlman JE, Teigen C, Ren H, et al. Amiodarone pulmonary toxicity: CT findings in symptomatic patients. *Radiology* 1990;177:121-125.

215. Akira M. Uncommon pneumoconioses: CT and pathologic findings. *Radiology* 1995;197:403-409.

216. Naidich DP. High-resolution computed tomography of cystic lung disease. *Semin Roentgenol* 1991;26:151-174.

217. Hogg JC. Benjamin Felson lecture. Chronic interstitial lung disease of unknown cause: a new classification based on pathogenesis. *AJR Am J Roentgenol* 1991;156:225-233.

218. Aquino SL, Webb WR, Zaloudek CJ, et al. Lung cysts associated with honeycombing: change in size on expiratory CT scans. *AJR Am J Roentgenol* 1994;162:583-584.

219. Worthy SA, Brown MJ, Müller NL. Technical report: Cystic airspaces in the lung: change in size on expiratory high-resolution CT in 23 patients. *Clin Radiol* 1998;53:515-519.
220. Lenoir S, Grenier P, Brauner MW, et al. Pulmonary lymphangiomyomatosis and tuberous sclerosis: comparison of radiographic and thin-section CT findings. *Radiology* 1990;175:329-334.
221. Templeton PA, McCloud TC, Müller NL, et al. Pulmonary lymphangiomyomatosis: CT and pathologic findings. *J Comput Assist Tomogr* 1989;13:54-57.
222. Sherrier RH, Chiles C, Roggli V. Pulmonary lymphangiomyomatosis: CT findings. *AJR Am J Roentgenol* 1989;153:937-940.
223. Rappaport DC, Weisbrod GL, Herman SJ, et al. Pulmonary lymphangiomyomatosis: high-resolution CT findings in four cases. *AJR Am J Roentgenol* 1989;152:961-964.
224. Müller NL, Chiles C, Kullnig P. Pulmonary lymphangiomyomatosis: correlation of CT with radiographic and functional findings. *Radiology* 1990;175:335-339.
225. Desai SR, Nicholson AG, Stewart S, et al. Benign pulmonary lymphocytic infiltration and amyloidosis: computed tomographic and pathologic features in three cases. *J Thorac Imaging* 1997;12:215-220.
226. Sanders C, Nath PH, Bailey WC. Detection of emphysema with computed tomography: correlation with pulmonary function tests and chest radiography. *Invest Radiol* 1988;23:262-266.
227. **Müller NL, Staples CA, Miller RR, et al. "Density mask": an objective method to quantitate emphysema using computed tomography. *Chest* 1988;94:782-787.**

228. Miller RR, Müller NL, Vedal S, et al. Limitations of computed tomography in the assessment of emphysema. *Am Rev Respir Dis* 1989;139:980-983.
229. Kinsella N, Müller NL, Vedal S, et al. Emphysema in silicosis: a comparison of smokers with nonsmokers using pulmonary function testing and computed tomography. *Am Rev Respir Dis* 1990;141:1497-1500.
230. Stern EJ, Webb WR, Weinacker A, et al. Idiopathic giant bullous emphysema (vanishing lung syndrome): imaging findings in nine patients. *AJR Am J Roentgenol* 1994;162:279-282.
231. Feuerstein I, Archer A, Pluda JM, et al. Thin-walled cavities, cysts, and pneumothorax in *Pneumocystis carinii* pneumonia: further observations with histopathologic correlation. *Radiology* 1990;174:697-702.
232. Panicek DM. Cystic pulmonary lesions in patients with AIDS [editorial]. *Radiology* 1989;173:12-14.
233. Gurney JW, Bates FT. Pulmonary cystic disease: comparison of *Pneumocystis carinii* pneumatoceles and bullous emphysema due to intravenous drug abuse. *Radiology* 1989;173:27-31.
234. Grenier P, Cordeau MP, Beigelman C. High-resolution computed tomography of the airways. *J Thorac Imag* 1993;8:213-229.
235. Lynch DA, Newell JD, Tschomper BA, et al. Uncomplicated asthma in adults: comparison of CT appearance of the lungs in asthmatic and healthy subjects. *Radiology* 1993;188:829-833.
236. Kim JS, Müller NL, Park CS, et al. Cylindrical bronchiectasis: diagnostic findings on thin-section CT. *AJR Am J Roentgenol* 1997;168:751-754.

237. Kang EY, Miller RR, Müller NL. Bronchiectasis: comparison of preoperative thin-section CT and pathologic findings in resected specimens. *Radiology* 1995;195:649-654.
238. Marti-Bonmati L, Ruiz PF, Catala F, et al. CT findings in Swyer-James syndrome. *Radiology* 1989;172:477-480.
239. Martin KW, Sagel SS, Siegel BA. Mosaic oligemia simulating pulmonary infiltrates on CT. *AJR Am J Roentgenol* 1986;147:670-673.
240. Worthy SA, Park CS, Kim JS, et al. Bronchiolitis obliterans after lung transplantation: high resolution CT findings in 15 patients. *AJR Am J Roentgenol* 1997;169:673-677.

P.192

241. Arakawa H, Webb WR. Expiratory high-resolution CT scan. *Radiol Clin North Am* 1998;36:189-209.
242. Webb WR. Radiology of obstructive pulmonary disease. *AJR Am J Roentgenol* 1997;169:637-647.
243. King MA, Bergin CJ, Yeung DWC, et al. Chronic pulmonary thromboembolism: detection of regional hypoperfusion with CT. *Radiology* 1994;191:359-363.
244. Schwickert HC, Schweden F, Schild HH, et al. Pulmonary arteries and lung parenchyma in chronic pulmonary embolism: preoperative and postoperative CT findings. *Radiology* 1994;191:351-357.
245. Im JG, Kim SH, Chung MJ, et al. Lobular low attenuation of the lung parenchyma on CT: evaluation of forty-eight patients. *J Comput Assist Tomogr* 1996;20:756-762.

246. Arakawa H, Webb WR, McCowin M, et al. Inhomogeneous lung attenuation at thin-section CT: diagnostic value of expiratory scans. *Radiology* 1998;206:89-94.
247. Worthy SA, Müller NL, Hartman TE, et al. Mosaic attenuation pattern on thin-section CT scans of the lung: differentiation among infiltrative lung, airway, and vascular diseases as a cause. *Radiology* 1997;205:465-470.
248. Bergin CJ, Rios G, King MA, et al. Accuracy of high-resolution CT in identifying chronic pulmonary thromboembolic disease. *AJR Am J Roentgenol* 1996;166:1371-1377.
249. Sherrick AD, Swensen SJ, Hartman TE. Mosaic pattern of lung attenuation on CT scans: frequency among patients with pulmonary artery hypertension of different causes. *AJR Am J Roentgenol* 1997;169:79-82.
250. Franquet T, Giménez A, Monill JM, et al. Primary Sjögren's syndrome and associated lung disease: CT findings in 50 patients. *AJR Am J Roentgenol* 1997;169:655-658.
251. Stern EJ, Swensen SJ, Hartman TE, et al. CT mosaic pattern of lung attenuation: distinguishing different causes. *AJR Am J Roentgenol* 1995;165:813-816.
252. Stern EJ, Webb WR. Dynamic imaging of lung morphology with ultrafast high-resolution computed tomography. *J Thorac Imag* 1993;8:273-282.
253. Stern EJ, Webb WR, Gamsu G. Dynamic quantitative computed tomography: a predictor of pulmonary function in obstructive lung diseases. *Invest Radiol* 1994;29:564-569.
254. Chen D, Webb WR, Storto ML, et al. Assessment of air trapping using postexpiratory high-resolution computed tomography. *J Thorac Imaging* 1998;13:135-143.

255. Lucidarme O, Coche E, Cluzel P, et al. Expiratory CT scans for chronic airway disease: correlation with pulmonary function test results. *AJR Am J Roentgenol* 1998;170:301-307.
256. Chung MH, Edinburgh KJ, Webb EM, et al. Mixed infiltrative and obstructive disease on high-resolution CT: differential diagnosis and functional correlates in a consecutive series. *Society of Thoracic Radiology*, 1998.
257. Arakawa H, Webb WR. Air trapping on expiratory high-resolution CT scans in the absence of inspiratory scan abnormalities: correlation with pulmonary function tests and differential diagnosis. *AJR Am J Roentgenol* 1998;170:1349-1353.
258. Hansell DM, Milne DG, Wilsher ML, et al. Pulmonary sarcoidosis: morphologic associations of airflow obstruction at thin-section CT. *Radiology* 1998;209:697-704.
259. Hansell DM, Wells AU, Padley SP, et al. Hypersensitivity pneumonitis: correlation of individual CT patterns with functional abnormalities. *Radiology* 1996;199:123-128.
260. Knudson RJ, Standen JR, Kaltenborn WT, et al. Expiratory computed tomography for assessment of suspected pulmonary emphysema. *Chest* 1991;99:1357-1366.
261. Kitahara Y, Takamoto M, Maruyama M, et al. Differential diagnosis of pulmonary emphysema using the CT index: LL% (in Japanese). *Nippon Kyobu Shikkan Gakkai Zasshi* 1989;27:689-695.
262. Newman KB, Lynch DA, Newman LS, et al. Quantitative computed tomography detects air trapping due to asthma. *Chest* 1994;106:105-109.

263. Park CS, Müller NL, Worthy SA, et al. Airway obstruction in asthmatic and healthy individuals: inspiratory and expiratory thin-section CT findings. *Radiology* 1997;203:361-367.
264. Lynch DA. Imaging of asthma and allergic bronchopulmonary mycosis. *Rad Clin N Amer* 1998;36:129-142.
265. Garg K, Newell JD, King TE, et al. Proliferative and constrictive bronchiolitis: classification and radiologic features. *AJR Am J Roentgenol* 1994;162:803-808.
266. Padley SPG, Adler BD, Hansell DM, et al. Bronchiolitis obliterans: high-resolution CT findings and correlation with pulmonary function tests. *Clin Radiol* 1993;47:236-240.
267. Moore ADA, Godwin JD, Dietrich PA, et al. Swyer-James syndrome: CT findings in eight patients. *AJR Am J Roentgenol* 1992;158:1211-1215.
268. Sweatman MC, Millar AB, Strickland B, et al. Computed tomography in adult obliterative bronchiolitis. *Clin Radiol* 1990;41:116-119.
269. Aquino SL, Webb WR, Golden J. Bronchiolitis obliterans associated with rheumatoid arthritis: findings on HRCT and dynamic expiratory CT. *J Comput Assist Tomogr* 1994;18:555-558.
270. Leung AN, Fisher K, Valentine V, et al. Bronchiolitis obliterans after lung transplantation: detection using expiratory HRCT. *Chest* 1998;113:365-370.
271. Yang CF, Wu MT, Chiang AA, et al. Correlation of high-resolution CT and pulmonary function in bronchiolitis obliterans: a study based on 24 patients associated with consumption of *Sauropus Androgynus*. *AJR Am J Roentgenol* 1997;168:1045-1050.

272. Stern EJ, Webb WR, Golden JA, et al. Cystic lung disease associated with eosinophilic granuloma and tuberous sclerosis: air trapping at dynamic ultrafast high-resolution CT. *Radiology* 1992;182:325-329.
273. Hansell DM, Wells AU, Rubens MB, et al. Bronchiectasis: functional significance of areas of decreased attenuation at expiratory CT. *Radiology* 1994;193:369-374.
274. Gelman M, King MA, Neal DE, et al. Focal air trapping in patients with HIV infection: CT evaluation and correlation with pulmonary function test results. *AJR Am J Roentgenol* 1999;172:1033-1038.
275. Small JH, Flower CD, Traill ZC, et al. Air-trapping in extrinsic allergic alveolitis on computed tomography. *Clin Radiol* 1996;51:684-688.
276. Gleeson FV, Traill ZC, Hansell DM. Evidence of expiratory CT scans of small-airway obstruction in sarcoidosis. *AJR Am J Roentgenol* 1996;166:1052-1054.
277. Ringertz HG, Brasch RC, Gooding CA, et al. Quantitative density-time measurements in the lungs of children with suspected airway obstruction using ultrafast CT. *Pediatr Radiol* 1989;19:366-370.
278. Webb WR, Stern EJ, Kanth N, et al. Dynamic pulmonary CT: findings in normal adult men. *Radiology* 1993;186:117-124.
279. Gevenois PA, Scillia P, de Maertelaer V, et al. The effects of age, sex, lung size, and hyperinflation on CT lung densitometry. *AJR Am J Roentgenol* 1996;167:1169-1173.
280. Adams H, Bernard MS, McConnochie K. An appraisal of CT pulmonary density mapping in normal subjects. *Clin Radiol* 1991;43:238-242.
281. Ng CS, Desai SR, Rubens MB, et al. Visual quantitation and observer variation of signs of small airways disease at

inspiratory and expiratory CT. *J Thorac Imaging* 1999;14:279-285.

282. Lee KW, Chung SY, Yang I, et al. Correlation of aging and smoking with air trapping at thin-section CT of the lung in asymptomatic subjects. *Radiology* 2000;214:831-836.

283. Robinson PJ, Kreel L. Pulmonary tissue attenuation with computed tomography: comparison of inspiration and expiration scans. *J Comput Assist Tomogr* 1979;3:740-748.

284. Gurney JW. Cross-sectional physiology of the lung. *Radiology* 1991;178:1-10.

285. Grenier P, Chevret S, Beigelman C, et al. Chronic diffuse infiltrative lung disease: determination of the diagnostic value of clinical data, chest radiography, and CT with Bayesian analysis. *Radiology* 1994;191:383-390.

286. Gurney JW, Schroeder BA. Upper lobe disease: physiological correlates. *Radiology* 1988;167:359-366.

Rheumatoid Arthritis and Lung Disease: From Mechanisms to a Practical Approach

Fiona Lake, MD, FRACP¹ Susanna Proudman, MB, BS, FRACP²

¹School of Medicine and Pharmacology, SCGH Unit, University of Western Australia, Nedlands, Western Australia, Australia

²Rheumatology Unit, Royal Adelaide Hospital, The University of Adelaide, Adelaide, South Australia, Australia

Address for correspondence Fiona Lake, MD, FRACP, School of Medicine and Pharmacology, SCGH Unit, University of Western Australia, QEII Medical Centre, 6 Verdun Street, Nedlands, WA 6009, M503, Australia (e-mail: Fiona.Lake@uwa.edu.au).

Semin Respir Crit Care Med 2014;35:222–238.

Abstract

Rheumatoid arthritis (RA) is a common chronic systemic autoimmune disease characterized by joint inflammation and, in a proportion of patients, extra-articular manifestations (EAM). Lung disease, either as an EAM of the disease, related to the drug therapy for RA, or related to comorbid conditions, is the second commonest cause of mortality. All areas of the lung including the pleura, airways, parenchyma, and vasculature may be involved, with interstitial and pleural disease and infection being the most common problems. High-resolution computed tomography of the chest forms the basis of investigation and when combined with clinical information and measures of physiology, a multidisciplinary team can frequently establish the diagnosis without the need for an invasive biopsy procedure. The most frequent patterns of interstitial lung disease (ILD) are usual interstitial pneumonia (UIP) and nonspecific interstitial pneumonia (NSIP), with some evidence for the prognosis being better than for the idiopathic equivalents. Risk factors depend on the type of disease but for ILD (mainly UIP and NSIP) include smoking, male gender, human leukocyte antigen haplotype, rheumatoid factor, and anticitrullinated protein antibodies (ACPAs). Citrullination of proteins in the lung, frequently thought to be incited by smoking, and the subsequent development of ACPA appear to play an important role in the development of lung and possibly joint disease. The biologic and nonbiological disease modifying antirheumatic drugs (DMARDs) have had a substantial impact on morbidity and mortality from RA, and although there multiple reports of drug-related lung toxicity and possible exacerbation of underlying ILD, overall these reactions are rare and should only preclude the use of DMARDs in a minority of patients. Common scenarios facing pulmonologists and rheumatologists are addressed using the current best evidence; these include screening the new patient; monitoring and choosing RA treatment in the presence of subclinical disease; treating deteriorating ILD; and establishing a diagnosis in a patient with an acute respiratory presentation.

Keywords

- ▶ rheumatoid arthritis
- ▶ lung
- ▶ interstitial
- ▶ drug induced
- ▶ anticitrullinated protein antibodies
- ▶ biologic disease modifying antirheumatic drugs
- ▶ prognosis

Rheumatoid arthritis (RA), a systemic autoimmune process characterized by a chronic symmetrical erosive synovitis, is frequently progressive and results in significant disability, especially if treatment is delayed.¹ In addition to articular disease, multiple other organ systems may be involved, with extra-articular manifestations (EAM) in the heart and vascu-

lar system, lungs, skin, and eyes, contributing to the excess morbidity and mortality of patients with RA.^{2,3} The lung and pleura are frequently involved and contribute to 10 to 20% of overall mortality.^{2–7} The type of involvement is very varied and can precede the development of joint symptoms or diagnosis of RA.^{7–9} With improvements in imaging of the

lung, we now have a better understanding of the amount, severity, and type of lung and pleural disease that occurs in patients with RA. Recent findings provide fascinating insights into the pathogenesis of lung disease and how it may relate to the development of RA. The role of antibodies to specific citrullinated proteins in the diagnosis of early RA, as markers of RA-associated interstitial lung disease (ILD) and in the pathogenesis of both lung and joint disease is intriguing and may offer new options for detection, monitoring, and therapy.¹⁰ Second, despite the availability of highly sensitive tools such as the high-resolution computed tomography (HRCT), the questions of which pleuropulmonary abnormalities are important, how screening and monitoring should be performed, and whether treatment directed at the RA should be modified because of the presence of subclinical or clinically apparent lung abnormalities is not clear.^{3,4,11,12} Outcome from the interplay between lung disease and the new biological disease modifying antirheumatic drugs (bDMARDs) used to treat joint disease is unclear^{11,13,14} and hence the risk versus benefit of bDMARDs in an individual patient with pulmonary EAM is uncertain.¹¹ Systematic reviews, however, suggest concerns about pulmonary complications with the use of DMARDs in patients with RA may be overstated.¹¹ This review will outline the breadth of lung involvement in patients with RA, but focus on the commonest forms in terms of pathogenesis, treatment, and uncertainties as outlined earlier. Interstitial, pleural, airway, and vascular disease and infection are either the most common or the most difficult to manage lung problems in patients with RA. Drug-induced lung disease is of importance and may complicate the management of patients with RA.^{15,16} On the basis of this review, we aim to provide a guide as to how to approach patients with possible lung involvement, whether as a rheumatologist managing someone presenting with predominately joint disease, or as a pulmonologist needing to determine the type, significance, and management of lung disease.

Overview of Lung Involvement in Rheumatoid Arthritis

Prevalence and Type of Lung Disease

Almost all components of the respiratory system have been shown to have the potential to be abnormal in patients with RA. These changes appear to be a result of the systemic inflammatory process in RA, as evidenced by the frequency, temporal relationship, pathogenesis, and pathology^{2,3,16}; or arise as a result of the treatment used for RA^{13,14,16–18}; or comorbidities that involve the lung.^{19,20}

Abnormalities involve the following:

- Pleura^{21,22}
- Airways—upper and lower, large and small airways²³
- Parenchyma with ILD and nodules^{3,4,13,16}
- Vasculature²⁴
- Infection related to RA or immunosuppressive therapy¹⁷
- Drug-related lung disease secondary to treatment of RA, for example, with DMARDs^{11,16,25,26}

- Comorbid medical conditions such as venous thromboembolism^{27,28} and lung cancer.^{19,29}

The specific conditions associated with RA are shown in **Table 1**, which summarizes their importance and impact on patients.

In general, patients with RA have an increased standardized mortality rate, which is higher in hospital cohorts when compared with inception cohorts and higher with increased age, male gender, presence of comorbidities, higher activity of joint disease, and presence of EAM of RA.^{4–6} In an inception cohort of 1,429 people with symptoms of < 2 years, there were 459 deaths during 18 years of follow-up.⁵ The greatest cause of early mortality was cardiovascular death (31%), but lung problems were the next biggest contributor (29%).⁵ Lung problems with significant mortality include infection (12% overall deaths), ILD (4%), and lung cancer (7%).⁵ Some forms of lung involvement, such as obliterative bronchiolitis, are rare but associated with a high mortality.^{2,44} In terms of morbidity, significant contributors are infection, ILD, pleural disease, and drug-related reactions.^{3,4}

It is difficult to confirm the exact prevalence of the different types of RA-associated respiratory disease but it can vary widely, with ILD, for example, ranging from 5 to 60% in various reports. Differences in prevalence are seen between autopsy, hospital, and community-based studies.^{46–51} Studies contain heterogeneous populations with differences in proportions with early or late stage disease, severity of disease, treatment, the method used to detect pulmonary abnormalities, sensitivity of equipment, expertise of those interpreting the tests used, and how “abnormal” is defined. The prevalence is undoubtedly influenced by smoking rates, other diseases in the community, genetic, and environmental factors.^{2,3,16} Most published studies have used multifaceted assessment, but some tests are consistently better at detecting abnormalities than others. In a study of 36 patients with new onset RA, abnormalities consistent with ILD were found in 58% of patients (physiology 22%, chest X-ray [CXR] 6%, HRCT 33%, bronchoalveolar lavage [BAL] 52%, 99mTc-DTPA [technetium-99m diethylenetriamine pentaacetic acid] radionuclide scan 15%).⁴⁶ Despite all these abnormalities, only 14% were felt to have clinically significant ILD. Similarly, a large number of patients with RA have pleural abnormalities on HRCT, but a minority of patients have clinically troublesome disease.⁵² Tests may be complementary, reflecting different aspects of structure or function. As much disease is subclinical and progression varied,^{6,9} the significance of many of these abnormalities in terms of future morbidity and mortality is not clear and in the absence of validated prognostic indicators, it is the complete clinical picture, with the combination of symptoms and structural and functional abnormalities in terms of both presence, severity, and change over time,⁵⁵ which helps determine the importance of any one finding and the need for intervention.

Risk Factors for Lung Disease

Understanding risk factors for pulmonary EAM in patients with RA has led to insights into pathogenesis and may provide

Table 1 Frequency and impact of EAM in the lung in patients with RA^a

	Frequency	Impact if present
Pleural ^{21,22,30–34}		
Pleuritis	++	++
Effusion ^a	++	++
Pleural thickening	+++	+
Other—unexpandable lung, empyema, chyloform effusion, ^b pneumothorax, ^b hemothorax, ^b pyopneumothorax, ^b bronchopleural fistula ^b	+	+++
Airway ^{2,23,35–42}		
Upper—cricothyroid immobility with vocal cord abnormality, cord nodules, recurrent laryngeal, or vagus nerve vasculitis and cord paralysis	+	++
Lower		
Airflow obstruction	++	+
Obliterative bronchiolitis	+	+++
Bronchiectasis ⁴³	+	+
Parenchymal ^{3,4,8,9,12,13,44–48}		
Interstitial lung disease	+++	+ +++
Apical fibrosis and Caplan syndrome	+	+
Nodules	+++	+
Vascular ^{24,49–51}		
Pulmonary hypertension	+	+++
Vasculitis	+	+++
Musculoskeletal related ^{3,18}		
Chest wall immobility and respiratory failure	+	+
Infection ^{17,52–54}		
Related to RA	+	+
Related to treatment	++	++
Treatment related ^{13–17,25,26}		
Pneumonitis	++	+++
Pleuritis/effusion (methotrexate, infliximab, adalimumab)	+	+
Increased risk ^{19,27–29}		
Lung cancer	+	+++
Pulmonary thromboembolism	+	++

Abbreviations: EAM, extra-articular manifestation; RA, rheumatoid arthritis.

^a+ (infrequent or unimportant) to +++ (frequent or important).

^bMay be associated with a ruptured nodule.

guidance for screening and surveillance. Although RA is more prevalent in females, in most but not all studies,⁴⁵ males more commonly developed ILD^{44,56} and nodules.⁵⁷ The findings with respect to smoking are mixed with evidence that current or previous smoking is a risk factor for ILD⁵⁸ (odds ratio [OR] 3.8 for > 25 pack years),⁵⁹ although some studies have reported no association.⁶⁰ It is important to note RA-ILD can occur in nonsmokers.³⁹ The severity and duration of joint disease is associated with the presence of both airflow

obstruction and ILD,⁵¹ and older age with ILD.⁶¹ The shared epitope human leukocyte antigen (HLA)-DRB1 allele is associated with ILD⁶² and in other studies, HLA-DRB1*1502 with ILD (relative risk [RR] ratio = 4.02; $p = 0.013$) but not airways disease (RR ratio = 0.15; $p = 0.08$).⁶¹ Rheumatoid factor is associated with a low diffusing capacity for carbon monoxide (DLCO),^{47,61} anticitrullinated protein antibodies (ACPAs) with ILD⁶³ and airways disease,⁶¹ and antibodies against anticitrullinated Hsp90 α/β with ILD.⁶⁴

Anticitrullinated Peptide Antibodies and Pathogenesis of Rheumatoid Arthritis

The role of ACPAs in joint inflammation and EAMs of RA has been a focus of much research over the last decade.¹⁰ Citrullination is a posttranslational modification of proteins by the enzymes peptidyl arginine deaminase-1 and -2 (PAD-1 and -2), in which arginine is converted to citrulline, thereby changing the tertiary structure and charge of the protein, increasing its immunogenicity. Several diseases have been associated with abnormal citrullination of peptides, including psoriasis, multiple sclerosis, and idiopathic pulmonary fibrosis (IPF).^{10,63} In RA, a range of synovial proteins, including vimentin, filaggrin, and fibronectin, can become citrullinated and incite an antibody response. Antibodies to citrullinated peptides are quite specific for RA and may play a role in the disease process. Furthermore, citrullinated peptides are found within the lungs of patients with RA, especially in smokers where citrullination is triggered in the context of smoking-induced inflammation.⁶² This is one mechanism by which smoking is a risk factor for RA. The early commercial assay for ACPAs was an enzyme-linked immunosorbent assay which used various filaggrin epitopes. The second, improved assay uses cyclic epitopes that mimic true conformational epitopes, which were selected from libraries of citrullinated peptides. This widely available commercial kit (second-generation anticyclic citrullinated peptide2 assay [anti-CCP2]) has been shown to have a moderate sensitivity (approximately 65%) and high specificity (approximately 95%) for RA.⁶⁵

ACPAs could contribute to synovial inflammation through the deposition of immune complexes and targeting of synovial antigens. With regard to the lungs and ACPAs, there are several interesting observations. First, a range of interstitial and airway abnormalities were documented in a group of patients with ACPAs in the absence of clinical or serological evidence of RA or other connective tissue disorders (CTD).⁶⁶ Over time, joint inflammation did develop in a small number of these patients, demonstrating that generation of ACPAs can precede the development of joint disease.⁶⁶ In patients diagnosed with RA by clinical and serological methods, ACPAs have been associated with a variety of lung abnormalities including a low DLCO,⁴⁷ ILD,^{61,63,64,67} bronchial wall thickening,⁴⁷ airflow obstruction,⁶¹ and nodules.^{47,63} Mori et al found high levels of ACPAs associated with RA-related airways disease (RR, 3.8; $p < 0.005$) and less so with RA-ILD (RR, 2.7; $p < 0.07$).⁶¹

The strength of these associations may be influenced by the type of ACPA measured. In recent work looking at ACPAs identified in the serum using a “reverse immunophenotyping” approach, Harlow et al demonstrated that a specific ACPA, against citrullinated Hsp90 has a high specificity (> 95%) and moderate sensitivity (20–30%) for RA-ILD relative to RA without lung disease or IPF.⁶⁴ In another study of 177 patients with RA, ACPAs were measured with both the anti-CCP2 commercial kit and by using a range of specific ACPAs that had been identified in previous studies. They found that RA-ILD was associated with both higher levels and a greater number of specific ACPAs than RA without ILD.⁶⁷ It is possible that an association between specific ACPAs and lung disease is

hidden when the broad range, rather than specific ACPAs, is studied.

The interaction between smoking, the lungs, and RA is intriguing. Smoking increases pulmonary PAD-2 and is also a recognized risk factor for airways disease and idiopathic and RA-related ILD. Citrullinated proteins are found in the BAL of smokers but not in nonsmokers.⁶² ACPAs have been identified in the lungs of smokers, with elevated levels in the BAL and airways. Willis et al identified ACPAs in the sputum of a group of patients at risk for RA (based on family history) in the absence of seropositivity, which along with increased ACPA to total immunoglobulin (Ig) ratios in sputa, supports the lung being the site of autoantibody generation in the early development of RA.⁶⁸ It is possible immune responses to citrullinated proteins may occur and indeed start in the lung. Clearly, this is not the whole answer as RA-ILD can occur in nonsmokers.⁶⁹

At this stage, apart from their use in the diagnosis of RA, these antibodies remain in the research domain. However, this work raises the possibility that specific antibodies may help predict ILD as an EAM in RA, as is seen in the anti-synthetase syndrome where anti-Jo-1 is strongly predictive of ILD in the inflammatory myopathies.¹⁰

Interstitial Lung Disease in Rheumatoid Arthritis

Importance and Clinical Presentation

ILD is the most important pulmonary manifestation of rheumatoid disease, being the commonest pulmonary cause of death in RA and a significant contributor to morbidity.^{5–7,70,71} An autopsy study of 81 patients with longstanding RA noted that 16% died of respiratory failure, while 34% had evidence of ILD.⁷⁰ In a large inception cohort in the United Kingdom followed for 18 years, excess mortality was seen for pulmonary disease overall (18%) and specifically ILD (4%).⁶ Apart from the clinical consequences of ILD, the presence of either clinically overt or subclinical ILD may influence the choice of DMARDs although it should be noted that the majority of patients with RA are not troubled by lung disease.

The clinical presentation and disease spectrum of RA-ILD are generally similar to that of the idiopathic interstitial pneumonias (IIPs)⁷² although differences have been noted in the pathology.⁷³ The classification of the idiopathic forms is regularly updated with progressive teasing apart of previously combined categories (cellular and fibrotic nonspecific interstitial pneumonia [NSIP]) and the addition of newly recognized IIP,^{74,75} but all recommendations emphasize that the diagnosis is best made through multidisciplinary discussion (MDD) between pulmonologists, radiologists, and pathologists.^{75,76} Castellino et al has emphasized the need for rheumatologists and pulmonologists to work together to enhance the accuracy of disease classification.⁷⁷ In a study of 50 patients referred with ILD, reclassification from idiopathic to CTD-associated ILD (CTD-ILD), or CTD-ILD to a different form of ILD occurred in a significant number (54%), with changes in therapy occurring in the majority of patients with CTD-ILD (84%). For those patients with

supposed idiopathic ILD, a number with predominately usual interstitial pneumonia (UIP) pattern, on review were reclassified as having an autoimmune featured-ILD, with manifestations of an undifferentiated CTD.⁷⁸ As ILD can predate the development of joint or serological manifestations,⁷⁻⁹ supported by the finding that 21 of 603 patients in a population cohort had ILD diagnosed before the appearance of RA,⁷ ongoing monitoring of presumed idiopathic ILD is warranted and ACPA measurement should form part of the screen for patients presenting with what appears to be idiopathic ILD.

For a patient with RA, an acute respiratory presentation may represent acute interstitial pneumonia (AIP), an exacerbation of ILD (with known or previously unknown pre-existing disease), infection in an immunosuppressed host, a drug reaction, or a mixture of these. The differential diagnosis needs to remain broad, with a range of investigations covering the possibilities being included (see section "Approach to Patients with RA-ILD") and discussions should be held within a multidisciplinary team.³ Diagnosis is based on clinical presentation, blood gases, and pulmonary function tests, if the latter can be performed, and HRCT scan, blood tests, sputum, possibly BAL, and very occasionally, a lung biopsy. Bronchoscopy and BAL are primarily useful in the exclusion of infection or diagnosis of other diffuse lung diseases (e.g., sarcoidosis, drug reaction). Nuclear imaging with gallium scans or DTPA scans do not have a useful role. With regard to a biopsy, transbronchial biopsies (TBBs) may be diagnostic with organizing pneumonia (OP) or confirm infection (fungal) but for most other possibilities are inadequate for diagnosis. Old HRCTs, including abdominal films, where upper slices may include the lung bases, are invaluable in determining if there is longstanding disease.

In the patient with RA presenting with chronic respiratory symptoms or the asymptomatic patient with RA, a range of interstitial patterns may be present. Modalities used to look for

disease vary in sensitivity and frequently detect changes which may not be clinically significant. Of 36 patients with early rheumatoid disease, 33% had a DLCO < 80% of predicted, but only 14% had symptoms.⁴⁴ It is the clinical picture with symptoms and crackles⁷⁹ and changes on HRCT, backed by a restrictive pattern on physiology, that are the key for confirming the type and significance of ILD, with the majority with significant disease showing abnormalities on all measures.

The common pathological and HRCT patterns of RA-associated ILD are shown in ► **Table 2**. These changes vary in terms of prevalence, prognosis, and histology but based on histological and HRCT-based studies, UIP and NSIP are the most common patterns found (44–56 and 33–44%, respectively), followed by mixed disease (0–12%).^{80,81} OP and AIP are seen less commonly (0–11%),^{82–84} and lymphocytic interstitial pneumonia (LIP) and desquamative interstitial pneumonia (DIP) are rare.^{3,4,18,56,80,81,90} Most studies of prognosis are likely to include patients with a mix of UIP and NSIP, making recommendations for a specific pattern difficult. A poor prognosis is associated with more extensive fibrosis or worsening of the extent of disease on HRCT, although reliable techniques which minimize interobserver variation are still being developed^{91–94} with the aim of better prediction of outcome. Goh et al have proposed a simple system classifying disease as extensive (> 30% of lungs affected) or limited (< 10% of lungs affected), with the significance in indeterminate category (10–30%) being determined by the forced vital capacity (FVC), with values > 70% suggesting limited disease. A recent study showed traction bronchiectasis and honeycombing were related to mortality in CTD-ILD, and interobserver agreement was greatest for traction bronchiectasis.^{95,96} The importance of asymptomatic changes will be discussed later.

Physiological abnormalities include a reduction in lung volumes, with total lung capacity (TLC) and FVC, a low DLCO, and oxygen desaturation during a 6-minute walk test

Table 2 Clinicopathological subtypes of RA-associated ILD^{3,4,7,16,18,72,75,80–90}

	Prevalence ^a	Prognosis	Radiological pattern	Histological pattern
Usual interstitial pneumonia	+++	Poor	Subpleural, basal predominance, reticular abnormality, honeycombing with or without traction bronchiectasis, absence of inconsistent features	Subpleural and paraseptal interstitial fibrosis, fibroblastic foci, architectural distortion with honeycombing, temporal heterogeneity, patchy involvement
Nonspecific interstitial pneumonia	+++	Intermediate to good	Bilateral ground glass change may have traction bronchiectasis and bronchiolectasis	Ground glass opacification (cellular) through to interstitial fibrosis (fibrotic) without honeycombing, uniform process
Organizing pneumonia	++	Good	Patchy peripheral consolidation, subpleural and peribronchial, often migratory	Intraluminal organization in alveolar ducts, occasionally alveoli and bronchioles with preservation of background lung tissues; variable interstitial inflammation
Acute interstitial pneumonia/DAD	+	Poor	Patchy ground glass changes with basal consolidation, rapid progression	Acute DAD with edema and hyaline membranes.

Abbreviations: DAD, diffuse alveolar damage; ILD, interstitial lung disease; RA, rheumatoid arthritis.

^aPrevalence + (rarest) to +++ (commonest).

(6MWT).^{3,4,15,55} Both DLCO and desaturation with walking can be influenced by the coexistence of emphysema or pulmonary hypertension.⁵⁵ A low DLCO is the measure best associated with the extent of disease in ILDs and a poorer prognosis in RA-ILD and FVC alone is not useful for predicting prognosis in ILD. Dawson et al found that a low DLCO was an indicator of a poor prognosis, with 80% of patients whose disease progressed having a DLCO less than 54%, and 93% of patients whose disease did not progress had a DLCO greater than 54% (i.e., 80% sensitivity and 93% specificity).⁴⁵ Desaturation < 88% is associated with a worse prognosis in ILD and is useful for guiding need for oxygen therapy or referral for transplantation. In terms of monitoring disease, comprehensive tests rather than FVC should be measured to increase the accuracy.⁵⁵ A significant fall would be accepted as a decrease in DLCO by 15% and FVC by 10% from baseline values. If abnormalities are present, initial monitoring should be 3 to 6 monthly, then yearly if stable.⁵⁵

The importance of investigations, in particular the HRCT and physiological assessment, is in determining the type of lung disease, the severity, and the change over time. It is extremely important to determine what type of underlying ILD is present in the IIPs because of differing prognoses and treatment,⁹⁵ but the importance of determining the subtype of ILD in RA is less clear. As in the IIPs, when the radiological picture is not classical, the diagnosis can be inaccurate when compared with histology.^{74,96,97} One report in RA noted a UIP-like picture on HRCT but NSIP on histology, but this is uncommon.⁹⁸

Outcomes in RA-ILD

Bongartz et al found in a longitudinal study that the 10, 20, and 30 years cumulative incidence of definite and probable ILD in patients with RA was 3.5, 6.3, and 7.7%, respectively, with a lifetime risk of 10%, suggesting disease can develop or progress late in the disease process.⁷ Dawson et al noted 34% of patients with RA-ILD progressed⁴⁵ and Kim et al noted those with a definite UIP pattern on HRCT had a worse prognosis.⁹⁰ Hakala showed hospitalization was not common among patients with RA-ILD (one case per 3,500 patient-years), but those hospitalized for ILD had a median survival of only 3.5 years.⁹⁸ Solomon et al retrospectively reviewed 48 patients with RA-ILD proven on biopsy, 31% of them having UIP. Age and fibrosis predicted a poor outcome.⁹⁹

In a retrospective review of 84 patients with RA-UIP who were monitored for 33 months, Song et al found respiratory abnormalities remained stable over that period in 50%, progressed in 30%, deteriorated with an acute exacerbation in 17%, and improved in 6%. A high TLC predicted stability.⁹⁷ Importantly, the stable group remained stable for a median of 45 months. Tsuchiya et al used HRCT and where available, pathology to retrospectively review outcome in 144 patients with RA-ILD, according to pathological patterns.¹⁰⁰ As expected the poorest prognosis was in those with diffuse alveolar damage (20.0% 5-year survival), followed by UIP (36.6%), OP (60.0%), bronchiectasis (87.1%), and bronchiolitis (88.9%), with the best prognosis in the patients with NSIP (93.8%). Importantly, diagnosis of NSIP was based on HRCT

findings of predominant bibasilar ground-glass attenuation with limited reticulation and absent honeycombing.

Studies on the outcomes in RA-related UIP, NSIP, or unclassifiable patterns compared with the idiopathic forms, although not sufficiently powered to provide robust conclusions, suggest a better prognosis with RA than in IIP, including with a range of immunosuppressive therapies.^{94,96,99-101} In one case-control study comparing 18 patients with RA-ILD versus 18 patients with IPF, the median survival was greater for patients with RA-ILD (60 vs. 27 months).⁸⁵ In a study of 86 patients with RA-ILD and 872 with IPF, survival was similar between the two groups.⁸⁷ Song et al reported a retrospective study where the prognosis of RA-UIP was significantly better than IPF, after matching for age, sex, smoking, and baseline lung function, with a median survival of 53 versus 41 months, respectively ($p = 0.015$).⁹⁷ Although the evidence is mixed, it does suggest that a substantial number of patients with RA-ILD have abnormalities that do not progress and a better outcome with RA-ILD than IPF.¹⁰⁰⁻¹⁰³ These findings hold when the subgroup of RA-UIP is compared with IPF. Studies also show much heterogeneity in progression among patients, irrespective of the pathological picture.⁸⁰⁻⁹⁴

In view of the variability in outcomes, combined with significant comorbidities in patients with RA, unlike in the IIPs, a surgical lung biopsy is usually not sought. As will be discussed, a more pragmatic approach to diagnosis is tending to be taken and prognosis and need for treatment is guided more by the extent of disease on HRCT, severity of physiology impairment, and rate of progression determined during a period of observation, than histology.¹⁰³ This approach may change with information from better longitudinal studies regarding the clinical course and response to treatment with the different histological subtypes.

Treatment of RA-ILD

With regard to treatment, the evidence is of low quality or absent. Nondrug treatment to be considered includes education, psychological support, and exercise rehabilitation, the latter used in IPF, but in patients with RA is likely to be limited by joint disease. There are no randomized controlled trials for drug treatment of RA-ILD. The limited data come from series or case reports, or small trials, the most recent with rituximab, which was inconclusive.

In general, the approach to treatment is based on evidence from the IIPs, where OP is usually very responsive to glucocorticoids and treatment would be given, NSIP somewhat responsive, and treatment given especially if features suggested a nonfibrotic type, and UIP is poorly responsive and drug treatment would be avoided unless given as part of a clinical trial. In the retrospective study of Song et al, 41% of patients with RA-UIP were treated due to poor initial lung function or progression of the disease. Treatment was with high-dose corticosteroids combined with azathioprine, cyclophosphamide, or cyclosporine and median follow-up of 33 months.⁹⁷ Of the patients, 50% improved or had stable lung function and there was no difference in outcome between the treated and untreated groups, despite worse starting lung function in the treated group. Predictors of poor outcome

were age, low FVC, and a decrease in DLCO over time. This study was not prospective, randomized, or controlled but would suggest either the outlook with treatment is better in RA-UIP than IPF, or the clinical diagnosis of RA-UIP is not accurate and the group probably includes patients with RA-NSIP, shown to have a better prognosis and response to treatment.

Approach to Patients with RA-ILD

How does this translate into practical advice for the clinician? An approach taken by Ryerson et al with unclassifiable ILDs was to categorize disease by behavior, taking into account independent predictors of survival with low DLCO and high radiological fibrosis score from the HRCT.¹⁰³ To quote Cottin, in an editorial linked to the article of Ryerson et al,¹⁰⁴ the classification as “self-limited, reversible, stable, or progressive and irreversible (with and without the potential for long-term stabilisation with therapy) may help to adapt treatment goals and the monitoring strategy.” The approach is used in recent guidelines on IIPs and can be usefully applied to RA-ILD with heterogeneous outcomes, infrequent pathological confirmation, and little data to guide treatment other than on clinical behavior.⁷² An adaptation of the approach for RA-ILD, incorporating drug-induced lung problems, is shown in ▶Table 3. Using this as a guide, the treatment for drug reactions and RA-OP is relatively clear. For the many forms of RA-ILD, we would recommend the following be considered, in deciding whether or not to treat with drugs:

- MDD to confirm the diagnosis and review severity of ILD based on extent of fibrosis on HRCT and DLCO (< 54%).
- Unless severe symptomatic disease, monitor comprehensive lung function (spirometry, lung volumes, DLCO, and

6MWT) for 3 to 6 months if initial measurements are abnormal.

- Consider potential impact (positive or negative) of drugs required for joint disease (DMARDs) and monitor lung function during therapy.¹⁰⁵
- Consider treatment if extensive disease (extent of fibrosis on HRCT > 30%, DLCO < 54%, desaturation with exercise), deteriorating (decrease from baseline in FVC by 10% or DLCO by 15%) or very symptomatic.
- Review age and comorbidities (obesity, osteoporosis, cardiovascular disease, infection risk, diabetes, coexisting lung disease such as chronic obstructive pulmonary disease [COPD]).
- Determine patient’s informed wish.

Treatment may be considered, irrespective of whether the pattern of ILD is UIP or NSIP, if disease is clinically significant (symptoms, severity of abnormalities), progressive and if the patient is younger, has minimal comorbidities, and is keen for treatment.

There are no randomized controlled trials for the treatment of RA-ILD. There are reports of the benefits of prednisolone/azathioprine, prednisolone/cyclophosphamide, cyclophosphamide, azathioprine, hydroxychloroquine, d-penicillamine, and cyclosporine,^{3,4,18,94,97,106–108} but there are no data as yet on N-acetyl cysteine or pirfenidone, although a study of the former is underway. Outcome was poorer when methotrexate (MTX) was part of therapy. In acute severe disease, pulsed intravenous methylprednisolone is recommended. There are reports of bDMARDs resulting in an improvement in ILD; however, as discussed later, reports have also documented rapid, occasionally fatal progression of lung disease and the development of new ILD.

Table 3 RA-associated interstitial pneumonias: classification according to disease behavior, adapted from Travis et al,⁷² classification for the idiopathic interstitial pneumonias^a

Clinical behavior	Treatment and treatment goal	Monitoring strategy
Potentially reversible with risk of irreversible disease (e.g., cases of drug-related lung disease in RA)	Remove cause, treat to obtain a response to reverse changes	Short-term (3–6 mo) observation to confirm disease regression, or occasionally need for palliation
Reversible disease with risk of progression (e.g., RA-cellular NSIP and some RA-fibrotic NSIP, RA-OP)	Treat to initially achieve response and then rationalize longer term therapy	Short-term observation to confirm treatment response. Long-term observation to ensure that gains are preserved
Stable with residual disease (e.g., some RA-fibrotic NSIP, some RA-UIP)	No treatment if stable, aiming to maintain status	Long-term observation to assess disease course
Progressive, irreversible disease with potential for stabilization (e.g., some RA-fibrotic NSIP, some RA-UIP)	Consider treatment trial to stabilize	Long-term observation to assess disease course
Progressive, irreversible disease despite therapy (e.g., RA-DAD, most RA-UIP, some RA-fibrotic NSIP)	In absence of contraindications, consider treatment trial in selected patients to slow progression	Short (DAD) or long-term observation to assess disease course, and need for transplant or effective palliation

Abbreviations: DAD, diffuse alveolar damage; NSIP, nonspecific interstitial pneumonia; OP, organizing pneumonia; RA, rheumatoid arthritis; UIP, usual interstitial pneumonia.

^aBased on a diagnosis established by a multidisciplinary team and with disease behavior classification reviewed with longitudinal measurement.

If a patient fails to respond or deteriorates, different immunosuppression could be considered but if the patient is young, early referral for lung transplantation is required and for others, following extensive discussion with the patient and family, active palliation may be instituted.¹⁰⁹⁻¹¹¹ Lung transplantation is often not possible because of age, immobility, osteoporosis, and EAM. Palliative measures include oxygen, titrated to reduce the exercise-induced hypoxia, treatment for cough, reflux, and breathlessness.¹⁰⁹⁻¹¹¹

Subclinical RA-ILD and Progression

Subclinical disease is frequent and the best way to approach a patient with abnormalities but no symptoms is unclear.^{8,9,59} In practical terms, subclinical disease is when HRCT shows interstitial changes, but symptoms and other tests do not support clinically important disease. The importance of subclinical disease is that early disease can progress and there is hope that deterioration can be prevented. RA patients who were older at the time of disease onset, male and who had more severe RA, were on MTX⁵⁹ or continued to smoke were at highest risk of progression.⁶ Although these studies demonstrate progression, the majority of patients do not have problems so how aggressively patients should be monitored, with investigations such as HRCT which carry some risk with radiation, is not clear. Doyle et al have outlined an algorithm for those with idiopathic disease, but also those seen to be at higher risk, as in the setting of familial ILD and CTD-related ILD.¹² This investigating all patients with RA as they are “at risk” would result in a large number of investigations. To minimize unnecessary tests, a threshold for instigating further investigations needs to be considered. Cottin and Cordier have argued crackles may be a useful screen, which should lead to a CXR, and comprehensive lung function, as spirometry (FVC) alone may underestimate abnormalities.^{55,79} A history of smoking should lead to investigation with a CXR and spirometry (looking for airflow obstruction) in the first instance. When DMARDs, such as MTX, should be avoided in patients with subclinical ILD will be discussed in the next section.

Drug-Induced Lung Disease in Rheumatoid Arthritis

Developments in drug therapy, with earlier use of conventional nonbiologic DMARDs and bDMARDs, often in combination or with a rules-based treat-to-target strategy, has had a profound impact on the morbidity and mortality of RA.^{1,12-14} Infrequently, DMARDs have been associated with drug-related pulmonary disease with significant mortality, which needs to be considered when choosing treatment.^{112,113} The most common problems are infection (discussed elsewhere),^{16,17} diffuse interstitial processes,¹⁶ and less commonly, airway disease or the development of nodules.¹¹⁴ The risk of pneumonitis, in particular, in the presence of pre-existing lung disease, may be over-emphasized, especially in the context of the benefits of DMARDs.

Differentiating between a drug reaction, underlying RA-associated lung disease, infection, or another problem can be difficult so a careful history and clinical assessment is important.¹² The Web site, www.pneumotox.com¹¹³ provides a comprehensive collection of the published literature relating to adverse drug effects involving the lungs. **Table 4** summarizes the drugs, their reactions, and predisposing factors. However, with new drugs entering the market on a regular basis, up to date information on adverse reactions should be obtained if there is any concern.

Nonbiologic DMARDs

MTX remains the most commonly used DMARD in patients with RA and is recommended as first-line therapy. The most common noninfectious pulmonary complication is AIP, with uncommon reports of interstitial fibrosis, nodules, asthma, and air trapping.^{16,119-125} Importantly, MTX has been associated with progression of preclinical interstitial disease,⁶³ raising the issue of screening and avoidance of MTX in certain patients. However, this is a rare occurrence and with the high prevalence of minor abnormalities and the significant benefit of MTX, a decision as to whether to avoid the drug or not should be based on both the severity of the joint disease and underlying lung disease. Acute pneumonitis may be an idiosyncratic reaction, as it does not always recur on challenge with MTX. Pneumonitis can occur with low doses (< 20 mg per week), usually within 2 years but can begin early after commencement and on changing from oral to parenteral,¹²⁰ or in one case, a month after it was discontinued. In patients with RA, the overall likelihood of developing acute pneumonitis during MTX therapy is 0.3 to 11.6%.¹²⁷ A multicenter, case-control study of 29 patients and 82 controls¹²² found older age (OR, 5.1), diabetes mellitus (OR, 35.6), hypoalbuminemia (OR, 19.5), pre-existing pleural or lung involvement with RA (OR, 7.1), and smoking and use of other DMARDs, in particular penicillamine (OR, 5.6) which is rarely used now, were risk factors for MTX-induced pneumonitis. In general, patients respond to MTX withdrawal and the prognosis is usually good, although the reaction can be fatal in some cases. Uncontrolled studies suggest glucocorticoids may be important in severely ill patients. Cautious rechallenge is an option if the drug is essential for management.¹⁶ Concern over the long-term effects of MTX upon lung function have not been supported by studies and although a mild reduction in spirometry has been reported, it is not clinically important.^{12,125}

Leflunomide blocks pyrimidine synthesis in activated lymphocytes and has been associated with ILD and nodule formation, with a RR of ILD of 1.9 compared with other DMARDs,¹²⁶⁻¹²⁸ although the risk was insignificant if there was no prior diagnosis of ILD or MTX use. Similar findings were reported in a large observational study with 1.2% of patients treated with leflunomide developing new or worsening ILD. As with MTX, safe prescribing requires assessment of risk factors with severity of pre-existing lung disease being the most important factor¹²⁸ as well as smoking, low body weight, and use of a loading dose.

Table 4 Reported adverse pulmonary reactions to drugs used to treat RA

Drug group	Adverse reaction	Risk factors for adverse reaction
Anti-inflammatory drugs		
NSAID (high-dose) anti-inflammatory ^{114,115}	Eosinophilic pneumonia (naproxen)	n/a
Corticosteroids ^{116–118}	Infection	<ul style="list-style-type: none"> • Dose related • Pre-existing severe lung disease • Biologic DMARD
Nonbiologic DMARD		
MTX ^{119–125}	Pneumonitis	<ul style="list-style-type: none"> • Abnormal lungs (DLCO < 70% increased risk by 10%) • Smoking, low albumin, previous use of DMARD
Leflunomide ^{112,126–128}	Pneumonitis—ALI/DAD Nodulosis	<ul style="list-style-type: none"> • Pre-existing ILD • Previous MTX—OR, 8.17; 95% CI, 4.63–14.4 • Japanese origin
Sulphasalazine, gold, penicillamine ^{16,129}	Pneumonitis—OP and NSIP	
Biologic DMARD ^{134,135}		
TNF blockade ^{130–139} <ul style="list-style-type: none"> • Etanercept (soluble p75 TNFα receptor fusion protein) • Infliximab (dimeric anti-TNFα) • Adalimumab (anti-TNFα monoclonal antibody) • Golimumab • Certolizumab 	Infection including TB (pneumonia 0.8%) Pneumonitis—ALI/UIP/NSIP (0.6%) Noninfectious granulomatous disease New lung nodules	<ul style="list-style-type: none"> • Previous lung disease • Low body weight • Older age • Previous MTX pneumonitis • CXR and Mantoux or QuantiFERON Gold before therapy
Anakinra (IL-1 blocker) ^{140,141}	Infection	No reports of pneumonitis
Rituximab (anti-B cell monoclonal antibody) ^{141–146}	Rare—rapidly progressive, OP	
Abatacept (a selective costimulation modulator which prevents T cell CD28 binding) ¹⁴¹	Pneumonitis	
Tocilizumab (humanized anti-IL-6 receptor mAb)	Rare exacerbation of pre-existing ILD	

Abbreviations: ALI, acute lung injury; CI, confidence interval; CXR, chest X-ray; DAD, diffuse alveolar damage; IL, interleukin; NSIP, nonspecific interstitial pneumonia; OP, organizing pneumonia; OR, odds ratio; TNF α , tumor necrosis factor alpha; UIP, usual interstitial pneumonia.

Biologic DMARDs

Biological DMARDs are used second line after MTX and work in a variety of ways.^{13,14,16,24,130,131} They have been shown to improve symptoms, joint disease, and possibly lung disease in patients with RA; however, pulmonary toxicity with a high mortality has also been described.^{14–16} Overall, however, the rate of adverse reactions is low. A variety of lung toxicities are shown in **Table 4**.

Useful information comes from the many biologic registers around the world.^{130–132} The British Society for Rheumatology Biologics Register (BSRBR) prospectively collects data on all patients in the United Kingdom receiving bDMARDs (> 8,000 patients).¹⁴⁰ The OR for mortality was 4.4 times higher (95% confidence interval [CI], 1.8–10.7) for those patients with RA and pre-existing pulmonary disease who were treated with bDMARDs compared with those without pul-

monary disease,¹⁴⁰ although some case reports show an improvement in ILD with bDMARDs.¹⁰⁵ Overall, the risk is low at around 1% although the mortality with a reaction appears to be high at 35.5%.¹¹ Despite case reports, it is not clear if combination therapy, such as with MTX and leflunomide, significantly increases the risk of an adverse reaction with bDMARDs.¹¹

Use of DMARDs in the Presence of Subclinical or Clinically Apparent Lung Disease in RA

The overall risk of pneumonitis from MTX, leflunomide, or tumor necrosis factor (TNF) inhibitors has been estimated from a systematic literature review, at around 1%.¹¹ The fatality rate from the reaction is reported to be 13% with MTX, 18% with leflunomide, and 35.5% with TNF inhibitors. In recognizing the significant impact, these drugs have had on

joint disease and overall morbidity and mortality,¹ the oft recommended avoidance of these drugs in the setting of any pulmonary abnormality seems inappropriate. Important considerations are pulmonary reserve and other comorbidities, and whether the patient would tolerate the development of pneumonitis.¹¹ With significant abnormalities with symptoms, signs (crackles), and abnormal HRCT and physiology, the drugs should be avoided or used with caution, but most other patients are likely to tolerate therapy without pulmonary consequences. Patients should understand the small risk and be educated to seek early review with the development of any new pulmonary symptoms. If DMARDs are used in patients with lung disease, regular monitoring with comprehensive lung function, initially at 3 to 6, then 12-month intervals if stable, is recommended.⁵⁵ Repeat HRCT should be used if deterioration in lung function is noted.

Infection in Rheumatoid Arthritis

The reported prevalence of infection in patients with RA varies substantially among studies and although it is not clear if there is an increase in mild infections in patients with RA, several studies confirm an increase in severe infections with probably worse outcomes.^{137,139,141} Most of these studies have not reported on infection by site,¹⁴² but pulmonary infection, in particular bacterial pneumonia, is the commonest form of severe infection.^{146,147} Other forms of pulmonary infection include bronchitis, exacerbations of bronchiectasis, empyema, or infected nodules. Predisposing factors for severe infection include host defense abnormalities related to RA (e.g., premature aging of the immune system), more active disease, comorbidities (e.g., underlying lung disease, smoking, diabetes, kidney disease),^{53,54} and RA-related drug therapy.¹⁴⁷⁻¹⁵⁰ It is estimated that corticosteroids increase the risk of serious infection fourfold.¹¹⁸ Nonbiologic DMARDs such as MTX and low-dose azathioprine have not been shown to consistently increase the risk of infection,⁵⁻⁵⁴ but may delay recovery from an infection, and although there is no clear evidence, some recommend the drug should be stopped during the episode of severe infection.

Cohort studies from registries show an increased risk of infection with bDMARDs^{53,54,135,151} with suggestions TNF α inhibitors increase risk twofold. However, results from the German bDMARD registry RABBIT of TNF α inhibitors use have shown, over 3 years of observation, that the risk of severe infection fell from 4.8 to 2.2/100 patient-years.¹⁴⁷ This, in part, relates to the drop out of high-risk patients, but is likely to also relate to the bDMARD with improvement in RA with therapy resulting in better mobility and less need for corticosteroids.¹⁴⁷ In terms of disease control and reduction in corticosteroid use, the use of bDMARDs outweigh the risk of infection with these drugs.^{53,150} With respect to corticosteroids in RA, it is estimated a dose of 5 mg/d is associated with a RR for severe infection of 1.4 (95% CI, 1.2, 1.6), for 5 to 10 mg/day a RR of 1.9 (95% CI, 1.7, 2.2), and for 10 to 20 mg/day a RR of 3.0 (95% CI, 1.9, 4.7),^{23,54,119,120} so minimizing the dose should be a priority.

It is important to be aware of the possible infectious agents when caring for an individual unwell with respiratory symptoms. Many infections reflect the organisms endemic to a geographical area. From cohorts and case series treated with corticosteroids and DMARDs, both common organisms such as pneumococcus, and opportunistic infections such as *Pneumocystis jiroveci* pneumonia (PJP), cryptococcal pneumonia, invasive pulmonary aspergillosis and disseminated histoplasmosis, other fungal species, *Nocardia*, *Listeria*, and viral pneumonia caused by parainfluenza and cytomegalovirus and tuberculosis have been reported.¹⁴⁹⁻¹⁵⁷ Kameda from Japan showed, in a study of patients on bDMARDs presenting with acute onset ILD thought to be drug related, 13/26 had definite and 11/26 had probable *P. jiroveci*,¹⁵² with good outcomes with treatment.

The development of tuberculosis, with both mycobacterium tuberculosis (MTB) and nontuberculous mycobacteria (non-TBM) has been associated with bDMARDs. From the British Biologics Register, the development of MTB was greatest in those treated infliximab and adalimumab, and lowest with etanercept.¹⁴⁰ The majority of the disease was extrapulmonary (62%) with a significant number presenting with disseminated disease. Appropriate screening (history, CXR, and Interferon Gold/Mantoux) before the start of treatment has had a significant impact on the development of active TB during therapy.⁵⁸ The development of non-TBM, most commonly due to *Mycobacterium avium*, probably relates to pre-existing disease, with a range of CT abnormalities being evident before treatment commenced, from small nodular lesions, bronchial abnormalities, and bronchiectasis to alveolar abnormalities.¹⁵² Outcome for non-TBM with treatment was favorable and it has been suggested the bDMARD could be continued during treatment for the non-TBM with successful outcome for both RA and the non-TBM.^{154,155} Monitoring for at least 6 months after anti-TNF therapy is stopped is required.^{153,157}

Attempts have been made to estimate the size of the contribution each of these factors, such as severity of RA, comorbidities, and RA therapy, to infection risk,^{117,118,147-150} and to provide a guide when considering RA treatment options in any individual. For example, in patients with comorbidities such as COPD and older age, and a dose of glucocorticoids which cannot be reduced despite other therapy, the risk of bDMARDs probably outweighs the benefit. The most important measure to reduce risk appears to be minimizing the dose of corticosteroids in all patients, and selective use of other immunosuppressive drugs. Other general measures which are important are vaccination with pneumococcus and influenza vaccines,⁵³ which appear to reduce morbidity and mortality.^{146,150} The responses to pneumococcal vaccination is not significantly diminished by bDMARDs. Prophylaxis against PJP during treatment for RA is not routine but could be considered when high-dose corticosteroids (≥ 20 mg of prednisone daily for 1 month or longer) are required, especially when combined with a TNF α inhibitor or another immunosuppressive drug. When rituximab is considered, low IgG levels increase risk of infection and so levels should be measured.^{153,157}

Bronchiectasis

An association between diffuse bronchiectasis and RA (RA-BB) has been noted, but for many, the disease is not troublesome.⁴³ As with other forms of lung disease, the HRCT is a sensitive way of detecting airway abnormalities. In a study of 26 patients with extensive bronchiectasis, the delta F508 mutation of the transmembrane conductance regulator gene (*CFTR*) was seen in 15.4%, significantly higher ($p < 0.05$) when compared with patients with RA but no bronchiectasis (0%) or the general population (2.8%).¹⁵⁸ In a family study, the *CFTR* mutation cosegregated with RA-DB (sib transmission disequilibrium test = 10.82, $p = 0.005$), indicating that a mutation unrelated to RA is linked to EAMs of RA.¹⁵⁹ Treatment of symptomatic disease does not differ from bronchiectasis unrelated to RA but significant disease and ongoing infection would be a contraindication to the use of bDMARDs.

Changes in Extra-articular Lung Disease over Time and with New Therapies

There have been significant changes in the management of RA over the past 25 years and as a result the development of disabling joint disease is much less common.¹ A shift has occurred from simple symptom management, to anti-inflammatories such as corticosteroids, to the consistent and early use of DMARDs, such as MTX, and bDMARDs, alone or in combination.^{11,15} The aim with early treatment is to reduce the inflammation and structural joint damage, and this has resulted in improvement in long-term outcomes, with significantly reduced mortality and morbidity.^{13,160–163} As the EAMs of RA are related to the activity, severity, and duration of the joint disease, one would predict early treatment of joint disease, with better drugs, may reduce the incidence or severity of EAM. This predicted improvement, however, could be masked by adverse effects of the DMARDs.

Earlier longitudinal cohort studies did not show any change over time in the prevalence of severe EAM or vasculitis (up to 1995).¹⁶¹ Recently, however, several studies have shown a reduction in amyloidosis and vasculitis but not nodules or ILD. Glace et al followed 10 patients on the French AutoImmunity and Rituximab/Rheumatoid Arthritis registry, who had lung nodules found at recruitment. A significant reduction in nodule size was seen after treatment.¹⁶² However, the major focus is on ILD. As noted, there are numerous case reports or case series of the development of a variety of forms of ILD in patients with RA treated with MTX and with biological modifiers, but also reports showing substantial improvement in pre-existing lung disease with MTX and bDMARDs. In a group of 122 patients with RA, with and without lung disease before treatment, Perez-Alvarez et al found worsening or new ILD of various histological types developing after commencement of anti-TNF α agents.¹⁶³ As noted, both new and worsening of pre-existing ILD after anti-TNF therapy carried a high mortality.¹¹ Conversely, a study in 1993 of 59 patients with RA who had no pulmonary symptoms showed 18% who were taking DMARDs (MTX, chloroquine, gold, penicillamine) had abnormal histology on TBB

but 42% who were not on DMARDs had abnormal histology.¹⁶⁴

Large studies from registries,¹² including from the BSRBR, with patients with known RA-ILD on DMARDs and bDMARDs, found after adjustment for age, sex, and other potential confounders, the adjusted mortality rate ratio was 0.81 (95% CI, 0.38–1.73) for the bDMARD cohort compared with the DMARD cohort. RA-ILD, however, was a more common cause of death in the TNF α blockers cohort.¹⁶⁵ Two large cohorts from Japan involving over 10,000 patients found a low prevalence of ILD and good outcomes when treated with etanercept and infliximab combined with MTX.¹¹ As noted previously, although there is a range of potential biases, the recent systematic literature review would support the safety of these agents, showing pulmonary toxicity was rare.

How to balance the risk of adverse lung reactions, including from infection and the possible benefit in terms of “treating” underlying lung disease will require more data from longitudinal studies, but as recommended, a sensible approach is to assess the risk factors for adverse effects (smoking, significant pre-existing lung disease, older age, comorbidities such as diabetes mellitus, need for high-dose corticosteroids) and closely monitor patients, through educating patients to seek help early with symptoms and monitoring of lung function. Longer and larger studies of the use of biologic DMARDs in a range of stages of RAILD and in combination with a variety of risk factors will better guide our ability to accurately predict risk.

Summary: A Practical Clinical Approach to Patients

The importance of lung disease in patients with RA has been recognized for some time, and the extent highlighted by improvements in the sensitivity and accuracy of investigations such as the HRCT. Numerous case reports raise concerns about drug toxicity with the DMARDs in patient with no lung disease, subclinical or clinically important lung disease. However, reactions are rare and overall, there does not appear to be worse outcomes. ► **Table 5** outlines an approach for either pulmonologists or rheumatologists for the commonest clinical scenarios they will see, namely, a new patient presenting with RA; a patient with RA and subclinical pulmonary abnormalities; a patient with known RA with pulmonary symptoms and interstitial abnormalities referred for assessment by pulmonologist; and finally, a patient with known RA treated with nonbiologic or biologic DMARDs. More data are required to allow us to accurately predict the risk of worsening RA-related lung problems or adverse lung reactions to therapy. In considering infection in the setting of RA, progress has been made in modeling risk and estimating the impact of being on corticosteroids at varying levels, additional DMARDs in the presence of other comorbidities and underlying lung disease (including ILD and COPD). With more data, we should be able to take a similar approach with estimating the risk of the development or worsening of ILD in the setting of treatment for RA. Until that time, the need for effective RA

Table 5 Approach to patients with RA and possible pulmonary EAM

<i>Scenario 1: Patient with new onset RA presenting to a rheumatologist</i>
<p>In patient with new onset RA, it is important to determine the type and severity of lung involvement as part of the EAM, or presence of other lung disease, which may impact choice of RA treatment.</p> <p>A recommended approach would be to assess</p> <ul style="list-style-type: none"> • Symptoms (breathlessness, cough, chest pain), smoking status, occupational, or other exposures • Signs (crackles) • Ensure receives yearly influenza vaccination and 5 yearly pneumococcal vaccination^{153,166} • If considering biologic DMARD, obtain history of TB exposure, and perform CXR and Mantoux or QuantiFERON Gold^{153,166} <p>If normal and nonsmoker</p> <ul style="list-style-type: none"> • Nil apart from ongoing monitoring of symptoms and signs <p>If normal but significant smoking history (previous or current)</p> <ul style="list-style-type: none"> • Smoking cessation • Spirometry • CXR • Monitor if abnormalities <p>If significant abnormalities</p> <ul style="list-style-type: none"> • Smoking cessation • Comprehensive lung function (spirometry, lung volumes, diffusion capacity) and 6MWT • CXR and HRCT • Consider review by a pulmonologist • Monitor 3–6 monthly (comprehensive pulmonary function tests), then yearly if stable • If evidence of latent TB and/or TB exposure, consider TB prophylaxis if using biologic DMARD
<i>Scenario 2: Patient with known RA with subclinical or clinically apparent interstitial pulmonary abnormalities (rheumatologist or pulmonologist)</i>
<p>Consider</p> <ul style="list-style-type: none"> • Initial assessment to include clinical assessment, comprehensive lung function and 6MWT, CXR and HRCT, autoantibodies, ACPA • Consider multidisciplinary review to establish <ul style="list-style-type: none"> ◦ Pattern and severity of lung disease ◦ Treatment options for RA • Ensure receives yearly influenza vaccination and 5 yearly pneumococcal vaccination • If considering biologic DMARDs, obtain history of TB exposure and perform Mantoux or QuantiFERON Gold^{153,166} • Monitor symptoms, comprehensive lung function, 6MWT initially 3–6 monthly, 12 monthly if stable • HRCT if decline in lung function. • Avoid MTX if clinically significant lung disease and comorbid factors • If biologic DMARD, close monitoring¹⁶⁶ of symptoms and 3–6 monthly lung function, and if evidence of latent TB and/or TB exposure, consider TB prophylaxis. Avoid if severe chronic lung infection
<i>Scenario 3: Patient with known RA with pulmonary symptoms and interstitial abnormalities referred for assessment by pulmonologist</i>
<p>Consider the possible diagnoses</p> <ul style="list-style-type: none"> • New onset ILD associated with RA • Known or unknown pre-existing ILD with <ul style="list-style-type: none"> ◦ Worsening/exacerbation of disease ◦ Superimposed infection or other problem (e.g., pulmonary embolism, heart failure) ◦ Superimposed drug reaction • Drug reaction • Other problem (pulmonary embolism, heart failure) <p>Approach to assessment</p> <ul style="list-style-type: none"> • History looking for timing of start of symptoms or decline, examination for crackles • Look for pre-existing disease with old X-rays, including abdominal or spinal CTs, which may include basal lung fields • Sputum for culture, blood tests exploring infection and RA • HRCT, lung function, oxygenation, 6MWT • Consider bronchoscopy, washings (infection, drug reaction) • Multidisciplinary review of type and extent of disease • Consider surgical lung biopsy if unusual or if felt it would change management (rarely required) <p>If deteriorating</p> <ul style="list-style-type: none"> • Multidisciplinary discussion to confirm the diagnosis and review severity of ILD based on extent of fibrosis on HRCT and DLCO (< 54%) • Unless severe symptomatic disease, monitor comprehensive lung function (spirometry, lung volumes, DLCO, and 6MWT) for 3–6 mo if initial measurements are abnormal • Consider potential impact (positive or negative) of drugs required for joint disease (DMARDs) and monitor lung function during therapy • Consider treatment if extensive disease (extent of fibrosis on HRCT > 30%, DLCO < 54%, desaturation with exercise), deteriorating (decrease from baseline in FVC by 10% or DLCO by 15%) or very symptomatic

- Review age and comorbidities (obesity, osteoporosis, cardiovascular disease, infection risk, diabetes, coexisting lung disease such as COPD)
- Determine patient's informed wish

Scenario 4. Patient with known RA treated with nonbiologic or biologic DMARD

- Educate patient to seek advice early with any new unexplained symptom
- Monitor for new symptoms or signs (crackles) 3–6 monthly initially
- If subclinical interstitial disease, monitor lung function
- Ensure receives yearly influenza vaccination and 5 yearly pneumococcal vaccination¹⁶⁶
- If evidence of latent TB and/or TB exposure, monitor for TB for at least 6 mo after discontinuing anti-TNF therapy¹⁶⁶

Abbreviations: ACPA, anticitrullinated protein antibody; CT, computed tomography; CXR, chest X-ray; DLCO, low diffusing capacity for carbon monoxide; DMARD, disease modifying antirheumatic drug; EAM, extra-articular manifestation; FVC, forced vital capacity; HRCT, high-resolution computed tomography; ILD, interstitial lung disease; MTX, methotrexate; RA, rheumatoid arthritis; 6MWT, 6-minute walk test; TNF, tumor necrosis factor.

therapy should drive treatment decisions and therapy avoided only in those patients with severe or worsening lung disease. The rest can be monitored closely during therapy and have a good outcome.

References

- van Nies JA, Krabben A, Schoones JW, Huizinga TW, Kloppenburg M, van der Helm-van Mil AH. What is the evidence for the presence of a therapeutic window of opportunity in rheumatoid arthritis? A systematic literature review. *Ann Rheum Dis* 2013; 0:1–10
- Tureson C. Extra-articular rheumatoid arthritis. *Curr Opin Rheumatol* 2013;25(3):360–366
- Brown KK. Rheumatoid lung disease. *Proc Am Thorac Soc* 2007; 4(5):443–448
- O'Dwyer DN, Armstrong ME, Cooke G, Dodd JD, Veale DJ, Donnelly SC. Rheumatoid arthritis (RA) associated interstitial lung disease (ILD). *Eur J Intern Med* 2013;24(7):597–603
- Kelly C, Hamilton J. What kills patients with rheumatoid arthritis? *Rheumatology (Oxford)* 2007;46(2):183–184
- Young A, Koduri G, Batley M, et al; Early Rheumatoid Arthritis Study (ERAS) group. Mortality in rheumatoid arthritis. Increased in the early course of disease, in ischaemic heart disease and in pulmonary fibrosis. *Rheumatology (Oxford)* 2007;46(2): 350–357
- Bongartz T, Nannini C, Medina-Velasquez YF, et al. Incidence and mortality of interstitial lung disease in rheumatoid arthritis: a population-based study. *Arthritis Rheum* 2010;62(6):1583–1591
- Gizinski AM, Mascolo M, Loucks JL, et al. Rheumatoid arthritis (RA)-specific autoantibodies in patients with interstitial lung disease and absence of clinically apparent articular RA. *Clin Rheumatol* 2009;28(5):611–613
- Chen J, Shi Y, Wang X, Huang H, Ascherman D. Asymptomatic preclinical rheumatoid arthritis-associated interstitial lung disease. *Clin Dev Immunol* 2013;2013:406927
- Deane KD, Nicolls MR. Developing better biomarkers for connective tissue disease-associated interstitial lung disease: citrullinated hsp90 autoantibodies in rheumatoid arthritis. *Arthritis Rheum* 2013;65(4):864–868
- Roubille C, Haraoui B. Interstitial lung diseases induced or exacerbated by DMARDs and biologic agents in rheumatoid arthritis: A systematic literature review. *Semin Arthritis Rheum* 2013 pii: S0049-0172(13)00201-1
- Doyle TJ, Hunninghake GM, Rosas IO. Subclinical interstitial lung disease: why you should care. *Am J Respir Crit Care Med* 2012; 185(11):1147–1153
- Picchianti Diamanti A, Germano V, Bizzi E, Laganà B, Migliore A. Interstitial lung disease in rheumatoid arthritis in the era of biologics. *Pulm Med* 2011;2011:931342
- Ruderman EM. Overview of safety of non-biologic and biologic DMARDs. *Rheumatology (Oxford)* 2012;51(Suppl 6):vi37–vi43
- Upchurch KS, Kay J. Evolution of treatment for rheumatoid arthritis. *Rheumatology (Oxford)* 2012;51(Suppl 6):vi28–vi36
- Atzeni F, Boiardi L, Sallì S, Benucci M, Sarzi-Puttini P. Lung involvement and drug-induced lung disease in patients with rheumatoid arthritis. *Expert Rev Clin Immunol* 2013;9(7): 649–657
- van Dartel SAA, Fransen J, Kievit W, et al. Predictors for the 5-year risk of serious infections in patients with rheumatoid arthritis treated with anti-tumour necrosis factor therapy: a cohort study in the Dutch Rheumatoid Arthritis Monitoring (DREAM) registry. *Rheumatology (Oxford)* 2013;52(6):1052–1057
- Marigliano B, Soriano A, Margiotta D, Vadacca M, Afeltra A. Lung involvement in connective tissue diseases: a comprehensive review and a focus on rheumatoid arthritis. *Autoimmun Rev* 2013;12(11):1076–1084
- Khurana R, Wolf R, Berney S, Caldito G, Hayat S, Berney SM. Risk of development of lung cancer is increased in patients with rheumatoid arthritis: a large case control study in US veterans. *J Rheumatol* 2008;35(9):1704–1708
- Bruzzese V, Hassan C, Ridola L, Zullo A. Rheumatoid arthritis and cardiovascular risk: between lights and shadows. *Curr Rheumatol Rev* 2013;9(2):100–104
- Corcoran JP, Ahmad M, Mukherjee R, Redmond KC. Pleuro-Pulmonary Complications of Rheumatoid Arthritis. *Respir Care* 2013 (e-pub ahead of print). doi:10.4187/respcare.02597
- Balbir-Gurman A, Yigla M, Nahir AM, Braun-Moscovici Y. Rheumatoid pleural effusion. *Semin Arthritis Rheum* 2006;35(6): 368–378
- Perez T, Remy-Jardin M, Cortet B. Airways involvement in rheumatoid arthritis: clinical, functional, and HRCT findings. *Am J Respir Crit Care Med* 1998;157(5 Pt 1):1658–1665
- Shahane A. Pulmonary hypertension in rheumatic diseases: epidemiology and pathogenesis. *Rheumatol Int* 2013;33(7): 1655–1667
- Ramos-Casals M, Perez-Alvarez R, Perez-de-Lis M, Xaubet A, Bosch X; BIOGEAS Study Group. Pulmonary disorders induced by monoclonal antibodies in patients with rheumatologic autoimmune diseases. *Am J Med* 2011;124(5):386–394
- Hadjinicolaou AV, Nisar MK, Bhagat S, Parfrey H, Chilvers ER, Ostör AJ. Non-infectious pulmonary complications of newer biological agents for rheumatic diseases—a systematic literature review. *Rheumatology (Oxford)* 2011;50(12):2297–2305
- Holmqvist ME, Neovius M, Eriksson J, et al. Risk of venous thromboembolism in patients with rheumatoid arthritis and

- association with disease duration and hospitalization. *JAMA* 2012;308(13):1350–1356
- 28 Kim SC, Schneeweiss S, Liu J, Solomon DH. Risk of venous thromboembolism in patients with rheumatoid arthritis. *Arthritis Care Res (Hoboken)* 2013;65(10):1600–1607
 - 29 Mercer LK, Davies R, Galloway JB, et al; British Society for Rheumatology Biologics Register (BSRBR) Control Centre Consortium. Risk of cancer in patients receiving non-biologic disease-modifying therapy for rheumatoid arthritis compared with the UK general population. *Rheumatology (Oxford)* 2013;52(1):91–98
 - 30 Rueth N, Andrade R, Groth S, D'Cunha J, Maddaus M. Pleuro-pulmonary complications of rheumatoid arthritis: a thoracic surgeon's challenge. *Ann Thorac Surg* 2009;88(3):e20–e21
 - 31 Avnon LS, Abu-Shakra M, Flusser D, Heimer D, Sion-Vardy N. Pleural effusion associated with rheumatoid arthritis: what cell predominance to anticipate? *Rheumatol Int* 2007;27(10):919–925
 - 32 Chapman PT, O'Donnell JL, Moller PW. Rheumatoid pleural effusion: response to intrapleural corticosteroid. *J Rheumatol* 1992;19(3):478–480
 - 33 Nishida C, Yatera K, Kunimoto M, et al. [A case of rheumatoid arthritis with pneumothorax due to subpleural pulmonary rheumatoid nodules]. *Nihon Kokyuki Gakkai Zasshi* 2008;46(11):934–939
 - 34 Ahmed R, Ahmed U, Syed I. Pneumothorax necessitans in a patient with trapped lung and rheumatoid arthritis. *BMJ Case Rep* 2013;2013;pii: bcr2013009263. doi: 10.1136/bcr-2013-009263
 - 35 Nannini C, Medina-Velasquez YF, Achenbach SJ, et al. Incidence and mortality of obstructive lung disease in rheumatoid arthritis: a population-based study. *Arthritis Care Res (Hoboken)* 2013;65(8):1243–1250
 - 36 Greco A, Fusconi M, Macri GF, et al. Cricoarytenoid joint involvement in rheumatoid arthritis: radiologic evaluation. *Am J Otolaryngol* 2012;33(6):753–755
 - 37 Mori S, Koga Y, Sugimoto M. Small airway obstruction in patients with rheumatoid arthritis. *Mod Rheumatol* 2011;21(2):164–173
 - 38 Fuld JP, Johnson MK, Cotton MM, et al. A longitudinal study of lung function in nonsmoking patients with rheumatoid arthritis. *Chest* 2003;124(4):1224–1231
 - 39 Ayhan-Ardic FF, Oken O, Yorgancioglu ZR, Ustun N, Gokharman FD. Pulmonary involvement in lifelong non-smoking patients with rheumatoid arthritis and ankylosing spondylitis without respiratory symptoms. *Clin Rheumatol* 2006;25(2):213–218
 - 40 Hayakawa H, Sato A, Imokawa S, Toyoshima M, Chida K, Iwata M. Bronchiolar disease in rheumatoid arthritis. *Am J Respir Crit Care Med* 1996;154(5):1531–1536
 - 41 Devouassoux G, Cottin V, Lioté H, et al; Groupe d'Etudes et de Recherche sur les Maladies "Orphelines" Pulmonaires (GERM"O"P). Characterisation of severe obliterative bronchiolitis in rheumatoid arthritis. *Eur Respir J* 2009;33(5):1053–1061
 - 42 Schwarz MI, Lynch DA, Tuder R. Bronchiolitis obliterans: the lone manifestation of rheumatoid arthritis? *Eur Respir J* 1994;7(4):817–820
 - 43 Wilczynska MM, Condliffe AM, McKeon DJ. Coexistence of bronchiectasis and rheumatoid arthritis: revisited. *Respir Care* 2013;58(4):694–701
 - 44 Gabbay E, Tarala R, Will R, et al. Interstitial lung disease in recent onset rheumatoid arthritis. *Am J Respir Crit Care Med* 1997;156(2 Pt 1):528–535
 - 45 Dawson JK, Fewins HE, Desmond J, Lynch MP, Graham DR. Fibrosing alveolitis in patients with rheumatoid arthritis as assessed by high resolution computed tomography, chest radiography, and pulmonary function tests. *Thorax* 2001;56(8):622–627
 - 46 Youssef AA, Machaly SA, El-Dosoky ME, El-Maghraby NM. Respiratory symptoms in rheumatoid arthritis: relation to pulmonary abnormalities detected by high-resolution CT and pulmonary functional testing. *Rheumatol Int* 2012;32(7):1985–1995
 - 47 Wilsher M, Voight L, Milne D, et al. Prevalence of airway and parenchymal abnormalities in newly diagnosed rheumatoid arthritis. *Respir Med* 2012;106(10):1441–1446
 - 48 Schreiber J, Koschel D, Kekow J, Waldburg N, Goette A, Merget R. Rheumatoid pneumoconiosis (Caplan's syndrome). *Eur J Intern Med* 2010;21(3):168–172
 - 49 Sharma S, Vaccharajani A, Mandke J. Severe pulmonary hypertension in rheumatoid arthritis. *Int J Cardiol* 1990;26(2):220–222
 - 50 Castro GW, Appenzeller S, Bertolo MB, Costallat LT. Isolated pulmonary hypertension secondary to rheumatoid arthritis. *Clin Rheumatol* 2006;25(6):901–903
 - 51 Udayakumar N, Venkatesan S, Rajendiran C. Pulmonary hypertension in rheumatoid arthritis—relation with the duration of the disease. *Int J Cardiol* 2008;127(3):410–412
 - 52 Blumentals WA, Arreglado A, Napalkov P, Toovey S. Rheumatoid arthritis and the incidence of influenza and influenza-related complications: a retrospective cohort study. *BMC Musculoskelet Disord* 2012;13:158–168
 - 53 Listing J, Gerhold K, Zink A. The risk of infections associated with rheumatoid arthritis, with its comorbidity and treatment. *Rheumatology (Oxford)* 2013;52(1):53–61
 - 54 Coyne P, Hamilton J, Heycock C, Saravanan V, Coulson E, Kelly CA. Acute lower respiratory tract infections in patients with rheumatoid arthritis. *J Rheumatol* 2007;34(9):1832–1836
 - 55 Wells AU, Ward S. Pulmonary function tests in idiopathic pulmonary fibrosis. In: Meyer KC, Nathan SD, eds. *Idiopathic Pulmonary Fibrosis: A Comprehensive Clinical Guide, Respiratory Medicine*. Vol. 9. Springer Science + Business Media: New York; 2014
 - 56 Koduri G, Norton S, Young A, et al; ERAS (Early Rheumatoid Arthritis Study). Interstitial lung disease has a poor prognosis in rheumatoid arthritis: results from an inception cohort. *Rheumatology (Oxford)* 2010;49(8):1483–1489
 - 57 Weyand CM, Schmidt D, Wagner U, Goronzy JJ. The influence of sex on the phenotype of rheumatoid arthritis. *Arthritis Rheum* 1998;41(5):817–822
 - 58 Saag KG, Kolluri S, Koehnke RK, et al. Rheumatoid arthritis lung disease. Determinants of radiographic and physiologic abnormalities. *Arthritis Rheum* 1996;39(10):1711–1719
 - 59 Gochuico BR, Avila NA, Chow CK, et al. Progressive preclinical interstitial lung disease in rheumatoid arthritis. *Arch Intern Med* 2008;168(2):159–166
 - 60 Biederer J, Schnabel A, Muhle C, Gross WL, Heller M, Reuter M. Correlation between HRCT findings, pulmonary function tests and bronchoalveolar lavage cytology in interstitial lung disease associated with rheumatoid arthritis. *Eur Radiol* 2004;14(2):272–280
 - 61 Mori S, Koga Y, Sugimoto M. Different risk factors between interstitial lung disease and airway disease in rheumatoid arthritis. *Respir Med* 2012;106(11):1591–1599
 - 62 Klareskog L, Stolt P, Lundberg K, et al. A new model for an etiology of rheumatoid arthritis: smoking may trigger HLA-DR (shared epitope)-restricted immune reactions to autoantigens modified by citrullination. *Arthritis Rheum* 2006;54(1):38–46
 - 63 Bongartz T, Cantaert T, Atkins SR, et al. Citrullination in extra-articular manifestations of rheumatoid arthritis. *Rheumatology (Oxford)* 2007;46(1):70–75
 - 64 Harlow L, Rosas IO, Gochuico BR, et al. Identification of citrullinated hsp90 isoforms as novel autoantigens in rheumatoid arthritis-associated interstitial lung disease. *Arthritis Rheum* 2013;65(4):869–879
 - 65 Nishimura K, Sugiyama D, Kogata Y, et al. Meta-analysis: diagnostic accuracy of anti-cyclic citrullinated peptide antibody and rheumatoid factor for rheumatoid arthritis. *Ann Intern Med* 2007;146(11):797–808
 - 66 Fischer A, Solomon JJ, du Bois RM, et al. Lung disease with anti-CCP antibodies but not rheumatoid arthritis or connective tissue disease. *Respir Med* 2012;106(7):1040–1047
 - 67 Giles JT, Danoff SK, Sokolove J, et al. Association of fine specificity and repertoire expansion of anticitrullinated peptide antibodies

- with rheumatoid arthritis associated interstitial lung disease. *Ann Rheum Dis* 2013 (e-pub ahead of print). doi:10.1136/annrheumdis-2012-203160
- 68 Willis VC, Demoruelle MK, Derber LA, et al. Sputum autoantibodies in patients with established rheumatoid arthritis and subjects at risk of future clinically apparent disease. *Arthritis Rheum* 2013;65(10):2545–2554
 - 69 Tureson C, Jacobsson LT, Sturfelt G, Matteson EL, Mathsson L, Rönnelid J. Rheumatoid factor and antibodies to cyclic citrullinated peptides are associated with severe extra-articular manifestations in rheumatoid arthritis. *Ann Rheum Dis* 2007;66(1):59–64
 - 70 Suzuki A, Ohosone Y, Obana M, et al. Cause of death in 81 autopsied patients with rheumatoid arthritis. *J Rheumatol* 1994;21(1):33–36
 - 71 Sihvonen S, Korpela M, Laippala P, Mustonen J, Pasternack A. Death rates and causes of death in patients with rheumatoid arthritis: a population-based study. *Scand J Rheumatol* 2004;33(4):221–227
 - 72 Travis WD, Costabel U, Hansell DM, et al; ATS/ERS Committee on Idiopathic Interstitial Pneumonias. An official American Thoracic Society/European Respiratory Society statement: update of the international multidisciplinary classification of the idiopathic interstitial pneumonias. *Am J Respir Crit Care Med* 2013;188(6):733–748
 - 73 Flaherty KR, Colby TV, Travis WD, et al. Fibroblastic foci in usual interstitial pneumonia: idiopathic versus collagen vascular disease. *Am J Respir Crit Care Med* 2003;167(10):1410–1415
 - 74 Vij R, Noth I, Streck ME. Autoimmune-featured interstitial lung disease: a distinct entity. *Chest* 2011;140(5):1292–1299
 - 75 Larsen BT, Colby TV. Update for pathologists on idiopathic interstitial pneumonias. *Arch Pathol Lab Med* 2012;136(10):1234–1241
 - 76 Wells AU. The revised ATS/ERS/JRS/ALAT diagnostic criteria for idiopathic pulmonary fibrosis (IPF)—practical implications. *Respir Res* 2013;14(Suppl 1):S2
 - 77 Castelino FV, Goldberg H, Dellaripa PF. The impact of rheumatological evaluation in the management of patients with interstitial lung disease. *Rheumatology (Oxford)* 2011;50(3):489–493
 - 78 Vij R, Streck ME. Diagnosis and treatment of connective tissue disease-associated interstitial lung disease. *Chest* 2013;143(3):814–824
 - 79 Cottin V, Cordier JF. Subclinical interstitial lung disease: no place for crackles? *Am J Respir Crit Care Med* 2012;186(3):289, author reply 289–290
 - 80 Lee HK, Kim DS, Yoo B, et al. Histopathologic pattern and clinical features of rheumatoid arthritis-associated interstitial lung disease. *Chest* 2005;127(6):2019–2027
 - 81 Yoshinouchi T, Ohtsuki Y, Fujita J, et al. Nonspecific interstitial pneumonia pattern as pulmonary involvement of rheumatoid arthritis. *Rheumatol Int* 2005;26(2):121–125
 - 82 Rees JH, Woodhead MA, Sheppard MN, du Bois RM. Rheumatoid arthritis and cryptogenic organising pneumonitis. *Respir Med* 1991;85(3):243–246
 - 83 Cohen AJ, King TE Jr, Downey GP. Rapidly progressive bronchiolitis obliterans with organizing pneumonia. *Am J Respir Crit Care Med* 1994;149(6):1670–1675
 - 84 Ippolito JA, Palmer L, Spector S, Kane PB, Gorevic PD. Bronchiolitis obliterans organizing pneumonia and rheumatoid arthritis. *Semin Arthritis Rheum* 1993;23(1):70–78
 - 85 Rajasekaran A, Shovlin D, Saravanan V, Lord P, Kelly C. Interstitial lung disease in patients with rheumatoid arthritis: comparison with cryptogenic fibrosing alveolitis over 5 years. *J Rheumatol* 2006;33(7):1250–1253
 - 86 Tansey D, Wells AU, Colby TV, et al. Variations in histological patterns of interstitial pneumonia between connective tissue disorders and their relationship to prognosis. *Histopathology* 2004;44(6):585–596
 - 87 Hamblin MJ, Horton MR. Rheumatoid arthritis-associated interstitial lung disease: diagnostic dilemma. *Pulm Med* 2011;2011:872120
 - 88 de Lauretis A, Veeraraghavan S, Renzoni E. Review series: aspects of interstitial lung disease: connective tissue disease-associated interstitial lung disease: how does it differ from IPF? How should the clinical approach differ?. *Chron Respir Dis* 2011;8(1):53–82
 - 89 Mori S, Cho I, Koga Y, Sugimoto M. Comparison of pulmonary abnormalities on high-resolution computed tomography in patients with early versus longstanding rheumatoid arthritis. *J Rheumatol* 2008;35(8):1513–1521
 - 90 Kim EJ, Collard HR, King TE Jr. Rheumatoid arthritis-associated interstitial lung disease: the relevance of histopathologic and radiographic pattern. *Chest* 2009;136(5):1397–1405
 - 91 Wells AU. Managing diagnostic procedures in idiopathic pulmonary fibrosis. *Eur Respir Rev* 2013;22(128):158–162
 - 92 Schmidt SL, Sundaram B, Flaherty KR. Diagnosing fibrotic lung disease: when is high-resolution computed tomography sufficient to make a diagnosis of idiopathic pulmonary fibrosis? *Respirology* 2009;14(7):934–939
 - 93 Tanaka N, Kim JS, Newell JD, et al. Rheumatoid arthritis-related lung diseases: CT findings. *Radiology* 2004;232(1):81–91
 - 94 Fischer A, du Bois R. Interstitial lung disease in connective tissue disorders. *Lancet* 2012;380(9842):689–698
 - 95 Goh NS, Desai SR, Veeraraghavan S, et al. Interstitial lung disease in systemic sclerosis: a simple staging system. *Am J Respir Crit Care Med* 2008;177(11):1248–1254
 - 96 Walsh SLF, Sverzellati N, Devaraj A, Keir GJ, Wells AU, Hansell DM. Connective tissue disease related fibrotic lung disease: high resolution computed tomographic and pulmonary function indices as prognostic determinants. *Thorax* 2013
 - 97 Song J-W, Lee H-K, Lee Et Al CK. Clinical course and outcome of rheumatoid arthritis-related usual interstitial pneumonia. *Sarcoidosis Vasc Diffuse Lung Dis* 2013;30(2):103–112
 - 98 Hakala M. Poor prognosis in patients with rheumatoid arthritis hospitalized for interstitial lung fibrosis. *Chest* 1988;93(1):114–118
 - 99 Solomon JJ, Ryu JH, Tazelaar HD, et al. Fibrosing interstitial pneumonia predicts survival in patients with rheumatoid arthritis-associated interstitial lung disease (RA-ILD). *Respir Med* 2013;107(8):1247–1252
 - 100 Tsuchiya Y, Takayanagi N, Sugiura H, et al. Lung diseases directly associated with rheumatoid arthritis and their relationship to outcome. *Eur Respir J* 2011;37(6):1411–1417
 - 101 Hubbard R, Venn A. The impact of coexisting connective tissue disease on survival in patients with fibrosing alveolitis. *Rheumatology (Oxford)* 2002;41(6):676–679
 - 102 Park JH, Kim DS, Park IN, et al. Prognosis of fibrotic interstitial pneumonia: idiopathic versus collagen vascular disease-related subtypes. *Am J Respir Crit Care Med* 2007;175(7):705–711
 - 103 Ryerson CJ, Urbani TH, Richeldi L, et al. Prevalence and prognosis of unclassifiable interstitial lung disease. *Eur Respir J* 2013;42(3):750–757
 - 104 Cottin V. Pragmatic prognostic approach of rheumatoid arthritis-associated interstitial lung disease. *Eur Respir J* 2010;35(6):1206–1208
 - 105 Vassallo R, Matteson E, Thomas CF Jr. Clinical response of rheumatoid arthritis-associated pulmonary fibrosis to tumor necrosis factor-alpha inhibition. *Chest* 2002;122(3):1093–1096
 - 106 Chang HK, Park W, Ryu DS. Successful treatment of progressive rheumatoid interstitial lung disease with cyclosporine: a case report. *J Korean Med Sci* 2002;17(2):270–273
 - 107 Kobayashi A, Okamoto H. Treatment of interstitial lung diseases associated with connective tissue diseases. *Expert Rev Clin Pharmacol* 2012;5(2):219–227
 - 108 Puttick MP, Klinkhoff AV, Chalmers A, Ostrow DN. Treatment of progressive rheumatoid interstitial lung disease with cyclosporine. *J Rheumatol* 1995;22(11):2163–2165

- 109 Danoff SK, Schonhoft EH. Role of support measures and palliative care. *Curr Opin Pulm Med* 2013;19(5):480–484
- 110 Gilbert CR, Smith CM. Advanced lung disease: quality of life and role of palliative care. *Mt Sinai J Med* 2009;76(1):63–70
- 111 Meyer KC. Management of interstitial lung disease in elderly patients. *Curr Opin Pulm Med* 2012;18(5):483–492
- 112 Kim SH, Yoo WH. Recurrent pneumothorax associated with pulmonary nodules after leflunomide therapy in rheumatoid arthritis: a case report and review of the literature. *Rheumatol Int* 2011;31(7):919–922
- 113 Camus P. The Drug-Induced Respiratory Disease Web site. Available at: www.pneumotox.com. Accessed October 21, 2013
- 114 Goodwin SD, Glenn RW. Nonsteroidal anti-inflammatory drug-associated pulmonary infiltrates with eosinophilia. Review of the literature and Food and Drug Administration Adverse Drug Reaction reports. *Arch Intern Med* 1992;152(7):1521–1524
- 115 Vogts N, Young S. Pulmonary infiltrates with eosinophilia syndrome in ibuprofen overdose. *N Z Med J* 2012;125(1360):74–75
- 116 Ethgen O, de Lemos Esteves F, Bruyere O, Reginster JY. What do we know about the safety of corticosteroids in rheumatoid arthritis? *Curr Med Res Opin* 2013;29(9):1147–1160
- 117 Dixon WG, Suissa S, Hudson M. The association between systemic glucocorticoid therapy and the risk of infection in patients with rheumatoid arthritis: systematic review and meta-analyses. *Arthritis Res Ther* 2011;13(4):R139
- 118 Dixon WG, Abrahamowicz M, Beauchamp ME, et al. Immediate and delayed impact of oral glucocorticoid therapy on risk of serious infection in older patients with rheumatoid arthritis: a nested case-control analysis. *Ann Rheum Dis* 2012;71(7):1128–1133
- 119 Chikura B, Sathi N, Lane S, Dawson JK. Variation of immunological response in methotrexate-induced pneumonitis. *Rheumatology (Oxford)* 2008;47(11):1647–1650
- 120 Collins K, Aspey H, Todd A, Saravanan V, Rynne M, Kelly C. Methotrexate pneumonitis precipitated by switching from oral to parenteral administration. *Rheumatology (Oxford)* 2008;47(1):109–110
- 121 Kremer JM, Alarcón GS, Weinblatt ME, et al. Clinical, laboratory, radiographic, and histopathologic features of methotrexate-associated lung injury in patients with rheumatoid arthritis: a multicenter study with literature review. *Arthritis Rheum* 1997;40(10):1829–1837
- 122 Alarcón GS, Kremer JM, Macaluso M, et al; Methotrexate-Lung Study Group. Risk factors for methotrexate-induced lung injury in patients with rheumatoid arthritis. A multicenter, case-control study. *Ann Intern Med* 1997;127(5):356–364
- 123 Kramer N, Chuzhin Y, Kaufman LD, Ritter JM, Rosenstein ED. Methotrexate pneumonitis after initiation of infliximab therapy for rheumatoid arthritis. *Arthritis Rheum* 2002;47(6):670–671
- 124 Dayton CS, Schwartz DA, Sprince NL, et al. Low-dose methotrexate may cause air trapping in patients with rheumatoid arthritis. *Am J Respir Crit Care Med* 1995;151(4):1189–1193
- 125 Dawson JK, Graham DR, Desmond J, Fewins HE, Lynch MP. Investigation of the chronic pulmonary effects of low-dose oral methotrexate in patients with rheumatoid arthritis: a prospective study incorporating HRCT scanning and pulmonary function tests. *Rheumatology (Oxford)* 2002;41(3):262–267
- 126 Suissa S, Hudson M, Ernst P. Leflunomide use and the risk of interstitial lung disease in rheumatoid arthritis. *Arthritis Rheum* 2006;54(5):1435–1439
- 127 Chikura B, Lane S, Dawson JK. Clinical expression of leflunomide-induced pneumonitis. *Rheumatology (Oxford)* 2009;48(9):1065–1068
- 128 Sawada T, Inokuma S, Sato T, et al; Study Committee for Leflunomide-induced Lung Injury, Japan College of Rheumatology. Leflunomide-induced interstitial lung disease: prevalence and risk factors in Japanese patients with rheumatoid arthritis. *Rheumatology (Oxford)* 2009;48(9):1069–1072
- 129 Tomioka R, King TE Jr. Gold-induced pulmonary disease: clinical features, outcome, and differentiation from rheumatoid lung disease. *Am J Respir Crit Care Med* 1997;155(3):1011–1020
- 130 van de Laar MA, Westermann CJ, Wagenaar SS, Dinant HJ. Beneficial effect of intravenous cyclophosphamide and oral prednisone on D-penicillamine-associated bronchiolitis obliterans. *Arthritis Rheum* 1985;28(1):93–97
- 131 Furst DE, Keystone EC, So AK, et al. Updated consensus statement on biological agents for the treatment of rheumatic diseases, 2012. *Ann Rheum Dis* 2013;72(Suppl 2):ii2–ii34
- 132 Mariette X, Gottenberg JE, Ravaud P, Combe B. Registries in rheumatoid arthritis and autoimmune diseases: data from the French registries. *Rheumatology (Oxford)* 2011;50(1):222–229
- 133 Koike T, Harigai M, Inokuma S, et al. Postmarketing surveillance of the safety and effectiveness of etanercept in Japan. *J Rheumatol* 2009;36(5):898–906
- 134 Peno-Green L, Lluberas G, Kingsley T, Brantley S. Lung injury linked to etanercept therapy. *Chest* 2002;122(5):1858–1860
- 135 Ognenovski VM, Ojo TC, Fox DA. Etanercept-associated pulmonary granulomatous inflammation in patients with rheumatoid arthritis. *J Rheumatol* 2008;35(11):2279–2282
- 136 Toussiot E, Berthelot JM, Pertuiset E, et al. Pulmonary nodulosis and aseptic granulomatous lung disease occurring in patients with rheumatoid arthritis receiving tumor necrosis factor- α -blocking agent: a case series. *J Rheumatol* 2009;36(11):2421–2427
- 137 Ostör AJ, Chilvers ER, Somerville MF, et al. Pulmonary complications of infliximab therapy in patients with rheumatoid arthritis. *J Rheumatol* 2006;33(3):622–628
- 138 Tai TL, O'Rourke KP, McWeeney M, Burke CM, Sheehan K, Barry M. Pneumocystis carinii pneumonia following a second infusion of infliximab. *Rheumatology (Oxford)* 2002;41(8):951–952
- 139 Huggett MT, Armstrong R. Adalimumab-associated pulmonary fibrosis. *Rheumatology (Oxford)* 2006;45(10):1312–1313
- 140 Dixon WG, Hyrich KL, Watson KD, et al; B S R B R Control Centre Consortium; BSR Biologics Register. Drug-specific risk of tuberculosis in patients with rheumatoid arthritis treated with anti-TNF therapy: results from the British Society for Rheumatology Biologics Register (BSRBR). *Ann Rheum Dis* 2010;69(3):522–528
- 141 Fleischmann RM, Tesser J, Schiff MH, et al. Safety of extended treatment with anakinra in patients with rheumatoid arthritis. *Ann Rheum Dis* 2006;65(8):1006–1012
- 142 Salliot C, Dougados M, Gossec L. Risk of serious infections during rituximab, abatacept and anakinra treatments for rheumatoid arthritis: meta-analyses of randomised placebo-controlled trials. *Ann Rheum Dis* 2009;68(1):25–32
- 143 Soubrier M, Jeannin G, Kemeny JL, et al. Organizing pneumonia after rituximab therapy: Two cases. *Joint Bone Spine* 2008;75(3):362–365
- 144 Matteson EL, Bongartz T, Ryu JH, et al. Open-label, pilot study of the safety and clinical effects of rituximab in patients with rheumatoid arthritis-associated interstitial pneumonia. *Open J Rheumatol Autoimmun Dis* 2012;2(3):53–58
- 145 Teichmann LL, Woenckhaus M, Vogel C, Salzberger B, Schölmerich J, Fleck M. Fatal Pneumocystis pneumonia following rituximab administration for rheumatoid arthritis. *Rheumatology (Oxford)* 2008;47(8):1256–1257
- 146 Lee YH, Bae SC, Song GG. The efficacy and safety of rituximab for the treatment of active rheumatoid arthritis: a systematic review and meta-analysis of randomized controlled trials. *Rheumatol Int* 2011;31(11):1493–1499
- 147 Strangfeld A, Eveslage M, Schneider M, et al. Treatment benefit or survival of the fittest: what drives the time-dependent decrease in serious infection rates under TNF inhibition and what does this imply for the individual patient? *Ann Rheum Dis* 2011;70(11):1914–1920
- 148 Gottenberg JE, Ravaud P, Bardin T, et al; Autoimmunity and Rituximab registry and French Society of Rheumatology. Risk factors for severe infections in patients with rheumatoid arthritis

- treated with rituximab in the autoimmunity and rituximab registry. *Arthritis Rheum* 2010;62(9):2625–2632
- 149 Franklin J, Lunt M, Bunn D, Symmons D, Silman A. Risk and predictors of infection leading to hospitalisation in a large primary-care-derived cohort of patients with inflammatory polyarthritis. *Ann Rheum Dis* 2007;66(3):308–312
- 150 McLean-Tookey A, Aldridge C, Waugh S, Spickett GP, Kay L. Methotrexate, rheumatoid arthritis and infection risk: what is the evidence? *Rheumatology (Oxford)* 2009;48(8):867–871
- 151 Housden MM, Bell G, Heycock CR, Hamilton J, Saravanan V, Kelly CA. How to reduce morbidity and mortality from chest infections in rheumatoid arthritis. *Clin Med* 2010;10(4):326–329
- 152 Kameda H, Tokuda H, Sakai F, et al. Clinical and radiological features of acute-onset diffuse interstitial lung diseases in patients with rheumatoid arthritis receiving treatment with biological agents: importance of *Pneumocystis pneumonia* in Japan revealed by a multicenter study. *Intern Med* 2011;50(4):305–313
- 153 Singh JA, Furst DE, Bharat A, et al. 2012 Update of the 2008 American College of Rheumatology recommendations for the use of disease-modifying antirheumatic drugs and biologic agents in the treatment of rheumatoid arthritis. *Arthritis Care Res* 2012;64:625–639
- 154 Mori S, Tokuda H, Sakai F, et al; NTM-BIORA (NTM infection in Biologic-treated RA patients) Study Investigators. Radiological features and therapeutic responses of pulmonary nontuberculous mycobacterial disease in rheumatoid arthritis patients receiving biological agents: a retrospective multicenter study in Japan. *Mod Rheumatol* 2012;22(5):727–737
- 155 Mori S, Sugimoto M. Is continuation of anti-tumor necrosis factor- α therapy a safe option for patients who have developed pulmonary mycobacterial infection?: Case presentation and literature review *Clin Rheumatol* 2012;31(2):203–210
- 156 Yamakawa H, Takayanagi N, Miyahara Y, et al. Prognostic factors and radiographic outcomes of nontuberculous mycobacterial lung disease in rheumatoid arthritis. *J Rheumatol* 2013;40(8):1307–1315
- 157 Lacaille D, Guh DP, Abrahamowicz M, Anis AH, Esdaile JM. Use of nonbiologic disease-modifying antirheumatic drugs and risk of infection in patients with rheumatoid arthritis. *Arthritis Rheum* 2008;59(8):1074–1081
- 158 Puéchal X, Fajac I, Bienvenu T, et al. Increased frequency of cystic fibrosis deltaF508 mutation in bronchiectasis associated with rheumatoid arthritis. *Eur Respir J* 1999;13(6):1281–1287
- 159 Puéchal X, Bienvenu T, Génin E, et al. Mutations of the cystic fibrosis gene in patients with bronchiectasis associated with rheumatoid arthritis. *Ann Rheum Dis* 2011;70(4):653–659
- 160 Mikuls TR. Rheumatoid arthritis incidence: what goes down must go up? *Arthritis Rheum* 2010;62(6):1565–1567
- 161 Gabriel SE, Crowson CS, Kremers HM, et al. Survival in rheumatoid arthritis: a population-based analysis of trends over 40 years. *Arthritis Rheum* 2003;48(1):54–58
- 162 Glace B, Gottenberg JE, Mariette X, et al. Efficacy of rituximab in the treatment of pulmonary rheumatoid nodules: findings in 10 patients from the French Autoimmunity and Rituximab/Rheumatoid Arthritis registry (AIR/PR registry). *Ann Rheum Dis* 2012;71(8):1429–1431
- 163 Perez-Alvarez R, Perez-de-Lis M, Diaz-Lagares C, et al. Interstitial lung disease induced or exacerbated by TNF-targeted therapies: analysis of 122 cases. *Semin Arthritis Rheum* 2011;41(2):256–264
- 164 Scherak O, Popp W, Kolarz G, Wottawa A, Ritschka L, Braun O. Bronchoalveolar lavage and lung biopsy in rheumatoid arthritis. In vivo effects of disease modifying antirheumatic drugs. *J Rheumatol* 1993;20(6):944–949
- 165 Dixon WG, Hyrich KL, Watson KD, Lunt M, Symmons DP; BSRBR Control Centre Consortium; British Society for Rheumatology Biologics Register. Influence of anti-TNF therapy on mortality in patients with rheumatoid arthritis-associated interstitial lung disease: results from the British Society for Rheumatology Biologics Register. *Ann Rheum Dis* 2010;69(6):1086–1091
- 166 Baughman RP, Meyer KC, Nathanson I, et al. Monitoring of nonsteroidal immunosuppressive drugs in patients with lung disease and lung transplant recipients: American College of Chest Physicians evidence-based clinical practice guidelines. *Chest* 2012;142(5):e1S–e11S

Rheumatoid arthritis

Josef S Smolen, Daniel Aletaha, Iain B McInnes



Rheumatoid arthritis is a chronic inflammatory joint disease, which can cause cartilage and bone damage as well as disability. Early diagnosis is key to optimal therapeutic success, particularly in patients with well-characterised risk factors for poor outcomes such as high disease activity, presence of autoantibodies, and early joint damage. Treatment algorithms involve measuring disease activity with composite indices, applying a treatment-to-target strategy, and use of conventional, biological, and new non-biological disease-modifying antirheumatic drugs. After the treatment target of stringent remission (or at least low disease activity) is maintained, dose reduction should be attempted. Although the prospects for most patients are now favourable, many still do not respond to current therapies. Accordingly, new therapies are urgently required. In this Seminar, we describe current insights into genetics and aetiology, pathophysiology, epidemiology, assessment, therapeutic agents, and treatment strategies together with unmet needs of patients with rheumatoid arthritis.

Introduction

Rheumatoid arthritis is one of the most prevalent chronic inflammatory diseases. It primarily involves the joints, but should be considered a syndrome that includes extra-articular manifestations, such as rheumatoid nodules, pulmonary involvement or vasculitis, and systemic comorbidities. A therapeutic revolution in the treatment of rheumatoid arthritis in the past decade—with the advent of novel therapeutics, introduction of early therapy, development of new classification criteria, and application of new effective treatment strategies—has transformed articular and systemic outcomes.^{1–6} In this Seminar, we highlight recent insights into most aspects of rheumatoid arthritis, from diagnosis to treatment strategies, and from aetiology to novel therapies. There is still a considerable unmet need in rheumatoid arthritis; full or stringent remission is not typical, nor is it usually sustained without continuing treatment, and as such it should now be the priority of research efforts.

Epidemiology, genetics, and aetiology

Rheumatoid arthritis is a chronic disease that carries a substantial burden for both the individual and society.⁷ The individual burden results from musculoskeletal deficits, with attendant decline in physical function, quality of life, and cumulative comorbid risk.⁸ The socioeconomic burden, aside from major direct medical costs, is a consequence of functional disability, reduced work capacity, and decreased societal participation.⁹ Efforts to establish the diagnosis early, initiate treatment promptly, and design novel treatment strategies to control inflammation and reduce or prevent consequent damage are paramount.

Rheumatoid arthritis has an incidence of 0.5% to 1%, with an apparent reduction from north to south (in the northern hemisphere) and from urban to rural areas.^{10,11} Some Native American populations have a very high prevalence.¹⁰ A positive family history increases the risk of rheumatoid arthritis roughly three to five times; concordance rates in twins are increased, implicating genetic factors in pathogenesis.^{10,12} The heritability of rheumatoid arthritis is currently estimated as 40–65% for seropositive

rheumatoid arthritis, but lower (20%) for seronegative disease.^{13,14}

Modern genetic technologies combined with large, well-characterised clinical cohorts have advanced our understanding of the genetics of the disease. Genome-wide association studies using single nucleotide polymorphisms have characterised more than a hundred loci associated with rheumatoid arthritis risk, most of which implicate immune mechanisms (figure 1), some of which are shared with other chronic inflammatory diseases.¹⁵ The HLA system (particularly HLA-DRB1) remains the dominant influence, strongly implicating peptide (and self-peptide) binding in pathogenesis.¹⁶ Disease-associated alleles share common amino acid sequences in the peptide-binding groove (the so-called shared epitope).¹⁷ Moreover, some HLA genotypes particularly associate with more aggressive erosive disease and with higher mortality, pointing to a crucial role of peptide binding.¹⁸

Other genetic loci probably contribute smaller functional effects that are presumably singly or cumulatively mediated,¹⁹ for example, via altered costimulatory pathways (eg, CD28, CD40), cytokine signalling, lymphocyte receptor activation threshold (eg, PTPN22), and innate immune activation (figure 1). The increased risk for rheumatoid arthritis in patients with the shared epitope is linked with seropositivity for autoantibodies against citrullinated peptides (ACPs) and autoantibodies against IgG (rheumatoid factor [RF]). These characteristic autoantibodies for rheumatoid

Lancet 2016; 388: 2023–38

Published Online

May 3, 2016

[http://dx.doi.org/10.1016/S0140-6736\(16\)30173-8](http://dx.doi.org/10.1016/S0140-6736(16)30173-8)

This online publication has been corrected. The corrected version first appeared at thelancet.com on June 10, 2016

Division of Rheumatology, Department of Medicine 3, Medical University of Vienna, Vienna, Austria (Prof J S Smolen MD, D Aletaha MD); 2nd Department of Medicine, Hietzing Hospital Vienna, Vienna, Austria (Prof J S Smolen); and Institute of Infection, Immunity and Inflammation, University of Glasgow, Glasgow, UK (Prof I B McInnes MD)

Correspondence to:

Prof Josef S Smolen, Division of Rheumatology, Department of Medicine 3, Medical University of Vienna, A-1090 Vienna, Austria
josef.smolen@wienkav.at

Search strategy and selection criteria

We searched MEDLINE using the terms “rheumatoid arthritis” in conjunction with “diagnosis”, “classification”, “epidemiology”, and “pathogenesis”. For treatment, we used recent systematic literature searches, and updated the respective searches in October, 2015, including terms on novel therapies and “treatment strategy”. Selection of articles was based on our personal judgment of relevance within the scope of this Seminar.

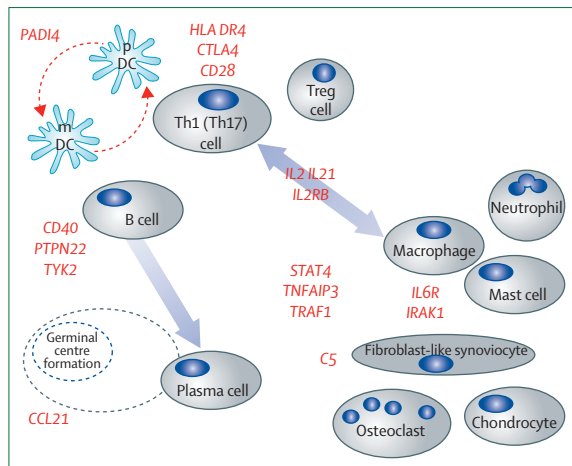


Figure 1: Important loci associated with risk and progression of rheumatoid arthritis

Key immune cells implicated in the pathogenesis of rheumatoid arthritis.

Th1=T-helper-1. Th17=T-helper-17. Treg=regulatory T. mDC=myeloid dendritic cell. pDC=plasmacytoid dendritic cell.

arthritis are present in 50–70% of patients at diagnosis, with remarkable stability throughout the disease course.^{20,21} The shared epitope has only poor association with ACPA-negative and RF-negative rheumatoid arthritis.¹⁸

Epigenetics contribute to pathogenesis, probably by integrating environmental and genetic effects.²² A recent epigenome-wide association study identified ten differentially methylated positions that could promote genetic risk in rheumatoid arthritis.²³ Altered histone acetylation and DNA methylation can regulate the biology of synovial fibroblasts and leucocytes.²² MicroRNAs represent an additional epigenetic aspect by targeting mRNA for degradation, thereby fine-tuning cellular responses.^{24,25} Many microRNAs have been identified as key regulators of lymphocytes, macrophages, and synovial fibroblasts (eg, miR146a or miR155).²⁵ Whether microRNAs will offer therapeutic utility in rheumatoid arthritis is as yet unclear.²²

Development of rheumatoid arthritis is associated with environmental factors. Consistently reported risk factors include smoking^{26,27} and low socioeconomic status or educational attainment.^{28,29} Rheumatoid arthritis is associated with periodontal disease, although the causality and nature of this relationship remains ill defined.³⁰ One hypothesis proposes that *Porphyromonas gingivalis* (a bacterium frequently found in periodontitis) promotes aberrant citrullination and provokes local breach of tolerance to citrullinated peptides via endogenous expression of its PADI4, which converts arginine to citrulline.³¹ Indeed, other infectious agents (eg, *Proteus mirabilis*, *Escherichia coli*, and Epstein-Barr virus) have been suggested to trigger rheumatoid arthritis,³² generally via molecular mimicry; however these proposed mechanisms have not yet been substantiated.

As is the case with many autoimmune diseases, there is now considerable interest in the effect of the microbiome on disease risk and progression (figure 2).^{30,35} Data from animal models of arthritis suggest an essential role for the gut microbiome in the development of disease.³⁵ Initial studies in humans have implicated gastrointestinal dysbiosis in rheumatoid arthritis, particularly in early disease.³⁰ One study³⁶ detected alterations in common microbial populations in oral, salivary, and gastrointestinal sites, which were associated with C-reactive protein and ACPA status, and further altered by therapy with disease-modifying antirheumatic drugs. The mechanisms underpinning such observations and their importance remain to be elucidated.

Pathophysiology of rheumatoid arthritis Autoimmune response

Rheumatoid arthritis is pathologically heterogeneous. The presence of autoantibodies (seropositivity) is associated with more severe symptoms and joint damage, and increased mortality.^{35–39} This is most likely due to formation of immune complexes by ACPAs with citrulline-containing antigens and subsequent binding of RF, which can lead to abundant complement activation.^{40–42} The detection of autoimmune responses to citrullinated self-proteins is a major advance.^{43,44} ACPAs can bind citrullinated residues on many self-proteins including vimentin, α -enolase, fibronectin, fibrinogen, histones, and type II collagen. The tissue in which these immune responses are activated is uncertain, but the lung is an attractive candidate, which is consistent with a role for smoking in rheumatoid arthritis and the presence of shared citrullinated peptides in lung and synovial tissue biopsies (figure 2).⁴⁵ Circulating ACPAs can be detected up to 10 years before diagnosis—so-called pre-rheumatoid arthritis.⁴⁶ Over time, the concentration and epitope diversity of ACPAs increases, as do serum cytokine concentrations, especially before onset of articular involvement. ACPAs can be of IgG, IgA, or IgM isotype, are indicative of T-cell help, and have an altered glycosylation status that confers enhanced Fc-receptor and citrullinated antigen binding.^{47,48} ACPA-producing B cells are present in the synovium and in the circulation.^{47,49} ACPAs themselves can be pathogenic, either by activating macrophages (eg, by ligating to toll-like receptors via the bound antigen, or by Fc-receptor engagement, or both), or by activating osteoclasts via immune complex formation and Fc-receptor engagement or, possibly, by binding membrane citrullinated vimentin,⁵⁰ thus promoting bone loss. With effective therapy, both RF and ACPA concentrations decrease, but patients rarely become ACPA negative, whereas RF decreases more profoundly and more frequently and patients may seroconvert to RF negativity.⁵¹ Anti-carbamylated and acetylated peptide autoantibodies have also been identified in patients with rheumatoid arthritis;⁵² additional autoantibodies, directed against other post-translational protein modifications,

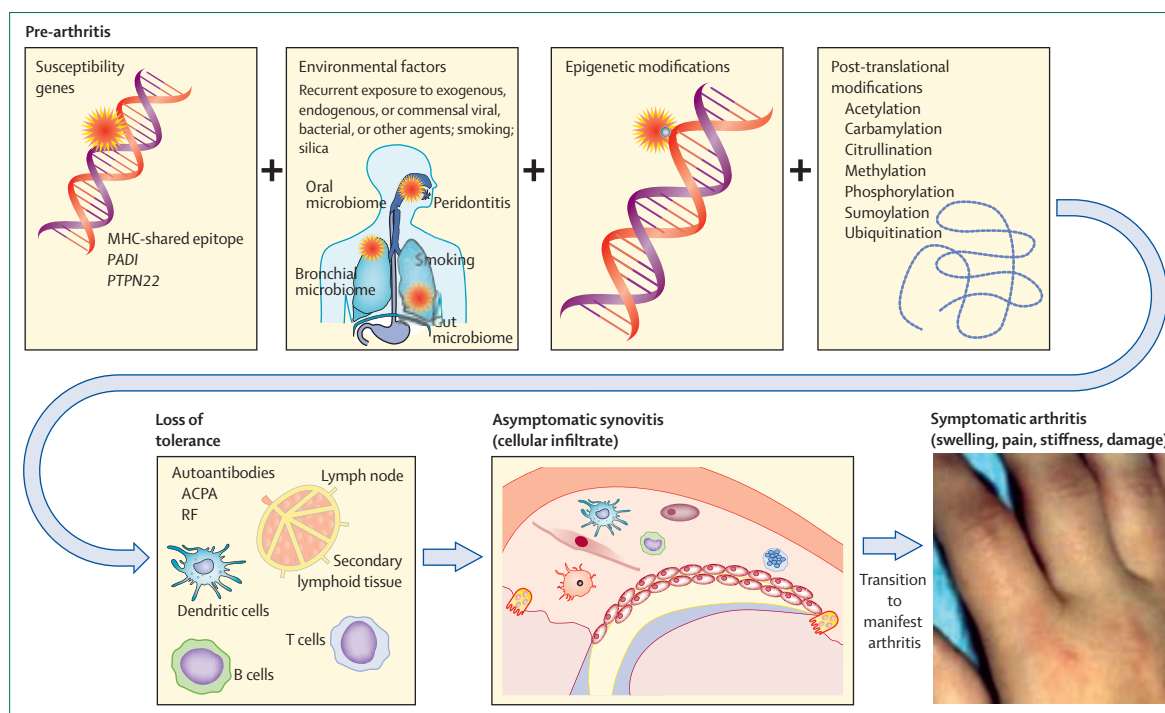


Figure 2: Pathways to rheumatoid arthritis

In a genetically predisposed host with susceptibility genes, environmental insults, epigenetic modifications, and post-translational modifications can lead to loss of tolerance with subsequent asymptomatic synovitis, ultimately leading to clinically overt arthritis. ACPA=autoantibodies against citrullinated peptides. RF=rheumatoid factor. Adapted from Smolen and colleagues³³ by permission of Elsevier, and McInnes and Schett³⁴ by permission of the Massachusetts Medical Society.

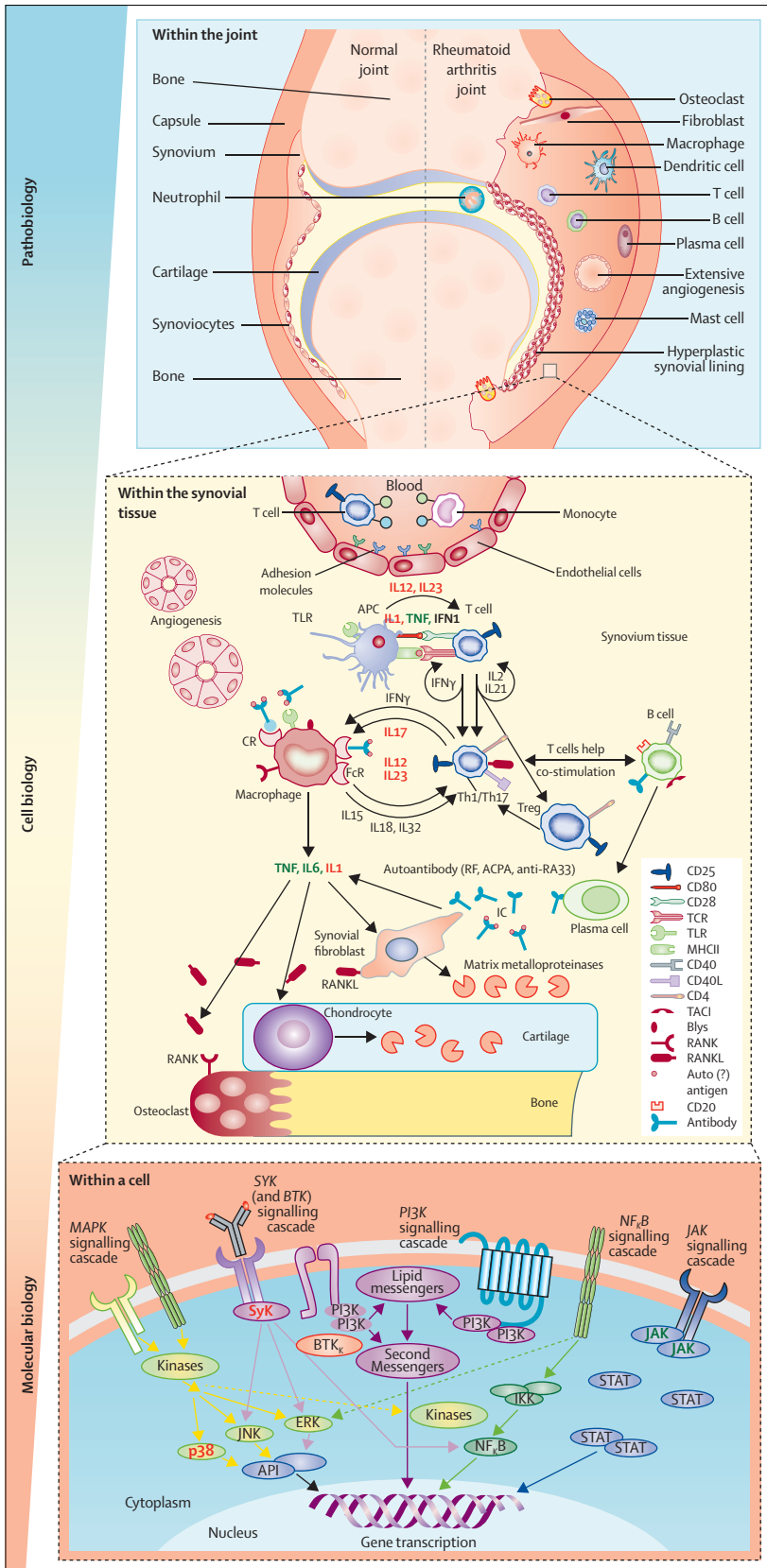
might emerge. RF is more directly involved in mechanisms of macrophage activation and induction of cytokine activation than ACPAs.^{42,53} ACPAs might form immune complexes that interact with RF, thus potentiating the effect on the inflammatory and destructive response.^{37,53} Less is known of the T-cell response that supports these processes.⁵⁴ Using HLA-DRB1*0401 tetramers, elevated numbers of citrulline-specific T-helper-1 cells have been found in the circulation of patients with rheumatoid arthritis, particularly in those with early disease,⁵⁵ although their contribution to autoimmune mechanisms remains uncertain. Lymph node biopsies in early rheumatoid arthritis suggest T-cell activation distant from the synovium.⁵⁶

Inflammation

Joint swelling in rheumatoid arthritis reflects synovial membrane inflammation consequent to immune activation, and is characterised by leucocyte infiltration into the normally sparsely populated synovial compartment (figure 3). The cellular composition of synovitis in rheumatoid arthritis includes innate immune cells (eg, monocytes, dendritic cells, mast cells, and innate lymphoid cells) and adaptive immune cells (eg, T-helper-1 and T-helper-17 cells, B cells, plasmablasts, and plasma cells). A robust tissue response—whereby synovial fibroblasts assume an aggressive inflammatory, matrix regulatory, and invasive phenotype, together with

enhanced chondrocyte catabolism and synovial osteoclastogenesis—promotes articular destruction.^{33,34} Findings from ultrasound-guided biopsies of small joints and detailed molecular (particularly transcriptomic) analyses suggest that myeloid-dominant, lymphocytic-dominant, and fibroid-dominant synovial subtypes might exist, which could be of therapeutic significance.⁵⁹

The inflammatory milieu in the synovial compartment is regulated by a complex cytokine and chemokine network; clinical interventions clearly demonstrate that of these components, tumour necrosis factor (TNF), interleukin 6, and probably granulocyte-monocyte colony stimulating factor are essential to the process, whereas others (such as interleukin 1 and various lymphokines) may be less important.⁶⁰ Cytokines and chemokines lead to the induction or aggravation of the inflammatory response by activating endothelial cells and attracting immune cells to accumulate within the synovial compartment. Activated fibroblasts, together with the accumulated activated T cells and B cells, and monocytes and macrophages, ultimately trigger osteoclast generation via receptor activator of nuclear factor κ B ligand (RANKL) expressed on T cells, B cells, and fibroblasts, with its receptor RANK on macrophages, dendritic cells, and pre-osteoclasts.^{61,62} Bony erosions ensue, arising from the so-called bare area at the junction between cartilage, periosteal synovial membrane insertion, and bone. Cartilage undergoes damage by catabolic effects in



chondrocytes after their stimulation by cytokines. Cartilage matrix is degraded by matrix metalloproteinases and other enzymes.⁶³ Cytokines bind cognate receptors to trigger various intracellular signal transduction events, the intermediaries between extracellular events and activation of an array of genes that lead to or aggravate inflammation and damage (figure 3).

Learning from success and failure of therapies

Many of these cells and molecules have been tested as therapeutic targets with notable success in rheumatoid arthritis and subsequently other inflammatory diseases, whereas targeting of other molecules rendered low or no therapeutic success. Thus, whereas the pathogenic events initiating and mediating chronicity of synovitis are not yet fully understood, remarkable insights have arisen from genetic, epidemiological, translational biological, and therapeutic studies.

Taken together, this evidence suggests that rheumatoid arthritis probably arises from multiple hits, whereby an initial combination of environmental, lifestyle, and stochastic insults occurring in a genetically predisposed, epigenetically modified individual leads to breach of immunological tolerance. An additional trigger, perhaps infectious (facilitated particularly by pathways associated with HLA class II), drives expansion of T-cell-mediated autoimmunity, and thereafter articular localisation via currently obscure mechanisms (eg, neurological, vascular, biomechanical). This crucial transition to chronic (non-resolving) synovitis is characterised by leucocyte and stromal cell dysregulation and wider comorbidity affecting various organs, such as the heart and the bone. Importantly, this transition must occur quite early, because treatment of very early, clinically incipient but overt rheumatoid arthritis usually does not reverse arthritis, and because synovial infiltration by inflammatory cells can occur before clinical signs and symptoms.^{64,65} Therefore, diagnosis of preclinical rheumatoid arthritis has become a focus of research activity,^{66,67} with the goal of using preventive therapy; the term “window of opportunity” increasingly refers to preventive aspects rather than interventions in early but clinically already manifest disease.

Diagnostic approach and differential diagnosis

No diagnostic criteria exist for rheumatoid arthritis. The typical patient presents with tender and swollen joints of recent onset, morning joint stiffness, and abnormal laboratory tests such as elevated concentrations of C-reactive protein or erythrocyte sedimentation rate. Unfortunately, this presentation is not specific to

Figure 3: Pathogenic pathways in rheumatoid arthritis
 Green text shows molecules or cells which are successfully targeted by respective therapies. Red text relates to molecules or cells for which targeting was not effective. Adapted from Smolen and colleagues³³ by permission of Elsevier, Mavers and colleagues²⁷ by permission of Springer, and Smolen and Steiner²⁸ by permission of Nature Publishing Group.

rheumatoid arthritis. Other causes of arthritis need to be considered, such as reactive arthritis, osteoarthritis, psoriatic arthritis, infectious arthritis (viral or bacterial, and particularly Lyme disease depending on geographic region), or some rarer autoimmune conditions such as connective tissue diseases if additional suggestive signs or symptoms are present (eg, rash, mouth ulcers, alopecia, Raynaud's phenomenon, Sicca syndrome, antinuclear antibodies, elevated muscle enzymes). In fact, in many patients no specific diagnosis can be made at first presentation, and the diagnosis of exclusion is undifferentiated arthritis. Providing such preliminary diagnosis, while leaving the future evolution to a distinct diagnosis open, is important, because disease-modifying treatment is indicated and necessary for any type of chronic inflammatory arthritis.

New classification criteria for rheumatoid arthritis were presented in 2010¹ to eliminate shortcomings of the former American College of Rheumatology (ACR) criteria, particularly inclusion of features of chronicity and poor prognosis.⁶⁸ Briefly, the new criteria, developed using cohorts and case scenarios of patients with early arthritis, require at least a single clinically swollen joint as entry criterion in the absence of other diseases explaining the clinical symptoms. Thereafter, the classification criteria allow for sensitive assessment of extent of joint involvement (tender joints or joints positive by ultrasound or MRI can be classified as active joints, just as well as clinically swollen joints). Additional features are serological markers (RF and ACPA), long symptom duration, and laboratory markers of systemic inflammation. The criteria have been validated in many settings and offer 21% higher sensitivity than the former criteria, at the cost of 16% lower specificity.⁶⁹ However, classification is not synonymous with diagnosis. Whereas diagnosis has the ultimate goal of being correct at the level of the individual patient, classification aims to maximise homogeneous populations for study purposes, but can be used to support diagnosis.

Extra-articular manifestations and comorbidities

Patients with insufficiently treated rheumatoid arthritis can have various extra-articular manifestations, including vasculitis or interstitial lung disease.⁶⁹ Moreover, the chronic inflammatory state of rheumatoid arthritis has been associated with secondary amyloidosis, lymphoma,⁷⁰ and cardiovascular disease⁸ and increased mortality.⁷¹ All these risks appear to be strikingly reduced with modern therapeutic strategies.^{72,73} Of note, methotrexate can induce nodulosis, which is indistinguishable from rheumatoid nodules,⁷⁴ and TNF inhibitors can elicit psoriasis-like lesions⁷⁵ that only subside after cessation of the drugs.

Disease assessment and definition of treatment targets

Assessment of disease activity is crucial in the follow-up of patients with rheumatoid arthritis.^{76,77} Composite measures that include joint counts have been

recommended for daily practice.⁷⁷ The ACR improvement criteria⁷⁸ distinguish a change from baseline of several defined variables by at least 20% (ACR20, minimal response), 50% (ACR50, moderate response), or 70% (ACR70, major response). They were developed to differentiate active therapy from placebo in clinical trials (in particular, ACR20), but cannot be used in practice because they are not based on a continuous scale; improvement is related to baseline values of the respective variable, which differ between individual patients or within patients at different treatment starts. By contrast with the DAS28, a disease activity score using 28 joint counts along with other components in a complex calculation (table 1),⁸⁰ the simplified disease activity index (SDAI) and clinical disease activity index (CDAI)^{81,82} provide continuous numerical scales reflecting disease activity (higher is worse; table 1).^{80,83} These measures can also classify disease activity states (high, moderate, low, and remission). There is an almost linear relationship between these disease activities and impairment of physical function^{77,82,84} or damage progression.^{82,85-87} Other disease activity measures that do not include joint counts⁸⁸

Components	Cutpoints	Remission			
		Low disease activity	Moderate disease activity	High disease activity	High disease activity
DAS28-ESR* Tender joint count (of 28), swollen joint count (of 28), erythrocyte sedimentation rate (in mm), global health	<2.6	2.6 to 3.2	>3.2 to ≤5.1	>5.1	
DAS28-CRP† Tender joint count (of 28), swollen joint count (of 28), C-reactive protein (in mg/dL), global health	<2.6	2.6 to 3.2	>3.2 to ≤5.1	>5.1	
SDAI‡ Tender joint count (of 28), swollen joint count (of 28), patient global assessment, evaluator (physician) global assessment both in cm, C-reactive protein (in mg/dL)	≤3.3	>3.3 to 11	>11 to ≤26	>26	
CDAI§ Tender joint count (of 28), swollen joint count (of 28), patient global assessment, evaluator (physician) global assessment both in cm	≤2.8	>2.8 to 10	>10 to ≤22	>22	
ACR-EULAR remission¶ Index: SDAI, CDAI; Boolean: swollen joint count (of 28), tender joint count (of 28), patient global assessment, C-reactive protein (in mg/dL)	SDAI ≤3.3, CDAI ≤2.8, Boolean all ≤1	

Patient global assessment reflects global health in DAS28; mm in DAS28; cm in CDAI, SDAI, Boolean. ACR=American College of Rheumatology. EULAR=European League against Rheumatism. DAS28=disease activity score using 28 joint counts. SDAI=simplified disease activity index. CDAI=clinical disease activity index. TJC28=tender joint count (of 28). SJC28=swollen joint count (of 28). ESR=erythrocyte sedimentation rate (in mm). GH=global health. CRP=C-reactive protein (in mg/dL). *DAS28-ESR calculated according to the following equation: $0.56 \times \sqrt{(TJC28)} + 0.28 \times \sqrt{(SJC28)} + 0.70 \times \log_{10}(\text{ESR}) + 0.014 \times \text{GH}$. †DAS28-CRP calculated according to the following equation: $0.56 \times \sqrt{(TJC28)} + 0.28 \times \sqrt{(SJC28)} + 0.36 \times \log_{10}(\text{CRP} + 1) + 0.014 \times \text{GH} + 0.96$. ‡SDAI calculated according to the following equation: $TJC28 + SJC28 + PtGA + EGA + CRP$. §CDAI calculated according to the following equation: $TJC28 + SJC28 + PtGA + EGA$.

Table 1: Composite measures of disease activity including joint counts, and ACR-EULAR remission criteria

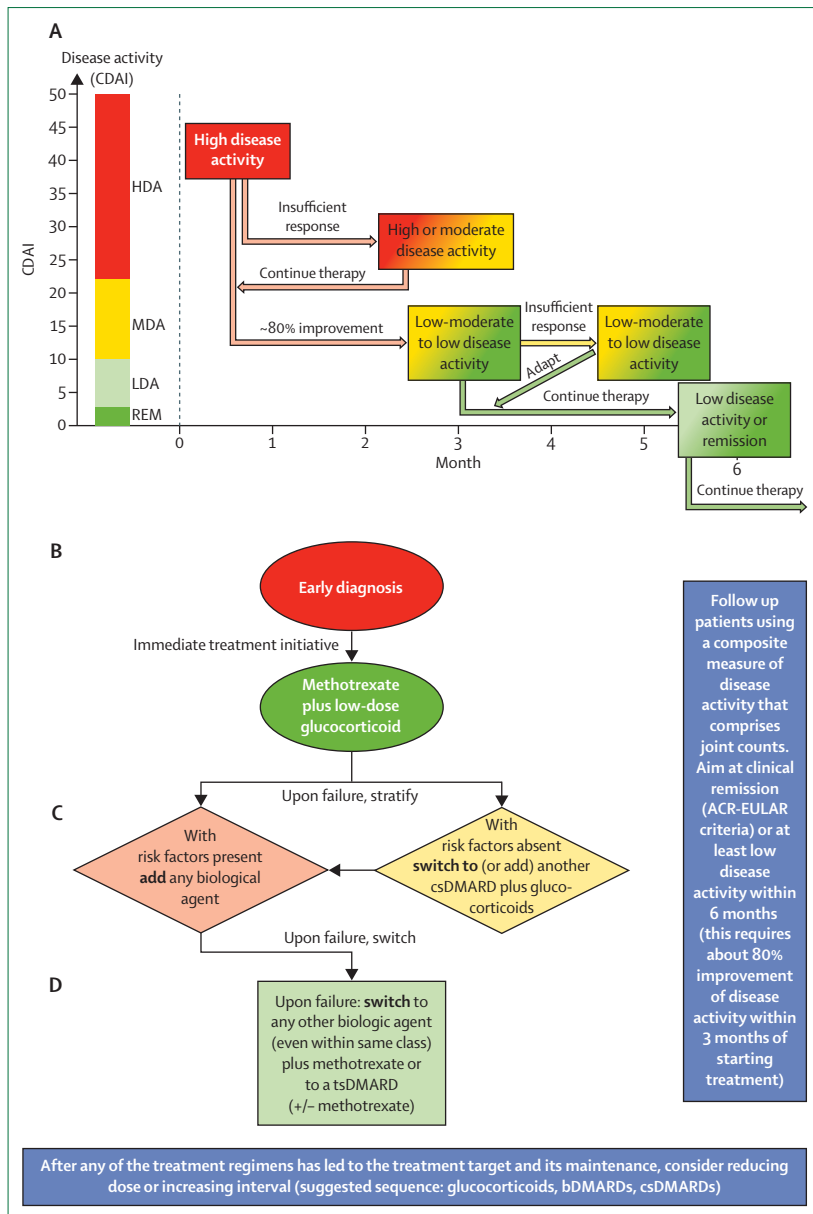


Figure 4: Therapeutic approaches to rheumatoid arthritis

(A) General strategy. (B) Early treatment phase. (C) Treatment approach if methotrexate (plus glucocorticoid) does not achieve the treatment target. (D) Treatment approach after a first biologic has failed. The recommendation to potentially use a TNF inhibitor after another TNF inhibitor has failed is based on the available evidence for biological DMARDs, but in some countries switching to another mode of action is recommended or mandated (against this evidence). Treatment algorithm based on EULAR recommendations.^{89,100} DMARD=disease-modifying antirheumatic drug. tsDMARD=targeted synthetic DMARD. csDMARD=conventional synthetic DMARD. bDMARD=biological DMARD. ACR=American College of Rheumatology. EULAR=European League Against Rheumatism. CDAI=clinical disease activity index. HDA=high disease activity. MDA=moderate disease activity. LDA=low disease activity. REM=remission. TNF=tumour necrosis factor.

have also been developed but are not widely recommended because of insufficient evidence for reliability across all patient populations and reflection of all outcomes.

Remission (primarily for early rheumatoid arthritis) or low disease activity (especially in long-standing disease) have been established as treatment targets.^{89,90} The ACR

and the European League Against Rheumatism (EULAR) recently developed new remission criteria, based on a Boolean approach or on an index approach using the criteria of the SDAI or CDAI (table 1).⁷⁹ Other definitions of remission (eg, remission according to DAS28-ESR criteria; table 1) might not correspond to true remission, because they are associated with progression of joint damage,⁹¹ presence of comorbidities,⁹² and significant residual activity in many patients,^{93,94} even if the established cutpoint of 2.6 is lowered.^{79,95} Although this issue is controversial, our analyses^{96,97} suggest that classification of remission according to DAS28-ESR or DAS28-CRP criteria (table 1) results in high frequency of false-positive responses, particularly when drugs affecting the acute-phase response are used. Indeed, sometimes major differences between DAS28-ESR and DAS28-CRP activity states are observed.^{98,99} Importantly, with the development of the new remission criteria, remission—either index-based or Boolean-based—is now closely related to the absence of residual inflammatory disease activity,¹⁰⁰ leaving other definitions consistent with a state of low disease activity.^{96,101}

Finally, it is important to evaluate structural progression of the disease. Treatment of rheumatoid arthritis should prevent or halt structural changes and thereby minimise or reverse physical disability. In routine practice, radiographs are usually done annually and evaluated semi-quantitatively. Formal scoring of radiographs for progression of erosions and joint space narrowing, as done in trials, is more accurate and sensitive.¹⁰² Other imaging modalities are being increasingly used, especially for diagnostic purposes. MRI scans detect bone marrow oedema as a potential area of (early or future) erosions,¹⁰³ but erosions also correlate well with clinical joint swelling. Ultrasound can quantify the degree and extent of synovial inflammation by using greyscale and power Doppler measurements.^{95,104,105} However, in follow-up, targeting sonographic remission does not provide any benefit over targeting clinical remission or even low disease activity, but is associated with substantial overtreatment.^{106,107}

Notably, many healthy people have detectable ultrasound and MRI signals of synovitis and vascularity.¹⁰⁸ Physical function is typically assessed using the Health Assessment Questionnaire Disability Index,¹⁰⁹ usually at every clinical visit.

Treatment strategies

Because inflammation is at the apex of clinical events (driving clinical symptoms, joint damage, disability, and comorbidity),³³ its reversal is the major therapeutic target; if inflammation subsides rapidly, damage or its progression are prevented, and physical function can be maximally improved without further sequelae. Treatment of rheumatoid arthritis thus requires a strategic approach whereby regular assessment of disease activity drives therapeutic adaptations or changes of drugs in accordance with such activity (treat to target).¹⁰⁰ Composite measures of disease activity that include joint counts are preferred

Timepoint	Methotrexate plus glucocorticoid		Methotrexate plus other csDMARDs plus glucocorticoid, or methotrexate plus bDMARD	
	Dose	LDA (% of patients)	Dose	LDA (% of patients)
CareRA ¹¹³ 4 months	15 mg methotrexate plus 30 mg prednisone (tapered)	87%	15 mg methotrexate plus 2 g sulfasalazine plus 60 mg prednisone (tapered)	85%
tREACH ¹¹⁴ 6 months	25 mg methotrexate plus 15 mg prednisone (tapered)	68%	25 mg methotrexate plus 2 g sulfasalazine plus 400 mg hydroxychloroquine plus 15 mg prednisone (tapered)	71%
IDEA ¹¹⁵ 6 months	20 mg methotrexate plus single intravenous dose of 250 mg methylprednisolone	67%	20 mg methotrexate plus infliximab	65%
BeSt ¹¹⁶ 6 months	7.5 mg methotrexate (increased to 30 mg if needed) plus 2 g sulfasalazine plus 60 mg prednisone	67%	25 mg methotrexate plus infliximab	64%

LDA=low disease activity. DMARD=disease-modifying antirheumatic drug. csDMARD=conventional synthetic DMARD. bDMARD=biological DMARD.

Table 2: Achievement of low disease activity using methotrexate monotherapy (with glucocorticoids) or combination therapy

tools in treat-to-target approaches. In practice, if a state of low disease activity or approximately 80% improvement in SDAI or CDAI has been attained by 3 months, the likelihood of reaching the target at 6 months from therapy initiation is very high.¹¹⁰ If improvement is small at 3 months (figure 4), treatment should be adapted. Likewise, if the state of low disease activity (or remission) is not attained at 6 months, treatment should be re-evaluated. However, escalation of therapy needs to be balanced against patient factors and treatment-related risks.¹⁰⁰

Therapies

Therapeutic approaches

Disease-modifying antirheumatic drugs (DMARDs) target inflammation and by definition must reduce structural damage progression. Non-steroidal anti-inflammatory drugs (NSAIDs), while reducing pain and stiffness and improving physical function, do not interfere with joint damage and are thus not disease modifying. Glucocorticoids offer rapid symptomatic and disease-modifying effects,¹¹¹ but are associated with serious long-term side-effects.

There are two major classes of DMARDs: synthetic and biological. Synthetic DMARDs are further defined as conventional synthetic or targeted synthetic.¹¹² The use of conventional synthetic DMARDs has evolved empirically and their modes of action are still largely unknown. By contrast, targeted synthetic DMARDs have been developed to modulate a particular target implicated in the generation of inflammation. Key examples include janus kinase (JAK) inhibitors, such as tofacitinib or baricitinib (Eli Lilly, Indianapolis, IN, USA).

Conventional synthetic DMARDs and glucocorticoids

According to EULAR recommendations,⁸⁹ treatment should be initiated with a conventional synthetic DMARD, ideally methotrexate, plus low-dose glucocorticoids (figure 4). There is compelling evidence that this is

the optimal approach. First, clinical trials comparing methotrexate plus glucocorticoids with combinations of methotrexate plus a biological agent have shown no significant difference in outcomes (table 2).^{115,116} Clearly, the dose of all conventional synthetic DMARDs should be optimised, escalating methotrexate to 25–30 mg per week (about 0.3 mg/kg)—either orally or subcutaneously—or sulfasalazine up to 3 g per day. Second, comparing methotrexate plus glucocorticoids with combinations of conventional synthetic DMARDs plus glucocorticoids revealed similar efficacy with less toxicity (table 2).^{113,114} Glucocorticoids are given at low to intermediate oral doses or parenterally as single intravenous or intramuscular applications. Low doses of glucocorticoids (<7.5 mg daily) combined with methotrexate confer additive structural protection when compared with methotrexate alone.¹¹⁷ Oral glucocorticoids should be tapered and then stopped within 6 months, when conventional synthetic DMARDs should have induced significant improvement.⁸⁹ With respect to the choice of a conventional synthetic DMARD, methotrexate is considered the anchor drug that also optimises efficacy of biological DMARDs.^{89,90} However, it has not yet been conclusively shown that methotrexate is superior to other conventional synthetic DMARDs clinically or structurally; rather, comparisons with sulfasalazine or leflunomide revealed similar outcomes, but the doses of methotrexate in these studies were low compared with those in current use.¹¹⁸ Other conventional synthetic DMARDs include sulfasalazine, leflunomide, and (for very mild disease) hydroxychloroquine or chloroquine, although these antimalarials have few structural effects.¹¹⁹ In some countries parenteral gold is still used,¹²⁰ but it can have serious side-effects.¹²¹

Table 2 summarises the most recent data on conventional synthetic DMARD monotherapy and combination therapy. These data suggest some uncertainty as to general use of conventional synthetic DMARD combinations. By comparison with methotrexate

	Molecule type	Usual dose*	Loading dose	Comments
Conventional synthetic DMARDs				
Methotrexate	Small chemical	25 mg once weekly*	No	Starting dose 10 mg—escalation to 25 mg within 4–8 weeks; folate use important (suggest 10 mg/week or 1 mg/day)
Sulfasalazine	Small chemical	3 g/day*	No	Starting dose 1 g, escalation to 3 g/day within 4–8 weeks
Leflunomide	Small chemical	20 mg/day	Optional	Loading dose associated with more gastrointestinal side-effects
Hydroxychloroquine	Small chemical	400 mg/day	No	For mild arthritis or as combination therapy
Biological DMARDs				
TNF inhibitors				
Adalimumab	Human monoclonal antibody	40 mg every 2 weeks subcutaneously	No	Biosimilars expected
Certolizumab pegol	F(ab') fragment of a humanised monoclonal antibody	200 mg every 2 weeks subcutaneously	Yes	
Etanercept	IgG-Fc-receptor construct (fusion protein)	50 mg/week subcutaneously	No	Biosimilar approved
Golimumab	Human monoclonal antibody	50 mg/month subcutaneously	No	
Infliximab	Chimeric monoclonal antibody	3–10 mg/kg intravenously every 4–8 weeks	Yes	Biosimilars approved
Anti-B-cell				
Rituximab	Chimeric monoclonal antibody	1000 mg intravenously every 6 months	No	Biosimilars expected
Anti-T-cell co-stimulation				
Abatacept	IgG-Fc-receptor construct (fusion protein)	125 mg/week subcutaneously	No	Intravenous dosing available
Anti-IL 6R				
Tocilizumab	Humanised monoclonal antibody	162.6 mg/week subcutaneously		Intravenous dosing available; sarilumab (anti-IL6R [Regeneron, Tarrytown, NY, USA]) and anti-IL6 cytokine antibodies (sirukumab [Janssen, Springhouse, PA, USA]) in development
Targeted synthetic DMARDs				
Janus kinase inhibitors				
Tofacitinib	Small chemical	5 mg twice daily	No	JAK1/2/3 inhibitor; once daily medication in development; baricitinib (Eli Lilly, Indianapolis, IN, USA), a JAK1/2 inhibitor, has completed phase 3 trials
<small>IL6R=interleukin 6 receptor. IL6=interleukin 6. DMARD=disease-modifying antirheumatic drug. TNF=tumour necrosis factor. *Contraindicated or dose reductions needed with renal or hepatic impairment; for adverse events see package inserts.</small>				

Table 3: DMARDs and recommended doses

monotherapy, there might be no added efficacy of conventional synthetic DMARD combinations at the potential cost of more toxicity. By comparison with biological agents used after methotrexate, conventional synthetic DMARD combination confers profound responses (eg, ACR70) at only low frequencies.¹²² This is a controversial issue,^{118,123} and triple therapy (methotrexate plus sulfasalazine plus hydroxychloroquine) was thought to be more efficacious than monotherapy. Several reviews that addressed higher glucocorticoid doses in the triple therapy arm arrive at different conclusions.^{4,124} Indeed, if the same dose of glucocorticoids is applied across both study groups, the most recent randomised controlled trials show no significant clinical, functional, or structural advantage of conventional synthetic DMARD

combinations compared with methotrexate monotherapy, but more toxicity and discontinuations.^{113,114}

Notably, the new ACR guidelines no longer advocate an early use of combination conventional synthetic DMARD therapy.³⁰ Many studies of such combination therapies were investigator initiated and these trials could have limitations, as discussed by Landewé and colleagues.¹²⁵ However, in patients with low risk of progressive disease, adding a conventional synthetic DMARD when methotrexate has not sufficiently improved disease activity is a possible therapeutic option, although switching the conventional synthetic DMARD is just as good an option.¹¹⁶

When the first treatment cycle fails, EULAR recommends stratification for predictors of severe disease as suggested by high disease activity despite the

previous therapy, autoantibodies (ACPA or RF, especially at high titres), and early joint damage on radiography (figure 4).⁸⁹ Patients with these risk factors should receive a biological DMARD, whereas those without should receive another conventional synthetic DMARD again in combination with glucocorticoids.

Biological DMARDs

Currently approved biological therapeutics for rheumatoid arthritis have four different modes of action:³ TNF inhibition, interleukin 6 receptor inhibition, T-cell co-stimulation blockade, and B-cell depletion (table 3, figures 3, 4, 5). A small proportion of patients respond to inhibition of interleukin 1 pathways.³ Among the TNF inhibitors, five compounds are currently approved, one for intravenous use (infliximab) and four for subcutaneous application (adalimumab, certolizumab pegol, etanercept, and golimumab). Etanercept is a TNF-receptor construct, whereas the others are monoclonal antibodies or fragments of monoclonal antibodies (certolizumab). Etanercept appears to have a lower (but not absent) risk of reactivating tuberculosis than monoclonal antibodies.¹²⁷ Patients with a positive tuberculosis test should receive appropriate prophylactic therapy. Biosimilar infliximab is already available and a biosimilar etanercept has been approved in Europe and other countries (table 3). Interleukin 6 inhibition is currently achieved by treatment with tocilizumab, a humanised monoclonal antibody directed at the interleukin 6 receptor; sarilumab (Bridgewater, NJ, USA), a human interleukin 6 receptor inhibitor, has completed phase 3 trials. Interleukin 6 itself is targeted by several monoclonal antibodies, including sirukumab (Janssen, Springhouse, PA, USA), which has completed phase 3 trials (eg, NCT01606761). Abatacept is presently the only T-cell co-stimulation inhibitor approved for rheumatoid arthritis; intriguingly its efficacy might result not only from T-cell targeting but also from inhibition of myeloid cell function.^{128,129} Rituximab is the only B-cell-directed monoclonal antibody approved for the treatment of rheumatoid arthritis, targeting CD20; biosimilars are expected in the near future.

These mechanistically discrete therapies seem to convey similar efficacy.³ Patients who have not previously received methotrexate have the highest ACR70 response rates (a surrogate for achieving low disease activity) with these therapies. Overall, ACR70 response rates to biological DMARDs in combination with methotrexate in these patients are around 30–40% (figure 5). However, embedded within this group of responders are those who would experience efficacy with methotrexate alone (20–25%). These data informed the decision of EULAR and, more recently, ACR to recommend starting treatment with methotrexate.^{89,90} Importantly, despite differences in targets, all four major modes of action of targeted biologics (in combination with methotrexate) have similar response rates, decreasing with increasing previous drug experience (figures 4, 5).^{3,130,131} This suggests

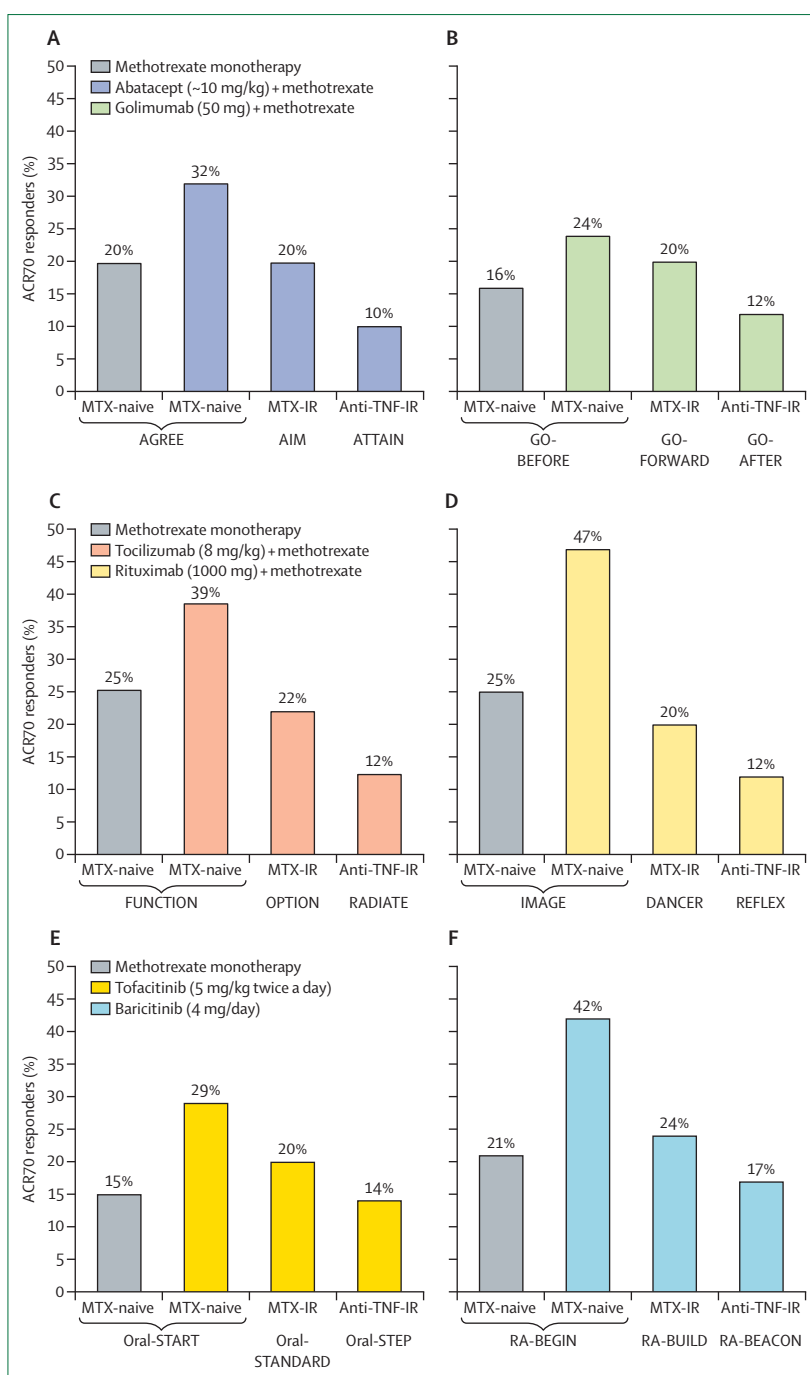


Figure 5: Response to different DMARD therapies

(A) Abatacept (inhibition of T-cell co-stimulation). (B) Golimumab (TNF inhibitor). (C) Tocilizumab (anti-interleukin 6 receptor antibody). (D) Rituximab (anti-CD20 mediated B-cell depletion). (E) Tofacitinib (pan-JAK inhibitor). (F) Baricitinib (JAK1/2 inhibitor; Eli Lilly, Indianapolis, IN, USA). ACR70 improvement rates as a surrogate for profound treatment responses. Baricitinib is not yet approved by regulatory authorities but has completed phase 3 trials. For the full list of references, see appendix. DMARD=disease-modifying antirheumatic drug. MTX=methotrexate. Adapted from Smolen and Aletaha² by permission of Nature Publishing Group.

that all these drugs might mediate their efficacy by interfering with a common final pathway—namely, proinflammatory cytokine production.¹³² See Online for appendix

All biological DMARDs exhibit enhanced efficacy when combined with methotrexate and presumably any other conventional synthetic DMARD, especially leflunomide.^{133,134} No biological DMARD used as monotherapy has shown consistent statistically significant clinical or functional superiority compared with methotrexate.^{126,135,136} Progression of structural damage is inhibited more strongly with biological monotherapy than with methotrexate monotherapy, albeit to a lesser extent than with the combination therapies. Also, combination of biologics with methotrexate has shown clinical and functional superiority to biological monotherapy.^{135–138} Moreover, methotrexate (plus glucocorticoids) conveys similar clinical, functional, and structural efficacy as methotrexate plus biological agent (table 2).^{115,116} However, if a monotherapy of a biological DMARD must be given because of intolerance of all conventional synthetic DMARDs, then tocilizumab would be the biologic of choice, since it has better efficacy than TNF inhibitor monotherapy¹³⁹ and also somewhat better efficacy than methotrexate.^{126,140}

Clinical and structural efficacy is similar across all types of biological DMARDs. This has been shown in meta-analyses, as well as in head-to-head studies.^{3,130,141} When a patient does not achieve the treatment target on a biological DMARD (plus methotrexate), then any other biological DMARD or a targeted synthetic DMARD can be used.⁸⁹ Indeed, even sequential use of TNF-inhibitors after initial lack of response appears to provide similar outcomes as biologics targeting other molecules, at least in clinical trials.^{130,131,142} Of note, in most recommendations or guidelines, rituximab should be used after other biologics have failed; however, it is highly effective in early rheumatoid arthritis¹⁴³ and is often used as a first biologic when others are contraindicated.

Targeted synthetic DMARDs

The first approved targeted synthetic DMARD is tofacitinib, a pan-JAK inhibitor; JAK inhibition interferes with signal transduction and thus cell activation elicited by interleukin 6, granulocyte-monocyte colony stimulating factor, interferons (type I and type II), and common γ -chain cytokines (such as interleukin 2 or interleukin 15).¹⁴⁴ Tofacitinib has been approved in the USA and many other countries, but is not yet approved for use within the European Union. The efficacy of tofacitinib plus methotrexate at the approved dose of 5 mg twice a day appears to be similar to that of biologics (figure 5). Intriguingly, tofacitinib monotherapy is clinically superior to methotrexate,¹⁴⁵ by contrast with most biological DMARDs. In phase 3 clinical trials the JAK 1/2 inhibitor baricitinib, which is not yet approved in any jurisdiction, appears to convey a similar range of efficacy as the biological DMARDs and tofacitinib (figure 5). Interestingly, however, baricitinib plus methotrexate elicited a superior clinical and functional (although not structural) outcome compared with

adalimumab plus methotrexate;¹⁴⁶ moreover, the roughly 15% ACR70 response rate in patients whose disease had previously not responded to or not tolerated a TNF inhibitor was similar to the response rate in patients who had not responded to multiple biologics.¹⁴⁷

Tapering therapy

After the desired treatment target (low disease activity or remission) has been reached, it should be sustained over time. Maintenance of a good outcome will normalise or at least maximise physical function, quality of life, and ability to work. When remission (or a targeted low disease activity) is sustained on biological DMARDs for some time (usually about 6 months), the treating clinician should consider tapering therapeutics. Glucocorticoid should be reduced and discontinued within about 6 months, and this should be done first. For biological therapies, the risk of a flare in disease activity after halving dose or doubling the interval between doses is low, whereas complete withdrawal often leads most patients to experience a flare in disease activity; however, the rate of flares decreases with increasingly lower disease activity and longer duration of sustained response.^{148–150} Importantly, when a flare occurs, patients usually respond very well to re-introduction of the same agent. However, more than 10% of the patients do not regain their original good outcome and, therefore, subjecting patients to abrupt stopping of biologics and thus risking potentially permanent deterioration of their status may be regarded as ethically unsound. Therefore, gradual dose reduction, rather than sudden stopping of biologics, should be the norm.

Adverse event profiles

The biological agents and the targeted synthetic DMARDs induce more adverse events than do conventional synthetic DMARDs. In particular, the incidence of serious infections is increased, although it decreases over time.^{5,151} A special risk relates to reactivation of tuberculosis,¹²⁷ although this has not been reported with rituximab. Rituximab is also the drug of choice in patients with concomitant multiple sclerosis, because it has shown efficacy in this disease,¹⁵² whereas TNF inhibitors can elicit flares of multiple sclerosis.¹⁵³ Patients with hepatitis B or hepatitis C, whose disease is well controlled with antiviral therapy, can be treated with biologics, but hepatologists should be consulted to introduce and monitor antiviral therapy.¹⁵⁴ However, the introduction of curative treatment for hepatitis C is likely to eliminate the potential risk for these patients. Biological agents (except rituximab) should be avoided within 5 years after malignant disease has been cured, although registry data do not suggest increased risks.¹⁵⁵ However, in patients with a history of lymphoma, rituximab or possibly tocilizumab would be drugs of choice.

During pregnancy, the drugs of choice are sulfasalazine or possibly azathioprine, which is approved for rheumatoid arthritis although it seems to have little efficacy.⁴ Methotrexate and leflunomide are contraindicated.¹⁵⁶ The use of biological therapies in pregnancy is controversial.^{157,158} Recent data suggest that use of TNF inhibitors is not associated with effects on conception or teratogenic risk. Similar data have been reported for abatacept and tocilizumab.^{159,160}

Open questions, unmet needs, and future therapeutics

Despite advances made over the past two decades, many open issues remain. First, we do not understand how therapies targeting different molecules achieve such similar efficacies, and we do not even know if profound responses are elicited by these agents in the same, totally different, or overlapping patient populations. Second, we cannot predict optimal responses or toxic risk for a given treatment; molecular analyses have failed to answer this question,^{161–163} although we firmly believe that predictors to permit precision medicine approaches in rheumatology will emerge. Third, although stringent remission (or at least low disease activity) is today's therapeutic goal for rheumatoid arthritis, many patients do not reach this target or achieve it but remain dependent on medication, implying that new therapies are still needed. Fourth, many patients lose responsiveness over time, the reasons for which are not known but might include immunogenicity, or non-adherence. Finally, therapeutics are not delivered via a pathogenetically coherent protocol that takes account of early dominant autoimmunity and later damage-related effector pathways. In this context, early treatment might be highly effective at preventing manifestation of rheumatoid arthritis, but how to detect pre-rheumatoid arthritis or patients at increased risk is unknown. Future diagnostic approaches and therapeutics must address these issues. We contend that there is value in studying the mechanisms of therapeutic failure—for example, interleukin 1, interleukin 12, interleukin 17, interleukin 20, interleukin 21, interleukin 23, anti-CD4, anti-BAFF, and inhibitors of p38-MAPK and SYK. The panel shows new therapeutics that are currently being developed on the basis of pathogenic insights and are being tested in early trials. The ultimate goal is to develop cause-directed, curative therapies, but this will not be possible without better understanding of the cause—or causes—of rheumatoid arthritis.

Conclusions

The therapeutic insights presented in this Seminar constitute the basis for recommendations for the management of rheumatoid arthritis (figure 4).⁸⁹ Early diagnosis and initiation of DMARD therapy are pivotal to prevent damage from occurring or becoming

Panel: Potential future therapeutics for rheumatoid arthritis

Biologics

- Cytokine inhibitors (human, or humanised; eg, targeting interleukin 6, interleukin 21, interferons, granulocyte-monocyte colony stimulating factor or its receptor)
- Cytokine-IgG fusion proteins (eg, interleukin 4-IgG)
- Bi-specific antibodies
- miRNA targeting
- Cell-targeting agents (eg, B-cell depletion, co-stimulatory blockade)

Intracellular signal inhibitors

- Janus kinase inhibitors (eg, baricitinib [Eli Lilly, Indianapolis, IN, USA], filgotinib)
- Bruton's tyrosine kinase inhibitors
- PI3 kinase inhibitors

Cellular therapies

- Tolerogenic dendritic cell transfer
- Stem cell transfer
- T-regulatory-cell activation

Miscellaneous approaches

- Toll-like receptor inhibitors
- PADI4 inhibitors
- Epigenetic modifiers (eg, histone deacetylase inhibitors)
- GnRH antagonists
- Vagus nerve stimulation

clinically significant.¹⁶⁴ The lower the disease activity achieved at 6 months, the better the long-term outcome; reaching stringent clinical remission within 3–6 months halts damage progression independent of the type of therapy used.^{85,91} Setting a treatment target of low disease activity or remission, following up patients regularly using composite disease activity measures (especially joint counts) to determine the disease activity status, and modulating DMARD therapy rapidly if the targeted state has not been achieved within a period of few months lead to better outcomes than routine care.^{165,166} Adding low-dose glucocorticoids to conventional synthetic DMARDs maximises clinical, functional, and structural benefit.^{117,167} In higher-risk patients, using methotrexate as a first DMARD and adding a biologic, for those who do not attain at least low disease activity within 6 months and have high progression risk, optimises benefit.¹⁶⁸ And finally, if a state of low disease activity or an 80% reduction of disease activity is achieved within 3 months from start of treatment, attainment of the target of low disease activity or remission at 6 months is highly likely. Rigorous attention to this regimen, coupled with the development of further therapeutic options for patients who remain unresponsive, should ensure within the next 10 years that most patients will achieve cessation of disease progression and disability, and retention of high levels of quality of life.

Contributors

JSS wrote the first versions of the introduction, the sections on treatment strategies, therapies, tapering, adverse events, failed therapies and open questions, and contributed to all other parts of the manuscript. DA performed the search and wrote the first versions of the sections on epidemiology, differential diagnosis and assessment, and contributed to all other parts of the manuscript. IBM wrote the first versions of the sections on genetics and pathophysiology, contributed to all other parts of the manuscript, and amended language aspects. All authors performed several rounds of amendments and also had a face-to-face meeting to finalise the manuscript. All authors have seen and approved of the final text.

Declaration of interests

JSS has received grants and/or personal fees from Abbvie, Lilly, MSD, Pfizer, Roche, personal fees from Amgen, AstraZeneca, Astro, Celgene, Chugai, GSK, ILTOO, Janssen, Novartis, Samsung, Sanofi, UCB, all outside the submitted work. DA has received personal fees from AbbVie, BMS, and MSD and personal fees from UCB, Janssen, AstraZeneca, Pfizer, Medac, Roche, Eli Lilly & Co, all outside the submitted work. IBM has received grants and/or personal fees from AbbVie, AstraZeneca, BMS, Celgene, Crescendo Bioscience, Janssen, MSD, Novartis, Lilly, UCB, Amgen, and Pfizer, all outside the submitted work.

References

- Aletaha D, Neogi T, Silman A, et al. 2010 rheumatoid arthritis classification criteria: an American College of Rheumatology/European League Against Rheumatism collaborative initiative. *Ann Rheum Dis* 2010; **69**: 1580–88.
- Smolen JS, Aletaha D. Rheumatoid arthritis therapy reappraisal: strategies, opportunities and challenges. *Nat Rev Rheum* 2015; **11**: 276–89.
- Nam JL, Ramiro S, Gaujoux-Viala C, et al. Efficacy of biological disease-modifying antirheumatic drugs: a systematic literature review informing the 2013 update of the EULAR recommendations for the management of rheumatoid arthritis. *Ann Rheum Dis* 2014; **73**: 516–28.
- Gaujoux-Viala C, Nam J, Ramiro S, et al. Efficacy of conventional synthetic disease-modifying antirheumatic drugs, glucocorticoids and tofacitinib: a systematic literature review informing the 2013 update of the EULAR recommendations for management of rheumatoid arthritis. *Ann Rheum Dis* 2014; **73**: 510–15.
- Ramiro S, Gaujoux-Viala C, Nam JL, et al. Safety of synthetic and biological DMARDs: a systematic literature review informing the 2013 update of the EULAR recommendations for management of rheumatoid arthritis. *Ann Rheum Dis* 2014; **73**: 529–35.
- Stoffer MA, Schoels M, Smolen JS, et al. Evidence for treating rheumatoid arthritis to target: results of a systematic literature search update. *Ann Rheum Dis* 2016; **75**: 16–22.
- Cross M, Smith E, Hoy D, et al. The global burden of rheumatoid arthritis: estimates from the global burden of disease 2010 study. *Ann Rheum Dis* 2014; **73**: 1316–22.
- Kitas GD, Gabriel SE. Cardiovascular disease in rheumatoid arthritis: state of the art and future perspectives. *Ann Rheum Dis* 2011; **70**: 8–14.
- Sokka T, Kautiainen H, et al. Work disability remains a major problem in rheumatoid arthritis in the 2000s: data from 32 countries in the QUEST-RA study. *Arthritis Res Ther* 2010; **12**: R42.
- Silman AJ, Pearson JE, Pincus T, et al. Epidemiology and genetics of rheumatoid arthritis. *Arthritis Res* 2002; **4** (suppl 3): S265–72.
- Alamanos Y, Voulgari PV, Drosos AA. Incidence and prevalence of rheumatoid arthritis, based on the 1987 American College of Rheumatology criteria: a systematic review. *Semin Arthritis Rheum* 2006; **36**: 182–88.
- Silman AJ, MacGregor AJ, Thomson W, et al. Twin concordance rates for rheumatoid arthritis: results from a nationwide study. *Br J Rheumatol* 1993; **32**: 903–07.
- Jiang X, Frisell T, Askling J, et al. To what extent is the familial risk of rheumatoid arthritis explained by established rheumatoid arthritis risk factors? *Arthritis Rheumatol* 2015; **67**: 352–62.
- Frisell T, Heggren K, Alfredsson L, Raychaudhuri S, Klareskog L, Askling J. Familial aggregation of arthritis-related diseases in seropositive and seronegative rheumatoid arthritis: a register-based case-control study in Sweden. *Ann Rheum Dis* 2016; **75**: 183–89.
- Roberson ED, Bowcock AM. Psoriasis genetics: breaking the barrier. *Trends Genet* 2010; **26**: 415–23.
- Okada Y, Wu D, Trynka G, et al. Genetics of rheumatoid arthritis contributes to biology and drug discovery. *Nature* 2014; **506**: 376–81.
- Gregersen PK, Silver J, Winchester RJ. The shared epitope hypothesis: an approach to understanding the molecular genetics of susceptibility to rheumatoid arthritis. *Arthritis Rheum* 1987; **30**: 1205–13.
- Viatte S, Plant D, Han B, et al. Association of HLA-DRB1 haplotypes with rheumatoid arthritis severity, mortality, and treatment response. *JAMA* 2015; **313**: 1645–56.
- Lenz TL, Deutsch AJ, Han B, et al. Widespread non-additive and interaction effects within HLA loci modulate the risk of autoimmune diseases. *Nat Genet* 2015; **47**: 1085–90.
- Barra L, Pope J, Bessette L, Haraoui B, Bykerk V. Lack of seroconversion of rheumatoid factor and anti-cyclic citrullinated peptide in patients with early inflammatory arthritis: a systematic literature review. *Rheumatology (Oxford)* 2011; **50**: 311–16.
- Nell-Duxneuner V, Machold K, Stamm T, et al. Autoantibody profiling in patients with very early rheumatoid arthritis: a follow-up study. *Ann Rheum Dis* 2010; **69**: 169–74.
- Klein K, Gay S. Epigenetics in rheumatoid arthritis. *Curr Opin Rheumatol* 2015; **27**: 76–82.
- Liu Y, Aryee MJ, Padyukov L, et al. Epigenome-wide association data implicate DNA methylation as an intermediary of genetic risk in rheumatoid arthritis. *Nat Biotechnol* 2013; **31**: 142–47.
- Baxter D, McInnes IB, Kurowska-Stolarska M. Novel regulatory mechanisms in inflammatory arthritis: a role for microRNA. *Immunol Cell Biol* 2012; **90**: 288–92.
- Bluml S, Bonelli M, Niederreiter B, et al. Essential role of microRNA-155 in the pathogenesis of autoimmune arthritis in mice. *Arthritis Rheum* 2011; **63**: 1281–88.
- Silman AJ, Newman J, MacGregor AJ. Cigarette smoking increases the risk of rheumatoid arthritis. Results from a nationwide study of disease-discordant twins. *Arthritis Rheum* 1996; **39**: 732–35.
- Klareskog L, Malmstrom V, Lundberg K, Padyukov L, Alfredsson L. Smoking, citrullination and genetic variability in the immunopathogenesis of rheumatoid arthritis. *Semin Immunol* 2011; **23**: 92–98.
- Millar K, Lloyd SM, McLean JS, et al. Personality, socio-economic status and inflammation: cross-sectional, population-based study. *PLoS One* 2013; **8**: e58256.
- Callahan LF, Pincus T. Education, self-care, and outcomes of rheumatic diseases: further challenges to the “biomedical model” paradigm. *Arthritis Care Res* 1997; **10**: 283–88.
- Scher JU, Littman DR, Abramson SB. Review: microbiome in inflammatory arthritis and human rheumatic diseases. *Arthritis Rheumatol* 2016; **68**: 35–45.
- Wegner N, Wait R, Sroka A, et al. Peptidylarginine deiminase from *Porphyromonas gingivalis* citrullinates human fibrinogen and α -enolase: implications for autoimmunity in rheumatoid arthritis. *Arthritis Rheum* 2010; **62**: 2662–72.
- Ebringer A, Wilson C. HLA molecules, bacteria and autoimmunity. *J Med Microbiol* 2000; **49**: 305–11.
- Smolen JS, Aletaha D, Koeller M, Weisman M, Emery P. New therapies for the treatment of rheumatoid arthritis. *Lancet* 2007; **370**: 1861–74.
- McInnes IB, Schett G. The pathogenesis of rheumatoid arthritis. *N Engl J Med* 2011; **365**: 2205–19.
- Honda K, Littman DR. The microbiome in infectious disease and inflammation. *Annu Rev Immunol* 2012; **30**: 759–95.
- Scher JU, Ubeda C, Artacho A, et al. Decreased bacterial diversity characterizes the altered gut microbiota in patients with psoriatic arthritis, resembling dysbiosis in inflammatory bowel disease. *Arthritis Rheumatol* 2015; **67**: 128–39.
- Aletaha D, Alasti F, Smolen JS. Rheumatoid factor, not antibodies against citrullinated proteins, is associated with baseline disease activity in rheumatoid arthritis clinical trials. *Arthritis Res Ther* 2015; **17**: 229.
- Gonzalez A, Icen M, Kremers HM, et al. Mortality trends in rheumatoid arthritis: the role of rheumatoid factor. *J Rheumatol* 2008; **35**: 1009–14.
- van Gaalen FA, van Aken J, Huizinga TW, et al. Association between HLA class II genes and autoantibodies to cyclic citrullinated peptides (CCPs) influences the severity of rheumatoid arthritis. *Arthritis Rheum* 2004; **50**: 2113–21.

- 40 Zhao X, Okeke NL, Sharpe O, et al. Circulating immune complexes contain citrullinated fibrinogen in rheumatoid arthritis. *Arthritis Res Ther* 2008; **10**: R94.
- 41 Sabharwal UK, Vaughan JH, Fong S, Bennett PH, Carson DA, Curd JG. Activation of the classical pathway of complement by rheumatoid factors. Assessment by radioimmunoassay for C4. *Arthritis Rheum* 1982; **25**: 161–67.
- 42 Anquetil F, Clavel C, Offer G, Serre G, Sebbag M. IgM and IgA rheumatoid factors purified from rheumatoid arthritis sera boost the Fc receptor- and complement-dependent effector functions of the disease-specific anti-citrullinated protein autoantibodies. *J Immunol* 2015; **194**: 3664–74.
- 43 Schellekens GA, de Jong BA, van den Hoogen FH, van de Putte LB, van Venrooij WJ. Citrulline is an essential constituent of antigenic determinants recognized by rheumatoid arthritis-specific autoantibodies. *J Clin Invest* 1998; **101**: 273–81.
- 44 Girbal-Neuhausser E, Durieux JJ, Arnaud M, et al. The epitopes targeted by the rheumatoid arthritis-associated antifilaggrin autoantibodies are posttranslationally generated on various sites of (pro)filaggrin by deimination of arginine residues. *J Immunol* 1999; **162**: 585–94.
- 45 Reynisdottir G, Olsen H, Joshua V, et al. Signs of immune activation and local inflammation are present in the bronchial tissue of patients with untreated early rheumatoid arthritis. *Ann Rheum Dis* 2015; published online Nov 3. DOI:10.1136/annrheumdis-2015-208216.
- 46 Nielen MM, van Schaardenburg D, Reesink WH, et al. Specific autoantibodies precede the symptoms of rheumatoid arthritis: a study of serial measurements in blood donors. *Arthritis Rheum* 2004; **50**: 380–86.
- 47 Rombouts Y, Willemze A, van Beers JJ, et al. Extensive glycosylation of ACPA-IgG variable domains modulates binding to citrullinated antigens in rheumatoid arthritis. *Ann Rheum Dis* 2016; **75**: 578–85.
- 48 Rombouts Y, Ewing E, van de Stadt LA, et al. Anti-citrullinated protein antibodies acquire a pro-inflammatory Fc glycosylation phenotype prior to the onset of rheumatoid arthritis. *Ann Rheum Dis* 2015; **74**: 234–41.
- 49 Kerkman PF, Fabre E, van der Voort EI, et al. Identification and characterisation of citrullinated antigen-specific B cells in peripheral blood of patients with rheumatoid arthritis. *Ann Rheum Dis* 2015; published online June 1. DOI:10.1136/annrheumdis-2014-207182.
- 50 Harre U, Georgess D, Bang H, et al. Induction of osteoclastogenesis and bone loss by human autoantibodies against citrullinated vimentin. *J Clin Invest* 2012; **122**: 1791–802.
- 51 Bohler C, Radner H, Smolen JS, Aletaha D. Serological changes in the course of traditional and biological disease modifying therapy of rheumatoid arthritis. *Ann Rheum Dis* 2013; **72**: 241–44.
- 52 Shi J, van Veelen PA, Mahler M, et al. Carbamylation and antibodies against carbamylated proteins in autoimmunity and other pathologies. *Autoimmun Rev* 2014; **13**: 225–30.
- 53 Sokolove J, Johnson DS, Lahey LJ, et al. Rheumatoid factor as a potentiator of anti-citrullinated protein antibody-mediated inflammation in rheumatoid arthritis. *Arthritis Rheumatol* 2014; **66**: 813–21.
- 54 Klarenbeek PL, de Hair MJ, Doorenspleet ME, et al. Inflamed target tissue provides a specific niche for highly expanded T-cell clones in early human autoimmune disease. *Ann Rheum Dis* 2012; **71**: 1088–93.
- 55 James EA, Rieck M, Pieper J, et al. Citrulline-specific Th1 cells are increased in rheumatoid arthritis and their frequency is influenced by disease duration and therapy. *Arthritis Rheumatol* 2014; **66**: 1712–22.
- 56 de Hair MJ, Zijlstra IA, Boumans MJ, et al. Hunting for the pathogenesis of rheumatoid arthritis: core-needle biopsy of inguinal lymph nodes as a new research tool. *Ann Rheum Dis* 2012; **71**: 1911–12.
- 57 Mavers M, Ruderman EM, Perlman H. Intracellular signal pathways: potential for therapies. *Curr Rheum Rep* 2009; **11**: 378–85.
- 58 Smolen JS, Steiner G. Therapeutic strategies for rheumatoid arthritis. *Nat Rev Drug Discov* 2003; **2**: 473–88.
- 59 Humby F, Kelly S, Hands R, et al. Use of ultrasound-guided small joint biopsy to evaluate the histopathologic response to rheumatoid arthritis therapy: recommendations for application to clinical trials. *Arthritis Rheumatol* 2015; **67**: 2601–10.
- 60 Feldmann M, Maini SR. Role of cytokines in rheumatoid arthritis: an education in pathophysiology and therapeutics. *Immunol Rev* 2008; **223**: 7–19.
- 61 Pettit AR, Ji H, von Stechow D, et al. TRANCE/RANKL knockout mice are protected from bone erosion in a serum transfer model of arthritis. *Am J Pathol* 2001; **159**: 1689–99.
- 62 Redlich K, Hayer S, Ricci R, et al. Osteoclasts are essential for TNF- α -mediated joint destruction. *J Clin Invest* 2002; **110**: 1419–27.
- 63 Martel-Pelletier J, Welsch DJ, Pelletier JP. Metalloproteases and inhibitors in arthritic diseases. *Best Pract Res Clin Rheumatol* 2001; **15**: 805–29.
- 64 Kraan MC, Versendaal H, Jonker M, et al. Asymptomatic synovitis precedes clinically manifest arthritis. *Arthritis Rheum* 1998; **41**: 1481–88.
- 65 Hayer S, Redlich K, Korb A, Hermann S, Smolen J, Schett G. Tenosynovitis and osteoclast formation as the initial preclinical changes in a murine model of inflammatory arthritis. *Arthritis Rheum* 2007; **56**: 79–88.
- 66 Raza K, Saber TP, Kvien TK, Tak PP, Gerlag DM. Timing the therapeutic window of opportunity in early rheumatoid arthritis: proposal for definitions of disease duration in clinical trials. *Ann Rheum Dis* 2012; **71**: 1921–23.
- 67 Gerlag DM, Raza K, van Baarsen LG, et al. EULAR recommendations for terminology and research in individuals at risk of rheumatoid arthritis: report from the Study Group for Risk Factors for Rheumatoid Arthritis. *Ann Rheum Dis* 2012; **71**: 638–41.
- 68 Radner H, Neogi T, Smolen JS, Aletaha D. Performance of the 2010 ACR/EULAR classification criteria for rheumatoid arthritis: a systematic literature review. *Ann Rheum Dis* 2014; **73**: 114–23.
- 69 Hurd ER. Extraarticular manifestations of rheumatoid arthritis. *Semin Arthritis Rheum* 1979; **8**: 151–76.
- 70 Baecklund E, Iliadou A, Askling J, et al. Association of chronic inflammation, not its treatment, with increased lymphoma risk in rheumatoid arthritis. *Arthritis Rheum* 2006; **54**: 692–701.
- 71 Listing J, Kekow J, Manger B, et al. Mortality in rheumatoid arthritis: the impact of disease activity, treatment with glucocorticoids, TNF α inhibitors and rituximab. *Ann Rheum Dis* 2015; **74**: 415–21.
- 72 Choi HK, Hernan MA, Seeger JD, Robins JM, Wolfe F. Methotrexate and mortality in patients with rheumatoid arthritis: a prospective study. *Lancet* 2002; **359**: 1173–77.
- 73 Jacobsson LT, Turesson C, Nilsson JA, et al. Treatment with TNF blockers and mortality risk in patients with rheumatoid arthritis. *Ann Rheum Dis* 2007; **66**: 670–75.
- 74 Patatianian E, Thompson DF. A review of methotrexate-induced accelerated nodulosis. *Pharmacotherapy* 2002; **22**: 1157–62.
- 75 Lee HH, Song IH, Friedrich M, et al. Cutaneous side-effects in patients with rheumatic diseases during application of tumour necrosis factor- α antagonists. *Br J Dermatol* 2007; **156**: 486–91.
- 76 van der Heijde DM, Van't Hof MA, van Riel PL, van Leeuwen MA, van Rijswijk MH, van de Putte LB. Validity of single variables and composite indices for measuring disease activity in rheumatoid arthritis. *Ann Rheum Dis* 1992; **51**: 177–81.
- 77 Welsing PM, van Gestel AM, Swinkels HL, Kiemeny LA, van Riel PL. The relationship between disease activity, joint destruction, and functional capacity over the course of rheumatoid arthritis. *Arthritis Rheum* 2001; **44**: 2009–17.
- 78 Felson DT, Anderson JJ, Boers M, et al. American College of Rheumatology preliminary definition of improvement in rheumatoid arthritis. *Arthritis Rheum* 1995; **38**: 727–35.
- 79 Felson DT, Smolen JS, Wells G, et al. American College Of Rheumatology/European League Against Rheumatism provisional definition of remission in rheumatoid arthritis for clinical trials. *Ann Rheum Dis* 2011; **70**: 404–13.
- 80 Prevoo MLL, van't Hof MA, Kuper HH, van de Putte LBA, van Riel PLCM. Modified disease activity scores that include twenty-eight-joint counts. Development and validation in a prospective longitudinal study of patients with rheumatoid arthritis. *Arthritis Rheum* 1995; **38**: 44–48.
- 81 Smolen JS, Breedveld FC, Schiff MH, et al. A simplified disease activity index for rheumatoid arthritis for use in clinical practice. *Rheumatology* 2003; **42**: 244–57.

- 82 Aletaha D, Nell VPK, Stamm T, et al. Acute phase reactants add little to composite disease activity indices for rheumatoid arthritis: validation of a clinical activity score. *Arthritis Res Ther* 2005; 7: R796–06.
- 83 Aletaha D, Martinez-Avila J, Kvien TK, Smolen JS. Definition of treatment response in rheumatoid arthritis based on the simplified and the clinical disease activity index. *Ann Rheum Dis* 2012; 71: 1190–96.
- 84 Radner H, Smolen JS, Aletaha D. Remission in rheumatoid arthritis: benefit over low disease activity in patient reported outcomes and costs. *Arthritis Res Ther* 2014; 16: R56.
- 85 Smolen JS, Han C, Van der Heijde DM, et al. Radiographic changes in rheumatoid arthritis patients attaining different disease activity states with methotrexate monotherapy and infliximab plus methotrexate: the impacts of remission and TNF-blockade. *Ann Rheum Dis* 2009; 68: 823–27.
- 86 Welsing PM, Landewe RB, van Riel PL, et al. The relationship between disease activity and radiologic progression in patients with rheumatoid arthritis: a longitudinal analysis. *Arthritis Rheum* 2004; 50: 2082–93.
- 87 Smolen JS, van der Heijde DMFM, St Clair EW, et al. Predictors of joint damage in patients with early rheumatoid arthritis treated with high-dose methotrexate without or with concomitant infliximab. Results from the ASPIRE trial. *Arthritis Rheum* 2006; 54: 702–10.
- 88 Pincus T, Swearingen CJ, Bergman M, Yazici Y. RAPID3 (Routine Assessment of Patient Index Data 3), a rheumatoid arthritis index without formal joint counts for routine care: proposed severity categories compared to disease activity score and clinical disease activity index categories. *J Rheumatol* 2008; 35: 2136–47.
- 89 Smolen JS, Landewe R, Breedveld FC, et al. EULAR recommendations for the management of rheumatoid arthritis with synthetic and biological disease-modifying antirheumatic drugs: 2013 update. *Ann Rheum Dis* 2014; 73: 492–509.
- 90 Singh JA, Saag KG, Bridges SL, et al. 2015 American College of Rheumatology guideline for the treatment of rheumatoid arthritis. *Arthritis Care Res* 2016; 68: 1–25.
- 91 Kavanaugh A, Fleischmann RM, Emery P, et al. Clinical, functional and radiographic consequences of achieving stable low disease activity and remission with adalimumab plus methotrexate or methotrexate alone in early rheumatoid arthritis: 26-week results from the randomised, controlled OPTIMA study. *Ann Rheum Dis* 2013; 72: 64–71.
- 92 Thiele K, Huscher D, Bischoff S, et al. Performance of the 2011 ACR/EULAR preliminary remission criteria compared with DAS28 remission in unselected patients with rheumatoid arthritis. *Ann Rheum Dis* 2013; 72: 1194–99.
- 93 Makinen H, Kautiainen H, Hannonen P, Sokka T. Is DAS28 an appropriate tool to assess remission in rheumatoid arthritis? *Ann Rheum Dis* 2005; 64: 1410–13.
- 94 Fleischmann R, van der Heijde D, Koenig AS, et al. How much does Disease Activity Score in 28 joints ESR and CRP calculations underestimate disease activity compared with the Simplified Disease Activity Index? *Ann Rheum Dis* 2015; 74: 1132–37.
- 95 Balsa A, de Miguel E, Castillo C, Peiteado D, Martin-Mola E. Superiority of SDAI over DAS-28 in assessment of remission in rheumatoid arthritis patients using power Doppler ultrasonography as a gold standard. *Rheumatology (Oxford)* 2010; 49: 683–90.
- 96 Smolen JS, Aletaha D. Interleukin-6 receptor inhibition with tocilizumab and attainment of disease remission in rheumatoid arthritis: the role of acute-phase reactants. *Arthritis Rheum* 2011; 63: 43–52.
- 97 Smolen JS, Collaud Basset S, Boers M, et al, for the European Society for Clinical and Economic Aspects of Osteoporosis, Osteoarthritis and Musculoskeletal Diseases (ESCEO). Clinical trials of new drugs for the treatment of rheumatoid arthritis: focus on early disease. *Ann Rheum Dis* 2016; published online April 1. DOI:10.1136/annrheumdis-2016-209429.
- 98 Fleischmann R, Kremer J, Cush J, et al. Placebo-controlled trial of tofacitinib monotherapy in rheumatoid arthritis. *N Engl J Med* 2012; 367: 495–507.
- 99 Smolen JS, Aletaha D, Gruben D, et al. Remission rates with tofacitinib treatment in rheumatoid arthritis: a comparison of various remission criteria. *Arthritis Rheum* 2012; 64 (suppl): S334.
- 100 Smolen JS, Breedveld FC, Burmester GR, et al. Treating rheumatoid arthritis to target: 2014 update of the recommendations of an international task force. *Ann Rheum Dis* 2016; 75: 3–15.
- 101 Food and Drug Administration. Guidance for industry—rheumatoid arthritis: Developing drug products for treatment. Draft Guidance May 2013. <http://www.fda.gov/downloads/Drugs/GuidanceComplianceRegulatoryInformation/Guidances/UCM354468.pdf> (accessed Jan 18, 2016).
- 102 van der Heijde D, Simon L, Smolen J, et al. How to report radiographic data in randomized clinical trials in rheumatoid arthritis: guidelines from a roundtable discussion. *Arthritis Rheum* 2002; 47: 215–18.
- 103 Jimenez-Boj E, Nobauer-Huhmann I, Hanslik-Schnabel B, et al. Bone erosions and bone marrow edema as defined by magnetic resonance imaging reflect true bone marrow inflammation in rheumatoid arthritis. *Arthritis Rheum* 2007; 56: 1118–24.
- 104 Mandl P, Balint PV, Brault Y, et al. Metrologic properties of ultrasound versus clinical evaluation of synovitis in rheumatoid arthritis: results of a multicenter, randomized study. *Arthritis Rheum* 2012; 64: 1272–82.
- 105 Sakellariou G, Scire CA, Verstappen SM, Montecucco C, Caporali R. In patients with early rheumatoid arthritis, the new ACR/EULAR definition of remission identifies patients with persistent absence of functional disability and suppression of ultrasonographic synovitis. *Ann Rheum Dis* 2013; 72: 245–49.
- 106 Dale J, Striling A, McInnes IB, Porter D. Targeting ultrasound remission in early rheumatoid arthritis—results of the Taser study. *Arthritis Rheum* 2013; 65 (suppl): S338–39.
- 107 Nordberg Lena B, Lie E, Lillegraven S, et al. Ultrasonography versus clinical examination in early DMARD-naive rheumatoid arthritis—a comparative study of synovitis on the individual joint level. *Arthritis Rheumatol* 2015; 67 (suppl 10): 162 (abstr).
- 108 Terslev L, Torp-Pedersen S, Qvistgaard E, von der RP, Bliddal H. Doppler ultrasound findings in healthy wrists and finger joints. *Ann Rheum Dis* 2004; 63: 644–48.
- 109 Fries JF, Spitz P, Kraines RG, Holman HR. Measurement of patient outcome in arthritis. *Arthritis Rheum* 1980; 23: 137–45.
- 110 Aletaha D, Alasti F, Smolen JS. Optimisation of a treat-to-target approach in rheumatoid arthritis: strategies for the 3-month time point. *Ann Rheum Dis* 2015; published online Sept 29. DOI:10.1136/annrheumdis-2015-208324.
- 111 Kirwan JR. The effect of glucocorticoids on joint destruction in rheumatoid arthritis. The Arthritis and Rheumatism Council Low-Dose Glucocorticoid Study Group. *N Engl J Med* 1995; 333: 142–46.
- 112 Smolen JS, van der Heijde D, Machold KP, Aletaha D, Landewe R. Proposal for a new nomenclature of disease-modifying antirheumatic drugs. *Ann Rheum Dis* 2014; 73: 3–5.
- 113 Verschuere P, De CD, Corluy L, et al. Methotrexate in combination with other DMARDs is not superior to methotrexate alone for remission induction with moderate-to-high-dose glucocorticoid bridging in early rheumatoid arthritis after 16 weeks of treatment: the CareRA trial. *Ann Rheum Dis* 2015; 74: 27–34.
- 114 de Jong PH, Hazes JM, Han HK, et al. Randomised comparison of initial triple DMARD therapy with methotrexate monotherapy in combination with low-dose glucocorticoid bridging therapy: 1-year data of the tREACH trial. *Ann Rheum Dis* 2014; 73: 1331–39.
- 115 Nam JL, Villeneuve E, Hensor EM, et al. Remission induction comparing infliximab and high-dose intravenous steroid, followed by treat-to-target: a double-blind, randomised, controlled trial in new-onset, treatment-naive, rheumatoid arthritis (the IDEA study). *Ann Rheum Dis* 2014; 73: 75–85.
- 116 Goekoop-Ruiterman YP, De Vries-Bouwstra JK, Allaart CF, et al. Clinical and radiographic outcomes of four different treatment strategies in patients with early rheumatoid arthritis (the BeSt study): a randomized, controlled trial. *Arthritis Rheum* 2005; 52: 3381–90.
- 117 Wassenberg S, Rau R, Steinfeld P, Zeidler H. Very low-dose prednisolone in early rheumatoid arthritis retards radiographic progression over two years: a multicenter, double-blind, placebo-controlled trial. *Arthritis Rheum* 2005; 52: 3371–80.
- 118 Dougados M, Combe B, Cantagrel A, et al. Combination therapy in early rheumatoid arthritis: a randomised, controlled, double blind 52 week clinical trial of sulphasalazine and methotrexate compared with the single components. *Ann Rheum Dis* 1999; 58: 220–25.
- 119 van der Heijde DM, van Riel PL, Nuver-Zwart IH, Gribnau FW, van de Putte LB. Effects of hydroxychloroquine and sulphasalazine on progression of joint damage in rheumatoid arthritis. *Lancet* 1989; 333: 1036–38.

- 120 Rau R, Herborn G, Menninger H, Sangha O. Radiographic outcome after three years of patients with early erosive rheumatoid arthritis treated with intramuscular methotrexate or parenteral gold. Extension of a one-year double-blind study in 174 patients. *Rheumatology* 2002; **41**: 196–204.
- 121 Ward JR, Williams JF, Egger MJ, et al. Comparison of auranofin, gold sodium thiomalate, and placebo in the treatment of rheumatoid arthritis. A controlled clinical trial. *Arthritis Rheum* 1983; **26**: 1303–15.
- 122 O'Dell JR, Mikuls TR, Taylor TH, et al. Therapies for active rheumatoid arthritis after methotrexate failure. *N Engl J Med* 2013; **369**: 307–18.
- 123 Capell HA, Madhok R, Porter DR, et al. Combination therapy with sulfasalazine and methotrexate is more effective than either drug alone in patients with rheumatoid arthritis with a suboptimal response to sulfasalazine: results from the double-blind placebo-controlled MASCOT study. *Ann Rheum Dis* 2007; **66**: 235–41.
- 124 Smolen JS, Aletaha D, Keystone E. Superior efficacy of combination therapy for rheumatoid arthritis: fact or fiction? *Arthritis Rheum* 2005; **52**: 2975–83.
- 125 Landewe RB, Smolen JS, Weinblatt ME, et al. Can we improve the performance and reporting of investigator-initiated clinical trials? Rheumatoid arthritis as an example. *Ann Rheum Dis* 2014; **73**: 1755–60.
- 126 Burmester GR, Rigby WF, van Vollenhoven RF, et al. Tocilizumab in early progressive rheumatoid arthritis: FUNCTION, a randomised controlled trial. *Ann Rheum Dis* 2015; published online Oct 28. DOI:10.1136/annrheumdis-2015-207628.
- 127 Winthrop KL, Siegel JN, Jereb J, Taylor Z, Iademarco MF. Tuberculosis associated with therapy against tumor necrosis factor α . *Arthritis Rheum* 2005; **52**: 2968–74.
- 128 Patakas A, Ji RR, Weir W, et al. Abatacept inhibition of T cell priming in mice by induction of a unique transcriptional profile that reduces their ability to activate antigen-presenting cells. *Arthritis Rheumatol* 2016; **68**: 627–38.
- 129 Bonelli M, Ferner E, Goschl L, et al. Abatacept (CTLA-4IG) treatment reduces the migratory capacity of monocytes in patients with rheumatoid arthritis. *Arthritis Rheum* 2013; **65**: 599–607.
- 130 Schoels M, Aletaha D, Smolen JS, Wong JB. Comparative effectiveness and safety of biological treatment options after tumour necrosis factor α inhibitor failure in rheumatoid arthritis: systematic review and indirect pairwise meta-analysis. *Ann Rheum Dis* 2012; **71**: 1303–08.
- 131 Smolen JS, Kay J, Matteson EL, et al. Insights into the efficacy of golimumab plus methotrexate in patients with active rheumatoid arthritis who discontinued prior anti-tumour necrosis factor therapy: post-hoc analyses from the GO-AFTER study. *Ann Rheum Dis* 2014; **73**: 1811–18.
- 132 Smolen JS, Aletaha D. Forget personalised medicine and focus on abating disease activity. *Ann Rheum Dis* 2013; **72**: 3–6.
- 133 Burmester GR, Mariette X, Montecucco C, et al. Adalimumab alone and in combination with disease-modifying antirheumatic drugs for the treatment of rheumatoid arthritis in clinical practice: the Research in Active Rheumatoid Arthritis (ReAct) trial. *Ann Rheum Dis* 2007; **66**: 732–39.
- 134 De SR, Frati E, Nargi F, et al. Comparison of combination therapies in the treatment of rheumatoid arthritis: leflunomide-anti-TNF- α versus methotrexate-anti-TNF- α . *Clin Rheumatol* 2010; **29**: 517–24.
- 135 Breedveld FC, Weisman MH, Kavanaugh AF, et al. The PREMIER study—a multicenter, randomized, double-blind clinical trial of combination therapy with adalimumab plus methotrexate versus methotrexate alone or adalimumab alone in patients with early, aggressive rheumatoid arthritis who had not had previous methotrexate treatment. *Arthritis Rheum* 2006; **54**: 26–37.
- 136 Klareskog L, van der Heijde D, de Jager JP, et al. Therapeutic effect of the combination of etanercept and methotrexate compared with each treatment alone in patients with rheumatoid arthritis: double-blind randomised controlled trial. *Lancet* 2004; **363**: 675–81.
- 137 Dougados M, Kissel K, Conaghan PG, et al. Clinical, radiographic and immunogenic effects after 1 year of tocilizumab-based treatment strategies in rheumatoid arthritis: the ACT-RAY study. *Ann Rheum Dis* 2014; **73**: 803–09.
- 138 Kaneko Y, Atsumi T, Tanaka Y, et al. Comparison of adding tocilizumab to methotrexate with switching to tocilizumab in patients with rheumatoid arthritis with inadequate response to methotrexate: 52-week results from a prospective, randomised, controlled study (SURPRISE study). *Ann Rheum Dis* 2016; published online Jan 5. DOI:10.1136/annrheumdis-2015-208426.
- 139 Gabay C, Emery P, van Vollenhoven R, et al. Tocilizumab monotherapy versus adalimumab monotherapy for treatment of rheumatoid arthritis (ADACTA): a randomised, double-blind, controlled phase 4 trial. *Lancet* 2013; **381**: 1541–50.
- 140 Jones G, Sebba A, Gu J, et al. Comparison of tocilizumab monotherapy versus methotrexate monotherapy in patients with moderate to severe rheumatoid arthritis: the AMBITION study. *Ann Rheum Dis* 2010; **69**: 88–09.
- 141 Weinblatt ME, Schiff M, Valente R, et al. Head-to-head comparison of subcutaneous abatacept versus adalimumab for rheumatoid arthritis: findings of a phase IIIb, multinational, prospective, randomized study. *Arthritis Rheum* 2013; **65**: 28–38.
- 142 Manders SH, Kievit W, Adang E, et al. Cost-effectiveness of abatacept, rituximab, and TNFi treatment after previous failure with TNFi treatment in rheumatoid arthritis: a pragmatic multi-centre randomised trial. *Arthritis Res Ther* 2015; **17**: 134.
- 143 Tak PP, Rigby WF, Rubbert-Roth A, et al. Inhibition of joint damage and improved clinical outcomes with rituximab plus methotrexate in early active rheumatoid arthritis: the IMAGE trial. *Ann Rheum Dis* 2011; **70**: 39–46.
- 144 O'Shea JJ, Schwartz DM, Villarino AV, Gadina M, McInnes IB, Laurence A. The JAK-STAT pathway: impact on human disease and therapeutic intervention. *Annu Rev Med* 2015; **66**: 311–28.
- 145 Lee EB, Fleischmann R, Hall S, et al. Tofacitinib versus methotrexate in rheumatoid arthritis. *N Engl J Med* 2014; **370**: 2377–86.
- 146 Taylor PC, Keystone EC, van der Heijde D, et al. Baricitinib versus placebo or adalimumab in patients with active rheumatoid arthritis (RA) and an inadequate response to background methotrexate therapy: results of a phase 3 study. *Arthritis Rheum* 2015; **67** (suppl 10): L2 (abstr).
- 147 Genovese MC, Kremer J, Zamani O, et al. Baricitinib in patients with refractory rheumatoid arthritis. *N Engl J Med* 2016; **374**: 1243–52.
- 148 Smolen JS, Nash P, Durez P, et al. Maintenance, reduction, or withdrawal of etanercept after treatment with etanercept and methotrexate in patients with moderate rheumatoid arthritis (PRESERVE): a randomised controlled trial. *Lancet* 2013; **381**: 918–29.
- 149 Emery P, Burmester GR, Bykerk VP, et al. Evaluating drug-free remission with abatacept in early rheumatoid arthritis: results from the phase 3b, multicentre, randomised, active-controlled AVERT study of 24 months, with a 12-month, double-blind treatment period. *Ann Rheum Dis* 2015; **74**: 19–26.
- 150 Smolen JS, Emery P, Ferraccioli GF, et al. Certolizumab pegol in rheumatoid arthritis patients with low to moderate activity: the CERTAIN double-blind, randomised, placebo-controlled trial. *Ann Rheum Dis* 2014; published online Jan 15. DOI:10.1136/annrheumdis-2013-204632.
- 151 Listing J, Strangfeld A, Kary S, et al. Infections in patients with rheumatoid arthritis treated with biologic agents. *Arthritis Rheum* 2005; **52**: 3403–12.
- 152 Hauser SL, Waubant E, Arnold DL, et al. B-cell depletion with rituximab in relapsing-remitting multiple sclerosis. *N Engl J Med* 2008; **358**: 676–88.
- 153 Mohan N, Edwards ET, Cupps TR, et al. Demyelination occurring during anti-tumor necrosis factor α therapy for inflammatory arthritides. *Arthritis Rheum* 2001; **44**: 2862–69.
- 154 Nard FD, Todoerti M, Grosso V, et al. Risk of hepatitis B virus reactivation in rheumatoid arthritis patients undergoing biologic treatment: extending perspective from old to newer drugs. *World J Hepatol* 2015; **7**: 344–61.
- 155 Strangfeld A, Hiese F, Rau R, et al. Risk of incident or recurrent malignancies among patients with rheumatoid arthritis exposed to biologic therapy in the German biologics register RABBIT. *Arthritis Res Ther* 2010; **12**: R5.
- 156 Ostensen M, Forger F. Management of RA medications in pregnant patients. *Nat Rev Rheumatol* 2009; **5**: 382–90.

- 157 Verstappen SM, King Y, Watson KD, Symmons DP, Hyrich KL. Anti-TNF therapies and pregnancy: outcome of 130 pregnancies in the British Society for Rheumatology Biologics Register. *Ann Rheum Dis* 2011; **70**: 823–26.
- 158 Raja H, Matteson EL, Michet CJ, Smith JR, Pulido JS. Safety of tumor necrosis factor inhibitors during pregnancy and breastfeeding. *Transl Vis Sci Technol* 2012; **1**: 6.
- 159 Gotestam SC, Hoeltzenbein M, Tincani A, et al. The EULAR points to consider for use of antirheumatic drugs before pregnancy, and during pregnancy and lactation. *Ann Rheum Dis* 2016; **75**: 795–810.
- 160 Flint J, Panchal S, Hurrell A, et al. BSR and BHRP guideline on prescribing drugs in pregnancy and breastfeeding—Part I: standard and biologic disease modifying anti-rheumatic drugs and corticosteroids. *Rheumatology* 2016; published online Jan 10.
- 161 Ducreux J, Durez P, Galant C, et al. Global molecular effects of tocilizumab therapy in rheumatoid arthritis synovium. *Arthritis Rheumatol* 2014; **66**: 15–23.
- 162 Ortea I, Roschitzki B, Ovalles JG, et al. Discovery of serum proteomic biomarkers for prediction of response to infliximab (a monoclonal anti-TNF antibody) treatment in rheumatoid arthritis: an exploratory analysis. *J Proteomics* 2012; **77**: 372–82.
- 163 Semerano L, Romeo PH, Boissier MC. Metabolomics for rheumatic diseases: has the time come? *Ann Rheum Dis* 2015; **74**: 1325–26.
- 164 Combe B, Landewe R, Lukas C, et al. Eular recommendations for the management of early arthritis: Report of a task force of the European Standing Committee for International Clinical Studies Including Therapeutics (ESCSIT). *Ann Rheum Dis* 2006; **66**: 34–45.
- 165 Grigor C, Capell H, Stirling A, et al. Effect of a treatment strategy of tight control for rheumatoid arthritis (the TICORA study): a single-blind randomised controlled trial. *Lancet* 2004; **364**: 263–69.
- 166 Gullick NJ, Oakley SP, Zain A, et al. Goal-directed therapy for RA in routine practice is associated with improved function in patients with disease duration up to 15 years. *Rheumatology (Oxford)* 2012; **51**: 759–61.
- 167 Bakker MF, Jacobs JW, Welsing PM, et al. Low-dose prednisone inclusion in a methotrexate-based, tight control strategy for early rheumatoid arthritis: a randomized trial. *Ann Intern Med* 2012; **156**: 329–39.
- 168 Smolen JS, Emery P, Fleischmann R, et al. Adjustment of therapy in rheumatoid arthritis on the basis of achievement of stable low disease activity with adalimumab plus methotrexate or methotrexate alone: the randomised controlled OPTIMA trial. *Lancet* 2014; **383**: 321–32.